Lanthanide Tetraisobutylaluminate Complexes: Structures, Single Component Catalysts, and Isoprene Polymerization

DISSERTATION

der Mathematisch-Naturwissenschaftlichen Fakultät

der Eberhard Karls Universität Tübingen

zur Erlangung des Grades eines

Doktors der Naturwissenschaften

(Dr. rer. nat.)

vorgelegt von

M. Sc. Eric C. Moinet

aus Freudenstadt

Tübingen

2023

Gedruckt mit Genehmigung der Mathematisch-Naturwissenschaftlichen Fakultät der Eberhard Karls Universität Tübingen.

Tag der mündlichen Qualifikation:	20.12.2023
Dekan:	Prof. Dr. Thilo Stehle
1. Berichterstatter:	Prof. Dr. Reiner Anwander
2. Berichterstatter:	Prof. Dr. Lars Wesemann
3. Berichterstatter:	Prof. Dr. Marc Visseaux

Lanthanide Tetraiosbutylaluminate Complexes: Structures, Single Component Catalysts, and Isoprene Polymerization

Eric C. Moinet

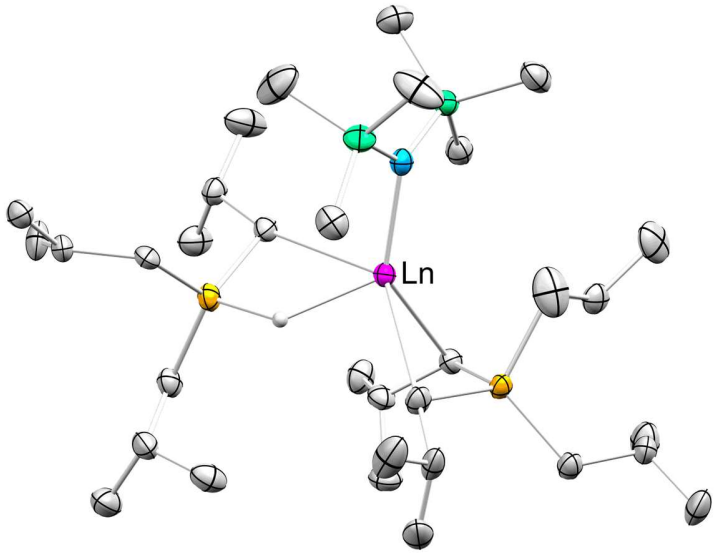

Preface

This PhD thesis consists of a general introduction into conjugated diene polymerization and polymers focusing on polyisoprene, and a research study examining the reactivity of rare-earth metal complexes towards higher organoaluminum reagent comprising residues larger than methyl, and evolving complexes characterized in the solid state by single X-ray diffraction, a summary of the main results, and original scientific papers.

This work has been performed at the Institut für Anorganische Chemie, Eberhard Karls Universität Tübingen, Germany in the period from May 2019 to June 2023 under supervision of Prof. Dr. Reiner Anwander. We are grateful for the generous support by Bridgestone Japan.

Parts of this thesis have been presented at both national, and international conferences as poster presentations.

Contents

List of Abbreviations

°C Degree Celsius

Å Ångström (10^{-10} m)

A Trityl Tetrakis(pentafluorophenyl)borate $[Ph_3C]^+[B(C_6F_5)_4]^-$

Ar Aryl

B *N*,*N*-Dimethylanilinium Tetrakis(pentafluorophenyl)borate $[C_6H_5NMe_2H]^+[B(C_6F_5)_4]^-$

Bn Benzyl

b. p. Boiling Point

C Tris(pentafluorophenyl)boron $[B(C_6F_5)_3]$

$Car^{Mes}PyCar^{Mes}$ 2,6-bis(3-mesitylimidazol-2-ylidene)pyridine

CN Coordination Number

COD 1,5-Cyclooctadiene

COSY Correlated Spectroscopy

Cp Cyclopentadienyl

Cp* Pentamethylcyclopentadienyl

D Dimethylaluminum Chloride $[Me_2AlCl]$

deg Degree

DFB 1,2-Difluorobenzene

DIBAH Diisobutylaluminum Hydride $[i Bu_2AlH]$

Diglyme 1-Methoxy-2-(2-methoxyethoxy)ethane

DME 1,2-Dimethoxyethane

Do Donor

DRIFTS Diffuse Reflectance Infrared Fourier Transform Spectroscopy

DSC Differential Scanning Calorimetry

E Diethylaluminum Chloride $[Et_2AlCl]$

EA Elemental Analysis

equiv. Equivalent

Et	Ethyl
F	Diisobutylaluminum Chloride [iBu$_2$AlCl]
Flu	Fluorenide, Fluorenyl
GPC	Gel Permeation Chromatography
h	Hour
HMBC	Heteronuclear Multiple Bond Correlation
HSQC	Heteronuclear Single Quantum Coherence
Hz	Hertz
iBu	Isobutyl
IP	Isoprene
iPr	Isopropyl
IR	Infrared
L	(Spectator)Ligand
Ln	Rare-earth Metals (Sc, Y, La-Lu)
L3	1,3-bis[O-4,6-di-tBu-C$_6$H$_2$-2-CH$_2$][C(NCH$_2$CH$_2$N)]
MAO	Methylaluminoxane
Me	Methyl
MMA	Methyl Methacrylate
M_n	Number Average Molar Mass
M_w	Mass Average Molar Mass
MWD	Molecular Weight Distribution
NN	2-(2,6-iPr$_2$C$_6$H$_3$N=CH)-5-tBuC$_4$H$_2$N$^-$
NMR	Nuclear Magnetic Resonance
NR	Natural Rubber
o	ortho
PBD	Polybutadiene
PDI	Polydispersity Index
Ph	Phenyl
Phen	Phenanthroline

PIP Polyisoprene

py Pyridine

r. t. Room Temperature

SIR Sterically Induced Reduction

*t*Bu *tert*-butyl

TCyTAC 1,3,5-Tricyclohexyl-1,3,5-triazacyclohexan

THF Tetrahydrofuran

TIBA Triisobutylaluminum

TMEDA Tetramethylethylenediamine

TOF Turnover frequency

$TP^{tBu,Me}$ Tris(3,5-dimethyl-pyrazolyl)borato

Triglyme Triethylene glycol dimethyl ether

V Volt

VT Variable Temperature

δ Chemical Shift

Summary

Nowadays, synthetic high-performance rubbers are indispensable for tire production. Neodymium-based catalysts provide the most efficient way to gain access to this kind of material, achieving desired physical properties and polymer selectivities. However, mechanisms involved for active catalyst formation are far from understood, especially the role of triisobutylaluminum comprised in inherently complicated catalyst mixtures, and only very few solid-state structures give insight into lanthanide-isobutyl interactions.

The present work reports on the first homoleptic Ln(II) tetraisobutylaluminates Ln(Al*i*Bu$_4$)$_2$ (Ln = Sm, Eu, Yb). Characterization in the solid state revealed an unprecedented bis-η^3-coordination of both tetraisobutylaluminato anions. Remarkably, Ln(Al*i*Bu$_4$)$_2$ (Ln = Sm, Eu, Yb) turned out to be single-component catalysts for isoprene polymerization, whereas a number of derivatization products of Ln(Al*i*Bu$_4$)$_2$ (Ln = Sm, Yb) did not lead to species active in polymerization. Activation of Ln(Al*i*Bu$_4$)$_2$ (Ln = Sm, Eu, Yb) with borate cocatalyst [PhNMe$_2$H][B(C$_6$F$_5$)$_4$] led to polymers with very narrow molecular weight distributions, i.e. for the Yb(Al*i*Bu$_4$)$_2$/[PhNMe$_2$H][B(C$_6$F$_5$)$_4$] mixture, a living polymerization was observed. NMR-spectroscopic studies gave evidence on species involved.

For the synthesis of Ln(III) tetraisobutylaluminates, we employed an amide elimination protocol starting from trivalent Ln[N(SiMe$_3$)$_2$]$_3$ and triisobutylaluminum. Ln[N(SiMe$_3$)$_2$](HAl*i*Bu$_3$)(Al*i*Bu$_4$) could be crystallized for the rare-earth elements lanthanum, praseodymium, neodymium, and gadolinium and characterized in the solid state. Hydride formation by β-H-elimination from isobutyl groups was found to be an important reactivity, and is highlighted by derivatization products such as [(μ-fluorenyl)$_3$La$_2$(μ-H)(HAl*i*Bu$_3$)$_2$]. Reaction of Nd[N(SiMe$_3$)$_2$](HAl*i*Bu$_3$)(Al*i*Bu$_4$) with [PhNMe$_2$H][B(C$_6$F$_5$)$_4$] led to the formation of [Nd{N(SiMe$_3$)$_2$}(PhNMe$_2$)$_2$][B(C$_6$F$_5$)$_4$]$_2$, which was active in isoprene polymerization without additional cocatalyst, and polymer data allowed to suggest a possible mechanistic scenario. In isoprene polymerization, the catalyst system Gd[N(SiMe$_3$)$_2$](HAl*i*Bu$_3$)(Al*i*Bu$_4$)/*i*Bu$_2$AlCl yielded high molecular weight polyisoprene with an impressively high *cis*-selectivity of >99.5%.

To obtain mixed chlorido/isobutylaluminato precatalysts, we treated [Ln{N(SiMe$_3$)$_2$}$_2$(μ-Cl)(thf)]$_2$ (Ln = La, Nd) with triisobutylaluminum. Accordingly, [Ln{N(SiMe$_3$)$_2$}(Al*i*Bu$_4$)(μ-Cl)]$_2$ was

obtained as a single component catalyst for stereoselective isoprene polymerization. In contrast, reaction of $[La\{N(SiMe_3)_2\}_2(\mu\text{-}Cl)(thf)]_2$ with trimethylaluminum yielded $[La\{N(SiMe_3)_2\}\{AlMe_3N(SiMe_3)_2\}(\mu\text{-}Cl)]_2$, highlighting the tremendous role of the organoaluminum reagent.

Zusammenfassung

Synthetischer Hochleistungskautschuk ist für die Reifenproduktion unverzichtbar. Die Neodym-basierte Polymerisation konjugierter Diene stellt derzeit den effizientesten Zugang zu diesem Material dar und ermöglicht die Synthese von Polyisopren mit der gewünscht hohen Stereoselektivität. Die zugrundeliegenden Mechanismen sind jedoch noch immer weitgehend unverstanden, was insbesondere für die Rolle von Triisobutylaluminium in Katalysatormischungen gilt. Zudem gewähren nur wenige Festkörperstrukturen Einblick in Lanthanid-Isobutyl-Wechselwirkungen.

Im Rahmen der vorliegenden Arbeit wurden die ersten homoleptischen Ln(II)-Tetraisobutylaluminate $Ln(Al\mathit{i}Bu_4)_2$ (Ln = Sm, Eu, Yb) strukturell charakterisiert, wobei im Festkörper eine η^3-Koordination der beiden Tetraisobutylaluminato-Anionen beobachtet wurde. Bemerkenswerterweise erwies sich $Ln(Al\mathit{i}Bu_4)_2$ (Ln = Sm, Eu, Yb) als Einkomponentenkatalysator für die Isoprenpolymerisation. Eine Reihe von Derivatisierungsprodukten von $Ln(Al\mathit{i}Bu_4)_2$ (Ln = Sm, Yb) erwiesen sich als nicht aktiv in der Isoprenpolymerisation. Die Aktivierung von $Ln(Al\mathit{i}Bu_4)_2$ (Ln = Sm, Yb) mit dem Borat-Cokatalysator $[PhNMe_2H][B(C_6F_5)_4]$ führte zu Polymeren mit sehr engen Molekulargewichtsverteilungen, d. h. für die $Yb(Al\mathit{i}Bu_4)_2/[PhNMe_2H][B(C_6F_5)_4]$-Mischung wurde eine lebende Polymerisation beobachtet. NMR-spektroskopische Studien ermöglichten Rückschlüsse auf beteiligte Spezies.

Die Synthese von Ln(III)-Tetraisobutylaluminaten gelang ausgehend von $Ln[N(SiMe_3)_2]_3$ und Triisobutylaluminium, wobei $Ln[N(SiMe_3)_2](HAl\mathit{i}Bu_3)(Al\mathit{i}Bu_4)$ als Produkt erhalten wurde. Dieses konnte für die Seltenerdelementmetalle Lanthan, Praseodym, Neodym, und Gadolinium kristallisiert und im Festkörper charakterisiert werden. Die Hydridbildung durch β-H-Eliminierung von Isobuten aus den Isobutylliganden konnte als wichtige Reaktivität identifiziert werden. Deren Relevanz wird durch Derivatisierungsprodukte wie $[(\mu\text{-Fluorenyl})_3La_2(\mu\text{-H})(HAl\mathit{i}Bu_3)_2]$ verdeutlicht. Die Reaktion von $Nd[N(SiMe_3)_2](HAl\mathit{i}Bu_3)(Al\mathit{i}Bu_4)$ mit $[PhNMe_2H][B(C_6F_5)_4]$ führte zur Bildung von $[Nd\{N(SiMe_3)_2\}(PhNMe_2)_2][B(C_6F_5)_4]_2$. Dieses stellte sich als Einkomponentenkatalysator für die Isoprenpolymerisation heraus; die Mikrostrukturen erhaltener Polymere ließen auf ein mögliches mechanistisches Szenario schließen.

Zudem konnte das Gd[$N(SiMe_3)_2$](HAl*i*Bu_3)(Al*i*Bu_4)/*i*Bu_2AlCl-Katalysatorsystem für die Polymerisation von Isopren entwickelt werden. Dieses lieferte hochmolekulares Polyisopren mit beeindruckend hoher *cis*-Selektivität >99,5 %.

Um Chlorido- und Isobutylaluminato-Einheiten in einem Lanthanoidkomplex zu vereinen, setzten wir [Ln{$N(SiMe_3)_2$}$_2$(μ-Cl)(thf)]$_2$ (Ln = La, Nd) mit Triisobutylaluminium um. Das Produkt [Ln{$N(SiMe_3)_2$}(Al*i*Bu_4)(μ-Cl)]$_2$ erwieß sich als Einkomponentenkatalysator für die stereoselektive Isoprenpolymerisation. Dagegen ergab die Reaktion von [La{$N(SiMe_3)_2$}$_2$(μ-Cl)(thf)]$_2$ mit Trimethylaluminium [La{$N(SiMe_3)_2$}{$AlMe_3N(SiMe_3)_2$}(μ-Cl)]$_2$ was die herausragende Rolle des Organoaluminiumreagens unterstreicht.

Publications

Paper I Divalent Lanthanide Tetraisobutylaluminates: Reactivity and Living Isoprene Polymerization

Zweiwertige Lanthanoid-Tetraisobutylaluminate: Reaktivität und lebende Isoprenpolymerisation

Eric C. Moinet, Benjamin M. Wolf, Olivier Tardif, Cäcilia Maichle-Mössmer, and Reiner Anwander

Angew. Chem. Int. Ed. 2023, 62, e202219316

Angew. Chem. 2023, 135, e2022193

https://doi.org/10.1002/anie.202219316

https://doi.org/10.1002/ange.202219316

Paper II Triisobutylaluminium-promoted formation of lanthanide hydrides

Eric C. Moinet, Olivier Tardif, Cäcilia Maichle-Mössmer and Reiner Anwander

Chem. Commun., 2023,59, 5261-5264

https://doi.org/10.1039/d3cc01330h

Paper III Discrete Trivalent Lanthanide Isobutylaluminates in Isoprene Polymerization: Elucidation of Cationized Active Species

Eric C. Moinet, Olivier Tardif, Lea-Sophie Hornberger, Friederike Adams, Cäcilia Maichle-Mössmer, and Reiner Anwander

ACS Catal. 2023, 13, 12826-12834.

Manuscript IV Structurally Defined Chloride/Isobutylaluminato Lanthanide Complexes in Isoprene Polymerisation

Eric C. Moinet, Philipp Wetzel, Olivier Tardif, Cäcilia Maichle-Mössmer, and Reiner Anwander

Poster Presentations

Poster I Rare-Earth-Metal Tetraisobutylaluminates

Eric C. Moinet, Benjamin M. Wolf, Cäcilia Maichle-Mössmer, and Reiner Anwander

XXX. Tage der Seltenen Erden - Terrae Rarae 2021, Montpellier, France

Poster II Chlorido-bridged early lanthanide tetraisobutylaluminate complexes: structures and performance in isoprene polymerization

Eric C. Moinet, Cäcilia Maichle-Mössmer, and Reiner Anwander

XXXI. Tage der Seltenen Erden - Terrae Rarae 2022, Leipzig, Germany

Objectives of this Thesis

The main objective of this work was to develop synthesis routes to discrete, crystalline rare-earth-metal isobutylaluminates and related compounds to elucidate the nature of conjugated diene polymerization catalysts, and to explore the so far elusive lanthanide-isobutylaluminate chemistry. Furthermore, discrete, both Ln(II)- and Ln(III)-isobutylaluminates were examined toward the polymerization of isoprene. The polymer analysis revealed trends in catalytic activity and selectivity of various lanthanide isobutylaluminate-catalysts, and indicated possible mechanistic scenarios.

Chapter A introduces both polyisoprene-related topics and mechanistic aspects of conjugated diene polymerization mediated by rare-earth element (pre)catalysts, as it does give a survey on structurally characterized tetraalkylaluminates with higher alkyl residues across the periodic table.

Chapter B consists of the summary of the main results, divided into the following three parts:

- Chemistry of divalent, homoleptic lanthanide tetraisobutylaluminates, derivatization products, and isoprene polymerization, and polymer analytics
- Silylamido elimination pathways to trivalent lanthanide isobutylaluminates and -hydrides, covering synthesis, structures, and isoprene polymerization
- Chlorido-bridged mixed tetraisobutylaluminato/silylamido lanthanide complexes

Chapter C contains results of this work that are not published so far, including

- Synthesis of isobutyl complexes
- Synthesis of alkaline-earth tetraisobutylaluminates

Chapter E consists of a compilation of publications

A

Polyisoprene and Higher Tetraalkyl-Aluminates

A. Introduction

Natural Rubber: Of Properties and Challenges

Among natures' most important biomolecules, (poly)isoprenoids are indispensable for all life. Though "only" considered secondary metabolites, isoprenoids cover a wide range of functional molecules, including membrane lipids, terpenes, vitamins, fragrances, hormones, or toxic compounds. Many of these chemicals formally derived from isoprene have become part of our every day's live, whereas others have inspired mankind to synthetic variants, for example neoprene as synthetic equivalent for polyisoprene ("natural rubber"). However, one challenge still remains partially unsolved today: How can the synthesis of these compounds be achieved? Although the synthesis of small molecules is well explored, polymers such as polyisoprene still pose challenges, and yet cannot be synthesized with the same selectivity as found in nature.

The most relevant example is natural rubber (NR). Its main constituent is highly stereoregular *cis*-1,4-polyisoprene, which is an indispensable polymer to date. First applications date back to ancient cultures in Mesoamerica long before the arrival of the first Europeans.[1] [2] For centuries, possible applications remained very limited due to the poor material properties.[2] The discovery of the vulcanization process by Charles Goodyear in 1839, however, marked the beginning of a new era.[2] Before, caoutchouc had been of little use,[2] being a brittle material when cold, and soft and sticky at higher temperatures.[3] [4] By reaction with elemental sulfur, it could be transformed into an elastic, resilient material, by cross-linking of polyisoprene molecules, which greatly improved its properties. Alongside with the rising demand in the early 1900s fueled by the emerging automobile industry and technological advances, natural rubber became a scare and sought-after commodity, quickly gaining industrial relevance.[2] Increasing demand and exorbitant prices, alongside with growing strategic relevance, not only led to the creation of plantations for rubber trees in south-east Asia, but also to increased efforts to generate synthetic equivalents. Despite of several attempts, merely oligomeric products were obtained in the beginning of the 20th century,[5] featuring very poor material properties, and the first polymerization of dimethylbutadiene, butadiene, and isoprene by emulsion polymerization was achieved by Hofmann only as late as 1909.[6] The rapid increase in knowledge of polymer materials in the 1920s was however spurred

not only due to synthetical advances, such as the introduction of styrene-butadiene rubber, but especially because of Hermann Staudinger's groundbreaking macromolecular hypothesis, that replaced the misconception of rubber being composed of "di- or trimers of isoprene" that were thought to be "aggregated to an immeasurable molecular weight".[5] However, synthetic polymers at that time were far from competitive, due to inferior polymer properties compared to natural rubber, and uneconomic monomer preparation.[7] One of the major challenges, to achieve a stereoselectivity similar to natural rubber, that consists of *cis*-1,4-polyisoprene (cf. Scheme 1), could not be achieved until the discovery of Ziegler-type mixed catalysts.[8] Synthetic *cis*-1,4-polyisoprene was produced from 1956 using Ziegler catalysts based on titanium tetrachloride, and aluminum alkyls or *n*-butyllithium, leading to 92% *cis*-stereoselectivity for the latter, which later could be improved up to 98% stereoselectivities for other transition metal catalyst systems,[9] [10] and first catalyst systems could be established that yielded polyisoprene resembling natural rubber in its properties.[11] Considering polymer characteristics, and selectivities, the rare-earth metal-based catalysis discovered shortly after, accounts for the highest quality polydienes to the present day, clearly excelling transition metal catalysis in terms of *cis*-selectivity (> 98%).[12] These technological advances finally made synthetic rubber competitive with natural rubber since the 1970s.[2]

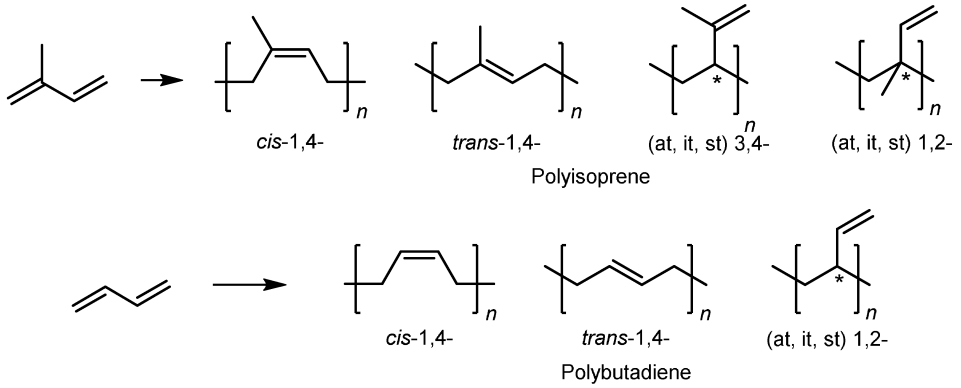

Scheme 1. Possible stereoisomers of polyisoprene, and (synthetic) polybutadiene. Examples of rubbers naturally occurring in plants are *cis*-1,4-polyisoprene (as found in *H. brasiliensis*), or *trans*-1,4-polyisoprene (which can be obtained from *Palaquium gutta*).

Nonetheless, still to date, some properties of NR are unmatched.[4] In contrast, natural rubber features excellent properties. Although more than 2500 different plant species, and some fungi are known to produce polyisoprenes, only *Hevea brasiliensis* is used for large-scale commercial

applications.[4] [13] [14] Natural rubber (meaning *Hevea* rubber in the following) almost entirely consists of *cis*-1,4-linked polyisoprene. Due to the biochemical synthesis, two trans-linked units per polymer chain,[4] [9] [13] [14] alongside with an ω-terminal dimethylallyl group, and an α-terminal fatty acid and phospholipid ester, are part of the polymer.[14] Furthermore, natural rubber possesses a broad and uncontrollable molecular weight distribution ($M_w/M_n \approx$ 2-10).[4] [9] [13] [15] [16] [17] Rubber obtained from *H. brasiliensis* features very high molecular weight ($M_n > 10^6$ g/mol).[18] It is commonly accepted that a high molecular weight of $>10^6$ g/mol (degree of polymerization $X_n >$ 15,000) is required for a high quality rubber.[13] Mechanical properties of natural rubber are still superior to synthetic polyisoprenes in terms of stress-strain properties, both unvulcanized, and vulcanized.[9] This is primarily caused by the *cis*-1,4-structure, that allows crystallization of the polymer chains upon stretching.[11] In contrast, small contents of 3,4-linked units, as found in synthetic polyisoprene, may interrupt crystallization on stretching, worsening mechanical properties.[9] The properties of natural rubber are also influenced by other components found in *Hevea* rubber, which contains approximately 6% of other constituents (proteins, fatty acids, neutral lipids, glycolipids, phospholipids, carbohydrates, and salts), which also influence mechanical properties (e. g. *via* enhancement of crystallization), but also account for the allergenic properties of *Hevea* rubber.[9]

Environmental and Economical Challenges associated with Rubbers

The large-scale production of natural rubber was made possible by Henry Wickham, who managed to sequester 70 000 seeds of *H. brasiliensis* from the Amazon rainforest in 1876, and (much fewer) plants grown in botanical gardens were later introduced to South-East Asia, laying the foundation for modern-day rubber plantations,[2] that still cover the natural rubber supply to date. The resulting, low genetic diversity of *H. brasiliensis* grown in plantations jeopardizes global rubber supply, due to susceptibility to diseases.[13] Nowadays, modern plantations consist of monocultures of high yielding *Hevea* clones.[2] However, *H. brasiliensis* is endemic in central America, especially the Amazon region, where large-scale plantations are not possible due to pathogens (especially *Microcyclus ulei*, that causes the South American Leaf Blight, a disease fatal to rubber trees), and spreading of pathogens remains a constant threat.[2] Besides, the creation of plantations for rubber

trees has ecologically devastating consequences. Especially in developing countries, tropical rain forest is cleared to generate acreage, and followed by a loss in biodiversity.[19] Furthermore, plantations of *H. brasiliensis* causes monoterpene emissions.[20] Its effect on climate is not yet fully understood. Isoprene for example does have an effect on climate, being a factor frequently overlooked.[21] This is especially relevant when it comes to arctic warming.[21] Mechanisms assumed consist in tropospheric formation of ozone, as well as secondary organic aerosols, which are caused by isoprene.[21]

The reliance on one single rubber source on one hand, and rising demand for this strategic commodity accompanied by the inability to satisfy the ever-increasing demand, illustrates the need for synthetic alternatives.[15] Steadily increasing demand can not be satisfied by rubber gained from *H. brasiliensis* exclusively, which may lead to adverse economic consequences in future.[13] Still, it needs to be noted that natural rubber obtained from different plants is not simply substituable, even if it features the same *cis*-stereoregularity, due to different polymer properties.[13] Using other plants containing *cis*-stereoregular polyisoprene such as *P. argentatum* bring disadvantages (*e.g.* large resin contents, which requires laborious removal, technical challenges, or deteriorates aging properties of cured rubber products),[9] making it only relevant for high-value nieche applications, e.g. when natural rubber from *H. brasiliensis* cannot be applied, for example due to the content of allergenic proteins in *Hevea* rubber. The global production of natural rubber is constantly increasing. Already from 2000 to 2014, rubber consumption increased by over 60 %,[13] and further increased from approx. 12 million tons in 2017 to 13.9 million tons in 2018.[13] [14] [22] Natural rubber accounts for approximately half of the total rubber consumption, and is a strategic raw material for more than 40 000 products.[23] Major applications include (high performance) airplane and truck tires, alongside with over 400 medical devices such as gloves, where natural rubber still is indispensable, and not fully replaceable by synthetic analogs.[9] [23] [24] Furthermore, it is problematic that tire material requires additives to achieve and maintain its performance.[25] For instance, oxidation of polydienes decreases durability and causes material fatigue and brittleness, which is reduced by addition of antioxidants. These additives, just as remaining monomers still contained in the polymer, may be environmentally harmful. For example, antioxidative additives were proven to cause mass die-offs of Coho salmon in the Pacific Northwest.[26]

Another challenge in the field of elastomer chemistry consists in recycling of rubbery materials. Both biological, and chemical devulcanization has been tackled,[25] but both devulcanization, and depolymerization, or recycling of the polydiene, is still challenging. The *cis*-1,4-microstructure does not only determine mechanical properties, but also environmental persistence. Only natural rubber, and to some extent synthetic rubber consisting mainly of *cis*-1,4-polyisoprene, can undergo biodegradation by several bacteria, or fungi, which are capable of (enzymatic) oxidative cleavage of double bonds in polyisoprene to generate low molecular weight oligo-*cis*-1,4 isoprene with ketone/aldehyde end groups, followed by further breakdown.[9, 14] Biological degradation is especially important, since erosion of rubber tires is the main source of microplastic particles in air beside synthetic textiles decomposition products, and urban dust.[27] Biological breakdown of rubbery materials however does not apply for most synthetic polydienes, especially not for copolymers and modified polymers. A major challenge is therefore the development of not only devulcanization techniques, but also polymer chain degradation, or recycling as well as environmental protection.

Synthetic Polydiene Rubber

In contrast to natural rubber, synthetic alternatives allow to adjust polymer properties. Characteristics such as glass transition temperature, molecular weight, molecular weight distribution, and especially stereoregularity are decisive factors, inevitably determining the quality of any application. In a wide range, the selectivity of synthetic polydienes can be steered by reaction conditions and the components constituting the catalyst, especially metal, and ligand environment.[28] Besides the choice of the monomer (especially 1,3-butadiene and isoprene), copolymerization of different monomers offer further options to influence polymer properties. For instance, block copolymers containing polybutadiene- or polyisoprene moieties are of enormous commercial value, such as styrene-butadiene copolymers.[28] Besides crosslinking processes (also called curing or vulcanization), which are conventionally employing sulphur or peroxides,[29] modification of polymers may also help to achieve desired polymer properties.

The polymerization of conjugated dienes displays one of the most effective catalytic transformation involving rare-earth elements.[12] Transition metals (especially cobalt and nickel) have been

investigated prior to lanthanide-based catalysts[8], but deliver much poorer catalytic performances in terms of stereoselectivity, and s-block metals are far less examined.[28] One of the rare examples of alkaline-earth catalysis comprises Okuda's work on butadiene polymerization with bis(allyl)calcium.[30]

To date, industrial procedures for synthesizing polydienes employ ill-defined catalyst mixtures.[12, 24] These Ziegler-Natta-type catalysts compose of a neodymium compound (e.g. of neodymium carboxylates, alkoxides, or halides), an organoaluminum cocatalyst such as triethyl-, or triisobutylaluminum (TIBA), a halide source (i.e. diethylaluminum chloride, or ethylaluminum sesquichloride), in some cases followed by treatment with diisobutylaluminum hydride or other additives, and some compounds may be used in excess.[12, 28] Despite of decades of intensive research and large-scale application, catalysts, and mechanistic details thereof are still far from understood,[12, 24] and catalyst systems are still found empirically. Different potential active species are described, that comprise allyl, alkyl, alkylaluminate, or hydride complexes, often paired with chlorido ligands, which are considered essential for obtaining a high *cis*-stereoselectivity. Understanding the sheer complexity of ternary catalyst mixtures is even complicated by the fact that, even when the same components in a ternary mixture are used, completely different results may be observed when the order of mixing is changed.[31] For example, Cui *et al*. describe that mixing the same catalyst precursors in different order results in very different catalytic behavior, yielding either traces of polymer, or quantitative yield in a short time.[32]

Still, challenges remain to be addressed besides elucidation of the active species: First, synthetic rubber production does rely on non-renewable resources.[9] Future alternatives exploit "green" and renewable dienes occurring naturally such as myrcene, farnesene, and ocimene. These monomers have gained attention only recently, and could further enrich the range of available polydienes.[33] Albeit polydienes have been synthetically available for decades, the chemistry is by no means fully explored, and challenges still need to be tackled, especially concerning environmental imperatives such as recycling and biodegradability. These new challenges add to technical requirements for high performance polydienes.

Another problem associated with synthetic polymers is catalyst productivity. In most mixed catalysts, only a small percentage of metal complexes is catalytically active. At a rough estimate, the share in neodymium-based systems lies between 0.4% and 7%,[34] implying that a large amount of precatalyst is wasted. On the other hand, mining of rare-earth elements, including neodymium,

results in vast environmental pollution, including tailings contaminated by radioactive and toxic heavy metals, especially thorium, and uranium, since monazite ore not only provides a host for lanthanides, but also for actinindes.[35] Therefore, reducing the amounts of required catalysts in polymerization procedures, or catalyst recycling, are desirable. Switching to more abundant elements, such as transition metals like titanium, is limited by the poorer catalytic performance. Similarly, cocatalyst productivity is equally if not more important than catalyst productivity in catalyst economics, but is often ignored.[36] The significant reduction of energy-consuming, pyrophoric organoaluminum equivalents not only implies an ecological benefit, but also an economical advantage, which could be feasible with a better understanding of involved species. Still, improvements in these processes are desirable, but are limited by the lack of understanding of mechanistic details of the polymerization process.

Mechanistic Aspects of Isoprene Polymerization

To address the above-mentioned challenges, it is immanent to understand the nature of polymerization mechanisms in detail, and organometallic catalysts are the key to control catalytic performances.[28] Recent works state that catalysts are monomeric, cationic neodymium complexes, with the polymer chain coordinated to the neodymium center by allyl- and olefin interactions.[24] In this context, it is notable that frequently applied cocatalyst triisobutylaluminum can also be used to achieve cationization of chloride complexes by formation of a $Cl(Al\mathit{i}Bu_3)_2^-$-anion.[32] Active species generated in Ziegler-Natta catalysts for conjugated diene polymerization may be regarded as an "in situ generation of lanthanide alkyls". However, as indicated by molecular weight distributions of polymers obtained with numerous catalysts, multiple active sites or active species with varying catalytic activities are formed.[24, 37] In addition, the transfer of the growing chain from the active site to organoaluminum moieties and *vice versa* is possible.[24, 38]

Mechanistically, like polymerization of (mono)olefins, polymerization of conjugated dienes such as butadiene or isoprene can proceed by the Cossee-Arlman mechanism. However, diene polymerization is by far more complicated than α-olefin polymerization:[28] First, stereochemistry involved with polymers formed from conjugated dienes is inherently more difficult. Second, a number of neutral lanthanide (alkyl) metallocene catalysts such as Cp^*_2LnR are very active for

polar monomer polymerization, including lactones and MMA, just as for the polymerization of ethylene without activation with additional cocatalyst, in some cases showing indication of living polymerization as shown by several works from many scientists including Marks, Evans, Teuben, Bercaw, and Yasuda.[28] [39] [40] In contrast, for conjugated dienes such as 1,3-butadiene, formation of η^3-allyl, or -crotyl complexes are responsible of the fast deactivation, resulting in no polymerization activity for conjugated dienes for metallocene systems.[39] On the other hand, Carpentier later showed that e.g. allylyttrium catalysts are able to homopolymerize isoprene.[41] Divalent samarocene derivatives such as $Cp^*_2Sm(THF)_2$ are reported to be efficient precursors for ethylene polymerization, but are considered almost inert toward dienes, due to the formation of stable η^3-allyl complexes. For example, the Cp^*_2Sm/butadiene reaction only leads to dimerization of butadiene (Scheme 2).[42]

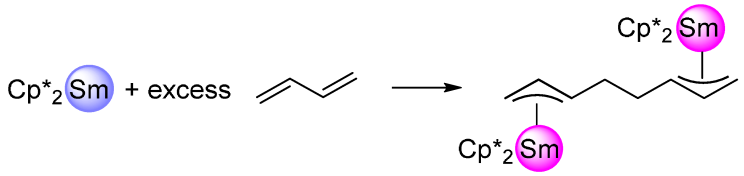

Scheme 2. Cp^*_2Sm/butadiene reaction leading to dimerization of butadiene, which impedes polymerization activity.[42]

Not only stereochemistry, but also regioselectivity of the insertion has to be controlled, posing challenges to both industrial production, and scientific research.[28] Possible products of butadiene and isoprene polymerization are shown in Scheme 1. 1,4-Polymerization of conjugated dienes gives rise to either *cis*- or *trans*-linked monomer units, whereas 1,2-polymerization (butadiene, very rarely isoprene), or 3,4-polymerization (isoprene) affords polymers bearing chiral carbon atoms, and the resulting properties thus are determined by the resulting tacticity (atactic, isotactic, and syndiotactic).[28] Mechanistically, it has been proposed that conjugated dienes bind large vacant coordination sites *via* η^4-coordination, and thus undergo 1,4-insertion.[28] Coordination *via* η^2-coordination (due to steric hindrance) may favor 1,2-insertion (or 3,4-insertion in case of isoprene).[28] However, also isomerization processes of the growing polymer chain may contribute to insertion selectivity, making the process much more complicated.[28] A mechanism involving allyl complexes was proposed in the 1960s, when transition-metal allyl complexes were discovered as putative catalyst precursors for diene polymerization,[43] [44] and later, the allyl-insertion

mechanism was proposed based on NMR studies.[45] Later, Taube and co-workers could show that neodymium allyl complexes are single component catalysts, and conducted mechanistic, and kinetic studies,[46] [47] [48] [49] [50] further substantiating the allyl-insertion mechanism. Scheme 3 summarizes possible insertion mechanisms of isoprene into a π-allyl lanthanide complex, resulting in *cis*- or *trans*-linked isoprene units, depending on the *anti*- or *syn*-conformation of the allylic species, whereas σ-bonded species can engage in olefin polymerization, resulting in 3,4-insertion. Although the preconformation of the diene inserted influences the generated allyl species, *syn-anti*-isomerization, or σ-π-shifts can lead to *cis*-or *trans*-regulation.[51]

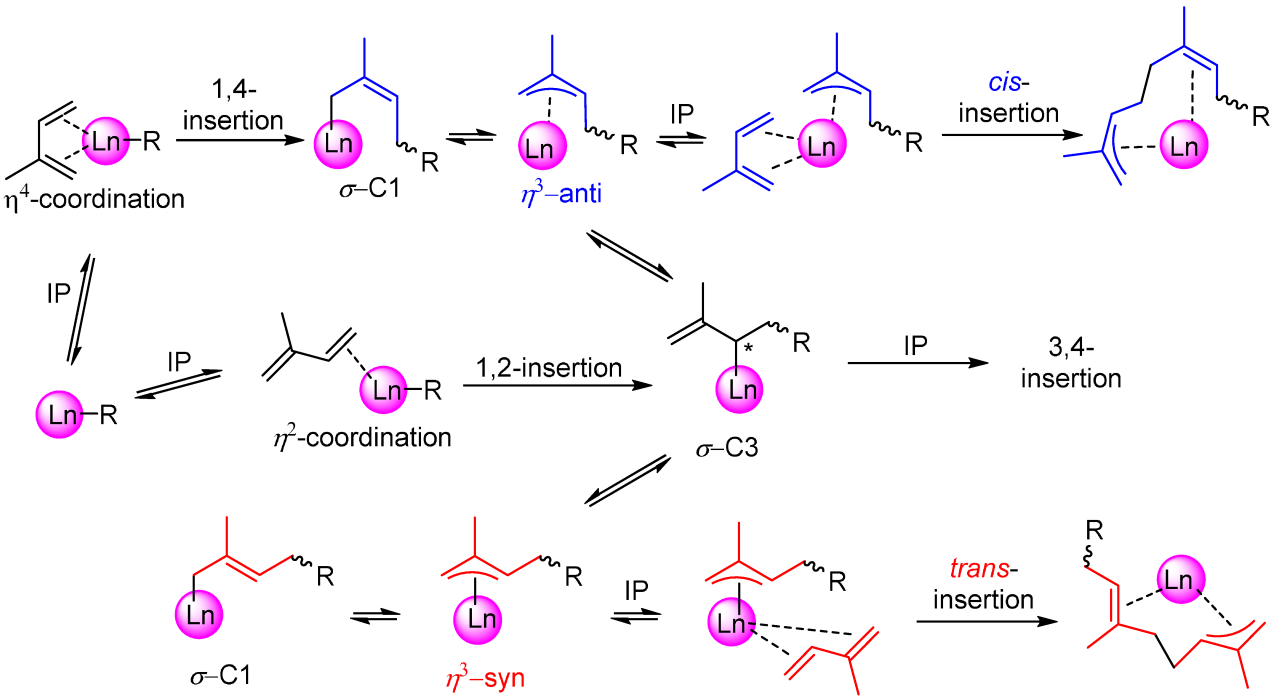

Scheme 3. Stereoselectivity arising from different coordination modes, and subsequent insertion into the π-allyl complex. Scheme is adapted from ref. [52].

Taubes' Allyl Complexes: Evidence for the Allyl-insertion Mechanism

Before organolanthanide catalysts were well examined as catalysts for conjugated diene polymerization, Rudolf Taube and coworkers managed to isolate a series of cationic allyl nickel(II) complexes published in 1977. The complexes of the form $[Ni(\eta^3\text{-}C_3H_5)L_2]X$ (L = $P(OPh)_3$, P(O-*o*-Tol)$_3$, PPh_3, 0.5 COD; X: BF_4, PF_6) were found to be single-component catalysts for butadiene polymerization.[47] Later studies on neodymium-allyl complexes, supported by kinetic studies by Taube *et al*. suggest that polymerization of butadiene is dependent on the coordination of the monomer to the catalytic Nd(III) center in proximity to the allyl anion, and concludes that the polymerization ability relies on the ability of neodymium to form π-complexes with the diene, which may occur in an η^2- or η^4-coordination.[47] [48] [49] In line with this mechanistic suggestion, Taube reports that $Nd(\pi\text{-}C_3H_5)_3$, and the donor adduct $Nd(\pi\text{-}C_3H_5)_3$(dioxane) were both found to polymerize butadiene in toluene at 50 °C without further additives, or cocatalysts.[47] [48] [49] It is notable that the dioxane adduct features a decreased polymerization activity, which was explained by the reduced space available for the diene coordination. Taubes' neutral tris(allyl) lanthanide complexes also display the first examples of single-component lanthanide catalysts, catalyzing the *trans*-1,4-selective polymerization.

The cationic compound $[Nd(\pi\text{-}C_3H_5)Cl(thf)_5][B(C_6H_5)_4]$, however, was not active in polymerization, and could not be converted into an active system, not even when organoaluminum Lewis acidic cocatalysts such as methylaluminoxane (MAO) were utilized,[49] whereas precatalysts such as $Nd(\eta^3\text{-}C_3H_5)Cl_2 \cdot 2$ thf gave extremely reactive catalysts when combined with 30 equivalents of MAO with *cis*-selectivities up to 98%.[47] In contrast, cationic allyl complexes $[Ln(\eta^3\text{-}C_3H_5)_2L_4][B(C_6H_5)_4]$ (Ln = La, Nd; L = THF, dioxane) were active in single-component polymerization of butadiene at 50 °C. It is notable that the THF adducts generally gave smaller turnover frequencies, which may be explained with the stronger coordination of THF compared to dioxane, and resulting blockage of the free coordination site. Compared to the lanthanum congeners, the neodymium complexes feature a higher *cis*-selectivity. However, polymer data suggest that, in case of the lanthanum complexes, two polymer chains per lanthanum center evolve, whereas only one chain is formed with neodymium. Taube concluded that this may indicate the formation of a dicationic monoallyl lanthanide complex fragment, that could also explain the higher

cis-selectivity for neodymium.[47] This also suggests that *cis*-1,4-selective polymerization is a result of catalysis carried out by a monoallyl neodymium complex.[47] [49]

Putative Active Species and Single-Component Catalysts

Despite of decades of intensive research, the nature of active rare-earth-metal catalysts in Ziegler-Natta type catalysts remain a matter of dispute.[24] [53] Nevertheless, it is generally accepted that Ln-alkyl, or Ln-H species are involved, whereas cationic species generated *i.e.* by Al→Ln chloride transfer are also possible candidates for active species.[54] The alkylation of the metal center in Ziegler-Nata type catalysts also is said to play a key role,[55] and species such as $[Me_2LnCl]_n$ or $[MeLnCl_2]_n$ are postulated as putative active species.[56] One example proposed by Cui *et al.* on the basis of NMR studies is $[i\text{BuYCl}]^+_n$, could partly transform into $[(H)YCl]^+_n$ by releasing isobutene.[57] Both compounds may be cationic, and possibly form a cluster, or an Al*i*Bu_3 adduct. ^{19}F-NMR spectroscopy indicates that there is no coordination of the borate moiety $[B(C_6F_5)_4]^-$ to the lanthanide center, indicating a spatial separation of the borate anion from the catalytically active center.[32] A number of other putative active species proposed in literature is shown in Scheme 4. A proposed mechanistic scenario for the cationization of $Nd[N(SiMe_3)_2]_3$ with $[PhNMe_2H][B(C_6F_5)_4]$ is shown as representative example in Scheme 5.[58]

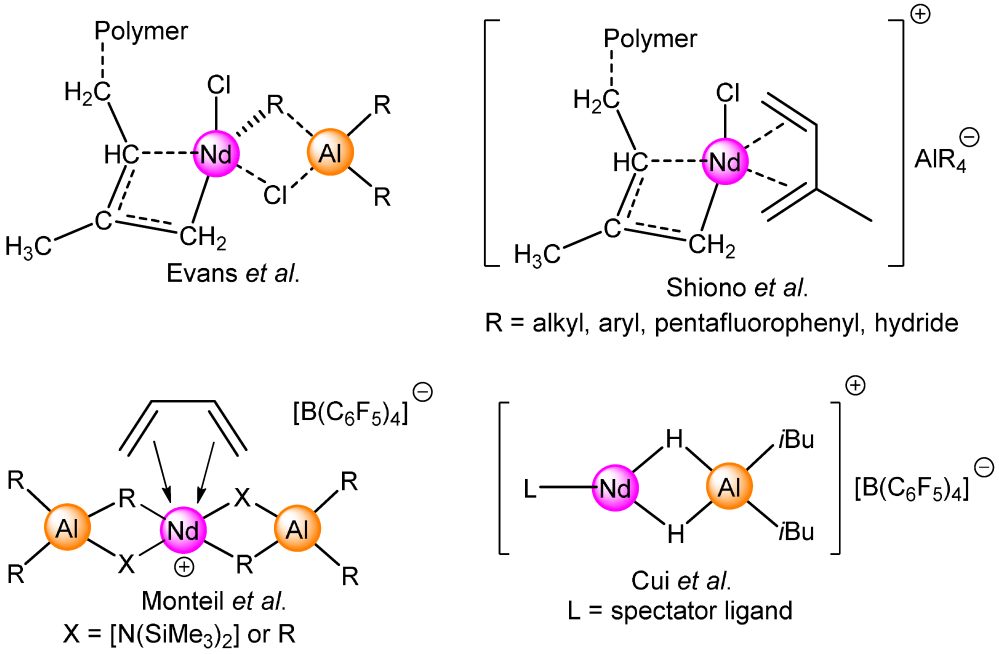

Scheme 4. Examples of proposed active species suggested by Evans *et al.*[12], Shiono *et al.*[59], Monteil *et al.*[58], and Cui *et al.*[57]

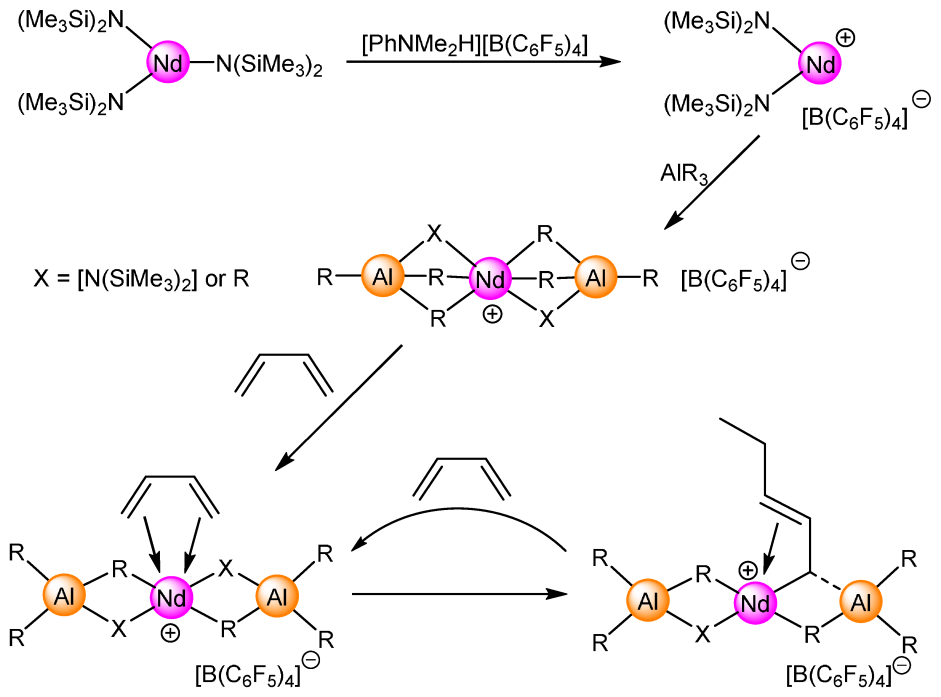

Scheme 5. Activation mechanism of $Nd[N(SiMe_3)_2]_3$ with $[PhNMe_2H][B(C_6F_5)_4]$ as proposed by Monteil *et al.*, and proposed mechanistic scenario.[58]

So far, only very few active compounds formed within Ziegler-Natta-type catalysts are structurally characterized, and initiating species are still ambiguous.[12, 32] Crystallizing active species from ternary catalyst mixtures may seem appropriate to elucidate the structures involved. However, this is almost impossible due to the low tendency to form crystals, and very likely the instability of active species involved. To date, there is only one example of a discrete crystallized product from a ternary mixture to our knowledge, that was published already in 1987 by Shan and co-workers. Crystalline material could be obtained after several months from the highly polymerization active ternary mixture comprised of Nd(O*i*Pr$_3$)/AlEt$_3$/AlEt$_2$Cl in a 1/10/1.5 ratio.[60] The complicated polynuclear product [Al$_3$Nd$_6$(μ_2-Cl)$_6$(μ_3-Cl)$_6$(μ_2-Et)$_9$Et$_5$(O*i*Pr)]$_2$, that consists of twelve neodymium centers linked by bridging chlorido ligands, alongside with aluminato moieties,[60] also features the first crystallographically characterized η^3-coordinated tetraethylaluminato moiety, though, regrettably, the crystallographic data are of poor quality.[61] The compound directly engages in polymerization,[60] and the difficult crystallization process of the complex product may explain why so many active catalysts escape crystallization and characterization.

Single-component catalysts, that may be used in order to study active species, may fill this gap. To date, a limited number of single component catalysts for the polymerization of conjugated dienes has been reported (*cf.* Scheme 6). These structurally diverse compounds include neutral or cationic allyl complexes,[41] [46] [48] [49] [62] [63] [64] and cationic mixed aluminate/borate compounds previously reported by our group.[18] [65] [66] In contrast to the trivalent lanthanide complexes, that are highly active in conjugated diene polymerization, complexes of the "classically divalent" lanthanides samarium, europium, and ytterbium are generally considered as not active in polymerization of conjugated dienes, often giving low yields, and reduction to a divalent complex is sometimes considered a putative inactivation mechanism for these elements.[34] [54] Hence, it is surprising that Evans reported on single-component catalysts LnI$_2$ (Ln = Nd, Sm, Dy, Tm), and LnI$_2$(thf)$_x$ (Ln = Sm, Tm).[67] However, no more work on divalent lanthanide catalysts has been published since.

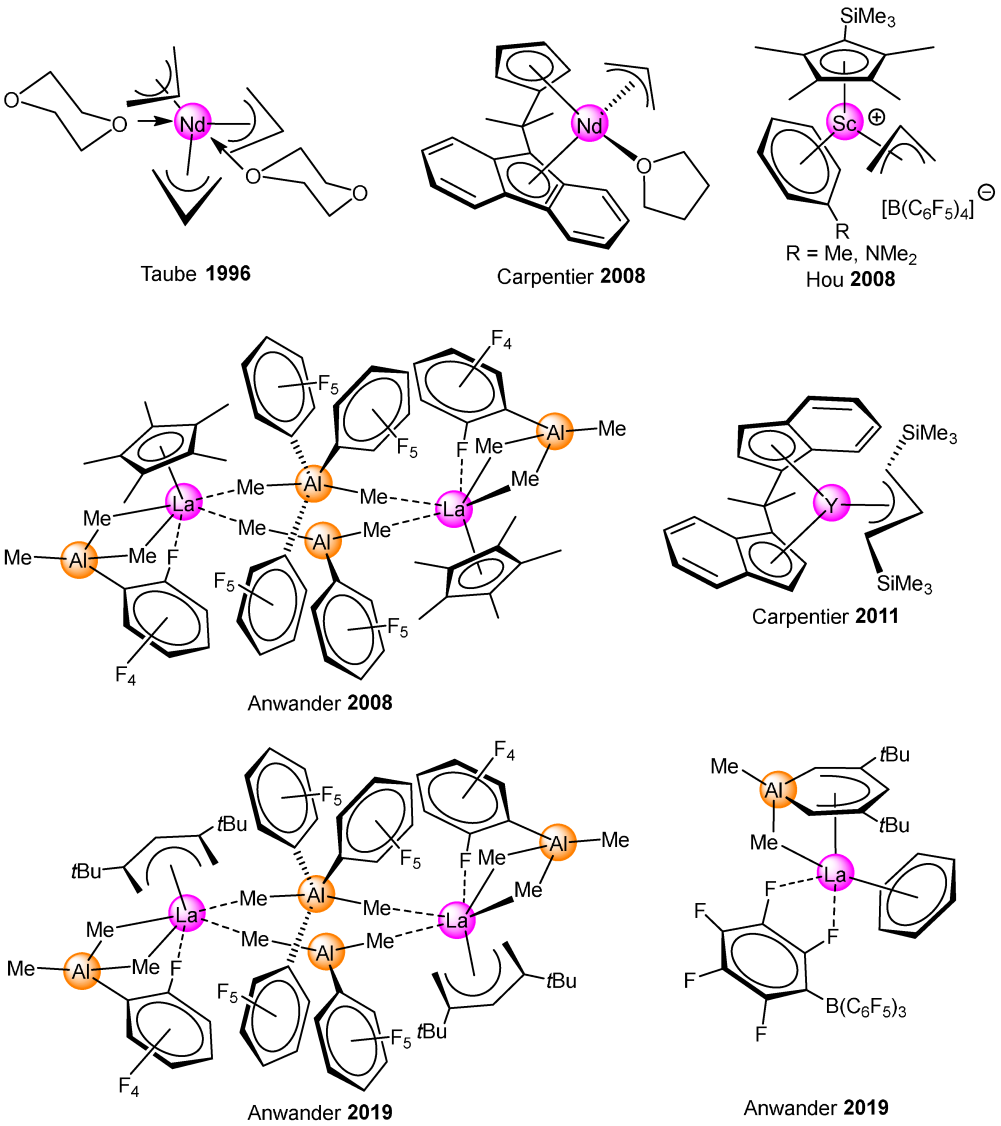

Scheme 6. Single-component catalysts for conjugated diene polymerization characterized in the solid state.[18] [41] [46] [63] [64] [65] [66]

Reaction Conditions Influencing Polymer Microstructure

The polydiene microstructure is influenced by several factors. Donor molecules occupy the coordination site, thus enforcing a change in *syn*/*anti* equilibrium, hence leading to changes in microstructure. For example, THF, and TMEDA were shown to reduce *cis*-selectivity and catalytic activity of a catalyst system comprised of neodymium versatate, DIBAH, and *tert*-butyl

chloride.[68] Little surprisingly, the solvent utilized may influence polymer microstructure, yield, and TOF,[24] which may be ascribed on the same donor effect. Systematic studies with mixed catalysts (comprised of neodymium versatate, diisobutylaluminum hydride and *tert*-butyl chloride) were performed by Coutinho, who could show that elevated temperature decreases catalyst activity, though without changing its selectivity, or polymer properties.[69] In terms of stereoselectivity, best results are usually obtained with DIBAH/TIBA compared to other organoaluminum compounds. DIBAH and TIBA yield higher *cis* selectivities, and higher molecular weight polymers compared to trihexyl- and trioctylaluminum.[70] However, the nature of the alkyl substituent does not seem to change the polymerization mechanism, although the molecular weight of polymers obtained is strongly determined by the alkylaluminum source employed, and large molecular masses are especially generated with bulky organoaluminum compounds.[70] It is assumed that the more "monomeric" nature of AlR_3, which is said to correspond with a higher "alkylating power" and thus higher activity. However, this statement must be treated with caution, given the fact that TIBA is, despite its sterically demanding alkyl chains, *not* entirely monomeric. Compared to trimethylaluminum, which is almost exclusively dimeric at ambient conditions, TIBA exists in an equilibrium with its dimer, however, this is largely governed by steric effects.[71]

In general, the reaction of aluminum carboxylates with excess trialkylaluminum reagent AlR_3 leads to the nucleophilic attack of the alkyl residue on the carboxylate $R'CO_2^-$, followed by subsequent attack on the ketone RR'CO formed, resulting in the formation of a tertiary alkoholate [$R_2R'CO^-$]. [72] However, the above-mentioned reactivity is not observed for discrete lanthanide carboxylate complexes. These feature distinct reactivities, as demonstrated by the works of Fischbach. Upon reaction with trimethylaluminum, tetramethylaluminato-, and dimethylaluminumcarboxylato moieties are formed.[34] A similar behavior was reported by Evans one year prior, who could show that, upon excess organoaluminum reagent, tetraalkylaluminates are formed, whereas stoichiometric amounts lead to Lewis acid-base adducts of carboxylato ligands, and triisobutylaluminum. Remarkably, crystal structures reveal a comparable Lewis acidity of Sm(III), and Al(III), as indicated by binding behavior of the formed triisobutylaluminum/carboxylato adduct.[73]

Higher Aluminates of Alkali Metals, Alkaline-Earth Metals, Transition Metals, and Lanthanides

The discovery of Ziegler-Natta type catalysts has spurred organoaluminum chemistry. Especially tetraorganoaluminato complexes have moved into the focus of research shortly after the discovery of Ziegler-type catalysts. Numerous discrete aluminate species have been employed as polymerization precatalysts alongside with organoaluminum/borate cocatalysts as "model systems" to study structure-reactivity relationships in Ziegler type catalyst-based polymerization.[74] Promising candidates that were studied comprise cationic and dicationic lanthanide allyl systems resembling proposed “active species”, but these complexes still require additional organoaluminum compounds to achieve polymerization activity.[24] Given this, alkylaluminates are key compounds to explore and understand Ziegler-Natta catalysts.

In the context of above-mentioned Ziegler mixed catalysts, the use of ethyl and isobutylaluminum compounds excels methylaluminum cocatalysts in many areas. First, higher alkylaluminum compounds can be obtained from aluminum, hydrogen, and ethylene (or higher olefins) in a straight forward, and cost-effective synthesis.[75] [76] Second, higher organoaluminum/aluminate compounds provide higher solubility, which often also enhances polymerization activity.[75] Even so, the investigation of ethyl- and isobutylaluminum chemistry poses major challenges. Besides difficulties in characterization of higher aluminates, complexes of the early transition metals and rare-earth metals engage in degradation reactions.[75] Especially without stabilizing ancillary ligands, possible decomposition pathways include α- and β-hydrogen abstraction, as well as β-alkyl transfer.[75, 77] Ligand redistribution is a common problem, i. e. when using lanthanide alkylaluminate precursors for the synthesis of discrete cationic hydride species.[78] In contrast, methylaluminates are well explored for the whole rare-earth element series (excluding promethium), especially their reactivity in isoprene polymerization.[74] [79]

Furthermore, the nature of the alkylaluminum cocatalyst employed determines properties of the products formed. For example, $[Sm(AlMe_4)_2]_n$ and $[Sm(AlEt_4)_2]_n$ are featuring a polymeric structure, but the methyl congener is insoluble in aliphatic, and aromatic solvents, whereas the ethylaluminate complex is readily soluble.[80] Utilization of different alkylaluminum compounds often results in diverse structural motifs. For instance, Evans and co-workers report that divalent

samarocene precursors undergo oxidation with trialkylaluminum reagents,[81] which leads to the -at least in the solid state- monomeric species [Cp*$_2$Sm{(μ-Et)$_2$AlEt$_2$}]. In contrast, when the less bulkier trimethylaluminum is employed, the bridging methylaluminate species [Cp*$_2$Sm{(μ-Me)AlMe$_2$(μ-Me)}$_2$SmCp*$_2$] is obtained.[55, 82] [81]

Tetramethylaluminates, despite the easy crystallizability, are not always suitable as models for catalysis, since they lack integral properties that commercial catalysts may exhibit, such as the ability to form hydride complexes via β-hydride elimination or -transfer. Higher alkylaluminum compounds feature different properties in polymerization, e.g. in terms of catalyst activity, compared to trimethylaluminum.[83] On the other hand, "higher" aluminates (meaning tetraalkylaluminates with R > Me) show bad crystallization behavior, or completely escape solid-state analysis. These difficulties in crystallization of "higher" alkylaluminates such as tetraethyl- and tetraisobutylaluminates arise from the fluxional behavior of the alkyl residues, thus hampering isolation, and purification by crystallization.[61] Additionally, bulky ethyl- or isobutyl groups greatly enhance solubility in both aliphatic and aromatic solvents. Therefore, prior works state that removing equimolarly formed, excellently soluble side products is "almost impossible".[61] The bulky higher alkyl groups in aluminate moieties suffer exchange by sterically less demanding alkyl groups. For example, alkaline earth tetraethylaluminates [Ae(AlEt$_4$)$_2$] (Ae = Ca, Sr, Ba), readily exchange ethyl groups for methyl groups upon reaction with trimethylaluminum.[84]

Besides ethyl- and tetraisobutylaluminate compounds, other "higher" alkylaluminates have been synthesized. The following list of compounds primarily emphasizes crystallographically characterized complexes featuring at least one tetraalkylaluminate moiety.

Higher Aluminates of Alkali Metals

Early works on alkali-metal alkylaluminates were tackled alongside the development of Ziegler's mixed catalysts. Encouraged by the thermal stability of alkali-metal aluminate derivatives such as $[M(AlEt_4)_2]$ (M = Li, Na),[85] [86] [87] [88] a number of syntheses were established beginning the 1960s, following different synthesis strategies including direct reaction from sodium and triethylaluminum, reaction of sodium hydride, triethylaluminum, and ethylene, or alkoxide elimination. Starting from $[Na(AlEt_4)]$ obtained this way, a transmetalation protocol allows the exchange of sodium against other alkali metals with alkali-metal amalgams until an equilibrium is reached.[84] A brief summary of these synthesis pathways is given in Scheme 7.

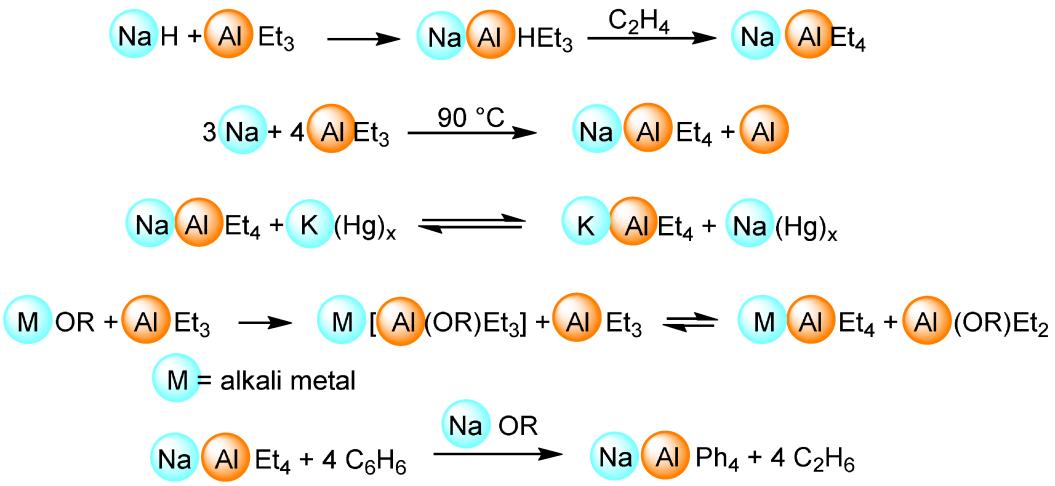

Scheme 7. Synthesis pathways leading to alkaline-metal tetraethylaluminates.[89] [90] [91] [92]

Ever since, alkali-metal aluminates are versatile synthesis precursors for salt-metathesis protocols, for instance for the synthesis of $[Y(AlMe_4)_3]$ starting from yttrium chloride and $[Li(AlMe_4)]$.[74] A number of higher aluminates has been structurally characterized in the solid state, among these the homoleptic aluminates $[Li(AlEt_4)]$,[88] $[Na(AlEt_4)]$,[93] $[Na(Al(n\text{Pr})_4)]$,[93] $Na[Al(SiMe_3)_4]$,[94] and $[K(AlEt_4)]$.[95] Besides, the donor adducts $[Li(\text{dioxane})_4][Al(i\text{Bu})_4]$,[96] $[Li(12\text{-c-}4)_2][Al(CH_2SiMe_3)_4]$,[97] and $[K(15\text{-c-}5)_2][Al(\eta^1\text{-}C_3H_5)_4]$,[98] as well as $[\{Ln(2,4\text{-}Me_2C_5H_5)_3\}\cdot(NaAlEt_4)_4]$ (Ln = La, Nd)[99] were characterized in the solid state.

Higher Aluminates of Alkaline-Earth Metals

Even though a first work on ethylaluminum compounds prepared from aluminum and ethyl iodide in a sealed glass ampoule has been published as early as 1859,[100] organoaluminum compounds finally were exhaustively examined about 100 years later in the context of Karl Zieglers seminal works on mixed catalyst for olefin polymerizations,[76] accompanied by Ziegler's work on trialkylaluminum compounds, including hydrides and decomposition processes.[101] Ziegler and Holzkamp also reported the synthesis of $[Mg(AlEt_4)_2]$ already in 1957 from diethyl magnesium, or ethylmagnesium chloride, and triethylaluminum.[85, 102] Alongside Zieglers' works, Herbert Lehmkuhl has been a pioneer both in the field of organoaluminum and organoaluminate synthesis, especially in terms of alkaline, and alkaline-earth element aluminates.[84, 91-92, 103] With respect to this, a number of different syntheses for alkaline-earth metal tetraethylaluminates has been published by Lehmkuhl and co-workers in the 1960s. As shown in Scheme 8, salt metathesis from metal chlorides with $[Na(AlEt_4)]$ provides the corresponding tetraethylaluminate after extraction with benzene from the insoluble residue.[91] A further possibility to purify the product was distillation. Lehmkuhl notes that $[Ba(AlEt_4)_2]$, in stark contrast to calcium and strontium homologues, features more salt-like characteristics. For instance, $[Ca(AlEt_4)_2]$ and $[Sr(AlEt_4)_2]$ can easily be distilled, and do only show little conductivity in solution, whereas $[Ba(AlEt_4)_2]$ does more resemble $[Na(AlEt_4)]$ in its properties.[84] Besides salt metathesis, an alkoxide-elimination protocol was established, followed by distillation of the products, which is feasible for Ca, Sr, and Ba. In contrast, magnesium tends to form the decomposition product EtMgOEt. Besides, the direct synthesis starting from alkaline-earth metal, diethyl mercury, and triethylaluminum also affords the alkaline-earth tetraethylaluminates and was conducted by Lehmkuhl and co-workers in a several hundred gram scale.[84] [92]

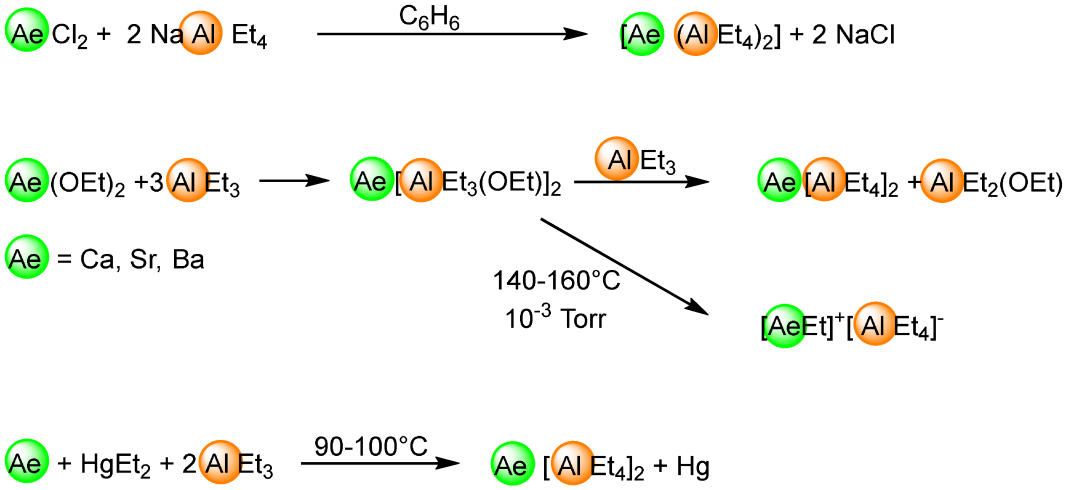

Scheme 8 Synthesis of various alkaline-earth metal tetraethylaluminates as published by Lehmkuhl and coworkers.[92] [84]

To date, other tetraethylaluminates including [{Ca(AlEt$_4$)$_2$}$_n$][85] and [{Ba(AlEt$_4$)$_2$}$_n$][104] are characterized in the solid state, alongside their donor adducts, ate complexes, and derivatives including [Ca(thf)$_2$(AlEt$_4$)$_2$],[85] [(Me$_2$NCH$_2$NMe$_2$)Ca(AlEt$_4$)$_2$],[89] [Ca(1,4-dimethylpiperazine)(AlEt$_4$)$_2$],[89] [Ca(tmeda)(AlEt$_4$)$_2$],[89] [Ca(1,3,5-trialkyl-1,3,5-triazacyclohexane)$_2$(AlEt$_4$)$_2$],[89] [{Ca(N(*i*Pr)$_2$)(AlEt$_4$)}$_2$],[89] [Ba(AlEt$_4$)$_2$(toluene)]$_2$,[105] [Ba(PhCHN=NCHPh)(AlEt$_4$)$_2$],[106] [BaK(AlEt$_4$)$_3$]$_n$,[95] (Tp^{tBu,Me})Ca(AlEt$_4$),[107] [Ca{μ-(N(SiMe$_3$)$_2$)(Al(CH$_2$SiMe$_3$)$_4$)}$_2$],[108] and [(Tp^{Ad,iPr})Ba(AlEt$_4$)]$_n$.[109] While in most cases μ_2-coordination is observed for the above-mentioned ethylaluminates in the solid state, and μ_2-coordination may be observed sporadically with sterically demanding ligands, as in the case of [Ca(μ_2-AlEt$_4$)(AlEt$_4$)(TCyTAC)] (TCyTAC = 1,3,5-tricyclohexyl-1,3,5-triazacyclohexane).[89] In contrast the fluxional behavior of coordinating tetraethylaluminato moieties was impressively demonstrated by Crimmin *et al.*, who examined the reaction of β-diketiminato calcium silylamides with triethylaluminum.[110] In this study, compound [{ArNC(Me)C(AlEt$_3$)HC(Me)NAr}Ca{AlEt$_4$}] was synthesized following an amide-elimination protocol. The fluctuating switch of the coordination modes has been shown by single-crystal structures of both the μ_2-coordinated, and μ_3-coordinated isomers of [{ArNC(Me)C(AlEt$_3$)HC(Me)NAr}Ca{AlEt$_4$}] (Scheme 9), with both isomers being present in an approximately 1 : 1 mixture. In solution, ^{1}H-NMR data suggested a rapid interconversion at

ambient temperature, highlighting the mobility of coordinating aluminato moieties, whereas a dissociative loss of triethylaluminum from the diketiminato "spectator" ligand was observed at low temperature.

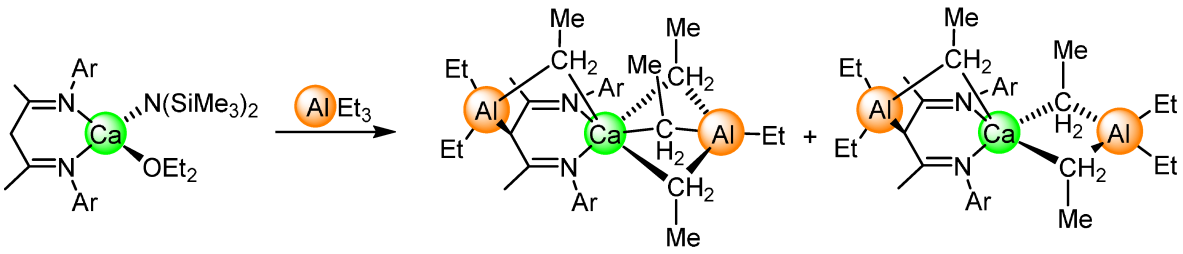

Scheme 9. Synthesis and structures of crystallographically characterized μ_2-, or μ_3-coordinated isomers of β-diketiminato calcium ethylaluminate compound [{ArNC(Me)C($AlEt_3$)HC(Me)NAr}Ca{$AlEt_4$}].[110]

Besides the aluminates mentioned above, it is noteworthy that a small number of solvent-separated alkaline earth tetraalkylaluminate compounds was published. These complexes are of great interest, especially when it comes to alkaline earth batteries. Among the candidates tested, [{$(thf)_3Mg(\mu$-$Cl)_3$)$Mg(thf)_3$}{$AlPh_4$}][111] stands out, featuring redox potentials as high as 2.5 V (vs Mg). This clearly excels first generation magnesium batteries by more than 1 V,[111] and may be a potential application of cheap, and excellently soluble, higher aluminates of readily abundant alkaline-earth metals. Similar structurally characterized complexes include [$Ca(thf)_5I$][$AlPh_4$],[112] [(CarMesPyCarMes)$Ca(thf)_2I$][$AlPh_4$] ($Car^{Mes}PyCar^{Mes}$ = 2,6-bis(3-mesitylimidazol-2-ylidene)pyridine),[113] and [$Sr(thf)_7$][$AlPh_4$]$_2$.[114]

Higher Aluminates of Transition Metals

In contrast to s- and f-block element compounds, transition-metal alkyls tend to be exceedingly unstable.[115] This especially applies to later transition metal alkyls, which tend to decompose by β-H elimination, whereas d^0-complexes feature less kinetic lability regarding β-H elimination,[75] which is crucial for the importance of early-transition metals in Ziegler–Natta-type polymerization catalysts.[75] In the solid state, there are almost no notable examples of (higher) transition metal tetralalkylaluminates, demonstrating the instability of transition metal alkyls.[115] One of the scarce examples of higher transition metal tetraalkylaluminates has been stabilized with electron deficient, weakly coordinating anion $[Al(C_6F_5)_4]$ alongside with cyclopentadienyl ligands, as in the case of the complexes $[Me_2C(Cp)(Flu)Zr(\mu_2\text{-}Br)]_2[Al(C_6F_5)_4]_2$ (Cp = C_5H_5, Flu = fluorenyl),[116] $[Cp^*_2Fe][Al(C_6F_5)_4]$,[117] and $[Cp_2Ta(CH_2)MeAl(C_6F_5)_2][Al(C_6F_5)_4]$.[118] The only structurally characterized example of exceedingly unstable tetraethylaluminates is the donor separated ion pair $[Co(2,2'\text{-bipyridine})_2Me_2][AlEt_4]$.[119] The tendency of transition-metal alkyls to decompose *via* β-H elimination is impressively demonstrated by complexes such as $Cp^*_2Ta(H)(C_2H_4{\cdot}AlEt_3)$ [120] which may be seen as a decomposition product of a putative intermediately formed, elusive "tetraethylaluminate".

Higher Aluminates of Divalent Rare-Earth Metals

Both di- and trivalent rare-earth metal ethylaluminates have been reported (see Scheme 10). Of the "classically divalent" lanthanide elements samarium, europium, and ytterbium, homoleptic and isomorphous tetraethylaluminates $[Sm(AlEt_4)_2]_n$,[80] $[Eu(AlEt_4)_2]_n$,[121] and $[Yb(AlEt_4)_2]_n$[122] have been structurally characterized. As the corresponding methyl congeners, the polymeric divalent ethylaluminates are accessible following an amide-elimination protocol by reaction of $Ln[N(SiMe_3)_2]_2(thf)_2$ with excess of $AlEt_3$. In contrast to the corresponding, insoluble divalent homoleptic metylaluminates $[Ln(AlMe_4)_2]_n$ (Ln = Sm, Eu, Yb), the polymeric ethylaluminates $[Ln(AlEt_4)_2]_n$ feature excellent solubility in aliphatic solvents.[80] In the solid state, polymeric $[Sm(AlEt_4)_2]_n$ comprises of an anionic moiety, and of a cationic fragment. The anionic $[Sm(AlEt_4)_3]$ -fragment features a η^2-coordination, compared to a η^3-coordination in the cationic $[Sm(AlEt_4)]$- fragment. Alongside with the homoleptic divalent ethylaluminates, their donor adducts have been reported. The tetrahydrofuran adducts $Ln(AlEt_4)_2(thf)_2$ was obtained for both samarium, and ytterbium.[123] Both are isostructural, with the ethyl aluminates again featuring a η^2-coordination mode. The same publication also reports on the synthesis of $Ln(AlEt_4)_2(py)_2$ (Ln = Sm, Yb) and $Ln(AlEt_4)_2(phen)$ (Ln = Sm, Yb), yet these complexes were not characterized in the solid state.[123] The donor addition strongly contrasts the reactivity of trivalent aluminates, that tend to undergo donor-induced aluminate cleavage instead of forming donor adducts.

Derivatization of $[Yb(AlEt_4)_2]_n$ with 0.5 equivalents of the oxidation agent Cp^*_2Pb in *n*-hexane yielded a mixture of products, from which only the trivalent ethylaluminate complex $Cp^*_2Yb(AlEt_4)$ could be identified.[124] When the same reaction was performed in a toluene/diethyl ether mixture, the divalent product $[Cp^*Yb(Et_2O)_2(AlEt_4)]$ was obtained alongside with elemental lead.[124] The protonolylsis of $[Ln(AlEt_4)_2]$ (Ln = Sm, Yb) employing 2,6-di-isopropyl phenol ($HOAr^{iPr}$) led to $[Et_2Al(\mu\text{-}OAr^{iPr})_2Yb(\mu\text{-}Et)_2AlEt(\mu\text{-}Et)]_2$, and a series of related, phenolato bridged triethylaluminum complexes.[125] As for the synthesis of homoleptic divalent tetraethylaluminates $[Ln(AlEt_4)_2]_n$, the silylamide eliminination protocol proved suitable for the synthesis of heteroleptic complex $(Tp^{tBu,Me})Yb(AlEt_4)$, which was synthesized from $(Tp^{tBu,Me})Yb[N(SiMe_3)_2]$ and >2 equivalents of triethylaluminum.[126] In the solid state, the tris(pyrazolyl)borate ligand $Tp^{tBu,Me}$ is κ^3-coordinated, whereas the $[AlEt_4]$-ligand is η_2-coordinated.[126]

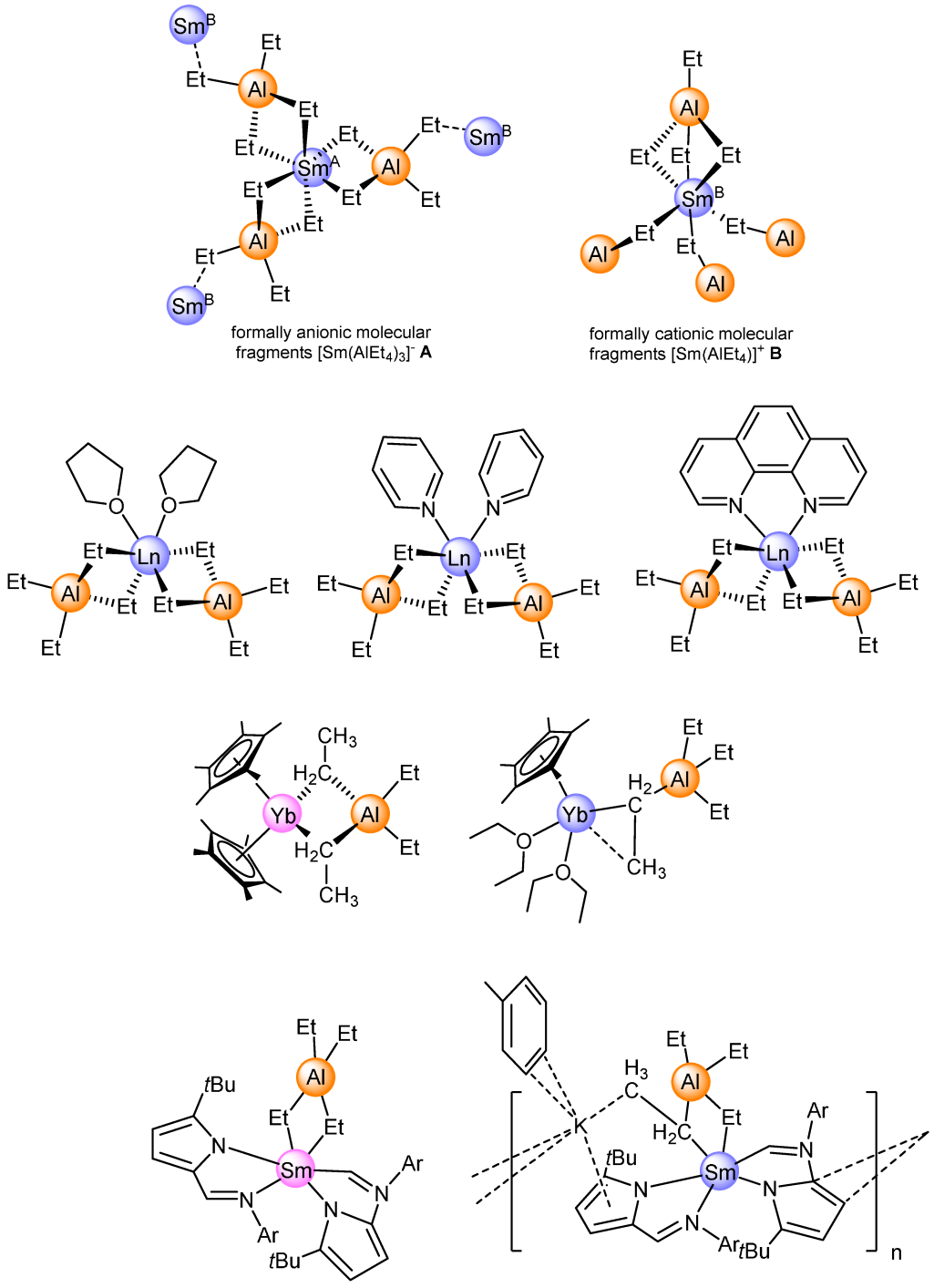

Scheme 10. Lanthanide tetraethylaluminates of samarium and ytterbium characterized in the solid state. Structural motifs found in $[Sm(AlEt_4)_2]_n$ as example for the structure of divalent homoleptic lanthanide ethylaluminates $[Sm(AlEt_4)_2]_n$,[80] $[Eu(AlEt_4)_2]_n$,[121] and $[Yb(AlEt_4)_2]_n$.[122] Donor adducts of $[Ln(AlEt_4)_2]_n$ (Ln = Sm, Yb).[123] Products obtained from the reaction of $[Yb(AlEt_4)_2]_n$ with 0.5 equivalents of Cp^*_2Pb,[124] and tri-, and divalent samarium ethylaluminate complexes $[NN]_2Sm(AlEt_4)$, and $[NN]_2SmAlEt_4K(toluene)\}_n$ ([NN] = [2-(2,6-$iPr_2C_6H_3N$=CH)-5-$tBuC_4H_2N$]$^-$).[127]

In solution, low temperature ^{1}H-NMR spectroscopy reveled that agostic Yb···H from the bridging methylene groups of the tetraethylaluminato moieties are not strong enough to maintain a rigid structure, as shown by only one signal set for the highly fluxional ligands $Tp^{tBu,Me}$, and the tetraethylaluminato moiety at temperatures as low as –80 °C.[126] Independently, another samarium ethylaluminate congener has been reported, which was synthesized from $[NN]_2SmCH_2SiMe_3$ ([NN] = [2-(2,6-*i*Pr$_2$C$_6$H$_3$N=CH)-5-*t*BuC$_4$H$_2$N]$^-$) with 3 equivalents of triethyl aluminum, that led to the formation of the trivalent ethylaluminate $[NN]_2Sm(AlEt_4)$, which was reduced with potassium in toluene to yield the linear, polymeric divalent ate complex $[\{NN\}_2Sm(AlEt_4)K(toluene)]_n$.[127]

The reaction of well-defined trivalent samarocene systems such as $[(C_5Me_5)_2Sm(O_2CC_6H_5)]_2$, $(C_5Me_5)_2Sm(thf)_2$, or $(C_5Me_5)_2Sm$ with dialkylaluminum chlorides R_2AlCl (R = Me, Et, *i*Bu) yielded complexes of the form $[(C_5Me_5)_2Ln(\mu\text{-}Cl)_2AlR_2]$, or $\{(C_5Me_5)_2Ln[(\mu\text{-}Cl)(\mu\text{-}R)AlR_2\}_x$ as stable products, and the dichlorides are apparently favored.[12] In terms of comparison of different alkyl residues, it is noteworthy that ethyl residues are capable of η^1-, η^2-, and η^3-coordination. This does have direct implications for conjugated diene polymerization, since this offers the possibility to (reversibly) protect a coordination site prior to the attack of a monomer during polymerization. Besides, the importance of agostic interactions metal-alkyl-interactions may play a role in stabilizing reactive intermediates in polymerization. Furthermore, the tendency for residues larger than methyl to form alkyl-bridged dimers is decreased, indicating that the higher sterical demand may decrease the tendency to dimerize. Another crucial aspect is the possibility of ethyl- or isobutyl groups to form hydride species following a β-elimination pathway, a scenario not possible for methyl congeners.

Trivalent Lanthanide Ethylaluminates Characterized in the Solid State

To date, only one type of homoleptic, higher aluminate complex of trivalent lanthanides of the form $[Ln(AlEt_4)_3]$ has been reported to our knowledge (*cf.* Scheme 11). Compound $[La(AlEt_4)_3]$ has been initially synthesized from $[La\{N(SiHMe_2)_2\}_3(thf)_2]$ and triethylaluminum,[128] wheras a synthesis was published later employing an amide elimination protocol starting from $[La(NMe_2)_3(LiCl)_3)_3]$.[75] The same protocol has later been applied to obtain homologous

complexes [Ln(AlEt$_4$)$_3$] for Ln = La, Ce, Pr, Nd, and Gd.[129] The diamagnetic probe [La(AlEt$_4$)$_3$] revealed high mobility in solution according to ^{1}H-NMR spectroscopy, and decoalescence of bridging, and terminal ethyl groups can not be observed even at at 190 K.[75] In contrast, lanthanide tetramethylaluminates, [Ln(AlMe$_4$)$_3$] show a different behavior.[74] Decoalescence of methyl resonances is already observed at 225 K for [Lu(AlMe$_4$)$_3$], but does not occur for large Ln^{3+} size aluminates such as [La(AlMe$_4$)$_3$]. This temperature dependence is ascribed to the increasing steric saturation, and the thus arising, more rapid alkyl exchange at the larger lanthanide centers.[74]

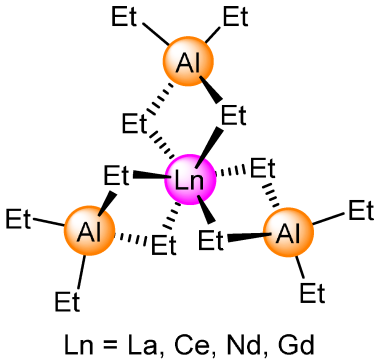

Scheme 11. Schematic structure of [La(AlEt$_4$)$_3$] and related compounds.[75] [128] [129]

The Decomposition of [La(AlEt$_4$)$_3$] in solution was observed after ten days at ambient temperature, whereas complete decomposition of [La(AlEt$_4$)$_3$] was observed when heated >1 h (cyclohexane-d_{12}), leading to the formation of degradation products [(AlEt$_4$)La{(μ-Et)(AlEt$_2$)}$_2$(μ-CH$_2$CH$_2$)] and [La{(Et$_3$Al)(μ-CH$_2$CH$_2$)(AlEt$_2$)(μ-CH$_2$CH$_2$)$_2$(AlEt$_3$)}] by β-H activation, as depicted in Scheme 12. As known for d^0 metal-ethyl complexes that readily undergo σ-bond metathesis, the C-H bond leads to the activation of neighboring alkyl ligands. Alongside with β-hydride transfer, β-hydride elimination is one of the major decomposition pathways.[75] For the decomposition of [La(AlEt$_4$)$_3$], no hydride complexes were postulated.[75] Instead, NMR studies suggested that the decomposition of [La(AlEt$_4$)$_3$] occurs by β-H abstraction *via* ethane elimination, forming degradation products [(AlEt$_4$)La{(μ-Et)(AlEt$_2$)}$_2$(μ-CH$_2$CH$_2$)] and [La{(Et$_3$Al)(μ-CH$_2$CH$_2$)-(AlEt$_2$)(μ-CH$_2$CH$_2$)$_2$(AlEt$_3$)}][75] alongside with ethane, following a mechanism suggested in literature.[75, 130] These findings also highlight the relevance of β-hydride transfer over the frequently assumed β-hydride elimination as putative degradation pathway for higher aluminates.

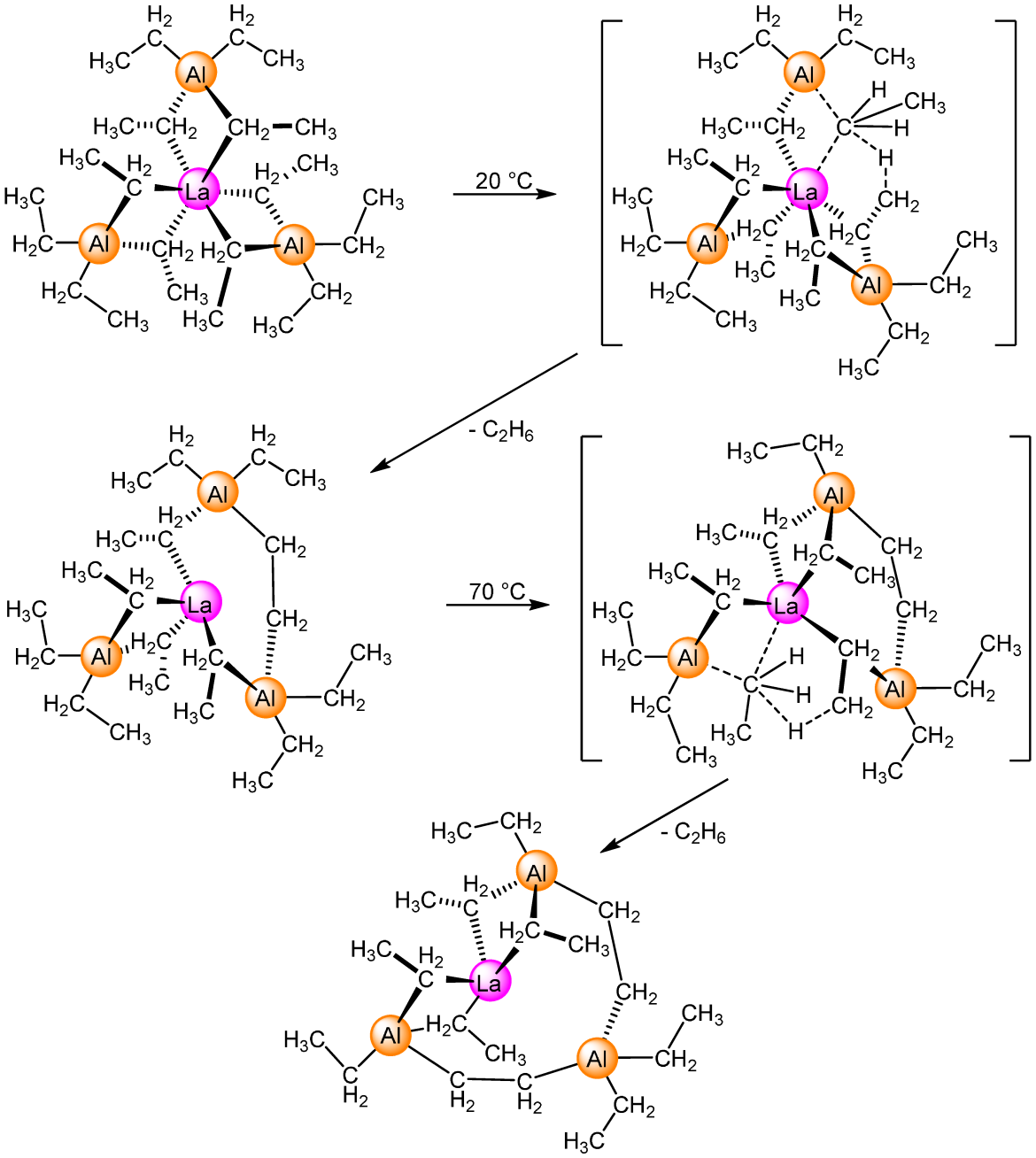

Scheme 12. Decomposition of [La(AlEt$_4$)$_3$] based on ^{1}H-NMR spectra as proposed in literature.[75] Figure is adapted from [75].

Heteroleptic trivalent rare-earth-metal ethylaluminates have been generated, either *via* oxidation of samarocene(II) precursors, or by derivatization of homoleptic trivalent ethylaluminate precursors. Starting from Cp*$_2$Sm, and Cp*$_2$Sm(thf)$_2$, and excess triethylaluminum, complexes Cp*$_2$Sm(AlEt$_4$),[55] and Cp*$_2$Sm(thf)[(μ-η^2-Et)AlEt$_3$][12] were obtained. It is remarkable that

complex [Cp*$_2$Sm(thf){(μ-η^2-Et)AlEt$_3$}], given the steric saturation of the complex, only one ethyl group of the tetraethylaluminate moiety coordinates (cf. Scheme 13), but in an η^2-coordination,[12] compared to the coordination of two ethyl groups in Cp*$_2$Sm(AlEt$_4$),[55] again highlighting the flexible coordination potential of the [AlEt$_4$] moiety. Besides, few heteroleptic ethylaluminates were synthesized, such as Cp*$_2$La(AlEt$_4$),[75] which could be generated by protonolysis using HCp* and La(AlEt$_4$)$_3$, whereas Tp^{Me,Me}La(AlEt$_4$)$_2$ was prepared from La(AlEt$_4$)$_3$ by salt metathesis using the potassium salt KTp^{Me,Me}.[129] In the context of lanthanide carboxylate based polymerization, a series of carboxylate/ethylaluminate complexes has been structurally characterized, such as La[(O$_2$CAr*i*Pr)$_4$(μ-AlEt$_2$)]$_2$[AlEt$_4$],[131] and much later La(Ph$_3$CCO$_2$)$_2$(AlEt$_4$) and Ln$_2$(Ph$_3$CCO$_2$)$_4$(AlEt$_4$)$_2$ (Ln = La, Nd).[132] [133] Both complexes feature a rather unusual η^3-coordination of the terminal ethylaluminate. However, both were dependent on an additional organoaluminum source for conjugated diene polymerization activity.

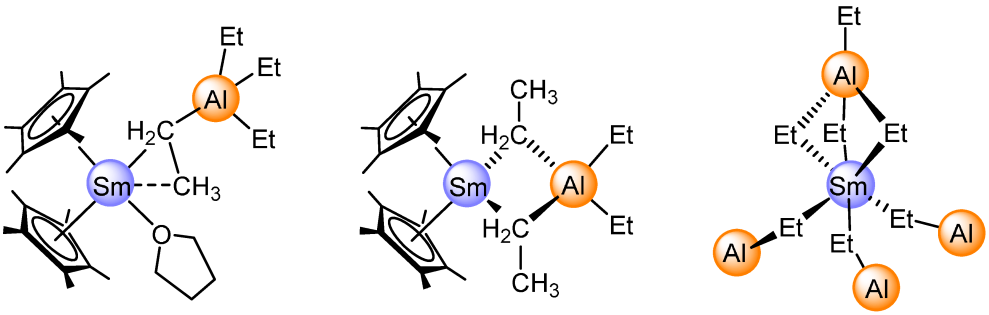

Scheme 13. Examples of versatile coordination of the tetraethylaluminato moieties in complexes Cp*$_2$Sm(AlEt$_4$),[55] [Cp*$_2$Sm(thf){(μ-η^2-Et)AlEt$_3$}],[12] and the cationic fragment of [Sm(AlEt$_4$)$_2$]$_n$.[80]

Lanthanide Isobutylaluminates Characterized in the Solid State

In mixed catalysts for conjugated diene polymerization, TIBA, and/or DIBAH are almost ubiquitously present in both academic- and industrially applied catalysts. For this reason, it is even more astonishing that only a handful of lanthanide isobutylaluminate complexes were published so far. Besides the donor adduct [(thf)$_2$Sm(O*t*Bu)$_2$(μ-O*t*Bu)$_2$Al(*i*Bu)$_2$],[134] all were obtained in the context of polymerization by the Evans group (*cf.* Scheme 14).[12, 73] So far, only one lanthanide complex containing a tetraisobutylaluminate moiety, (C$_5$Me$_5$)$_2$Sm[(μ-CH$_2$CHMe$_2$)$_2$Al(CH$_2$CHMe$_2$)$_2$], was crystallographically characterized by Evans *et al.*[81] In the

solid state structure, a η^2-coordination of the tetraisobutyl aluminate moiety was reported. Two more types of lanthanide compounds containing a triisobutylaluminum moiety were reported, and all are stabilized by pentamethylcyclopentadienyl ligands $(C_5Me_5)_2Ln[(\mu\text{-}Cl)(\mu\text{-}CH_2CHMe_2)Al(CH_2CHMe_2)_2]$ (Ln = Sm, Y), and $(C_5Me_5)_2Ln[(\mu\text{-}O_2CPh)(\mu\text{-}CH_2CHMe_2)Al(CH_2CHMe_2)_2]$.[12, 73] The latter is formed in the reaction of $[(C_5Me_5)_2Sm(\mu\text{-}O_2CPh)]_2$ with Al*i*Bu$_3$. It is remarkable that complex $(C_5Me_5)_2Ln[(\mu\text{-}O_2CPh)(\mu\text{-}CH_2CHMe_2)Al(CH_2CHMe_2)_2]$ displays two different carboxylate orientations toward the metals in a single crystal, indicating that the Lewis acidity for both Sm(III) *vs*. Al(III) may be very similar.[73] Apparently, all complexes reported by Evans feature the bulky Cp*-Ligand (C_5Me_5), which helps crystallizing the complexes, but also blocks access to the lanthanide core, thus preventing diene coordination to the metal center. It is thus little surprising that no polymerization activity has been reported for any of these compounds.

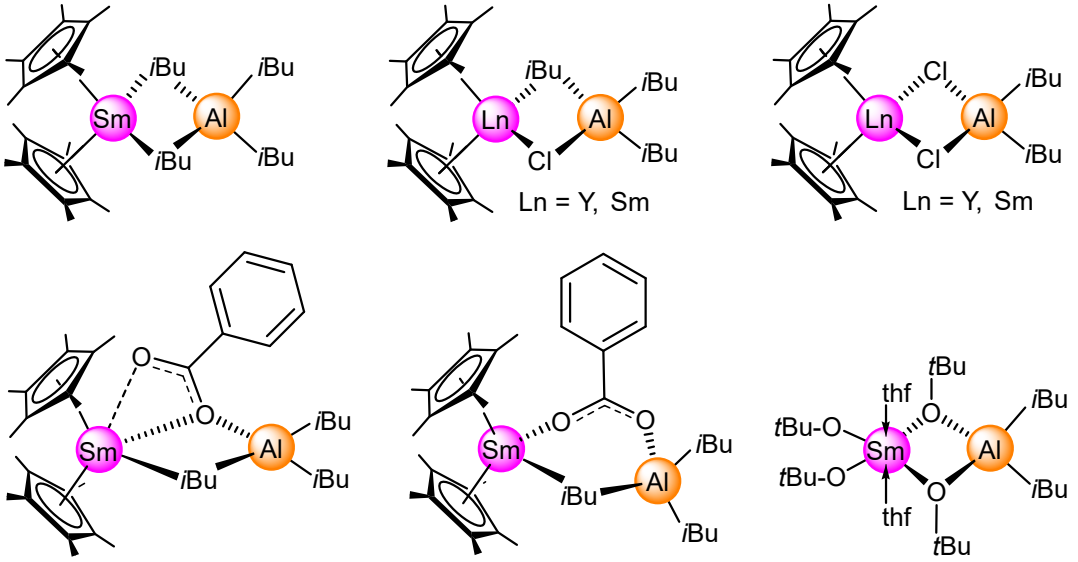

Scheme 14. Isobutylaluminum complexes of rare-earth elements characterized in the solid state.[12, 73, 134]

Besides homoleptic tetraethylaluminates, such as $[Nd(AlEt_4)_3]$, which has been extensively studied in isoprene polymerization in our group, leading to high-yield high-*cis* selective 1,4-polymerization,[129] higher aluminates of rare-earth elements are reported as putative model complexes for active species in polymerization. As reported for the decomposition of $[La(AlEt_4)_3]$,[75] showing the formation of difficult-to-crystallize products, species formed during

aging of a catalytic mixture, e.g. comprising an rare-earth-metal aluminate and organoaluminum cocatalyst, tend to be almost impossible to structurally characterize, due to their high reactivity, diversity, and flexibility.

Besides these first lanthanide isobutylaluminates, only one higher tetraphenylaluminate was characterized in the solid state, and published only recently. [Cp*$_2$Y(AlPh$_4$)] was obtained by heating the corresponding [Cp*$_2$Y(AlMe$_4$)] in benzene for six days at 120 °C.[135]

In the context of polymerization, [Y(CH$_2$Me$_3$)$_2$(thf)$_4$][Al(CH$_2$SiMe$_3$)$_4$] has been synthesized.[136] This more bottom up approach to analyze active species in catalytic mixtures consisted in synthesizing discrete complexes containing structural features commonly assumed to be present in active catalyst species. This route was followed by the group of Okuda, postulating the activity of dicationic lanthanide monoalkyl complexes as active species in ethylene polymerization. This assumption is based on the observation that alkyl complexes of the type [Ln(CH$_2$SiMe$_3$)$_3$(thf)$_2$](Ln = Tm, Er, Y, Ho, Dy, Tb) catalyze ethylene polymerization in toluene upon activation with [PhNMe$_2$H][B(C$_6$F$_5$)$_4$], and Al*i*Bu$_3$.[136] The authors propose the activation mechanism forming a "dicationic active species" as shown below (Scheme 15).

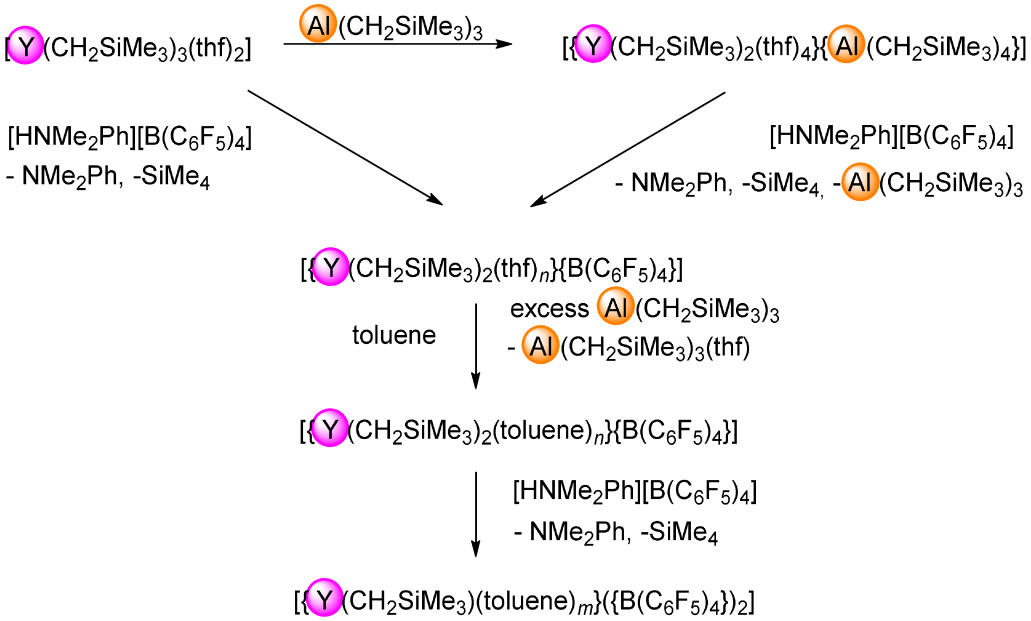

Scheme 15. Proposed activation of [Y(CH$_2$SiMe$_3$)$_3$(thf)$_2$] with dimethylanilinium/organoaluminum cocatalysts as proposed by the group of Okuda.[136] Scheme is adapted from[136].

However, it is obvious that tetraalkylaluminates may be forming in the proposed scheme, that implies solely arene is available for coordination to sterically stabilize the complex. In another work of Okuda, polynuclear yttrium hydride compound $[YH_2(thf)_2]_n[Al(CH_2SiMe_3)_4]_n$ was obtained *via* hydrogenolysis of $[Y(CH_2SiMe_3)_2(thf)_4][Al(CH_2SiMe_3)_4]$, which has subsequently been used to manufacture *trans*-$[Y(OCHPh_2)_2(triglyme)(thf)][(Al(CH_2SiMe_3)_4)]$, and subsequently $[YH_2(12\text{-crown-}4)]_4[Al(CH_2SiMe_3)_4]_4$.[78] The authors state that solubility problems of yttrium hydride complexes may be overcome using bulky aluminate anions.[78] Still, a synthetic challenge is the invariably formed mixtures of cationic hydrides, whose composition depended on the choice of the respective precursor, hydride source, and solvent.[78] Despite a large number of structurally characterized cationic rare-earth-metal complexes, no single component catalyst comprising of a (di)cationic complex has been reported to date to our knowledge, which is able to achieve conjugated diene polymerization without the need of additional cocatalyst.[78] [137] [138] [139] [140]

Aims of this Work

The main emphasis of this work was to synthesize discrete, crystalline rare-earth-metal isobutylaluminates and related compounds to elucidate the nature of 1,3-diene polymerization catalysts, and to explore the so far not well-established lanthanide-isobutylaluminate chemistry. However, the branched isobutyl ligands prevent crystallization, featuring increased mobility compared to the much easier crystallizing tetramethylaluminates. Main challenges involve:

- high mobility of isobutyl residues in solution/low tendency to crystallize[61]
- high boiling point of TIBA (46 °C/1 mm Hg[141], 86 °C/10 mmHg, according to the supplier Merck KGaA)
- very high solubility of isobutylaluminates in aliphatic, and aromatic solvents[61]
- equimolarly formed, almost inseparable side products[61]

Given the challenges involved with crystallizing discrete isobutylaluminate species, stabilizing spectator ligands, such as Cp*, or [$N(SiMe_3)_2$] were possible candidates to access the previously elusive isobutylaluminate congeners. It is remarkable that, among the initially reported, structurally characterized trivalent isobutylaluminate congeners, none was generated following an amide-elimination protocol, which is a state-of-the-art protocol for lanthanide tetramethyl-, and tetraethylaluminates. In contrast, $Yb[N(SiMe_3)_2]_2(thf)_2$ was utilized to generate complexes $[Yb(AlMe_4)_2]_n$, $[Yb(AlEt_4)_2]_n$, and $Yb(Al\textit{i}Bu_4)_2$.[122] However, the latter could not be structurally characterized in the solid state, since the "crystals" did not produce a diffraction pattern in single crystal analysis. In general, the bulky [$N(SiMe_3)_2$]-ligand has found wide-spread use in lanthanide chemistry, due to its sterical demand, and stability. Rare-earth-metal silylamides $Ln[N(SiMe_3)_2]_3$ stand out due to the easy exchangeability of the silylamido ligands, accompanied by high Lewis acidity, and excellent solubility in organic solvents, enabling manifold applications in catalysis.[53] For instance, hydroamination, -silylation, -boration have ben reported. In polymerization, a vide variety of monomers, including methyl methacrylate, ethylene, and ε-caprolactone has been reported.[142] Especially, in butadiene and isoprene polymerization, rare-earth-metal silylamides have found application in combination with triisobutylaluminum,[58] [143] [144] and are subjects of several theoretical studies.[142] [145] [146] Both selectivity and activity of $Ln[N(SiMe_3)_2]_3$/TIBA systems were found to be superior or at least comparable with established catalyst systems based

on lanthanide carboxylates.[143] Polymerization of butadiene with $Nd[N(SiMe_3)_2]_3$, $[C_6H_5NMe_2H][B(C_6F_5)_4]$, and Al*i*$Bu_3$ is reported by Sadow *et al*. who highlights the enhanced stereoselectivity depending on the solvent (86 % *cis*-1,4 in heptane *vs*. 70 % *cis*-1,4 in toluene).[24] However, previous works (falsely!) claim that trivalent silylamide complexes $[Ln\{N(SiMe_3)_2\}_3]$ "do not even show reactivity towards organoaluminum reagents such as TMA, since the lanthanide center is sterically completely shielded, and bulky $[N(SiMe_3)_2]$ ligands cannot be attacked due to the sterical bulk of the amide ligands".[61] In contrast, the Gambarotta group previously reported on the reaction of $Sm[N(SiMe_3)_2]_3$ with 6 equivalents of $AlMe_3$ and 2,6-diphenylphenol in toluene. The darkening of the reaction mixture indicated reduction to Sm(II) species, and the product was identified as $Sm[\{\mu$-2,6-bis(phenylphenol)$\}]_2[(\mu$-Me)$(AlMe_2)]$ by X-ray analysis. Treatment of this compound with one atm. CO_2 atmosphere led to insertion of CO_2 into the [Sm-Me-Al] fragment, forming $[Sm\{\mu$-2,6-bis(phenylphenoxy))$_2AlMe_2\}$-$\{\mu$-(acetato)-(2,6-bis(phenylphenoxy))Al $Me_2\}$(1,2-dimethoxyethane)]. [Sm-μ-{6,6'-methylene-bis(2-*tert*-butyl-4-methylphenol)}$(\mu$-$Me_2AlMe_2)]_2$ was obtained following the above mentioned route, and featured significant activity as single-component ethylene polymerization catalyst without the need of further activation with a cocatalyst.[147] The same protocol was also applied to generate $[Tm(Me)\{\mu$-$CH_2AlMe_2(\eta^5$-$NC_4Me_4)\}_2]$ from $Tm[N(SiMe_3)_2]_3$, $AlMe_3$, and 2,3,4,5-tetramethylpyrrole.[147] For this reason, the reactivity of lanthanide silylamide complexes towards triisobutylaluminum was examined in the scope of this work.

B

B. Summary of the Main Results

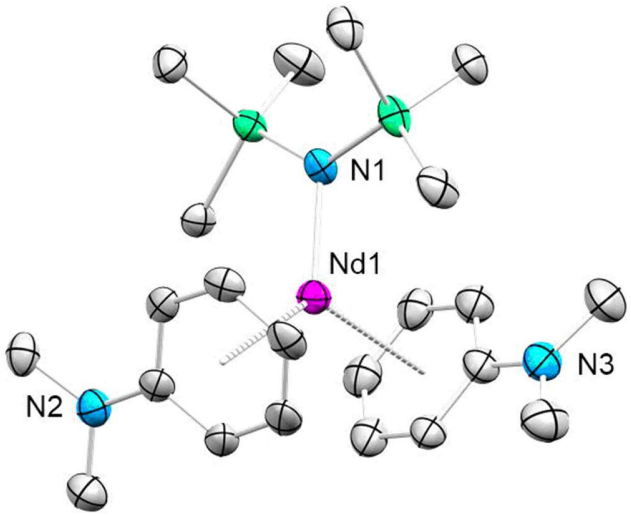

B. Summary of the Main Results

Divalent Homoleptic Lanthanide Tetraisobutylaluminates

Twenty years prior to this work, Yb(Al*i*Bu$_4$)$_2$ (**1^{Yb}**) was synthesized following an amide-elimination protocol, but the complex escaped solid-state characterization.[122] [147] It was noted that higher alkylaluminates are very hard to crystallize. This was ascribed to the mobility of higher alkyl residues of coordinated aluminato ligands, and to the equimolar formed side products which are "almost impossible" to remove due to excellent solubility of both products, and side products.[61] Following the protocol applied for the synthesis of Yb(Al*i*Bu$_4$)$_2$ (**1^{Yb}**), Benjamin Wolf almost two decades later succeeded in obtaining first single crystals of Sm(Al*i*Bu$_4$)$_2$ (**1^{Sm}**), [147] [148] but did not pursue this further.

In the context of this work, Sm(Al*i*Bu$_4$)$_2$ (**1^{Sm}**) was synthesized from Sm[N(SiMe$_3$)$_2$]$_2$(thf)$_2$, and Al*i*Bu$_3$. Repeated recrystallization afforded **1^{Sm}** as crystaline, purple-red solid (yield 75%). Similarly, the synthesis of Eu(Al*i*Bu$_4$)$_2$ (**1^{Eu}**) was tackled following the same amide-elimination protocol, accomplishing excellent crystalline yields (89%). The previously mentioned chemistry of Yb(Al*i*Bu$_4$)$_2$ (**1^{Yb}**) was revisited in this context, and we managed to finally obtain crystals of the so far elusive ytterbium aluminate **1^{Yb}**, which were of sufficient quality to reveal its solid-state structure. All three compounds, Sm(Al*i*Bu$_4$)$_2$ (**1^{Sm}**), Eu(Al*i*Bu$_4$)$_2$ (**1^{Eu}**), and Yb(Al*i*Bu$_4$)$_2$ (**1^{Yb}**), are isostructural, and revealed an unprecedented η^3-coordination of the tetraisobutylaluminato anions in the solid state (*cf*. Figure 1). The steric influence of the isobutyl residues are highlighted by slightly longer Sm–C distances of average 2.866 Å in Sm(Al*i*Bu$_4$)$_2$ (**1^{Sm}**), compared to Sm[AlEt$_4$)$_2$]$_2$(thf)$_2$, which features an η^2-coordination of the ethylaluminato ligand, and an average Ln–C distances of

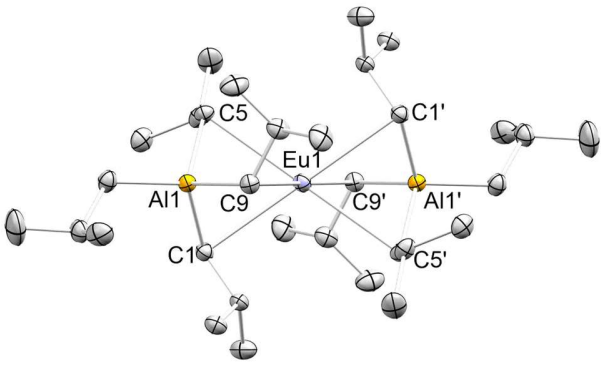

Figure 1. Crystal structure of Eu(AliBu$_4$)$_2$ (**1^{Eu}**) as representative exemple for the isostructural Ln(AliBu$_4$)$_2$ series (**1^{Ln}**). Ellipsoids are shown at the 50% probability level. Hydrogen atoms are omitted for clarity.

2.774 Å.[80] In contrast to the polymeric (insoluble) methyl- and (soluble) ethylaluminates $[Ln(AlR_4)_2]_n$ (Ln = Sm, Eu, Yb; R = Me, Et), complexes $Ln(Al\textit{i}Bu_4)_2$ (**1**$^{\mathbf{Ln}}$) feature excellent solubility, and a monomeric motif in the solid state, making them the first examples of homoleptic divalent lanthanide tetraisobutylaluminates structurally characterized in the solid state.

Reactivity of $Ln(Al\textit{i}Bu_4)_2$ (**1**$^{\mathbf{Ln}}$) Toward Oxidizing Agents

The reactivity of $Sm(Al\textit{i}Bu_4)_2$ (**1**$^{\mathbf{Sm}}$) and $Yb(Al\textit{i}Bu_4)_2$ (**1**$^{\mathbf{Yb}}$) toward chlorinating agents was probed in order to examine the accessibility of trivalent isobutylaluminate species, that could serve as putative isoprene polymerization catalysts. In this context, it is notable that transition of Sm(II) to Sm(III) is accompanied by a color change from deep purple to pale yellow, which is of great help to indicate oxidation.

Remarkably, reaction of $Sm(Al\textit{i}Bu_4)_2$ (**1**$^{\mathbf{Sm}}$) with hexachloroethane proceeded without a characteristic color change. From the reaction mixture, blackish-green crystals were formed that were identified as mixed-valent $Sm_6Cl_8(Al\textit{i}Bu_4)_6$ (**2**) (*cf.* Scheme 16) by XRD analysis. The same product was obtained upon oxidation of $Sm(Al\textit{i}Bu_4)_2$ (**1**$^{\mathbf{Sm}}$) with trityl chloride as identified by XRD analyses, though contaminated with cocrystallized Gomberg's Dimer.

Analogously, the reaction of $Yb(Al\textit{i}Bu_4)_2$ (**1**$^{\mathbf{Yb}}$) with hexachloroethane was probed, and X-ray diffraction revealed the formation of Yb(II) cluster $Yb_4Cl_4(Al\textit{i}Bu_4)_4$ (**3**), co-crystallized with the precursor $Yb(Al\textit{i}Bu_4)_2$ (**1**$^{\mathbf{Yb}}$). Both clusters $Sm_6Cl_8(Al\textit{i}Bu_4)_6$ (**2**), and $Yb_4Cl_4(Al\textit{i}Bu_4)_4$ (**3**), did undergo decomposition in solution. In case of $Sm_6Cl_8(Al\textit{i}Bu_4)_6$ (**2**), this was accompanied by a rapid color change from dark green to brown when dissolved in aromatic solvents, and over the period of several hours in aliphatic solvents. Decomposition products identified by ^{1}H-NMR spectroscopy include $Sm(Al\textit{i}Bu_4)_2$ (**1**$^{\mathbf{Sm}}$), triisobutylaluminum, and isobutene. $Yb_4Cl_4(Al\textit{i}Bu_4)_4$ (**3**) does show similar decomposition, however during the course of several days in aromatic solvents.

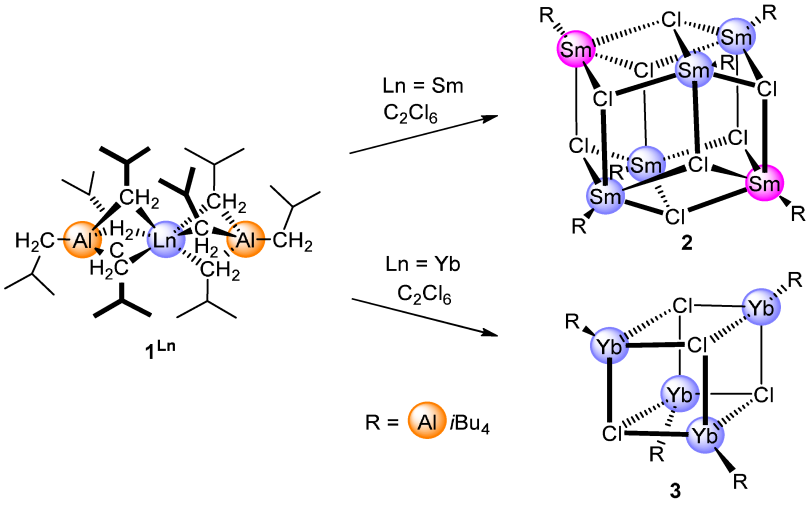

Scheme 16. Reactivity of Ln(Al*i*Bu$_4$)$_2$ (**1**^{Ln}) towards hexachloroethane, and formation of the products Sm$_6$Cl$_8$(Al*i*Bu$_4$)$_6$ (**2**) (mixed valent), and Yb$_4$Cl$_4$(Al*i*Bu$_4$)$_4$ (**3**) (divalent).

When treating Sm(Al*i*Bu$_4$)$_2$ (**1**^{Sm}) with tellurium(IV) chloride in toluene, a dark oil was obtained, and no product could be isolated. After treatment with tetrahydrofuran, few crystals were obtained. These were identified as the coordination polymer [{SmCl(thf)$_5$)(AlBn*i*Bu$_3$}]$_n$ (**4**), which consists of an almost linear chain of alternating samarium(II) and chlorido ions (Scheme 17). The Sm(II) centers are sterically saturated by five THF molecules, leading to a coordination number of 7. The charge-balancing heteroaluminato anion features a benzyl group alongside with three isobutyl groups. For the formation of divalent samarium polymer [{SmCl(thf)$_5$)(AlBn*i*Bu$_3$}]$_n$ (**4**), a ligand exchange mechanism can be assumed, most likely involving transient "SmCl$_2$" and “tellurium alkylaluminate” or alkyl tellurium species. Decomposition of an organotellurium species formed in situ may lead to radical formation, and subsequent activation of toluene in the favorable benzylic position, possibly causing the substitution of an isobutyl group for a benzyl unit. In stark contrast to the previously examined oxidation reagents, that did not result in the formation of (entirely) trivalent species, plumbocene Cp*$_2$Pb was successfully employed for the oxidation of Sm(Al*i*Bu$_4$)$_2$ (**1**^{Sm}), and Yb(Al*i*Bu$_4$)$_2$ (**1**^{Yb}), producing exclusively sandwich complexes Cp*$_2$Ln(Al*i*Bu$_4$) (**5**^{Ln}) in both cases in excellent yields.

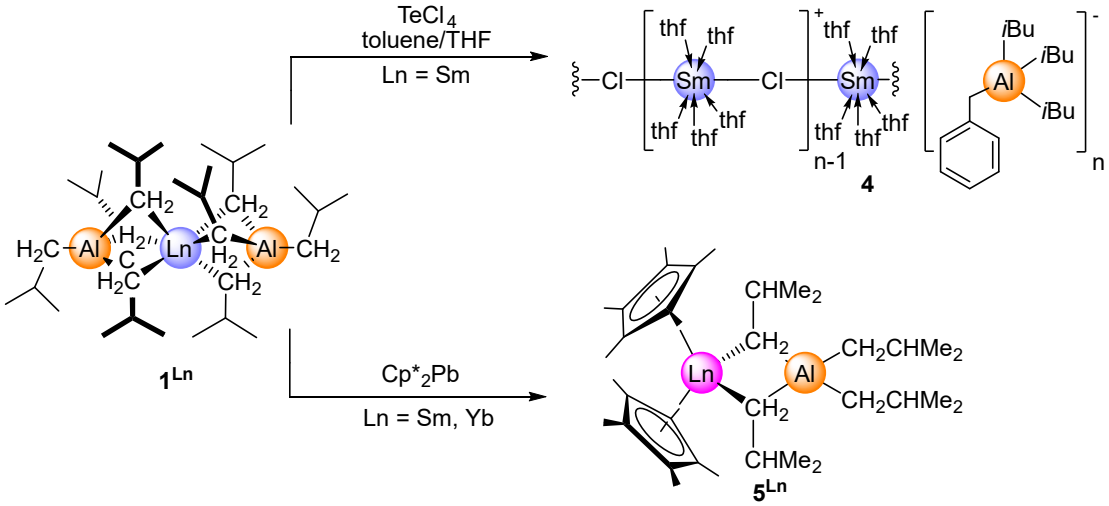

Scheme 17. Reactivity of Ln(Al*i*Bu$_4$)$_2$ (**1^{Ln}**) toward TeCl$_4$, and formation of the products [{SmCl(thf)$_5$}(AlBn*i*Bu$_3$}]$_n$ (**4**) and Cp*$_2$Sm(Al*i*Bu$_4$) (**5^{Ln}**).

Reactivity of Ln(Al*i*Bu$_4$)$_2$ (**1^{Ln}**) Toward Boranes, and 18-Crown-6

The reaction of Ln(Al*i*Bu$_4$)$_2$ (**1^{Ln}**) with [B(C$_6$F$_5$)$_3$] (**C**), a cocatalyst frequently employed in conjugated diene polymerization, led to the formation of the Lewis pair [Sm(PhMe)$_2${HB(C$_6$F$_5$)$_3$}$_2$] (**6**), and in case of the smaller ytterbium, [Yb(C$_6$D$_6$){HB(C$_6$F$_5$)$_3$}$_2$] (**7**) from a microscale reaction (*cf*. Scheme 18). These products were both obtained with one, and two equivalents of B(C$_6$F$_5$)$_3$ (**C**). Addition of diethyl ether to [Sm(PhMe)$_2${HB(C$_6$F$_5$)$_3$}$_2$] (**6**) led to [Sm(Et$_2$O)$_3${HB(C$_6$F$_5$)$_3$}$_2$] (**8**). Donor adducts of Ln(Al*i*Bu$_4$)$_2$ (**1^{Ln}**) could not be crystallized, and escaped isolation and purification, e.g. for donors such as thf, pyridine, diethyl ether, TMEDA, or diglyme. However, Yb(Al*i*Bu$_4$)$_2$ (**1^{Yb}**) and 18-crown-6 led afforded [Yb(18-crown-6)(Al*i*Bu$_4$)$_2$] (**9**). The steric demand of the tetraisobutylaluminato moieties seems to enforce an η^1-coordination in the solid state, featuring an 180° C(1)-Yb(1)-C(1)' angle. Little surprisingly, the Yb–C distance is elongated with 2.9159(19) Å in **9** compared to 2.735(16)-2.796(12) Å in Yb(Al*i*Bu$_4$)$_2$ (**1^{Yb}**).

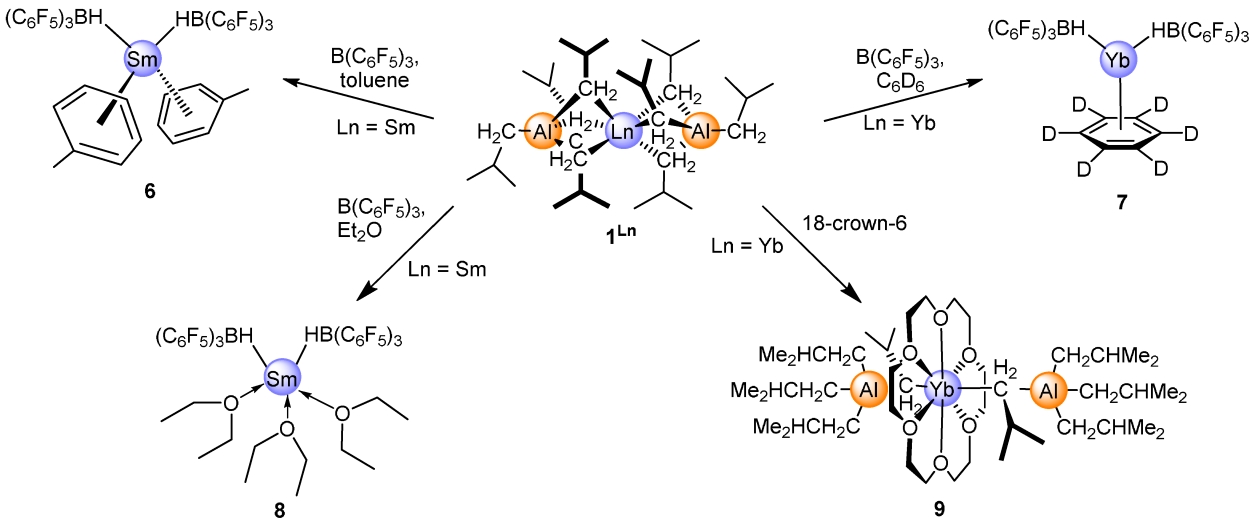

Scheme 18. Reactivity of Ln(Al*i*Bu$_4$)$_2$ (**1^{Ln}**) towards B(C$_6$F$_5$)$_3$ (**C**), and 18-crown-6, and formation of the products [Sm(PhMe)$_2${HB(C$_6$F$_5$)$_3$}$_2$] (**6**), [Yb(C$_6$D$_6$){HB(C$_6$F$_5$)$_3$}$_2$] (**7**), [Sm(Et$_2$O)$_3${HB(C$_6$F$_5$)$_3$}$_2$] (**8**), and [Yb(18-crown-6)(Al*i*Bu$_4$)$_2$] (**9**).

Isoprene Polymerization Employing Divalent Lanthanide Precatalysts

Divalent lanthanide complexes have been considered inactive in conjugated diene polymerization, and reduction of trivalent to divalent species was postulated to explain the relatively poor performance in conjugated diene polymerization of samarium, europium, and ytterbium.[34] Only one publication covering the subject of isoprene polymerization with divalent rare-earth metal iodides has been reported.[67]

We were therefore interested in probing the previously mentioned complexes in isoprene polymerization. Remarkably, complexes Ln(Al*i*Bu$_4$)$_2$ (**1^{Ln}**) engage in isoprene polymerization, even without cocatalyst (Table 1, entry 1, 6, 7, and 11). This astonishing result corresponds to the behavior of aforementioned LnI$_2$. Also in the case with Ln(Al*i*Bu$_4$)$_2$ (**1^{Ln}**) as precatalyst, no correlation between the redox potential and polymerization activity was observed, indicating that a divalent species is accountable for catalysis ($E_{1/2}$ vs. NHE [V]: Eu^{2+}: -0.35; Yb^{2+}: -1.15; Sm^{2+}: -1.55).

These findings that a divalent species is the active polymerization catalyst was further corroborated by the reactivity of Ln(Al*i*Bu$_4$)$_2$ (**1^{Ln}**) and borate cocatalysts. The activation reaction employing

1^{Yb} was examined by ^{1}H-NMR spectroscopy, revealing no paramagnetic broadening of the signals in accordance with the non-occurence of oxidation. Borate cocatalysts [CPh_3][$B(C_6F_5)_4$] (**A**) (*cf.* Table 1, entries 2, 8, 12) and [$C_6H_5NMe_2H$][$B(C_6F_5)_4$] (**B**) (*cf.* entries 3, 9, 12-17) activate **1^{Ln}** equimolar, delivering high yields of polymer. Upon activation of Ln(Al*i*$Bu_4)_2$ (**1^{Ln}**) with **A**, and **B**, very narrow molecular weight distributions were observed. Probing the system **1^{Yb}**/**B** with addition of the monomer in several portions, showed that the PDIs are in the range of 1.02-1.05, and molecular weight, and monomer consumption increases linearly after each monomer addition (*cf.* Table 2, entries 14-17; Figure 2), thus proving perfectly living polymerization for the binary catalyst system **1^{Yb}**/**B**. In contrast, $B(C_6F_5)_3$ (**C**)/Ln(Al*i*$Bu_4)_2$ (**1^{Ln}**) mixtures were (almost) inactive in isoprene polymerization (*cf.* Table 1 and Table 2, entries 4, 10, 18). Since [$Sm(PhMe)_2${$HB(C_6F_5)_3$}$_2$] (**6**), and [$Yb(C_6D_6)${$HB(C_6F_5)_3$}$_2$] (**7**) were identified as complexes not active in polymerization, the formation of these complexes is the most likely explanation. Similarly, reaction of **1^{Ln}** with dimethyl-, and diethylaluminum chloride do not produce polymers. In this case, it is likely that inactivation occurs by ligand exchange and subsequent precipitation of amorphous divalent lanthanide chloride.

Table 1. Isoprene polymerization employing $\mathbf{1^{Ln}}$ (Ln = Sm, Eu, Yb) as precatalysts

entry[a]	pre-catalyst	co-catalyst[b]	reaction time [h]	[IP]/[Ln]	yield [%]	*cis*-1,4[c] [%]	*trans*-1,4[c] [%]	3,4[c] [%]	M_n[d] [10^4 g·mol^{-1}]	PDI[d]	T_G[e] [°C]
1	$\mathbf{1^{Sm}}$	none	4h	1000	20	77.97	1.86	20.17	5.7	1.52	–53
2	$\mathbf{1^{Sm}}$	**A**	24	1000	> 99	16.87	74.69	8.44	4.0	1.30	–63
3	$\mathbf{1^{Sm}}$	**B**	1	1000	> 99	27.60	60.23	12.17	4.8	1.21	–59
4	$\mathbf{1^{Sm}}$	**C**	24	1000	12	37.49	55.51	7.00	1.4	5.15	–63
5	$\mathbf{1^{Sm}}$	**D**, or **E**	24	1000	0	-	-	-	-	-	-
6	$\mathbf{1^{Eu}}$	none	24	1000	> 99	76.68	0	23.32	39.0	1.62	–49
7	$\mathbf{1^{Eu}}$	none	1	1000	41	75.69	0	24.31	26.6	1.40	–48
8	$\mathbf{1^{Eu}}$	**A**	24	1000	> 99	18.16	70.80	11.04	3.7	1.29	–61
9	$\mathbf{1^{Eu}}$	**B**	24	1000	> 99	25.62	61.22	13.16	6.1	1.12	–58
10	$\mathbf{1^{Eu}}$	**C**, **D**, or **E**	24	1000	0	-	-	-	-	-	-
11	$\mathbf{1^{Yb}}$	none	1	1000	94	81.82	5.43	12.75	6.0	1.92	–58
12	$\mathbf{1^{Yb}}$	**A**	24	1000	33	46.23	25.42	28.35	2.1	1.24	–46
13	$\mathbf{1^{Yb}}$	**B**	1	1000	> 99	54.92	14.14	30.94	5.4	1.10	–41

[a] Conditions: 20 µmol of precatalyst, 20 µmol of cocatalyst, 20 mmol of isoprene, 8 mL of toluene, 500 rpm stirring velocity. [b] Aged with cocatalyst at ambient temperature for 30 min: **A** = $[Ph_3C][B(C_6F_5)_4]$; **B** = $[PhNMe_2H][B(C_6F_5)_4]$; **C** = $B(C_6F_5)_3$; **D** = Me_2AlCl, **E** = Et_2AlCl, 1 equivalent. [c] Determined by $^1H/^{13}C$-NMR spectroscopy in $CDCl_3$. [d] Determined by SEC. [e] Determined by DSC.

Table 2. Isoprene polymerization employing $\mathbf{1^{Ln}}$ (Ln = Sm, Eu, Yb) as precatalysts

entry[a]	pre-catalyst	co-catalyst[b]	reaction time [h]	[IP]/[Ln]	yield [%]	*cis*-1,4[c] [%]	*trans*-1,4[c] [%]	3,4[c] [%]	M_n[d] [10^4 g·mol^{-1}]	PDI[d]	T_G[e] [°C]
14[f]	$\mathbf{1^{Yb}}$	**B**	2	250	> 99	54.15	14.14	31.71	1.7	1.04	–45
15[f]	$\mathbf{1^{Yb}}$	**B**	3	500	> 99	53.27	15.29	31.44	2.7	1.02	–45
16[f]	$\mathbf{1^{Yb}}$	**B**	4	750	> 99	51.61	16.79	31.60	4.0	1.05	–44
17[f]	$\mathbf{1^{Yb}}$	**B**	5	1000	> 99	53.74	14.71	31.55	4.9	1.03	–43
18	$\mathbf{1^{Yb}}$	**C**, **D**, or **E**	24	1000	0	-	-	-	-	-	-
19[g]	**2**	none	24	1000	0	-	-	-	-	-	-
20[g]	**2**	**A**	2	1000	10	96.9	0	3.1	n.d.	n.d.	n.d.
21[g]	**2**	**C**	2	1000	9	95.1	0	4.9	18.5	2.09	n.d.
22[g]	**2**	**B**, **D**, or **E**	24	1000	0	-	-	-	-	-	-
23	**6**	none	24	1000	0	-	-	-	-	-	-

[a] Conditions: 20 µmol of precatalyst, 20 µmol of cocatalyst, 20 mmol of isoprene, 8 mL of toluene, 500 rpm stirring velocity. [b] Aged with cocatalyst at ambient temperature for 30 min: **A** = $[Ph_3C][B(C_6F_5)_4]$; **B** = $[PhNMe_2H][B(C_6F_5)_4]$; **C** = $B(C_6F_5)_3$; **D** = Me_2AlCl, **E** = Et_2AlCl, 1 equivalent. [c] Determined by $^1H/^{13}C$-NMR spectroscopy in $CDCl_3$. [d] Determined by SEC. [e] Determined by DSC. [f] 20 µmol of precatalyst, 20 µmol of **B** ($[PhNMe_2H][B(C_6F_5)_4]$), 10 mL toluene, aged at ambient temperature for 30 min, addition of 10 mmol of isoprene (0.5 mL, 5 mmol) after each hour, 500 rpm stirring velocity. [g] 3.3 µmol of precatalyst, 20 µmol of cocatalyst, 8 mL of *n*-hexane, 20 mmol of isoprene, n.d. not determined.

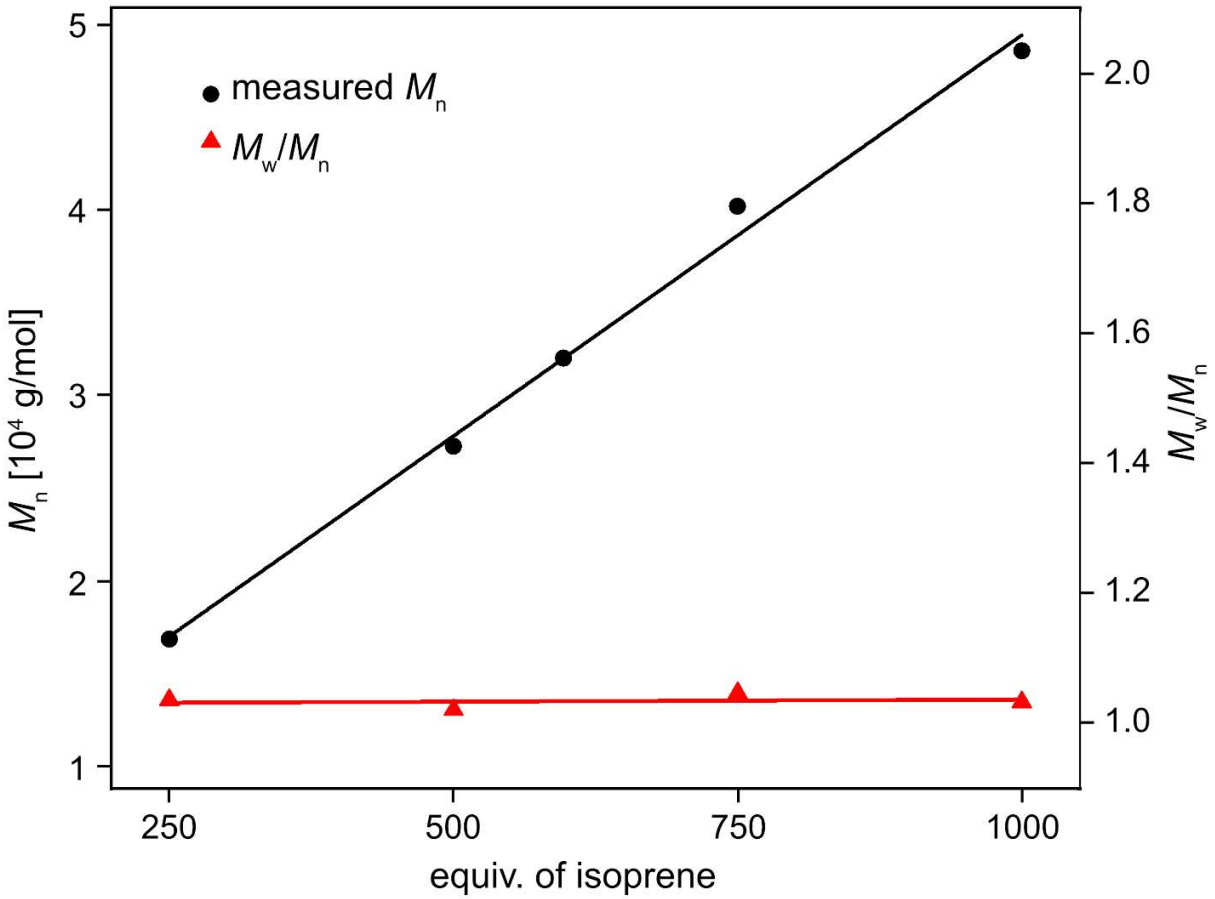

Figure 2. Molecular weight vs. equivalents of isoprene for polymers obtained with the $\mathbf{1^{Yb}}$/**B** catalyst mixture showing linearly increasing M_n and narrow PDIs after several monomer additions.

The reactions of Yb(Al*i*Bu$_4$)$_2$ ($\mathbf{1^{Yb}}$) with one equivalent **A**, or **B** in deuterated benzene were monitored using ^{1}H-NMR spectroscopy (Figure 3 and Figure 4). Activation of Yb(Al*i*Bu$_4$)$_2$ ($\mathbf{1^{Yb}}$) with [CPh$_3$][B(C$_6$F$_5$)$_4$] (**A**) leads to the formation of triphenylmethane, isobutene, and TIBA. The absence of paramagnetic broadening of proton resonances (as observed with the $\mathbf{1^{Yb}}$/**B** mixture) indicates that exclusively Yb(II) species are formed. The new isobutyl signal may be assigned to a putative active species "[{Yb(Al*i*Bu$_4$)}{B(C$_6$F$_5$)$_4$}] (**10**)". (see Scheme 19). Activation of Yb(Al*i*Bu$_4$)$_2$ ($\mathbf{1^{Yb}}$) with [C$_6$H$_5$NMe$_2$H][B(C$_6$F$_5$)$_4$] (**B**) led to the formation of isobutane, and the TIBA-dimethylaniline adduct. This indicates the protonolysis of one tetraisobutylaluminato ligand, without further decomposition *via* β-hydride elimination of the activation product (absence of isobutene resonances). The formation of a new isobutyl signal set was observed, that may be

assigned to the putative active species, most likely a cationized tetraisobutylaluminate complex "[{Yb(PhNMe$_2$-Al*i*Bu$_3$)(Al*i*Bu$_4$)}$^+${B(C$_6$F$_5$)$_4$}$^-$]" (**11A**). Even though activation products with both catalysts are similar, which explains similar microstructures of the polymers obtained, the slight differences in polymerization (e.g. yields in entries 12, and 13, Table 1) may be explained by the presence of a dimethylanillinium-triisobutylaluminum adduct, that enhances the solubility of the **1^{Yb}/B** mixture.

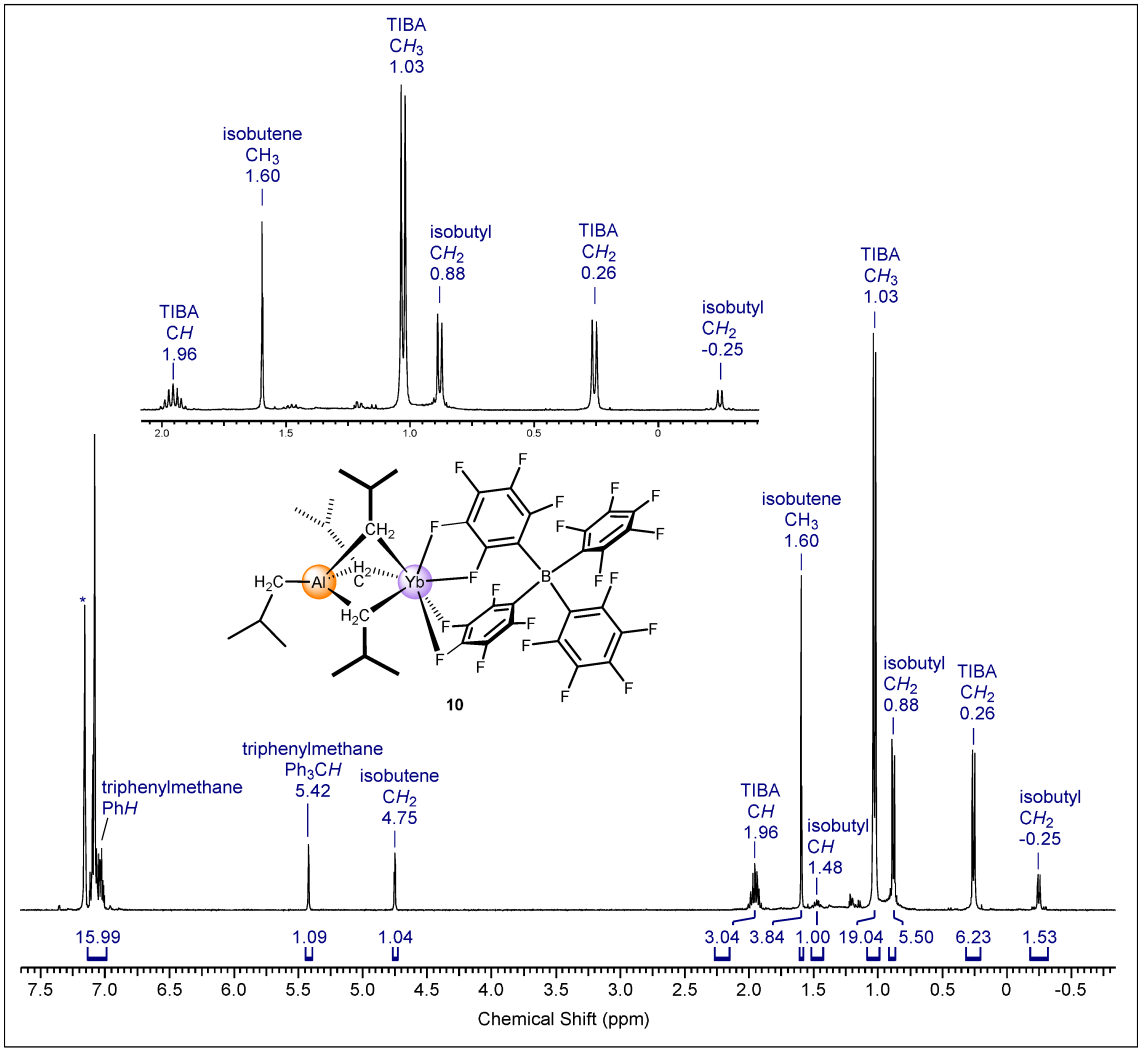

Figure 3. ^{1}H-NMR spectrum (400 MHz, C$_6$D$_6$, 26 °C) of the reaction of **1^{Yb}** with one equivalent of cocatalyst **A** and proposed active species **10**.

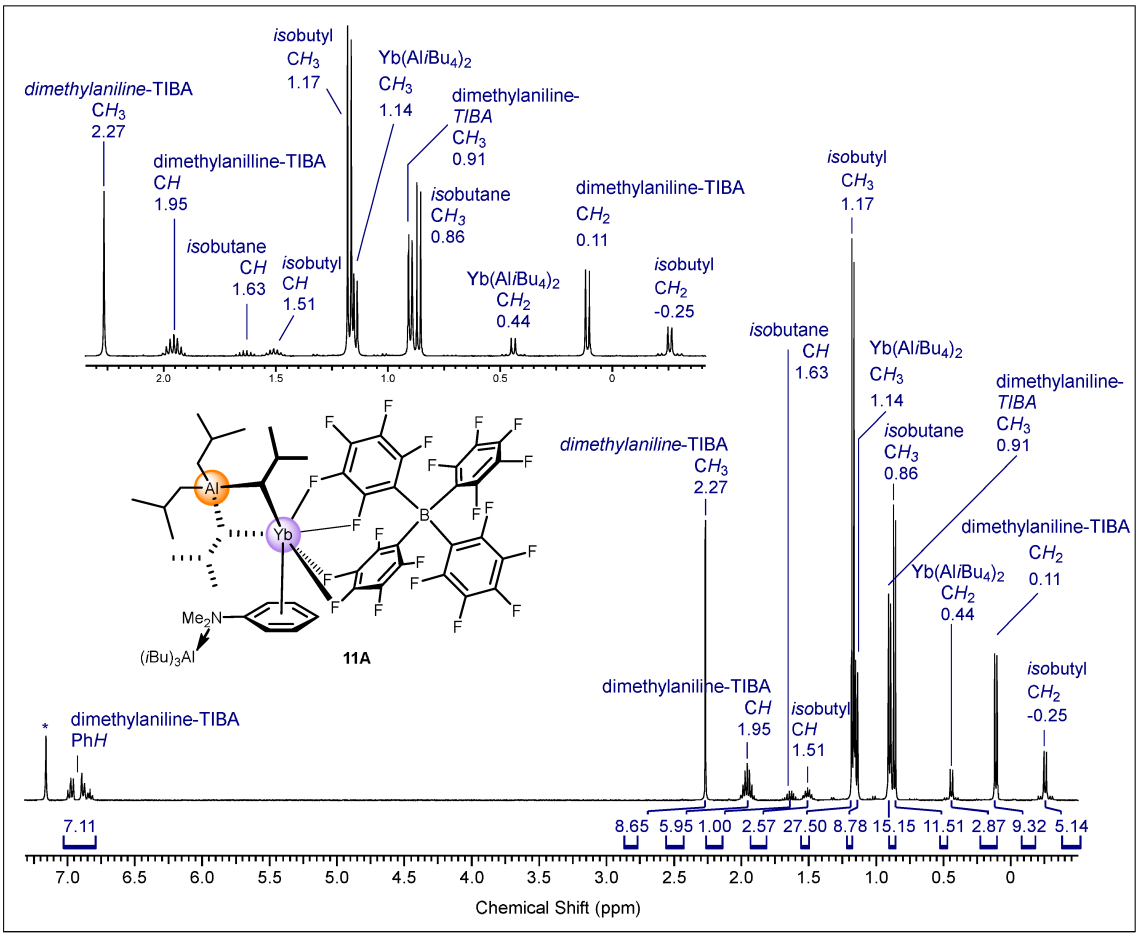

Figure 4. ^{1}H-NMR spectrum (400 MHz, C_6D_6, 26 °C) of the reaction of $\mathbf{1}^{\mathbf{Yb}}$ with one equivalent of cocatalyst **B** and proposed active species (**11A**).

The reaction of Yb(Al*i*Bu$_4$)$_2$ ($\mathbf{1}^{\mathbf{Yb}}$) with one equivalent of **B** in benzene was performed following procedures similar to the NMR experiments. However, no crystals or precipitate was obtained from the concentrated reaction mixture upon storing at –40 °C even after 1.5 years. The solution was then stored at ambient temperature, whereupon yellowish, needle-shaped crystaline product [Yb(C$_6$H$_6$)$_2$(Al*i*Bu$_4$)][B(C$_6$F$_5$)$_4$]/[Yb(C$_6$H$_6$)$_2${B(C$_6$F$_5$)$_4$}$_2$] (**11B**) identified by X-ray crystallography formed (*cf.* Scheme 19). It is notable that the aluminate unit [Yb(C$_6$H$_6$)$_2$(Al*i*Bu$_4$)][B(C$_6$F$_5$)$_4$] exhibits the coordination of two benzene molecules, similar to perfluorinated compounds **6** and **7**. In case of **11B**, the benzene molecules are not only satisfying the sterical demand of the Yb(II) center, but also likely occupying the catalytically active coordination site. Albeit **11B** may be a decomposition product, it supports the structure of proposed active species **11A**.

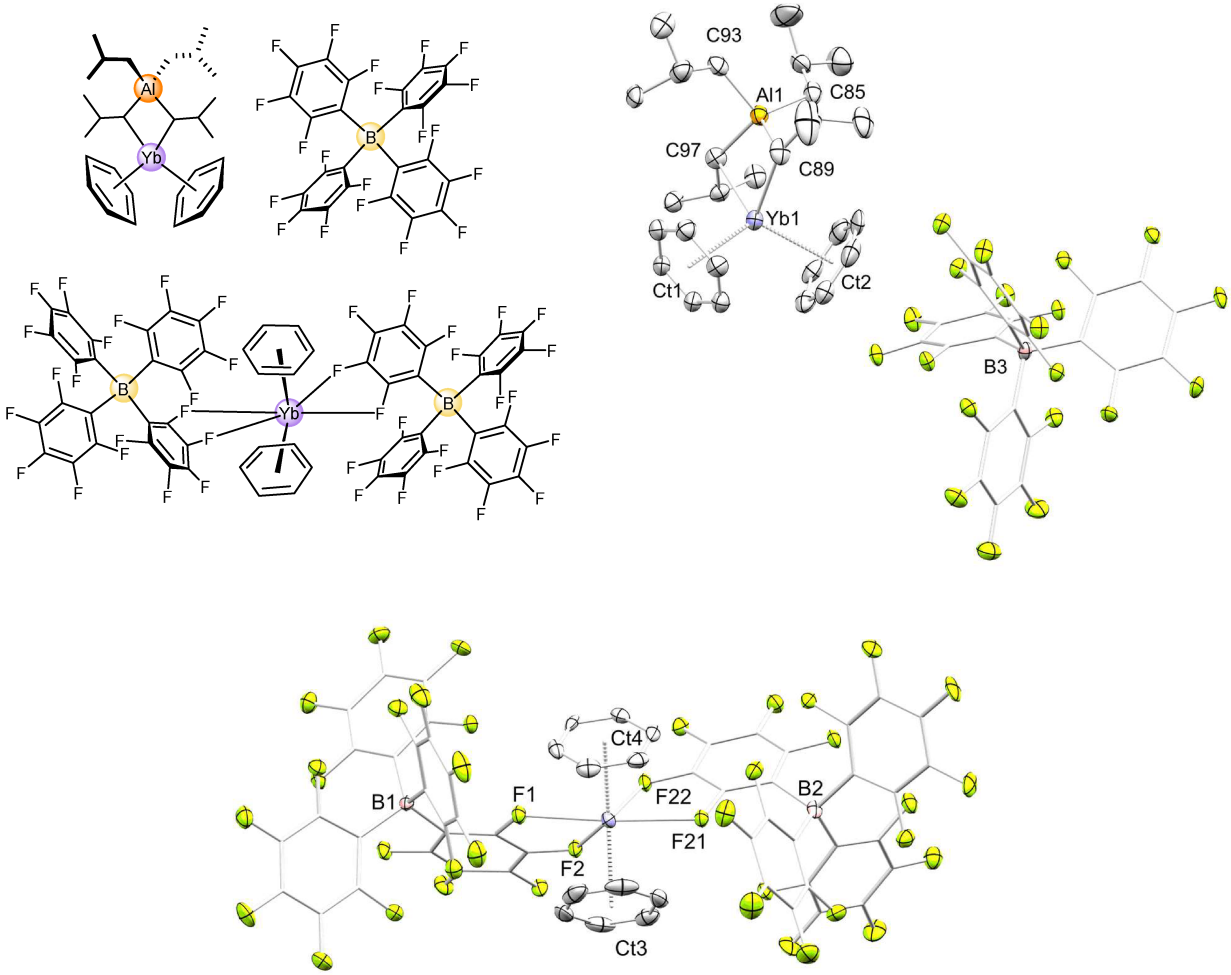

Scheme 19**.** Left: Schematic representation of product $[Yb(C_6H_6)_2(Al\textit{i}Bu_4)][B(C_6F_5)_4]$/$[Yb(C_6H_6)_2\{B(C_6F_5)_4\}_2]$ (**11B**) crystallized from a $Yb(Al\textit{i}Bu_4)_2$/**B** mixture. Right: Crystal structure of the aluminate moiety $[Yb(C_6H_6)_2(Al\textit{i}Bu_4)][B(C_6F_5)_4]$ of **11B**. Ellipsoids are shown at the 50% probability level. Hydrogen atoms are omitted for clarity. Selected interatomic distances [Å]: Yb(1)–C(89) 2.568(9), Yb(1)–C(97) 2.540(8), Yb(1)··Ct(1) 2.633, Yb(1)··Ct(2) 2.608. Bottom: $[Yb(C_6H_6)_2\{B(C_6F_5)_4\}_2]$ unit of **11B**. Ellipsoids are shown at the 50% probability level. Hydrogen atoms are omitted for clarity. Selected interatomic distances [Å]: Yb(2)–F(1) 2.543(4), Yb(2)–F(2) 2.593(4), Yb(2)–F(21) 2.606(4), Yb(2)–F(22) 2.521(4), Yb(1)··Ct(3) 2.553, Yb(1)··Ct(4) 2.584.

Trivalent Heteroleptic Lanthanide Isobutylaluminates

To date, only one trivalent lanthanide tetraisobutylaluminate, $Cp^*_2Sm(Al\textit{i}Bu_4)$, has been characterized in the solid state.[81] However, pentamethylcyclopentadienyl spectator ligands impede activity in conjugated diene polymerization, and redox-active samarium is hardly representative for the early lanthanides applied in industrial catalyst mixtures.

In order to isolate discrete trivalent tetraisobutylaluminates of early lanthanides, we employed a number of different amide precursors $Ln(NR_2)_3$ (R = Me, Et, *i*Pr, $SiHMe_2$, $SiMe_3$). However, excess triisobutylaluminum alongside with isobutylaluminum side products greatly hampered crystallization, and products did not crystallize in most cases despite different conditions and solvents, due to the very high mobility of isobutyl residues, and excellent solubility in aliphatic solvents.

However, the reaction of $La[N(SiMe_3)_2]_3$ with 6.5 equiv. triisobutylaluminum did yield a very viscous oil, from which we could obtain single crystals of $La[N(SiMe_3)_2](HAl\textit{i}Bu_3)(Al\textit{i}Bu_4)$ (**12**$^{\mathbf{La}}$) (Figure 5, Scheme 20), and the formation of a hydride was accompanied by slow isobutene evolution as visible in the ^{1}H-NMR spectrum (Figure 6). The same product could also be obtained with 4.1 equiv. TIBA, which improved the purification process. This protocol could be applied to generate isostructural early lanthanide isobutylaluminates $Ln[N(SiMe_3)_2](HAl\textit{i}Bu_3)(Al\textit{i}Bu_4)$ (**12**$^{\mathbf{Ln}}$) (Ln = La, Pr, Nd, Gd), whereas $Sm[N(SiMe_3)_2]_3$ did undergo reduction to $Sm(Al\textit{i}Bu_4)_2$ (**1**$^{\mathbf{Sm}}$). It is notable that the gadolinium aluminate was the smallest lanthanide aluminate that could still be isolated; however, it proved to be more difficult to crystallize than corresponding early lanthanide congeners with a larger metal center, and the gadolinium aluminate was obtained in a lower yield. In contrast, for example $Ho[N(SiMe_3)_2]_3$/TIBA reaction mixtures, did not yield crystalline products, indicating that smaller lanthanides escape crystallization, and characterization. ^{1}H-NMR spectra of the diamagnetic congener $La[N(SiMe_3)_2](HAl\textit{i}Bu_3)(Al\textit{i}Bu_4)$ (**12**$^{\mathbf{La}}$) provided evidence that, even at temperatures as low as 190 K, bridging and terminal isobutyl residues are still exchanging, which highlights the high mobility of isobutyl residues coordinated to the lanthanum center in solution.

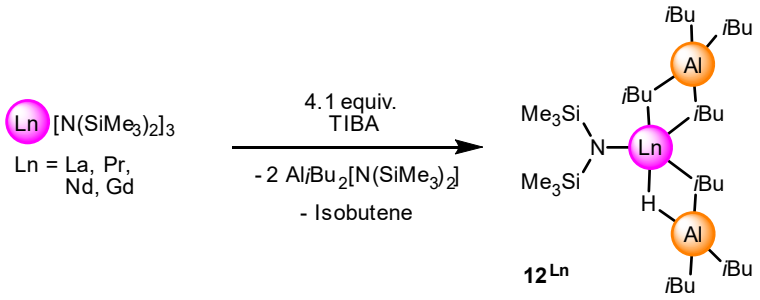

Scheme 20. Synthesis of Ln[N(SiMe$_3$)$_2$](HAl*i*Bu$_3$)(Al*i*Bu$_4$) (**12^{Ln}**) (Ln = La, Pr, Nd, Gd) following an silylamido-elimination protocol.

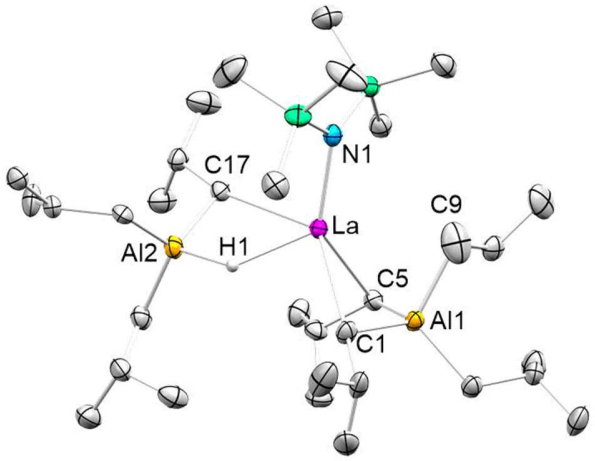

Figure 5. Crystal structure of the first structurally characterized trivalent lanthanide isobutylaluminate La[N(SiMe$_3$)$_2$](HAl*i*Bu$_3$)(Al*i*Bu$_4$) (**12^{La}**). Ellipsoids are shown at a 50% probability level. Hydrogen atoms expect the hydride, and the disorder in isobutyl groups are omitted for clarity.

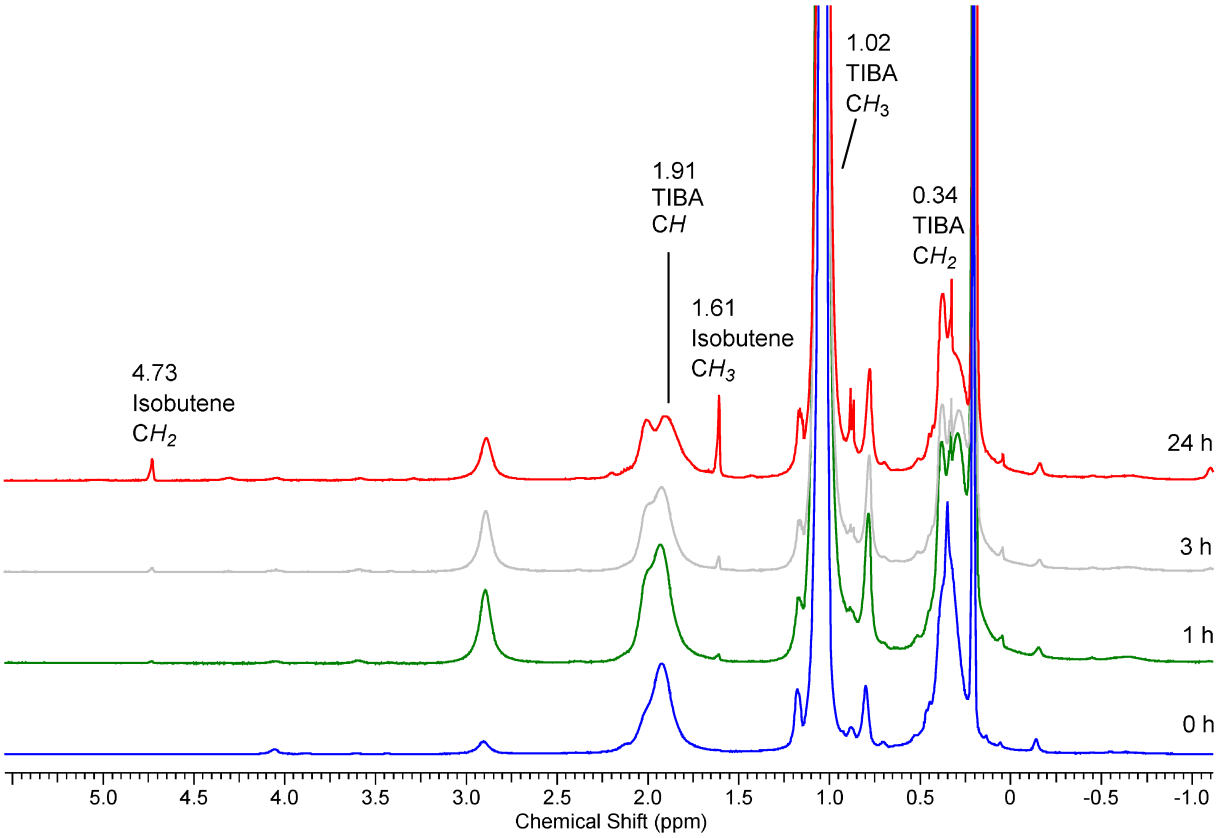

Figure 6. ^{1}H-NMR spectra (25°C, 400 MHz) of the reaction of Nd[N(SiMe$_3$)$_2$]$_3$ with 5 equivalents TIBA showing isobutene evolution after several hours at ambient temperature in benzene-d$_6$.

The heteroleptic complexes Ln[N(SiMe$_3$)$_2$](HAl*i*Bu$_3$)(Al*i*Bu$_4$) (**12^{Ln}**) (Ln = La, Pr, Nd, Gd) proved to be isostructural, containing one remaining silylamido ligand, alongside with a hydrido-bridged triisobutylaluminum moiety, and a tetraisobutylaluminato ligand. In contrast to the divalent tetraisobutylaluminates **1^{Ln}**, that did not show the propensity to form hydrides, it is notable that the far more Lewis acidic trivalent lanthanide precursors readily feature isobutene evolution when treated with triisobutylaluminum. The role of organoaluminum hydride compounds is of great relevance for industrially applied mixed catalysts, that often contain either triisobutylaluminum, or diisobutylaluminum hydride, or both compounds. The reactivity of TIBA to form hydrido complexes was shown for the first time with the synthesis of Ln[N(SiMe$_3$)$_2$](HAl*i*Bu$_3$)(Al*i*Bu$_4$) (**12^{Ln}**), and finally provides a link between both cocatalysts TIBA and DIBAH.

The role of the hydrido moiety is further highlighted by derivatization products of Ln[N(SiMe$_3$)$_2$](HAl*i*Bu$_3$)(Al*i*Bu$_4$) (**12^{Ln}**). Addition of 18-crown-6 to

Nd[N(SiMe$_3$)$_2$](HAl*i*Bu$_3$)(Al*i*Bu$_4$) (**12Nd**) led to the formation of [Nd(18-c-6){N(SiMe$_3$)$_2$}(HAl*i*Bu$_3$)][Al*i*Bu$_4$] (**13**) (*cf.* Scheme 21). Compound **13** features a completely separated tetraisobutylaluminato moiety, whereas the coordinated heteroaluminate moiety indicated a strong Nd–H binding. Besides, reaction of La[N(SiMe$_3$)$_2$](HAl*i*Bu$_3$)(Al*i*Bu$_4$) (**12^{La}**) with fluorene gave insoluble [(μ-fluorenyl)$_3$La$_2$(μ-H)(HAl*i*Bu$_3$)$_2$][(fluorenyl)$_2$La{N(SiMe$_3$)$_2$}] (**14**). It consists of a binuclear, hydrido-bridged moiety featuring an unusual η^6-coordination of the fluorenyl ligands, instead of a η^5-coordination as present in the cocrystallized [(fluorenyl)$_2$La{N(SiMe$_3$)$_2$}] molecule. The pre-formed [HAl*i*Bu$_3$] unit may remain coordinated while compound **14** is formed, due to a strong Ln-H interaction as observed with compound [Nd(18-c-6){N(SiMe$_3$)$_2$}(HAl*i*Bu$_3$)][Al*i*Bu$_4$] (**13**). The number of hydrides in **14** was confirmed by monitoring the protonolysis with isopropanol by ^{1}H-NMR spectroscopy, showing hydrogen formation. Referenced to the signal of hexamethyldisilazane co-formed in the mixture, the integral ratios of 6 (or 3 of the non-binomial triplet observed when instead *i*PrOD-d$_8$ was employed) hydrogen protons to 18 hexamethyldisilazane protons corroborate the presence of three hydrides in [(μ-fluorenyl)$_3$La$_2$(μ-H)(HAl*i*Bu$_3$)$_2$][(fluorenyl)$_2$La{N(SiMe$_3$)$_2$}] (**14**).

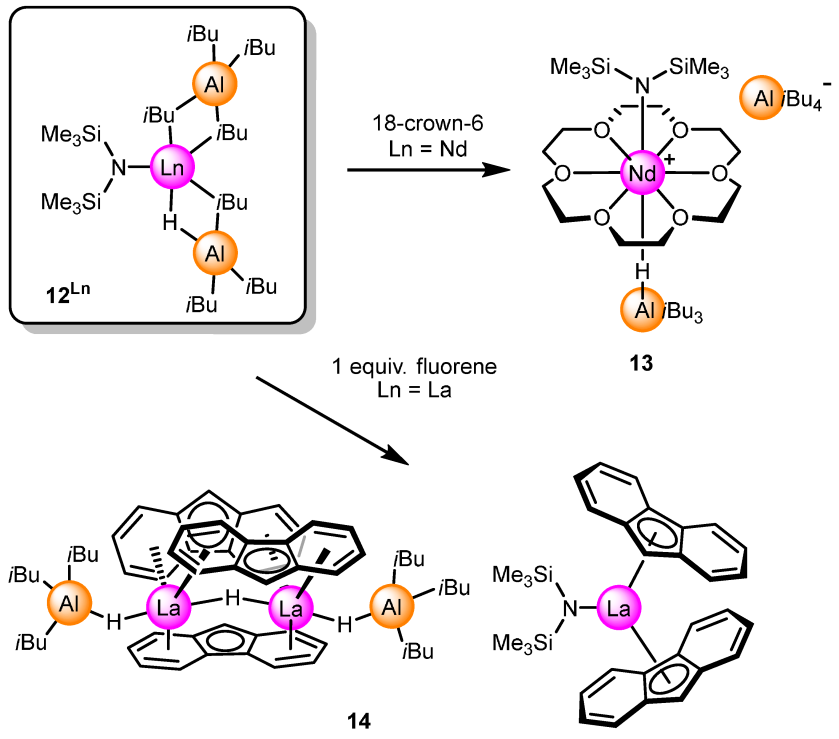

Scheme 21. Synthesis [Nd(18-c-6){N(SiMe$_3$)$_2$}(HAl*i*Bu$_3$)][Al*i*Bu$_4$] (**13**), and [(μ-fluorenyl)$_3$La$_2$(μ-H)(HAl*i*Bu$_3$)$_2$][(fluorenyl)$_2$La{N(SiMe$_3$)$_2$}] (**14**).

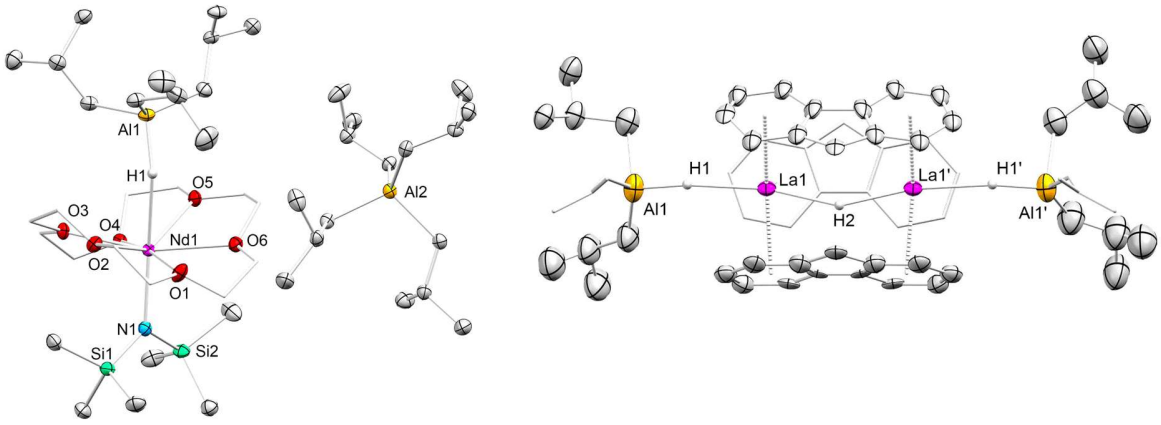

Figure 7. Crystal structures of compounds [Nd(18-c-6){N(SiMe$_3$)$_2$}(HAliBu$_3$)][AliBu$_4$] (**13**), and the heterobimetallic moiety of [(μ-fluorenyl)$_3$La$_2$(μ-H)(HAl*i*Bu$_3$)$_2$][(fluorenyl)$_2$La{N(SiMe$_3$)$_2$}] (**14**). Hydrogen atoms except bridging hydridos, as well as the disorder in isobutyl groups are omitted for clarity.

Trivalent Heteroleptic Lanthanide Isobutylaluminates in Isoprene Polyermization

Complexes Ln[N(SiMe$_3$)$_2$](HAl*i*Bu$_3$)(Al*i*Bu$_4$) (**12^{Ln}**) (Ln = La, Pr, Nd, Gd) were tested in isoprene polymerization, making them the first discrete trivalent lanthanide isobutylaluminates to be employed as precatalyst. A large part of the studies were conducted in both toluene, and *n*-hexane using Nd[N(SiMe$_3$)$_2$](HAl*i*Bu$_3$)(Al*i*Bu$_4$) (**12Nd**) as precatalyst. The neodymium complex was used since neodymium usually delivers high *cis*-polymers and is applied for large scale polyisoprene synthesis alongside with industrially relevant alkylaluminum chloride cocatalysts.

Surprisingly, Nd[N(SiMe$_3$)$_2$](HAl*i*Bu$_3$)(Al*i*Bu$_4$) (**12Nd**) did already exhibit a minor polymerization activity without additional cocatalyst (*cf.* Table 3, entry 1). Speculatively, the relatively high *trans*-content may be ascribed to the putative formation of an active allyl species, since works of Taube *et al.* showed that tris(allyl)neodymium(III) is a single component catalyst for selective *trans*-polymerization of butadiene as mentioned before, and the hydride compound

Nd[N(SiMe$_3$)$_2$](HAl*i*Bu$_3$)(Al*i*Bu$_4$) (**12Nd**) may form an allylic complex by isoprene insertion into the Nd–H bond.

Very active catalyst systems were generated by activation of precatalyst Nd[N(SiMe$_3$)$_2$](HAl*i*Bu$_3$)(Al*i*Bu$_4$) (**12Nd**) with borate cocatalysts. Employing [CPh$_3$][B(C$_6$F$_5$)$_4$] (**A**), [C$_6$H$_5$NMe$_2$H][B(C$_6$F$_5$)$_4$] (**B**), or B(C$_6$F$_5$)$_3$ (**C**) yielded polyisoprene quantitatively after 1 h (Table 3, entry 2-4). The polymers featured slightly higher *cis*-selectivities, alongside with improved yields compared to the homoleptic tetramethylaluminates under comparable conditions.[79] Nd[N(SiMe$_3$)$_2$](HAl*i*Bu$_3$)(Al*i*Bu$_4$) (**12Nd**) activated with cocatalysts Me$_2$AlCl (**D**), or Et$_2$AlCl (**E**) (*cf*. Table 3, entry 5 and 7) yielded selectivities similar to homoleptic lanthanide tetramethylaluminates. Probing different amounts of cocatalyst **E**, it was noted that the most active catalysts are obtained with two equivalents (*cf*. Table 3, entry 6-11), which is in good accordance with literature for comparable systems.[143] Polymerizations employing Nd[N(SiMe$_3$)$_2$](HAl*i*Bu$_3$)(Al*i*Bu$_4$) (**12Nd**) as precatalyst in *n*-hexane generally yielded lower *cis*-selectivity, and decreased polymerization activity (*cf*. Table 3, Table 4, entry 12-19), whereas polymerization activity was slightly higher for organoaluminum chloride cocatalysts with comparable *cis*-selectivity as found with homoleptic lanthanide tetramethylaluminates.[79]

The influence of the lanthanide center was further studied employing isostructural complexes Ln[N(SiMe$_3$)$_2$](HAl*i*Bu$_3$)(Al*i*Bu$_4$) (**12^{Ln}**) with each one, or two equivalents diisobutylaluminum chloride (**F**) as cocatalyst (*cf*. Table 4, entry 20-29). Several trends were observed: First, all complexes exhibited higher activities with 2 equiv. **F** compared to 1 equiv. **F**. Second, the activity of both **1^{Ln}**/**F**, and **1^{Ln}**/2**F** was found to increase in the order La<Pr<Nd≈Gd. More importantly, also the stereoselectivity was found to increase following the similar sequence La<Pr<Nd<Gd. Mixtures **1Nd**/**F**, but especially **1^{Gd}**/**F** (Table 4, entries 25-26, and 28-29) produced high molecular weight polyisoprene. Alongside with high molecular weight, especially the *cis*-selectivity is crucial for a high-performance rubber. With Gd[N(SiMe$_3$)$_2$](HAl*i*Bu$_3$)(Al*i*Bu$_4$) (**12^{Gd}**)/**F** catalyst mixtures, almost perfect *cis*-stereoselectivity of >99.5 % *cis* was observed, with no trans-linked isoprene resonances detected by ^{13}C{^{1}H}-NMR spectroscopy (see Figure 8).

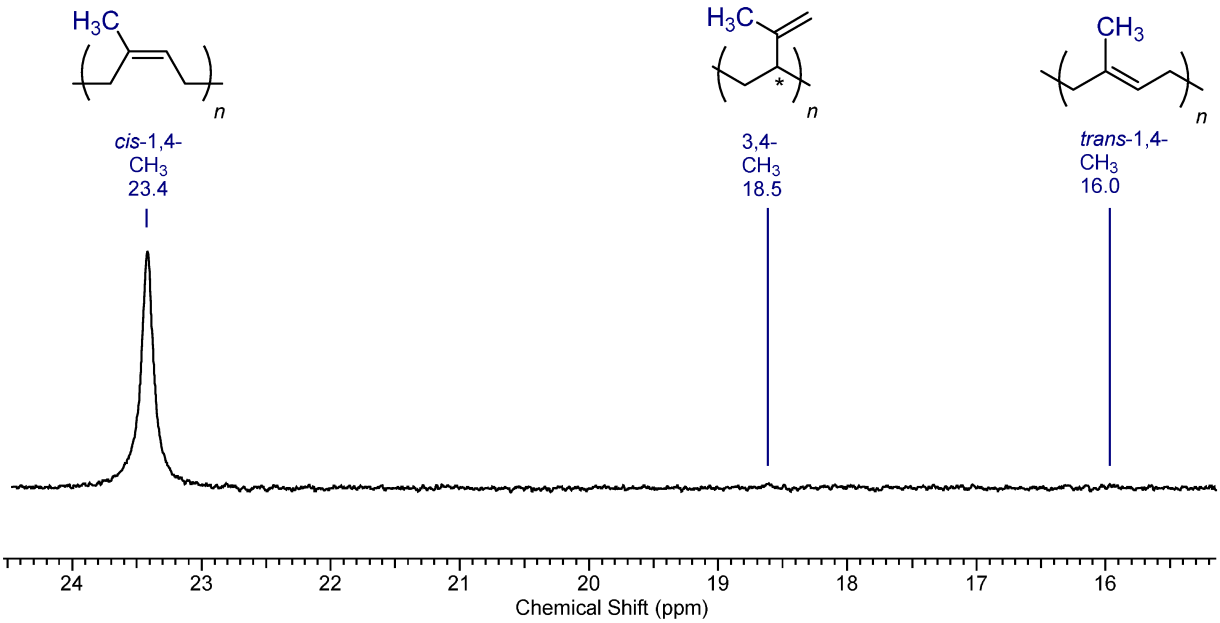

Figure 8. $^{13}C\{^{1}H\}$-NMR spectrum (25°C, 400 MHz) of polyisoprene obtained with catalyst mixture **12**^{Gd}/2**F** (cf. Table 2, entry 29).

Alongside ^{1}H-NMR spectroscopic experiments studying the reactivity of cocatalysts employed for isoprene polymerization towards La[N(SiMe$_3$)$_2$](HAl*i*Bu$_3$)(Al*i*Bu$_4$) (**12**^{La}), we also managed to crystallize a reaction product of Nd[N(SiMe$_3$)$_2$](HAl*i*Bu$_3$)(Al*i*Bu$_4$) (**12**Nd) with one equivalent [C$_6$H$_5$NMe$_2$H][B(C$_6$F$_5$)$_4$] (**B**), which was identified as [Nd{N(SiMe$_3$)$_2$}(PhNMe$_2$)$_2$][B(C$_6$F$_5$)$_4$]$_2$ (**15**) by XRD analysis (see Figure 9). Product [Nd{N(SiMe$_3$)$_2$}(PhNMe$_2$)$_2$][B(C$_6$F$_5$)$_4$]$_2$ (**15**) is composed of a dicationic [Nd{N(SiMe)$_3$)$_2$}(PhNMe$_2$)$_2$] moiety, and two spatially separated borato anions [B(C$_6$F$_5$)$_4$]. Of great help was that the same product [Nd{N(SiMe$_3$)$_2$}(PhNMe$_2$)$_2$][B(C$_6$F$_5$)$_4$]$_2$ (**15**) could be directly obtained from Nd[N(SiMe$_3$)$_2$]$_3$ and two equivalents of [C$_6$H$_5$NMe$_2$H][B(C$_6$F$_5$)$_4$] (**B**), and was the only derivatization product of Nd[N(SiMe$_3$)$_2$]$_3$ obtained with one, two, or three equivalents of [C$_6$H$_5$NMe$_2$H][B(C$_6$F$_5$)$_4$] (**B**). It needs to be noted that the η^6-coordination of *N*,*N*-dimethylanilline is governed by steric factors, whereas *N*,*N*-dimethylanilline coordinates to the smaller, and harder scandium also *via* the nitrogen atom instead of the aromatic ring,[149] or by η^6-coordination.[64]

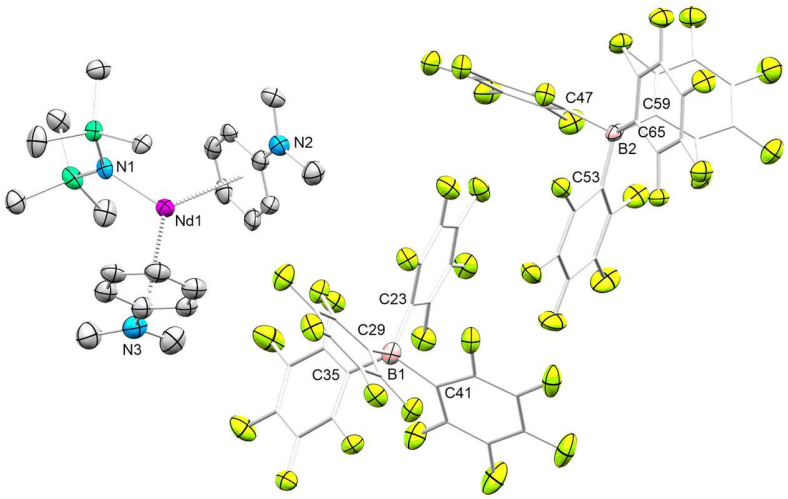

Figure 9. Crystal structure of $[Nd\{N(SiMe_3)_2\}(PhNMe_2)_2][B(C_6F_5)_4]_2$ (**15**). Ellipsoids are shown at the 50% probability level. Hydrogen atoms are omitted for clarity.

In isoprene polymerization, $[Nd\{N(SiMe_3)_2\}(PhNMe_2)_2][B(C_6F_5)_4]_2$ (**15**) proved to be a single-component catalyst (*cf*. Table 4, entry 30-31), yielding essentially *trans*-free polyisoprene in good yields with high molecular weights, though the overall catalytic activity was better in 1,2-difluorobenzene than in toluene due to the moderate solubility of **15**. Although mechanistic details have escaped characterization so far, alkylation of the neodymium center by a B→Nd transfer of a pentafluorophenyl group, amide insertion, or cationic polymerization may be considered. Employing $[Nd\{N(SiMe_3)_2\}(PhNMe_2)_2][B(C_6F_5)_4]_2$ (**15**) and two equivalents of triisobutylaluminum for isoprene polymerization only led to a slight increase of activity compared to pure $[Nd\{N(SiMe_3)_2\}(PhNMe_2)_2][B(C_6F_5)_4]_2$ (**15**) (23% vs. 17 % yield; *cf*. entries 32, and 31), thus showing little influence on the active species, and most likely, no further alkylation occurs, that would have further increased catalytic activity. The addition of triisobutylaluminum, however, led to a decrease in molecular weight (14.9 vs. 46.9 x 10^4 g mol^{-1}), due to the chain-transfer activity of triisobutylaluminum.

Microstructures of polyisoprenes obtained using Nd[N(SiMe$_3$)$_2$](HAl*i*Bu$_3$)(Al*i*Bu$_4$) (**12Nd**) with two equivalents [C$_6$H$_5$NMe$_2$H][B(C$_6$F$_5$)$_4$] (**B**) as catalyst mixture, and [Nd{N(SiMe$_3$)$_2$}(PhNMe$_2$)$_2$][B(C$_6$F$_5$)$_4$]$_2$ (**15**) however differed, suggesting that [Nd{N(SiMe$_3$)$_2$}(PhNMe$_2$)$_2$][B(C$_6$F$_5$)$_4$]$_2$ (**15**) is not the main species formed in **12Nd**/2**B** mixtures (entries 34-35). Possibly, compound [Nd{N(SiMe$_3$)$_2$}(PhNMe$_2$)$_2$][B(C$_6$F$_5$)$_4$]$_2$ (**15**) is formed as a decomposition product from the putative cationic species generated by cationization of Nd[N(SiMe$_3$)$_2$](HAl*i*Bu$_3$)(Al*i*Bu$_4$) (**12Nd**) with [C$_6$H$_5$NMe$_2$H][B(C$_6$F$_5$)$_4$] (**B**) (Scheme 22). This scenario is based on ^{1}H-NMR spectra of the reaction of diamagnetic La[N(SiMe$_3$)$_2$](HAl*i*Bu$_3$)(Al*i*Bu$_4$) (**12^{La}**) with one equivalent of [C$_6$H$_5$NMe$_2$H][B(C$_6$F$_5$)$_4$] (**B**) in deuterated benzene, which revealed the formation of several byproducts. Besides **12^{La}** still present in the mixture, isobutene, triisobutylaluminum, hydrogen, and isobutane were observed. In this case, a putative cationic species [Ln(PhNMe$_2$){N(SiMe$_3$)$_2$}{AlR$_4$}][B(C$_6$F$_5$)$_4$] (**16**) may be present. Based on decomposition product analysis, a putative mechanistic scenario was postulated as depicted in Scheme 22. In case of the neodymium congener Nd[N(SiMe$_3$)$_2$](PhNMe$_2$)$_2$[B(C$_6$F$_5$)$_4$]$_2$ (**15**), the same "cationic" active species could be formed by mixing Nd[N(SiMe$_3$)$_2$](HAl*i*Bu$_3$)(Al*i*Bu$_4$) (**12Nd**), and [Nd{N(SiMe$_3$)$_2$}(PhNMe$_2$)$_2$][B(C$_6$F$_5$)$_4$]$_2$ (**15**), yielding same polymers as a Nd[N(SiMe$_3$)$_2$](HAl*i*Bu$_3$)(Al*i*Bu$_4$) (**12Nd**)/**B** mixture. In fact, strikingly similar microstructures (*cis*/*trans*/3,4) were observed for polymerizations employing catalyst mixtures **12Nd**/**B** with 71.67/21.00/7.34 (Table 3, entry 3), compared to **12Nd** /**15** with 69.37/23.32/7.31 (Table 4, entry 33). Molecular weights of polymers in entry 3 (Table 3), and entry 33 (Table 4) are in accordance with the total amount of neodymium in each catalyst mixture (54 000 g/mol, 0.02 mmol Nd for **12Nd** /**B**, vs. 21 000 g/mol, 0.04 mmol Nd for **12Nd** /**15**), and molecular weight distributions are almost identical (1.28 vs. 1.16), giving evidence for the presence of the active species [Ln(PhNMe$_2$){N(SiMe$_3$)$_2$}{AlR$_4$}][B(C$_6$F$_5$)$_4$] (**16**).

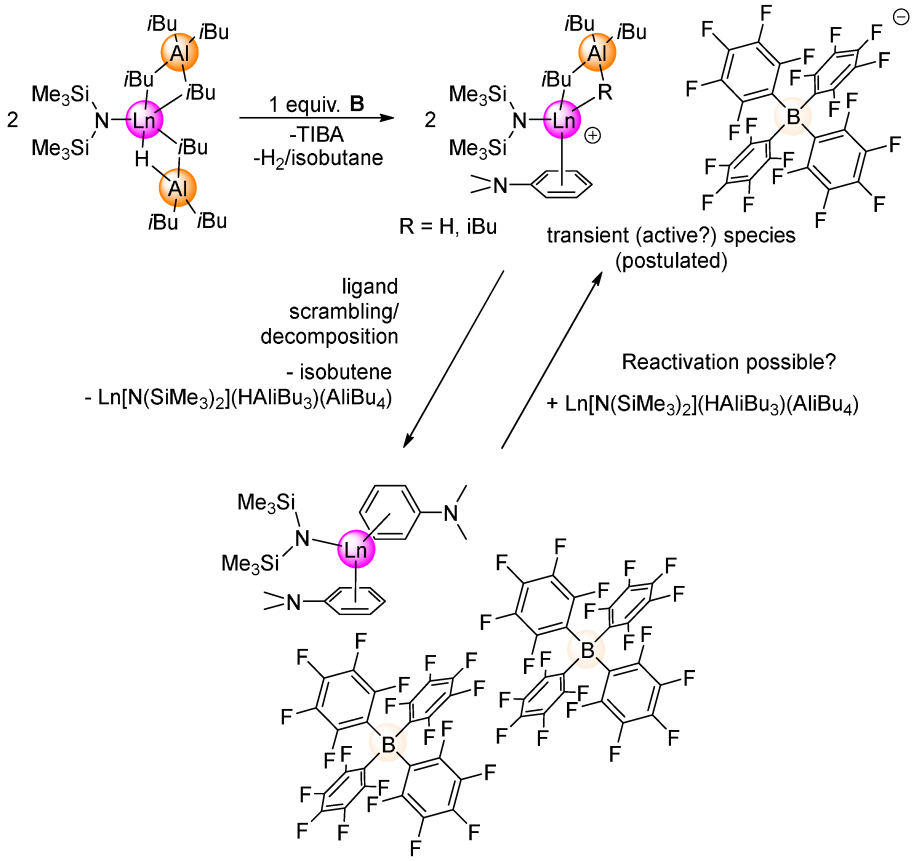

Scheme 22. Activation mechanism proposed for the reactiton of Ln[N(SiMe$_3$)$_2$](HAliBu$_3$)(AliBu$_4$) (**12**$^{\mathbf{Ln}}$), and **B**.

Table 3. Performance of complexe **12Nd** as precatalyst in isoprene polymerization.

entry	precatalyst	cocatalyst	reaction time [h]	solvent	yield [%]	*cis*-1,4[c] [%]	*trans*-1,4[c] [%]	3,4[c] [%]	M_n[d] [10^4 g·mol^{-1}]	PDI[d]	T_G[e] [°C]
1	**12Nd**	none	72	toluene	2	18.39	74.92	6.70	n.d.	n.d.	n.d.
2	**12Nd**	1**A**	1	toluene	> 99	86.07	5.86	8.07	6.3	1.49	-62
3	**12Nd**	1**B**	1	toluene	> 99	71.67	21.00	7.34	5.4	1.28	-62
4	**12Nd**	1**C**	1	toluene	> 99	92.68	2.57	4.75	8.8	3.48	-65
5	**12Nd**	1**D**	24	toluene	74	94.62	3.38	2.00	5.4	3.74	-65
6	**12Nd**	1**E**	10 min	toluene	1	97.55	0	2.45	n.d.	n.d.	n.d.
7	**12Nd**	1**E**	24	toluene	81	95.93	1.94	2.13	5.6	3.20	-64
8	**12Nd**	2**E**	1	toluene	96	97.62	0	2.38	3.4	6.04	-64
9	**12Nd**	2**E**	10 min	toluene	25	97.73	0	2.27	4.4	5.63	-64
10	**12Nd**	3**E**	30 min	toluene	34	96.44	0.95	2.61	1.8	3.66	-64
11	**12Nd**	4**E**	24	toluene	< 1	95.19	0	4.81	n.d.	n.d.	n.d.
12	**12Nd**	1**A**	1	*n*-hexane	88	55.75	38.20	6.05	3.7	1.70	-64
13	**12Nd**	1**B**	1	*n*-hexane	78	30.45	60.80	8.75	2.5	1.81	-65
14	**12Nd**	1**C**	1	*n*-hexane	94	90.66	5.15	4.19	9.2	2.30	-64
15	**12Nd**	1**D**	1	*n*-hexane	17	97.25	0	2.75	5.1	8.31	-65
16	**12Nd**	1**E**	1	*n*-hexane	10	97.05	0	2.95	3.2	9.54	-65
17	**12Nd**	2**E**	10 min	*n*-hexane	93	97.04	0	2.96	4.7	4.27	-64
18	**12Nd**	3**E**	10 min	*n*-hexane	87	97.09	0	2.91	7.1	6.48	-65

[a] Conditions: 20 µmol of precatalyst, 20 µmol of cocatalyst, 20 mmol of isoprene, 8 mL of solvent, 500 rpm stirring velocity. [b] Aged with cocatalyst at ambient temperature for 30 min: **A** = $[Ph_3C][B(C_6F_5)_4]$; **B** = $[PhNMe_2H][B(C_6F_5)_4]$; **C** = $B(C_6F_5)_3$; **D** = Me_2AlCl, **E** = Et_2AlCl, **F** = iBu_2AlCl, 1, 2, 3, or 4 equivalents. [c] Determined by $^1H/^{13}C$-NMR spectroscopy in $CDCl_3$. [d] Determined by SEC. [e] Determined by DSC. n.d. not determined due to low yield.

Table 4. Performance of complexes **12^{Ln}** (Ln = La, Nd, Pr, Gd) as precatalyst in isoprene polymerization.

entry	pre-catalyst	co-catalyst	reaction time [h]	solvent	yield [%]	*cis*-1,4[c] [%]	*trans*-1,4[c] [%]	3,4[c] [%]	M_n[d] [10^4 g·mol^{-1}]	PDI[d]	T_G[e] [°C]
19	**12Nd**	1**F**	1	*n*-hexane	16	97.58	0	2.42	3.4	7.99	-64
20	**12^{La}**	1**F**	2	toluene	5	92.64	3.90	3.46	1.1	4.00	-64.
21	**12^{La}**	2**F**	1	toluene	18	96.77	0	3.23	1.6	8.39	-63
22	**12^{Pr}**	1**F**	1	toluene	7	97.35	0	2.65	1.6	5.88	-64
23	**12^{Pr}**	2**F**	1	toluene	58	97.31	0	2.69	3.3	5.52	-63
24	**12Nd**	1**F**	1	toluene	22	97.73	0	2.27	2.0	4.68	-64
25	**12Nd**	2**F**	10 min	toluene	54	98.12	0	1.88	2.5	4.50	-63
26	**12Nd**	2**F**	30 min	toluene	> 99	97.59	0	2.41	5.2	3.35	-63
27	**12Nd**	3**F**	2	toluene	28	95.48	1.87	2.65	2.0	2.69	-64
28	**12^{Gd}**	1**F**	1	toluene	32	100	0	0	5.4	3.55	-63
29	**12^{Gd}**	2**F**	30 min	toluene	89	100	0	0	5.2	4.30	-63
30	**15**	none	10 min	1,2-difluoro-benzene	44	84.66	0	15.34	34.1	1.27	-58
31	**15**	none	30 min	toluene	17	82.21	0	17.79	46.9	1.12	-58
32	**15**	2 TIBA	30 min	toluene	23	84.56	0	15.44	14.9	1.49	-57
33[f]	**15**/**12Nd**	none	10 min	toluene	> 99	69.37	23.32	7.31	2.1	1.34	-64
34	**12Nd**	2B	10 min	toluene	> 99	83.37	8.13	8.50	2.9	1.38	-63
35	**12Nd**	2B	<1 min.	1,2-difluoro-benzene	> 99	92.40	0	7.60	12.7	2.00	-61

[a] Conditions: 20 µmol of precatalyst, 20 µmol of cocatalyst, 20 mmol of isoprene, 8 mL of solvent, 500 rpm stirring velocity. [b] Aged with cocatalyst at ambient temperature for 30 min: **A** = $[Ph_3C][B(C_6F_5)_4]$; **B** = $[PhNMe_2H][B(C_6F_5)_4]$; **C** = $B(C_6F_5)_3$; **D** = Me_2AlCl, **E** = Et_2AlCl, **F** = iBu_2AlCl, 1, 2, 3, or 4 equivalents. [c] Determined by $^1H/^{13}C$-NMR spectroscopy in $CDCl_3$. [d] Determined by SEC. [e] Determined by DSC. n.d. not determined due to low yield. [f]0.04 mmol Nd in total.

Mixed Heteroleptic Isobutylaluminato/chlorido Complexes of Redox-Inactive Rare-Earth Metals

Synthesis and structures

To elucidate whether early lanthanide chlorido-bridged isobutylaluminato complexes can be obtained for early lanthanide metals, the neodymium complex $[Nd\{N(SiMe_3)_2\}_2(\mu\text{-}Cl)(thf)]_2$ (**17Nd**) and the hitherto unknown complex $[La\{N(SiMe_3)_2\}_2(\mu\text{-}Cl)(thf)]_2$ (**17^{La}**) were synthesized (Scheme 23, Figure 10). $[Nd\{N(SiMe_3)_2\}_2(\mu\text{-}Cl)(thf)]_2$ (**17Nd**) was prepared from $NdCl_3(thf)_2$ and $Nd[N(SiMe_3)_2]_3$ following the slightly modified procedure reported by Berg and coworkers.[150] Similarly, we achieved the synthesis of $[La\{N(SiMe_3)_2\}_2(\mu\text{-}Cl)(thf)]_2$ (**17^{La}**) by heating a mixture of $La[N(SiMe_3)_2]_3$ (1.5 equiv.) with $LaCl_3(thf)$ in THF to 70 °C for several days, which led to quantitative formation of $[La\{N(SiMe_3)_2\}_2(\mu\text{-}Cl)(thf)]_2$ (**17^{La}**).[151] It is noteworthy that $[La\{N(SiMe_3)_2\}_2(\mu\text{-}Cl)(thf)]_2$ (**17^{La}**) displays the first diamagnetic compound of the type $[Ln\{N(SiMe_3)_2\}_2(\mu\text{-}Cl)(thf)]_2$ (**17^{Ln}**) for early lanthanides.

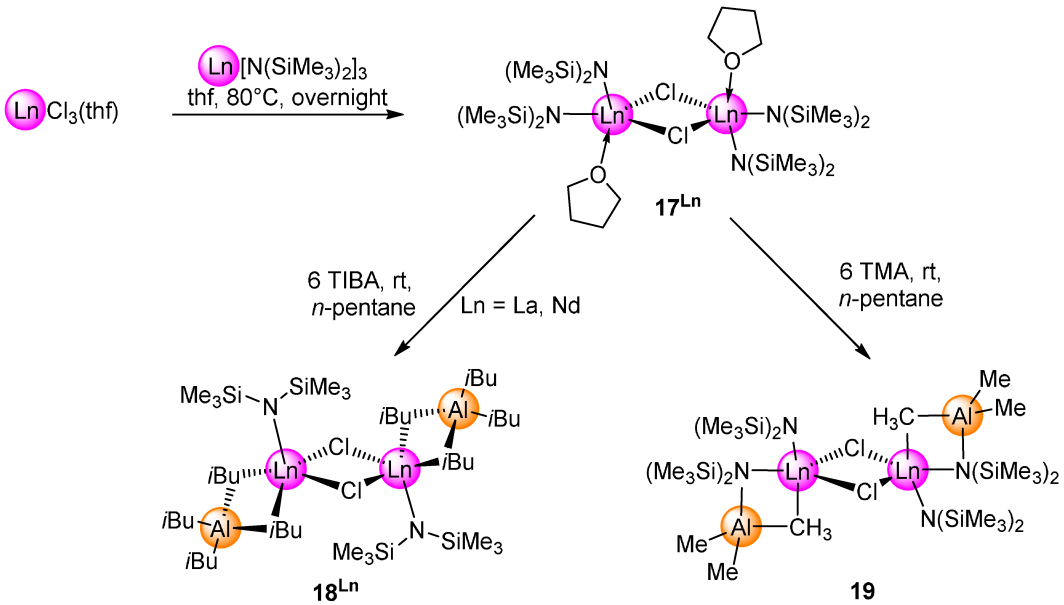

Scheme 23. Synthesis of $[Ln\{N(SiMe_3)_2\}_2(\mu\text{-}Cl)(thf)]_2$ (**17^{Ln}**) and products $[Ln\{N(SiMe_3)_2\}(AliBu_4)(\mu\text{-}Cl)]_2$ (**18^{Ln}**) $[La\{N(SiMe_3)_2\}\{(\mu\text{-}CH_3)(\mu\text{-}N(SiMe_3)_2)AlMe_2\}(\mu\text{-}Cl)]_2$ (**19**) obtained with triisobutylaluminum, and trimethylaluminum.

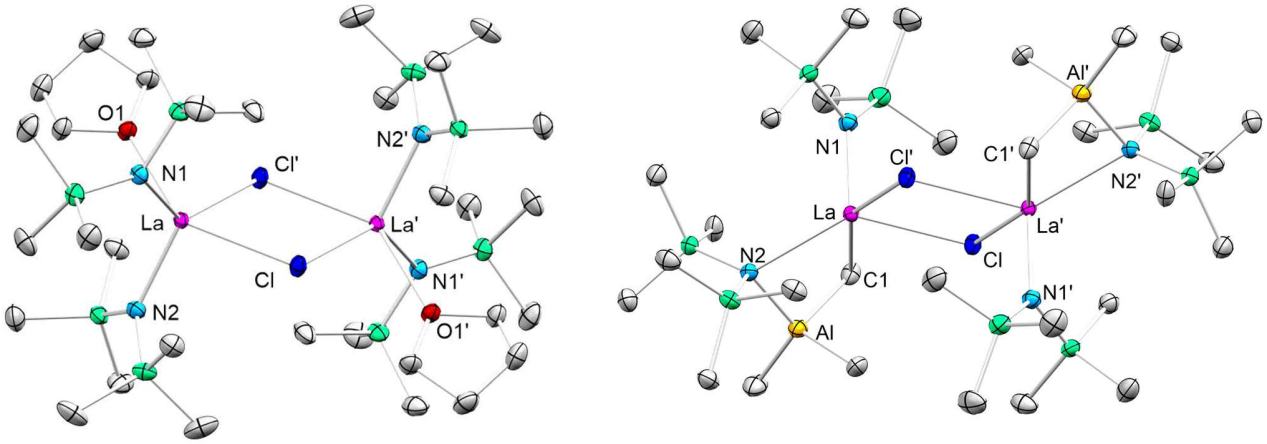

Figure 10. Crystal structures of complexes [La{N(SiMe$_3$)$_2$}$_2$(μ-Cl)(thf)]$_2$ (**17^{La}**), and [La{N(SiMe$_3$)$_2$}{(μ-CH$_3$)(μ-N(SiMe$_3$)$_2$)AlMe$_2$}(μ-Cl)]$_2$ (**19**). Hydrogen atoms are omitted for clarity. Atomic displacement ellipsoids were set at 50% probability.

Even though the synthesis of [Ln{N(SiMe$_3$)$_2$}$_2$(μ-Cl)(thf)]$_2$ (**17^{Ln}**) has been known for decades, these works initially involved smaller lanthanide metal sizes. Although the lanthanum congener is diamagnetic, it was not published so far. [La{N(SiMe$_3$)$_2$}$_2$(μ-Cl)(thf)]$_2$ (**17^{La}**) reacts with 6.5 equiv. TIBA to form [La{N(SiMe$_3$)$_2$}(Al*i*Bu$_4$)(μ-Cl)]$_2$ (**18^{La}**). With **17Nd** and TIBA, the isostructural complex [Nd{N(SiMe$_3$)$_2$}(Al*i*Bu$_4$)(μ-Cl)]$_2$ (**18Nd**) (Scheme 23, Figure 11) is obtained. Both complexes display a distorted η^3-coordination of the tetraisobutylaluminato ligand, with one Ln–C

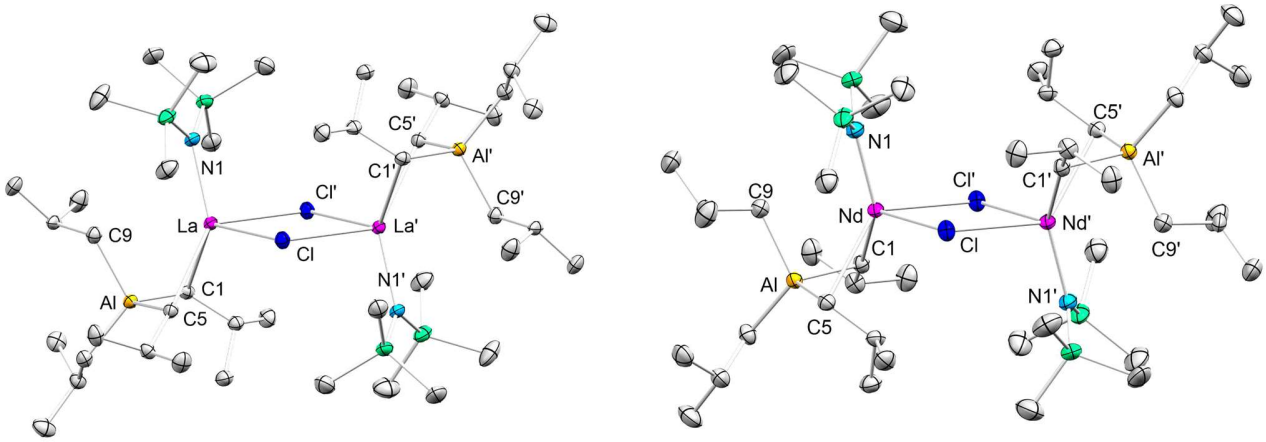

Figure 11. Crystal structures of [La(Al*i*Bu$_4$){N(SiMe$_3$)$_2$}(μ-Cl)]$_2$ (**18^{La}**), and [Nd(AliBu$_4$)[N(SiMe$_3$)$_2$](μ-Cl)]$_2$ (**18Nd**). Hydrogen atoms are omitted for clarity. Atomic displacement ellipsoids were set at 50% probability.

distance (Ln–C9) significantly elongated compared to the other two Ln–C bonds (i.e. 2.782(3), 2.809(2), and 3.132(3) Å for **18^{La}**). In contrast, the reaction of [La{N(SiMe$_3$)$_2$}$_2$(μ-Cl)(thf)]$_2$ (**17^{La}**) with 6 equiv. trimethylaluminum did not lead to the displacement of the silylamido ligands as observed with triisobutylaluminum. Most remarkably, we could isolate a crystal of [La{N(SiMe$_3$)$_2$}{(μ-CH$_3$)(μ-N(SiMe$_3$)$_2$)AlMe$_2$}(μ-Cl)]$_2$ (**19**) (Figure 10), featuring two Me$_3$Al–N(SiMe$_3$)$_2$ moieties. In contrast to TIBA, trimethylaluminum engaged with [La{N(SiMe$_3$)$_2$}$_2$(μ-Cl)(thf)]$_2$ (**17^{La}**) in the formation of an Lewis acid-base adduct, instead of displacing the silylamido ligand. The methyl homologue to [La{N(SiMe$_3$)$_2$}(Al*i*Bu$_4$)(μ-Cl)]$_2$ (**18^{La}**) could not be obtained. Compound [La{N(SiMe$_3$)$_2$}{(μ-CH$_3$)(μ-N(SiMe$_3$)$_2$)AlMe$_2$}(μ-Cl)]$_2$ (**19**) features a significant elongation of the two La–N distances in case of the TMA-silylamido moiety (2.677(2) Å), indicating weaker interactions due to a less basic silylamido ligand. In contrast, the other two La–N distances are much shorter with 2.285(2) Å, which could even indicate a strengthening of this bond. For selected interatomic distances, *cf.*

Table 5.

Similar silylamido-trimethylaluminum adducts have already been reported. For example, Andersen and Boncella reported the formation of Yb{N(SiMe$_3$)$_2$}$_2$(AlMe$_3$)$_2$ from donor-free ytterbium bis(trimethylsilyl)amide, and trimethylaluminum[152], whereas trimethylaluminum reacts with Mn{N(SiMe$_3$)$_2$}$_2$(thf) to form the methyl-bridged compound [{Mn(μ-Me){N(SiMe$_3$)$_2$AlMe$_3$}]$_2$].[153]

Table 5. Selected interatomic distances for the compounds **17^{La}**, **17Nd**, **18^{La}**, **18Nd**, **19** in Å. Interatomic distances of [Nd{N(SiMe$_3$)$_2$}$_2$(μ-Cl)(thf)]$_2$ (**17Nd**) are adapted from [150].

	17^{La}	**17Nd [150]**	**18^{La}**	**18Nd**	**19**
Ln–N	2.340(1)-2.379(1)	2.300(8)-2.335(8)	2.279(2)	2.220(1)	2.285(2) [N(SiMe$_3$)$_2$] 2.677(2) [N(SiMe$_3$)$_2$-AlMe$_3$]
Ln–O	2.566(1)	2.496(7)	-	-	-
Ln–C	-	-	2.782(3) 2.809(2) 3.132(3)	2.723(2) 2.746(2) 3.101(1)	2.769(3)
Ln–Cl	2.8531(4)-2.9031(5)	2.791(3)-2.854(3)	2.8397(6)-2.8514(6)	2.7804(5)-2.8000(5)	2.8513(8)-2.8631(7)
Ln···Al	-	-	3.0321(8)	2.9817(6)	3.144(1)

^{1}H-NMR spectroscopy of [La{N(SiMe$_3$)$_2$}(Al*i*Bu$_4$)(μ-Cl)]$_2$ (**18^{La}**) at 26°C revealed that a mixture of products was present, albeit **18^{La}** proved to be pure by elemental analysis. This indicated direct decomposition in deuterated benzene, leading to the formation of decomposition products identified as La[N(SiMe$_3$)$_2$](HAl*i*Bu$_3$)(Al*i*Bu$_4$) (**12^{La}**), La[N(SiMe$_3$)$_2$]$_3$, and isobutene by ^{1}H-NMR resonances (see Figure 12). This decomposition scenario possibly involves the formation $LaCl_3$. Since no precipitate of $LaCl_3$ was observed, this may indicate that $LaCl_2$[N(SiMe$_3$)$_2$] is formed, which is a possible explanation for the silylamido resonance observed at 0.33 ppm. Similar equilibrium phenomena are known for neodymium silylamido/chlorido complexes in solution observed by ^{1}H-NMR spectroscopy.[150, 154] The observed decomposition of [La(Al*i*Bu$_4$){N(SiMe$_3$)$_2$}(μ-Cl)]$_2$ (**18^{La}**) is little surprising, given the tendency of heteroleptic rare-earth metal complexes to undergo fast ligand redistribution, forming homoleptic complexes. In contrast, ^{1}H-NMR spectroscopy of [La(Al*i*Bu$_4$){N(SiMe$_3$)$_2$}(μ-Cl)]$_2$ (**18^{La}**) in deuterated toluene at – 50 °C revealed that the complex **18^{La}** is stable in solution at low temperatures (*cf*. Figure 13).

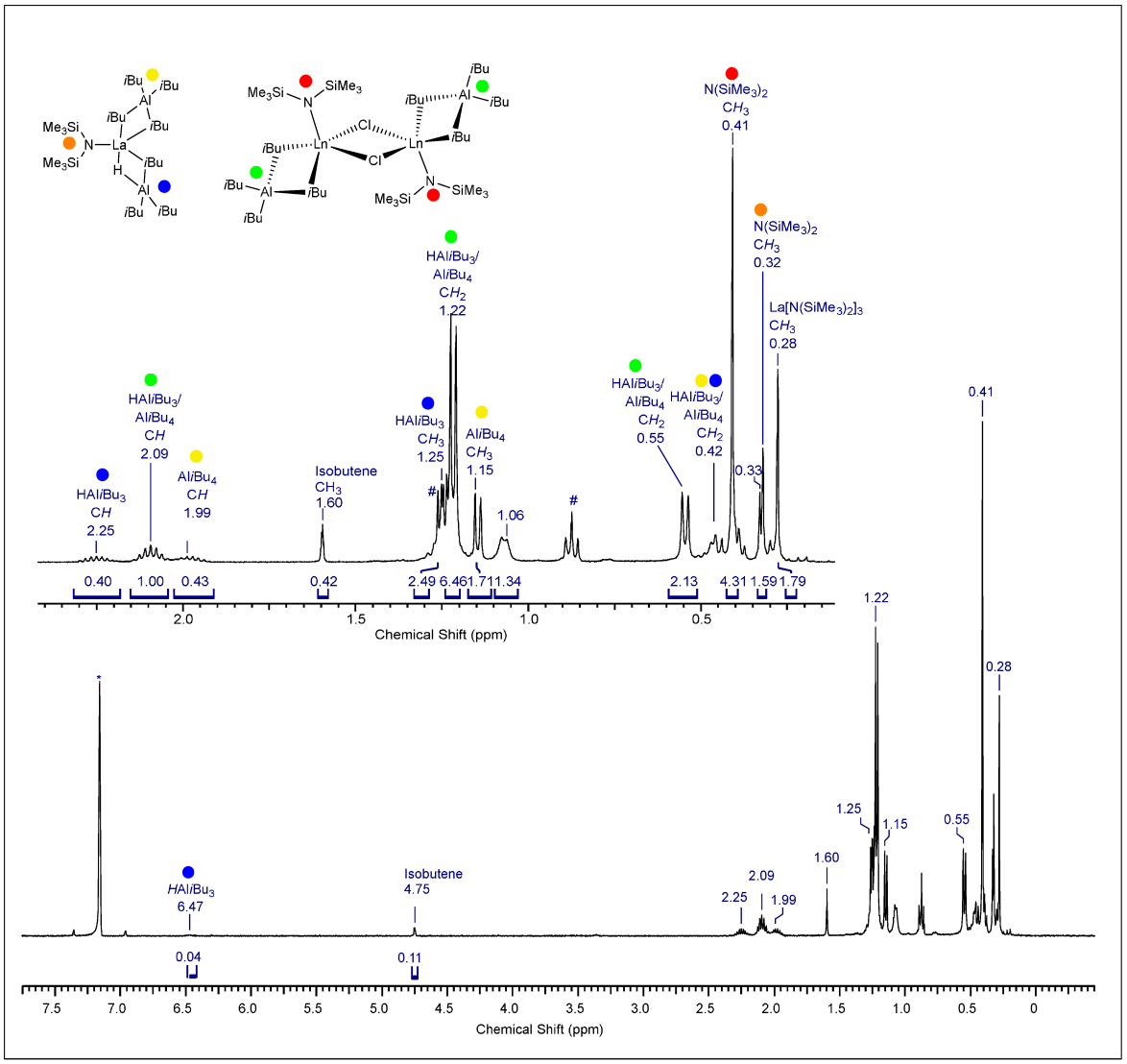

Figure 12. ^{1}H-NMR spectrum (25°C, 500 MHz) of [La(Al*i*Bu$_4$){N(SiMe$_3$)$_2$}(μ-Cl)]$_2$ (**18^{La}**) in deuterated benzene. Resonances assigned to the decomposition product La[N(SiMe$_3$)$_2$](HAl*i*Bu$_3$)(Al*i*Bu$_4$) (**12^{La}**), and [La(Al*i*Bu$_4$){N(SiMe$_3$)$_2$}(μ-Cl)]$_2$ (**18^{La}**) are labeled with colored dots. The signal of the solvent is marked with an asterisk, # denotes aliphatic alkane, resulting from the contamination of commercial C_6D_6.

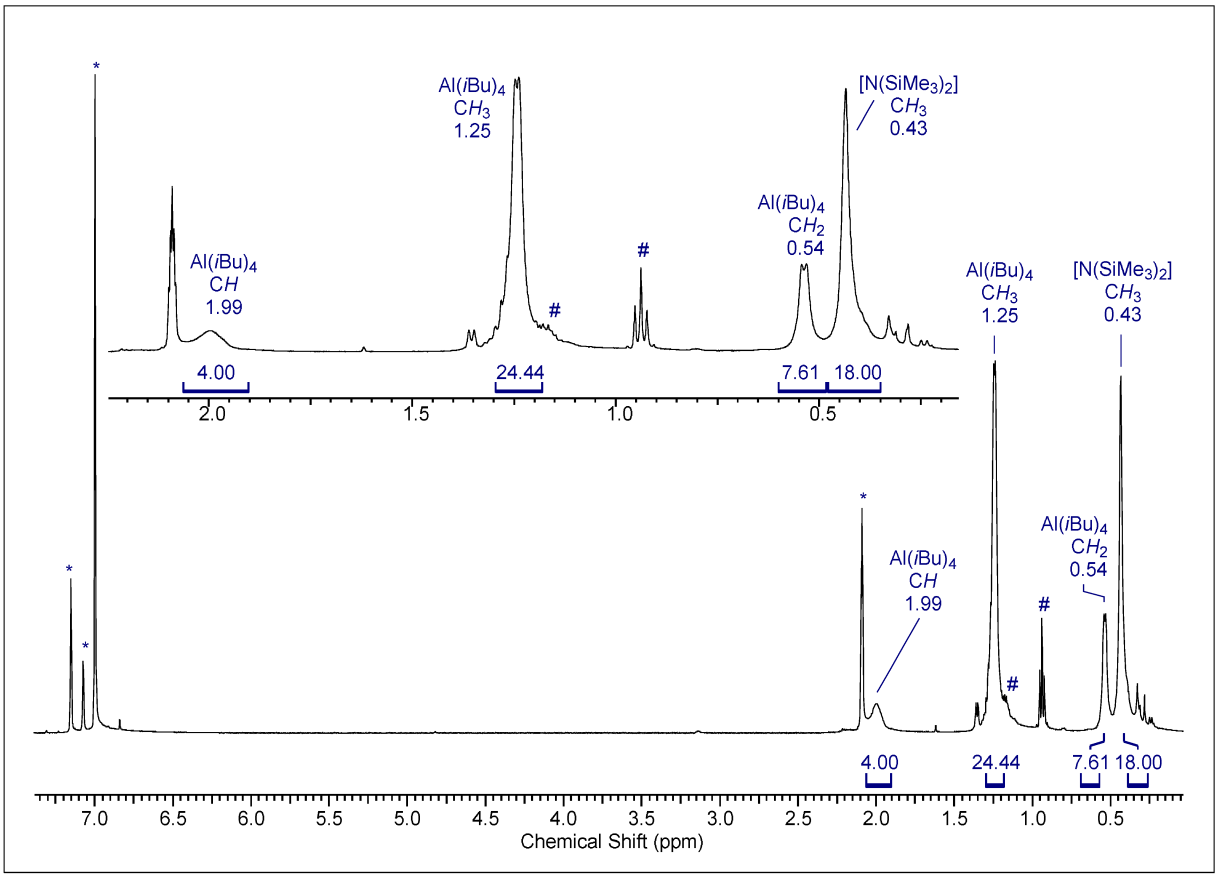

Figure 13. Low-temperature ^{1}H-NMR spectrum (-50 °C, 500 MHz) of [La(Al*i*Bu$_4$){N(SiMe$_3$)$_2$}(μ-Cl)]$_2$ (**18^{La}**) in deuterated toluene. The signal of the solvent is marked with an asterisk, # denotes aliphatic alkane, resulting from the contamination of commercial toluene-d_8.

Polymerization with [Nd{N(SiMe$_3$)$_2$}(Al*i*Bu$_4$)(μ-Cl)]$_2$

Compound [Nd{N(SiMe$_3$)$_2$}(Al*i*Bu$_4$)(μ-Cl)]$_2$ (**18Nd**) was found to polymerize isoprene as a single-component catalyst without the necessity of additional cocatalyst, and/or organoaluminum species (*cf.* entry 1). Data of polymers obtained using precatalyst [Nd{N(SiMe$_3$)$_2$}(Al*i*Bu$_4$)(μ-Cl)]$_2$ (**18Nd**) are shown in Table 6. As with neodymium tetramethylaluminate/organoaluminum chloride cocatalysts, high *cis*-1,4-selective polymerization was observed. The addition of additional chloride source proved pivotal for the overall polymerization activity. Interestingly, addition of 0.5, or 1 equivalent [Cl]/[Nd] in the form of aluminum trichloride decreased polymerization

activity to almost zero (entries 2-3), whereas addition of 1 equivalent [Cl]/[Nd] in the form of trimethylsilyl chloride did not affect the overall yield considerably (entry 4). In stark contrast, addition of one equivalent [Cl]/[Nd] in the form of diisobutylaluminum chloride increased the yield to 69% (entry 5; compared to 24% without addition of diisobutylaluminum chloride in entry 1). These findings are consistent with the results of [Nd{N(SiMe$_3$)$_2$}(Al*i*Bu$_4$)(HAl*i*Bu$_3$)] activated with dialkylaluminum chloride systems, showing highest activities in with 2-3 [Cl]/[Nd]. Similar findings have been reported for neodymium-catalyzed polymerization with the ill-defined mixture [Nd{N(SiMe$_3$)$_2$}$_3$]/x Et$_2$AlCl/40 Al*i*Bu$_3$ showing a maximum activity for x = 2-2.5 in heptane.[143] Although this polymerization was conducted at 70 °C, it is notable that a 93.1 *cis*/6.0 *trans*/0.9% 1,2 microstructure was observed in toluene (15 min, 38% conversion), whereas [Nd{N(SiMe$_3$)$_2$}(Al*i*Bu$_4$)(μ-Cl)]$_2$ (**18Nd**) delivers essentially *trans*-free polyisoprene. Generally, addition of two equivalents triisobutylaluminum enhance the polymerization activity of [Nd{N(SiMe$_3$)$_2$}(Al*i*Bu$_4$)(μ-Cl)]$_2$ (**18Nd**), to 31% vs. 24% without triisobutylaluminum (*cf*. entries 1, and 6). The addition of two equivalents triisobutylaluminum also increased the yield of [Nd{N(SiMe$_3$)$_2$}(Al*i*Bu$_4$)(μ-Cl)]$_2$ (**18Nd**)/2 equiv. *i*Bu$_2$AlCl (1 equiv. [Cl]/[Nd]) from 69 to 79% (*cf*. entries 5, and 7). This may suggest that further replacement of the remaining silylamido ligand still enhances the overall polymerization activity.

Table 6. Isoprene polymerization using [Nd{N(SiMe$_3$)$_2$}(Al*i*Bu$_4$)(μ-Cl)]$_2$ (**18Nd**) as precatalyst

entry[a]	pre-catalyst	co-catalyst[b]	yield [%]	*cis*-1,4[c] [%]	*trans*-1,4[c] [%]	3,4[c] [%]	M_n[d] [10^4 g·mol^{-1}]	PDI[d]	T_G[e] [°C]
1	**18Nd**	none	24	98.0	0	2.0	3.2	3.69	-66
2	**18Nd**	$AlCl_3$ (6.67 µmol) = 0.5 [Cl]/[Nd]	12	98.3	0	1.7	7.4	3.59	-65
3*	**18Nd**	$AlCl_3$ (12.0 µmol) = 1[Cl]/[Nd]	4	98.0	0	2.0	0.5	4.79	-65
4	**18Nd**	1 equiv. Me_3SiCl	21	97.9	0	2.1	2.6	4.67	-66
5	**18Nd**	1 **F**	69	98.0	0	2.0	19.2	1.57	-65
6	**18Nd**	2 TIBA	31	98.0	0	2.0	2.1	4.36	-67
7	**18Nd**	1**F**/2TIBA	79	98.0	0	2.0	11.3	2.04	-64

[a] Conditions: 20 µmol of precatalyst, 20 µmol of cocatalyst, 20 mmol of isoprene, 8 mL of toluene, 500 rpm stirring velocity. [b] Aged with cocatalyst at ambient temperature for 30 min: **F** = *i*Bu$_2$AlCl, equivalents are given as [Cl]/[Nd], one hour reaction time. [c] Determined by ^{1}H, ^{13}C NMR in $CDCl_3$. [d] Determined by SEC. [e] Determined by DSC.

Potassium Isobutylaluminate Side Product

In cases of contamination of silylamido precursors with low amounts of ate complex, or K[N(SiMe$_3$)$_2$], we noticed that after the reaction with TIBA fine, colorless needles crystallized prior to the main product [La{N(SiMe$_3$)$_2$}(Al*i*Bu$_4$)(μ-Cl)]$_2$ (**18^{La}**) upon cooling to –40 °C. The side product was identified as potassium isobutylaluminate [K(*i*Bu$_3$Al-μ-H-Al*i*Bu$_3$)]$_n$ (**20**) by X-ray diffraction analysis (see Figure 14), and elemental analysis (calc. C 66.00, H 12.69; obs. C 65.81, H 12.55, N 0.00). In the solid state, the compound exhibits a polymeric structure, with CH$_2$-moieties of the isobutyl groups bridging to potassium ions. ^{1}H-NMR spectroscopy revealed the hydride resonance at 2.55 ppm, alongside with one set of isobutyl resonances.

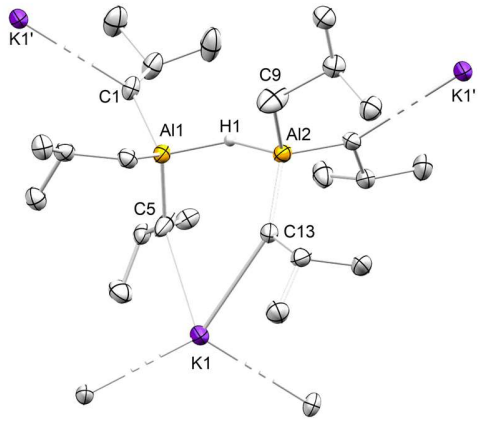

Figure 14. Connectivity of polymeric [K(*i*Bu$_3$Al-μ-H-Al*i*Bu$_3$)]$_n$ (**20**). Hydrogen atoms are omitted for clarity. Atomic displacement ellipsoids were set at 50% probability.

C.

Unpublished

Results

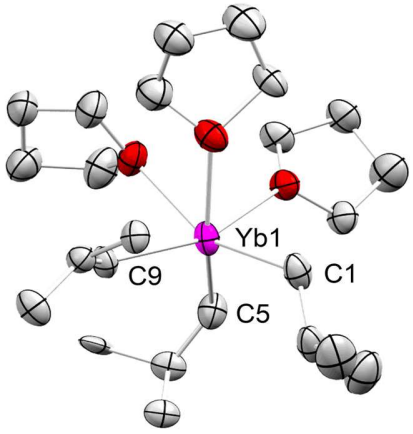

C. Unpublished Results

Synthesis of Trivalent Lanthanide Isobutyl Complexes

Tris(isobutyl)ytterbium Tetrahydrofuran Solvate

A possible pathway to trivalent tetraisobutylaluminates could involve the reaction of a triisobutyl lanthanide complex, and triisobutylaluminum. To date, according to the Cambridge Crystallographic Data Centre, no triisobutyl lanthanide compound of the form Ln(*i*Bu)$_3$(do)$_x$, or Ln(*i*Bu)$_3$ (Ln = Sc, Y, La-Lu) was reported. However, M. Niemeyer reported a procedure for the synthesis of the neopentyl complex Yb(CH$_2$*t*Bu)$_3$-THF solvate.[155] According to this procedure, trivalent tris(neopentyl) ytterbium was synthesized from the equimolar mixture of elemental ytterbium, and the corresponding alkyl iodide in THF, forming divalent ytterbium iodide as a side product.[155] However, an ytterbium(III) alkyl complex featuring a β-hydride was not yet reported following this protocol to the best of our knowledge. For this reason, we were curious whether discrete trivalent lanthanide isobutyl complexes can be synthesized.

Following Niemeyer's procedure, the reaction of ytterbium metal flakes with isobutyl iodide at –40 °C in tetrahydrofuran yielded a dark red, crystalline solid, which rapidly decomposed at ambient temperature, as indicated by a color change from dark red to brown. We managed to identify the very temperature-sensitive dark-red product, as Yb(*i*Bu)$_3$(thf)$_3$ (**21**) by X-ray diffraction (Figure 15).

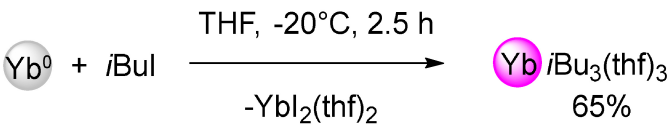

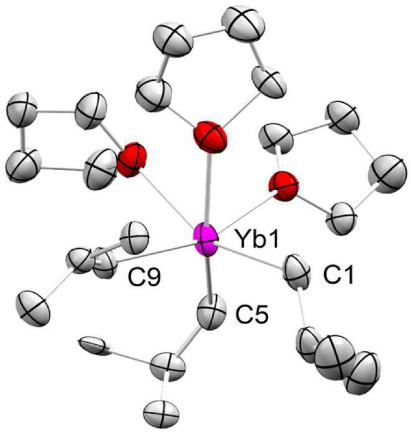

Figure 15. Synthesis and crystal structure of of Yb(*i*Bu$_3$)(thf)$_3$ (**21**) from ytterbium metal and isobutyl iodide. Atomic displacement parameters are set at 50% probability level. Hydrogen atoms are omitted for clarity.

We also sought to apply this protocol to synthesize other rare-earth-metal isobutyl complexes as novel precursors for isobutylaluminate chemistry. However, due to the much lower reactivity of other metals, e.g. neodymium powder, compared to ytterbium metal flakes, this reaction was not yet successful. Therefore, we did not exploit this promising synthetic route further.

Approaches to Alkaline Earth Tetraisobutylaluminates

Diisobutylmagnesium Dioxanate and TIBA-Dioxane Adduct

For the synthesis of a putative magnesium aluminate "Mg(Al*i*Bu$_4$)$_2$", we sought to gain access through a diisobutyl magnesium solvate. In contrast to the heavier alkaline-earth homologues, dialkylmagnesium congeners can be readily obtained from Grignard reagents *via* the Schlenk-equilibrium.[156] Following this protocol, polymeric [Mg*i*Bu$_2$(dioxane)]$_n$ (**22**, *cf.* Scheme 24) was synthesized from isobutylmagnesium bromide by addition of dioxane to the ethereal solution. However, upon treatment of [Mg*i*Bu$_2$(dioxane)]$_n$ (**22**) with TIBA, the sought-after magnesium isobutylaluminate escaped isolation and purification, due to the formation of large amounts of almost inseparable colorless crystals of the dioxane adduct [(Al*i*Bu$_3$)$_2$(dioxane)] (**23**), as identified by X-ray diffraction.

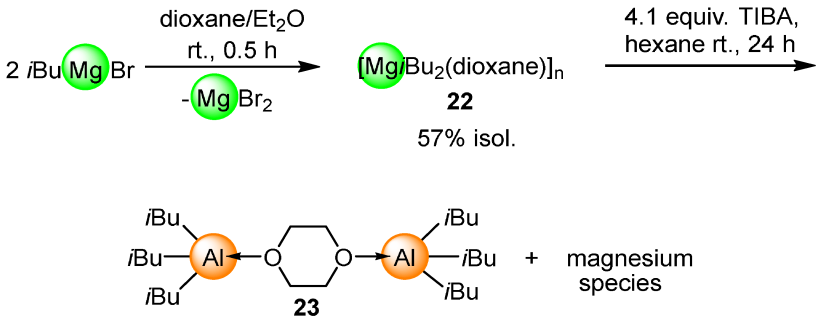

Scheme 24. Synthesis of [Mg*i*Bu$_2$(dioxane)]$_n$ (**22**), and reaction with TIBA.

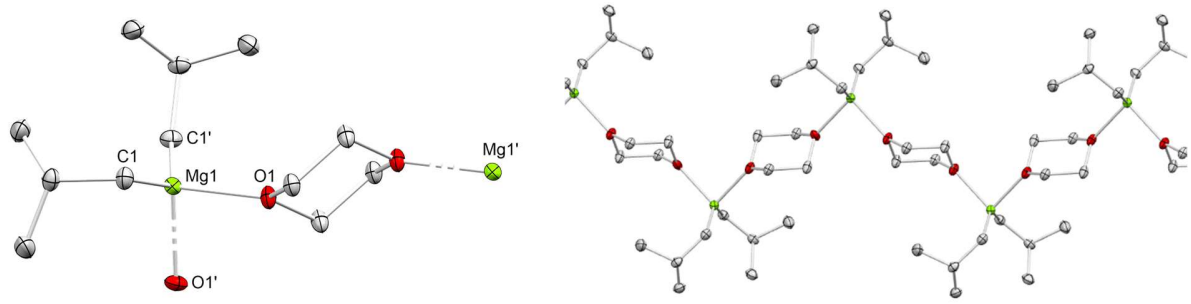

Figure 16. Segment of the polymeric crystal structure, and coordination polymer of $[Mg(i)Bu_2(dioxane)]_n$ (**22**). Atomic displacement parameters are set at 50% probability level. Hydrogen atoms are omitted for clarity.

Alkaline-Earth Metal Tetraisobutylaluminate Complexes

To examine whether the size of the central metal ion influences the coordination number, or the six-fold coordination is maintained with smaller ions, we set out to prepare alkaline-earth (Ae) isobutylaluminates. It needs to be noted that divalent lanthanide compounds of Sm, Eu, and Yb feature many similarities with the alkaline-earth analogues as indicated in Table 7, especially for the pairs Ca(II)-Yb(II), and Sr(II)-Sm(II)/Eu(II), which can be explained by negligible metal-ligand orbital interactions, almost same radii, and thus similar, and mainly ionic interactions. [157] [158] [159]

Table 7. Ionic radii for selected divalent lanthanide, and alkaline-earth ions for coordination number of 6.[160] [161] Table adapted from [157]

Metal	ionic radius [Å] (CN = 6)
Mg^{2+}	0.72
Ca^{2+}	1.00
Sr^{2+}	1.18
Ba^{2+}	1.35
Sm^{2+}	1.15
Eu^{2+}	1.14
Yb^{2+}	1.03

Following the protocol established for the synthesis of Ln(Al*i*Bu$_4$)$_2$ (**1**$^{\mathbf{Ln}}$, Ln = Sm, Eu, Yb), starting from divalent bis(trimethylsilylamido) alkaline-earth metal precursors, silylamide elimination led to the formation of bis η^3-coordinated, molecular homoleptic tetraisobutylaluminate complexes (see Scheme 25). For calcium, and strontium, excellent yields were obtained, e. g. Sr(Al*i*Bu$_4$)$_2$ (**24**$^{\mathbf{Sr}}$) was obtained in the form of a white powder in 84% crystalline yield after recrystallization. However, in case of the barium congener, the synthesis of the silylamide precursor Ba[N(SiMe$_3$)$_2$]$_2$(thf)$_2$ *via* salt metathesis from barium iodide, and potassium bis(trimethylsilylamide), resulted in inevitable formation of the "ate" complex, as shown by both elemental analyses and ICP-OES, and separation of Ba(Al*i*Bu$_4$)$_2$ (**24**$^{\mathbf{Ba}}$) from potassium isobutylaluminate was possible by fractional crystallization. Just as observed for Yb(Al*i*Bu$_4$)$_2$ (**1**$^{\mathbf{Yb}}$) which has been published over twenty years ago,[123] Ca(Al*i*Bu$_4$)$_2$ (**24**$^{\mathbf{Ca}}$) proved to be very challenging to analyze by X-ray diffraction analysis, resembling the problems observed with isostructural Yb(Al*i*Bu$_4$)$_2$ (**1**$^{\mathbf{Yb}}$), that features a similar cation size.[123]

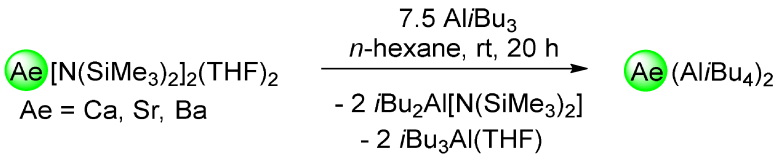

Scheme 25. Synthesis of divalent alkaline-earth-metal tetraisobutylaluminates.

As reported by Harder *et al.*, samarium(II) and strontium(II) complexes are isomorphous due to almost identic ionic radii, and exhibit striking similarities in terms of cell constants, and bonding situations, as does the pair Ca/Yb.[159] In fact, X-ray crystallography revealed that all divalent tetraisobutylaluminates displayed the η^3-coordination of the tetraisobutylaluminate anions in the solid state as observed for corresponding lanthanide congeners such as Sm(Al*i*Bu$_4$)$_2$ (**1**$^{\mathbf{Sm}}$). The diamagnetic alkaline-earth-metal isobutylaluminates allow a conclusive NMR analysis; in the case of Ca(Al*i*Bu$_4$)$_2$ (**24**$^{\mathbf{Ca}}$), only one signal set for the isobutyl protons was observed, and no decoalescence of the isobutyl resonances occured in the accessible temperature range (down to 190 K) just as observed for comparable **1**$^{\mathbf{Yb}}$. This indicates that isobutylaluminate moieties display a high mobility, indicating a highly fluxional behavior of the aluminates in solution even at low temperature. Despite the long known and structurally characterized homoleptic magnesium tetramethylaluminate[162], as well as calcium, strontium, and barium bis(tetraethylaluminate)[163], alkaline-earth-metal isobutylaluminates have escaped characterization, and identification so far.

Neither Ca(Al*i*Bu$_4$)$_2$ (**24^{Ca}**) nor Sr(Al*i*Bu$_4$)$_2$ (**24^{Sr}**) were found to be of comparable activity as the lanthanide congeners in isoprene polymerization. Although the cause for the inactivity remains unclear, and no obvious correlation of redox potential, and polymerization activity was observed in the case of the corresponding lanthanide congeners, the formation of more stable allyl complexes could prevent polymerization for alkaline-earth metal complexes. A possible explanation may be the initiation *via* an allylic compound, that may be more stable than its lanthanide counterparts, making it a thermodynamic sink. Analogously, other divalent alkaline-earth-metal tetraisobutylaluminates were generated on this occasion as shown in Figure 12. All complexes share the η^3-coordination mode observed with [Ln(Al*i*Bu$_4$)$_2$] (**1^{Ln}**) and display bond lengths as shown in Table 8.

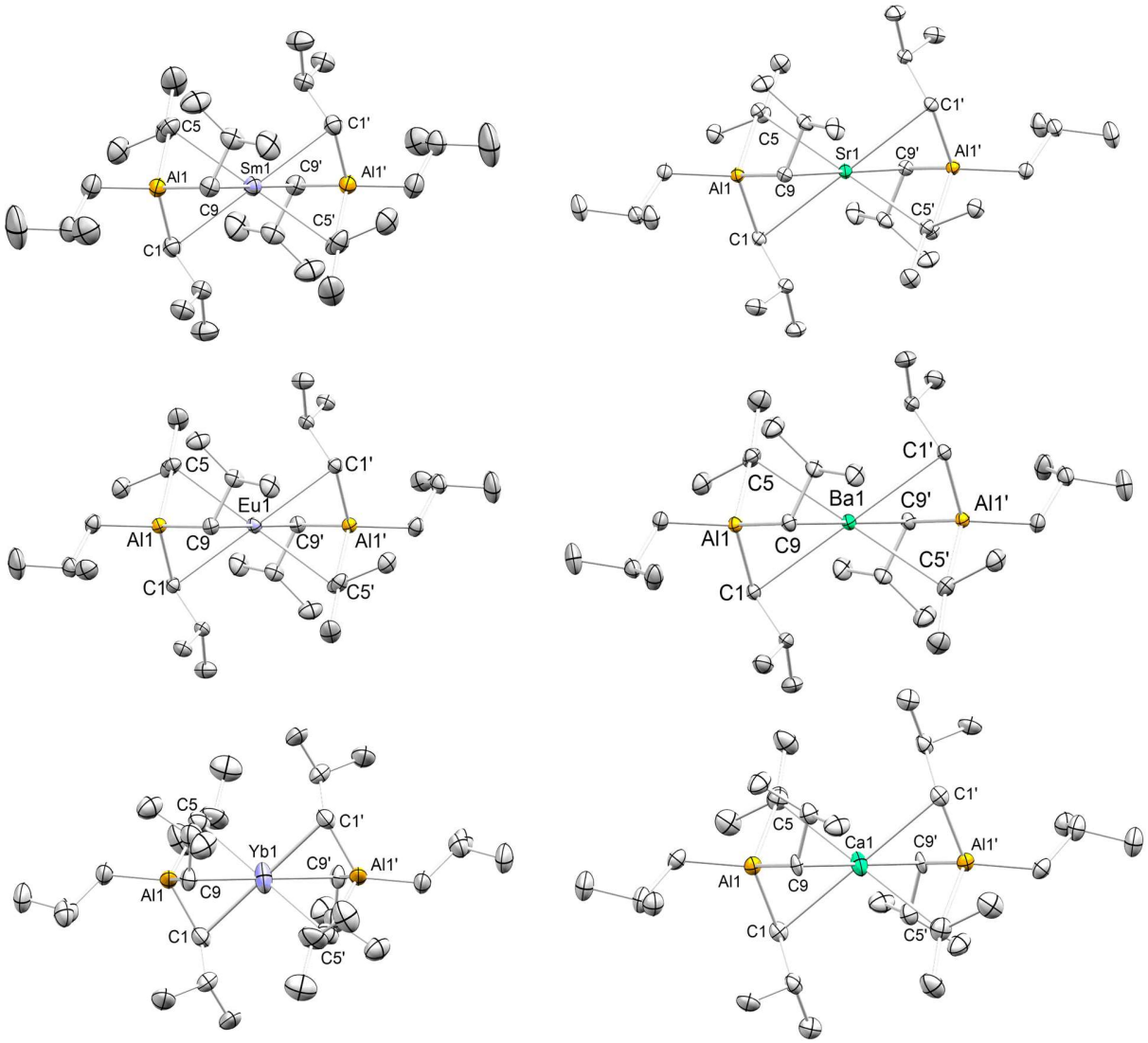

Figure 17. Crystal structures of [Sm(Al*i*Bu$_4$)$_2$] (**1**^{Sm}), [Eu(Al*i*Bu$_4$)$_2$] (**1**^{Eu}), [Yb(Al*i*Bu$_4$)$_2$] (**1**^{Yb}), [Ca(Al*i*Bu$_4$)$_2$] (**24**^{Ca}), [Sr(Al*i*Bu$_4$)$_2$] (**24**^{Sr}), and [Ba(Al*i*Bu$_4$)$_2$] (**24**^{Ba}). For [Ca(Al*i*Bu$_4$)$_2$] (**24**^{Ca}), only a connectivity was obtained. Atomic displacement parameters are set at 50 % probability level. Hydrogen atoms are omitted for clarity.

Table 8. Selected interatomic distances for the compounds **24**^{Ca}, **24**^{Sr}, **24**^{Ba}, **1**^{Sm}, **1**^{Eu}, and **1**^{Yb} in Å.

	24^{Ca}*	**24**^{Sr}	**24**^{Ba}	**1**^{Sm}	**1**^{Eu}	**1**^{Yb}
M–C	2.707-2.760*	2.8986(12)-3.2545(12)	2.9959(17)-3.3893(18)	2.8514(18)-2.8854(18)	2.850(2)-2.878(2)	2.735(16)-2.796(12)

*[Ca(Al*i*Bu$_4$)$_2$] (**24**^{Ca}): connectivity only.

Redox Chemistry Involving Samarium Silylamides, and Organoaluminum Reagents

Since divalent $Sm[N(SiMe_3)_2]_2(thf)_2$ proved a valuable precursor for the synthesis of $Sm(Al\textit{i}Bu_4)_2$ (**1**^{Sm}), we were curious whether the corresponding trivalent congeners could exhibit a similar reactivity. Since an attempt to generate a half-sandwich isobutylaluminate complex by oxidation of $Sm(Al\textit{i}Bu_4)_2$ with Cp^*_2Pb led to $Cp^*_2Sm(Al\textit{i}Bu_4)$, we employed $Cp^*Sm[N(SiMe_3)_2]_2$ which was synthesized according to literature.[124] The reaction with TIBA yielded red crystals of the heteroleptic complex $[Cp^*Sm\{N(SiMe_3)_2\}(Al\textit{i}Bu_4)]$ (**25**), featuring a distorted η^3-coordination of the $[Al\textit{i}Bu_4]$-Ligand as depicted in Figure 14. However, all attempts to isolate complex **25** failed due to the challenging purification by repeated crystallization, especially since the isobutylaluminum sideproduct mixture greatly hampered crystallization. Elemental analysis confirmed that the desired product was not obtained in pure form. In general, heteroleptic lanthanide complexes are challenging to obtain, due to ligand scrambling scenarios. In this case, the formation of heteroleptic complex **25** may indicate that the steric demand of the pentamethylcyclopentadienyl, and the bis(trimethylsilyl)amido ligands are affecting the outcome of the reaction. However, it is likely that the remaining amido ligand may be replaced as well, possibly explaining why $[Cp^*Sm\{N(SiMe_3)_2\}(Al\textit{i}Bu_4)]$ (**25**) was not obtained in pure form according to elemental analyses.

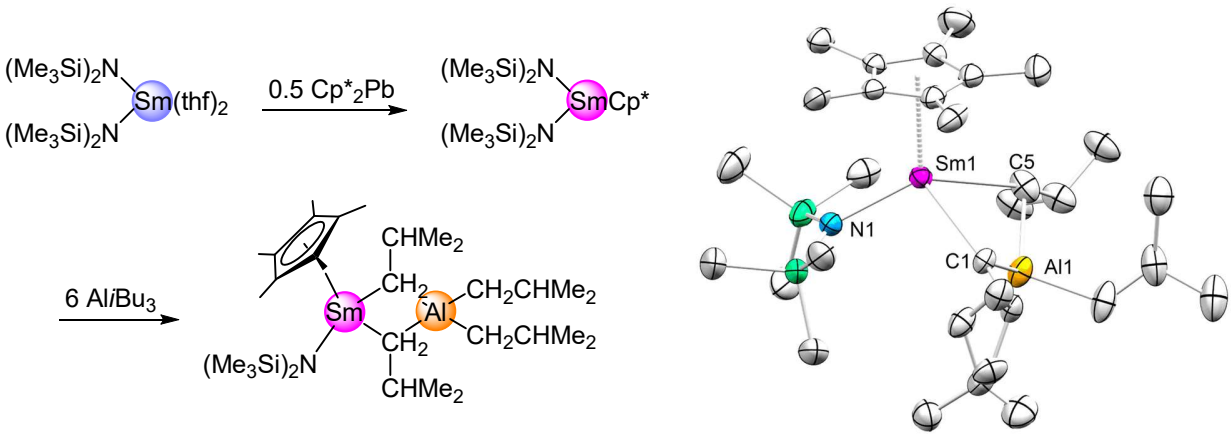

Figure 18. Synthesis and crystal structure of $[Cp^*Sm\{N(SiMe_3)_2\}(Al\textit{i}Bu_4)]$ (**25**). Atomic displacement parameters are set at 50 % probability level. Hydrogen atoms are omitted for clarity. Selected interatomic distances [Å]: Sm–N 2.261(4), Sm–C(1) 2.628(4), Sm–C(5) 2.807(5) and Sm–C(9) 3.797(5).

Reaction of $Sm[N(SiMe_3)_2]_3$ with Trialkyl Aluminum Compounds

Due to the formation of trivalent [Cp*Sm{N(SiMe$_3$)$_2$}(Al*i*Bu$_4$)] (**25**), we were curious whether other trivalent samarium isobutylaluminates would be accessible following the same silylamide elimination protocol. Starting from $Sm[N(SiMe_3)_2]_3$, the reaction with 7.5 equiv. TIBA in a J. Young tube was monitored by ^{1}H-NMR spectroscopy. The initially yellowish solution adopted a brownish color after one hour, which turned to a dark violet color after 12 h, indicating the reduction to a divalent species. In fact, ^{1}H-NMR spectroscopy revealed the formation of complex $Sm(Al\textit{i}Bu_4)_2$ (**1^{Sm}**) as main product, alongside with isobutene (*cf.* Figure 20). In contrast to the reaction of $Sm[N(SiMe_3)_2]_3$ with triisobutylaluminum, we did not observe a color change when applying $Sm[N(SiMe_3)_2]_3$ and trimethylaluminum. The dark yellow solution formed with trimethylaluminum in a J. Young tube maintained its color for several weeks at ambient temperature, without a sign of reduction. Several products are observed upon reaction of $Sm[N(SiMe_3)_2]_3$ with TMA, including $Me_2Al[N(SiMe_3)_2]$, and $Sm(AlMe_4)_3$ according to the shift given in literature (observed shift: -3.08 ppm, C*H*$_3$, see Figure 21; literature shift -3.06 ppm [74]). From the reaction mixture, we managed to isolate crystals that were identified as $Sm[N(SiMe_3)_2](AlMe_4)_2$ (**26**) by X-ray crystallography, which likely is a reaction intermediate (*cf.* Figure 19, Scheme 26). This reactivity underlines a reductive pressure of the bulky isobutyl moieties on the lanthanide center, and in case of samarium, a sterically induced reduction can be assumed, as it is for several cases in literature.[164]

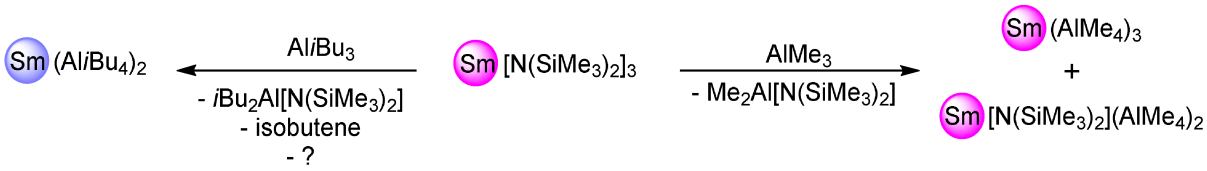

Scheme 26. Reactivity of $Sm[N(SiMe_3)_2]_3$ towards triisobutylaluminum, and trimethylaluminum.

It is noteworthy that in case of the $Sm[N(SiMe_3)_2]_3$/TIBA mixture, the reduction to the divalent samarium species $Sm(Al\textit{i}Bu_4)_2$ took place, which was not observed with [Cp*Sm{N(SiMe$_3$)$_2$}(Al*i*Bu$_4$)] (**25**). As described by Evans, the synthesis of $Cp^*_2Sm(Al\textit{i}Bu_4)$ from Cp^*_2Sm with TIBA leads to the oxidation of a divalent to the trivalent samarium species, with elemental aluminum formed. It is remarkable that both oxidation, and reduction are feasible with

similar complexes, dependent on the presence of sterically demanding pentamethylcyclopentadienide ligands.

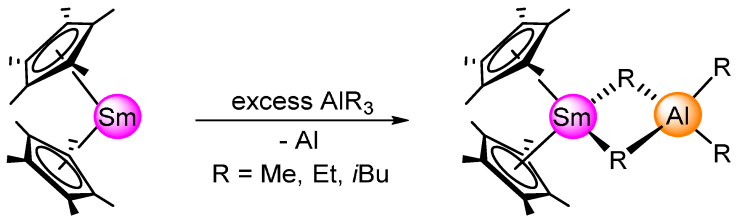

Scheme 27. Evans' synthesis of [Cp*$_2$Sm(AlR$_4$)] (R = Me, Et, *i*Bu) by oxidative addition of decamethylsamarocene with trialkylaluminum reagent.[12]

This reactivity entirely disproves the claim that complexes Ln[N(SiMe$_3$)$_2$]$_3$ do not react with organoaluminum reagents. In previous works, it is falsely claimed that trivalent silylamide complexes Ln[N(SiMe$_3$)$_2$]$_3$, in contrast to divalent silylamide compounds, do not react with alkylating agents, especially trimethylaluminum, even in large excess. It is reported that Ln[N(SiMe$_3$)$_2$]$_3$ can even be "recovered" from reaction mixtures with TMA, and it is concluded that this is caused by the "sterical inaccessibility" caused by the bulky silylamido ligands, thus entirely shielding the central ion, and prohibiting an attack on the basic amido ligand by the Lewis acidic organoaluminum reagent.[61] This statement is little convincing, given numerous donor adducts of complexes Ln[N(SiMe$_3$)$_2$]$_3$, of which many are characterized in the solid state. In the context of this work, we obtained trivalent samarium tetramethylaluminato complexes from Sm[N(SiMe$_3$)$_2$]$_3$, whereas reaction of Nd[N(SiMe$_3$)$_2$]$_3$ with TMA led to crystallization of Nd(AlMe$_4$)$_3$ x Al$_2$Me$_6$ as identified by X-ray diffraction.

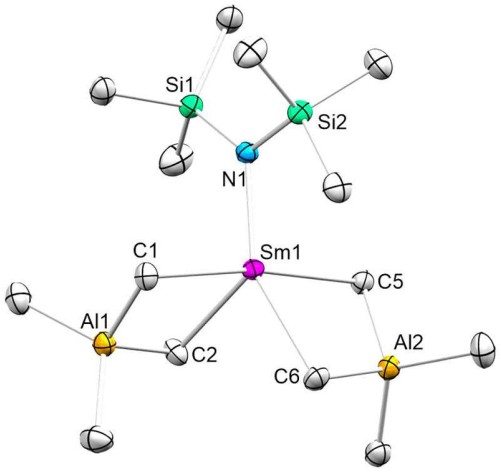

Figure 19. Crystal structure of $Sm[N(SiMe_3)_2](AlMe_4)_2$ (**26**). Hydrogen atoms are omitted for clarity. Atomic displacement ellipsoids were set at 50% probability. Selected interatomic distances [Å] and angles [°]: C(1)-Sm(1) 2.589(4), C(2)-Sm(1) 2.566(4), C(5)-Sm(1) 2.610(4), C(6)-Sm(1) 2.647(3), N(1)-Sm(1) 2.211(3).

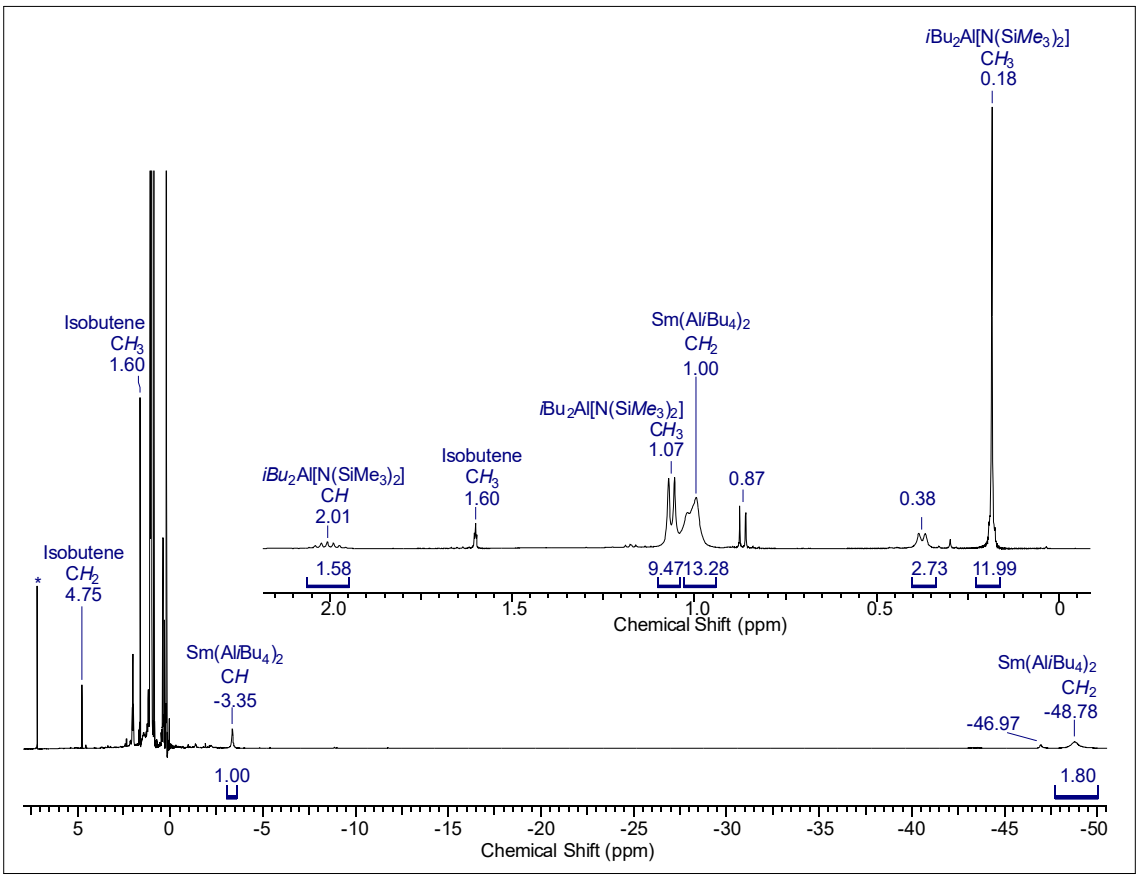

Figure 20. ^{1}H-NMR spectrum (400 MHz, C_6D_6, 25 °C) of the reaction of $Sm[N(SiMe_3)_2]_3$ with 7.5 equivalents of triisobutylaluminum after 48 h reaction time, proving reduction to $[Sm(Al\textit{i}Bu_4)_2]$ (**1^{Sm}**).

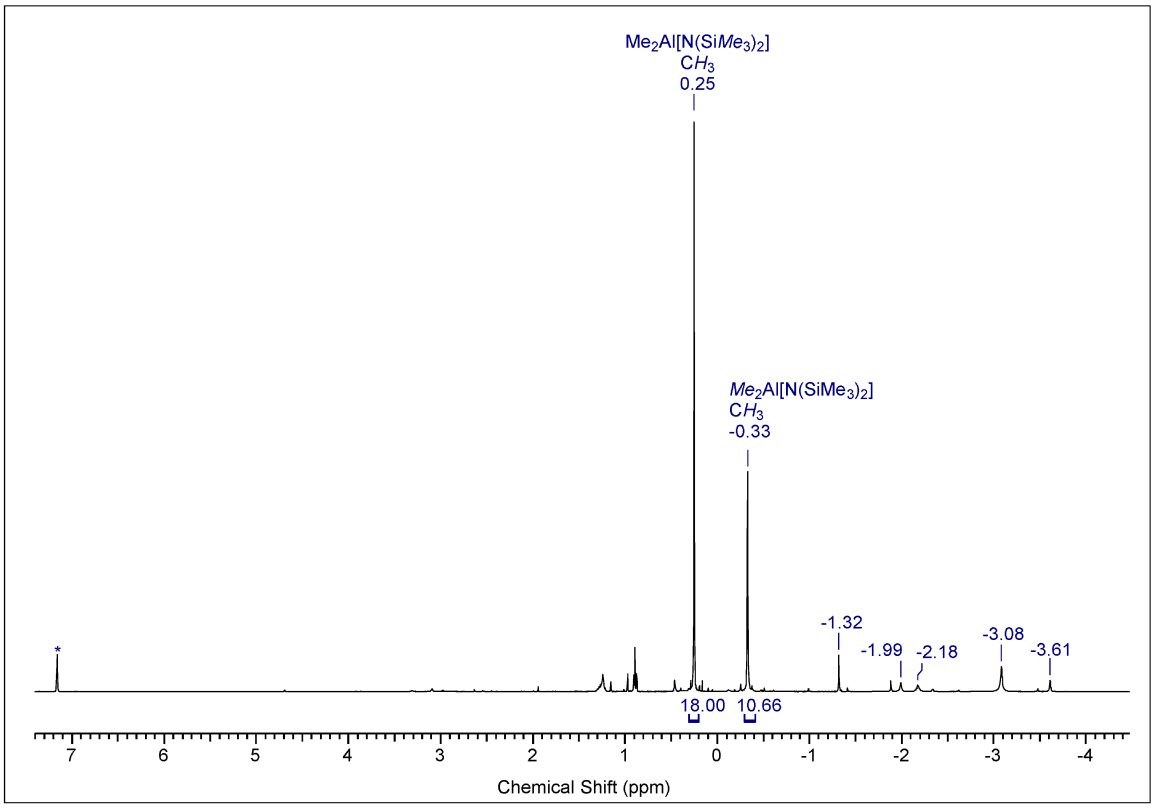

Figure 21. ^{1}H-NMR spectrum (400 MHz, C_6D_6, 25 °C) of the reaction of $Sm[N(SiMe_3)_2]_3$ with 6 equivalents of trimethylaluminum after 48 h reaction time.

Samarium Oxide as Precursors for Isobutyl Aluminates

Spurred by the remarkable redox chemistry of samarium isobutylaluminate complexes, we sought to gain access to a halogenido-bridged samarium complex, since halogenide ions play a pivotal role in Ziegler-Natta-type conjugated diene polymerization catalysts. For industrial polymerization, rare-earth-metal oxides are a cheap and well accessible starting material. Only recently, a facile procedure for the direct activation of rare-earth-metal oxides has been reported, which can easily be converted to the corresponding halides.[165] It involves activation of rare-earth-metal oxides with Me_3SiX (X = Cl, Br, I) for several lanthanides such as La, Pr, Nd, Sm, and Eu. Besides the "activated" chlorides $LnCl_3(thf)_x$, more expensive, or commercially unavailable bromides such as $LaBr_3(thf)_4$, $NdBr_3(thf)_4$, and $SmBr_3(thf)_2$ can be synthesized.[165] This procedure does not only allow the use of cheap oxide precursors, but also yields donor adducts of the corresponding trihalogenido compounds, thus avoiding the time-consuming step of activating rare-

earth-metal chlorides by extraction with THF employing a Soxhlet apparatus. So far, the use of rare-earth-metal oxides as starting materials in organolanthanide chemistry in academics is essentially limited to the preparation of donor-free rare-earth-metal chlorides $LnCl_3$ employing the "ammonium chloride route".

Following an adapted procedure (as shown in Scheme 28), a mixture of samarium oxide and 15 equivalents of trimethylsilyl bromide in tetrahydrofuran was refluxed under argon atmosphere for 2.5 h. Drying under reduced pressure yielded a slightly yellowish $SmBr_3(thf)_2$, which was treated without further purification with 1.5 equivalents of $K[N(SiMe_3)_2]$ in tetrahydrofuran. After removal of the solvent, extraction of the residual solid with *n*-pentane and cooling of the solution to –40 °C, colorless crystals were obtained. Identification *via* X-ray diffraction analysis confirmed that the product was $[Sm\{N(SiMe_3)_2\}_2(\mu\text{-Br})(thf)]_2$ (**27**) according to cell constants as reported in literature.[166] The reaction of the bromido-bridged silylamide complex with six equivalents triisobutylaluminum led to formation of the heteroleptic complex $[Sm\{N(SiMe_3)_2\}(Al\textit{i}Bu_4)(\mu\text{-Br})]_2$ (**28**) (Figure 22). As already observed for the reaction of $Sm[N(SiMe_3)_2]_3$ with TIBA, the reaction of $[Sm\{N(SiMe_3)_2\}_2(\mu\text{-Br})(thf)]_2$ (**27**) and TIBA was accompanied by a partial reduction to $Sm(Al\textit{i}Bu_4)_2$ (**1**$^{\mathbf{Sm}}$), which was identified by X-ray diffraction analysis of cell constants. With this synthesis protocol, we finally succeeded in establishing a procedure leading to a previously not accessible, heteroleptic halogenido-bridged isobutylaluminate species.

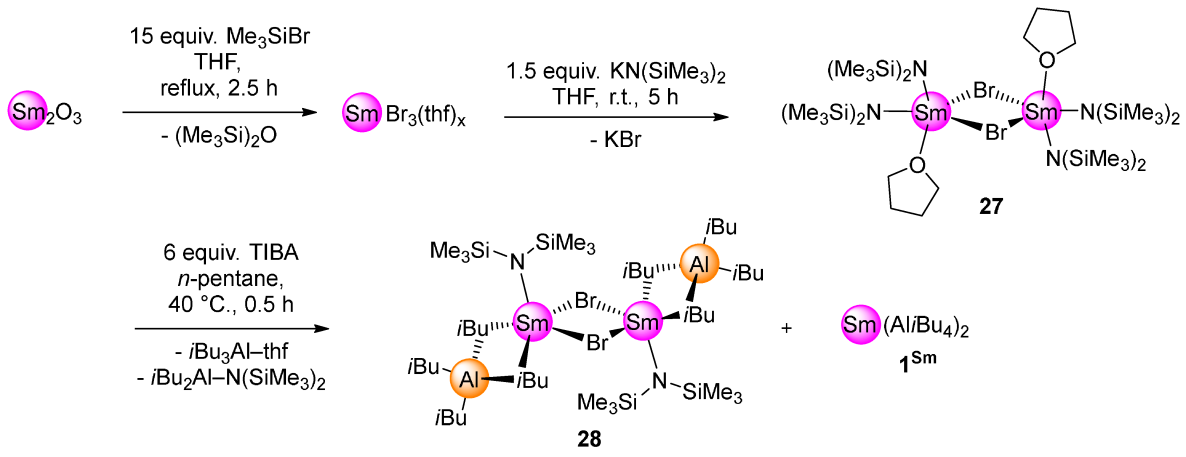

Scheme 28. Activation of samarium oxide, synthesis of $[Sm\{N(SiMe_3)_2\}_2(\mu\text{-Br})(thf)]_2$ (**27**), and partial amide elimination with TIBA yielding $[Sm\{N(SiMe_3)_2\}(Al\textit{i}Bu_4)(\mu\text{-Br})]_2$ (**28**) and $[Sm(Al\textit{i}Bu_4)_2]$ (**1**$^{\mathbf{Sm}}$).

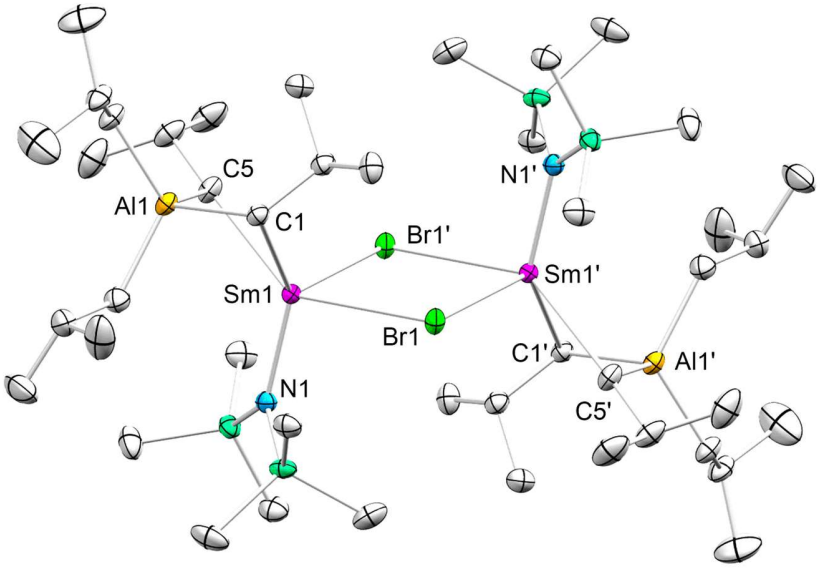

Figure 22. Crystal structure of $[Sm\{N(SiMe_3)_2\}(Al\textit{i}Bu_4)(\mu\text{-}Br)]_2$ (**28**). Hydrogen atoms are omitted for clarity. Atomic displacement ellipsoids were set at 50% probability.

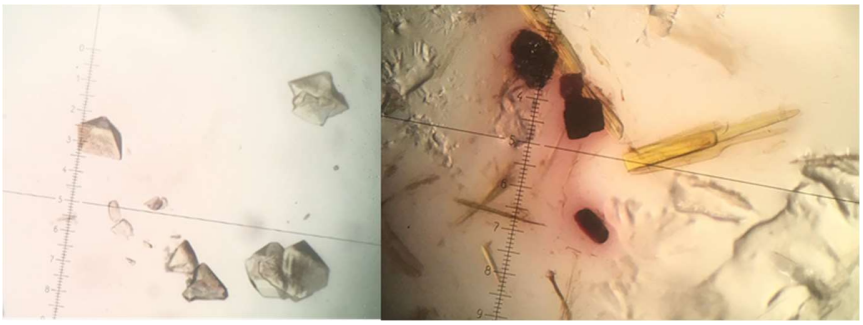

Figure 23. Colorless crystals of $[Sm\{N(SiMe_3)_2\}_2(\mu\text{-}Br)(thf)]_2$ (**27**) (left), and mixture of yellowish $[Sm\{N(SiMe_3)_2\}(Al\textit{i}Bu_4)(\mu\text{-}Br)]_2$ (**28**) and red crystals consisting of divalent $Sm(Al\textit{i}Bu_4)_2$ (**1**$^{\mathbf{Sm}}$).

Experimental Data for Unpublished Results

General Considerations

All manipulations were performed under rigorous exclusion of air and moisture, using standard Schlenk, high-vacuum, and glovebox techniques (MBraun MB200B <1 ppm O_2, <1 ppm H_2O, argon atmosphere). Solvents were supplied by Merck KGaA, purified using a SPS solvent purification system (MBraun) and stored inside a glovebox. Tetrahydrofuran was dried over molecular sieves (3 Å). Benzene-d_6 and toluene-d_8 were obtained from Merck KGaA and dried over Na/K alloy prior to use. Isoprene was purchased from Merck KGaA, dried with trioctylaluminum and distilled under reduced pressure before polymerization. Dimethylaluminum chloride, diethylaluminum chloride, hexachloroethane, potassium bis(trimethylsilyl)amide, triisobutylaluminum (TIBA), trioctylaluminum, *n*-butyllithium, and trityl chloride were purchased from Merck KGaA and used as received. Bis(trimethylsilyl)amine, diethylamine, 1,2-difluorobenzene, diisopropylamine, trimethylsilylbromide, samarium powder, ytterbium chips, tellurium tetrachloride, 18-crown-6, isobutyl iodide, and iodine were purchased from abcr and used without further purification. 1,2-Diiodoethane was obtained from abcr and recrystallized from diethyl ether prior to use. Rare-earth-metal chlorides $LaCl_3$, $PrCl_3$, $NdCl_3$, $SmCl_3$, $GdCl_3$, $HoCl_3$, and YCl_3 were obtained from abcr and used as received. Isobutyl magnesium bromide solution was obtained from Merck KGaA. Alkaline-earth metal diiodides CaI_2, SrI_2, and BaI_2 were obtained from abcr and used as received. $[CPh_3][B(C_6F_5)_4]$, $[C_6H_5NMe_2H][B(C_6F_5)_4]$, and $[B(C_6F_5)_3]$ were purchased from Boulder Scientific and used as received. Argon (99.999 Vol%) was supplied by Westfalen AG. Precursors $LnI_2(thf)_2$ (Ln = Sm, Eu, Yb) were prepared from elemental metal and 1,2-diiodoethane following Kagan's procedure.[167] $Ln\{N(SiMe_3)_2\}_2(thf)_2$ (M = Sm, Eu, Yb), and $Cp^*Sm\{N(SiMe_3)_2\}_2$ were prepared according to literature procedure.[124] [168] Lithium diethylamide and –diisopropylamide were prepared using standard protonolysis protocols. Complexes $Ln[N(SiMe_3)_2]_3$ (Ln = La, Pr, Nd, Gd) were prepared following standard procedures.[169]

Chemicals were stored at −40 °C. Glassware and polymer fittings were dried prior to use for several hours at 120 °C or 80 °C, respectively. IR spectra were recorded on a Nicolet 6700 FTIR

spectrometer (Thermo Fisher Scientific), and samples were mixed with KBr powder and measured in a DRIFT cell equipped with KBr windows. Elemental analyses were performed on an Elementar vario MICRO cube. NMR spectra of air and moisture sensitive compounds were recorded using J. Young valve NMR tubes on a Bruker AVII+400 spectrometer (^{1}H: 400.13 MHz; ^{13}C{^{1}H}: 100.61 MHz). ^{1}H and ^{13}C{^{1}H} NMR chemical shifts are referenced to solvent residual resonances and reported in parts per million, relative to tetramethylsilane. Coupling constants are given in Hertz. The microstructures of polyisoprenes were determined by ^{1}H and ^{13}C{^{1}H} NMR-spectroscopy in $CDCl_3$ on a Bruker AVBII+400 spectrometer (^{1}H: 400.13 MHz) at ambient temperatures. Low temperature NMR spectra were recorded on Bruker AVII+500 spectrometer (^{1}H: 500.13 MHz). Size-exclusion chromatography (SEC) was performed on a Viscotek GPCmax VE2001 device equipped with a TDA305 detector (Viscotek) against a polystyrene standard in THF (35 °C) with a flow rate of 1 mL/min. Sample solutions (1.0 mg polymer per mL THF) were filtered through a 0.45 µm syringe filter prior to injection. M_n and M_w were determined by means of the integrated OmniSec software. Glass transition temperatures T_g were determined by differential scanning calorimetry (DSC) under nitrogen atmosphere on a DSC8000 device equipped with a CLN2 cooler (PerkinElmer) calibrated with cyclohexane and indium standards, by scanning from –100 °C up to +100 °C with heating rates of 20 K/min and cooling rates of 60 K/min. The monomer conversion was determined gravimetrically.

Caution! Note that organoaluminum compounds react very vigorously upon contact with air or moisture and may explode with water!

Procedures

$[Yb(C_6H_6)_2(Al\mathit{i}Bu_4)][B(C_6F_5)_4]/[Yb(C_6H_6)_2\{B(C_6F_5)_4\}_2]$ (11B)

To a mixture of $Yb(Al\mathit{i}Bu_4)_2$ ($\mathbf{1^{Yb}}$) (92.8 mg, 0.136 mmol, 1 equiv.) and cocatalyst **B** (108.8 mg, 0.136 mmol), 2 mL of benzene were added. The resulting solution was stirred at ambient temperature for 30 minutes, concentrated to approx. 0.3 mL volume, and stored for 1.5 years at -40°C. Since no crystals were obtained upon storing in the cold, the solution was stored at ambient temperature. Crystals of $[Yb(C_6H_6)_2(Al\mathit{i}Bu_4)][B(C_6F_5)_4]/[Yb(C_6H_6)_2\{B(C_6F_5)_4\}_2]$ (**11B**) suitable for X-ray analysis formed after three weeks at ambient temperature, yielding 11.5 mg of crystalline product (4%).

$Yb(\mathit{i}Bu)_3(thf)_3$ (21)

The procedure was adapted from similar procedures reported by Niemeyer.[155] Ytterbium (987 mg, 5.703 mmol, 1 equiv.) in 5 mL of THF, and isobutyliodide (1.050 g, 5.703 mmol, 1 equiv.) in 5 mL of THF were cooled to –40 °C. The isobutyliodide solution was added in portions to the ytterbium metal under stirring. The reaction mixture was allowed to stir for 2.5 h at –20°C. After removal of the solvent, the reddish brown residue was extracted with *n*-hexane precooled to –40 °C, filtered, and allowed to crystallize at –40 °C, yielding very temperature sensitive, dark red crystals of **21** as identified by X-ray analysis (690 mg, 65%).

$[Mg\mathit{i}Bu_2(dioxane)]_n$ (22)

A solution of *i*BuMgBr in diethyl ether (2 M, 40 mL) was diluted in additional diethyl ether (80 mL). Under stirring, dioxane (10 mL) was added. The resulting suspension was centrifugated, the supernatant filtered, and concentrated *in vacuo*. Colorless crystals formed overnight at –40 °C. Recrystallization from diethyl ether afforded 5.130 g product (57%). Crystals suitable for X-ray crystallography were grown from a concentrated solution of $[Mg\mathit{i}Bu_2(dioxane)]_n$ (**22**) in diethyl ether at –40 °C. ^{1}H-NMR (400.1 MHz, C_6D_6, 25 °C): δ 3.37 (s, 8 H, dioxane-CH_2); 2.22 (m, 2 H, CH); 1.31 (d, 12 H, CH_3); 0.09 (d, 4 H, isobutyl-CH_2) ppm. $^{13}C\{^1H\}$ NMR (100.6 MHz, C_6D_6, 25

°C): δ 67.6 (dioxane-*C*H_2); 30.9 (*C*H_3); 29.3 (*C*H); 24.0 (*C*H_2) ppm. DRIFTS (KBr, cm^{-1}): 2985 (vw), 2934 (vs), 2849 (m), 2817 (vs), 2771 (w), 2750 (m), 2639 (vw), 1457 (m), 1399 (w), 1289 (m), 1259 (m), 1106 (s), 1174 (s), 1040 (w), 1010 (w), 984 (w), 949 (m), 893 (w), 877 (m), 864 (m), 796 (w), 615 (m), 550 (s). $C_{12}H_{26}MgO_2$ (226.64 g/mol): calcd. C 63.59, H 11.56; found C 63.35, H 11.28.

[Ca(Al*i*Bu$_4$)$_2$] (24^{Ca})

Triisobutylaluminum (24.865 g, 125.534 mmol, 6.2 equiv.) in 50 mL *n*-pentane was added dropwise to a solution of Ca[N(SiMe$_3$)$_2$]$_2$(thf)$_2$ (10.210 g, 20.216 mmol) in *n*-pentane (50 mL) under stirring. After stirring for two hours, the solution was concentrated in vacuum. The solution was cooled to –40 °C. White crystals of [Ca(Al*i*Bu$_4$)$_2$] (**24^{Ca}**) were obtained and purified by repeated recrystallization, yielding 7.885 g (14.318 mmol, 71%). ^{1}H-NMR (400.1 MHz, C_6D_6, 25 °C): δ 1.98 (m, 1H, C*H*); 1.14 (d, 6H, CH_3); 0.17 (d, 2H, CH_2) ppm. ^{13}C{^{1}H} NMR (100.6 MHz, C_6D_6, 25 °C): δ 29.5 (*C*H), 28.7 (*C*H_3), 28.3 (*C*H_2) ppm. DRIFTS (KBr, cm^{-1}): 2950 (vs), 2919 (vs), 2862 (vs), 2738 (s), 2648 (w), 2563 (w), 1462 (vs), 1380(s), 1362 (s), 1317 (m), 1250 (w), 1178 (s), 1160 (s), 1066 (vs), 1018 (m), 992 (s), 944 (m), 914 (w), 809 (s), 879 (vs), 660 (vs), 596 (vs), 415 (vs). $C_{32}H_{72}Al_2Ca$ (550.96 g/mol): calcd. C 69.76, H 13.17; found C 69.41, H 13.31.

[Sr(Al*i*Bu$_4$)$_2$] (24^{Sr})

To a suspension of Sr[N(SiMe$_3$)$_2$]$_2$(thf)$_2$ (2.500 g, 4.52 mmol) in *n*-hexane (25 mL), TIBA (6.730 g, 33.93 mmol) was added dropwise under stirring. The resulting clear solution was stirred 6 h at ambient temperature, and concentrated *in vacuo*. Crystals suitable for X-ray characterization were obtained after several days at –40 °C. Repeated crystallization afforded 2.282 g spectroscopically pure [Sr(Al*i*Bu$_4$)$_2$] (**24^{Sr}**) as white solid (84%). ^{1}H-NMR (400.1 MHz, C_6D_6, 25 °C): δ 1.85 (m, 1H, C*H*); 1.14 (d, 6H, CH_3); 0.15 (d, 2H, CH_2) ppm. ^{13}C{^{1}H} NMR (100.6 MHz, C_6D_6, 25 °C): δ 29.5 (*C*H), 28.8 (*C*H_3), 28.7 (*C*H_2) ppm. DRIFTS (KBr, cm^{-1}): 2949 (vs), 2924 (s), 2860 (s), 2832 (m), 2750 (m), 2645 (w), 2560 (vw), 1463 (m), 1381 (w), 1362 (m), 1339 (w), 1315 (vw), 1293 (vw), 1170 (m), 1059 (m), 1018 (vw), 994 (w), 913 (vw), 808 (w), 680 (s), 658 (s), 622 (s), 609 (m), 599

(m), 580 (m), 440 (m), 431 (vs), 420 (m). $C_{32}H_{72}Al_2Sr$ (598.50 g/mol): calcd. C 64.22, H 12.13; found C 63.94, H 11.74.

[Ba(Al*i*Bu$_4$)$_2$] (24^{Ba})

Triisobutylaluminum (19.278 g, 97.216 mmol, 6 equiv.) in 30 mL *n*-hexane was added dropwise to a solution of Ba[N(SiMe$_3$)$_2$]$_2$(thf)$_2$ (19.278 g, 16.203 mmol) in *n*-hexane (20 mL) under stirring. After stirring for three hours, the solution was concentrated in vacuum and cooled to –40 °C, yielding 7.920 g white solid after recrystallization. However, elemental analyses and ICP-OES showed that the product was not pure and contained potassium, originating from the synthesis of Ba[N(SiMe$_3$)$_2$]$_2$(thf)$_2$ from BaI_2 and 1.8 equiv. of K[N(SiMe$_3$)$_2$]. It has been reported that "ate"complex formation is a common problem in salt metathesis protocols for barium hexamethylsilazide chemistry.[170]

[Sm{N(SiMe$_3$)$_2$}$_2$(thf)(μ-Br)]$_2$ (27)

The protocol follows a slightly modified procedure for the activation of rare-earth metal oxides reported in literature.[165, 171] To a suspension of Sm_2O_3 (0.800 g, 2.29 mmol, 1 equiv.) in THF (25 mL), a solution of Me_3SiBr (5.300 g, 34.62 mmol, 7.5 equiv.) in THF (25 mL) was added dropwise over thirty minutes under vigorous stirring. The solution was heated under reflux for 1.5 hours, and dried in vacuum, yielding a yellowish solid. After dissolving in THF (50 mL), K[N(SiMe$_3$)$_2$] (1.373 g, 6.88 mmol, 1.5 equiv.) was added in small portions. The suspension was stirred for five hours at ambient temperature, dried in vacuum, and extracted with *n*-pentane, yielding pyramidally shaped crystals of [Sm{N(SiMe$_3$)$_2$}$_2$(thf)(μ-Br)]$_2$ (**27**) upon cooling of the filtered, yellowish *n*-pentane solution to –40 °C, which were identified by X-ray diffraction by comparison of cell parameters to literature.[166]

[Sm(Al*i*Bu$_4$){N(SiMe$_3$)$_2$}(μ-Br)]$_2$ (28)

To [Sm{N(SiMe$_3$)$_2$}$_2$(thf)(μ-Br)]$_2$ (**27**) (260 mg, 209 mmol, 1 equiv.) in *n*-pentane (1 mL), a solution of triisobutylaluminum (248 mg, 1.252 mmol, 6 equiv.) in *n*-pentane (2 mL) was added dropwise under stirring at ambient temperature, whereupon the initially yellowish solution underwent a color change from yellowish to greenish-black. After stirring for ten minutes at ambient temperature, the solution was cooled to to –40 °C, yielding purple crystals of Sm(Al*i*Bu$_4$)$_2$, and yellowish crystals of [Sm(Al*i*Bu$_4$){N(SiMe$_3$)$_2$}(μ-Br)]$_2$ (**28**) identified by X-ray diffraction.

Crystallographic Data

X-ray crystallography and crystal structure determination

For X-ray structure analyses, crystals suitable for X-ray diffraction were selected in a glovebox, coated with Parabar 10312 (Hampton Research), and fixed on a nylon/loop glass fiber. X-ray data for all compounds was collected on a Bruker APEX II DUO diffractometer equipped with an IμS microfocus sealed tube and QUAZAR optics for MoKα (λ = 0.71073 Å). The data collection strategy was determined using COSMO,[172] employing ω-scans. Raw data were processed using APEX,[173] and SAINT.[173] Corrections for absorption effects were applied using SADABS.[174] The structures were solved by direct methods and refined against all data by full-matrix least-squares methods on F2 using SHELXTL[175], and ShelXle.[176] Disorder models were calculated using DSR, a program for refining structures in ShelXl.[177] All graphics were produced employing Mercury 4.2.011[178] and POV-Ray12.[179]

Table 9. Crystallographic Data for $[Yb(C_6H_6)_2(Al\textit{i}Bu_4)][B(C_6F_5)_4]/[Yb(C_6H_6)_2\{B(C_6F_5)_4\}_2]$ (**11B**), $Yb(\textit{i}Bu)_3(thf)_3$ (**21**) and $[Mg\textit{i}Bu_2(dioxane)]_n$ (**22**)

	11B	**21**	**22**
formula	$C_{154}H_{102}AlB_3F_{60}Yb_2$	$C_{24}H_{51}O_3Yb$	$C_{12}H_{26}MgO_2$
M [g mol^{-1}]	3497.84	560.68	226.64
color/shape	yellow/needle	red/block	colorless/block
crystal dimensions [mm]	0.140 x 0.057 x 0.047	0.391 x 0.219 x 0.180	0.358 x 0.315 x 0.242
cryst. system	monoclinic	monoclinic	monoclinic
space group	*P2₁/c*	*P2₁/n*	*C2/c*
a [Å]	17.3220(11)	9.938(3)	14.8406(8)
b [Å]	21.4959(13)	15.821(4)	9.1327(5)
c [Å]	37.669(2)	17.314(5)	10.7894(6)
α [°]	90	90	90
β [°]	98.331(2)	90.314(4)	108.1080(10)
γ [°]	90	90	90
V [Å^3]	13878.2(15)	2722.3(13)	1389.91(13)
Z	4	4	4
T [K]	100(2)	100(2)	100(2)
wavelength [Å]	0.71073	0.71073	0.71073
ρ_{calcd} [Mg m^{-3}]	1.674	1.368	1.083
μ [mm^{-1}]	1.481	3.454	0.111
F (000)	6936	1156	504
θ range [°]	1.188 to 26.429	4.291 to 29.163	2.657/29.970
unique reflns	28478	7303	2014
observed reflns	181559	39197	16240
R1/*w*R2 (I>2σ)[a]	0.0672/0.1388	0.0461/0.1022	0.0301/0.0797
R1/*w*R2 (all data)[a]	0.1179/0.1598	0.0681/0.1129	0.0327/0.0822
GOF[a]	1.028	1.104	1.065

[a] $R1 = \Sigma(||F_0|-|F_c||)/\Sigma|F_0|$, $F_0 > 4\sigma(F_0)$. $wR2 = \{\Sigma[w(F_0^2-F_c^2)^2/\Sigma[w(F_0^2)^2]\}^{1/2}$.

Table 10. Crystallographic data for compounds [Ca(Al*i*Bu$_4$)$_2$] (**24^{Ca}**)*, [Sr(Al*i*Bu$_4$)$_2$] (**24^{Sr}**), and [Ba(Al*i*Bu$_4$)$_2$] (**24^{Ba}**)

	24^{Ca}*	**24^{Sr}**	**24^{Ba}**
formula	$C_{32}H_{72}Al_2Ca$	$C_{32}H_{72}Al_2Sr$	$C_{32}H_{72}Al_2Ba$
M [g mol^{-1}]	550.93	598.47	648.19
color/shape	colorless/needle	colorless/needle	colorless/needle
crystal dimensions [mm]	0.100 x 0.100 x 0.100	0.466 x 0.138 x 0.096	0.185 x 0.178 x 0.146
cryst. system	triclinic	monoclinic	triclinic
space group	$P\bar{1}$	$P2_1/n$	$P\bar{1}$
a [Å]	10.870(7)	9.4859(6)	9.797(4)
b [Å]	10.969(7)	18.5497(12)	10.714(4)
c [Å]	17.816(11)	10.6821(7)	10.989(4)
α [°]	87.509(12)	90	115.519(5)
β [°]	88.110(13)	96.4930(10)	92.389(6)
γ [°]	60.886(11)	90	110.152(7)
V [Å^3]	1854(2)	1867.6(2)	952.4(7)
Z	2	2	1
T [K]	100(2)	100(2)	100(2)
wavelength [Å]	0.71073	0.71073	0.71073
ρ_{calcd} [Mg m^{-3}]	-	1.064	1.130
μ [mm^{-1}]	-	1.507	1.105
F (000)	-	656	346
θ range [°]	-	2.196/28.799	2.107/30.294
unique reflns	-	4856	5667
observed reflns	-	48090	5667
R1/*w*R2 (I>2σ)[a]	-	0.0267/0.0668	0.0231/0.0617
R1/*w*R2 (all data)[a]	-	0.0332/0.0701	0.0233/0.0618
GOF[a]	-	1.036	1.140

[a] $R1 = \Sigma(||F_0|-|F_c||)/\Sigma|F_0|$, $F_0 > 4\sigma(F_0)$. $wR2 = \{\Sigma[w(F_0^2-F_c^2)^2/\Sigma[w(F_0^2)^2]\}^{1/2}$.

* Note that only a connectivity was obtained due to poor crystal quality.

Table 11. Crystallographic data for compound Compound **26** and **28**

	26	**28**
formula	$C_{14}H_{42}Al_2NSi_2Sm$	$C_{44}H_{108}Al_2Br_2N_2Si_4Sm_2$
M [g mol^{-1}]	484.97	1292.16
color/shape	colorless/needle	orange/needle
crystal dimensions [mm]	0.264 x 0.081 x 0.079	0.173 x 0.099 x 0.049
cryst. system	monoclinic	triclinic
space group	$P2_1/c$	$P\bar{1}$
a [Å]	17.214(6)	9.3478(5)
b [Å]	10.490(4)	12.2609(7)
c [Å]	14.626(5)	27.3915(15)
α [°]	90	92.0630(10)
β [°]	110.547(6)	94.6560(10)
γ [°]	90	90.3650(10)
V [Å^3]	2473.1(15)	3126.9(3)
Z	4	2
T [K]	100(2)	100(2)
wavelength [Å]	0.71073	0.71073
ρ_{calcd} [Mg m^{-3}]	1.303	1.372
μ [mm^{-1}]	2.537	3.269
F (000)	996	1324
θ range [°]	2.316/29.103	1.493/28.361
unique reflns	6591	15644
observed reflns	19906	156664
R1/wR2 (I>2σ)[a]	0.0352/0.0814	0.0299/0.0604
R1/wR2 (all data)[a]	0.0522/0.0919	0.0418/0.0660
GOF[a]	1.021	1.034

[a] $R1 = \Sigma(||F_0|-|F_c||)/\Sigma|F_0|$, $F_0 > 4\sigma(F_0)$. $wR2 = \{\Sigma[w(F_0^2-F_c^2)^2/\Sigma[w(F_0^2)^2]\}^{1/2}$.

NMR Spectra

In general, solvent residual signals are labeled with an asterisk (*). In some cases, the paramagnetic nature of Pr(III), Nd(III), Gd(III) and Yb(III), or poor solubility did not allow a conclusive NMR analysis.

[Mg*i*Bu$_2$(dioxane)]$_n$ (22)

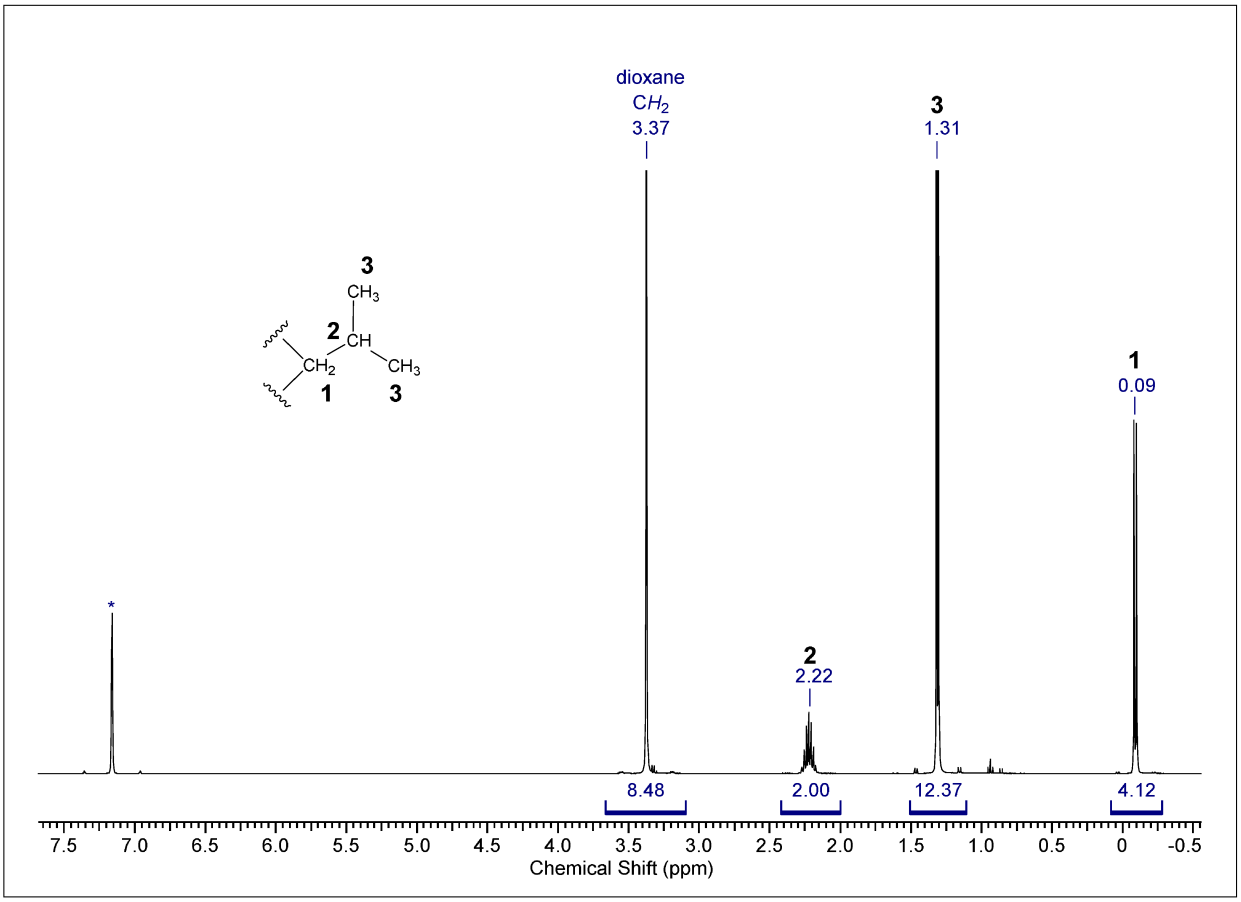

Figure 24. ^{1}H-NMR spectrum (400 MHz, C_6D_6, 25 °C) of [Mg*i*Bu$_2$(dioxane)]$_n$ (**22**).

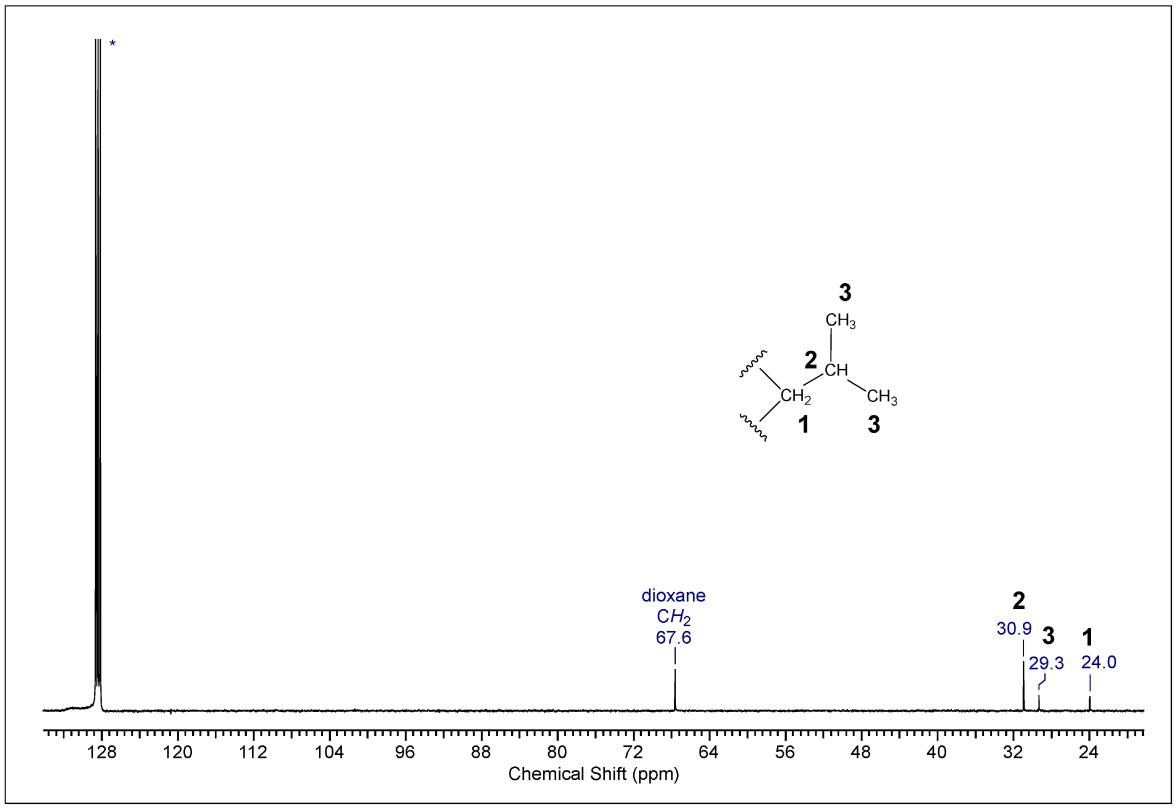

Figure 25. $^{13}C\{^{1}H\}$-NMR spectrum (101 MHz, C_6D_6, 25 °C) of [Mg*i*Bu$_2$(dioxane)]$_n$ (**22**).

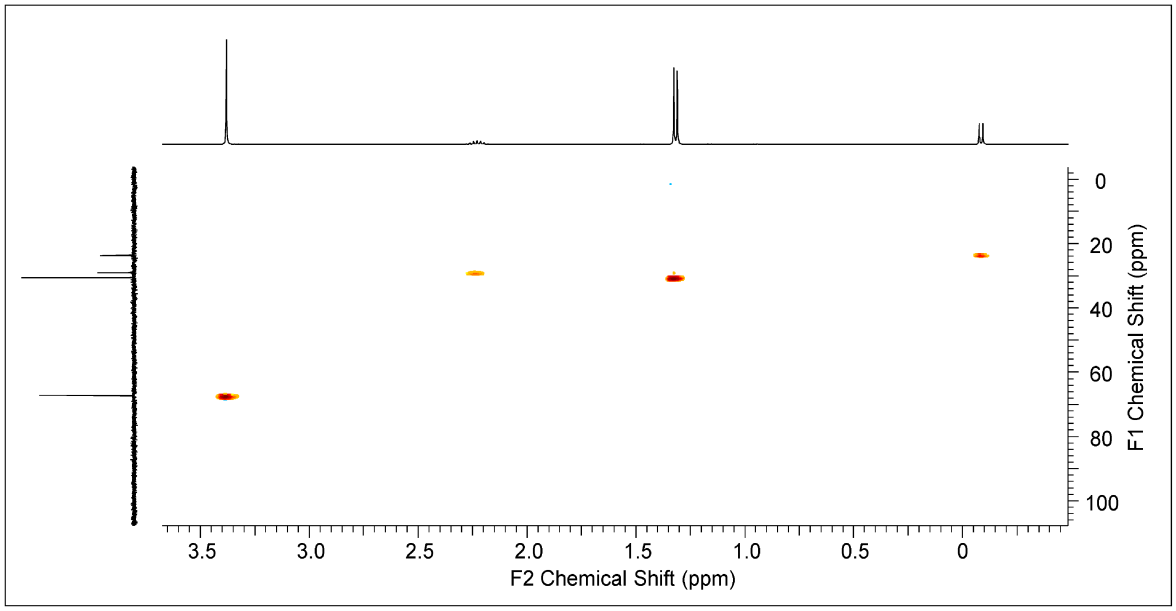

Figure 26. ^{1}H-^{13}C HSQC NMR spectrum (400/101 MHz, C_6D_6, 25 °C) of [Mg*i*Bu$_2$(dioxane)]$_n$ (**22**).

Homoleptic Alkaline Earth Tetraisobutylaluminates [Ae(Al*i*Bu$_4$)$_2$] (24^{Ae})

[Ca(Al*i*Bu$_4$)$_2$] (24^{Ca})

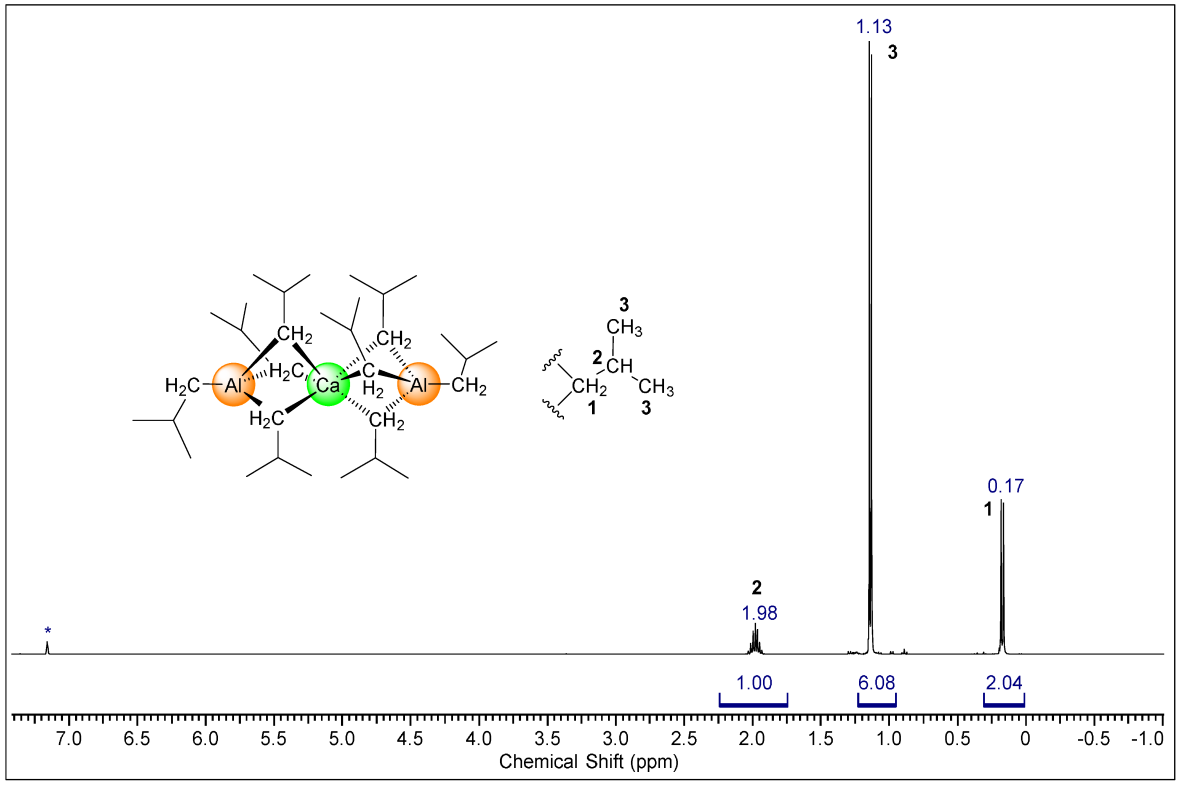

Figure 27. ^{1}H-NMR spectrum (400 MHz, C_6D_6, 25 °C) of Ca(Al*i*Bu$_4$)$_2$ (**24^{Ca}**).

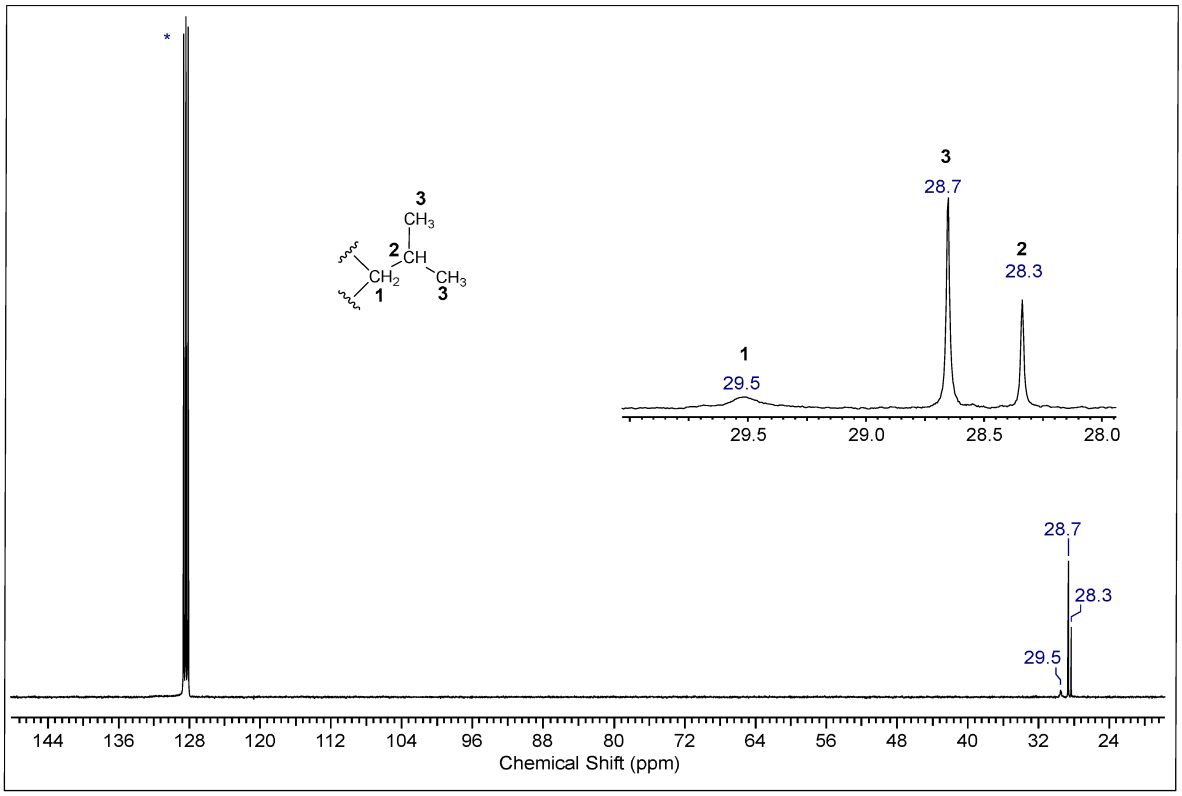

Figure 28. $^{13}C\{^{1}H\}$-NMR spectrum (101 MHz, C_6D_6, 25 °C) of $Ca(Al\textit{i}Bu_4)_2$ (**24**^{Ca}).

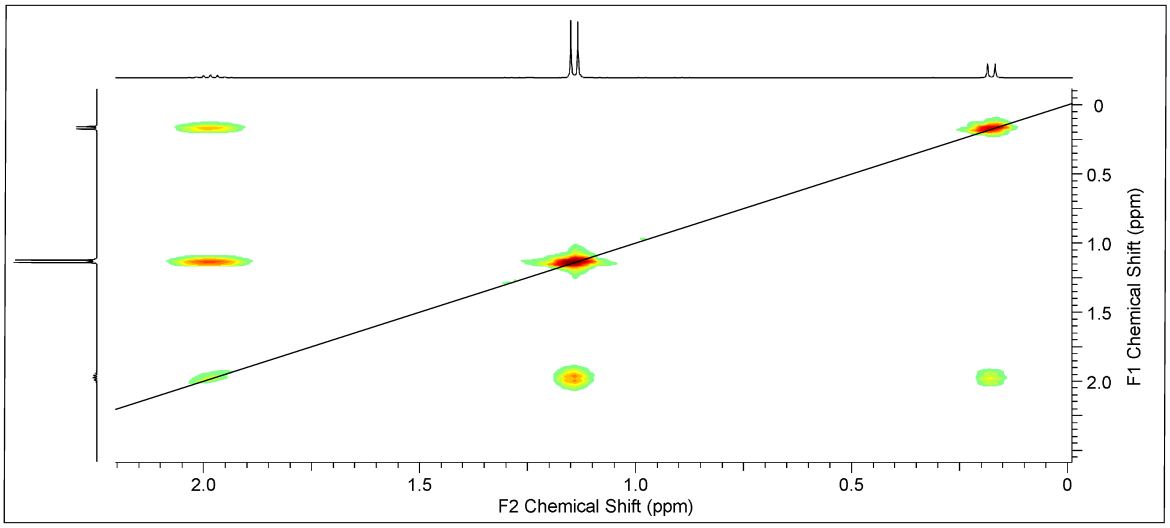

Figure 29. ^{1}H-^{1}H COSY NMR spectrum (400 MHz, C_6D_6, 25 °C) of $Ca(Al\textit{i}Bu_4)_2$ (**24**^{Ca}).

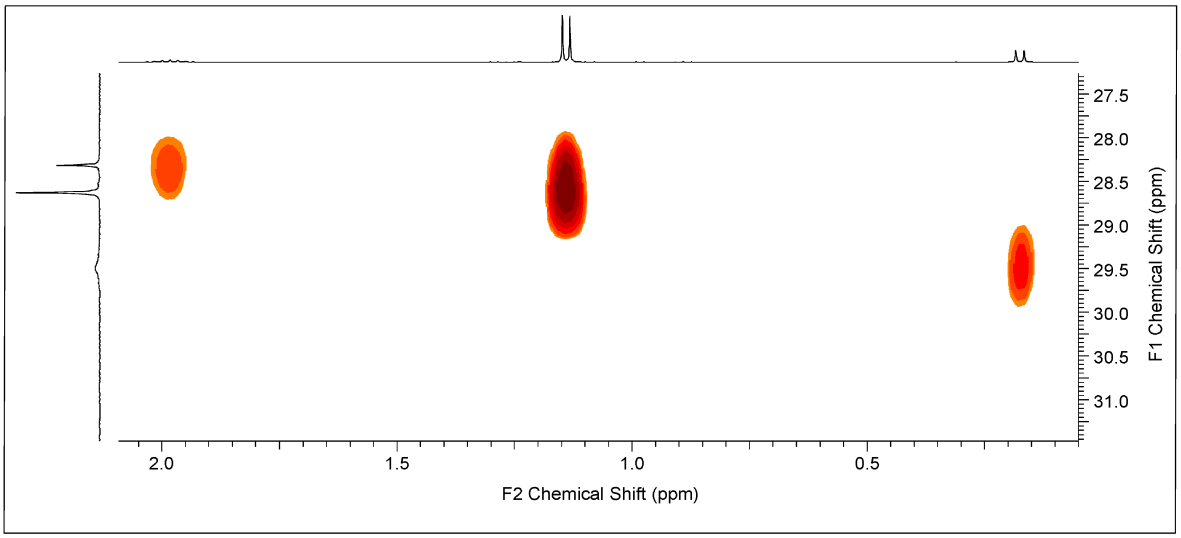

Figure 30. ^{1}H-^{13}C HSQC NMR spectrum (400/101 MHz, C_6D_6, 25 °C) of Ca(Al*i*Bu$_4$)$_2$ (**24^{Ca}**).

[Sr(Al*i*Bu$_4$)$_2$] (24^{Sr})

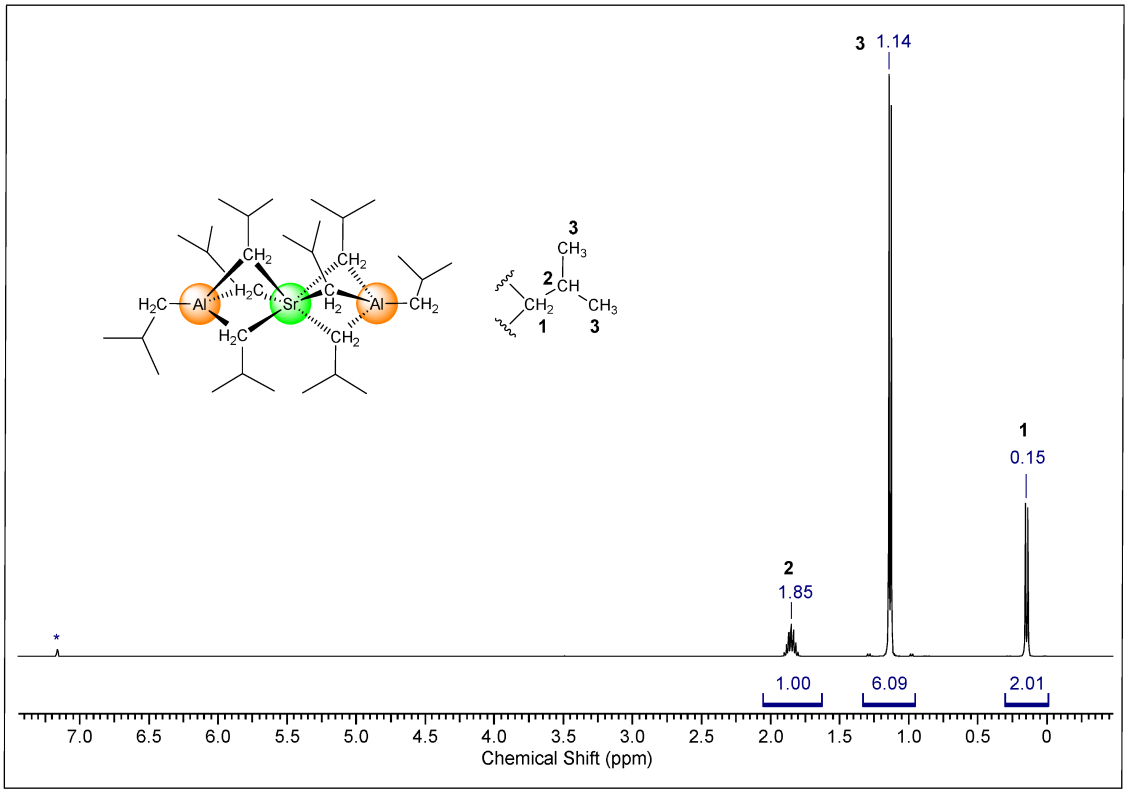

Figure 31. ^{1}H-NMR spectrum (400 MHz, C_6D_6, 25 °C) of Sr(Al*i*Bu$_4$)$_2$ (**24^{Sr}**).

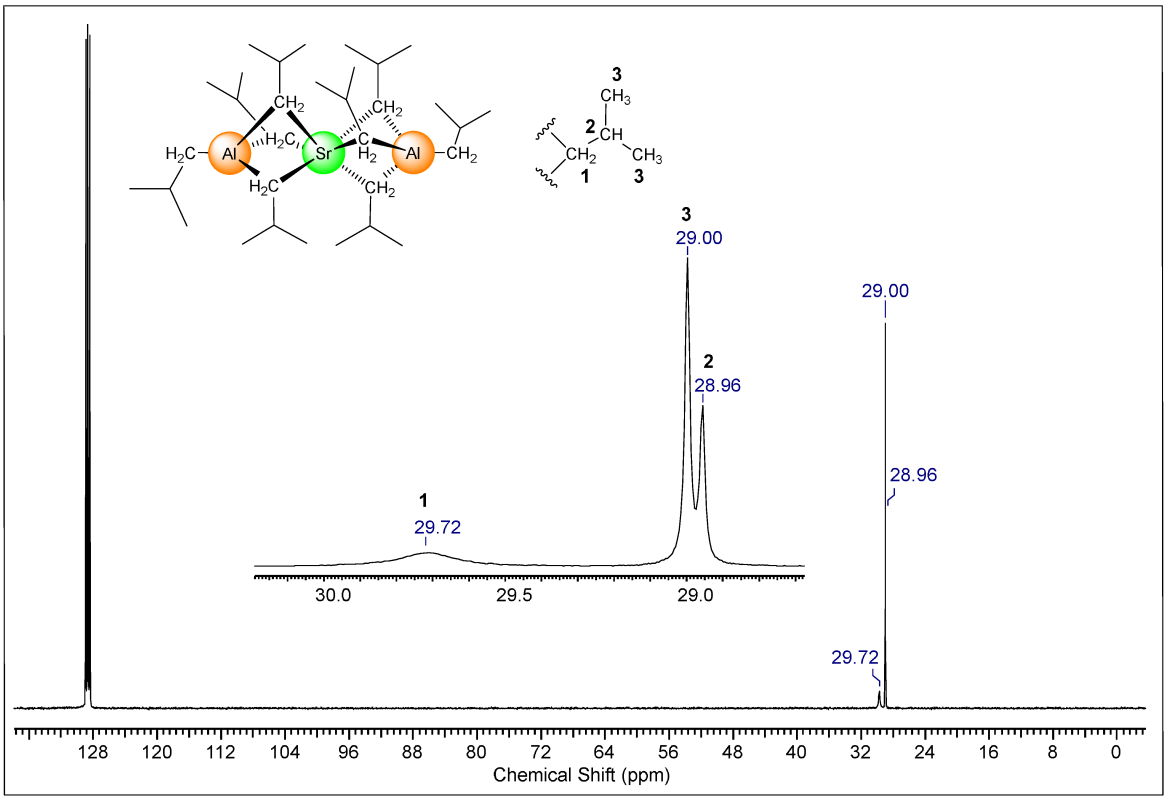

Figure 32. $^{13}C\{^{1}H\}$-NMR spectrum (101 MHz, C_6D_6, 25 °C) of $Sr(Al\textit{i}Bu_4)_2$ (**24**^{Sr}).

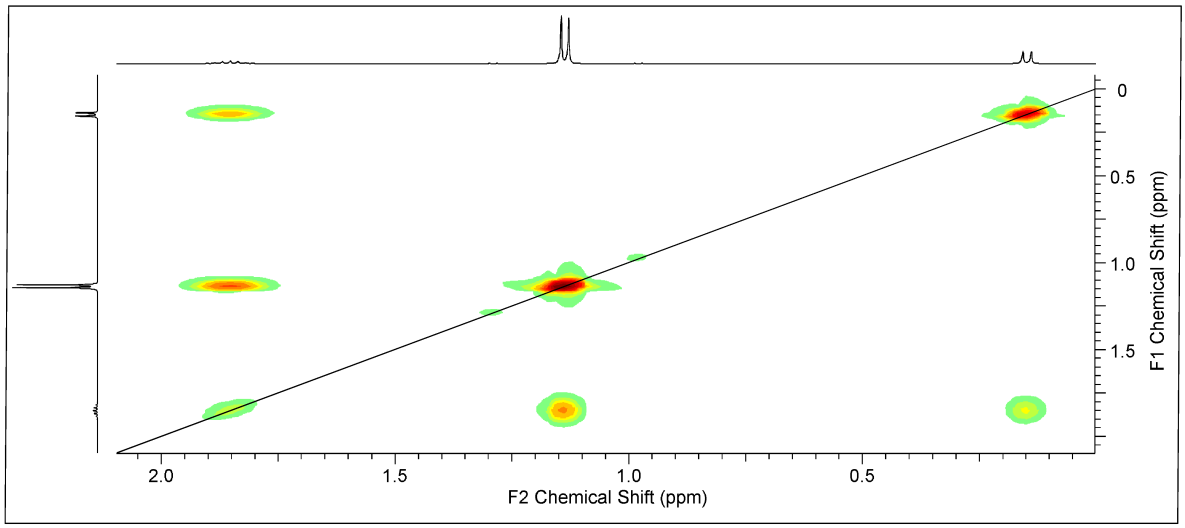

Figure 33. ^{1}H-^{1}H COSY NMR spectrum (400 MHz, C_6D_6, 25 °C) of $Sr(Al\textit{i}Bu_4)_2$ (**24**^{Sr}).

D

D. Bibliography

D. Bibliography

[1] D. Hosler, S. L. Burkett, M. J. Tarkanian, *Science* **1999**, *284*, 1988-1991.

[2] P. E. Hurley, *J. Macromol. Sci. A* . **1981**, *15*, 1279-1287.

[3] C. Goodyear, *Gum-Elastic and Its Varieties*, New Haven, **1855**.

[4] J. E. Puskas, E. Gautriaud, A. Deffieux, J. P. Kennedy, *Progr. Polym. Sci.* **2006**, *31*, 533-548.

[5] M. Morton, *J. Macromol. Sci. A* . **1981**, *15*, 1289-1302.

[6] F. Hofmann, *Angew. Chem.* **1912**, *25*, 1462-1467.

[7] H. M. Dietrich, Technische Universität München **2006**.

[8] G. Ricci, G. Pampaloni, A. Sommazzi, F. Masi, *Macromolecules* **2021**, *54*, 5879-5914.

[9] A. S. T. Koyama, *Biopolymers - Polyisoprenoids, Vol. 2*, Wiley-VCH, Weinheim, **2001**.

[10] T. Sone, *Int. Pol. Sci. Tech.* **2016**, *43*, 49-54.

[11] S. E. Horne, J. P. Kiehl, J. J. Shipman, V. L. Folt, C. F. Gibbs, E. A. Willson, E. B. Newton, M. A. Reinhart, *Ind. Eng. Chem. Res.* **1956**, *48*, 784-791.

[12] W. J. Evans, T. M. Champagne, D. G. Giarikos, J. W. Ziller, *Organometallics* **2005**, *24*, 570-579.

[13] K. Cornish, *Technology & Innovation* **2017**, *18*, 244-255.

[14] D. Kasai, *Biosci. Biotechnol. Biochem.* **2020**, *84*, 1089-1097.

[15] L. Zhang, T. Suzuki, Y. Luo, M. Nishiura, Z. Hou, *Angew. Chem. Int. Ed.* **2007**, *46*, 1909-1913.

[16] R. A. Backhaus, *Isr. J. Plant Sci.* **1985**, *34*, 283-293.

[17] C. L. Swanson, R. A. Buchanan, F. H. Otey, *J. Appl. Polym. Sci.* **1979**, *23*, 743-748.

[18] M. Zimmermann, K. W. Törnroos, R. Anwander, *Angew. Chem. Int. Ed.* **2008**, *47*, 775-778.

[19] E. Warren-Thomas, P. M. Dolman, D. P. Edwards, *Conserv. Lett.* **2015**, *8*, 230-241.

[20] Y.-F. Wang, S. M. Owen, Q.-J. Li, J. Peñuelas, *Glob. Change Biol.* **2007**, *13*, 2270-2282.

[21] K. Vasquez, *C&EN* **2022**, *100*.

[22] Y. C. Fong, A. A. Khin, C. S. Lim, *AJEM* **2018**, *6*, 403-418.

[23] H. Mooibroek, K. Cornish, *Appl. Microbiol. Biotechnol.* **2000**, *53*, 355-365.

[24] B. M. Schmidt, A. Pindwal, A. Venkatesh, A. Ellern, A. J. Rossini, A. D. Sadow, *ACS Catal.* **2019**, *9*, 827-838.

[25] J. K. Kim, J. W. Park, *J. Appl. Polym. Sci.* **1999**, *72*, 1543-1549.

[26] Z. Tian, H. Zhao, K. T. Peter, M. Gonzalez, J. Wetzel, C. Wu, X. Hu, J. Prat, E. Mudrock, R. Hettinger, A. E. Cortina, R. G. Biswas, F. V. C. Kock, R. Soong, A. Jenne, B. Du, F. Hou, H. He, R. Lundeen, A. Gilbreath, R. Sutton, N. L. Scholz, J. W. Davis, M. C. Dodd, A. Simpson, J. K. McIntyre, E. P. Kolodziej, *Science* **2021**, *371*, 185.

[27] C. Wang, J. Zhao, B. Xing, *J. Hazard. Mater.* **2021**, *407*, 124-357.

[28] S. Harder, *Early Main Group Metal Catalysis Concepts and Reactions*, 1 ed., Wiley-VCH, Weinheim, Germany, **2020**.

[29] I. Rivera, R. Lopez, F. J. Enríquez-Medrano, S. Kumar, A. Aguilar-Sanchez, R. Handa, R. E. D. de León-Gómez, L. Valencia, *J. Mater. Chem.* **2022**, *10*, 5019-5043.

[30] P. Jochmann, T. S. Dols, T. P. Spaniol, L. Perrin, L. Maron, J. Okuda, *Angew. Chem.* **2009**, *121*, 5825-5829.

[31] W. Dong, K. Endo, T. Masuda, *Macromol. Chem. Phys.* **2003**, *204*, 104-110.

[32] D. Li, S. Li, D. Cui, X. Zhang, *Organometallics* **2010**, *29*, 2186-2193.

[33] B. Liu, S. Li, M. Wang, D. Cui, *Angew. Chem. Int. Ed.* **2017**, *56*, 4560-4564.

[34] A. Fischbach, R. Anwander, *Adv. Polym. Sci.* **2006**, *204*, 155-281.

[35] H.-J. Förster, **1998**, *83*, 259-272.

[36] O. L. Sydora, *Organometallics* **2019**, *38*, 997-1010.

[37] L. Friebe, J. M. Müller, O. Nuyken, W. Obrecht, *J. Macromol. Sci. A* . **2006**, *43*, 841-854.

[38] L. Friebe, O. Nuyken, H. Windisch, W. Obrecht, *Macromol. Chem. Phys.* **2002**, *203*, 1055-1064.

[39] G. Jeske, H. Lauke, H. Mauermann, P. N. Swepston, H. Schumann, T. J. Marks, *J. Am. Chem. Soc.* **1985**, *107*, 8091-8103.

[40] S. Kaita, Z. Hou, Y. Wakatsuki, *Macromolecules* **1999**, *32*, 9078-9079.

[41] L. Annunziata, M. Duc, J.-F. Carpentier, *Macromolecules* **2011**, *44*, 7158-7166.

[42] W. J. Evans, T. A. Ulibarri, J. W. Ziller, *J. Am. Chem. Soc.* **1990**, *112*, 2314-2324.

[43] L. Porri, G. Natta, M. C. Gallazzi, *J. Polym. Sci. C* **1967**, *16*, 2525-2537.

[44] G. Wilke, B. Bogdanović, P. Hardt, P. Heimbach, W. Keim, M. Kröner, W. Oberkirch, K. Tanaka, E. Steinrücke, D. Walter, H. Zimmermann, *Angew. Chem. Int. Ed.* **1966**, *5*, 151-164.

[45] R. Warin, P. Teyssié, P. Bourdaudurq, F. Dawans, *J. Polym. Sci.: Polym. Letters Ed.* **1973**, *11*, 177-183.

[46] R. Taube, H. Windisch, S. Maiwald, H. Hemling, H. Schumann, *J. Organomet. Chem.* **1996**, *513*, 49-61.

[47] R. Taube, *Metalorganic Catalysts for Synthesis and Polymerization*, Springer, Berlin, **1999**.

[48] S. Maiwald, H. Weißenborn, C. Sommer, G. Müller, R. Taube, *J. Organomet. Chem.* **2001**, *640*, 1-9.

[49] R. Taube, S. Maiwald, J. Sieler, *J. Organomet. Chem.* **2001**, *621*, 327-336.

[50] S. Tobisch, H. Bögel, R. Taube, *Organometallics* **1996**, *15*, 3563-3571.

[51] L. N. Jende, Eberhard Karls Universität Tübingen, PhD Thesis, **2015**.

[52] L. N. Jende, C. Maichle-Mössmer, C. Schädle, R. Anwander, *J. Organomet. Chem.* **2013**, *744*, 74-81.

[53] C. Meermann, University of Bergen, Technische Universität München **2008**.

[54] D. Cui, *Vol. 137, Molecular catalysis of rare-earth elements* (Ed.: P. W. Roesky), Springer Science & Business Media, **2010**.

[55] W. J. Evans, L. R. Chamberlain, J. W. Ziller, *J. Am. Chem. Soc.* **1987**, *109*, 7209-7211.

[56] C. Meermann, K. W. Törnroos, W. Nerdal, R. Anwander, *Angew. Chem.* **2007**, *119*, 6628-6633.

[57] K. Lv, D. Cui, *Organometallics* **2010**, *29*, 2987-2993.

[58] V. Monteil, R. Spitz, C. Boisson, *Polym. Int.* **2004**, *53*, 576-581.

[59] R. Tanaka, Y. Nakayama, T. Shiono, *Organometallics* **2020**, *39*, 1855-1860.

[60] C. Shan, Y. Lin, J. Ouyang, Y. Fan, G. Yang, *Macromol. Chem.* **1987**, *188*, 629-635.

[61] M. G. Klimpel, Technische Universität München, PhD Thesis, **2001**.

[62] X. Li, M. Nishiura, K. Mori, T. Mashiko, Z. Hou, *Chem. Comm.* **2007**, 4137-4139.

[63] A.-S. Rodrigues, E. Kirillov, B. Vuillemin, A. Razavi, J.-F. Carpentier, *Polymer* **2008**, *49*, 2039-2045.

[64] N. Yu, M. Nishiura, X. Li, Z. Xi, Z. Hou, *Chem. Asian J.* **2008**, *3*, 1406-1414.

[65] D. Barisic, D. A. Buschmann, D. Schneider, C. Maichle-Mössmer, R. Anwander, *Chem. Eur. J.* **2019**, *25*, 4821-4832.

[66] D. Barisic, J. Lebon, C. Maichle-Mössmer, R. Anwander, *Chem. Comm.* **2019**, *55*, 7089-7092.

[67] W. J. Evans, D. G. Giarikos, N. T. Allen, *Macromolecules* **2003**, *36*, 4256-4257.

[68] F. M. B. Coutinho, T. C. J. Rocha, I. L. Mello, D. S. S. Nunes, B. G. Soares, M. A. S. Costa, *J. Appl. Polym. Sci.* **2005**, *98*, 2539-2543.

[69] I. L. Mello, F. M. B. Coutinho, *Eur. Polym. J.* **2008**, *44*, 2893-2898.

[70] T. C. J. Rocha, F. M. B. Coutinho, B. G. Soares, *Polymer Bulletin* **2009**, *62*, 1-10.

[71] M. B. Smith, *J. Organomet. Chem.* **1970**, *22*, 273-281.

[72] S. Inoue, Y. Yokoo, *Bull. Chem. Soc. Jpn* **1972**, *45*, 3651-3653.

[73] W. J. Evans, T. M. Champagne, J. W. Ziller, *Chem. Comm.* **2005**, 5925-5927.

[74] M. Zimmermann, N. Å. Frøystein, A. Fischbach, P. Sirsch, H. M. Dietrich, K. W. Törnroos, E. Herdtweck, R. Anwander, *Chem. Eur. J.* **2007**, *13*, 8784-8800.

[75] H. M. Dietrich, K. W. Törnroos, R. Anwander, *Angew. Chem. Int. Ed.* **2011**, *50*, 12089-12093.

[76] K. Ziegler, *Angew. Chem.* **1963**, *13*, 545-552.

[77] P. J. Shapiro, W. P. Schaefer, J. A. Labinger, J. E. Bercaw, W. D. Cotter, *J. Am. Chem. Soc.* **1994**, *116*, 4623-4640.

[78] S. Arndt, M. U. Kramer, W. Fegler, Y. Nakajima, I. Del Rosal, R. Poteau, T. P. Spaniol, L. Maron, J. Okuda, *Organometallics* **2015**, *34*, 3739-3747.

[79] C. O. Hollfelder, L. N. Jende, D. Diether, T. Zelger, R. Stauder, C. Maichle-Mössmer, R. Anwander, *Catalysts* **2018**, *8*.

[80] H.-M. Sommerfeldt, C. Meermann, M. G. Schrems, K. W. Törnroos, N. Å. Frøystein, R. J. Miller, E.-W. Scheidt, W. Scherer, R. Anwander, *Dalton Trans.* **2008**, 1899-1907.

[81] W. J. Evans, J. T. Leman, R. D. Clark, J. W. Ziller, *Main Group Met. Chem.* **2000**, *23*, 163-168.

[82] W. J. Evans, L. Chamberlain, T. A. Ulibarri, J. W. Ziller, *J. Am. Chem. Soc.* **1988**, *110*, 6423-6432.

[83] I. L. Mello, F. M. B. Coutinho, B. G. Soares, D. S. S. Nunes, M. A. S. Costa, L. C. d. S. Maria, *Quím. Nova* **2004**, *27*, 277-286.

[84] H. Lehmkuhl, W. Eisenbach, *Liebigs Ann. Chem.* **1967**, *705*, 42-53.

[85] O. Michel, C. Meermann, K. W. Törnroos, R. Anwander, *Organometallics* **2009**, *28*, 4783-4790.

[86] D. T. Hurd, *J. Org. Chem.* **1948**, *13*, 711-713.

[87] E. B. Baker, H. H. Sisler, *J. Am. Chem. Soc.* **1953**, *75*, 5193-5195.

[88] R. L. Gerteis, R. E. Dickerson, T. L. Brown, *Inorg. Chem.* **1964**, *3*, 872-875.

[89] M. Hülsmann, B. Neumann, H.-G. Stammler, N. W. Mitzel, *Eur. J. Inorg. Chem.* **2012**, 4200-4209.

[90] F. W. Frey, P. Koebetz, G. C. Robinson, T. O. Sistrunk, *J. Org. Chem.* **1961**, *26*, 2950-2953.

[91] H. Lehmkuhl, *Angew. Chem.* **1963**, *75*, 1090-1097.

[92] H. Lehmkuhl, W. Eisenbach, *Angew. Chem.* **1962**, *74*, 779-780.

[93] J. H. Medley, F. R. Fronczek, N. Ahmad, M. C. Day, R. D. Rogers, C. R. Kerr, J. L. Atwood, *J. Crystallogr. Spectrosc. Res.* **1985**, *15*, 99-107.

[94] G. A. L. Rosch, C.Kruger, Y.-H.Tsay, *Z. Naturforsch. B* **1983**, *38*.

[95] O. Michel, H. M. Dietrich, R. Litlabø, K. W. Törnroos, C. Maichle-Mössmer, R. Anwander, *Organometallics* **2012**, *31*, 3119-3127.

[96] J. García-Álvarez, E. Hevia, A. R. Kennedy, J. Klett, R. E. Mulvey, *Chem. Comm.* **2007**, 2402-2404.

[97] M. U. Kramer, D. Robert, Y. Nakajima, U. Englert, T. P. Spaniol, J. Okuda, *Eur. J. Inorg. Chem.* **2007**, 665-674.

[98] C. Lichtenberg, T. P. Spaniol, J. Okuda, *Organometallics* **2011**, *30*, 4409-4417.

[99] M. R. Kunze, J. Sieler, R. Taube, *Z. Anorg. Allg. Chem.* **2008**, *634*, 1045-1050.

[100] W. Hallwachs, A. Schafarik, *Liebigs Ann. Chem.* **1859**, *109*, 206-209.

[101] K. Ziegler, W.-R. Kroll, W. Larbig, O.-W. Steudel, *Liebigs Ann. Chem.* **1960**, *629*, 53-89.

[102] K. Ziegler, E. Holzkamp, *Liebigs Ann. Chem.* **1957**, *605*, 93-97.

[103] H. Lehmkuhl, O. Olbrysch, H. Nehl, *Liebigs Ann. Chem.* **1973**, 708-714.

[104] O. Michel, K. W. Törnroos, C. Maichle-Mössmer, R. Anwander, *Chem. Eur. J.* **2011**, *17*, 4964-4967.

[105] O. Michel, S. König, K. W. Törnroos, C. Maichle-Mössmer, R. Anwander, *Chem. Eur. J.* **2011**, *17*, 11857-11867.

[106] O. Michel, K. Yamamoto, H. Tsurugi, C. Maichle-Mössmer, K. W. Törnroos, K. Mashima, R. Anwander, *Organometallics* **2011**, *30*, 3818-3825.

[107] B. M. Wolf, C. Stuhl, C. Maichle-Mössmer, R. Anwander, *Organometallics* **2019**, *38*, 1614-1621.

[108] M. Westerhausen, C. Birg, H. Nöth, J. Knizek, T. Seifert, *Eur. J. Inorg. Chem.* **1999**, 2209-2214.

[109] X. Shi, Z. Liu, J. Cheng, *Dalton Trans.* **2019**, *48*, 17919-17924.

[110] M. R. Crimmin, M. S. Hill, P. B. Hitchcock, M. F. Mahon, *New J. Chem.* **2010**, *34*, 1572-1578.

[111] N. Pour, Y. Gofer, D. T. Major, D. Aurbach, *J. Am. Chem. Soc.* **2011**, *133*, 6270-6278.

[112] S. Krieck, H. Görls, M. Westerhausen, *Organometallics* **2008**, *27*, 5052-5057.

[113] A. Koch, S. Krieck, H. Görls, M. Westerhausen, *Organometallics* **2017**, *36*, 994-1000.

[114] J. Langer, S. Krieck, H. Görls, G. Kreisel, W. Seidel, M. Westerhausen, *New J. Chem.* **2010**, *34*, 1667-1677.

[115] G.-W. Parshall, J.-J. Mrowca, *Adv. Organomet. Chem.* **1969**, *7*, 157-209.

[116] M.-C. Chen, J. A. S. Roberts, A. M. Seyam, L. Li, C. Zuccaccia, N. G. Stahl, T. J. Marks, *Organometallics* **2006**, *25*, 2833-2850.

[117] L. L. Liu, L. L. Cao, Y. Shao, D. W. Stephan, *J. Am. Chem. Soc.* **2017**, *139*, 10062-10071.

[118] W. R. Mariott, L. O. Gustafson, E. Y. X. Chen, *Organometallics* **2006**, *25*, 3721-3729.

[119] S. Komiya, T. Yamamoto, A. Yamamoto, A. Takenaka, Y. Sasada, *Acta Cryst. Sect. B* **1979**, *35*, 2702-2704.

[120] C. McDade, V. C. Gibson, B. D. Santarsiero, J. E. Bercaw, *Organometallics* **1988**, *7*, 1-7.

[121] G. Occhipinti, C. Meermann, H. M. Dietrich, R. Litlabø, F. Auras, K. W. Törnroos, C. Maichle-Mössmer, V. R. Jensen, R. Anwander, *J. Am. Chem. Soc.* **2011**, *133*, 6323-6337.

[122] M. G. Klimpel, R. Anwander, M. Tafipolsky, W. Scherer, *Organometallics* **2001**, *20*, 3983-3992.

[123] M. G. Schrems, H. M. Dietrich, K. W. Törnroos, R. Anwander, *Chem. Comm.* **2005**, 5922-5924.

[124] A. M. Bienfait, B. M. Wolf, K. W. Törnroos, R. Anwander, *Organometallics* **2015**, *34*, 5734-5744.

[125] H.-M. Sommerfeldt, C. Meermann, K. W. Törnroos, R. Anwander, *Inorg. Chem.* **2008**, *47*, 4696-4705.

[126] R. Litlabø, K. Saliu, M. J. Ferguson, R. McDonald, J. Takats, R. Anwander, *Organometallics* **2009**, *28*, 6750-6754.

[127] J. Hao, H. Song, C. Cui, *Organometallics* **2009**, *28*, 3100-3104.

[128] A. Fischbach, M. G. Klimpel, M. Widenmeyer, E. Herdtweck, W. Scherer, R. Anwander, *Angew. Chem. Int. Ed.* **2004**, *43*, 2234-2239.

[129] A. Krenzer, Eberhard Karls Universität Tübingen, PhD Thesis, **2016**.

[130] P. M. Morse, Q. D. Shelby, D. Y. Kim, G. S. Girolami, *Organometallics* **2008**, *27*, 984-993.
[131] A. Fischbach, F. Perdih, E. Herdtweck, R. Anwander, *Organometallics* **2006**, *25*, 1626-1642.
[132] D. M. Roitershtein, A. A. Vinogradov, A. A. Vinogradov, K. A. Lyssenko, Y. V. Nelyubina, I. V. Anan'ev, I. E. Nifant'ev, V. A. Yakovlev, N. N. Kostitsyna, *Organometallics* **2013**, *32*, 1272-1286.
[133] D. M. Roitershtein, A. A. Vinogradov, K. A. Lyssenko, I. V. Ananyev, V. A. Yakovlev, N. N. Kostitsyna, I. E. Nifant'ev, *Inorg. Chim. Acta* **2019**, *487*, 153-161.
[134] G. R. Giesbrecht, J. C. Gordon, D. L. Clark, B. L. Scott, J. G. Watkin, K. J. Young, *Inorg. Chem.* **2002**, *41*, 6372-6379.
[135] M. Bonath, D. Schädle, C. Maichle-Mössmer, R. Anwander, *Inorg. Chem.* **2021**, *60*, 14952-14968.
[136] S. Arndt, T. P. Spaniol, J. Okuda, *Angew. Chem. Int. Ed.* **2003**, *42*, 5075-5079.
[137] S. Arndt, B. R. Elvidge, P. M. Zeimentz, T. P. Spaniol, J. Okuda, *Organometallics* **2006**, *25*, 793-795.
[138] Z. Hou, M. Nishiura, T. Shima, *Eur. J. Inorg. Chem.* **2007**, 2535-2545.
[139] M. Nishiura, F. Guo, Z. Hou, *Acc. Chem. Res.* **2015**, *48*, 2209-2220.
[140] P. M. Zeimentz, S. Arndt, B. R. Elvidge, J. Okuda, *Chem. Rev.* **2006**, *106*, 2404-2433.
[141] K. Suzuki, T. Nagasawa, L. Barriault, S. Arns, *Triisobutylaluminum*, **DOI 10.1002/047084289**.
[142] R. M. Gauvin, T. Chenal, R. A. Hassan, A. Addad, A. Mortreux, *J. Mol. Catal. A Chem.* **2006**, *257*, 31-40.
[143] C. Boisson, F. Barbotin, R. Spitz, *Macromol. Chem. Phys.* **1999**, *200*, 1163-1166.
[144] N. Martins, F. Bonnet, M. J. P. Visseaux, *Polymer* **2014**, *55*, 5013-5016.
[145] T. J. Woodman, Y. Sarazin, G. Fink, K. Hauschild, M. Bochmann, *Macromolecules* **2005**, *38*, 3060-3067.
[146] A. Bathellier, D. Moreno, L. Maron, C. Dinoi, I. Del Rosal, *Chem. Eur. J.* **2020**, *26*, 13213-13225.
[147] I. Korobkov, S. Gambarotta, *Organometallics* **2009**, *28*, 4009-4019.
[148] E. C. Moinet, Eberhard Karls Universität Tübingen, Master Thesis, **2019**.
[149] O. Tardif, S. Kaita, *Dalton Trans.* **2008**, 2531-2533.
[150] D. J. Berg, R. A. L. Gendron, *Can. J. Chem.* **2000**, *78*, 454-458.
[151] P. Wetzel, Eberhard Karls Universität Tübingen, Bachelor Thesis, **2020**.
[152] J. M. Boncella, R. A. Andersen, *Organometallics* **1985**, *4*, 205-206.
[153] M. Niemeyer, P. P. Power, *Chem. Comm.* **1996**, 1573-1574.
[154] D. J. Berg, R. A. L. Gendron, *Can. J. Chem.* **2000**, *78*, 454-458.
[155] M. Niemeyer, *Z. Anorg. Allg. Chem.* **2000**, *626*, 1027-1029.

[156] J. Langer, S. Krieck, R. Fischer, H. Görls, D. Walther, M. Westerhausen, *Organometallics* **2009**, *28*, 5814-5820.

[157] B. M. Wolf, Eberhard Karls Universität Tübingen **2018**.

[158] K. Izod, W. Clegg, S. T. Liddle, *Organometallics* **2000**, *19*, 3640-3643.

[159] S. Harder, **2004**, *43*, 2714-2718.

[160] R. Shannon, *Acta Cryst. Sect. A* **1976**, *32*, 751-767.

[161] Y. Q. Jia, *J. Solid State Chem.* **1991**, *95*, 184-187.

[162] J. Atwood, G. D. Stucky, *J. Am. Chem. Soc.* **1969**, *91*, 2538-2543.

[163] H. Lehmkuhl, W. Eisenbach, *Angew. Chem. Int. Ed.* **1962**, *1*, 590-591.

[164] W. J. Evans, *Coord. Chem. Rev.* **2000**, *206*, 263-283.

[165] A. R. Petrov, N. K. Pruß, A. V. Churakov, K. A. Rufanov, J. Sundermeyer, *Z. Anorg. Allg. Chem.* **2019**, *645*, 679-682.

[166] M. Karl, G. Seybert, W. Massa, S. Agarwal, A. Greiner, K. Dehnicke, *Z. Anorg. Allg. Chem.* **1999**, *625*, 1405-1407.

[167] P. Girard, J. L. Namy, H. B. Kagan, *J. Am. Chem. Soc.* **1980**, *102*, 2693-2698.

[168] W. J. Evans, D. K. Drummond, H. Zhang, J. L. Atwood, *Inorg. Chem.* **1988**, *27*, 575-579.

[169] D. C. Bradley, J. S. Ghotra, F. A. Hart, *Dalton Trans.* **1973**, *10*, 1021-1023.

[170] B. A. Vaartstra, J. C. Huffman, W. E. Streib, K. G. Caulton, *Inorg. Chem.* **1991**, *30*, 121-125.

[171] S. Petriček, *Z. Anorg. Allg. Chem.* **2005**, *631*, 1947-1952.

[172] COSMO v. 1.61, Bruker AXS Inc., Madison, WI., **2012**.

[173] APEX 3 v. 2017.3-0, Bruker AXS Inc., Madison, WI., **2017**.

[174] L. Krause, R. Herbst-Irmer, G. M. Sheldrick, D. Stalke, *J. Appl. Crystallogr.* **2015**, *48*, 3-10.

[175] G. Sheldrick, *Acta Crystallogr. Sect. C.* **2015**, *71*, 3-8.

[176] C. B. Hübschle, G. M. Sheldrick, B. Dittrich, *J. Appl. Crystallogr.* **2011**, *44*, 1281-1284.

[177] D. Kratzert, J. J. Holstein, I. Krossing, *J. Appl. Crystallogr.* **2015**, *48*, 933-938.

[178] C. F. Macrae, P. R. Edgington, P. McCabe, E. Pidcock, G. P. Shields, R. Taylor, M. Towler, J. van de Streek, *J. Appl. Crystallogr.* **2006**, *39*, 453-457.

[179] POV-Ray v. 3.6, Persistence of Vision Pty. Ltd., Williamstown, Victoria, Australia, **2004**.

E

E.

Publications

E. Publications

Paper I

Divalent Lanthanide Tetraisobutylaluminates: Reactivity and Living Isoprene Polymerization

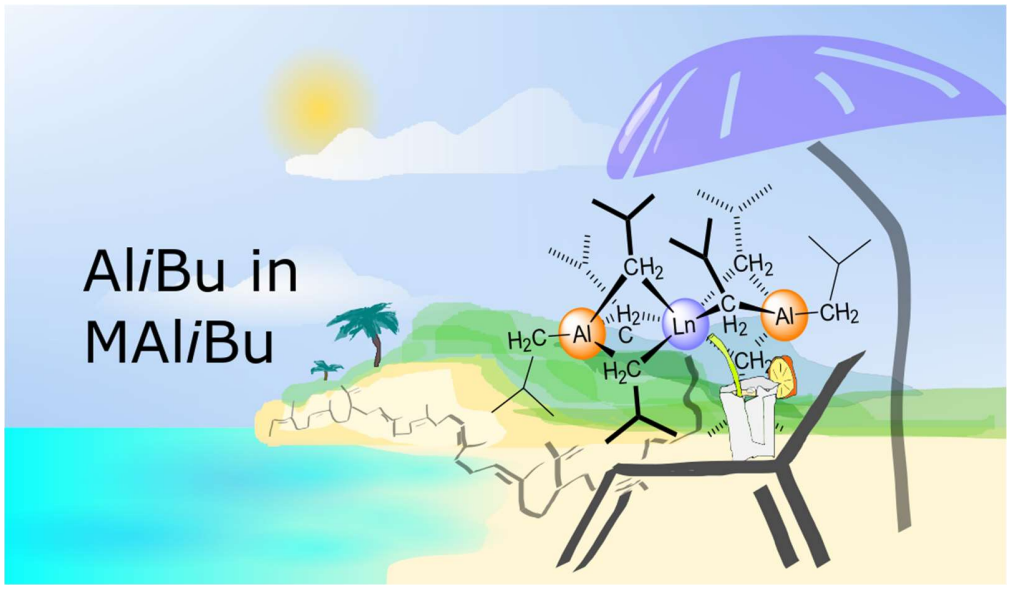

Polymerization Hot Paper

How to cite: *Angew. Chem. Int. Ed.* **2023**, *62*, e202219316
International Edition: doi.org/10.1002/anie.202219316
German Edition: doi.org/10.1002/ange.202219316

Divalent Lanthanide Tetraisobutylaluminates: Reactivity and Living Isoprene Polymerization

*Eric C. Moinet, Benjamin M. Wolf, Olivier Tardif, Cäcilia Maichle-Mössmer, and Reiner Anwander**

Abstract: Lanthanide (Ln) tetraisobutylaluminates constitute key components in commercial 1,3-diene polymerization catalysts, and likewise are the homogeneous rare-earth-metal catalysts of prime industrial importance. Discrete divalent rare-earth-metal complexes [Ln(Al*i*Bu$_4$)$_2$] (Ln = Sm, Eu, Yb) reported here display the first structurally characterized homoleptic metal tetraisobutylaluminates. Treatment of [Ln(Al*i*Bu$_4$)$_2$] with C_2Cl_6 gives access to Sm^{II}/Sm^{III} mixed-valence cluster [Sm$_6$Cl$_8$(Al*i*Bu$_4$)$_6$] and the Yb^{II} cluster [Yb$_4$Cl$_4$(Al*i*Bu$_4$)$_4$], respectively. Reaction with B(C$_6$F$_5$)$_3$ leads to hydride abstraction and formation of arene-coordinated hydroborates such as [Sm{HB(C$_6$F$_5$)$_3$}$_2$(toluene)$_2$]. Complexes [Ln(Al*i*Bu$_4$)$_2$] engage in single-component isoprene polymerization, affording high *cis*-1,4 polyisoprenes with narrow molecular weight distributions. Binary [Yb(Al*i*Bu$_4$)$_2$]/[HNPhMe$_2$][B(C$_6$F$_5$)$_4$] fabricates polyisoprene in a perfectly living manner. The catalytically active species are scrutinized by NMR spectroscopy.

Introduction

Industrial stereospecific 1,3-diene polymerization relies on empirically designed intricate catalyst mixtures.[1–7] Widely deployed rare-earth-metal-based catalysts consist of neodymium compounds (carboxylates, chlorides, alkoxides), Al*i*Bu$_3$ (TIBA), AlEt$_2$Cl, and/or HAl*i*Bu$_2$.[4,7] Highly active catalysts form by ambiguous pathways from these mixtures,[8] yet these are poorly defined.[7] Albeit these systems still lack the option to fine-tune desirable polymer properties, neodymium-based catalysis allows high performance synthetic rubber manufacturing for tires,[9–11] and clearly excels transition-metal catalysis in terms of *cis*-stereoselectivity.[1] Despite of this relevance, the intrinsic chemistry of such catalytic mixtures is still far from fully understood, and model systems usually do not provide information of the species involved in catalysis.[12,13] Albeit lanthanide-tetraisobutylaluminato or -hydrido/isobutyl-heteroaluminato moieties are proposed as active species in isoprene polymerization,[7,14,15] very few complexes involving lanthanide (Ln)-isobutyl moieties have been reported in the literature.[8,16–18] In particular and to the best of our knowledge, structurally authenticated homoleptic tetraisobutylaluminates of any transition/4f metal have remained elusive, and therefore any related reactivity studies. The only crystallographically characterized lanthanide compound featuring a tetraisobutylaluminato moiety according to the Cambridge Crystallographic Data Center (CCDC) was obtained by Evans et al. from the reaction of [Cp*$_2$Sm(THF)$_2$] (Cp* = C$_5$Me$_5$) with TIBA, generating [Cp*$_2$Sm(Al*i*Bu$_4$)] (*i*Bu = CH$_2$CHMe$_2$).[17] Evans et al. also reacted the samarocene(III) carboxylate [Cp*$_2$Sm(O$_2$CPh)]$_2$ with TIBA to obtain carboxylate/isobutyl heteroaluminates [Cp*$_2$Sm(μ-η^1:η^2-O$_2$CPh)(μ-*i*Bu)Al*i*Bu$_2$] and [Cp*$_2$Sm(μ-η^1:η^1-O$_2$CPh)(μ-*i*Bu)Al*i*Bu$_2$], respectively.[18] Moreover, treatment of [Cp*$_2$Sm(O$_2$CPh)]$_2$ with *i*Bu$_2$AlCl yielded the chorido/isobutyl heteroaluminate [Cp*$_2$Sm(μ-Cl)$_2$Al*i*Bu$_2$][18] and addition of TIBA to [Cp*$_2$YCl]$_2$ gave [Cp*$_2$Y(μ-Cl)(μ-*i*Bu)Al*i*Bu$_2$].[19] We have previously embarked on *ansa*-yttrocene alkyl/alkyl heteroaluminates of the type [*rac*-{Me$_2$Si(2-Me-C$_9$H$_5$)$_2$}Y(μ-Me)(μ-R)AlR$_2$] (R = Et, *i*Bu) to investigate into aluminum-mediated chain transfer, but could only obtain structural data on the ethyl derivative.[20] Young et al. characterized alkoxy/isobutyl heteroaluminates [(HO*i*Pr)Sm(μ-O*i*Pr){(μ-O*i*Pr)$_2$Al(*i*Bu)(O*i*Pr)}]$_2$ and [(THF)$_2$Sm(O*t*Bu)$_2${(μ-O*t*Bu)$_2$Al*i*Bu$_2$}] as the only ancillary ligand-free complexes, accessed by reacting [Sm{N(SiMe$_3$)$_2$}$_3$] with Al*i*Bu$_3$ in the presence of 6 equiv of isopropyl alcohol and *tert*-butanol, respectively.[21] Structural motifs observed within these isobutylaluminate complexes are shown in Scheme 1.[22]

Herein, we wish to present the first crystal structures of homoleptic metal tetraisobutylaluminates. The reactivity of compounds [Ln(Al*i*Bu$_4$)$_2$] (Ln = Sm, Eu, Yb) toward oxidizing and cationizing reagents is studied in detail. Particular attention is given to the performance of [Ln(Al*i*Bu$_4$)$_2$] in isoprene polymerization, providing the first well-defined Ln^{II} single-component catalysts.[23–25]

[*] E. C. Moinet, Dr. B. M. Wolf, Dr. C. Maichle-Mössmer, Prof. Dr. R. Anwander
Institut für Anorganische Chemie, Eberhard Karls Universität Tübingen
Auf der Morgenstelle 18, 72076 Tübingen (Germany)
E-mail: reiner.anwander@uni-tuebingen.de
Dr. O. Tardif
Bridgestone Corporation
Ogawahigashi-cho, Kodaira-shi, Tokyo, 187-8531 (Japan)

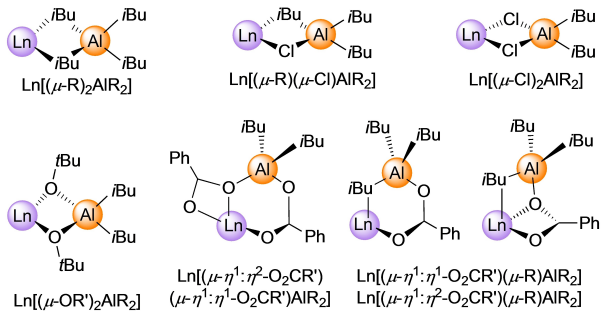

Scheme 1. Structural motifs involving rare-earth-metal isobutyl moieties. Adapted from ref. [3].

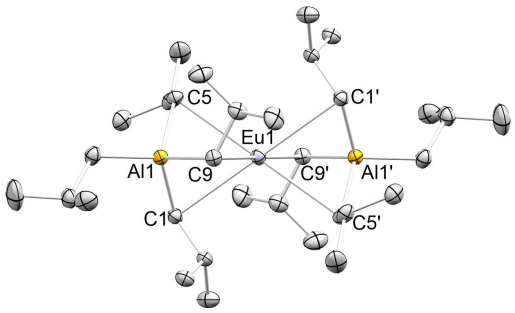

Figure 1. Crystal structure of [Eu(Al*i*Bu$_4$)$_2$] (**1^{Eu}**). Ellipsoids are shown at the 50% probability level. Hydrogen atoms are omitted for clarity. Selected interatomic distances [Å] and angles [°]: Eu(1)–C(1) 2.850(2), Eu(1)–C(5) 2.878(2), Eu(1)–C(9) 2.834(2), Eu(1)–Al(1) 2.9578(6), Al(1)–C(1) 2.065(2), C(1)–Eu(1)–C(1)′ 180.0.

Results and Discussion

Synthesis and Crystal Structure of Divalent Lanthanide Tetraisobutylaluminates [Ln(AliBu_4)$_2$] (Ln = Sm, Eu, Yb)

Twenty years ago, we have communicated that homoleptic divalent complex [Yb(Al*i*Bu$_4$)$_2$] can be obtained in "crystalline form", but that the obtained "crystals" did not produce a diffraction pattern at all.[26] The infeasibility of a solid-state structure was ascribed to the highly mobile/disordered isobutyl groups, which are assumed to counteract proper crystallization. Surprisingly, we now found access to single-crystalline [Sm(Al*i*Bu$_4$)$_2$] (**1^{Sm}**) and determined its crystal structure. Compound **1^{Sm}** was obtained via silylamido elimination from [Sm{N(SiMe$_3$)$_2$}$_2$(THF)$_2$] and TIBA as red-purple crystals.[27] Several recrystallization steps gave 75% yield. Following the same synthesis protocol (equation 1), treatment of [Eu{N(SiMe$_3$)$_2$}$_2$(THF)$_2$] with slight excess (ca. 7 equiv) TIBA gave [Eu(Al*i*Bu$_4$)$_2$] (**1^{Eu}**) in excellent yield (89%).[27] The synthesis of the corresponding methyl- and ethylaluminates [Ln(AlR$_4$)$_2$]$_n$ (Ln = Sm, Eu, Yb; R = Me, Et), which are accessible following a related silylamido elimination protocol with trimethylaluminum, or triethylaluminum, has already been described.[28–30]

$$[Ln\{N(SiMe_3)_2\}_2(THF)_2] + 6\ Al\textit{i}Bu_3 \rightarrow [Ln(Al\textit{i}Bu_4)_2]\ (\mathbf{1^{Ln}}) + 2\ Al\textit{i}Bu_2[N(SiMe_3)_2] + 2\ Al\textit{i}Bu_3(THF)_2 \quad (1)$$

However, [Ln(AlMe$_4$)$_2$]$_n$ are insoluble in aliphatic and aromatic solvents, limiting potential applications.[28–30] The corresponding homoleptic tetraethylaluminates are readily soluble in aliphatic solvents, but display a polymeric structure in the solid state. Isostructural [Ln(AlEt$_4$)$_2$]$_n$ feature agostically linked right-handed helices formally composed of ethyl-bridged [Ln(AlEt$_4$)$_3$]$^-$ and [Ln(AlEt$_4$)]$^+$ building units.[26]

In contrast, the isobutyl congeners [Ln(Al*i*Bu$_4$)$_2$] (**1^{Ln}**, Ln = Sm, Eu, Yb) show both excellent solubility in aliphatic and aromatic solvents and feature the first examples of Ln^{II} tetraalkylaluminate complexes with a discrete monomeric structural motif in the solid state (*cf.* Figure 1, Supporting Information: Figs. S18 and S20). Isostructural **1^{Ln}** revealed an unprecedented η^3-coordination of the monoanionic tetraisobutylaluminato ligands, accomplishing 6-coordinate Ln^{II} centers. For comparison, Evans' trivalent samarocene complex [Cp*$_2$Sm(Al*i*Bu$_4$)] exhibits η^2-coordinated tetraisobutylaluminato moieties.[19] The Ln–C distances in **1^{Ln}** average 2.866 Å (Ln = Sm), 2.854 Å (Ln = Eu), and 2.760 Å (Ln = Yb), in line with the decreasing metal ion radii. For further comparison, divalent 6-coordinate donor adducts like [Ln(AlEt$_4$)$_2$(THF)$_2$] (av. Sm–C 2.774 Å, av. Yb–C 2.663 Å)[28] and [Yb(AlMe$_4$)$_2$(Phen)$_2$] (av. Yb–C, 2.610 Å)[29] display η^2-coordinated alkylaluminato ligands with significantly shorter Ln–C contacts, while 8-coordinate azacrown complex [(TCyTAC)$_2$Sm(AlMe$_4$)$_2$] features η^1-coordinated methylaluminato ligands with elongated Sm–C distances of average 2.948 Å.[31]

Oxidation, Chlorination, and Cationization of [Ln(AliBu_4)$_2$] (Ln = Sm, Yb)

Since trivalent lanthanide complexes are widely used as 1,3-diene polymerization catalysts, we wondered whether complexes **1^{Ln}** (Ln = Sm, Yb) can act as precursors in targeted oxidation reactions. Plumbocene Pb(C$_5$Me$_5$)$_2$ was initially probed as a redox equivalent toward **1^{Ln}** (Ln = Sm, Yb), as it was already successfully used for accessing [(C$_5$Me$_5$)$_2$Ln(AlR$_4$)] from [Ln(AlR$_4$)$_2$]$_n$ (Ln = Sm, Yb; R = Me, Et).[32–35] Accordingly, single-crystalline [(C$_5$Me$_5$)$_2$Sm(Al*i*Bu$_4$)] (**2^{Sm}**) was obtained from treatment of **1^{Sm}** with 1 equiv Pb(C$_5$Me$_5$)$_2$ in quantitative yield (Scheme 2). Note that samarocene **2^{Sm}** was described previously by Evans et al. to form in the reaction of [(C$_5$Me$_5$)$_2$Sm(THF)$_2$] with TIBA (34% yield), including its solid-state structure (see above).[17] Analogously to **2^{Sm}**, the redox protocol gave the isostructural ytterbium congener [(C$_5$Me$_5$)$_2$Yb(Al*i*Bu$_4$)] (**2^{Yb}**) as large, royal blue crystals (Figure 2). Striking is the displacement of the cyclopentadienyl methyl carbon atoms from the cyclopentadienyl ring plane (0.130–0.389 Å),[27] indicating enhanced steric crowding at the Yb^{III} center, comparable to [(C$_5$Me$_5$)$_2$Yb(AlEt$_4$)] (0.059–0.442 Å).[34] This is also reflected in the Yb–C(*i*Bu) distances of 2.6089(18) Å (cf., [(C$_5$Me$_5$)$_2$Yb(AlEt$_4$)]: Yb–C(Et) av. 2.62 Å).

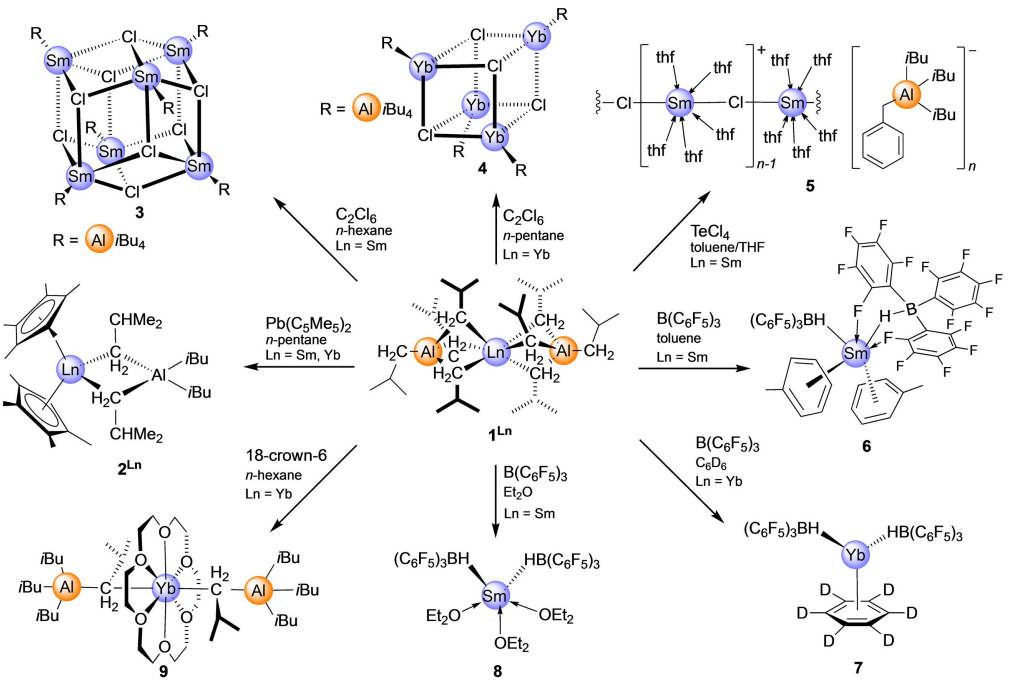

Scheme 2. Overview of derivatizations of [Sm(Al*i*Bu$_4$)$_2$] (**1^{Sm}**) and [Yb(Al*i*Bu$_4$)$_2$] (**1^{Yb}**) employing various oxidants, B(C$_6$F$_5$), and a crown ether.

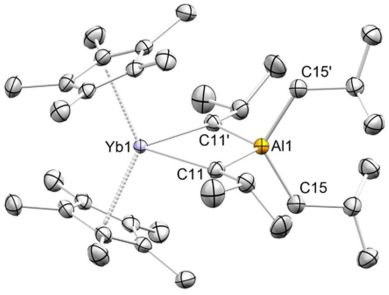

Figure 2. Crystal structure of [(C$_5$Me$_5$)$_2$Yb(Al*i*Bu)$_4$] (**2**). Ellipsoids are shown at the 50% probability level. Hydrogen atoms are omitted for clarity. Selected interatomic distances [Å] and angles [°]: Yb(1)–C(11) 2.6089(18), Yb(1)–Cnt 2.357; Cnt(1)–Yb(1)–Cnt(1)′ 133.74, C(11)′–Yb-(1)–C(11) 79.94(8).

Particular attention was given to the reaction and subsequent chemistry of **1^{Ln}** (Ln = Sm, Yb) with oxidizing chlorido donors. Electron-withdrawing, weakly coordinating chlorido coligands assume a crucial role in commercial Ln^{III}-based Ziegler-type catalysts for stereoselective 1,3-diene polymerization. For example, compounds of composition [Ln(alkyl)$_x$(Cl)$_y$]$_n$ ($x+y=3$) or [Ln$_a$Al$_b$(alkyl)$_c$(Cl)$_d$]$_n$ have been identified as single-component catalysts.[36,37] Noteworthy, trivalent [Sm(AlMe$_4$)$_3$] was previously shown to engage in redox chemistry with precatalyst Et$_2$AlCl forming a black solid ("Sm^{II}" species) exhibiting quite low catalytic activity in isoprene polymerization.[36,37] Fortunately, samarium redox chemistry is accompanied by a color change involving deep purple Sm^{II} and yellow Sm^{III} compounds. Surprisingly, purple-black [Sm(Al*i*Bu$_4$)$_2$] (**1^{Sm}**) proved to be remarkably resilient toward chlorinating reagents. Treatment of **1^{Sm}** with hexachloroethane proceeded without a characteristic color change. From the purple reaction mixture, blackish-green crystals of the Sm^{II}/Sm^{III} mixed-valence cluster [Sm$_6$Cl$_8$(Al*i*Bu$_4$)$_6$] (**3**) were obtained in moderate yield (47%, (Scheme 2).[27] The highly symmetric dodecametallic cluster **3** consists of a core formed by six samarium ions, each bridged by a total of eight μ_3-chlorido ions (Figure 3/left). Additionally, each samarium ion is flanked by a tetraisobutylaluminato moiety. In total, charge balance requires two Sm^{III} and four Sm^{II} cations. The mixed valency is also reflected in different sets of Sm–C and Sm–Cl distances. The Sm(2)–C (2.767(3), 2.776(3), 3.180 (3) Å; distorted η^3) and Sm(3)–C (2.842(3)-2.853(3) Å; η^3) match those in divalent **1^{Sm}** (2.851(2)–2.885(2) Å), whereas the Sm(1)–C distances amount to 2.576(3), 2.627(3), and 2.953(3) Å (cf., Sm^{III}(AlMe$_4$)$_3$: av. 2.565 Å). Additionally, the Sm–Cl distances are significantly shorter for Sm(1) (2.7370(7)-2.8076(7) Å) than for Sm(2) (2.9487(7)–3.0051 (7) Å), and Sm(3) (2.9291(7)–3.0719(7) Å), indicative of a trivalent Sm(1) center.

Analogously, divalent compound **1^{Yb}** was treated with hexachloroethane, and an X-ray diffraction analysis revealed the formation of Yb^{II} cluster [Yb$_4$Cl$_4$(Al*i*Bu$_4$)$_4$] (**4**) (Scheme 2; Figure 3/right).[27] The cuboid core structure with alternating 6-coordinate ytterbium(II) and μ_3-chlorido ions appears markedly distorted, but similar motifs have been reported previously,[38] also for Ln^{III} ions.[39–41] Since the {Yb$_4$Al$_4$} cluster **4** co-crystallized with precursor [Yb-(Al*i*Bu$_4$)$_2$] (**1^{Yb}**) showing similar solubility, its purification was hampered. The Yb–C(*i*Bu) distances of **4** range form 2.659(7) to 2.690(8) Å, being significantly shorter than those in **1^{Yb}** (av. 2.760 Å). Both clusters **3** and **4** undergo decomposition in solution (*cf.* Figure S5); for **3**, when

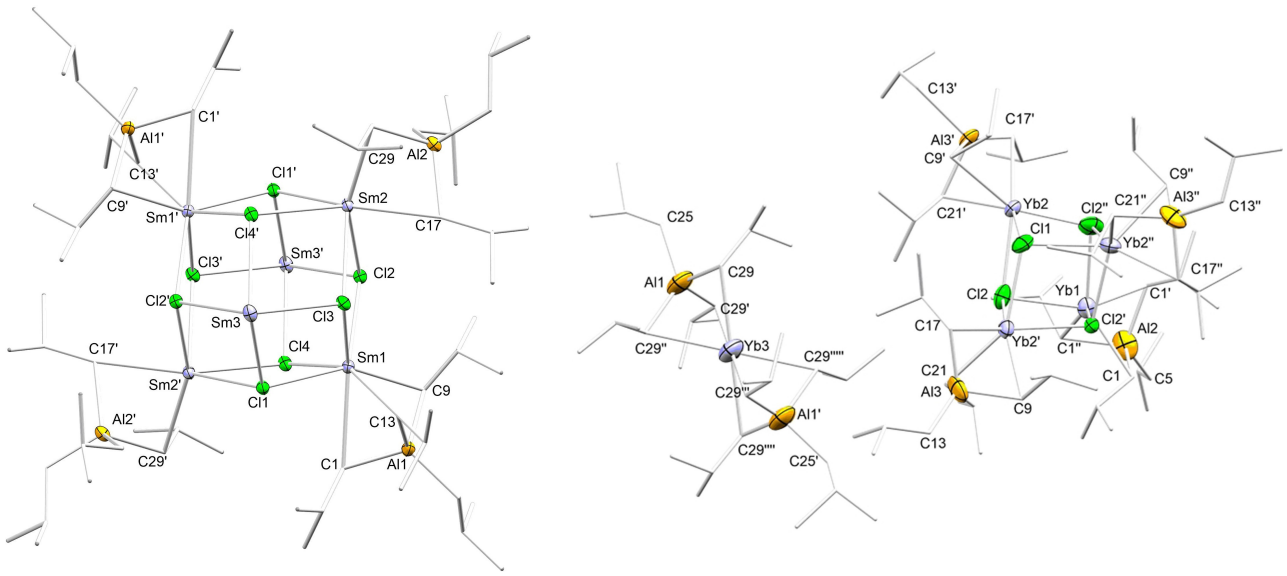

Figure 3. Left: Crystal structure of $[Sm_6Cl_8(AliBu_4)_6]$ (**3**); the tetraisobutylaluminato moiety at Sm(3) and hydrogen atoms are omitted for clarity. Right: $[YbCl_4(AliBu_4)_4]$ (**4**) and co-crystallized $[Yb(AliBu_4)_2]$ ($\mathbf{1^{Yb}}$). Ellipsoids are shown at the 50% probability level. Hydrogen atoms are omitted for clarity. For metrics, see Supporting Information.

dissolved in aromatic solvents decomposition could be observed within seconds at ambient temperature by a rapid color change from dark green to brown.

Decomposition products identified by ^{1}H NMR spectroscopy include TIBA, isobutene, and $\mathbf{1^{Sm/Yb}}$ in deuterated benzene. In aliphatic solvents, decomposition of **3** occurred within several hours, possibly indicating a kinetic effect of the decomposition of the metastable solution of **3**. Ytterbium cluster **4** displays higher stability in deuterated benzene at ambient temperature, but after several days slow decomposition was revealed by the disappearance of one isobutyl signal in the ^{1}H NMR spectrum.

Tellurium(IV) chloride was attempted as a stronger chlorinating oxidant, given its successful use in $Ce^{III}\rightarrow Ce^{IV}$ transformations.[42] Accordingly, treatment of $\mathbf{1^{Sm}}$ with $TeCl_4$ in toluene yielded a dark, oily substance, which could not be crystallized, but which readily dissolved in THF (Scheme 2). The dark purple solution yielded few crystals identified as $\{[SmCl(THF)_5][AlBn\mathit{i}Bu_3]\}_n$ (**5**).[27] The divalent coordination polymer consists of an almost linear chain of alternating samarium(II) and chlorido ions, with the 7-coordinate rare-earth-metal centers additionally coordinated by five THF molecules (Figure 4). The cationic polymeric chain displayed by **5** features a unique structural motif, according to a CCDC search. The Sm1–Cl1 distance of 2.8994(17) is comparable to those in crystalline $SmCl_2$ (2.928(2), CN = 9).[43] The heteroaluminato moiety of the solvent-separated ion pairs in **5** consists of a benzyl (Bn) group along with three isobutyl moieties. Since no oxidation product could be identified, it can be hypothesized that a ligand exchange mechanism applies, involving transient $SmCl_2$ and "tellurium alkylaluminate" or alkyl tellurium species. Rapid decom-

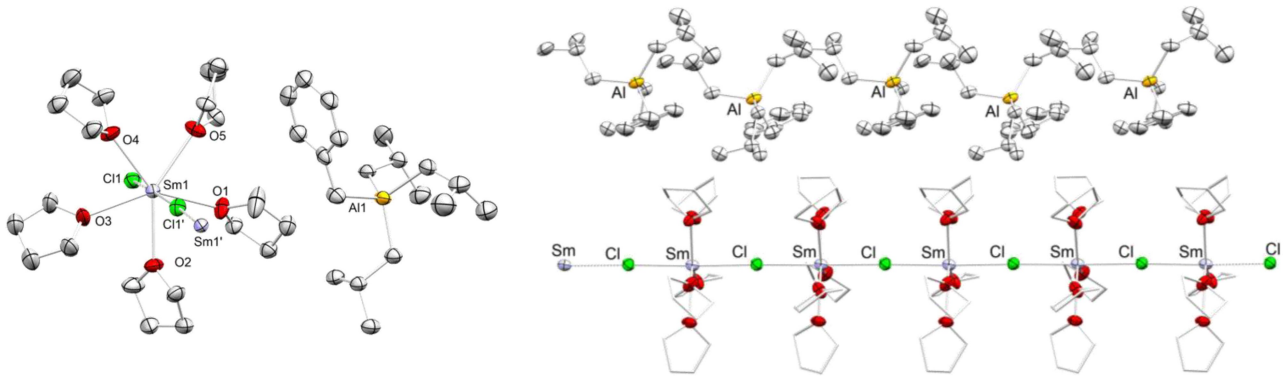

Figure 4. Section of the crystal structure of polymeric $\{[SmCl(THF)_5][AlBn\mathit{i}Bu_3]\}_n$ (**5**) (left), and polymer representation (right). Ellipsoids are shown at the 50% probability level. Hydrogen atoms and lattice THF are omitted for clarity. Selected interatomic distances [Å] and angles [°]: Sm1–Cl1 2.8994(17), Sm1′–Cl1 2.8969(17), av. Sm–O 2.577; Cl1–Sm–Cl1′ 174.80(2). For another view of the polymeric structure and more metrics, see Supporting Information.

position of tellurium alkyls would involve radical formation, followed by activation of toluene, and transfer of the benzyl unit to one of the aluminum centers. Exchange of the isobutylaluminato moiety for chlorido might be kinetically favored over the thermodynamically preferred oxidation of samarium. Alternatively, a transiently formed Sm^{III}–*i*Bu might deprotonate toluene[44] and benzyl/isobutyl heteroaluminato displacement forced by the donor solvent. For further comparison, it has been previously shown that the alkylaluminate complex $[(C_5Me_5)_2Y(AlMe_4)]$ activates benzene and toluene forming phenyl-incorporated heteroaluminato moieties, which can be displaced by a donor solvent like THF.[45] Although we did not succeed in fully characterizing compound **5**, mainly because NMR spectroscopy was not definitive due to the paramagnetic nature of divalent samarium, the solid-state structure of **5** gives evidence of ligand exchange as a scenario that might be favored over oxidation. Although one would generally assume that samarium(II) complexes should be easier to oxidize according to its more negative reduction potential, in some cases ytterbium(II) complexes get faster oxidized, whereas samarium congeners require a certain induction period.[34] Moreover, the reducing effect of the alkylaluminato environment in $\mathbf{1}^{Sm}$ may hinder oxidation to trivalent species.

Finally, cationization was probed as a viable means to prime complexes $\mathbf{1}^{Ln}$ for polymerization reactions. The strongly Lewis-acidic borane $B(C_6F_5)_3$ (**C**) and metal-ion-selective 18-crown-6 were selected as cationizing reactants (Scheme 2). Surprisingly, treatment of $\mathbf{1}^{Sm}$ with one or two equivalents of **C** in toluene both led to the formation of arene-stabilized bis(hydridoborato) complex $[Sm\{HB(C_6F_5)_3\}_2(\eta^6\text{-toluene})_2]$ (**6**) (Figure 5/left)[27] via release of isobutene and TIBA. Similarly, crystalline $[Yb\{HB(C_6F_5)_3\}_2(\eta^6\text{-}C_6D_6)]$ (**7**) (Figure 5/middle)[27] was obtained from the equimolar reaction of $\mathbf{1}^{Yb}$ and $B(C_6F_5)_3$ in C_6D_6 in a microscale reaction (NMR spectra, see Supporting Information). Apparently, the smaller Yb^{II} center in complex **7** allows for accommodation of only one additional arene ligand. The Ln–Centroid(η^6-toluene/benzene) distances in **6** and **7** account to 2.880 and 2.490 Å. η^6-Arene complexes are routinely observed for electron-deficient rare-earth-metal centers in the absence of donor solvent molecules.[46,47] Bis(arene) interactions are less common and are preferably detected for cationized trivalent metallocenes of the type $[(C_5Me_5)_2Ln][BPh_4]$.[48] Notably, divalent complexes $[Yb\{N(SiMe_3)_2\}(BPh_4)]$ and $[Yb\{t\text{Bu}_2\text{pz}\}](BPh_4)]$ exhibit a $\eta^6{:}\eta^6$-coordination of the tetraphenylborato ligands (Yb–centroid 2.489/2.515 Å and 2.513/2.602 Å).[49] Also, fluorenyl ligands are prone to Ln^{II}-size dependent $\eta^5\rightarrow\eta^6$-coordination switches, as revealed in heteroaluminates $Sm[\eta^6\text{-}AlR_3(Flu^{SiMe3})]_2$ (R = Me, Et; Sm–Centroid 2.74 and 2.76 Å) and $Yb[\eta^6\text{-}AlMe_3(Flu^{SiMe3})][\eta^5\text{-}Flu^{SiMe3}]$ (Yb–Centroid(η^6) 2.53 Å).[50] For further comparison, the divalent aryloxylethylalumoxane $[Sm\{O(AlEt_2(OC_6H_2t\text{Bu-2,6-Me-4}))_2\}(\eta^6\text{-toluene})]$ and the aryloxy/methyl heteroaluminate $Sm[AlMe_3(OC_6H_3Ph_2\text{-}2,6)]_2$ display Sm–Centroid(η^6-toluene/Ph) distances of 2.935(7) Å and of av. 2.955 Å, respectively.[51,52]

Addition of diethyl ether to **6** or conducting the reaction in diethyl ether led to samarium borohydride $[Sm\{HB(C_6F_5)_3\}_2(OEt_2)_3]$ (**8**) (Figure 5/right).[27] All complexes feature a tridentate κ^3-H(B),F,F coordination of the fluorinated tri(phenyl)hydridoborato ligand. The Ln^{II}–H and Ln^{II}–F distances in complexes **6–8** avarage 2.59 Å (Sm), 2.26 Å (Yb) and 2.670 Å (Sm), 2.418 Å (Yb), respectively. Calcium and ytterbium complexes $[M\{HB(C_6F_5)_3\}_2(THF)_2]$ (M = Ca, Yb) with similar bonding pattern were examined by the Sadow group.[53] These complexes were accessed from alkyls $[M\{C(SiHMe_2)_3\}_2(THF)_2]$ and **C** via β-hydride(SiH) abstraction. Sadow et al. reported also on discrete trivalent derivatives $[Ln\{C(SiHMe_2)_3\}_{3-x}\{HB(C_6F_5)_3\}_x]$ (Ln = La, Ce, Pr, Nd; $x = 1$, 2), which, when activated with Al*i*Bu_3, generated catalysts for butadiene polymerization, implying Ln–$C(SiHMe_2)_3$/Al*i*Bu_3 exchange.[54]

Like Lewis acids, oxygen-donor molecules were shown to produce cationic organorare-earth-metal moieties with charge-balancing separated tetraalkylaluminato anions. Representative examples include THF adducts $[\eta^5\text{-(fluorenyl)Yb(THF)}_4][AlMe_4]$,[50] $[Cp^*Yb(THF)_4][AlMe_4]$,[29] $[Y(CH_2SiMe_3)_2(THF)_4][Al(CH_2SiMe_3)_4]$[55] or the crown ether derivatives $[YMe(12\text{-crown-4})_2][AlMe_4]_2$ and

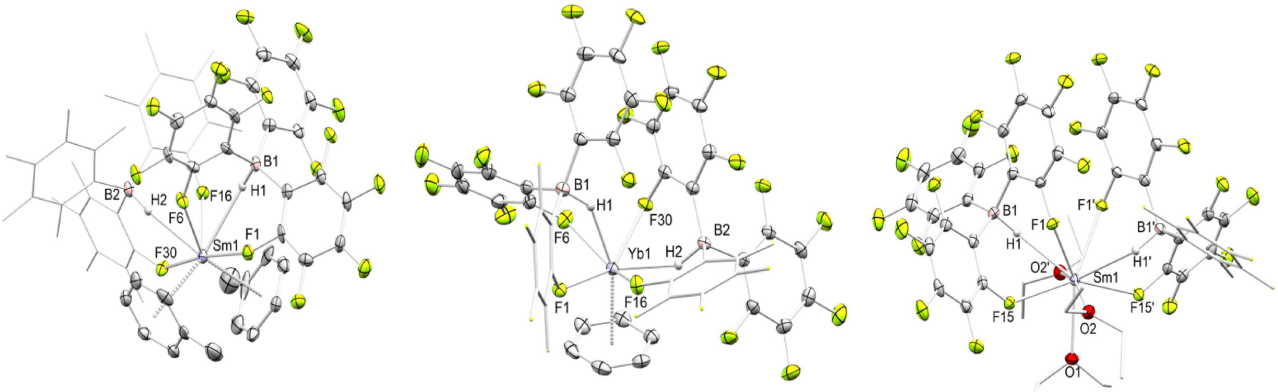

Figure 5. Crystal structures of $[Sm\{HB(C_6F_5)_3\}_2(\eta^6\text{-toluene})_2]$ (**6**), $[Yb\{HB(C_6F_5)_3\}_2(\eta^6\text{-benzene})]$ (**7**), and $[Sm\{HB(C_6F_5)_3\}_2(Et_2O)_3]$ (**8**). Ellipsoids are shown at the 50% probability level. Hydrogen atoms and lattice solvent are omitted for clarity. For metrics, see Supporting Information.

$[PrMe(18\text{-crown-}6)_2][AlMe_4]_2$.[56] The reaction of $\mathbf{1^{Yb}}$ with 18-crown-6 simply led to the coordination of the crown ether without displacement of the tetraisobutylaluminato moieties, affording $[Yb(18\text{-crown-}6)(Al\textit{i}Bu_4)_2]$ (**9**) (Figure 6).[27] The centric circular coordination of the crown ether enforces an unprecedented η^1-coordination of the tetraisobutylaluminato ligands and a linear C(1)-Yb(1)-C(1)′ angle. The Yb–C distance of 2.9159(19) Å in **9** is markedly longer than the 2.735(16)-2.796(12) Å in precursor $\mathbf{1^{Yb}}$. As observed for $\mathbf{1^{Yb}}$, **9** revealed no broadening or splitting of the ^{1}H NMR resonances even at 190 K, indicating high mobility of the isobutylaluminato groups in solution, even at very low temperature.

Lanthanide(II) Isobutylaluminates in Isoprene Polymerization

So far, very few studies have been reported dealing with the polymerization of conjugated dienes involving divalent lanthanide complexes. Such catalyst systems mainly exploit samarocene(II) derivatives $Cp^R{}_2Sm(THF)_2$ which form trivalent active species through cocatalyst-mediated oxidation (cocatalyst: $Al\textit{i}Bu_3/[Ph_3C][B(C_6F_5)_4]$, MAO or MMAO = modified MAO).[57,58] Unfortunately, samarocene(II) precatalysts are easily inactivated in the absence of suitable cocatalysts by forming thermodynamically favored η^3-allyl complexes.[59] On the other hand, Ln^{III}-based Ziegler-type catalysts, prone to reduction to divalent state (Sm, Eu, Yb), even gave minor quantities or no polymer at all.[3] It was therefore assumed that lanthanides exclusively in the trivalent state exhibit high polymerization activities.[3] Thus, it has been concluded for a long time, that divalent lanthanide complexes are inactive in conjugated diene polymerization, or at least that reduction to divalent species decreases polymerization activity and catalyst productivity. On the other hand, Evans et al. applied LnI_2 (Ln = Nd, Sm, Dy, Tm) or $LnI_2(THF)_2$ (Ln = Sm, Tm) as highly efficient catalysts for *cis*-1,4-selective isoprene polymerization, and noted that there was no correlation between reduction potential and catalyst activity.[60] The addition of triisobutylaluminum to LnI_2 enhanced the polymerization performance, accounting for a higher monomer conversion, higher molecular weight and even narrower molecular weight distribution, but was not required.[60]

Naturally, we were interested in examining the rare-earth-metal isobutylaluminates $[Ln(Al\textit{i}Bu_4)_2]$ ($\mathbf{1^{Ln}}$) (Ln = Sm, Eu, Yb) in isoprene polymerization. Main benefits of these systems comprise excellent solubility in aromatic and aliphatic solvents (compared to LnI_2), and the diamagnetic properties of $[Yb(Al\textit{i}Bu_4)_2]$ ($\mathbf{1^{Yb}}$), thus allowing monitoring with ^{1}H NMR spectroscopy. To probe $\mathbf{1^{Ln}}$ in isoprene polymerization, we applied borane/borate, or dialkylaluminum chloride cocatalysts, as well as using solely $\mathbf{1^{Ln}}$ for comparison. Application of an equimolar amount of borate cocatalysts $[CPh_3][B(C_6F_5)_4]$ (**A**) and $[C_6H_5NMe_2H][B(C_6F_5)_4]$ (**B**) activate $\mathbf{1^{Ln}}$, resulting in high polymer yields, especially with cocatalyst **B** (*cf.* entries 2–3, 8–9, and 12–13). Generally, the binary systems $\mathbf{1^{Sm}}$/**B** and $\mathbf{1^{Eu}}$/**B** gave predominantly 1,4-*trans* polymers whereas $\mathbf{1^{Yb}}$/**B** produced a lower *trans* content. Upon activation with **A**, and **B**, very narrow molecular weight distributions were observed. Especially catalyst system $\mathbf{1^{Yb}}$/**B** revealed an ideal living polymerization behavior (entry 13). Scrutinizing the binary system $\mathbf{1^{Yb}}$/**B** via addition of extra monomer after complete conversion of the previous batch, showed that the PDIs stayed in the range of 1.02–1.05, while the monomer consumption and hence molecular weight increased linearly after each additional monomer addition (Table 1, entry 14–17; *cf.* Figure 7), proving perfectly living polymerization for the binary system $\mathbf{1^{Yb}}$/**B**.

Polymers obtained from $\mathbf{1^{Ln}}$ activated with cocatalyst **C** did generally yield very little to no polymer at all (entry 4, 10, and 18). This is not surprising, taking into account that $[Sm\{HB(C_6F_5)_3\}_2(\eta^6\text{-toluene})_2]$ (**6**), obtained from $\mathbf{1^{Sm}}$/**C**, is inactive in isoprene polymerization (entry 23). The remaining side products may account for the (low) catalytic activity. This is also consistent with the relatively high PDI (entry 4), which indicates the formation of different catalytically active side products.

No polymers were obtained when complexes $\mathbf{1^{Ln}}$ were activated with cocatalyst **D** (dimethylaluminum chloride) or **E** (diethylaluminum chloride) (entries 5, 10, 18). As shown

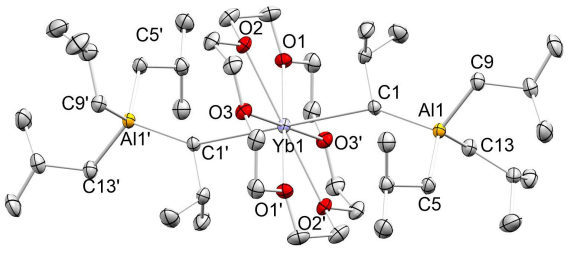

Figure 6. Crystal structure of $[Yb(Al\textit{i}Bu_4)_2(18\text{-crown-}6)]$ (**9**). Ellipsoids are shown at the 50% probability level. Hydrogen atoms and lattice THF are omitted for clarity. Selected interatomic distances [Å] and angles [°]: Yb1–C1 2.9159(19), av. Yb–O 2.6384; C1–Yb–C1′ 180.00(6). For more metrics, see Supporting Information.

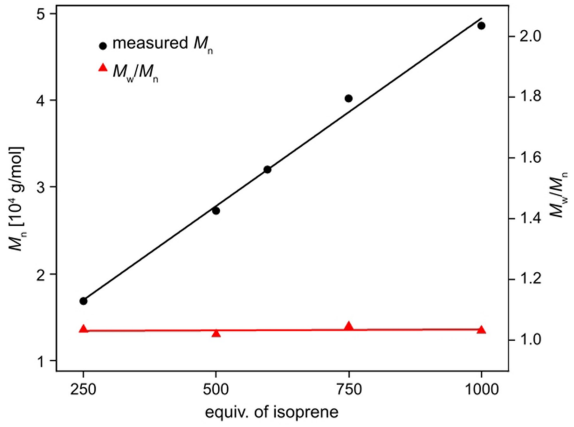

Figure 7. Isoprene polymerization with $\mathbf{1^{Yb}}$/**B**. Molecular weight vs. equiv. of isoprene.

Table 1: Isoprene homopolymerization

entry[a]	pre-catalyst	co-catalyst[b]	reaction time [h]	[IP]/[Ln]	yield [%]	*cis*-1,4[c] [%]	*trans*-1,4[c] [%]	3,4[c] [%]	M_n[d] [10^4 g mol^{-1}]	PDI[d]	T_G[e] [°C]
1	$\mathbf{1}^{Sm}$	none	4	1000	20	77.97	1.86	20.17	5.7	1.52	−53
2	$\mathbf{1}^{Sm}$	**A**	24	1000	>99	16.87	74.69	8.44	4.0	1.30	−63
3	$\mathbf{1}^{Sm}$	**B**	1	1000	>99	27.60	60.23	12.17	4.8	1.21	−59
4	$\mathbf{1}^{Sm}$	**C**	24	1000	12	37.49	55.51	7.00	1.4	5.15	−63
5	$\mathbf{1}^{Sm}$	**D**, or **E**	24	1000	0	–	–	–	–	–	–
6	$\mathbf{1}^{Eu}$	none	24	1000	>99	76.68	0	23.32	39.0	1.62	−49
7	$\mathbf{1}^{Eu}$	none	1	1000	41	75.69	0	24.31	26.6	1.40	−48
8	$\mathbf{1}^{Eu}$	**A**	24	1000	>99	18.16	70.80	11.04	3.7	1.29	−61
9	$\mathbf{1}^{Eu}$	**B**	24	1000	>99	25.62	61.22	13.16	6.1	1.12	−58
10	$\mathbf{1}^{Eu}$	**C**, **D**, or **E**	24	1000	0	–	–	–	–	–	–
11	$\mathbf{1}^{Yb}$	none	1	1000	94	81.82	5.43	12.75	6.0	1.92	−58
12	$\mathbf{1}^{Yb}$	**A**	24	1000	33	46.23	25.42	28.35	2.1	1.24	−46
13	$\mathbf{1}^{Yb}$	**B**	1	1000	>99	54.92	14.14	30.94	5.4	1.10	−41
14[f]	$\mathbf{1}^{Yb}$	**B**	2	250	>99	54.15	14.14	31.71	1.7	1.04	−45
15[f]	$\mathbf{1}^{Yb}$	**B**	3	500	>99	53.27	15.29	31.44	2.7	1.02	−45
16[f]	$\mathbf{1}^{Yb}$	**B**	4	750	>99	51.61	16.79	31.60	4.0	1.05	−44
17[f]	$\mathbf{1}^{Yb}$	**B**	5	1000	>99	53.74	14.71	31.55	4.9	1.03	−43
18	$\mathbf{1}^{Yb}$	**C**, **D**, or **E**	24	1000	0	–	–	–	–	–	–
19[g]	**3**	none	24	1000	0	–	–	–	–	–	–
20[g]	**3**	**A**	2	1000	10	96.9	0	3.1	n.d.	n.d.	n.d.
21[g]	**3**	**C**	2	1000	9	95.1	0	4.9	18.5	2.09	n.d.
22[g]	**3**	**B**, **D**, or **E**	24	1000	0	–	–	–	–	–	–
23	**6**	none	24	1000	0	–	–	–	–	–	–

[a] Conditions: 20 µmol of precatalyst, 20 µmol of cocatalyst, 20 mmol of isoprene, 8 mL of toluene, 500 rpm stirring velocity. [b] Aged with cocatalyst at ambient temperature for 30 min: **A** = $[Ph_3C][B(C_6F_5)_4]$; **B** = $[PhNMe_2H][B(C_6F_5)_4]$; **C** = $B(C_6F_5)_3$; **D** = Me_2AlCl, **E** = Et_2AlCl, 1 equivalent. [c] Determined by $^1H/^{13}C$ NMR spectroscopy in $CDCl_3$. [d] Determined by SEC. [e] Determined by DSC. [f] 20 µmol of precatalyst, 20 µmol of **B** ($[PhNMe_2H][B(C_6F_5)_4]$), 10 mL toluene, aged at ambient temperature for 30 min, addition of isoprene (0.5 mL, 5 mmol) after each hour, 500 rpm stirring velocity. [g] 3.3 µmol of precatalyst, 20 µmol of cocatalyst (which equals 1 equiv. of cocatalyst per [Sm] center), 8 mL of *n*-hexane, 20 mmol of isoprene, n.d. not determined.

above for the synthesis of compounds **3**, **4**, and **5**, the exchange of the isobutylaluminato moiety for chlorido is a likely scenario in this system. In fact, $[Sm(Al\mathit{i}Bu_4)_2]$ rapidly formed a dark-brownish precipitate when treated with chlorido donors **D**, **E**, and $\mathit{i}Bu_2AlCl$ (**F**), indicating that -according to the color- a presumably divalent chloride salt precipitates, which prevents the formation of species active in isoprene polymerization.

Much to our surprise, $[Sm(Al\mathit{i}Bu_4)_2]$ ($\mathbf{1}^{Sm}$) polymerized isoprene even in the absence of a cocatalyst, yielding a polyisoprene with high *cis*-1,4 content, and a relatively narrow molecular weight distribution (entry 1). To elucidate the effect of a possible redox scenario, we probed $\mathbf{1}^{Eu}$ and $\mathbf{1}^{Yb}$ without prior activation (entries 6, 7, and 11, respectively). Remarkably, $\mathbf{1}^{Eu}$ and $\mathbf{1}^{Yb}$ afforded much higher polymer yields than $\mathbf{1}^{Sm}$, with similar polymer microstructure. Oddly, very high molecular weight polymers were observed for $\mathbf{1}^{Eu}$ as a catalyst (entry 6, and 7), which may be caused by a small amount of catalytically active europium.

Investigations into the Catalytically Active Ln^{II} Species

Since $\mathbf{1}^{Sm}$ and $\mathbf{1}^{Eu}$ are paramagnetic, the reactivity of ytterbium(II) isobutylaluminate $\mathbf{1}^{Yb}$ was probed toward cocatalysts **A**, **B**, **C**, and **F**, and the reaction was monitored by ^1H NMR spectroscopy (Figures 8 and 9, Figures S11–S17). No paramagnetic broadening/shifting of proton resonances was observed with any cocatalyst, indicating that ytterbium remains in its divalent state entirely. The equimolar reaction of $\mathbf{1}^{Yb}$ with cocatalyst **A** in benzene-d_6 produced triphenylmethane, isobutene, and TIBA. Besides the complete consumption of $\mathbf{1}^{Yb}$, a new isobutyl signal set appeared, which is assigned to putative active species "$[Yb(Al\mathit{i}Bu_4)][B(C_6F_5)_4]$" (Figure 8). The hydride abstraction with cocatalyst **A** as indicated by isobutene formation is a little surprising, taking into account that similar reactivity was observed when $\mathbf{1}^{Ln}$ was treated with $B(C_6F_5)_3$, affording complexes $[Sm\{HB(C_6F_5)_3\}_2(\eta^6\text{-toluene})_2]$ (**6**) and $[Yb\{HB(C_6F_5)_3\}_2(\eta^6\text{-}C_6D_6)]$ (**7**) (see above).

The equimolar reaction of $\mathbf{1}^{Yb}$ with **B** in deuterated benzene was also monitored by ^1H NMR spectroscopy (Figure 9). Proceeding protonolysis of one tetraisobutylaluminato ligand was revealed by the formation of isobutane and the dimethylaniline adduct of TIBA. Isobutene was not formed, which indicated that no further decomposition by β-hydride elimination of the activation product occurred. Besides, a new isobutyl signal set appeared, which may be assigned to a cationized tetraisobutylaluminate complex "$[Yb(Al\mathit{i}Bu_4)\{Al\mathit{i}Bu_3(PhNMe_2)\}][B(C_6F_5)_4]$" as putative active species. This implies the formation of a similar activation product as obtained with cocatalyst **A**, however, the overall solubility of the mixture with cocatalyst **B** is slightly better, and also the polymer properties are different.

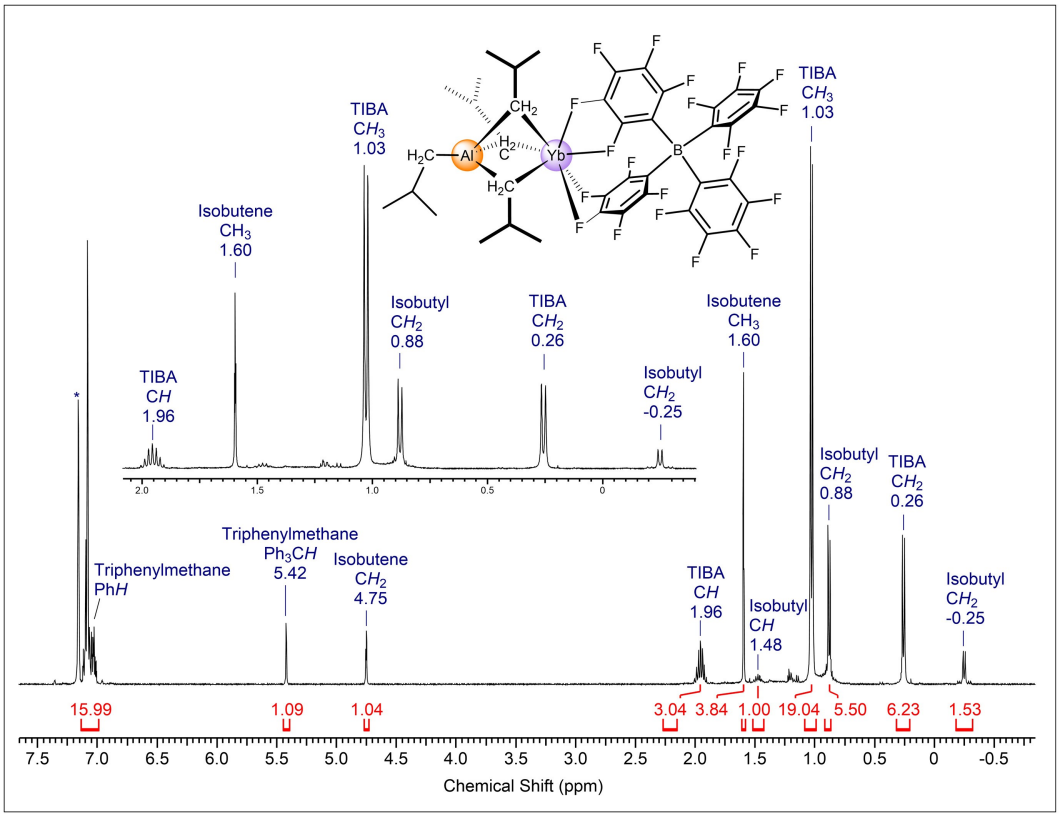

Figure 8. ^{1}H NMR spectrum (400 MHz, C_6D_6, 26 °C) of the reaction of $\mathbf{1}^{Yb}$ with one equivalent of cocatalyst **A**, and proposed active species.

Thus, it is likely that the TIBA-dimethylaniline adduct interacts with the active species, making it both more soluble, and thus more active. With cocatalyst **A**, a slightly broader molecular weight distribution was observed, which may indicate that the lower catalyst solubility hinders simultaneous polymerization initiation, while the growing polymer chains improve solubility. However, activation with **B** led to an ideal living polymerization, because the binary system $[Yb(Ali Bu_4)_2]/[PhNMe_2H][B(C_6F_5)_4]$ ($\mathbf{1}^{Yb}$/**B**) exhibits good solubility in toluene. Therefore, we propose "$[Yb(Ali Bu_4)\{Ali Bu_3(PhNMe_2)\}][B(C_6F_5)_4]$" (*cf.* Figure 9) as putative active species, which engages in living isoprene polymerization.

In contrast to the clear NMR spectra observed for the reactions of $\mathbf{1}^{Yb}$ with one equiv. **A** or **B**, the activation with **C** revealed the formation of several isobutyl signal sets, alongside with isobutene and TIBA (Figs. S15–S16). The mixture of different isobutyl species observed by ^{1}H NMR spectroscopy for $\mathbf{1}^{Yb}$/**C** is consistent with the broad molecular weight distribution of the respective polymer, indicating the presence of several active species. The formation of a large amount of isobutene indicates that hydride species are formed upon activation. Moreover, the ^{1}H NMR resonances of precursor $\mathbf{1}^{Yb}$ are still present in the spectra, indicating an incomplete consumption. In fact, $[Yb\{HB(C_6F_5)_3\}_2(C_6D_6)]$ (**7**) crystallized from a 1:1 reaction mixture of $\mathbf{1}^{Yb}$ and $B(C_6F_5)_3$ (**C**) in benzene-d_6 and the concomitant formation of isobutene was observed (see above). The reaction of $\mathbf{1}^{Yb}$ with one equiv. $i Bu_2AlCl$ (**F**) gave proton resonances of free TIBA and unreacted precursor $\mathbf{1}^{Yb}$ (Figure S17). This may underline the propensity of the system to form hardly soluble $[Yb^{II}Cl_x]_n$ species by ligand exchange, instead of putative $[Yb\text{-}(\mu\text{-}ClAli Bu_3)_x]$ heteroaluminato species. Strikingly, the binary system $\mathbf{1}^{Yb}$/**F** did not fabricate polymer despite of the presence of unreacted single-component catalyst $\mathbf{1}^{Yb}$. This may be ascribed to the effect of TIBA to decrease the degree of polymerization by chain transfer, or else that $[YbCl_x]_n$ species impede the polymerization activity of $\mathbf{1}^{Yb}$.

Again, the occurrence of a tentative scrambling reaction resembles the reactivity of $\mathbf{1}^{Sm}$ with tellurium(IV)-chloride, leading to $\{[SmCl(THF)_5][AlBn i Bu_3]\}_n$ (**5**), where ligand redistribution seems to be favored over oxidation of samarium. In contrast to $[Sm(Ali Bu_4)_2]$ ($\mathbf{1}^{Sm}$), $[Sm_6Cl_8(Ali Bu_4)_6]$ (**3**) behaved inert toward polymerization without prior activation with a cocatalyst (entry 19). This provides credible evidence that chlorido-bridged lanthanide(II) aluminates are inactive in polymerization, thus explaining the inactivity of equimolar mixtures of $\mathbf{1}^{Ln}$ (Ln = Sm, Eu, Yb) and R_2AlCl (R = Me, Et) in isoprene polymerization.

Upon activation of **3** with cocatalysts **B**, **D**, or **E**, brownish suspensions were obtained, which did not produce any polyisoprene (entry 22). Some polyisoprene obtained with the **3**/**A** catalyst mixture did not dissolve at all. Eventually, this may indicate the formation of a cross-linked polymer (entry 20). The microstructure therefore corre-

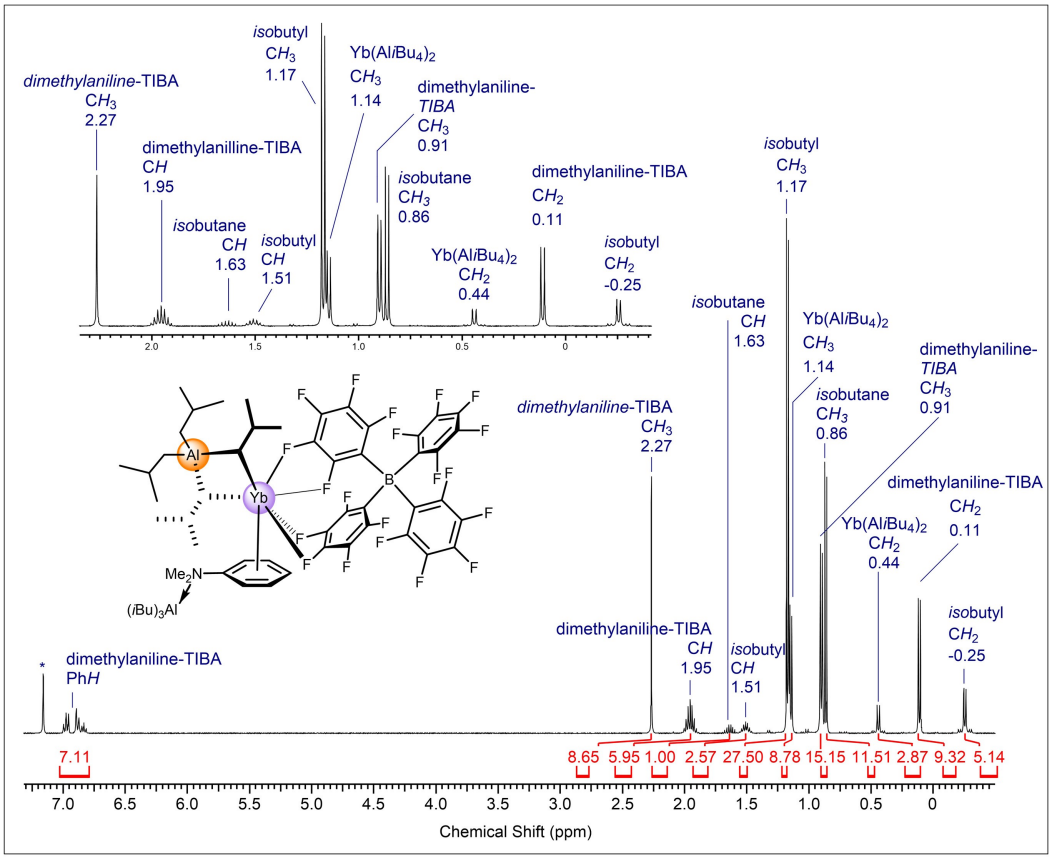

Figure 9. ^{1}H NMR spectrum (400 MHz, C_6D_6, 26 °C) of the reaction of $\mathbf{1}^{Yb}$ with one equivalent of cocatalyst **B**, and proposed active species.

sponds to the soluble polymer fraction. Additionally, the polyisoprene obtained with **3**/**A** maintained the orange color during quenching, and after drying. This suggests incorporation of non-dissolved "heterogeneous catalyst" **3** into the polymer, which possibly limits its activity and explains the low polymer yields. Remarkably, the polymers obtained with **3** and cocatalysts **A** and **C** consisted almost entirely of pure *cis*-1,4 polyisoprene (97 % and 95 %), with no *trans*-1,4 polyisoprene detected.

Conclusion

Discrete complexes $[Sm(Al\mathit{i}Bu_4)_2]$, $[Eu(Al\mathit{i}Bu_4)_2]$, and $[Yb(Al\mathit{i}Bu_4)_2]$ are well accessible from $[Ln\{N(SiMe_3)_2\}_2(THF)_2]$ (Ln = Sm, Eu, Yb) and excess $Al\mathit{i}Bu_3$ (TIBA) in high yield. For the first time, such homoleptic rare-earth-metal tetraisobutylaluminates have been fully characterized including X-ray structure analyses. Complexes $[Ln(Al\mathit{i}Bu_4)_2]$ (Ln = Sm, Yb) engage readily in a plethora of derivatization reactions, including oxidation, chlorination and cationization. Chlorinating reagents give predominantly $Al\mathit{i}Bu_4$/Cl ligand exchange as shown for the isolation of Yb^{II} cluster $[Yb_4Cl_4(Al\mathit{i}Bu_4)_4]$ and polymeric $[\{SmCl(THF)_5\}(AlBn\mathit{i}Bu_3)]_n$. However, involvement of the increasingly redox-active samarium(II) can also result in partial oxidation as revealed for the Sm^{II}/Sm^{III} mixed-valence cluster $[Sm_6Cl_8(Al\mathit{i}Bu_4)_6]$. Facile oxidations of $[Ln(Al\mathit{i}Bu_4)_2]$ (Ln = Sm, Yb) occurred with $Pb(C_5Me_5)_2$ giving trivalent lanthanidocenes $[Cp^*_2Ln(Al\mathit{i}Bu_4)]$. Attempted isobutylaluminato abstraction with $B(C_6F_5)_3$ led to β-hydride abstraction and formation of arene-stabilized hydroborato complexes $[Sm\{HB(C_6F_5)_3\}_2(toluene)_2]$ and $[Yb\{HB(C_6F_5)_3\}_2(benzene)]$. Isobutylaluminato displacement from $[Yb(Al\mathit{i}Bu_4)_2]$ with 18-crown-6 was not observed, but simply the donor adduct $[Yb(Al\mathit{i}Bu_4)_2(18\text{-crown-6})]$.

The Sm^{II}/Sm^{III} mixed-valence cluster $[Sm_6Cl_8(Al\mathit{i}Bu_4)_6]$ is not active in isoprene polymerization without cocatalyst, but fabricates 1,4-*trans*-free polyisoprene with a *cis* stereoselecivity up to 97 % with borane/borate cocatalysts. Remarkably, divalent $[Ln(Al\mathit{i}Bu_4)_2]$ display single-component catalysts for the homopolymerization of isoprene, yielding a high-*cis* polymer with a small PDI, with no *trans*-1,4 content detectable for $[Eu(Al\mathit{i}Bu_4)_2]$. Any correlation between redox potential and polymerization activity was not observed, indicating that divalent lanthanide species are highly active in isoprene polymerization. The absence of any catalytically active ytterbium(III) species is also supported by NMR-spectroscopic examination of the equimolar binary systems $[Yb(Al\mathit{i}Bu_4)_2]/[CPh_3][B(C_6F_5)_4]$ and $[Yb(Al\mathit{i}Bu_4)_2]/[PhNMe_2H][B(C_6F_5)_4]$. Therefore, the present work is one of the first to deal with divalent lanthanides in successful conjugated 1,3-diene polymerization. The binary system $[Yb(Al\mathit{i}Bu_4)_2]/[PhNMe_2H][B(C_6F_5)_4]$ features ideal

living polymerization behavior with polydispersity indices of 1.02–1.05, with "[Yb(Al*i*Bu$_4$){Al*i*Bu$_3$(PhNMe$_2$)}][B(C$_6$F$_5$)$_4$]" as the active species suggested by NMR spectroscopy.

Acknowledgements

We thank Bridgestone Corporation for generous support. Open Access funding enabled and organized by Projekt DEAL.

Conflict of Interest

The authors declare no conflict of interest.

Data Availability Statement

The data that support the findings of this study are available in the Supporting Information of this article.

Keywords: Cluster · Isobutylaluminate · Lanthanides · Living Isoprene Polymerization · Single-Component Catalyst

[1] G. Ricci, G. Pampaloni, A. Sommazzi, F. Masi, *Macromolecules* **2021**, *54*, 5879–5914.
[2] L. Friebe, O. Nuyken, W. Obrecht, *Adv. Polym. Sci.* **2006**, *204*, 1–154.
[3] A. Fischbach, R. Anwander, *Adv. Polym. Sci.* **2006**, *204*, 155–281.
[4] Z. Zhang, D. Cui, B. Wang, B. Liu, Y. Yang, in *Molecular Catalysis of Rare-Earth Elements* (Ed.: P. W. Roesky), Springer, Berlin, Heidelberg, **2010**, pp. 49–108.
[5] J. Jothieswaran, S. Fadlallah, F. Bonnet, M. Visseaux, *Catalysts* **2017**, *7*, 378.
[6] T. Sone, *Int. Pol. Sci. Tech.* **2016**, *43*, 49–54.
[7] a) W. Gao, D. Cui, *J. Am. Chem. Soc.* **2008**, *130*, 4984–4991; b) W. Rong, M. Wang, S. Li, J. Cheng, D. Liu, D. Cui, *Organometallics* **2018**, *37*, 971–978.
[8] Q. Shen, W. Chen, Y. Jin, C. Shan, *Pure Appl. Chem.* **1988**, *60*, 1251–1256.
[9] M. Nishiura, F. Guo, Z. Hou, *Acc. Chem. Res.* **2015**, *48*, 2209–2220.
[10] F. Yang, X. Li, *J. Polym. Sci. Part A* **2017**, *55*, 2271–2280.
[11] J. Huang, Z. Liu, D. Cui, X. Liu, *ChemCatChem* **2018**, *10*, 42–61.
[12] S. Arndt, K. Beckerle, P. M. Zeimentz, T. Spaniol, J. Okuda, *Angew. Chem. Int. Ed.* **2005**, *44*, 7473–7477; *Angew. Chem.* **2005**, *117*, 7640–7644.
[13] H. M. Dietrich, O. Schuster, K. W. Törnroos, R. Anwander, *Angew. Chem. Int. Ed.* **2006**, *45*, 4858–4863; *Angew. Chem.* **2006**, *118*, 4977–4982.
[14] K. Lv, D. Cui, *Organometallics* **2010**, *29*, 2987–2993.
[15] A. D. Oswald, L. Verrieux, P.-A. R. Breuil, H. Olivier-Bourbigou, J. Thuilliez, F. Vaultier, M. Taoufik, L. Perrin, C. Boisson, *Organometallics* **2022**, *41*, 2106–2118.
[16] For carboxylato/isobutyl heteroaluminates, see: F. Li, Y. Jin, C. Song, Y. Lin, F. Pei, F. Wang, N. Hu, *Appl. Organomet. Chem.* **1996**, *10*, 761–771.
[17] W. J. Evans, J. T. Leman, R. D. Clark, J. W. Ziller, *Main Group Met. Chem.* **2000**, *23*, 163–168.
[18] W. J. Evans, T. M. Champagne, D. G. Giarikos, J. W. Ziller, *Organometallics* **2005**, *24*, 570–579.
[19] W. J. Evans, T. M. Champagne, J. W. Ziller, *Chem. Commun.* **2005**, 5925–5927.
[20] M. G. Klimpel, J. Eppinger, P. Sirsch, W. Scherer, R. Anwander, *Organometallics* **2002**, *21*, 4021–4023.
[21] G. R. Giesbrecht, J. C. Gordon, D. L. Clark, B. L. Scott, J. G. Watkin, K. J. Young, *Inorg. Chem.* **2002**, *41*, 6372–6379.
[22] For the first structurally characterized Ln-*i*Bu complexes, see: T. Berger, D. Baschnagel, C. Maichle-Mössmer, R. Anwander, *Z. Anorg. Allg. Chem.* **2023**, *649*, e202200274.
[23] For the synthesis of *cis*-1,4 polyisoprene via Ln^{III}-single-component living polmerization, see: L. Zhang, T. Suzuki, Y. Luo, M. Nishiura, Z. Hou, *Angew. Chem. Int. Ed.* **2007**, *46*, 1909–1913; *Angew. Chem.* **2007**, *119*, 1941–1945.
[24] For the synthesis of *trans*-1,4 polyisoprene via Ln^{III}-single-component living polmerization, see: M. Zimmermann, K. W. Törnroos, R. Anwander, *Angew. Chem. Int. Ed.* **2008**, *47*, 775–778; *Angew. Chem.* **2008**, *120*, 787–790.
[25] For the synthesis of 3,4-polyisoprene via Ln^{III}-single-component living polmerization, see L. Zhang, Y. Luo, Z. Hou, *J. Am. Chem. Soc.* **2005**, *127*, 14562–14563.
[26] M. G. Klimpel, R. Anwander, M. Tafipolsky, W. Scherer, *Organometallics* **2001**, *20*, 3983–3992.
[27] Deposition numbers 2231690 (for **1^{Sm}**), 2231689 (for **1^{Eu}**), 2231688 (for **1^{Yb}**), 2231693 (for **2^{Yb}**), 2231697 (for **3**), 2231695 (for **4**), 2231696 (for **5**), 2231691 (for **6**), 2231694 (for **7**), 2231692 (for **8**), and 2231698 (for **9**) contain the supplementary crystallographic data for this paper. These data are provided free of charge by the joint Cambridge Crystallographic Data Centre and Fachinformationszentrum Karlsruhe Access Structures service.
[28] M. G. Schrems, H. M. Dietrich, K. W. Törnroos, R. Anwander, *Chem. Commun.* **2005**, 5922–5924.
[29] H.-M. Sommerfeldt, C. Meermann, M. G. Schrems, K. W. Törnroos, N. Å. Frøystein, R. J. Miller, E.-W. Scheidt, W. Scherer, R. Anwander, *Dalton Trans.* **2008**, 1899–1907.
[30] G. Occhipinti, C. Meermann, H. M. Dietrich, R. Litlabø, F. Auras, K. W. Törnroos, C. Maichle-Mössmer, V. R. Jensen, R. Anwander, *J. Am. Chem. Soc.* **2011**, *133*, 6323–6337.
[31] D. Bojer, A. Venogopal, B. Neumann, H.-G. Stammler, N. W. Mitzel, *Angew. Chem. Int. Ed.* **2010**, *49*, 2611–2614; *Angew. Chem.* **2010**, *122*, 2665–2669.
[32] W. J. Evans, K. J. Forrestal, J. T. Leman, J. W. Ziller, *Organometallics* **1996**, *15*, 527–531.
[33] M. P. Coles, P. B. Hitchcock, M. F. Lappert, A. V. Protchenko, *Organometallics* **2012**, *31*, 2682–2690.
[34] A. M. Bienfait, B. M. Wolf, K. W. Törnroos, R. Anwander, *Organometallics* **2015**, *34*, 5734–5744.
[35] B. M. Wolf, C. Stuhl, C. Maichle-Mössmer, R. Anwander, *Chem. Eur. J.* **2018**, *24*, 15921–15929.
[36] A. Fischbach, M. G. Klimpel, M. Widenmeyer, E. Herdtweck, W. Scherer, R. Anwander, *Angew. Chem. Int. Ed.* **2004**, *43*, 2234–2239; *Angew. Chem.* **2004**, *116*, 2284–2289.
[37] C. Meermann, K. W. Törnroos, W. Nerdal, R. Anwander, *Angew. Chem. Int. Ed.* **2007**, *46*, 6508–6513; *Angew. Chem.* **2007**, *119*, 6628–6633.
[38] B. M. Wolf, C. Stuhl, R. Anwander, *Chem. Commun.* **2018**, *54*, 8826–8829.
[39] W.-X. Zhang, Z. Wang, M. Nishiura, Z. Xi, Z. Hou, *J. Am. Chem. Soc.* **2011**, *133*, 5712–5715.
[40] M. B. Ley, D. B. Ravnsbæk, Y. Filinchuk, Y.-S. Lee, R. Janot, Y. W. Cho, J. Skibsted, T. R. Jensen, *Chem. Mater.* **2012**, *24*, 1654–1663.
[41] X.-J. Zhang, F.-Z. Su, D.-M. Chen, Y. Peng, W.-Y. Guo, C.-S. Liu, M. Du, *Dalton Trans.* **2019**, *48*, 1843–1849.

[42] O. Eisenstein, P. B. Hitchcock, A. G. Hulkes, M. F. Lappert, L. Maron, *Chem. Commun.* **2001**, 1560–1561.
[43] G. Meyer, T. Schleid, *J. Less-Common Met.* **1986**, *116*, 187–197.
[44] W. J. Evans, J. M. Perotti, J. W. Ziller, *J. Am. Chem. Soc.* **2005**, *127*, 3894–3909.
[45] M. Bonath, D. Schädle, C. Maichle-Mössmer, R. Anwander, *Inorg. Chem.* **2021**, *60*, 14952–14968.
[46] a) G. B. Deacon, Q. Shen, *J. Organomet. Chem.* **1996**, *506*, 1–17; b) Md. E. Hossain, Z. Guo, J. Wang, G. B. Deacon, P. C. Junk, D. Diether, R. Anwander, *Eur. J. Inorg. Chem.* **2022**, e202101009.
[47] P. M. Zeimentz, S. Arndt, B. R. Elvidge, J. Okuda, *Chem. Rev.* **2006**, *106*, 2404–2433.
[48] W. J. Evans, C. A. Seibel, J. W. Ziller, *J. Am. Chem. Soc.* **1998**, *120*, 6745–6752.
[49] G. B. Deacon, C. M. Forsyth, P. C. Junk, *Eur. J. Inorg. Chem.* **2005**, 817–821.
[50] H. Nakamura, Y. Nakayama, H. Yasuda, T. Maruo, N. Kanehisa, Y. Kai, *Organometallics* **2000**, *19*, 5392–5399.
[51] H.-M. Sommerfeldt, C. Meermann, K. W. Törnroos, R. Anwander, *Inorg. Chem.* **2008**, *47*, 4696–4705.
[52] I. Korobkov, S. Gambarotta, *Organometallics* **2009**, *28*, 4009–4019.
[53] K. Yan, B. M. Upton, A. Ellern, A. D. Sadow, *J. Am. Chem. Soc.* **2009**, *131*, 15110–15111.
[54] B. M. Schmidt, A. Pindwal, A. Venkatesh, A. Ellern, A. J. Rossini, A. D. Sadow, *ACS Catal.* **2019**, *9*, 827–838.
[55] S. Arndt, T. P. Spaniol, J. Okuda, *Angew. Chem. Int. Ed.* **2003**, *42*, 5075–5079; *Angew. Chem.* **2003**, *115*, 5229–5233.
[56] A. Nieland, A. Mix, B. Neumamm, H.-G. Stammler, N. W. Mitzel, *Dalton Trans.* **2010**, *39*, 6753–6760.
[57] S. Kaita, Z. Hou, Y. Wakatsuki, *Macromolecules* **1999**, *32*, 9078–9079.
[58] F. Bonnet, M. Visseaux, D. Barbier-Baudry, *J. Organomet. Chem.* **2004**, *689*, 264–269.
[59] W. J. Evans, T. A. Ulibarri, J. W. Ziller, *J. Am. Chem. Soc.* **1990**, *112*, 2314–2324.
[60] W. J. Evans, D. G. Giarikos, N. T. Allen, *Macromolecules* **2003**, *36*, 4256–4257.

Manuscript received: December 30, 2022
Accepted manuscript online: February 14, 2023
Version of record online: March 15, 2023

Zitierweise: *Angew. Chem. Int. Ed.* **2023**, *62*, e202219316
Internationale Ausgabe: doi.org/10.1002/anie.202219316
Deutsche Ausgabe: doi.org/10.1002/ange.202219316

Polymerisation | Hot Paper

Zweiwertige Lanthanoid-Tetraisobutylaluminate: Reaktivität und lebende Isoprenpolymerisation

*Eric C. Moinet, Benjamin M. Wolf, Olivier Tardif, Cäcilia Maichle-Mössmer, und Reiner Anwander**

Abstract: Lanthanoid (Ln)-Tetraisobutylaluminate sind Schlüsselkomponenten in kommerziell genutzten Katalysatoren für die 1,3-Dienpolymerisation und sind gleichsam Seltenerdmetall-Katalysatoren von wesentlicher industrieller Relevanz. Die hier beschriebenen, diskreten zweiwertigen Seltenerdmetall-Komplexe [Ln(Al*i*Bu$_4$)$_2$] (Ln = Sm, Eu, Yb) sind die ersten strukturell charakterisierten, homoleptischen Tetraisobutylaluminat-Komplexe. Durch Umsetzen von [Ln(Al*i*Bu$_4$)$_2$] mit C_2Cl_6 wird der gemischtvalente Sm^{II}/Sm^{III}-Cluster [Sm_6Cl_8(Al*i*Bu$_4$)$_6$], sowie der Yb^{II}-Cluster [Yb_4Cl_4(Al*i*Bu$_4$)$_4$] erhalten. Reaktion mit $B(C_6F_5)_3$ führt zur Hydridabstraktion und zur Bildung Aren-koordinierter Hydridoborate, wie beispielsweise [Sm{HB(C_6F_5)$_3$}$_2$(Toluol)$_2$]. Die Komplexe [Ln(Al*i*Bu$_4$)$_2$] sind Einkomponentenkatalysatoren für die *cis*-1,4-selektive Polymerisation von Isopren mit enger Molmassenverteilung. Das Zweikomponentenkatalysatorsystem [Yb(Al*i*Bu$_4$)$_2$]/[HNPhMe$_2$][B(C_6F_5)$_4$] katalysiert die lebende Isoprenpolymerisation, wobei die aktiven, zweiwertigen Spezies mittels NMR-Spektroskopie untersucht werden.

Einleitung

Die industrielle stereospezifische 1,3-Dien-Polymerisation beruht auf komplexen, empirisch entwickelten Mischkatalysatoren.[1–7] Gängige Katalysatorsysteme auf der Basis von Seltenerdmetallen bestehen aus Neodym-Verbindungen (Carboxylate, Chloride, Alkoxide), Al*i*Bu$_3$ (TIBA), $AlEt_2Cl$, und/oder HAl*i*Bu$_2$.[4,7] Hochaktive Katalysatorspezies bilden sich auf komplexe Weise aus diesen Mischungen,[8] allerdings sind diese nur unzureichend charakterisiert.[7] Obwohl diese Systeme die Möglichkeit zur Feinabstimmung gewünschter Polymereigenschaften vermissen lassen, erlaubt die Verwendung von Neodym-Katalysatoren die Herstellung von Hochleistungskautschuk, der überwiegend für Reifen Anwendung findet.[9–11] Dabei ist insbesondere die *cis*-Stereoselektivität ähnlichen, auf Übergangsmetallen-basierten Systemen deutlich überlegen.[1]

Dieser Relevanz ungeachtet ist die zugrundeliegende Chemie derartiger katalytisch aktiver Systeme noch bei Weitem nicht verstanden; zudem liefern verwendete Modellsysteme oft keine Information über in die Katalyse involvierte Metallspezies.[12,13] Obwohl Lanthanoid-Tetraisobutylaluminato- oder Hydrido-Isobutylaluminato-Einheiten als aktive Spezies in der Isoprenpolymerisation postuliert wurden,[7,14,15] sind bisher nur sehr wenige Komplexe mit Lanthanoid(Ln)-Isobutyl-Motiven literaturbekannt.[8,16–18]

Insbesondere wurde unseres Wissens nach bislang über keine strukturell charakterisierten homoleptischen Übergangsmetall- oder 4f-Tetraisobutylaluminat-Komplexe berichtet und dementsprechend gibt es auch keine Reaktivitätsstudien. Der laut Cambridge Crystallographic Data Center (CCDC) einzige kristallographisch charakterisierte Tetraisobutylaluminat-Lanthanoid-Komplex [Cp*$_2$Sm(Al*i*Bu$_4$)] (*i*Bu = CH_2CHMe_2) konnte von Evans et al. durch Reaktion von [Cp*$_2$Sm(THF)$_2$] (Cp* = C_5Me_5) mit TIBA erhalten werden.[17] Zudem gelang es Evans et al., aus dem Samarocen(III)carboxylat [Cp*$_2$Sm(O_2CPh)]$_2$ durch Reaktion mit Triisobutylaluminium die Carboxylato/Isobutyl-Heteroaluminate [Cp*$_2$Sm(μ-η^1:η^2-O_2CPh)(μ-*i*Bu)Al*i*Bu$_2$] sowie [Cp*$_2$Sm(μ-η^1:η^1-O_2CPh)(μ-*i*Bu)Al*i*Bu$_2$] zu gewinnen.[18] Die Reaktion von [Cp*$_2$Sm(O_2CPh)]$_2$ mit *i*Bu$_2$AlCl führte zur Bildung des Chlorido/Isobutyl-Heteroaluminats [Cp*$_2$Sm(μ-Cl)$_2$Al*i*Bu$_2$],[18] wohingegen [Cp*$_2$Y(μ-Cl)(μ-*i*Bu)Al*i*Bu$_2$] durch Umsetzen von [Cp*$_2$YCl]$_2$ mit TIBA isoliert werden konnte.[19]

Wir haben zuvor von *ansa*-Yttrocen-Alkyl/Alkyl-Heteroaluminaten des Typs [*rac*-{Me_2Si(2-Me-C_9H_5)$_2$}Y(μ-Me)(μ-R)AlR_2] (R = Et, *i*Bu) zur Untersuchung des Aluminium-vermittelten Kettentransfers berichtet, konnten allerdings nur das entsprechende Ethyl-Derivat strukturell charakterisieren.[20] Young et al. erhielten die Alkoxy/Isobutyl-Heteroaluminate [(HO*i*Pr)Sm(μ-O*i*Pr){(μ-O*i*Pr)$_2$Al(*i*Bu)(O*i*Pr)}]$_2$, sowie [(THF)$_2$Sm(O*t*Bu)$_2${(μ-O*t*Bu)$_2$Al*i*Bu$_2$}] als bislang einzige Isobutyl-Komplexe ohne stabilisierende Hilfsliganden. Dies gelang durch Reaktion von [Sm{N($SiMe_3$)$_2$}$_3$] mit

[*] E. C. Moinet, Dr. B. M. Wolf, Dr. C. Maichle-Mössmer, Prof. Dr. R. Anwander
Institut für Anorganische Chemie, Eberhard Karls Universität Tübingen
Auf der Morgenstelle 18, 72076 Tübingen (Deutschland)
E-mail: reiner.anwander@uni-tuebingen.de
Dr. O. Tardif
Bridgestone Corporation
Ogawahigashi-cho, Kodaira-shi, Tokyo, 187-8531 (Japan)

Al*i*Bu$_3$ in Gegenwart von sechs Äquivalenten Isopropanol, bzw. *tert*-Butanol.[21] Die in den oben beschriebenen Komplexen beobachteten Strukturmotive sind in Schema 1 gezeigt.[22]

In dieser Arbeit möchten wir die ersten Kristallstrukturen homoleptischer Metall-Tetraisobutylaluminate vom Typ [Ln(Al*i*Bu$_4$)$_2$] (Ln = Sm, Eu, Yb) vorstellen. Eingehend untersucht wird die Reaktivität der Komplexe gegenüber oxidierenden und kationisierenden Reagenzien. Zudem wird auf die katalytischen Eigenschaften der Komplexe [Ln(Al*i*Bu$_4$)$_2$] in der Isoprenpolymerisation eingegangen, welche sich als erste, wohldefinierte zweiwertige Einkomponentenkatalysatoren erwiesen haben.[23–25]

Ergebnisse und Diskussion

Synthese und Kristallstruktur zweiwertiger Lanthanoid-Tetraisobutylaluminate [Ln(Al*i*Bu$_4$)$_2$] (Ln = Sm, Eu, Yb)

Vor zwanzig Jahren berichteten wir über den Komplex [Yb(Al*i*Bu$_4$)$_2$], welcher in "kristalliner Form" erhalten wurde, wenngleich die erhaltenen "Kristalle" mittels Röntgenbeugung keine Reflexe zeigten.[26] Die Schwierigkeit, eine Festkörperstruktur zu erhalten wurde den sehr mobilen bzw. stark fehlgeordneten Isobutylgruppen zugeschrieben, wobei davon ausgegangen wurde, dass diese die Kristallisation beeinträchtigen. Zu unserer Überraschung gelang es nun, einkristallines [Sm(Al*i*Bu$_4$)$_2$] (**1^{Sm}**) und dessen Festkörperstruktur zu erhalten. Die Synthese von **1^{Sm}** gelang mittels einer Silylamido-Eliminierung (vgl. Gleichung 1) ausgehend von [Sm{N(SiMe$_3$)$_2$}$_2$(THF)$_2$] durch Reaktion mit TIBA, wobei **1^{Sm}** als rotviolette Kristalle erhalten wurde,[27] nach mehrfacher Umkristallisation in 75 %iger Ausbeute. Analog konnte aus [Eu{N(SiMe$_3$)$_2$}$_2$(THF)$_2$] mit geringfügigem Überschuss von TIBA (ca. 7 äq.) [Eu(Al*i*Bu$_4$)$_2$] (**1^{Eu}**) in sehr guter Ausbeute gewonnen werden (89 %).[27]

$$[\mathrm{Ln}\{\mathrm{N(SiMe_3)_2}\}_2(\mathrm{THF})_2] + 6\ \mathrm{Al}i\mathrm{Bu_3} \rightarrow [\mathrm{Ln}(\mathrm{Al}i\mathrm{Bu_4})_2]\ (\mathbf{1^{Ln}}) + 2\ \mathrm{Al}i\mathrm{Bu_2}[\mathrm{N(SiMe_3)_2}] + 2\ \mathrm{Al}i\mathrm{Bu_3}(\mathrm{THF}) \quad (1)$$

Die Synthese der Methyl- und Ethylderivate [Ln(AlR$_4$)$_2$]$_n$ (Ln = Sm, Eu, Yb; R = Me, Et), die nach einem ähnlichen Silylamido-Eliminierungsprotokoll mit Trimethyl- bzw. Triethylaluminium zugänglich sind, wurde bereits beschrieben.[28–30]

Als bedeutender Unterschied bleibt hervorzuheben, dass die Methylaluminate [Ln(AlMe$_4$)$_2$]$_n$ in aliphatischen und aromatischen Lösungsmitteln gänzlich unlöslich sind, was mögliche Anwendungen limitiert,[28–30] während die entsprechenden Ethylaluminate [Ln(AlEt$_4$)$_2$]$_n$ sich zwar bereitwillig in aliphatischen Lösungsmitteln lösen lassen, im Festkörper jedoch eine polymere Struktur aufweisen. Die isostrukturellen Komplexe [Ln(AlEt$_4$)$_2$]$_n$ weisen agostisch verknüpfte, rechtshändige Helices auf, welche aus ethylverbrückten [Ln(AlEt$_4$)$_3$]$^-$- und [Ln(AlEt$_4$)]$^+$-Einheiten bestehen.[26] Kontrastierend verfügen die entsprechenden Isobutylaluminate [Ln(Al*i*Bu$_4$)$_2$] (**1^{Ln}**, Ln = Sm, Eu, Yb) über hervorragende Löslichkeit in Aliphaten und Aromaten, und stellen zugleich auch die ersten bekannten Vertreter im Festkörper monomerer Ln^{II}-Tetraalkylaluminate dar. (vgl. Abbildung 1, S18 und S20). Die isostrukturellen Komplexe **1^{Ln}** weisen eine beispiellose η^3-Koordination der monoanionischen Tetraisobutylaluminato-Liganden auf, die zur Hexakoordination der Ln^{II}-Ionen führt.

Vergleichend dazu sind die Tetraisobutylaluminato-Anionen im von Evans publizierten dreiwertigen Samarocen-Komplex [Cp*$_2$Sm(Al*i*Bu$_4$)] η^2-koordiniert.[19] Durchschnittliche Ln–C-Abstände der Komplexe **1^{Ln}** betragen 2.866 Å (Ln = Sm), 2.854 Å (Ln = Eu) und 2.760 Å (Ln = Yb), wie durch die abnehmenden Ionenradien zu erwarten. Zum weiteren Vergleich sind die Ln–C-Abstände der η^2-koordinierten Alkylaluminato-Liganden in zweiwertigen, hexakoordinierten Donoraddukten durchschnittlich 2.774 Å (Sm–C) bzw. 2.663 Å (Yb–C) in [Ln(AlEt$_4$)$_2$(THF)$_2$],[28] und 2.610 Å in [Yb(AlMe$_4$)$_2$(Phen)$_2$][29] und somit signifikant kürzer, wohingegen der achtfach-koordinierte Azakronen-Komplex [(TCyTAC)$_2$Sm(AlMe$_4$)$_2$] η^1-koordinierte Methylaluminato-Liganden mit aufgeweiteten Sm–C-Abständen von durchschnittlich 2.948 Å aufweist.[31]

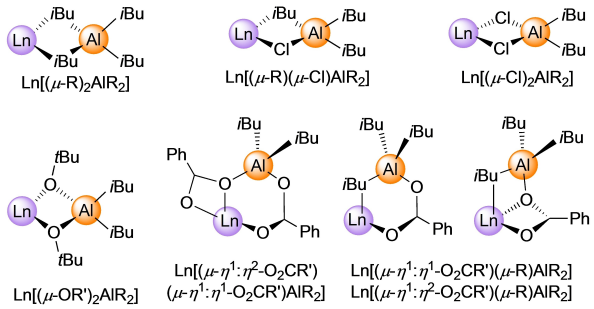

Schema 1. Seltenerdmetall-Isobutyl-Strukturmotive. Basierend auf Quelle 3.

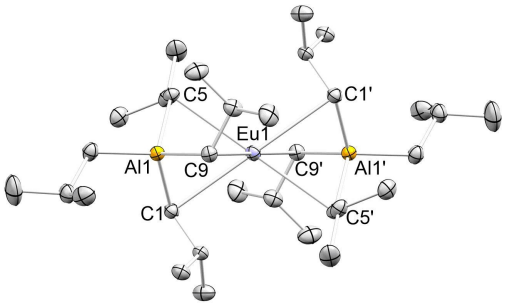

Abbildung 1. Kristallstruktur von [Eu(Al*i*Bu$_4$)$_2$] (**1^{Eu}**). Ellipsoide werden mit einer Wahrscheinlichkeit von 50 % angegeben, auf die Darstellung der Wasserstoffatome wird der Übersichtlichkeit halber verzichtet. Ausgewählte interatomare Abstände [Å] und Winkel [°]: Eu(1)–C(1) 2.850(2), Eu(1)–C(5) 2.878(2), Eu(1)–C(9) 2.834(2), Eu(1)–Al(1) 2.9578(6), Al(1)–C(1) 2.065(2), C(1)–Eu(1)–C(1)′ 180.0.

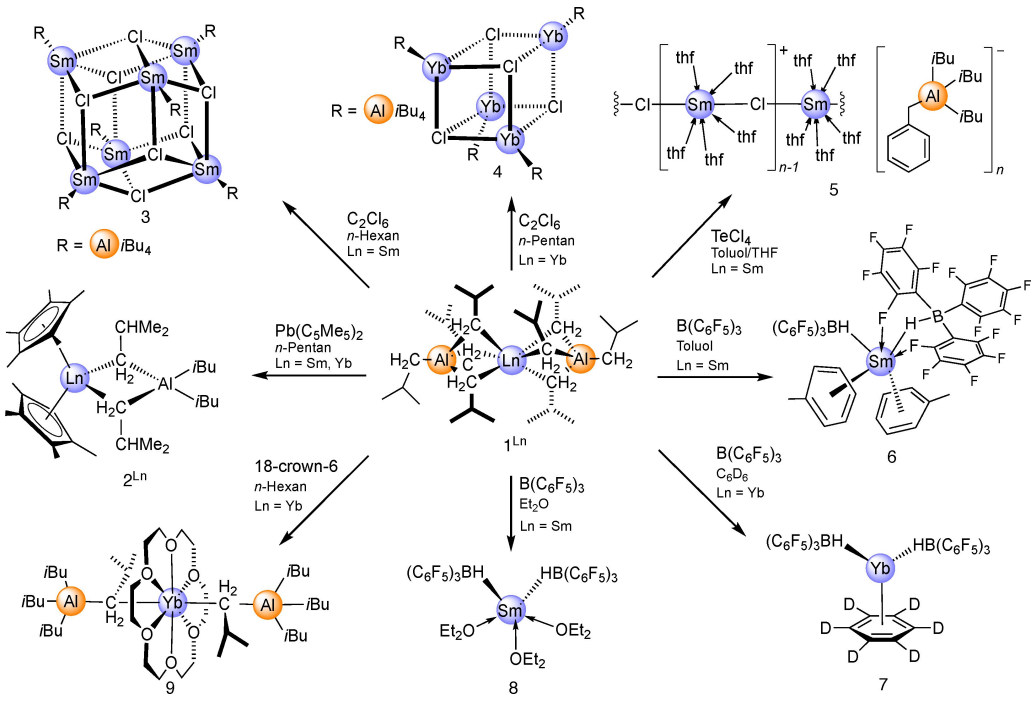

Schema 2. Überblick über die Reaktivität von [Sm(Al*i*Bu$_4$)$_2$] (**1^{Sm}**) und [Yb(Al*i*Bu$_4$)$_2$] (**1^{Yb}**) mit verschiedenen Oxidationsmitteln, B(C$_6$F$_5$), sowie einem Kronenether.

*Oxidation, Chlorierung, und Kationisierung von [Ln(Ali*Bu$_4$)$_2$]* (Ln = Sm, Yb)

Aufgrund der Relevanz dreiwertiger Lanthanoid-Komplexe in der 1,3-Dienpolymerisation stellte sich die Frage, ob die Komplexe **1^{Ln}** (Ln = Sm, Yb) als Edukte für gezielte Oxidationsreaktionen herangezogen werden können. Das Plumbocen-Derivat Pb(C$_5$Me$_5$)$_2$ wurde bereits erfolgreich für die Synthese von [(C$_5$Me$_5$)$_2$Ln(AlR$_4$)], ausgehend von [Ln(AlR$_4$)$_2$]$_n$ (Ln = Sm, Yb; R = Me, Et), eingesetzt.[32–35] Dementsprechend führte die Reaktion von Pb(C$_5$Me$_5$)$_2$ mit **1^{Ln}** (Ln = Sm, Yb) in quantitativer Ausbeute zu einkristallinem [(C$_5$Me$_5$)$_2$Sm(Al*i*Bu$_4$)] (**2^{Sm}**) (Schema 2). Samarocen **2^{Sm}** wurde bereits von Evans et al. durch die Reaktion von [(C$_5$Me$_5$)$_2$Sm(THF)$_2$] mit TIBA in 34 %iger Ausbeute erhalten und strukturell charakterisiert (*siehe weiter vorne*).[17] Analog zu **2^{Sm}** konnte ebenfalls der isostrukturelle Ytterbium-Komplex [(C$_5$Me$_5$)$_2$Yb(Al*i*Bu)$_4$] (**2^{Yb}**) in Form großer, königsblauer Kristalle erhalten werden (Abbildung 2). Bemerkenswert ist die Auslenkung der Methylgruppen des Cyclopentadienylrings aus der Cyclopentadienylringebene (0.130–0.389 Å),[27] was den hohen sterischen Anspruch um das Yb^{III}-Zentralion verdeutlicht, ähnlich wie in [(C$_5$Me$_5$)$_2$Yb(AlEt$_4$)] (0.059–0.442 Å).[34] Dies spiegelt sich auch in den Yb–C(*i*Bu)-Abständen von 2.6089(18) Å wieder (vgl., [(C$_5$Me$_5$)$_2$Yb(AlEt$_4$)]: Yb–C(Et) av. 2.62 Å).

Besonderes Augenmerk wurde auf die Derivatisierung von **1^{Ln}** (Ln = Sm, Yb) mit oxidativen Chlorido-donierenden Reagenzien gerichtet. Elektronenziehenden, schwach-koordinierenden Chlorido-Coliganden wird in kommerziell verwendeten Ln^{III}-Ziegler-Mischkatalysatoren für die stereoselektive Polymerisation konjugierter Diene eine entscheidende Rolle

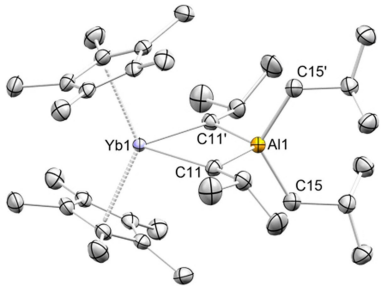

Abbildung 2. Kristallstruktur von [(C$_5$Me$_5$)$_2$Yb(Al*i*Bu)$_4$] (**2**). Ellipsoide werden mit einer Wahrscheinlichkeit von 50 % angegeben, auf die Darstellung der Wasserstoffatome wird der Übersichtlichkeit halber verzichtet. Ausgewählte interatomare Abstände [Å] und Winkel [°]: Yb(1)–C(11) 2.6089(18), Yb(1)–Cnt 2.357; Cnt(1)–Yb(1)–Cnt(1)′ 133.74, C(11)′–Yb(1)–C(11) 79.94(8). Weitere metrische Daten finden sich im Anhang.

zugeschrieben. Beispielsweise wurden Verbindungen der Zusammensetzung [Ln(alkyl)$_x$(Cl)$_y$]$_n$ ($x+y=3$) sowie [Ln$_a$Al$_b$(alkyl)$_c$(Cl)$_d$]$_n$ als Einkomponentenkatalysatoren identifiziert.[36,37] Interessanterweise konnte bereits gezeigt werden, dass dreiwertiges [Sm(AlMe$_4$)$_3$] eine Redoxreaktion mit dem Präkatalysator Et$_2$AlCl unter Bildung eines schwarzen Feststoffes eingeht ("Sm^{II}"-Spezies) und eine bemerkenswert niedrige katalytische Aktivität in der Isoprenpolymerisation aufweist.[36,37]

Glücklicherweise wird die Redoxaktivität von Samarium-Verbindungen von einem Farbwechsel von tief violettem Sm^{II} zu gelbem Sm^{III} begleitet. Überraschenderweise verhielt sich das schwarzviolette [Sm(Al*i*Bu$_4$)$_2$] (**1^{Sm}**) außerordentlich resistent gegenüber chlorierenden Reagenzien. So ergab die

Reaktion von $\mathbf{1}^{Sm}$ mit Hexachlorethan keine charakteristische Farbänderung. Aus der violetten Reaktionsmischung konnten jedoch schwarzgrüne Kristalle des gemischtvalenten Sm^{II}/Sm^{III}-Clusters $[Sm_6Cl_8(Ali Bu_4)_6]$ (**3**) in mäßigen Ausbeuten erhalten werden (47 %, Schema 2).[27] Der hochsymmetrische, dodekametallische Cluster **3** zeigt einen Kern aus sechs Samarium-Kationen und insgesamt acht verbrückenden Chlorido-Anionen (Abbildung 3 links). Zudem wird jedes Samarium-Ion von einem Tetraisobutylaluminato-Anion flankiert. Insgesamt erfordert die Summe der Ladungen zwei Sm^{III}-, sowie vier Sm^{II}-Zentren. Die unterschiedlichen Oxidationszustände spiegeln sich ferner in den verschiedenen Sm–C- und Sm–Cl-Abständen wider: Sm(2)–C (2.767(3), 2.776(3), 3.180 (3) Å; verzerrt η^3) sowie Sm(3)–C (2.842(3)-2.853(3) Å; η^3), welche mit den Sm–C-20en von $\mathbf{1}^{Sm}$ vergleichbar sind (2.851(2)-2.885(2) Å), wohingegen die Sm(1)–C-Abstände 2.576(3), 2.627(3), sowie 2.953(3) Å betragen (vergl., Sm^{III}-$(AlMe_4)_3$: durchschnittlich 2.565 Å). Außerdem sind die Sm–Cl-Abstände für Sm(1) (2.7370(7)-2.8076(7) Å) gegenüber Sm(2) (2.9487(7)-3.0051(7) Å) und Sm(3) (2.9291(7)-3.0719(7) Å) signifikant verkürzt, was auf ein dreiwertiges Sm(1) hindeutet.

Die Reaktion von $\mathbf{1}^{Yb}$ mit Hexachlorethan wurde analog durchgeführt. Die Röntgenbeugungsanalyse des kristallinen Produktes zeigte die Bildung des Yb^{II}-Clusters $[Yb_4Cl_4(Ali Bu_4)_4]$ (**4**) (Schema 2; Abbildung 3, rechts).[27] Die verzerrte, kubanartige Kernstruktur des Clusters besteht alternierend aus 6-fach koordinierten Ytterbium(II)-, sowie μ_3-Chloridionen, wobei ähnliche Strukturmotive bereits literaturbekannt sind,[38] auch für Ln^{III}-Ionen.[39–41] Aufgrund der Cokristallisation des $\{Yb_4Al_4\}$-Clusters **4** mit Edukt $[Yb(Ali Bu_4)_2]$ ($\mathbf{1}^{Yb}$) und der ähnlichen Löslichkeit konnten beide Komplexe nicht separiert werden. Die Yb–C(*i*Bu)-Abstände in **4** betragen zwischen 2.659(7) und 2.690(8) Å, womit sie wesentlich kürzer sind als in $\mathbf{1}^{Yb}$ beobachtet (durchschnittlich 2.760 Å). Sowohl Cluster **3** wie auch **4** zersetzen sich in Lösung (vgl. Abbildung S5); im Falle von Cluster **3** zeigt sich in aromatischen Lösungsmitteln bei Umgebungstemperatur Zersetzung innerhalb weniger Sekunden anhand eines raschen Farbwechsels von dunkelgrün nach braun. Mittels ^{1}H NMR-Spektroskopie in deuteriertem Benzol wurden die Zersetzungsprodukte TIBA, Isobuten und $\mathbf{1}^{Sm}$ identifiziert. Im Gegensatz dazu verlief die Zersetzung von **3** in aliphatischen Lösungsmitteln bei Raumtemperatur über mehrere Stunden, was auf einen kinetischen Einfluss der metastabilen Lösung von **3** hindeuten könnte. Im Gegensatz dazu ist Cluster **4** deutlich beständiger. Dieser ist in Lösung in deuteriertem Benzol bei Umgebungstemperatur kurzzeitig stabil, wobei sich erst nach mehreren Stunden im ^{1}H NMR-Spektrum langsam Zersetzung durch das Verschwinden eines Isobutylsignals zeigt.

Als stärkeres chlorierendes Oxidationsmittel wurde Tellur(IV)-chlorid eingesetzt, welches bereits für $Ce^{III}\rightarrow Ce^{IV}$-Transformationen erfolgreich verwendet wurde.[42] Die Reaktion von $\mathbf{1}^{Sm}$ mit $TeCl_4$ in Toluol ergab eine dunkle, ölige Substanz, die nicht zur Kristallisation gebracht werden konnte, sich aber gut in THF löste (Schema 2). Aus der dunkelvioletten Lösung konnten einige wenige Kristalle erhalten werden, welche als $\{[SmCl(THF)_5][AlBni Bu_3]\}_n$ (**5**) identifiziert werden konnten.[27] Das divalente Koordinationspolymer besteht aus einer annähernd linearen Kette alternierender Samarium(II)- und Chlorido-Ionen, wobei die 7-fach koordinierten Seltenerdmetallzentren zusätzlich von fünf Molekülen THF koordiniert werden (Abbildung 4). Die kationische Polymerkette in **5** ist laut einer CCDC-Recherche einmalig. Der Sm1–Cl1-Abstand von 2.8994(17) ist vergleichbar mit

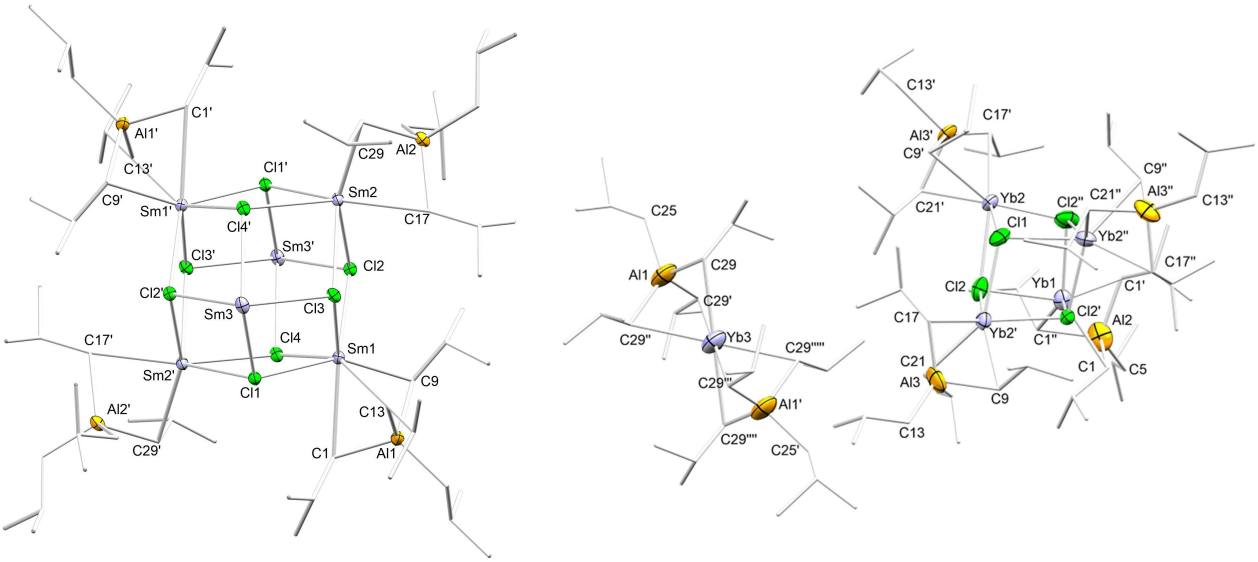

Abbildung 3. Links: Kristallstruktur von $[Sm_6Cl_8(Ali Bu_4)_6]$ (**3**); Ellipsoide werden mit einer Wahrscheinlichkeit von 50 % angegeben, auf die Darstellung der Tetraisobutylaluminateinheit an Sm(3), sowie der Wasserstoffatome wird der Übersichtlichkeit halber verzichtet. Rechts: $[YbCl_4(Ali Bu_4)_4]$ (**4**) und co-kristallisiertes $[Yb(Ali Bu_4)_2]$ ($\mathbf{1}^{Yb}$). Ellipsoide werden mit einer Wahrscheinlichkeit von 50 % angegeben, auf die Darstellung der Wasserstoffatome wird der Übersichtlichkeit halber verzichtet. Ausgewählte interatomare Abstände und Winkel finden sich im Anhang.

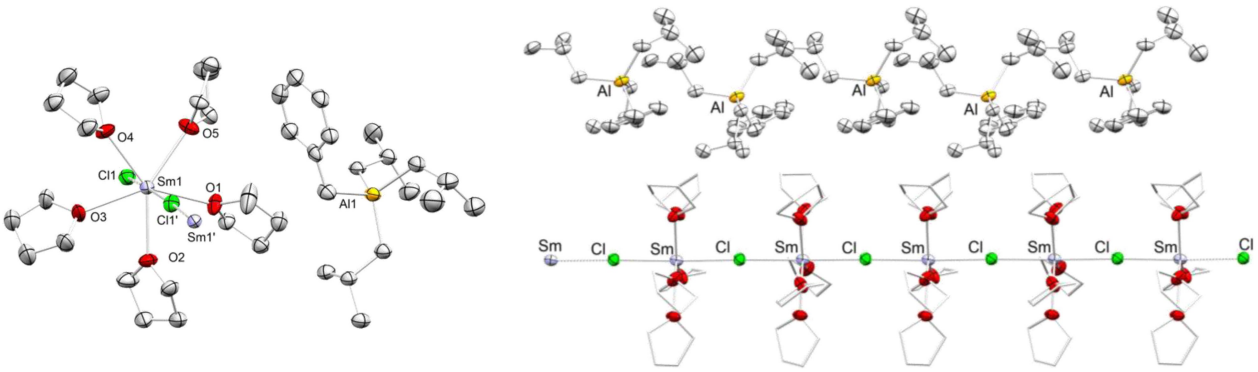

Abbildung 4. Ausschnitt der Kristallstruktur des Koordinationspolymers $\{[SmCl(THF)_5][AlBn_iBu_3]\}_n$ (**5**) (links), sowie Koordinationspolymer (rechts). Ellipsoide werden mit einer Wahrscheinlichkeit von 50% angegeben, auf die Darstellung der Wasserstoffatome und von cokristallisiertem Tetrahydrofuran wird der Übersichtlichkeit halber verzichtet. Ausgewählte interatomare Abstände [Å] und Winkel [°]: Sm1–Cl1 2.8994(17), Sm1′–Cl1 2.8969(17), av. Sm–O 2.577; Cl1–Sm–Cl1′ 174.80(2).

dem in der Festkörperstruktur von $SmCl_2$ gefundenem (2.928(2), KZ = 9).[43] Die Heteroaluminato-Einheit des lösungsmittelseparierten Ionenpaares in **5** enthält neben einer Benzyl(Bn)-Gruppe drei Isobutylreste. Da kein Oxidationsprodukt isoliert werden konnte, kann davon ausgegangen werden, dass es stattdessen zu einem Ligandenaustausch-Szenario kommt, welches vorrübergehend $SmCl_2$ und "Telluraluminat", oder eventuell Alkyltellur-Spezies involviert. Die rasche Zersetzung von Alkyltellur-Spezies könnte die Bildung von Radikalen beinhalten, gefolgt von der Aktivierung von Toluol sowie der Übertragung des Benzylrestes auf eines der Aluminiumzentren. Der Austausch einer Isobutylaluminato-Einheit gegen Chlorido könnte kinetisch über die thermodynamisch günstigere Oxidation bevorzugt sein; alternativ könnte eine kurzlebige Sm^{III}–*i*Bu-Spezies Toluol deprotonieren,[44] und die Abspaltung des resultierenden Benzyl/Isobutyl-Heteroaluminato-Liganden von dem Donor THF erzwungen werden.

Weiterhin wurde bereits gezeigt dass der Alkylaluminat-Komplex $(C_5Me_5)_2Y(AlMe_4)$ Benzol und Toluol unter Bildung von Phenylheteroaluminato-Einheiten aktiviert, die durch ein Donorlösungsmittel wie THF verdrängt werden können.[45] Obwohl es uns nicht gelungen ist, Komplex **5** vollständig zu charakterisieren, insbesondere da die NMR-Spektroskopie aufgrund der paramagnetischen Natur des zweiwertigen Samariums nicht aussagekräftig war, zeigt **5**, dass Ligandenaustausch ein Szenario darstellt, was gegenüber der Oxidation bevorzugt sein kann. Obwohl man im Allgemeinen aufgrund des negativeren Redoxpotentials davon ausgehen würde, dass Samarium(II)-Komplexe leichter oxidierbar sein sollten, werden Ytterbium(II)-Komplexe in einigen Fällen schneller oxidiert, wohingegen entsprechende Samarium-Verbindungen einer gewissen Induktionsperiode bedürfen.[34] Ferner könnte die reduzierende Wirkung der Alkylaluminato-Umgebung in $\mathbf{1}^{Sm}$ die Oxidation zu einer dreiwertigen Spezies behindern.

Schließlich wurde die Derivatisierung von $\mathbf{1}^{Sm}$ mit kationisierenden Reagenzien getestet. Das stark Lewis-azide Boran $B(C_6F_5)_3$ (**C**) sowie der Kronenether 18-Krone-6 wurden als kationisierende Reagenzien ausgewählt (Schema 2). Erstaunlicherweise führte die Reaktion von $\mathbf{1}^{Sm}$ sowohl mit einem, wie auch mit zwei Äquivalenten **C** zur Bildung des selben Aren-stabilisierten Bis(Hydridoborato)-Komplexes $[Sm\{HB(C_6F_5)_3\}_2(\eta^6\text{-Toluol})_2]$ (**6**) (Abbildung 5, links),[27] durch Elimi-

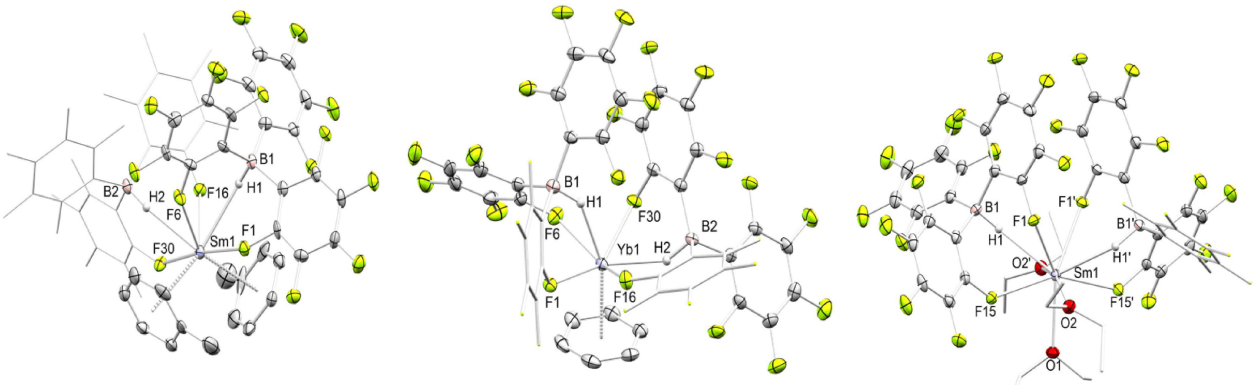

Abbildung 5. Kristallstrukturen von $[Sm\{HB(C_6F_5)_3\}_2(\eta^6\text{-Toluol})_2]$ (**6**), $[Yb\{HB(C_6F_5)_3\}_2(\eta^6\text{-Benzol})]$ (**7**), and $[Sm\{HB(C_6F_5)_3\}_2(Et_2O)_3]$ (**8**). Ellipsoide werden mit einer Wahrscheinlichkeit von 50% angegeben, auf die Darstellung der Wasserstoffatome wird der Übersichtlichkeit halber verzichtet. Ausgewählte interatomare Abstände und Winkel finden sich im Anhang.

nierung von Isobuten und TIBA. Kristalle von Komplex $[Yb\{HB(C_6F_5)_3\}_2(\eta^6\text{-}C_6D_6)]$ (**7**) (Abbildung 5, Mitte)[27] wurden auf ähnliche Weise aus einer äquimolaren Reaktionsmischung aus $\mathbf{1^{Yb}}$ und $B(C_6F_5)_3$ in C_6D_6 in einem NMR-Röhrchen gewonnen (NMR-Spektren im Anhang). Offenbar ist am kleineren Yb^{II}-Ion lediglich Platz für die Koordination eines weiteren Aren-Liganden. Die Ln–Centroid(η^6-Toluol/Benzol)-Abstände in **6** und **7** betragen 2.880, bzw. 2.490 Å. η^6-Aren-Komplexe werden in Abwesenheit von Donorlösungsmittel-Molekülen häufig für elektronenarme Seltenerdmetallzentren beobachtet.[46,47] Bis(Aren)-Wechselwirkungen hingegen sind deutlich seltener und werden meist für dreiwertige Metallocen-Komplexe des Typs $[(C_5Me_5)_2Ln][BPh_4]$ beobachtet.[48] Ferner weisen die zweiwertigen Komplexe $[Yb\{N(SiMe_3)_2\}(BPh_4)]$ und $[Yb\{tBu_2pz\}](BPh_4)]$ eine $\eta^6{:}\eta^6$-Koordination des Tetraphenylborates auf (Yb–Centroid 2.489/2.515 Å und 2.513/2.602 Å).[49] Auch neigen Fluorenyl-Liganden in Abhängigkeit der Ln^{II}-Ionengröße zu $\eta^5{\rightarrow}\eta^6$-Koordinationswechseln, wie die Heteroaluminate $Sm[\eta^6\text{-}AlR_3(Flu^{SiMe3})]_2$ (R = Me, Et; Sm–Centroid 2.74 und 2.76 Å) und $Yb[\eta^6\text{-}AlMe_3(Flu^{SiMe3})][\eta^5\text{-}Flu^{SiMe3}]$ (Yb–Centroid(η^6) 2.53 Å) zeigen.[50] Außerdem weist das divalente Aryloxyethylalumoxane $[Sm\{O(AlEt_2(OC_6H_2tBu\text{-}2,6\text{-}Me\text{-}4))_2\}(\eta^6\text{-}Toluol)]$ sowie das Aryloxy/Methyl-Heteroaluminat $Sm[AlMe_3(OC_6H_3Ph_2\text{-}2,6)]_2$ Sm–Centroid(η^6-Toluol/Ph)-Abstände von 2.935(7) Å bzw. 2.955 Å auf.[51,52] Die Zugabe von Diethylether zu **6** bzw. die Durchführung der Reaktion in Diethylether ermöglichten die Darstellung des Komplexes $[Sm\{HB(C_6F_5)_3\}_2(OEt_2)_3]$ (**8**) (Abbildung 5/rechts).[27]

Die Komplexe **6**–**8** weisen allesamt eine tridentate κ^3-H(B),F,F-Koordination der fluorierten Triphenylhydridoborato-Liganden auf. Die Ln^{II}–H- und Ln^{II}–F-Abstände in den Komplexen **6**–**8** betragen durchschnittlich 2.59 Å (Sm), 2.26 Å (Yb) und 2.670 Å (Sm), bzw. 2.418 Å (Yb). Ähnliche Calcium- und Ytterbium-Komplexe vom Typ $[M\{HB(C_6F_5)_3\}_2(THF)_2]$ (M = Ca, Yb) wurden von Sadow und Mitarbeitern publiziert.[53] Diese Komplexe bildeten sich ausgehend von $[M\{C(SiHMe_2)_3\}_2(THF)_2]$ und **C** via β-Hydrid(SiH)-Abstraktion. Sadow et al. berichteten zudem von diskreten, dreiwertigen Komplexen $[Ln\{C(SiHMe_2)_3\}_{3-x}\{HB(C_6F_5)_3\}_x]$ (Ln = La, Ce, Pr, Nd; $x = 1, 2$), welche nach Aktivierung mit TIBA aktive Dien-Polymerisationskatalysatoren lieferten, was einen $Ln\text{–}C(SiHMe_2)_3/AliBu_3$ Austausch impliziert.[54]

Sauerstoff-enthaltende Donormoleküle, ganz analog zu Lewissäuren, sind in der Lage, kationische Organoseltenerdmetall-Fragmente mit ladungsausgleichenden, räumlich separierten Tetraalkylaluminato-Anionen zu bilden. Repräsentative Vertreter sind die THF-Addukte $[\eta^5$-(Fluorenyl)$Yb(THF)_4][AlMe_4]$,[50] $[Cp^*Yb(THF)_4][AlMe_4]$,[29] $[Y(CH_2SiMe_3)_2(THF)_4][Al(CH_2SiMe_3)_4]$[55] oder Kronenether-Derivate $[YMe(12\text{-}Krone\text{-}4)_2][AlMe_4]_2$ und $[PrMe(18\text{-}Krone\text{-}6)_2][AlMe_4]_2$.[56] Die Reaktion von $\mathbf{1^{Yb}}$ mit 18-Krone-6 führte lediglich zur Koordination des Kronenethers, ohne die Tetraisobutylaluminato-Anionen zu separieren und zur Bildung von $[Yb(18\text{-}Krone\text{-}6)(AliBu_4)_2]$ (**9**) (Abbildung 6).[27] Dabei erzwingt die Koordination des Kronenethers die η^1-Koordination der Tetraisobutylaluminato-Liganden sowie einen linearen C(1)–Yb(1)–C(1′) Winkel. Der Yb–C-Abstand

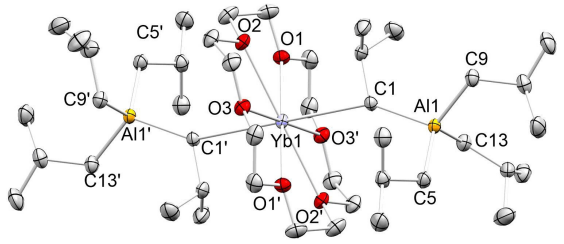

Abbildung 6. Kristallstruktur von $[Yb(AliBu_4)_2(18\text{-}crown\text{-}6)]$ (**9**). Ellipsoide werden mit einer Wahrscheinlichkeit von 50% angegeben, auf die Darstellung der Wasserstoffatome wird der Übersichtlichkeit halber verzichtet. Ausgewählte interatomare Abstände [Å] und Winkel [°]: Yb1–C1 2.9159(19), durchschn. Yb–O 2.6384; C1–Yb–C1′ 180.00(6). Weitere metrische Daten finden sich im Anhang.

von 2.9159(19) Å in **9** ist merklich länger als in Edukt $\mathbf{1^{Yb}}$ (2.735(16)–2.796(12) Å).

Wie bereits für $\mathbf{1^{Yb}}$ beobachtet, zeigt Komplex **9** keine Verbreiterung oder Aufspaltung der ^{1}H NMR-Resonanzen, sogar bei 190 K, was auf die hohe Mobilität der Isobutylaluminato-Gruppen in Lösung, selbst bei sehr tiefen Temperaturen, hindeutet.

Lanthanoid(II)-Isobutylaluminate in der Isopren-Polymerisation

Die Polymerisation konjugierter Diene mit zweiwertigen Lanthanoid-Komplexen wurde bisher nur in sehr wenigen Arbeiten untersucht. Zumeist wurden zweiwertige Samarocen-Derivate $Cp^R{}_2Sm(THF)_2$ eingesetzt, welche durch die Cokatalysatoren zu dreiwertigen Spezies oxidiert werden (Cokatalysatoren: $AliBu_3/[Ph_3C][B(C_6F_5)_4]$, MAO oder MMAO = modifiziertes MAO).[57,58] Unvorteilhafterweise werden divalente Samarocen-Präkatalysatoren leicht durch Bildung thermodynamisch günstiger η^3-Allylkomplexe inaktiviert.[59] Andererseits tendieren Ln^{III}-basierte (Sm, Eu, Yb) Ziegler–Natta-Katalysatoren dazu, durch Reduktion zweiwertige Spezies zu bilden, was zu geringen Ausbeuten, oder völliger Polymerisationsinaktivität führen kann.[3] Daher wurde lange postuliert, dass ausschließlich dreiwertige Lanthanoid-Spezies polymerisationsaktiv seien,[3] wohingegen zweiwertige Seltenerdmetall-Komplexe als inaktiv betrachtet wurden, bzw. dass die Reduktion zu zweiwertigen Spezies zumindest die Polymerisationsaktivität mindere.

Andererseits fanden Evans et al., dass zweiwertige Seltenerdmetall-Iodide LnI_2 (Ln = Nd, Sm, Dy, Tm) sowie $LnI_2(THF)_2$ (Ln = Sm, Tm) die *cis*-1,4-selektive Isoprenpolymerisation katalysieren, und dass wohl kein Zusammenhang zwischen Reduktionspotential und Katalysatoraktivität besteht.[60] Die Zugabe von Triisobutylaluminium verbesserte die Leistungsfähigkeit und erzielte einen höheren Umsatz sowie höhere Molekulargewichte, und sogar eine schmalere Molekulargewichtsverteilung, allerdings bedurfte die Polymerisationsaktivität keiner Zugabe von TIBA.[60]

Dementsprechend waren wir interessiert, die zweiwertigen Seltenerdmetall-Isobutylaluminate $[Ln(AliBu_4)_2]$ ($\mathbf{1^{Ln}}$) (Ln = Sm, Eu, Yb) in der Isoprenpolymerisation zu testen. Ein wesentlicher Vorteil dieses Systems ist neben der hervor-

Tabelle 1: Homopolymerisation von Isopren

Eintrag[a]	Präkatalysator	Cokatalysator[b]	Reaktionszeit [h]	[IP]/[Ln]	Ausbeute [%]	*cis*-1,4[c] [%]	*trans*-1,4[c] [%]	3,4[c] [%]	M_n[d] [10^4 g·mol^{-1}]	PDI[d]	T_c[e] [°C]
1	$\mathbf{1}^{Sm}$	kein	4	1000	20	77.97	1.86	20.17	5.7	1.52	−53
2	$\mathbf{1}^{Sm}$	**A**	24	1000	>99	16.87	74.69	8.44	4.0	1.30	−63
3	$\mathbf{1}^{Sm}$	**B**	1	1000	>99	27.60	60.23	12.17	4.8	1.21	−59
4	$\mathbf{1}^{Sm}$	**C**	24	1000	12	37.49	55.51	7.00	1.4	5.15	−63
5	$\mathbf{1}^{Sm}$	**D**, oder **E**	24	1000	0	–	–	–	–	–	–
6	$\mathbf{1}^{Eu}$	kein	24	1000	>99	76.68	0	23.32	39.0	1.62	−49
7	$\mathbf{1}^{Eu}$	kein	1	1000	41	75.69	0	24.31	26.6	1.40	−48
8	$\mathbf{1}^{Eu}$	**A**	24	1000	>99	18.16	70.80	11.04	3.7	1.29	−61
9	$\mathbf{1}^{Eu}$	**B**	24	1000	>99	25.62	61.22	13.16	6.1	1.12	−58
10	$\mathbf{1}^{Eu}$	**C**, **D**, oder **E**	24	1000	0	–	–	–	–	–	–
11	$\mathbf{1}^{Yb}$	kein	1	1000	94	81.82	5.43	12.75	6.0	1.92	−58
12	$\mathbf{1}^{Yb}$	**A**	24	1000	33	46.23	25.42	28.35	2.1	1.24	−46
13	$\mathbf{1}^{Yb}$	**B**	1	1000	>99	54.92	14.14	30.94	5.4	1.10	−41
14[f]	$\mathbf{1}^{Yb}$	**B**	2	250	>99	54.15	14.14	31.71	1.7	1.04	−45
15[f]	$\mathbf{1}^{Yb}$	**B**	3	500	>99	53.27	15.29	31.44	2.7	1.02	−45
16[f]	$\mathbf{1}^{Yb}$	**B**	4	750	>99	51.61	16.79	31.60	4.0	1.05	−44
17[f]	$\mathbf{1}^{Yb}$	**B**	5	1000	>99	53.74	14.71	31.55	4.9	1.03	−43
18	$\mathbf{1}^{Yb}$	**C**, **D**, oder **E**	24	1000	0	–	–	–	–	–	–
19[g]	**3**	kein	24	1000	0	–	–	–	–	–	–
20[g]	**3**	**A**	2	1000	10	96.9	0	3.1	n. b.	n. b.	n. b.
21[g]	**3**	**C**	2	1000	9	95.1	0	4.9	18.5	2.09	n. b.
22[g]	**3**	**B**, **D**, oder **E**	24	1000	0	–	–	–	–	–	–
23	**6**	kein	24	1000	0	–	–	–	–	–	–

[a] Bedingungen: 20 µmol Präkatalysator, 20 µmol Cokatalysator, 20 mmol Isopren, 8 mL Toluol, 500 rpm Rührgeschwindigkeit. [b] Inkubiert mit Cokatalysator bei Umgebungstemperatur für 30 min: **A** = $[Ph_3C][B(C_6F_5)_4]$; **B** = $[PhNMe_2H][B(C_6F_5)_4]$; **C** = $B(C_6F_5)_3$; **D** = Me_2AlCl, **E** = Et_2AlCl, 1 Äquivalent. [c] Bestimmt mittels ^{1}H- und ^{13}C-NMR-Spektroskopie in $CDCl_3$. [d] Bestimmt mittels SEC. [e] Bestimmt mittels DSC. [f] 20 µmol Präkatalysator, 20 µmol **B** ($[PhNMe_2H][B(C_6F_5)_4]$), 10 mL Toluol, inkubiert bei Umgebungstemperatur für 30 min, Isoprenzugabe (0.5 mL, 5 mmol) nach jeder Stunde, 500 rpm Rührgeschwindigkeit. [g] 3.3 µmol Präkatalysator, 20 µmol Cokatalysator (was 1 Äquivalent Cokatalyst/[Sm] entspricht), 8 mL *n*-Hexan, 20 mmol Isopren, n. b. nicht bestimmt.

ragenden Löslichkeit in aromatischen und aliphatischen Lösungsmitteln (im Vergleich zu LnI_2) der Diamagnetismus von $[Yb(Al\mathit{i}Bu_4)_2]$ ($\mathbf{1}^{Yb}$), welcher die Beobachtung beteiligter Spezies mittels ^{1}H NMR-Spektroskopie erlaubt. Für die Aktivierung von $\mathbf{1}^{Ln}$ für die Isoprenpolymerisation verwendeten wir Boran-/Borat-, oder Dialkylaluminiumchlorid-Cokatalysatoren, sowie zu Vergleichszwecken $\mathbf{1}^{Ln}$ ohne Zusatz eines Cokatalysators. Die Verwendung äquimolarer Mengen an Borat-Cokatalysatoren $[CPh_3][B(C_6F_5)_4]$ (**A**) bzw. $[C_6H_5NMe_2H][B(C_6F_5)_4]$ (**B**) mit $\mathbf{1}^{Ln}$ resultierte in hohen Polymerausbeuten, insbesondere mit Cokatalysator **B** (siehe Tabelle 1, Einträge 2–3, 8–9 und 12–13). Generell lieferten die binären Systeme $\mathbf{1}^{Sm}$/**B** und $\mathbf{1}^{Eu}$/**B** überwiegend 1,4-*trans*-Polymer, wohingegen $\mathbf{1}^{Yb}$/**B** Polymer mit niedrigerem *trans* Anteil ergab. Die Aktivierung mit **A** oder **B** führte generell zu sehr engen Molmassenverteilungen. Insbesondere mit $\mathbf{1}^{Yb}$/**B** zeigte sich das Verhalten einer idealen lebenden Polymerisation (Eintrag 13). Nähere Untersuchungen ergaben, dass auch bei mehrfacher Zugabe von Monomer zu $\mathbf{1}^{Yb}$/**B** Polydispersitätsindizes von 1.02–1.05 gemessen wurden, wobei Monomerverbrauch und Anstieg der Molmasse nach jeder Monomerzugabe durch einen linearen Zusammenhang gekennzeichnet waren, was die perfekt lebende Polymerisation für $\mathbf{1}^{Yb}$/**B** belegt (Table 1, Einträge 14–17; vgl. Abbildung 7).

Die Aktivierung von $\mathbf{1}^{Ln}$ mit **C** und nachfolgende Polymerisation lieferte hingegen kein oder nur sehr wenig Polymer

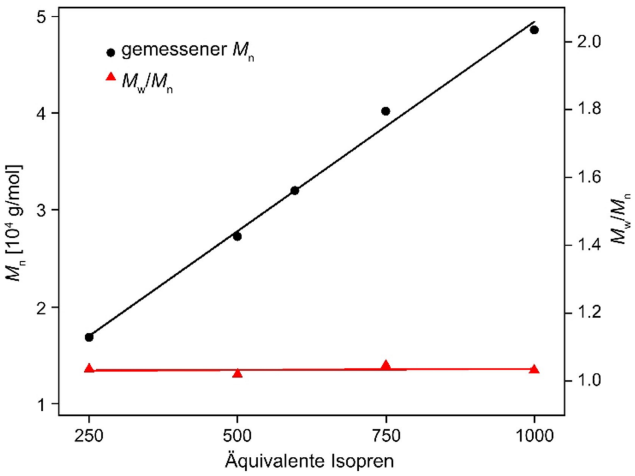

Abbildung 7. Isoprenpolymerisation mit $\mathbf{1}^{Yb}$/**B**. Molekulargewicht vs. eingesetzte Isoprenäquivalente.

(Einträge 4, 10 und 18). Angesichts der Bildung des polymerisationsinaktiven Komplexes $[Sm\{HB(C_6F_5)_3\}_2(\eta^6\text{-Toluol})_2]$ (**6**) aus $\mathbf{1}^{Sm}$/**C** ist die Inaktivität von $\mathbf{1}^{Sm}$/**C** in der Polymerisation wenig überraschend (Eintrag 23). Die geringe Polymerausbeute ist sehr wahrscheinlich auf gebildete Nebenprodukte zurückzuführen. Dies korreliert mit dem verhältnismäßig

hohen PDI (Eintrag 4), welcher die Bildung verschiedener, katalytisch aktiver Nebenprodukte andeutet.

Die binären Systeme **1^{Ln}/D** (**D** = Dimethylaluminiumchlorid) sowie **1^{Ln}/E** (**E** = Diethylaluminiumchlorid) waren nicht polymerisationsaktiv (Einträge 5, 10, 18). Wie bereits durch die Synthese der Verbindungen **3**, **4** und **5** gezeigt, ist der Isobutylaluminato-Austausch ein mögliches Szenario in diesem System. Tatsächlich wurde bei der Zugabe von **D** bzw. **E** oder **F** (iBu$_2$AlCl) zu einer Lösung von [Sm(AliBu$_4$)$_2$] in Toluol rasch ein dunkler, bräunlicher Niederschlag gebildet. Dies deutet auf die Bildung eines – der Farbe nach – divalenten Chloridsalzes hin, was die Bildung polymerisationsaktiver Spezies verhindert.

Zu unserer Überraschung polymerisierte [Sm(AliBu$_4$)$_2$] (**1^{Sm}**) Isopren auch ohne vorherige Aktivierung mit einem Cokatalysator, wobei Polyisopren mit relativ hohem *cis*-1,4-Anteil und einem relativ kleinen PDI entstand (Eintrag 1). Um den Einfluss eines möglichen Redoxszenarios zu prüfen, wurden **1^{Eu}** und **1^{Yb}** ohne vorherige Aktivierung als Katalysatoren eingesetzt (Einträge 6, 7 und 11). Bemerkenswerterweise lieferten die Katalysatoren **1^{Eu}** und **1^{Yb}** deutlich höhere Ausbeuten als **1^{Sm}** bei vergleichbarer Mikrostruktur der Polymere, wobei **1^{Eu}** ein Polymer mit sehr hohem Molekulargewicht lieferte (Einträge 6 und 7), was auf einen verhältnismäßig geringen Anteil katalytisch aktiver Europium-Zentren zurückgeführt werden kann.

Untersuchung der katalytisch aktiven Ln^{II}-Spezies

Aufgrund des Paramagnetismus von **1^{Sm}** und **1^{Eu}** wurde die Reaktivität des diamagnetischen Ytterbium(II)-Isobutylaluminats **1^{Yb}** gegenüber den Cokatalysatoren **A**, **B**, **C** und **F** getestet und mittels ^{1}H-NMR-Spektroskopie verfolgt (Abbildung 8, 9, S11–S17). Mit keinem der getesteten Cokatalysatoren wurde eine paramagnetische Verbreiterung, oder -Verschiebung der Protonresonanzen beobachtet, was darauf hindeutet, dass alle gebildete Spezies zweiwertig bleiben. Die äquimolare Reaktion von **1^{Yb}** mit dem Cokatalysator **A** in Benzol-d$_6$ ließ die Bildung von Triphenylmethan, Isobuten und TIBA erkennen. Neben dem vollständigen Verschwinden der Resonanzen des Eduktes **1^{Yb}** zeigte sich ein neuer Satz an Isobutyl-Resonanzen, welcher der möglichen aktiven Spezies "[Yb(AliBu$_4$)][B(C$_6$F$_5$)$_4$]" zugeordnet werden kann (Abbildung 8). Die Hydridabstraktion mit Cokatalysator **A**, die durch die Isobutenbildung angezeigt wird, ist etwas überraschend, bedenkt man, dass eine ähnliche Reaktivität auch bei der Reaktion von **1^{Ln}** mit B(C$_6$F$_5$)$_3$ und der Bildung der Komplexe [Sm{HB(C$_6$F$_5$)$_3$}$_2$(η^6-Toluol)$_2$] (**6**) und [Yb{HB(C$_6$F$_5$)$_3$}$_2$(η^6-C$_6$D$_6$)] (**7**) beobachtet wurde (*siehe weiter vorne*).

Die äquimolare Reaktion von **1^{Yb}** mit **B** in deuteriertem Benzol wurde ebenfalls mittels ^{1}H-NMR-Spektroskopie verfolgt (Abbildung 9). Die Protonolyse eines Tetraisobutylaluminats lässt sich anhand der Bildung von Isobutan und dem TIBA-Dimethylanillin-Addukt erkennen. Die Entstehung von Isobuten wurde nicht beobachtet, was zeigt, dass keine weitere Zersetzung gemäß einer β-Hydrideliminierung stattfindet. Ein neuer Isobutyl-Signalsatz kann dem kationisierten

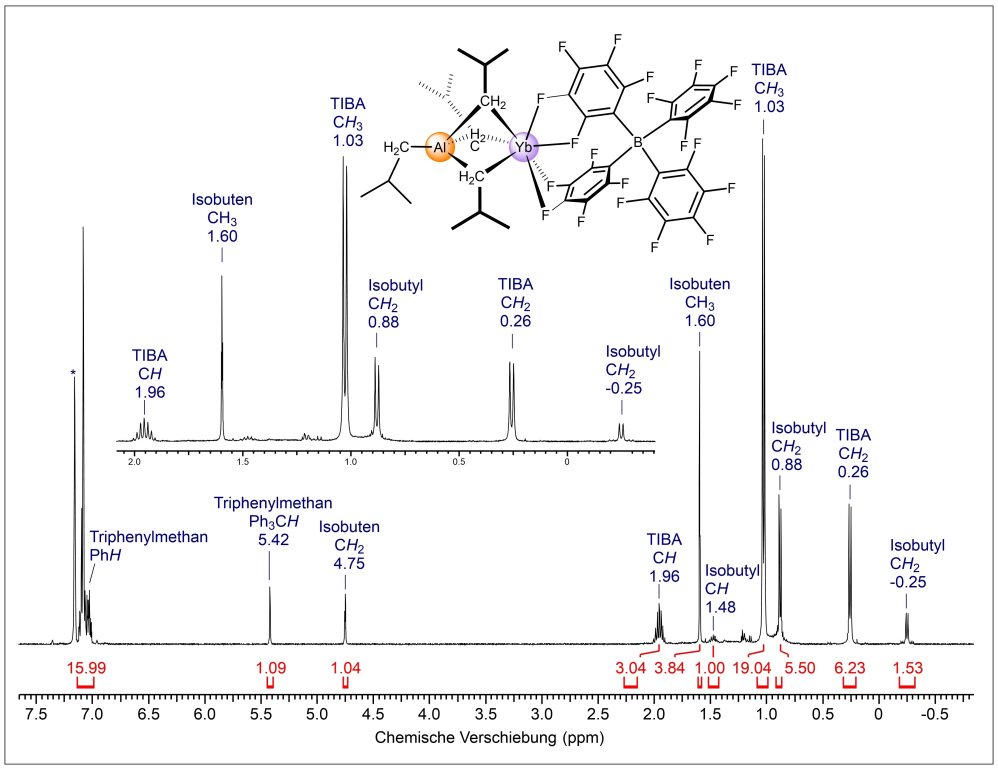

Abbildung 8. ^{1}H-NMR-Spektrum (400 MHz, C$_6$D$_6$, 26 °C) der äquimolaren Reaktion von **1^{Yb}** mit Cokatalysator **A** und vorgeschlagene aktive Spezies.

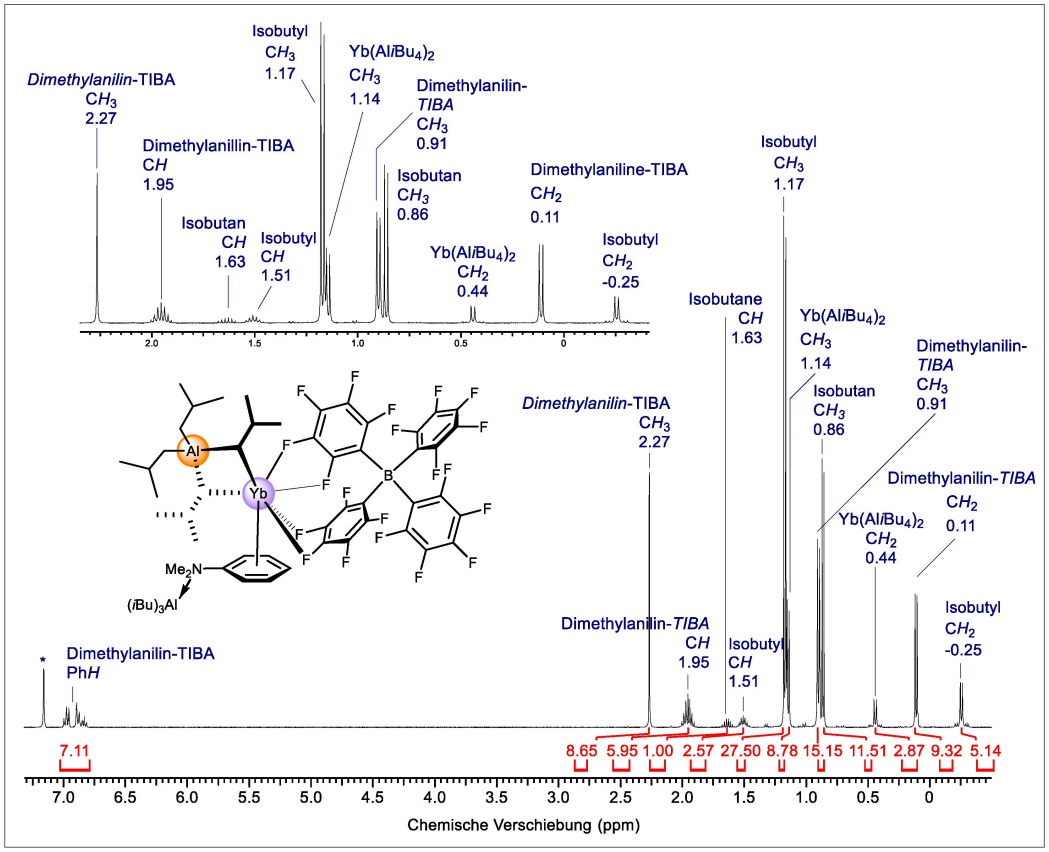

Abbildung 9. ^{1}H-NMR-Spektrum (400 MHz, C_6D_6, 26 °C) der äquimolaren Reaktion von $\mathbf{1}^{Yb}$ mit Cokatalysator **B** und vorgeschlagene aktive Spezies.

Tetraisobutylaluminat-Komplex "[Yb(Al*i*Bu$_4$){Al*i*Bu$_3$-(PhNMe$_2$)}][B(C$_6$F$_5$)$_4$]" als mögliche aktive Spezies zugeordnet werden. Dies impliziert, dass sich sowohl mit **A**, wie auch mit **B** ähnliche Produkte bilden, wobei die Löslichkeit des mit Cokatalysator **B** erhaltenen Produktes etwas besser ist. Es ist daher wahrscheinlich, dass das TIBA-Dimethylanilin-Addukt mit der aktiven Spezies interagiert, und diese besser löslich, und damit katalytisch aktiver macht. Mit Cokatalysator **A** wurde eine geringfügig breitere Molmassenverteilung beobachtet, was darauf hindeuten könnte, dass die etwas niedrigere Löslichkeit der aktiven Spezies eine gleichzeitige Initiierung der Polymerisation verhindert, wohingegen sich die Löslichkeit jedoch mit wachsender Polymerkette verbessert. Die Aktivierung mit **B** führt hingegen zur idealen lebenden Polymerisation, da das binäre System [Yb-(Al*i*Bu$_4$)$_2$]/[PhNMe$_2$H][B(C$_6$F$_5$)$_4$] ($\mathbf{1}^{Yb}$/**B**) in Toluol gut löslich ist. Daher postulieren wir "[Yb(Al*i*Bu$_4$){Al*i*Bu$_3$(PhNMe$_2$)}]-[B(C$_6$F$_5$)$_4$]" (vgl. Abbildung 9) als aktive Spezies, welche die lebende Polymerisation von Isopren katalysiert.

Im Gegensatz zu den übersichtlichen NMR-Spektren, welche für die Reaktion von $\mathbf{1}^{Yb}$ mit je einem Äquivalent **A** oder **B** erhalten wurden, zeigt die Aktivierung mit **C** die Entstehung mehrerer Isobutyl-Signalsätze, wie auch die Bildung von Isobuten und TIBA. (Abbildung S15–S16). Die Vielzahl verschiedener Spezies, die im ^{1}H-NMR-Spektrum für das binäre System $\mathbf{1}^{Yb}$/**C** beobachtet wurde, ist konsistent mit der breiten Molmassenverteilung des entsprechenden Polymers, das auf die Gegenwart mehrerer polymerisationsaktiver Spezies hindeutet. Die Entstehung größerer Isobutenmengen legt nahe, dass Hydridspezies im Zuge der Aktivierung gebildet werden. Darüber hinaus sind immer noch ^{1}H-NMR-Resonanzen des Eduktes $\mathbf{1}^{Yb}$ vorhanden, was dessen unvollständigen Umsatz anzeigt. Tatsächlich kristallisierte [Yb{HB(C$_6$F$_5$)$_3$}$_2$(C$_6$D$_6$)] (**7**) aus einer 1:1 Reaktionsmischung von $\mathbf{1}^{Yb}$ und B(C$_6$F$_5$)$_3$ (**C**) in Benzol-d$_6$ (*siehe weiter vorne*).

Die Reaktion von $\mathbf{1}^{Yb}$ mit einem Äquivalent *i*Bu$_2$AlCl (**F**) zeigte die Protonenresonanzen von freiem TIBA und nicht umgesetztem $\mathbf{1}^{Yb}$ (Abbildung S17). Dies könnte die Tendenz der Mischung zur Bildung schwerlöslicher [Yb^{II}Cl$_x$]$_n$-Spezies durch Ligandenaustausch, anstelle der Bildung potentieller [Yb-(μ-ClAl*i*Bu$_3$)$_x$] Heteroaluminat-Spezies unterstreichen. Bemerkenswerterweise lieferte das binäre System $\mathbf{1}^{Yb}$/**F** trotz der Anwesenheit des Einkomponentenkatalysators $\mathbf{1}^{Yb}$ kein Polymer. Dies könnte auf den Effekt von TIBA zurückzuführen sein, den Polymerisationsgrad durch Kettentransfer zu reduzieren, oder auf eine die Polymerisation hindernde Wirkung etwaiger [YbCl$_x$]$_n$-Spezies. Wiederum erinnert diese Ligandenaustauschreaktion an die Reaktivität von $\mathbf{1}^{Sm}$ gegenüber Tellur(IV)-chlorid und an die Bildung von {[SmCl-(THF)$_5$][AlBn*i*Bu$_3$]}$_n$ (**5**), wo der Ligandenaustausch gegenüber der Oxidation des Samariums bevorzugt wird.

Im Gegensatz zu [Sm(Al*i*Bu$_4$)$_2$] ($\mathbf{1}^{Sm}$) verhielt sich [Sm$_6$Cl$_8$(Al*i*Bu$_4$)$_6$] (**3**) inert in der Isoprenpolymerisation ohne vorherige Aktivierung (Eintrag 19). Dies ist ein glaubwürdi-

ger Beweis dafür, dass Chlorid-verbrückte Lantanoid(II)-Aluminate in der Isoprenpolymerisation inaktiv sind, und erklärt ebenso die Inaktivität der äquimolaren Mischung von $\mathbf{1^{Ln}}$ (Ln = Sm, Eu, Yb) mit R_2AlCl (R = Me, Et). Während der Aktivierung von **3** mit den Cokatalysatoren **B**, **D**, oder **E** entstanden bräunliche Suspensionen, die nicht polymerisationsaktiv waren (Eintrag 22). Mit **3**/**A** als Katalysator gewonnenes Polyisopren ließ sich nicht vollständig lösen, was auf teils quervernetztes Polymer hindeuten kann, weshalb die angegebenen Daten der löslichen Polymerfraktion entsprechen (Eintrag 20).

Interessanterweise behielt das mit **3**/**A** gewonnene Polymer seine orange Farbe auch während des Fällens in Methanol und auch nach dem Trockenen, dergestalt, dass davon ausgegangen werden kann, dass ungelöster, "Heterogen-Katalysator" in das Polymer eingeschlossen wurde, was möglicherweise auch die relativ niedere Katalysatoraktivität bzw. Polymerausbeute erklärt. Die mit **3** und den Cokatalysatoren **A** und **C** gewonnenen Polymere wiesen interessanterweise einen sehr hohen Anteil *cis*-1,4-verknüpfter Isopreneinheiten aus (97 % und 95 %), wohingegen kein *trans*-1,4-Anteil nachgewiesen werden konnte.

Zusammenfassung

Die diskreten Komplexe $[Sm(Ali Bu_4)_2]$, $[Eu(Ali Bu_4)_2]$ und $[Yb(Ali Bu_4)_2]$ lassen sich aus $[Ln\{N(SiMe_3)_2\}_2(THF)_2]$ (Ln = Sm, Eu, Yb) und Überschuss $Ali Bu_3$ (TIBA) mit sehr guten Ausbeuten darstellen. Zum ersten Mal konnten damit homoleptische Seltenerdmetall-Tetraisobutylaluminate synthetisiert und vollständig charakterisiert werden, einschließlich Röntgenstrukturanalyse. Die Komplexe $[Ln(Ali Bu_4)_2]$ (Ln = Sm, Yb) lassen sich in vielfältiger Weise derivatisieren, wie z. B. durch Oxidation, Chlorierung und Kationisierung. Chlorierende Reagenzien führen primär zum $Ali Bu_4$/Cl-Ligandenaustausch, wie der Yb^{II}-Cluster $[Yb_4Cl_4(Ali Bu_4)_4]$ und das Koordinationspolymer $[\{SmCl(THF)_5)(AlBn i Bu_3\}]_n$ zeigen. Das stärker redoxaktive Samarium(II) hingegen wird partiell oxidiert, wie der gemischtvalente Sm^{II}/Sm^{III}-Cluster $[Sm_6Cl_8(Ali Bu_4)_6]$ belegt. Mit $Pb(C_5Me_5)_2$ ließen sich die Aluminate $[Ln(Ali Bu_4)_2]$ (Ln = Sm, Yb) hingegen leicht zu den dreiwertigen Lanthanoidocenen $[Cp^*_2Ln(Ali Bu_4)]$ oxidieren. Die versuchte Abstraktion eines Isobutylaluminato-Liganden mit $B(C_6F_5)_3$ führt zur β-Hydrid-Abstraktion und der Bildung der Aren-stabilisierten Hydridoborat-Komplexe $[Sm\{HB(C_6F_5)_3\}_2(Toluol)_2]$ und $[Yb\{HB(C_6F_5)_3\}_2(Benzol)]$. Die Verdrängung der Isobutylaluminato-Liganden von $[Yb(Ali Bu_4)_2]$ mit dem Kronenether 18-Krone-6 wurde nicht beobachtet, hingegen bildete sich das Donoraddukt $[Yb(Ali Bu_4)_2$(18-Krone-6)].

Der gemischtvalente Sm^{II}/Sm^{III}-Cluster $[Sm_6Cl_8(Ali Bu_4)_6]$ polymerisiert Isopren nur im Beisein von Cokatalysator, liefert aber 1,4-*trans*-freies Polyisopren mit einer *cis*-Stereoselektivität von bis zu 97 % mit Boran/Borat-Cokatalysatoren. Faszinierenderweise agiert homoleptisches $[Ln(Ali Bu_4)_2]$ als Einkomponentenkatalysator und vermag Isopren ohne weitere Zusätze zu polymerisieren, wobei ein Polymer mit hohen *cis*-Anteilen und kleinem PDI erhalten wird; insbesondere für $[Eu(Ali Bu_4)_2]$ lässt sich kein *trans*-1,4-Anteil nachweisen.

Eine Korrelation zwischen dem Redoxpotential und der Polymerisationsaktivität wurde nicht beobachtet, was darauf hindeutet, dass zweiwertige Lanthanoid-Spezies sehr aktiv in der Isoprenpolymerisation sein können. Die Abwesenheit jeglicher katalytisch aktiver Yb^{III}-Spezies wurde mittels NMR-Spektroskopie für die äquimolaren binären Katalysatormischungen $[Yb(Ali Bu_4)_2]/[CPh_3][B(C_6F_5)_4]$ und $[Yb(Ali Bu_4)_2]/[PhNMe_2H][B(C_6F_5)_4]$ verifiziert, was diese Arbeit zu einer der ersten macht, die sich mit dem erfolgreichen Einsatz zweiwertiger Lanthanoide in der Polymerisation konjugierter Diene befasst. Das binäre System $[Yb(Ali Bu_4)_2]/[PhNMe_2H][B(C_6F_5)_4]$ vermag Isopren lebend zu polymerisieren, wobei Polydispersitätsindizes von 1.02–1.05 gemessen wurden; die anhand von NMR-spektroskopischen Untersuchungen vorgeschlagene aktive Spezies ist "$[Yb(Ali Bu_4)\{Ali Bu_3(PhNMe_2)\}][B(C_6F_5)_4]$".

Danksagung

Wir danken der Bridgestone Corporation für Ihre großzügige Unterstützung. Open Access Veröffentlichung ermöglicht und organisiert durch Projekt DEAL.

Interessenkonflikt

Die Autoren erklären, dass keine Interessenkonflikte vorliegen.

Erklärung zur Datenverfügbarkeit

Die Daten, die die Ergebnisse dieser Studie unterstützen, sind in den Hintergrundinformationen zu diesem Artikel verfügbar.

Stichwörter: Cluster · Einkomponentenkatalysator · Isobutylaluminate · Lanthanoide · Lebende Isoprenpolymerisation

[1] G. Ricci, G. Pampaloni, A. Sommazzi, F. Masi, *Macromolecules* **2021**, *54*, 5879–5914.
[2] L. Friebe, O. Nuyken, W. Obrecht, *Adv. Polym. Sci.* **2006**, *204*, 1–154.
[3] A. Fischbach, R. Anwander, *Adv. Polym. Sci.* **2006**, *204*, 155–281.
[4] Z. Zhang, D. Cui, B. Wang, B. Liu, Y. Yang, in *Molecular Catalysis of Rare-Earth Elements* (Ed.: P. W. Roesky), Springer Berlin Heidelberg, **2010**, 49–108.
[5] J. Jothieswaran, S. Fadlallah, F. Bonnet, M. Visseaux, *Catalysts* **2017**, *7*, 378.
[6] T. Sone, *Int. Pol. Sci. Tech.* **2016**, *43*, 49–54.
[7] a) W. Gao, D. Cui, *J. Am. Chem. Soc.* **2008**, *130*, 4984–4991; b) W. Rong, M. Wang, S. Li, J. Cheng, D. Liu, D. Cui, *Organometallics* **2018**, *37*, 971–978.

[8] Q. Shen, W. Chen, Y. Jin, C. Shan, *Pure Appl. Chem.* **1988**, *60*, 1251–1256.
[9] M. Nishiura, F. Guo, Z. Hou, *Acc. Chem. Res.* **2015**, *48*, 2209–2220.
[10] F. Yang, X. Li, *J. Polym. Sci. Part A* **2017**, *55*, 2271–2280.
[11] J. Huang, Z. Liu, D. Cui, X. Liu, *ChemCatChem* **2018**, *10*, 42–61.
[12] S. Arndt, K. Beckerle, P. M. Zeimentz, T. Spaniol, J. Okuda, *Angew. Chem. Int. Ed.* **2005**, *44*, 7473–7477; *Angew. Chem.* **2005**, *117*, 7640–7644.
[13] H. M. Dietrich, O. Schuster, K. W. Törnroos, R. Anwander, *Angew. Chem. Int. Ed.* **2006**, *45*, 4858–4863; *Angew. Chem.* **2006**, *118*, 4977–4982.
[14] K. Lv, D. Cui, *Organometallics* **2010**, *29*, 2987–2993.
[15] A. D. Oswald, L. Verrieux, P.-A. R. Breuil, H. Olivier-Bourbigou, J. Thuilliez, F. Vaultier, M. Taoufik, L. Perrin, C. Boisson, *Organometallics* **2022**, *41*, 2106–2118.
[16] Für Carboxylato/Isobutyl-Heteroaluminate, siehe: F. Li, Y. Jin, C. Song, Y. Lin, F. Pei, F. Wang, N. Hu, *Appl. Organomet. Chem.* **1996**, *10*, 761–771.
[17] W. J. Evans, J. T. Leman, R. D. Clark, J. W. Ziller, *Main Group Met. Chem.* **2000**, *23*, 163–168.
[18] W. J. Evans, T. M. Champagne, D. G. Giarikos, J. W. Ziller, *Organometallics* **2005**, *24*, 570–579.
[19] W. J. Evans, T. M. Champagne, J. W. Ziller, *Chem. Commun.* **2005**, 5925–5927.
[20] M. G. Klimpel, J. Eppinger, P. Sirsch, W. Scherer, R. Anwander, *Organometallics* **2002**, *21*, 4021–4023.
[21] G. R. Giesbrecht, J. C. Gordon, D. L. Clark, B. L. Scott, J. G. Watkin, K. J. Young, *Inorg. Chem.* **2002**, *41*, 6372–6379.
[22] Für erste strukturell charakterisierte Ln-*i*Bu-Komplexe, siehe: T. Berger, D. Baschnagel, C. Maichle-Mössmer, R. Anwander, *Z. Anorg. Allg. Chem.* **2023**, *649*, e202200274.
[23] Für die Synthese von *cis*-1,4-Polyisopren via lebender Ln^{III}-Einkomponentenpolymerisation, siehe: L. Zhang, T. Suzuki, Y. Luo, M. Nishiura, Z. Hou, *Angew. Chem. Int. Ed.* **2007**, *46*, 1909–1913; *Angew. Chem.* **2007**, *119*, 1941–1945.
[24] Für die Synthese von *trans*-1,4-Polyisopren via lebender Ln^{III}-Einkomponentenpolymerisation, siehe: M. Zimmermann, K. W. Törnroos, R. Anwander, *Angew. Chem. Int. Ed.* **2008**, *47*, 775–778; *Angew. Chem.* **2008**, *120*, 787–790.
[25] Für die Synthese von 3,4-Polyisopren via lebender Ln^{III}-Einkomponentenpolymerisation, siehe: L. Zhang, Y. Luo, Z. Hou, *J. Am. Chem. Soc.* **2005**, *127*, 14562–14563.
[26] M. G. Klimpel, R. Anwander, M. Tafipolsky, W. Scherer, *Organometallics* **2001**, *20*, 3983–3992.
[27] Die Hinterlegungsnummern 2231690 (für $\mathbf{1}^{Sm}$), 2231689 (für $\mathbf{1}^{Eu}$), 2231688 (für $\mathbf{1}^{Yb}$), 2231693 (für $\mathbf{2}^{Yb}$), 2231697 (für **3**), 2231695 (für **4**), 2231696 (für **5**), 2231691 (für **6**), 2231694 (für **7**), 2231692 (für **8**) und 2231698 (für **9**) erlauben Zugriff auf die ausführlichen kristallographischen Daten zu dieser Veröffentlichung. Die Daten sind kostenlos beim Access-Structures-Service des Cambridge Crystallographic Data Centre und des Fachinformationszentrums Karlsruhe erhältlich.
[28] M. G. Schrems, H. M. Dietrich, K. W. Törnroos, R. Anwander, *Chem. Commun.* **2005**, 5922–5924.
[29] H.-M. Sommerfeldt, C. Meermann, M. G. Schrems, K. W. Törnroos, N. Å. Frøystein, R. J. Miller, E.-W. Scheidt, W. Scherer, R. Anwander, *Dalton Trans.* **2008**, 1899–1907.
[30] G. Occhipinti, C. Meermann, H. M. Dietrich, R. Litlabø, F. Auras, K. W. Törnroos, C. Maichle-Mössmer, V. R. Jensen, R. Anwander, *J. Am. Chem. Soc.* **2011**, *133*, 6323–6337.
[31] D. Bojer, A. Venogopal, B. Neumann, H.-G. Stammler, N. W. Mitzel, *Angew. Chem. Int. Ed.* **2010**, *49*, 2611–2614; *Angew. Chem.* **2010**, *122*, 2665–2669.
[32] W. J. Evans, K. J. Forrestal, J. T. Leman, J. W. Ziller, *Organometallics* **1996**, *15*, 527–531.
[33] M. P. Coles, P. B. Hitchcock, M. F. Lappert, A. V. Protchenko, *Organometallics* **2012**, *31*, 2682–2690.
[34] A. M. Bienfait, B. M. Wolf, K. W. Törnroos, R. Anwander, *Organometallics* **2015**, *34*, 5734–5744.
[35] B. M. Wolf, C. Stuhl, C. Maichle-Mössmer, R. Anwander, *Chem. Eur. J.* **2018**, *24*, 15921–15929.
[36] A. Fischbach, M. G. Klimpel, M. Widenmeyer, E. Herdtweck, W. Scherer, R. Anwander, *Angew. Chem. Int. Ed.* **2004**, *43*, 2234–2239; *Angew. Chem.* **2004**, *116*, 2284–2289.
[37] C. Meermann, K. W. Törnroos, W. Nerdal, R. Anwander, *Angew. Chem. Int. Ed.* **2007**, *46*, 6508–6513; *Angew. Chem.* **2007**, *119*, 6628–6633.
[38] B. M. Wolf, C. Stuhl, R. Anwander, *Chem. Commun.* **2018**, *54*, 8826–8829.
[39] W.-X. Zhang, Z. Wang, M. Nishiura, Z. Xi, Z. Hou, *J. Am. Chem. Soc.* **2011**, *133*, 5712–5715.
[40] M. B. Ley, D. B. Ravnsbæk, Y. Filinchuk, Y.-S. Lee, R. Janot, Y. W. Cho, J. Skibsted, T. R. Jensen, *Chem. Mater.* **2012**, *24*, 1654–1663.
[41] X.-J. Zhang, F.-Z. Su, D.-M. Chen, Y. Peng, W.-Y. Guo, C.-S. Liu, M. Du, *Dalton Trans.* **2019**, *48*, 1843–1849.
[42] O. Eisenstein, P. B. Hitchcock, A. G. Hulkes, M. F. Lappert, L. Maron, *Chem. Commun.* **2001**, 1560–1561.
[43] G. Meyer, T. Schleid, *J. Less-Common Met.* **1986**, *116*, 187–197.
[44] W. J. Evans, J. M. Perotti, J. W. Ziller, *J. Am. Chem. Soc.* **2005**, *127*, 3894–3909.
[45] M. Bonath, D. Schädle, C. Maichle-Mössmer, R. Anwander, *Inorg. Chem.* **2021**, *60*, 14952–14968.
[46] a) G. B. Deacon, Q. Shen, *J. Organomet. Chem.* **1996**, *506*, 1–17; b) Md. E. Hossain, Z. Guo, J. Wang, G. B. Deacon, P. C. Junk, D. Diether, R. Anwander, *Eur. J. Inorg. Chem.* **2022**, e202101009.
[47] P. M. Zeimentz, S. Arndt, B. R. Elvidge, J. Okuda, *Chem. Rev.* **2006**, *106*, 2404–2433.
[48] W. J. Evans, C. A. Seibel, J. W. Ziller, *J. Am. Chem. Soc.* **1998**, *120*, 6745–6752.
[49] G. B. Deacon, C. M. Forsyth, P. C. Junk, *Eur. J. Inorg. Chem.* **2005**, 817–821.
[50] H. Nakamura, Y. Nakayama, H. Yasuda, T. Maruo, N. Kanehisa, Y. Kai, *Organometallics* **2000**, *19*, 5392–5399.
[51] H.-M. Sommerfeldt, C. Meermann, K. W. Törnroos, R. Anwander, *Inorg. Chem.* **2008**, *47*, 4696–4705.
[52] I. Korobkov, S. Gambarotta, *Organometallics* **2009**, *28*, 4009–4019.
[53] K. Yan, B. M. Upton, A. Ellern, A. D. Sadow, *J. Am. Chem. Soc.* **2009**, *131*, 15110–15111.
[54] B. M. Schmidt, A. Pindwal, A. Venkatesh, A. Ellern, A. J. Rossini, A. D. Sadow, *ACS Catal.* **2019**, *9*, 827–838.
[55] S. Arndt, T. P. Spaniol, J. Okuda, *Angew. Chem. Int. Ed.* **2003**, *42*, 5075–5079; *Angew. Chem.* **2003**, *115*, 5229–5233.
[56] A. Nieland, A. Mix, B. Neumamm, H.-G. Stammler, N. W. Mitzel, *Dalton Trans.* **2010**, *39*, 6753–6760.
[57] S. Kaita, Z. Hou, Y. Wakatsuki, *Macromolecules* **1999**, *32*, 9078–9079.
[58] F. Bonnet, M. Visseaux, D. Barbier-Baudry, *J. Organomet. Chem.* **2004**, *689*, 264–269.
[59] W. J. Evans, T. A. Ulibarri, J. W. Ziller, *J. Am. Chem. Soc.* **1990**, *112*, 2314–2324.
[60] W. J. Evans, D. G. Giarikos, N. T. Allen, *Macromolecules* **2003**, *36*, 4256–4257.

Manuskript erhalten: 30. Dezember 2022
Akzeptierte Fassung online: 14. Februar 2023
Endgültige Fassung online: 15. März 2023

Angewandte Chemie
Eine Zeitschrift der Gesellschaft Deutscher Chemiker

Supporting Information

Divalent Lanthanide Tetraisobutylaluminates: Reactivity and Living Isoprene Polymerization

*E. C. Moinet, B. M. Wolf, O. Tardif, C. Maichle-Mössmer, R. Anwander**

Supporting Information

69451 Weinheim, Germany

Table of Contents

Experimental Procedures

General Considerations. All manipulations were performed under rigorous exclusion of air and moisture, using standard Schlenk, high-vacuum, and glovebox techniques (MBraun MB200B <1 ppm O_2, <1 ppm H_2O, argon atmosphere). Glassware and polymer fittings were dried prior to use for several hours at 120 °C or 80 °C, respectively. Solvents were supplied by Merck KGaA, purified using a SPS solvent purification system (MBraun) and stored inside a glovebox. Argon (99.999 Vol%) was supplied by Westfalen AG. Tetrahydrofuran was dried over molecular sieves (3 Å). Benzene-d_6 and toluene-d_8 were obtained from Merck KGaA and dried over Na/K alloy prior to use. Isoprene was purchased from Merck KGaA, dried with trioctylaluminum and distilled under reduced pressure before polymerization. Dimethylaluminum chloride, diethylaluminum chloride, hexachloroethane, potassium bis(trimethylsilyl)amide, triisobutylaluminum (TIBA), trioctylaluminum and trityl chloride were purchased from Merck KGaA and used as received. Samarium powder, tellurium tetrachloride, 18-crown-6, and iodine were purchased from abcr and used without further purification. 1,2-Diiodoethane was obtained from abcr and recrystallized from diethyl ether prior to use. $[CPh_3][B(C_6F_5)_4]$, $[C_6H_5NMe_2H][B(C_6F_5)_4]$, and $[B(C_6F_5)_3]$ were purchased from Boulder Scientific and used as received. $[M\{N(SiMe_3)_2\}_2(THF)_2]$ (M = Sm, Eu, Yb) were prepared according to literature procedure,[1] and the precursors $LnI_2(THF)_2$ (Ln = Sm, Eu, Yb), were prepared from elemental metal and 1,2-diiodoethane following Kagan's procedure.[2] Chemicals were stored at −40 °C.

IR spectra were recorded on a Nicolet 6700 FTIR spectrometer (Thermo Fisher Scientific), and samples were mixed with KBr powder and measured in a DRIFT cell equipped with KBr windows. Elemental analyses were performed on an Elementar vario MICRO cube. NMR spectra of air and moisture sensitive compounds were recorded using J. Young-valved NMR tubes on a Bruker AVII+400 spectrometer (^{1}H: 400.13 MHz; $^{13}C\{^1H\}$: 100.61 MHz). ^{1}H and $^{13}C\{^1H\}$ NMR chemical shifts are referenced to solvent residual resonances and reported in parts per million, relative to tetramethylsilane. Coupling constants are given in Hertz. The microstructures of polyisoprenes were determined by ^{1}H- and $^{13}C\{^1H\}$-NMR spectroscopy in $CDCl_3$ on a Bruker AVBII+400 spectrometer (^{1}H: 400.13 MHz) at ambient temperatures. Low temperature NMR spectra were recorded on Bruker AVII+500 spectrometer (^{1}H: 500.13 MHz). Size-exclusion chromatography (SEC) was performed on a Viscotek GPCmax VE2001 device equipped with a TDA305 detector (Viscotek) against a polystyrene standard in THF (35 °C) with a flow rate of 1 mL/min. Sample solutions (1.0 mg polymer per mL THF) were filtered through a 0.45 µm syringe filter prior to injection. M_n and M_w were determined by means of the integrated OmniSec software. Glass-transition temperatures T_g were determined by differential scanning calorimetry (DSC) under nitrogen atmosphere on a DSC8000 device equipped with a CLN2 cooler (PerkinElmer) calibrated with cyclohexane and indium standards, by scanning from –100 °C up to +100 °C with heating rates of 20 K/min and cooling rates of 60 K/min. The monomer conversion was determined gravimetrically.

Caution! Note that organoaluminum compounds may react very vigorously upon contact with air or moisture and may explode with water!

Synthesis Procedures

[Sm(Al*i*Bu$_4$)$_2$] (1^{Sm}). Analogously to the reaction of [Yb{N(SiMe$_3$)$_2$}$_2$(THF)$_2$] with TIBA,[3] a solution of TIBA (0.967 g, 4.88 mmol) in *n*-hexane (1 mL) was added to a solution of [Sm{N(SiMe$_3$)$_2$}$_2$(THF)$_2$] (0.400 g, 0.65 mmol) in *n*-hexane (4 mL). The resulting dark purple solution was stirred for 2 h at ambient temperature and filtered. The remaining solution was concentrated *in vacuo* and stored at −40 °C. Complex **1^{Sm}** was obtained as dark purple crystals and purified by recrystallization from *n*-hexane (0.320 g, 75%). ^{1}H NMR (C$_6$D$_6$, 26 °C): δ 1.00 (s, 48H, C*H*$_3$), −3.33 (s, 8H, C*H*), −48.89 (s, 16H, C*H*$_2$) ppm. DRIFT (KBr, cm^{-1}): 2948 (vs), 2928 (vs), 2859 (s), 2834 (m), 2755 (m), 2642 (w), 2620 (vw), 1463 (m), 1416 (vw), 1381 (vs), 1362 (m), 1338 (w), 1314 (vw), 1291 (w), 1171 (m), 1059 (w), 994 (w), 808 (m), 660 (s), 616 (m), 434 (w). Elemental analysis calcd (%) for C$_{32}$H$_{72}$Al$_2$Sm (661.24 g/mol): C 58.12, H 10.98; found C 58.17, H 11.05.

[Eu(Al*i*Bu$_4$)$_2$] (1^{Eu}). [Eu{N(SiMe$_3$)$_2$}$_2$(THF)$_2$] (936 mg, 1.52 mmol) was dissolved in *n*-hexane (5 mL), and a solution of TIBA (2.106 g, 10.62 mmol) in *n*-hexane (2 mL) was added dropwise under stirring. The resulting clear solution was stirred 3 h at ambient temperature, and concentrated *in vacuo*. Single crystals suitable for X-ray characterization were obtained after several days at −40 °C from *n*-hexane. Repeated crystallization afforded 897 mg spectroscopically pure **1^{Eu}** as yellowish solid (1.35 mmol, 89%). DRIFT (KBr, cm^{-1}): 2949 (s), 2860 (m), 2745 (m), 2645 (w), 2554 (vw), 1463 (m), 1417 (vw), 1381 (w), 1362 (w), 1314 (w), 1291 (vw), 1171 (m), 1059 (m), 994 (m), 944 (vw), 912 (vw), 807 (m), 671 (vs), 658 (vs), 619 (s), 595 (m), 581 (m), 426 (m). Elemental analysis calcd (%) for C$_{32}$H$_{72}$Al$_2$Eu (662.84 g/mol): C 57.98, H 10.95; found C 57.88, H 11.32.

[Yb(Al*i*Bu$_4$)$_2$] (1^{Yb}). [Yb(Al*i*Bu$_4$)$_2$] (**1^{Yb}**) was prepared following literature procedures employing [Yb{N(SiMe$_3$)$_2$}$_2$(THF)$_2$] and TIBA.[3] Crystals suitable for X-ray analysis were obtained from 1,2-difluorobenzene.

[Cp*$_2$Yb(Al*i*Bu$_4$)] (2^{Yb}). To a solution of **1^{Yb}** (340 mg, 0.532 mmol) in *n*-pentane (1 mL), a solution of Cp*$_2$Pb (254.2 mg, 0.532 mmol) in *n*-pentane (4 mL) was added dropwise. The resulting dark solution was stirred for 15 minutes at ambient temperature, and chunks of elemental lead were removed from the black suspension by filtration. Dark blue crystals were grown from the filtrate at –40 °C. After recrystallization from *n*-pentane, analytically pure **2^{Yb}** (325 mg, 88%) was obtained. DRIFT (KBr, cm^{-1}): 2964 (s), 2945 (vs), 2914 (s), 2861 (s), 2767 (vw), 2731 (vw), 1488 (vw), 1457 (w), 1443 (w), 1379 (w), 1359 (w), 1312 (vw), 1251 (vw), 1207 (vw), 1173 (vw), 1157 (w), 1060 (w), 1020 (w), 937 (vw), 810 (w), 685 (m), 665 (w), 643 (w), 577 (vw), 550 (w), 432 (vw). C$_{36}$H$_{66}$AlYb (698.93 g/mol): calcd. C 61.86, H 9.52; found C 61.85, H 9.53.

[Cp*$_2$Sm(Al*i*Bu$_4$)] (2^{Sm}). To a solution of [Sm(Al*i*Bu$_4$)$_2$] (**1^{Sm}**, 200 mg, 0.303 mmol) in *n*-pentane (1 mL), a solution of Cp*$_2$Pb (144.5 mg, 0.303 mmol) in *n*-pentane (3 mL) was added dropwise, which led to a rapid color change from deep purple to red-orange. After stirring for 12 h at ambient temperature, the solution was filtrated from chunks of elemental lead, and concentrated in vacuum. Complex **2^{Sm}** rapidly crystallized at –40 °C, affording 201 mg (98%) as red-orange plates. C$_{36}$H$_{66}$AlSm (676.25 g/mol): calcd. C 63.94, H 9.84; found C 64.01, H 10.05. Further analytics in accord with literature data.[4]

[$Sm_6Cl_8(Al$*i*$Bu_4)_6$] (3). To a solution of [Sm(Al*i*Bu$_4$)$_2$] (**1^{Sm}**, 1.488 g, 2.25 mmol) in *n*-hexane (10 mL) cooled to −40 °C, a cooled solution of hexachloroethane (0.357 g, 1.51 mmol) in *n*-hexane (5 mL) was added dropwise over 30 minutes. The mixture was allowed to warm to ambient temperature, stirred for two hours, concentrated *in vacuo*, and stored at −40 °C. Complex **3** was obtained as dark green crystals suitable for X-ray diffraction analysis, and purified by repeated recrystallization from *n*-pentane (0.478 mg, 47%). DRIFT (KBr, cm^{-1}): 2948 (vs), 2861 (s), 2773 (w), 2730 (m), 2641 (vw), 1463 (s), 1448 (w), 1417 (vw), 1403 (w), 1384 (w), 1361 (w), 1317 (vw), 1174 (w), 1159 (w), 1063 (w), 1019 (vw), 953 (vw), 942 (vw), 814 (vw), 680 (m), 668 (m), 617 (vw), 596 (vw), 438 (vw). Elemental analysis calcd (%) for $C_{96}H_{216}Al_6Cl_8Sm_6$ (2718.84 g/mol): C 42.42, H 8.01, found: C 42.23, H 7.86.

[$Yb_4Cl_4(Al$*i*$Bu_4)_4$] (4). To a solution of [Yb(Al*i*Bu$_4$)$_2$] (**1^{Yb}**, 50.0 mg, 0.0783 mmol) in *n*-pentane (2 mL), a solution of hexachloroethane (12.0 mg, 0.051 mmol, 1.3 equiv.) in *n*-pentane (2 mL) was added dropwise under stirring. The yellowish solution was stirred overnight. Reducing the solvent in vacuum and cooling to −40 °C yielded pale yellow crystals of **4^{Yb}** co-crystallized with **1^{Yb}**. All attempts to recrystallize pure compounds failed due to contamination with by-products, and presumably slow decomposition of the product. Single crystals of **4** suitable for X-ray diffraction analysis were grown from *n*-pentane.

[{SmCl(THF)$_5$)(AlBn*i*Bu$_3$}]$_n$ (5). To a solution of [Sm(Al*i*Bu$_4$)$_2$] (**1^{Sm}**, 100.0 mg, 0.15 mmol) in toluene (1 mL), a suspension of $TeCl_4$ (13.6 mg, 0.05 mmol) in toluene (5 mL) was added in several portions. The resulting suspension was stirred for one day at ambient temperature. The slurry was filtrated, and the volume of the dark brown filtrate was reduced in vacuum. Since no crystalline material was obtained upon storage at −40 °C over several weeks, the solvent was removed in vacuum, and the residue was dissolved in THF (1mL). The resulting, purple solution was stored at −40 °C. Blue crystals of **5** suitable for X-ray analysis formed after overlaying the solution with of a small amount of *n*-hexane. However, the yield of crystalline material obtained was too low for recrystallization, and remaining TIBA hindered the characterization of the product.

[Sm{HB(C_6F_5)$_3$}$_2$(toluene)$_2$] (6). [Sm(Al*i*Bu$_4$)$_2$] (**1^{Sm}**) (100 mg, 0.151 mmol) was suspended in *n*-pentane (2 mL). After the addition of 1.8 equiv. B(C_6F_5)$_3$ (139 mg, 0.272 mmol) in toluene (4 mL), the suspension was stirred for 0.5 h at 40 °C. The remaining, brownish orange suspension was concentrated in vacuum and centrifuged. The resulting precipitate was washed three times with *n*-pentane (0.5 mL), affording **6** as an orange, hardly soluble powder (135 mg, 0.099 mmol, 73%). Crystals suitable for single crystal X-ray structure determination were obtained from a very diluted solution of **5** in 1,2-difluorobenzene layered with toluene at –40 °C. DRIFT (KBr, cm^{-1}): 2313 (vw), 2282 (vw), 2166 (vw), 2123 (vw), 1644 (vw), 1595 (vw), 1516 (s), 1496 (vs), 1374 (vw), 1279 (vw), 1112 (w), 1082 (w), 972 (m), 959 (s), 888 (vw), 769 (vw), 673 (vw). $C_{57}H_{26}B_2F_{30}Sm$ (1360.61 g/mol): calcd. C 44.14, H 1.33; found C 43.77, H 1.53.

[Yb{HB(C_6F_5)$_3$}$_2$(C_6H_6)] (7). With B(C_6F_5)$_3$ (= cocatalyst **C**), crystals of [Yb(C_6D_6){HB(C_6F_5)$_3$}$_2$] (**6**) formed from an equimolar solution in deuterated benzene in a J. Young-valved NMR tube after resting several days at ambient temperature.

[Sm{HB(C$_6$F$_5$)$_3$}$_2$(OEt$_2$)$_3$] (8). [Sm({HB(C$_6$F$_5$)$_3$}$_2$(toluene)$_2$] (**6**) (20 mg, 0.015 mmol) was dissolved in diethyl ether (5 mL), resulting in a clear orange-red solution. After stirring five minutes at ambient temperature, and evaporation of the solvent, orange red crystals of **8** were obtained (20.1 mg, 0.014 mmol, 98%). Crystals suitable for X-ray crystallography were grown from a diethyl ether solution at –40 °C. DRIFT (KBr, cm^{-1}): 2990 (vw), 2947 (vw), 2903 (vw), 2294 (vw), 2169 (vw), 2064 (vw), 1645 (vw), 1606 (vw), 1515 (s), 1468 (vs), 1389 (w), 1371 (vw), 1275 (w), 1110 (m), 1079 (m), 1047 (w), 998 (vw), 972 (s), 959 (vs), 892 (w), 777 (w), 669 (vw), 634 (vw), 604 (vw), 467 (vw). C$_{48}$H$_{32}$B$_2$F$_{30}$O$_3$Sm (1398.70 g/mol): calcd. C 41.22, H 2.31; found C 40.72, H 2.41.

[Yb(Al*i*Bu$_4$)$_2$(18-crown-6)] (9). To a solution of **1^{Yb}** (50.0 mg, 0.078 mmol, 1 equiv.) in *n*-hexane (0.5 mL), a solution of 18-crown-6 (10.3 mg, 0.039 mmol, 0.5 equiv.) in *n*-hexane (1.5 mL) was added dropwise under stirring. The immediately formed, almost colorless precipitate was washed twice with 2 mL *n*-hexane and dried *in vacuo*. The remaining powder was recrystallized from toluene at –40 °C, yielding complex **9** as colorless plates suitable for X-ray diffraction analysis (48.5 mg, 0.0512 mmol, 65%). ^{1}H NMR (400.1 MHz, C$_6$D$_6$, 26 °C): δ 3.06 (s, 24 H, 18-C-6-C*H*$_2$), δ 2.25 (m, 8H, C*H*), δ 1.40 (d, 48 H, C*H*$_3$), δ 0.09 (d, 16H, C*H*$_2$) ppm. ^{13}C{^{1}H} NMR (100.6 MHz, 26 °C): δ 70.1 (18-C-6-*C*H$_2$), 29.8 (*C*H$_3$); 29.1 (*C*H), 28.6 (*C*H$_2$) ppm. DRIFT (KBr, cm^{-1}): 2939 (vs), 2851 (s), 2832 (s), 2770 (m), 2584 (vw), 1461 (w), 1354 (w), 1306 (vw), 1286 (vw), 1251 (vw), 1203 (vw), 1162 (w), 1096 (vs), 1046 (w), 1010 (vw), 978 (m), 842 (vw), 809 (vw), 729 (vw), 665 (w), 643 (w), 449 (w). C$_{44}$H$_{96}$Al$_2$O$_6$Yb (948.23 g/mol): calcd. C 55.73, H 10.20; found C 55.49, H 10.00.

Activation of Precatalysts for ^{1}H-NMR Spectroscopy. A detailed procedure is described as a typical example. A J. Young-valved NMR tube was charged with [Yb(Al*i*Bu$_4$)$_2$] (**1^{Yb}**) (6.9 mg, 0.01 mmol), and [Ph$_3$C][B(C$_6$F$_5$)$_4$] (**A**) (1 equiv., 10.0 mg, 0.01 mmol). Deuterated benzene was added to the mixture, yielding a yellowish suspension, which was shaken gently. NMR spectra were recorded after sedimentation of the precipitate. Analogously, activation was performed with [C$_6$H$_5$NMe$_2$H][B(C$_6$F$_5$)$_4$] (**B**), B(C$_6$F$_5$)$_3$ (**C**), and *i*Bu$_2$AlCl (**F**).

Polymerization

Detailed procedures are described as typical examples.

Polymerization of Isoprene (Entries 1-13, 15-17, Table 1). (Table 1, entry 2). [Sm(Al*i*Bu$_4$)$_2$] (**1^{Sm}**) (13.22 mg, 0.02 mmol) and [CPh$_3$][B(C$_6$F$_5$)$_4$] (**A**) (1 equiv., 18.45 mg, 0.02 mmol) were dissolved in toluene (8 mL), and stirred at ambient temperature for 30 minutes. After addition of isoprene (20 mmol), the polymerization was carried out at ambient temperature for 24 h under stirring (500 rpm). The solution was quenched in methanol (20 mL) containing 0.1% (w/w) 2,6-di-*tert*-butyl-4-methylphenol as a stabilizer. The precipitated polymer was dried *in vacuo* at ambient temperature to constant weight.

Polymerization of Isoprene with [Yb(Al*i*Bu$_4$)$_2$] and [C$_6$H$_5$NMe$_2$H][B(C$_6$F$_5$)$_4$] (Entries 14-17, Table 1). [Yb(Al*i*Bu$_4$)$_2$] (**1^{Yb}**) (10 equiv., 136.78 mg, 0.20 mmol) and [C$_6$H$_5$NMe$_2$H][B(C$_6$F$_5$)$_4$] (**B**) (10 equiv., 160.24 mg, 0.20 mmol) were dissolved in 50 mL toluene and stirred at 500 rpm and ambient temperature for 30 minutes, whereupon a clear, orange colored solution had formed. Each 5 mL (0.02 mmol catalyst) of the aged catalyst solution was put in a vial and was diluted with each additional 5 mL of toluene. Each 0.5 mL isoprene (5 mmol), was added and stirred at 500 rpm for two hours. Two batches were quenched following the above-mentioned

procedure. Each 0.5 mL isoprene (5 mmol) was added to the remaining flasks, respectively. After stirring for one additional hour, two batches were quenched, and isoprene addition/stirring was repeated for the remaining four flasks. The same procedure was repeated, and the last batches were quenched 5 h after the initial isoprene addition. Further workup was performed as described above.

NMR Spectra

In general, solvent residual signals are labeled with an asterisk (*). In some cases, the paramagnetic nature of Eu(II), Sm(II) and Sm(III) did not allow a conclusive interpretation of the recorded NMR spectra (**1**^{Eu}, **2**, **5**, **7**).

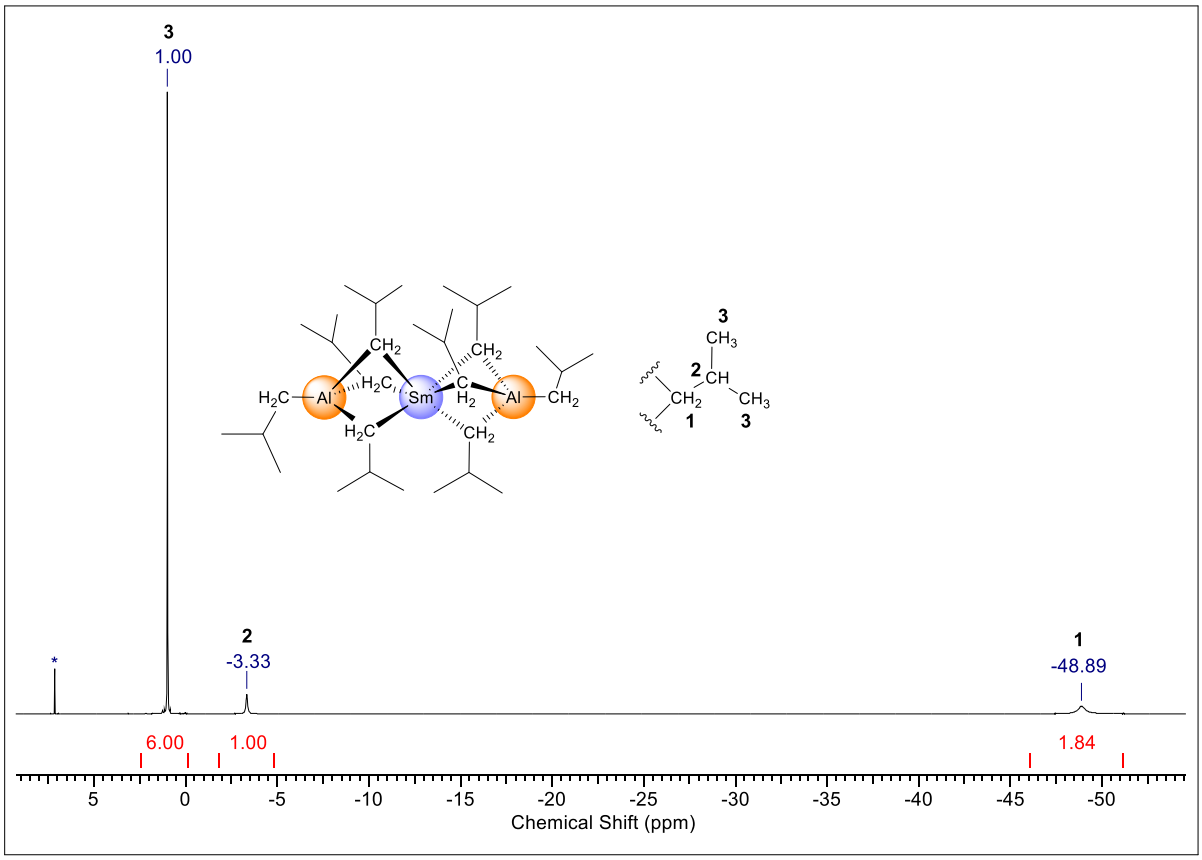

Figure S1. ^{1}H-NMR spectrum (400 MHz, C_6D_6, 26 °C) of [Sm(Al*i*Bu$_4$)$_2$] (**1**^{Sm}).

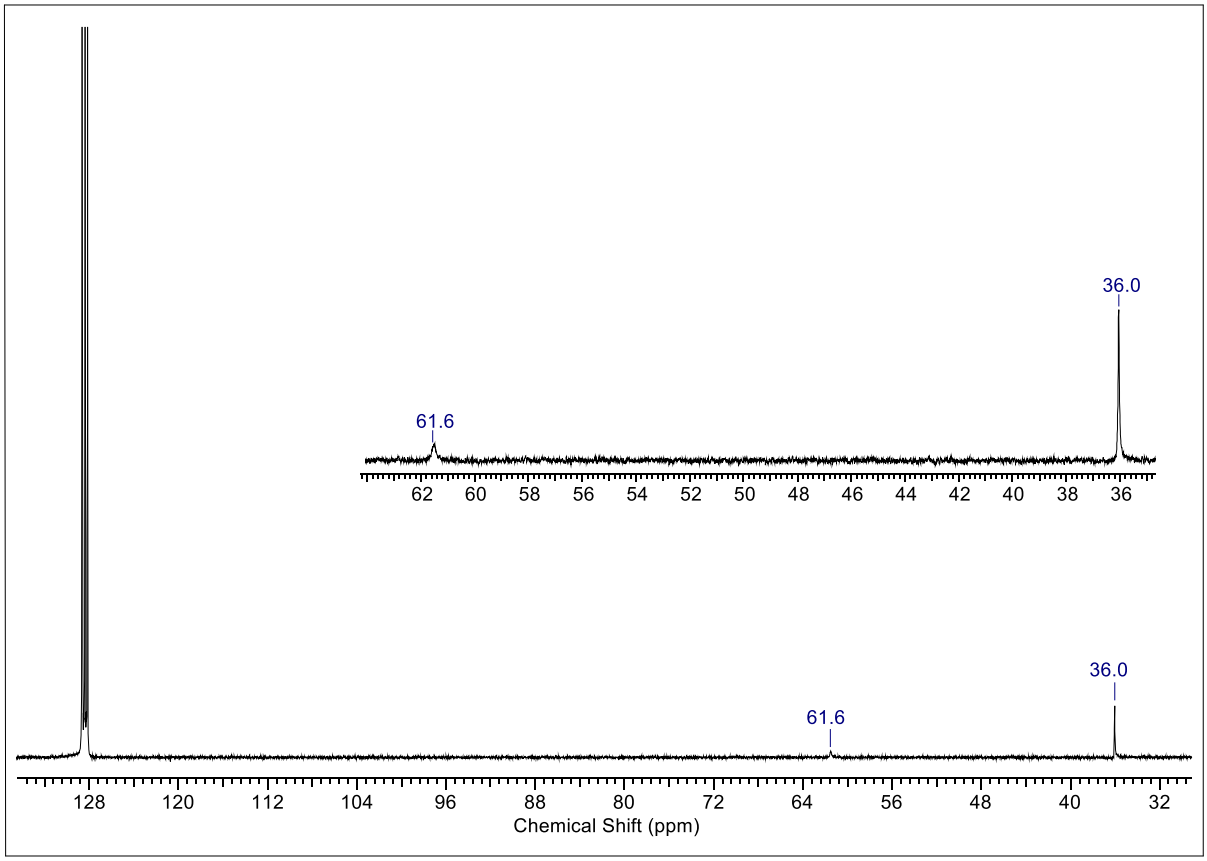

Figure S2. $^{13}C\{^{1}H\}$-NMR spectrum (101 MHz, C_6D_6, 26 °C) of [Sm(Al*i*Bu$_4$)$_2$] **(1^{Sm})**.

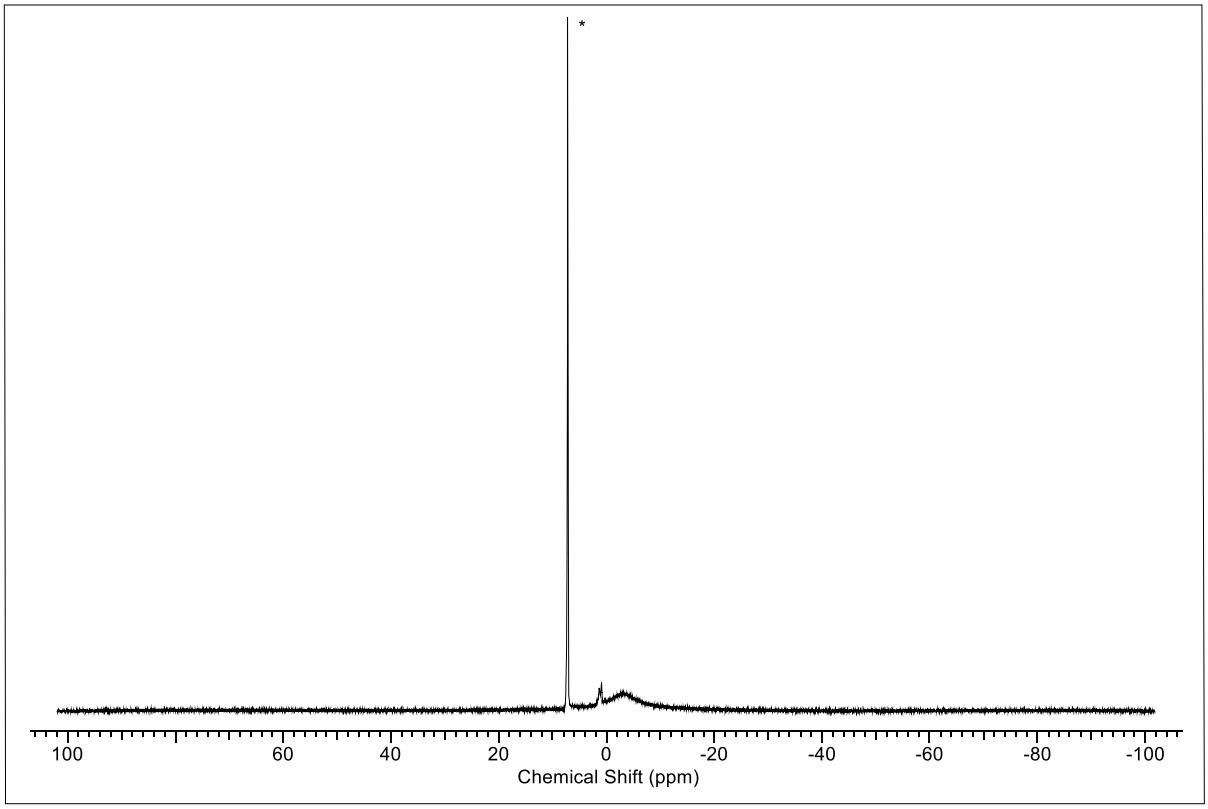

Figure S3. ^{1}H-NMR spectrum (400 MHz, C_6D_6, 26 °C) of [Eu(Al*i*Bu$_4$)$_2$] (**1^{Eu}**) showing traces of *n*-hexane and only very broadened resonances.

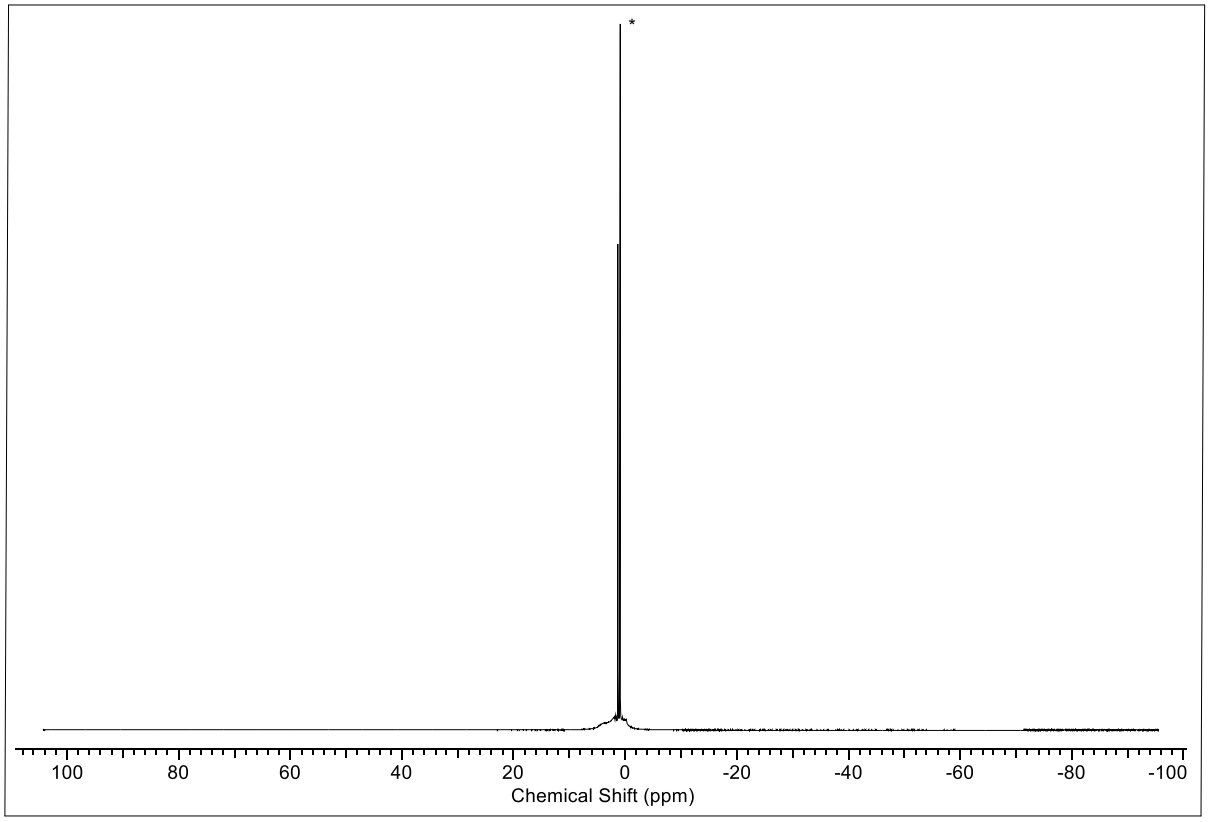

Figure S4. ^{1}H-NMR spectrum (400 MHz, *n*-C_6D_{14}, 26 °C) of $[Sm_6Cl_8(Al\textit{i}Bu_4)_6]$ (**3**).

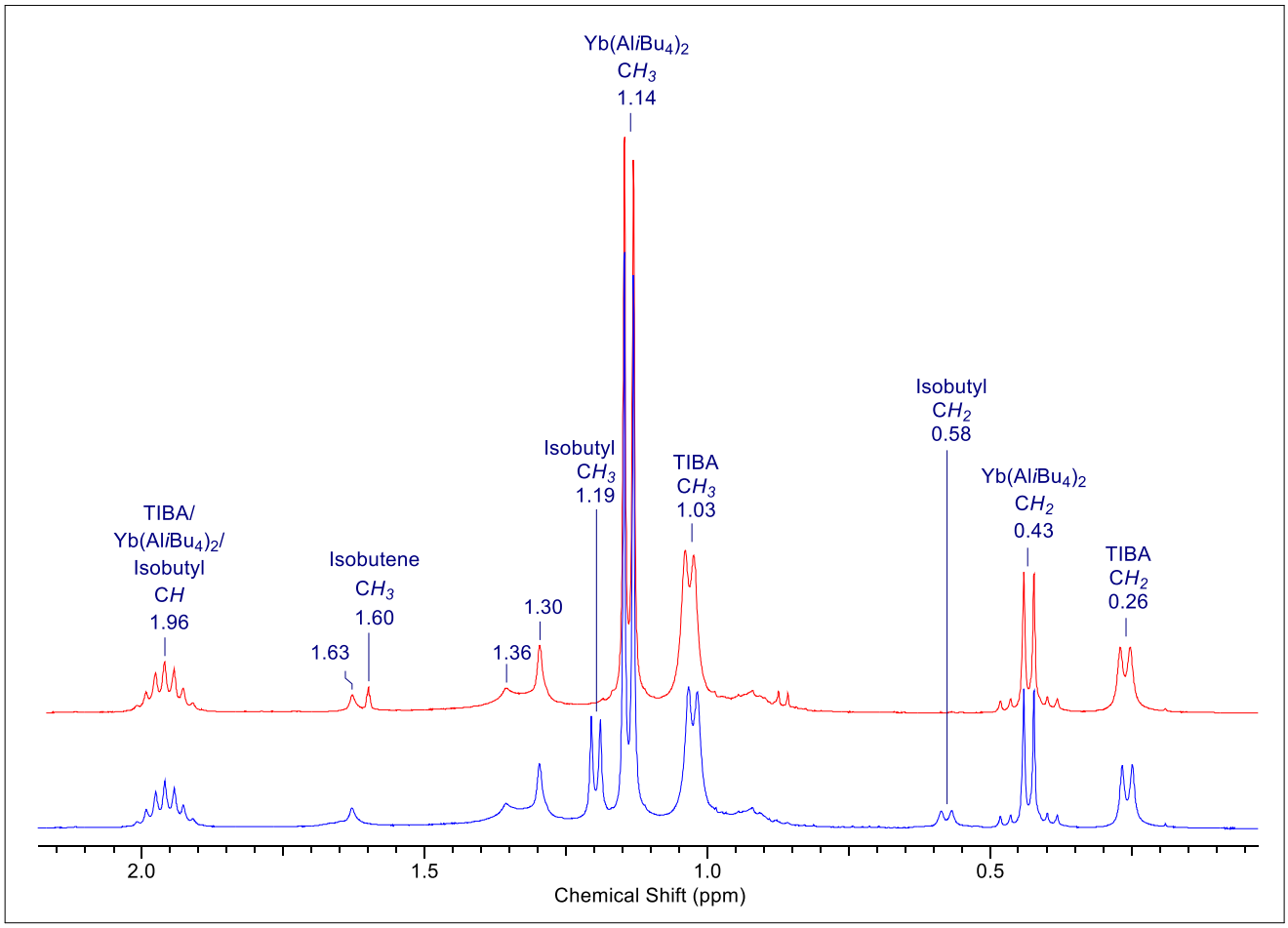

Figure S5. ^{1}H-NMR spectra (400 MHz, C_6D_6, 26 °C) of [Yb(Al*i*Bu$_4$)$_2$] (**1^{Yb}**) with 1.3 equiv. hexachloroethane measured directly (blue trace), and after two days (red trace). The reaction presumably yielded [Yb$_4$Cl$_4$(Al*i*Bu$_4$)$_4$] (**4**), [Yb(Al*i*Bu$_4$)$_2$] (**1^{Yb}**), and TIBA. Note the disappearance of the putative signals of [Yb$_4$Cl$_4$(Al*i*Bu$_4$)$_4$] (**4**) at 1.19 ppm and 0.58 ppm (red trace).

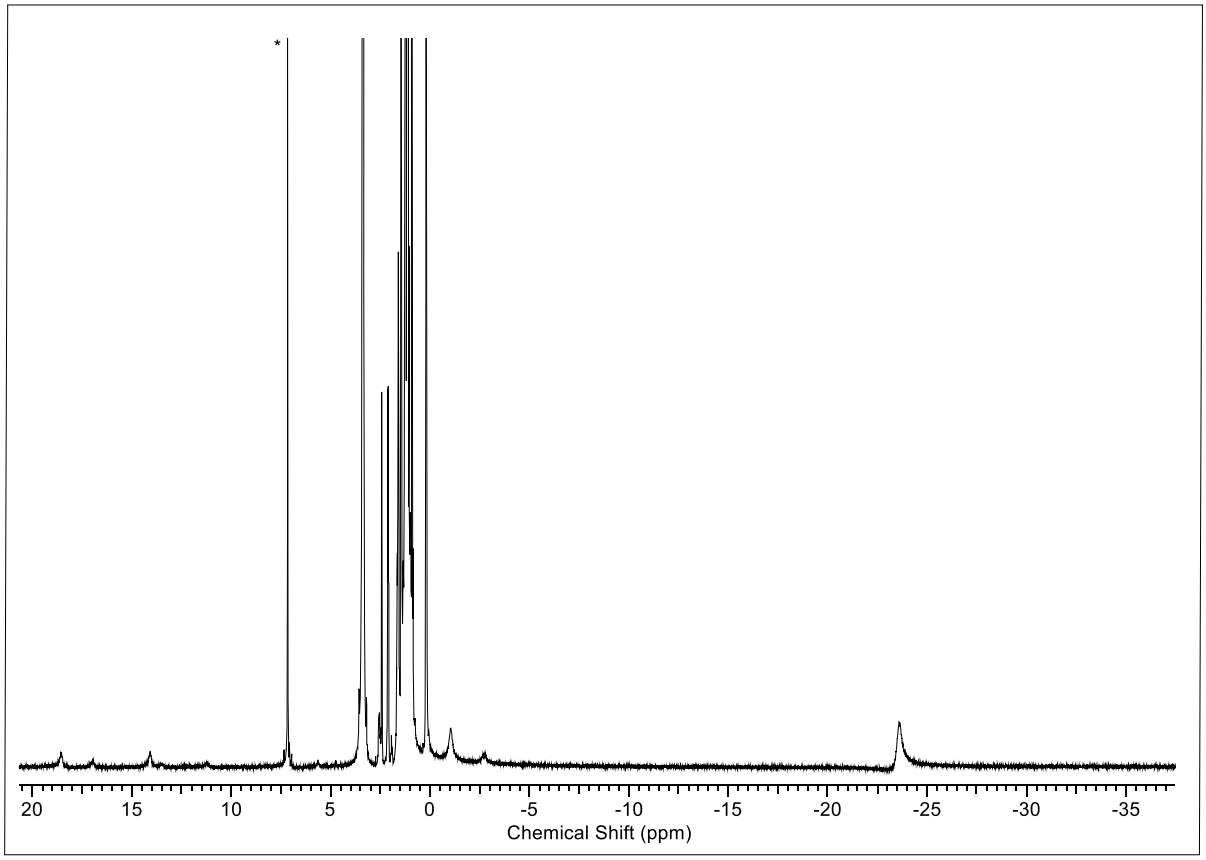

Figure S6. ^{1}H-NMR spectrum (400 MHz, C_6D_6, 26 °C) of the reaction of [Sm(Al*i*Bu$_4$)$_2$] (**1^{Sm}**) with $TeCl_4$ and THF.

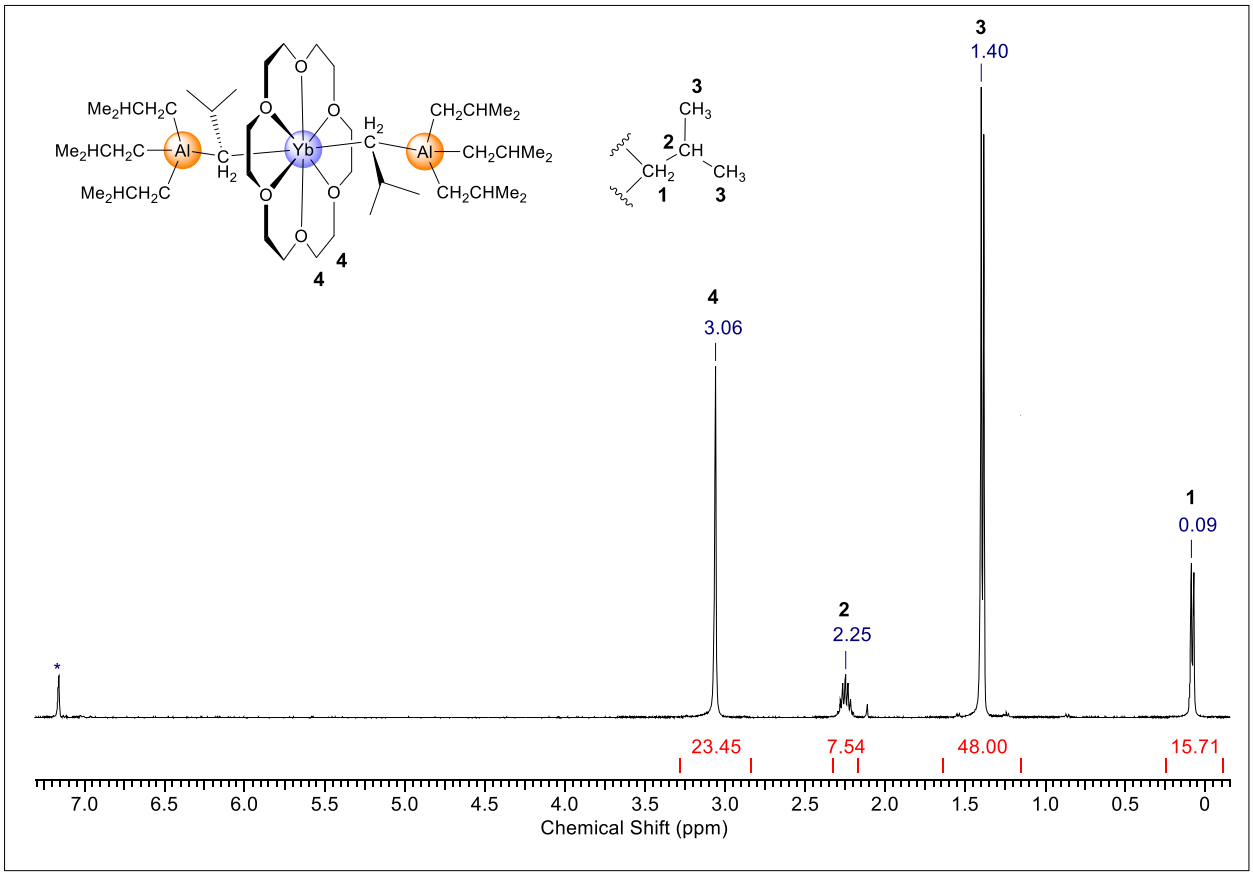

Figure S7. ^{1}H-NMR spectrum (400 MHz, C_6D_6, 26 °C) of [Yb(Al*i*Bu$_4$)$_2$(18-crown-6)] (**9**).

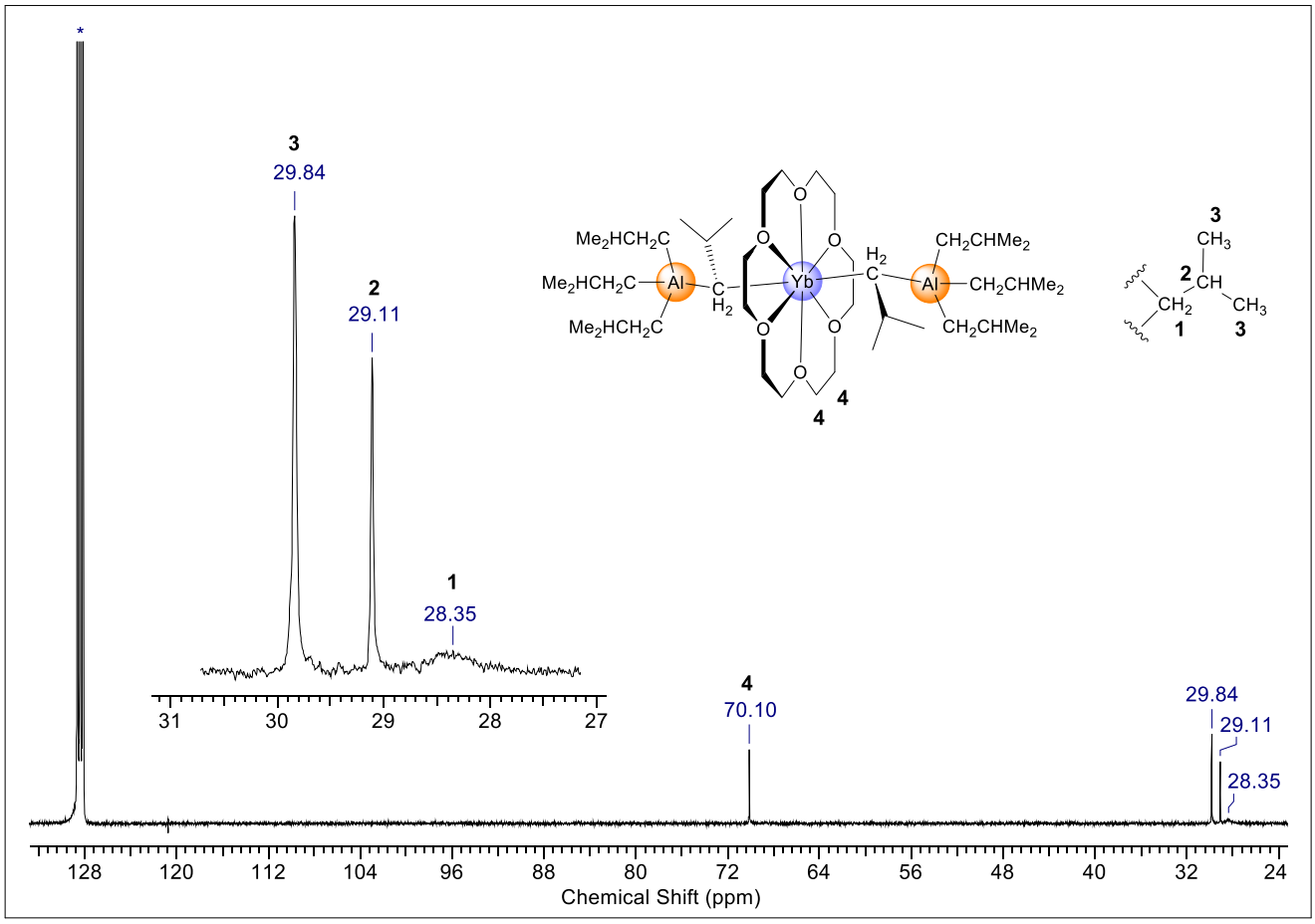

Figure S8. $^{13}C\{^{1}H\}$-NMR spectrum (101 MHz, C_6D_6, 26 °C) of [Yb(Al*i*Bu$_4$)$_2$(18-crown-6)] (**9**).

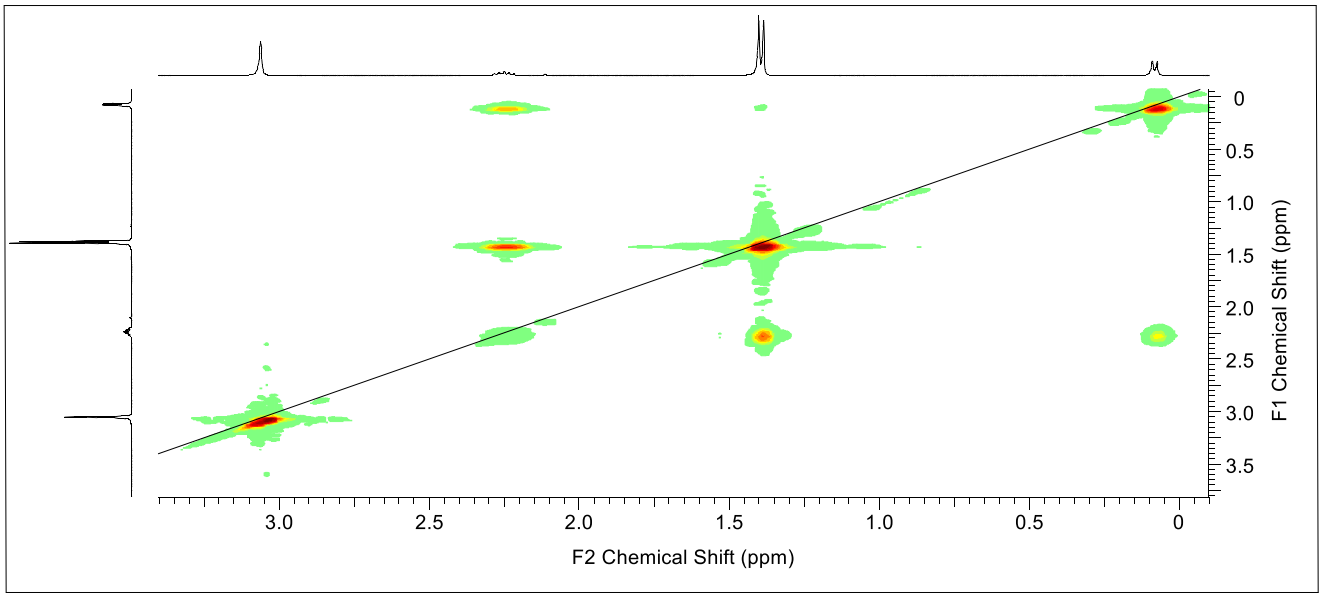

Figure S9. ^{1}H-^{1}H COSY spectrum (400/400 MHz) of [Yb(Al*i*Bu$_4$)$_2$(18-crown-6)] (**9**) in C_6D_6 at 26 °C.

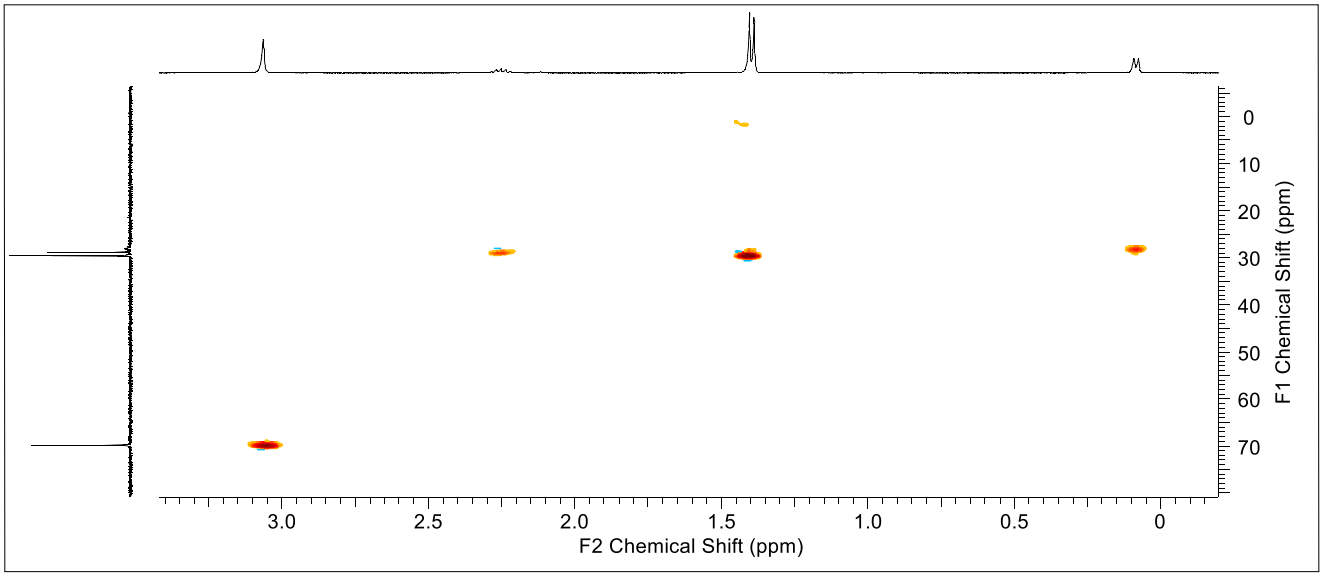

Figure S10. ^{1}H-^{13}C{^{1}H} HSQC (400/101 MHz) spectrum of [Yb(Al*i*Bu$_4$)$_2$(18-crown-6)] (**9**) in C_6D_6 at 26 °C.

Reactions of 1^{Yb} with 1 equiv. of cocatalysts

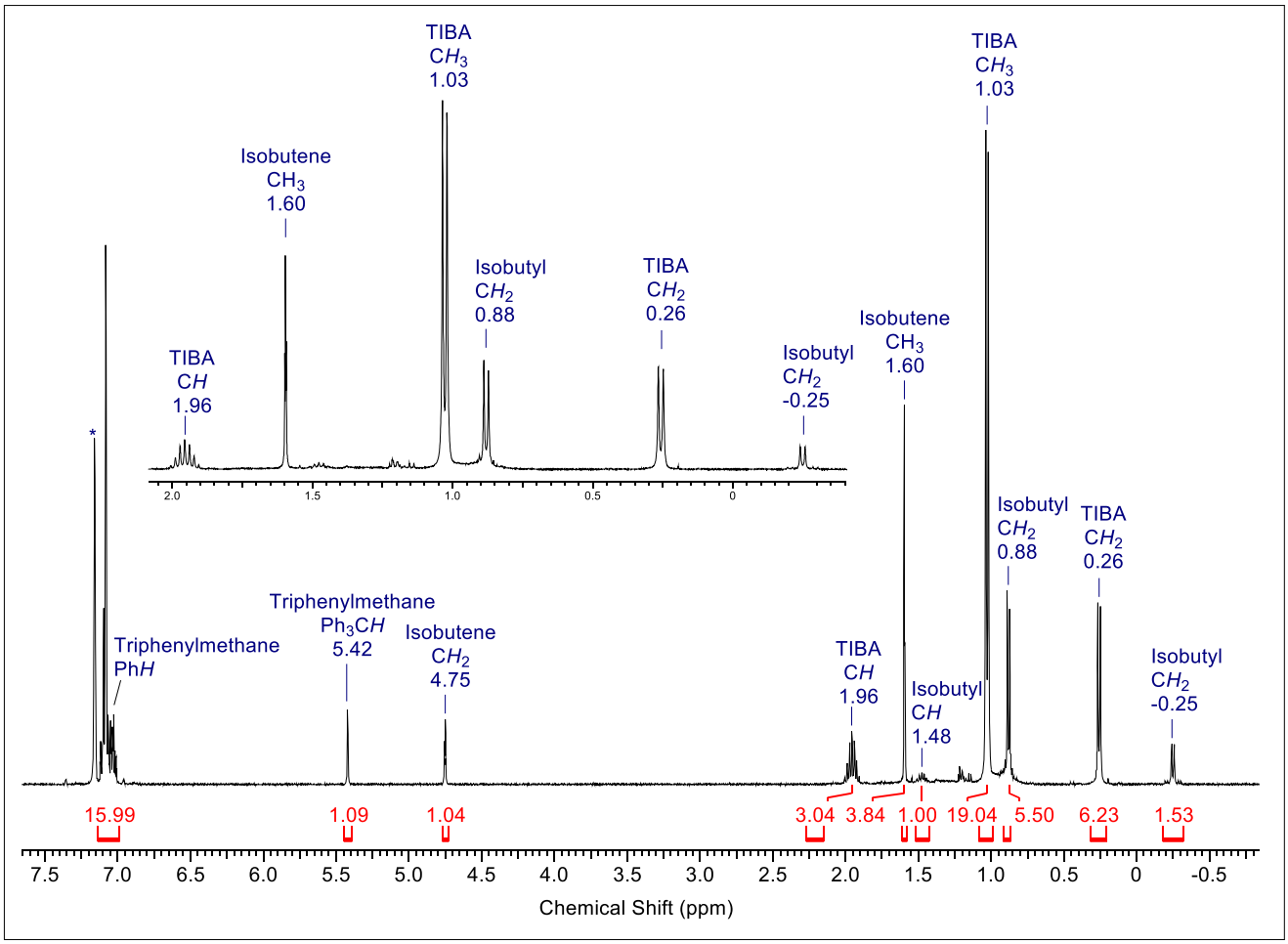

Figure S11. ^{1}H-NMR spectrum of the reaction of $\mathbf{1}^{Yb}$ with one equivalent of cocatalyst **A** (400 MHz, C_6D_6, 26 °C).

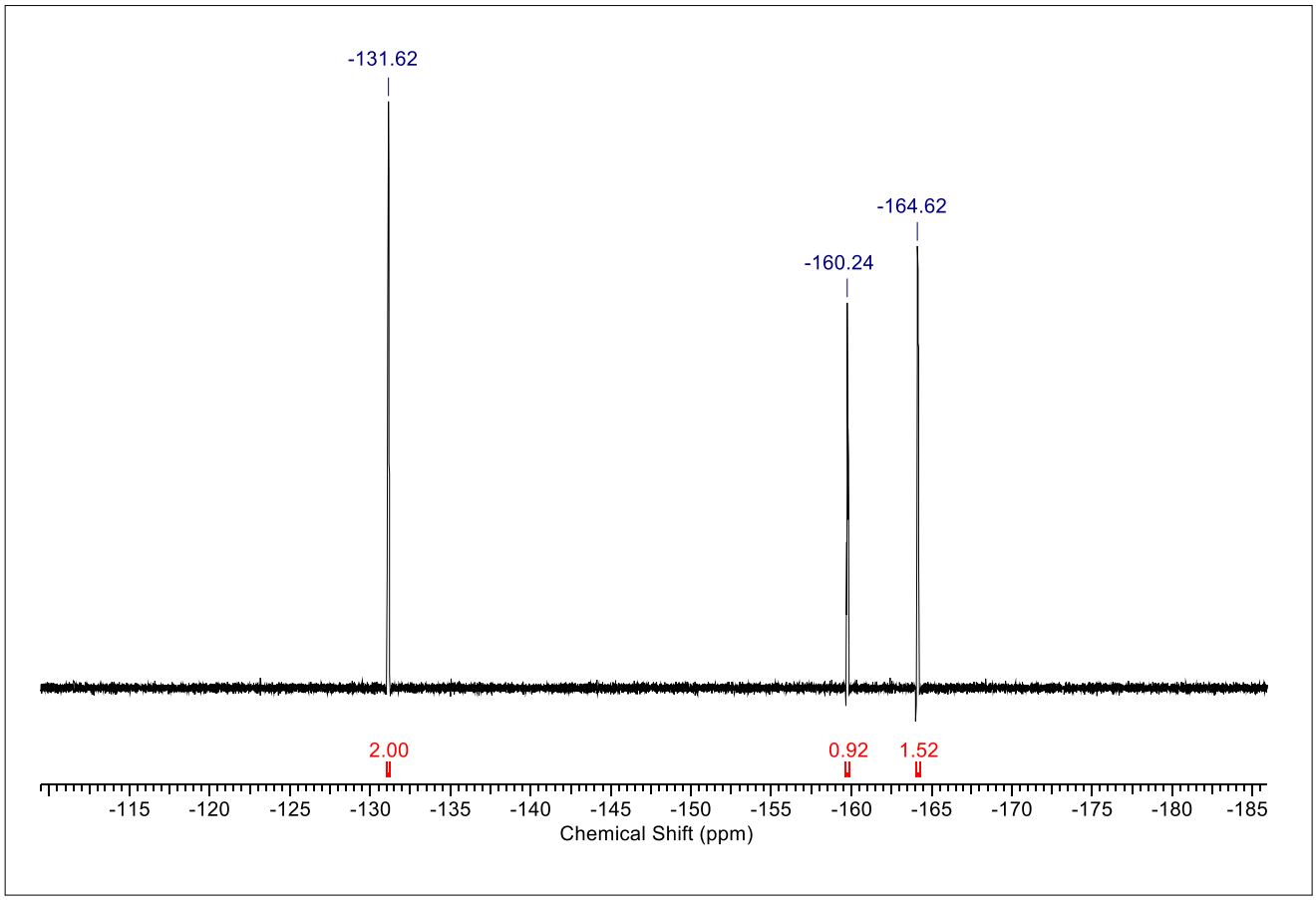

Figure S12. $^{19}F\{^{1}H\}$-NMR spectrum of the reaction of $\mathbf{1}^{\mathbf{Yb}}$ with one equivalent of cocatalyst **A** (400 MHz, C_6D_6, 26 °C).

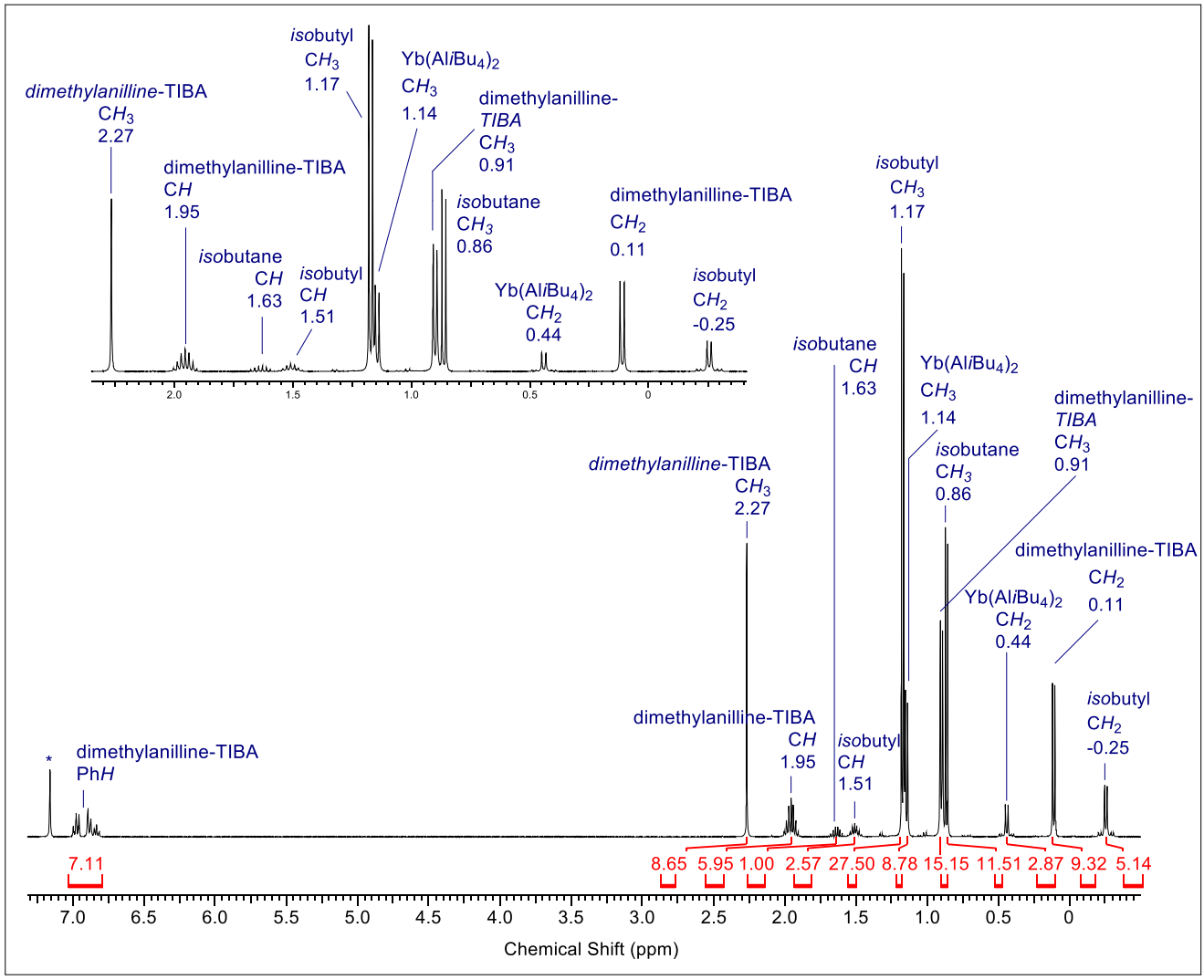

Figure S13. ^{1}H-NMR spectrum of the reaction of **1**^{Yb} with one equivalent of cocatalyst **B** (400 MHz, C_6D_6, 26 °C).

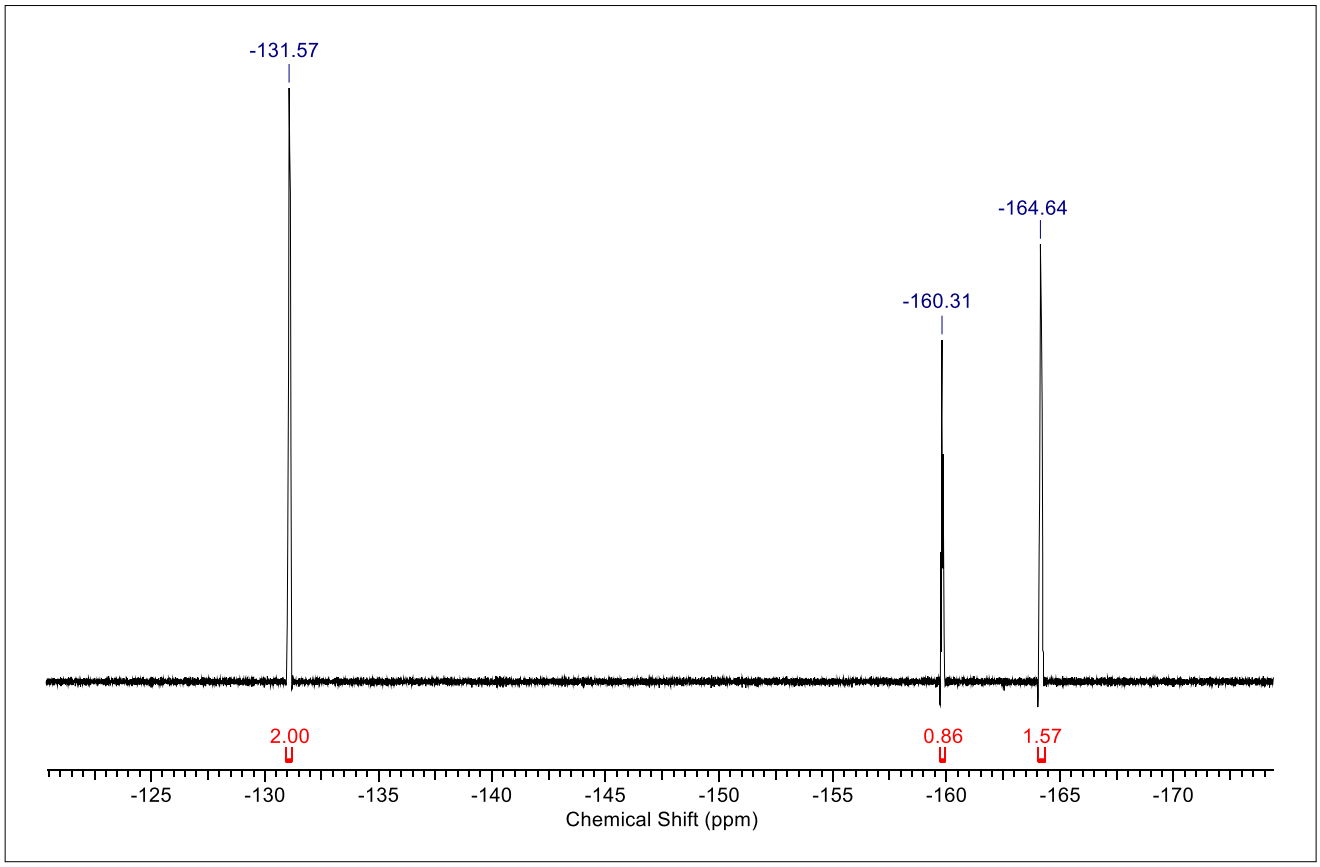

Figure S14. $^{19}F\{^{1}H\}$-NMR spectrum of the reaction of **1^{Yb}** with one equivalent of cocatalyst **B** (400 MHz, C_6D_6, 26 °C).

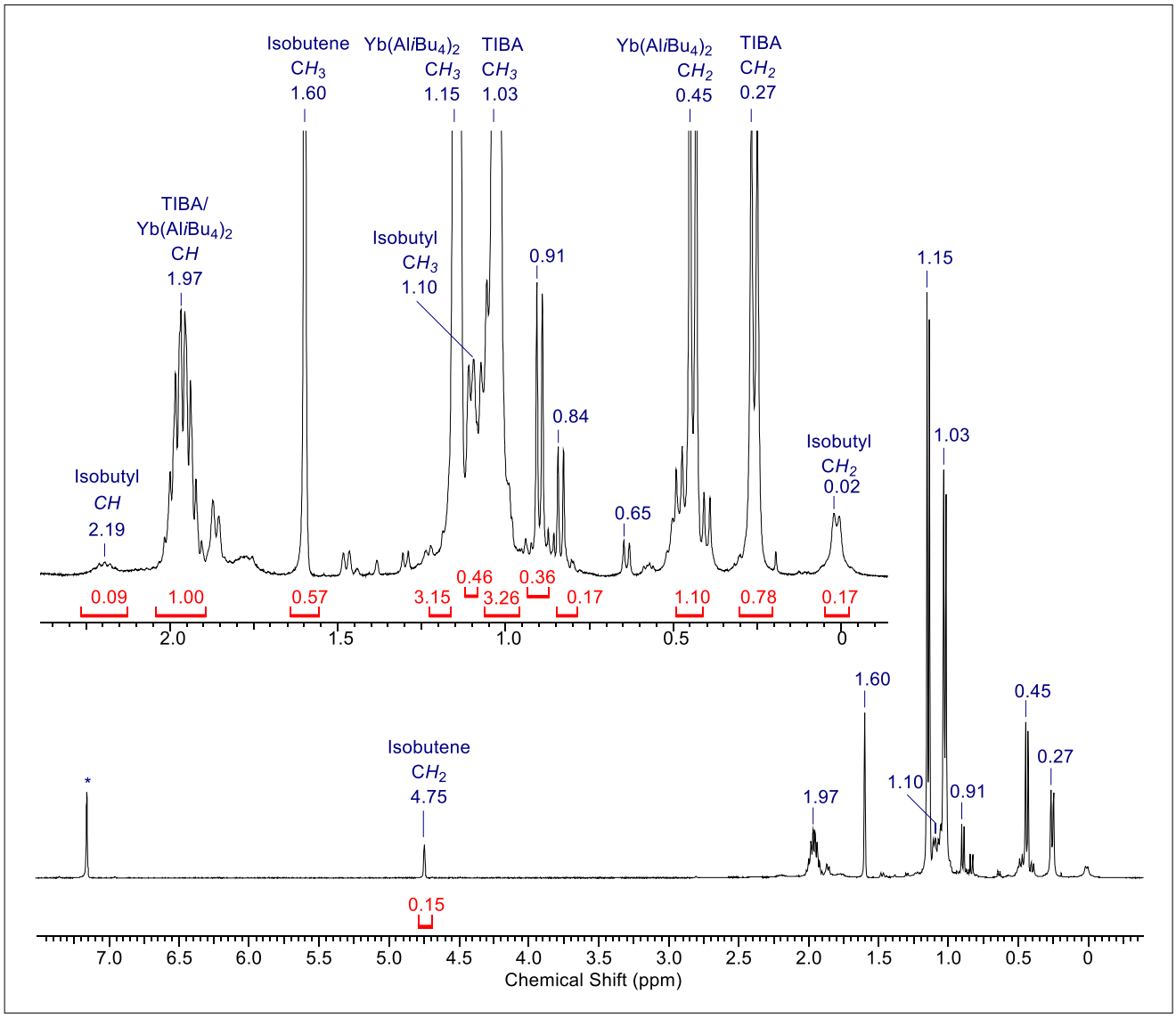

Figure S15. ^{1}H-NMR spectrum of the reaction of **1^{Yb}** with one equivalent of cocatalyst **C** (400 MHz, C_6D_6, 26 °C).

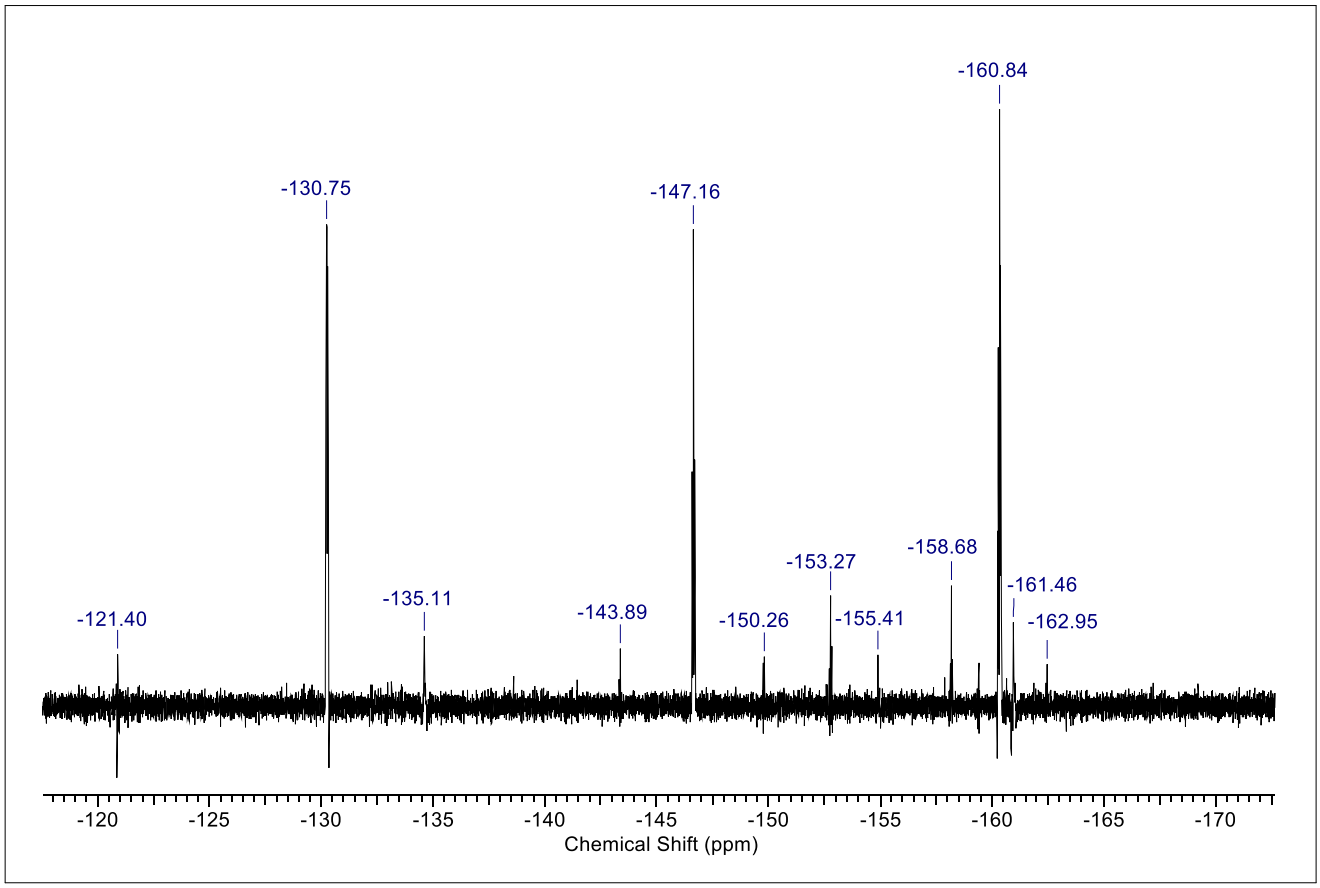

Figure S16. $^{19}F\{^{1}H\}$-NMR spectrum of the reaction of $\mathbf{1^{Yb}}$ with one equivalent of cocatalyst **C** (400 MHz, C_6D_6, 26 °C).

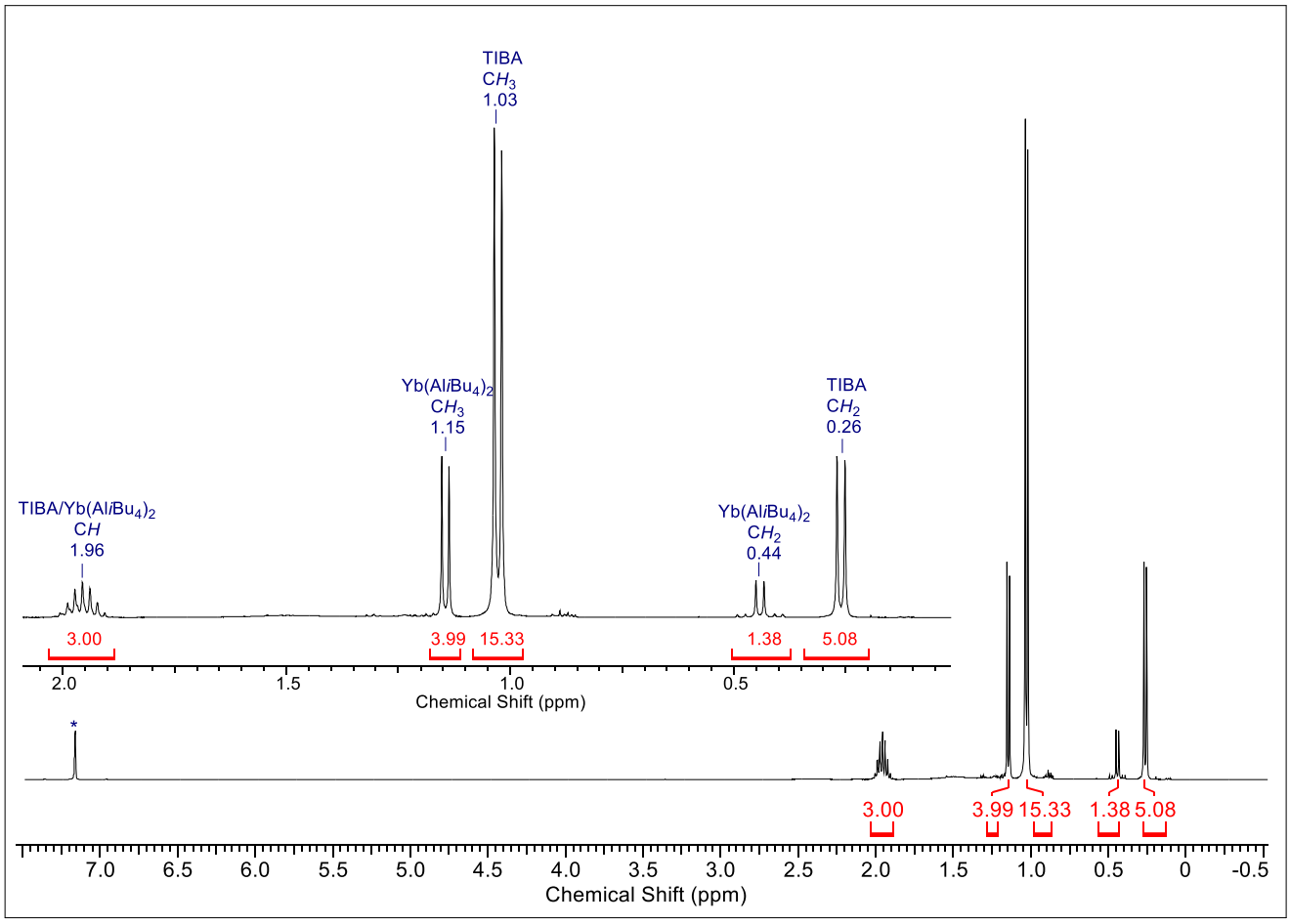

Figure S17. ^{1}H-NMR spectrum of the reaction of **1^{Yb}** with one equivalent of cocatalyst *i*Bu$_2$AlCl (**F**) (400 MHz, C_6D_6, 26 °C).

Crystallography

X-ray Crystallography and Crystal Structure Determination

For X-ray structure analyses, crystals suitable for X-ray diffraction were selected in a glovebox, coated with Parabar 10312 (Hampton Research), and fixed on a nylon/loop glass fiber. X-ray data for all compounds was collected on a Bruker APEX II DUO diffractometer equipped with an IμS microfocus sealed tube and QUAZAR optics for MoK_α (λ = 0.71073 Å). The data collection strategy was determined using COSMO,[5] employing ω-scans. Raw data were processed using APEX[6], and SAINT[6]. Corrections for absorption effects were applied using SADABS.[7] The structures were solved by direct methods and refined against all data by full-matrix least-squares methods on F2 using SHELXTL[8], and ShelXle.[9] Disorder models were calculated using DSR, a program for refining structures in ShelXl.[10] All graphics were produced employing Mercury 4.2.011[11] and POV-Ray12.[12]

For X-ray crystallography, single crystalline material of [Sm(Al*i*Bu$_4$)$_2$] (**1**^{Sm}), [Eu(Al*i*Bu$_4$)$_2$] (**1**^{Eu}) was grown from *n*-hexane at –40°C. [Yb(Al*i*Bu$_4$)$_2$] (**1**^{Yb}) was crystallized from o-difluorobenzene. Crystals of [Sm$_6$Cl$_8$(Al*i*Bu$_4$)$_6$] (**2**), [Yb$_4$Cl$_4$(Al*i*Bu$_4$)$_4$] (**3**), and [Cp*$_2$Yb(Al*i*Bu$_4$)] (**9**^{Yb}) were grown from *n*-pentane at –40°C. Crystals of [{SmCl(THF)$_5$)(AlBn*i*Bu$_3$}]$_n$ (**4**) were obtained from an *n*-hexane/THF mixture at –40 °C, [Yb(18-crown-6)(Al*i*Bu$_4$)$_2$] (**8**) was crystallized from toluene at –40 °C, whereas crystals of [Sm(PhMe)$_2${HB(C$_6$F$_5$)$_3$}$_2$] (**5**) were obtained from a o-difluorobenzene/toluene mixture at –40 °C. Complexes [Cp*$_2$Sm(Al*i*Bu$_4$)] (**9**^{Sm}), and [Yb(C$_6$H$_6$){HB(C$_6$F$_5$)$_3$}$_2$] (**5**) were crystallized from benzene at ambient temperature. [Sm(Et$_2$O)$_3${HB(C$_6$F$_5$)$_3$}$_2$] (**7**) was obtained from diethyl ether in crystalline form.

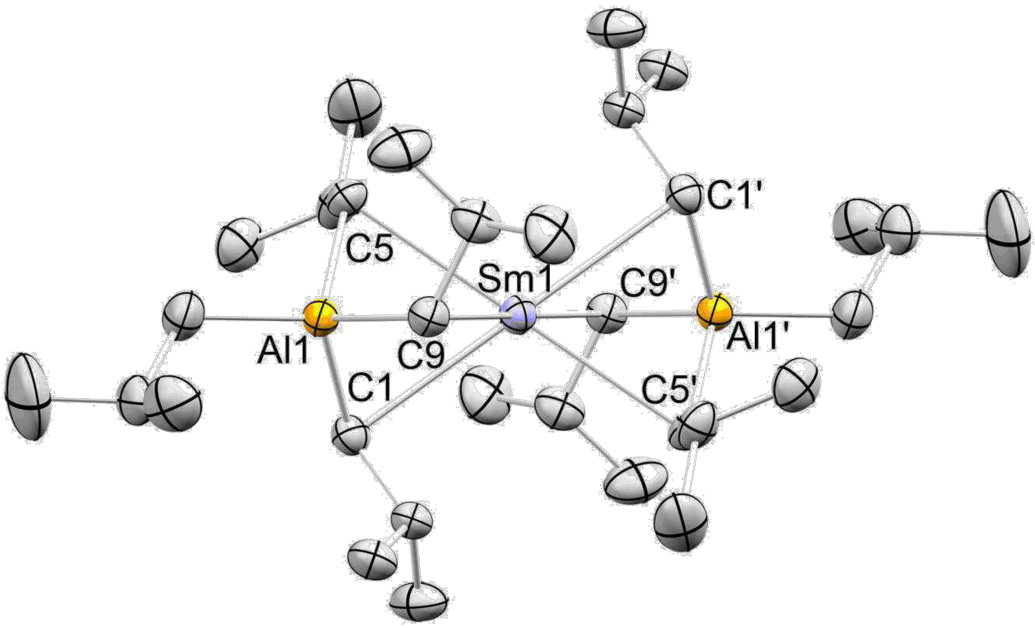

Figure S18. Crystal structure of [Sm(Al*i*Bu$_4$)$_2$] (**1^{Sm}**). Ellipsoids are shown at the 50% probability level. Hydrogen atoms are omitted for clarity. Selected interatomic distances [Å]: Sm(1)–C(1) 2.8514(18), Sm(1)–C(5) 2.8618(19), Sm(1)–C(9) 2.8854(18), Sm(1)···Al(1) 2.9690(6), Al(1)–C(1) 2.0670(19), Al(1)–C(5) 2.0695(19), Al(1)–C(9) 2.0674(18), Al(1)–C(13) 1.976(2). Selected angles [°]: C(1)-Sm(1)-C(1)‘ 180.0, C(5)-Sm(1)-C(5)‘ 180.0, C(9)-Sm(1) -C(9)‘ 180.0, C(1)-Sm(1)-C(5) 70.45(5), C(1)-Sm(1)-C(9) 69.78(5), C(5)-Sm(1)-C(9) 69.72(5).

‘-x+1, -y+1, -z+1

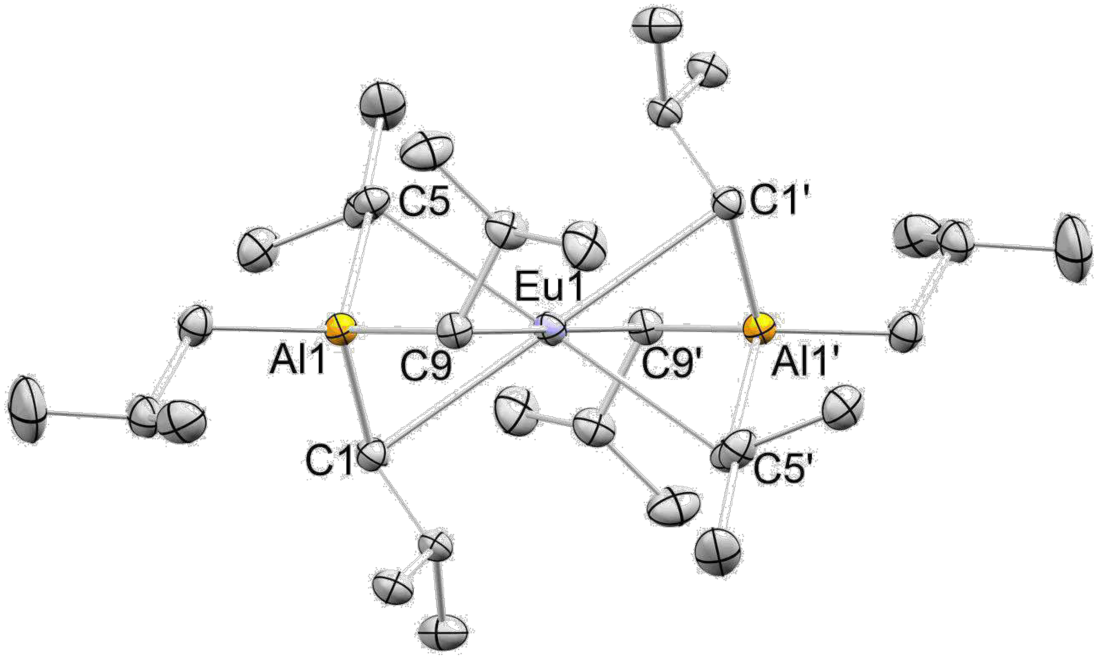

Figure S19. Crystal structure of [Eu(Al*i*Bu$_4$)$_2$] (**1^{Eu}**). Ellipsoids are shown at the 50% probability level. Hydrogen atoms are omitted for clarity. Selected interatomic distances [Å]: Eu(1)–C(1) 2.850(2), Eu(1)–C(5) 2.878(2), Eu(1)–C(9) 2.834(2), Al(1)···Eu(1) 2.9578(6), Al(1)–C(1) 2.065(2), Al(1)–C(5) 2.066(2), Al(1)–C(9) 2.067(2), Al(1)–C(13) 1.976(2). Selected angles [°]: C(1)-Eu(1)-C(1)‘ 180.0, C(5)-Eu(1)-C(5)‘ 180.0, C(9)‘-Eu(1)-C(9) 180.0, C(1)-Eu(1)-C(5) 69.88(6), C(9)-Eu(1)-C(1) 70.71(7), C(9)-Eu(1)-C(5) 69.99(6).

‘-x+1, -y+1, -z+1

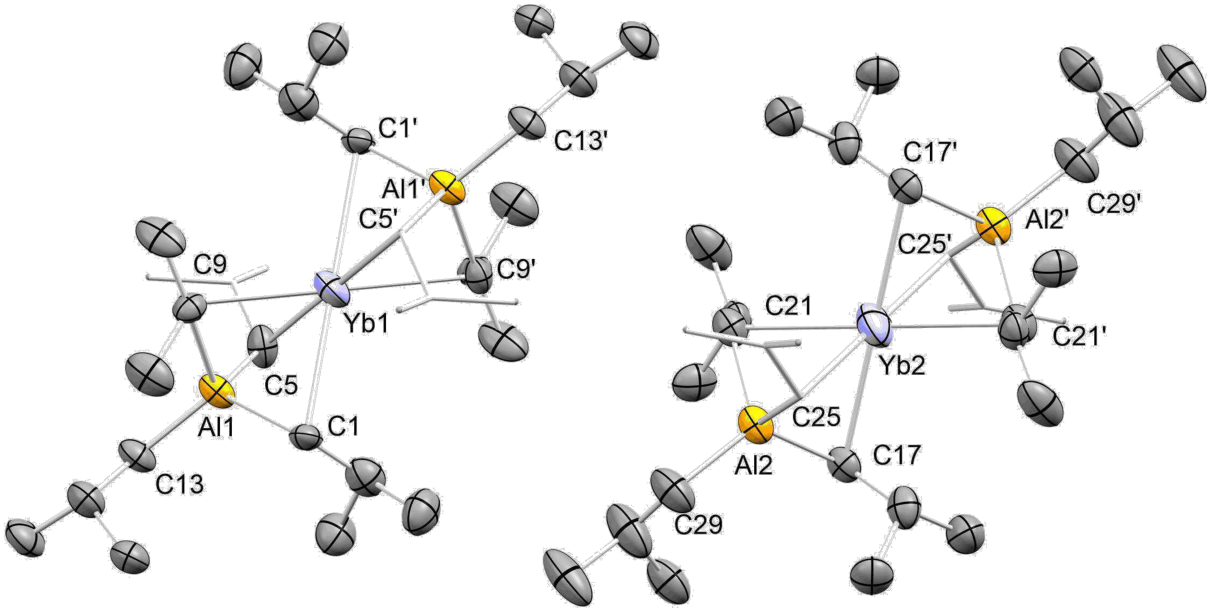

Figure S20. Crystal structure of [Yb(Al*i*Bu$_4$)$_2$] (**1^{Yb}**). Selected interatomic distances Yb(1)–C(1) 2.796(12), Yb(1)–C(5) 2.774(13), Yb(1)–C(9) 2.735(16), Yb(2)–C(17) 2.745(14), Yb(2)–C(21) 2.751(15), Yb(2)–C(25) 2.757(16), Al(1)···Yb(1) 2.853(4), Al(2) ···Yb(2) 2.840(4), Al(1)–C(1) 2.085(15), Al(1)–C(5) 2.087(13), Al(1)–C(9) 2.049(15), Al(1)–C(13) 1.973(13), Al(2)–C(17) 2.064(14), Al(2)–C(21) 2.079(16), Al(2)–C(25) 2.052(17), Al(2)–C(29) 1.970(15). Selected angles [°]: C(1)'1-Yb(1)-C(1) 180.0, C(5)-Yb(1)-C(5)‘ 180.0, C(9)-Yb(1)-C(9)‘ 180.0, C(17)-Yb(2)-C(17)’ 180.0, C(21)'-Yb(2)-C(21) 180.0, C(25)'-Yb(2)-C(25) 180.0(7), C(9)-Yb(1)-C(5) 73.7(4), C(5)-Yb(1)-C(1) 107.3(4), C(9)-Yb(1)-C(1) 72.0(4), C(9)'-Yb(1)-C(1) 108.0(4), C(5)'-Yb(1)-C(1) 107.3(4), C(5)-Yb(1)-C(1) 72.7(4), C(17)''-Yb(2)-C(21)' 107.1(4), C(17)'-Yb(2)-C(21)' 72.9(4), C(17)-Yb(2)-C(21) 72.9(4), C(17)''-Yb(2)-C(25) 107.9(4), C(21)-Yb(2)-C(25)'' 106.3(5), C(17)-Yb(2)-C(25) 72.1(4), C(21)-Yb(2)-C(25) 73.7(5), Al(1)'-Yb(1)-Al(1) 180.0, Al(2)-Yb(2)-Al(2)'' 180.00(13).

‘-x+1, -y+1, -z+1
‘‘-x+2, -y+1, -z

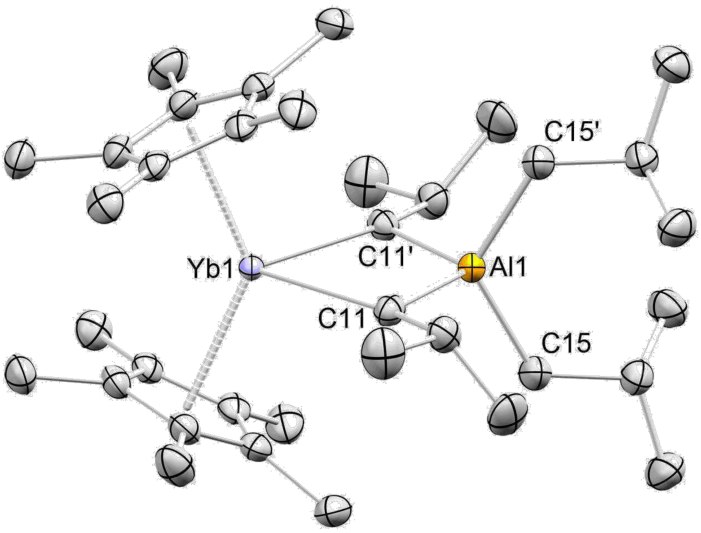

Figure S21. Crystal structure of [Cp*$_2$Yb(Al*i*Bu$_4$)] (**2^{Yb}**). Ellipsoids are shown at the 50% probability level. Hydrogen atoms are omitted for clarity. Selected bond lengths [Å]: Yb(1)–C(11) 2.6089(18), Al(1)–C(11) 2.0995(19), Al(1)–C(15) 2.021(2), Yb(1)–centroid(1) 2.357. Selected angles [°]: Centroid(1)-Yb(1)-centroid(1)' 133.74, C(11)'-Yb(1)-C(11) 79.94(8), C(15)'-Al(1)-C(15) 122.94(12).

' 1-x, +y, 3/2-z

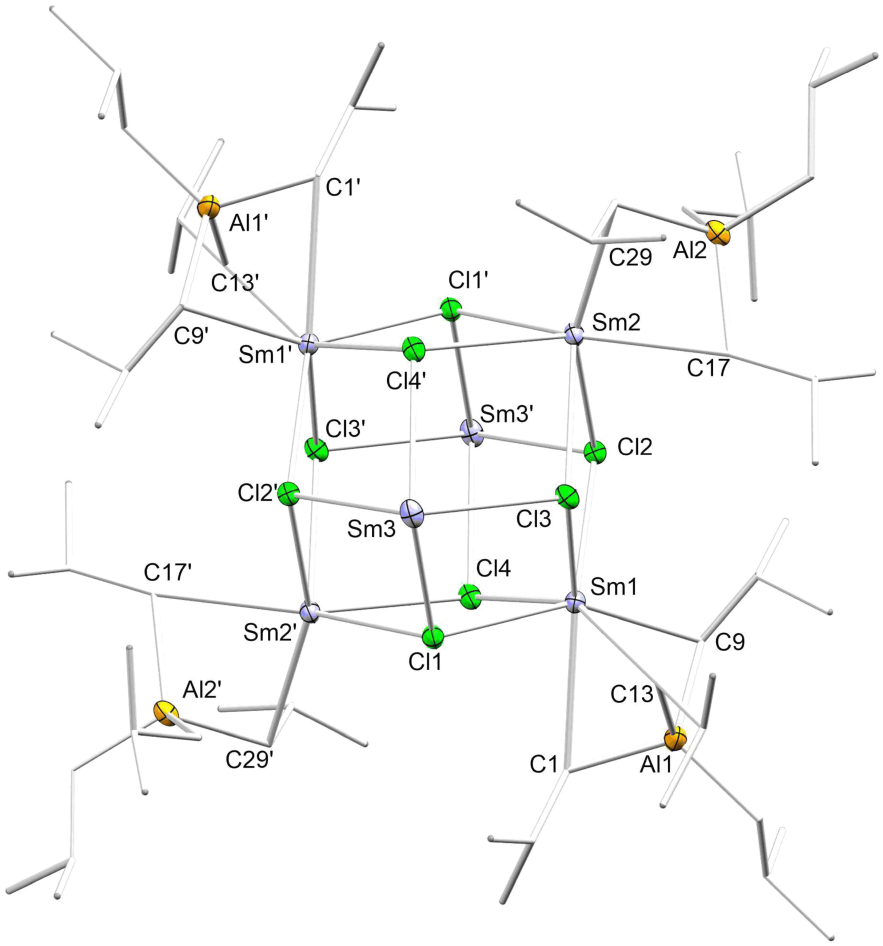

Figure S22. Crystal structure of $[Sm_6Cl_8(Al\textit{i}Bu_4)_6]$ (**3**). Ellipsoids are shown at the 50% probability level. Hydrogen atoms, and cocrystallized hexane are omitted for clarity. The isobutyl aluminate moieties at Sm(3) are omitted for clarity. Selected interatomic distances [Å]: Al(1)–C(1) 2.027(3), Al(1)–C(5) 1.974(3), Al(1)–C(9) 2.112(3), Al(1)–C(13) 2.097(3), Al(2)–C(17) 2.074(3), Al(2)–C(29) 2.073(3), Al(3)–C(33) 2.077(3), Al(3)–C(37) 2.060(5), Al(3)–C(45) 2.063(5), Sm(1)–C(1) 2.953(3), Sm(1)–C(9) 2.576(3), Sm(1)–C(13) 2.627(3), Sm(2)–C(17) 2.767(3), Sm(2)–C(29) 2.776(3), Sm(3)–C(33) 2.842(3), Sm(3)–C(37) 2.853(3), Sm(3)–C(45) 2.850(4), Al(1)···Sm(1) 2.8658(9), Al(2)···Sm(2) 3.0098(9), Al(3)···Sm(3) 2.9394(9), Sm(1)–Cl(1) 2.7370(7), Sm(2)'–Cl(1) 2.9576(6), Sm(3)–Cl(1) 3.0719(7), Sm(1)–Cl(2) 2.7879(7), Sm(2)–Cl(2) 2.9696(7), Sm(3)'–Cl(2) 2.9854(6), Sm(1)–Cl(3) 2.7798(7), Sm(3)–Cl(3) 2.9291(7), Sm(2)–Cl(3) 2.9487(7), Sm(1)–Cl(4) 2.8076(7), Sm(3)'–Cl(4) 2.9739(8), Sm(2)'–Cl(4) 3.0051(7), Sm(2)–Cl(1)' 2.9575(6), Sm(2)–Cl(4)' 3.0051(7), Sm(3)–Cl(4)' 2.9739(8), Sm(3)–Cl(2)' 2.9854(6). Selected angles [°]: Al(1)-C(1)-Sm(1) 67.32(8), Al(1)-C(9)-Sm(1) 74.63(9), Al(1)-C(13)-Sm(1) 73.73(9), Al(2)-C(17)-Sm(2) 75.37(9), Al(2)-C(29)-Sm(2) 75.17(9), Al(3)-C(33)-Sm(3) 71.48(9), Al(3)-C(37)-Sm(3) 71.43(11), Al(3)-C(45)-Sm(3) 71.47(12), Sm(1)-Cl(1)-Sm(2)' 106.65(2), Sm(1)-Cl(1)-Sm(3) 105.43(2), Sm(2)'-Cl(1)-Sm(3) 108.99(2), Sm(1)-Cl(2)-Sm(2) 107.547(19), Sm(1)-Cl(2)-Sm(3)' 107.60(2), Sm(2)-Cl(2)-Sm(3)' 111.04(2), Sm(1)-Cl(3)-Sm(3) 108.23(2), Sm(1)-Cl(3)-Sm(2) 108.349(19), Sm(3)-Cl(3)-Sm(2) 106.48(2), Sm(1)-Cl(4)-Sm(3)' 107.39(2), Sm(1)-Cl(4)-Sm(2)' 103.587(19), Sm(3)'-Cl(4)-Sm(2)' 103.92(2), C(9)-Sm(1)-C(1) 70.43(9), C(9)-Sm(1)-C(13) 76.69(9), C(13)-Sm(1)-C(1) 72.74(9), C(17)-Sm(2)-C(21) 69.11(9), C(17)-Sm(2)-C(29) 72.68(9), C(21)-Sm(2)-C(21) 63.75 (9), C(33)-Sm(3)-C(45) 69.92(9), C(33)-Sm(3)-C(37) 69.61(10), C(45)-Sm(3)-C(37) 71.92(14). '-x+1, -y+1, -z+1

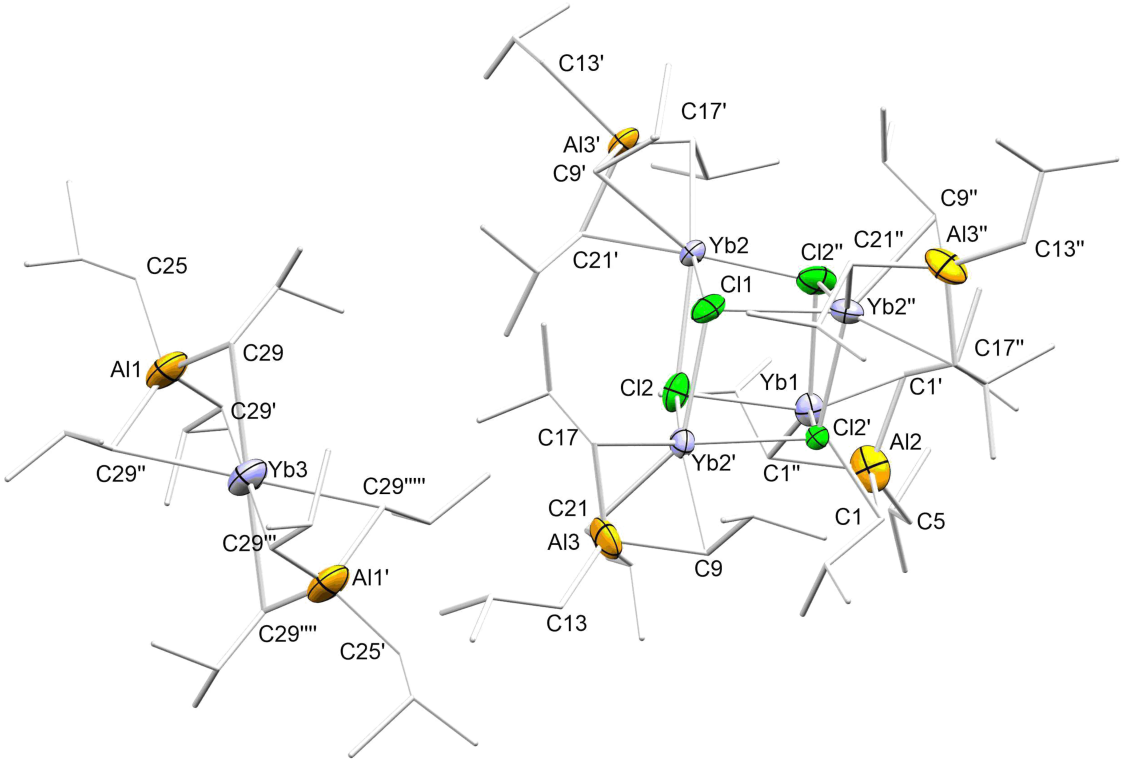

Figure S23. Crystal structure of $[Yb_4Cl_4(Al\textit{i}Bu_4)_4]$ (**4**) co-crystallized with $[Yb(Al\textit{i}Bu_4)_2]$ (**1**^{Yb}). Ellipsoids are shown at the 50% probability level. Hydrogen atoms are omitted for clarity. Selected interatomic distances [Å]: Al(1)–C(25) 2.03(2), Al(1)–C(29) 2.038(11), Al(2)–C(1) 2.07(3), Al(2)–C(5) 1.99(2), Al(3)–C(9) 2.065(8), Al(3)–C(13) 1.972(10), Al(3)–C(17) 2.068(9), Al(3)–C(21) 2.039(9), Yb(1)–C(1) 2.67(2), Yb(2)–C(9) 2.659(7), Yb(2)–C(17) 2.690(8), Yb(2)–C(21) 2.659(8), Yb(3)–C(29) 2.786(10), Al(2)···Yb(1) 2.779(5), Al(3)···Yb(2) 2.787(2), Al(1)···Yb(3) 2.806(4), Yb(1)–Cl(2) 2.836(6), Yb(2)–Cl(1) 2.7758(11), Yb(2)–Cl(2) 2.7925(17). Selected angles [°]: Yb(2)'-Cl(1)-Yb(2) 99.73(5), Yb(2)-Cl(2)-Yb(2)' 98.91(5), Yb(2)-Cl(2)-Yb(1) 92.68(7), C(1A)''-Yb(1)-C(1A)' 70.7(9), C(9)-Yb(2)-C(17) 74.3(3), C(9)-Yb(2)-C(21) 74.7(3), C(17)-Yb(2)-C(21) 74.0(3), C(29)'''-Yb(3)-C(29) 72.0(4).

' -y+1, x-y+1, z
'' -x+y, -x+1, z
''' -y+1, x-y, z

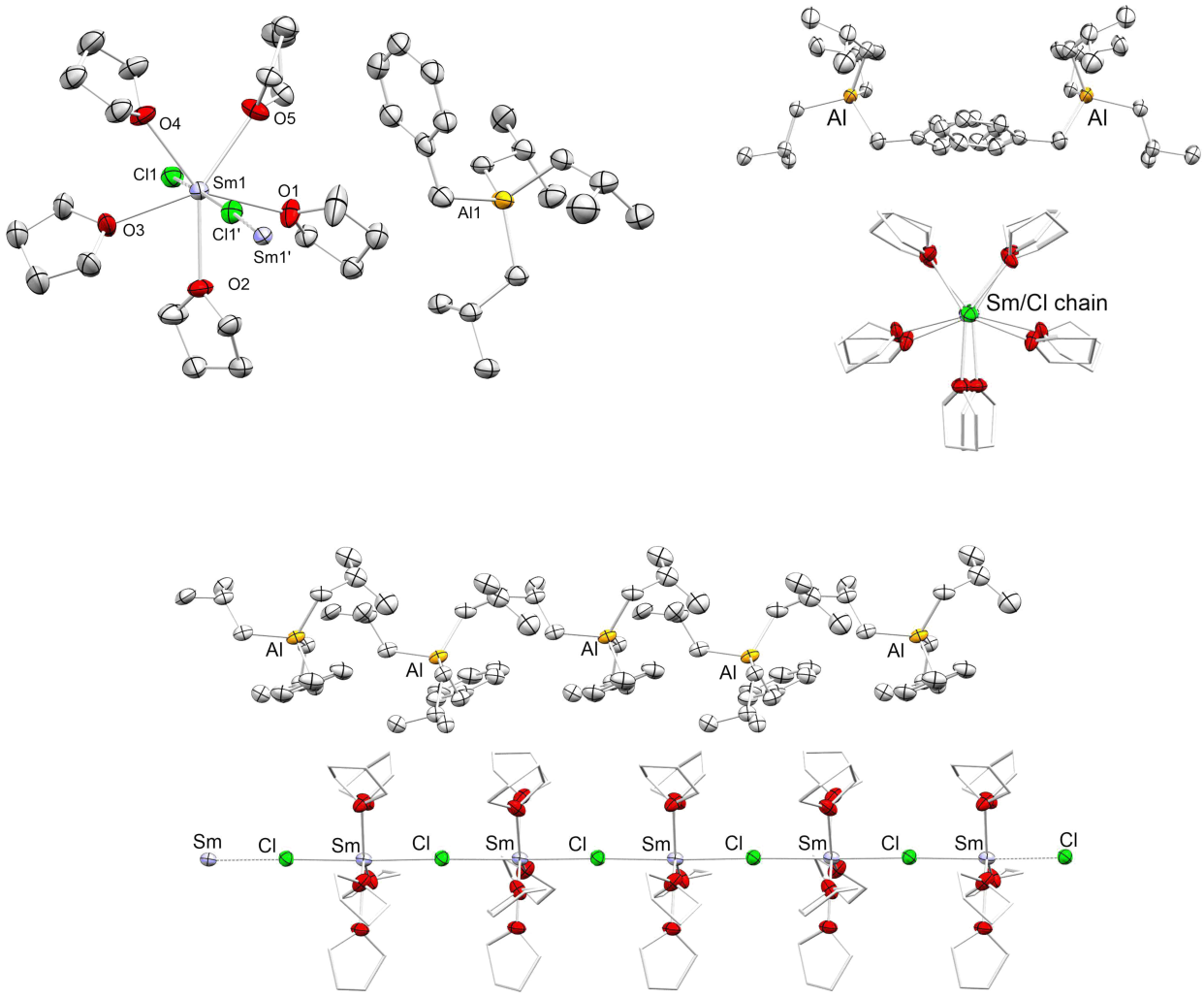

Figure S24. Different representations of the crystal structure of {[SmCl(THF)$_5$][AlBn*i*Bu$_3$]}$_n$ (**5**). Top left: repeat unit; top right: view along the Sm–Cl polymer axis; bottom: polymeric representation. Ellipsoids are shown at the 50% probability level. Hydrogen atoms are omitted for clarity. Selected interatomic distances [Å]: Sm(1)'–Cl(1) 2.8969(17), Sm(1)–Cl(1) 2.8994(17), Sm(1)–O(1) 2.569(4), Sm(1)–O(2) 2.578(4), Sm(1)–O(3) 2.582(4), Sm(1)–O(4) 2.580(4), Sm(1)–O(5) 2.574(4), Al(1)–C(25) 2.023(7), Al(1)–C(29) 2.017(7), Al(1)–C(33) 2.031(7), Al(1)–C(37) 2.046(7). Selected angles [°]: Sm(1)'–Cl(1)–Sm(1) 178.37(7), Cl(1)'–Sm(1)–Cl(1) 174.80(2), O(1)–Sm(1)–O(2) 73.30(16), O(1)–Sm(1)–O(5) 70.27(15), O(2)–Sm(1)–O(3) 72.06(16), O(4)–Sm(1)–O(3) 72.15(16), O(5)–Sm(1)–O(4) 72.47(16), O(1)–Sm(1)–Cl(1)' 86.94(12), O(2)–Sm(1)–Cl(1)' 88.85(11), O(4)–Sm(1)–Cl(1)' 94.21(12), O(3)–Sm(1)–Cl(1)' 87.56(12), O(5)–Sm(1)–Cl(1)' 91.24(11), O(1)–Sm(1)–Cl(1) 88.86(12), O(2)–Sm(1)–Cl(1) 87.01(11), O(3)–Sm(1)–Cl(1) 94.14(11), O(4)–Sm(1)–Cl(1) 90.98(12), O(5)–Sm(1)–Cl(1) 90.23(11).

' x, 1/2-y, 1/2+z

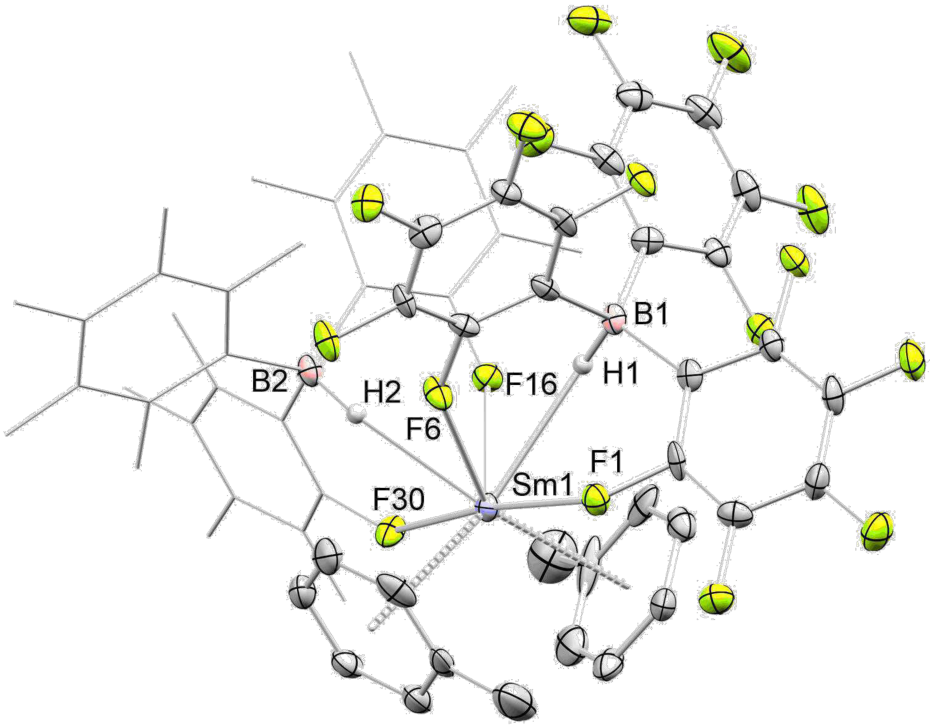

Figure S25. Crystal structure of [Sm{HB(C_6F_5)$_3$}$_2$(toluene)$_2$] (**6**). Ellipsoids are shown at the 50% probability level. Hydrogen atoms are omitted, and one borato moiety is shown as stick presentation for clarity. Selected interatomic distances [Å]: Sm(1)–F(1) 2.731(4), Sm(1)–F(6) 2.650(4), Sm(1)–F(16) 2.670(4), Sm(1)–F(30) 2.660(4), Sm(1)–H(1) 2.68 (6), Sm(1)–H(2) 2.50(7), B(1)–H(1) 1.14(6), B(2)–H(2) 1.12(7), Sm(1)–centroid(1) 2.880, Sm(1)–centroid(2) 2.811, Sm(1)–C(toluene)$_{range}$ 3.110(8)-3.218(8), Sm(2)–C(toluene)$_{range}$ 3.074(8)-3.185(8). Selected angles [°]: F(6)-Sm(1)-F(16) 88.99(12), F(6)-Sm(1)-F(30) 120.02(12), F(6)-Sm(1)-F(1) 65.88(12), F(16)-Sm(1)-F(1) 120.17(12), F(6)-Sm(1)-H(2) 60.4(15), F(30)-Sm(1)-H(2) 59.9(15), F(16)-Sm(1)-H(2) 57.8(15), F(1)-Sm(1)-H(2) 126.2(15).

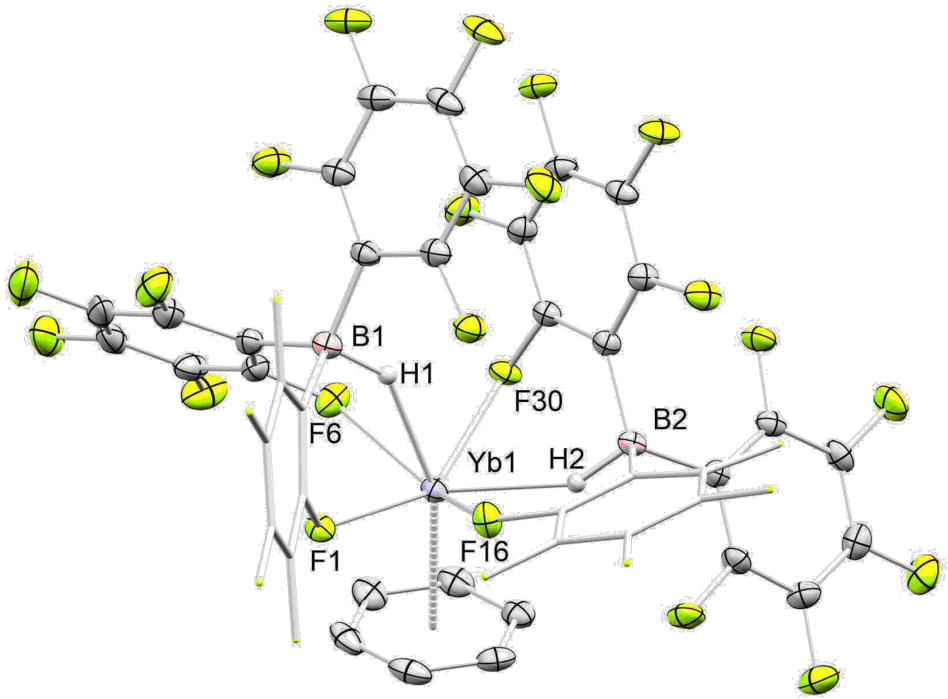

Figure S26. Crystal structure of [Yb{HB(C_6F_5)$_3$}$_2$(C_6D_6)] (**7**) Ellipsoids are shown at the 50% probability level. Hydrogen atoms are omitted for clarity. Selected interatomic distances [Å]: Yb(1)–F(1) 2.4267(17), Yb(1)–F(6) 2.4295(18), Yb(1)–F(16) 2.3974(18), Yb(1)–F(30) 2.4179(17), Yb(1)–H(1) 2.27 (3), Yb(1)–H(2) 2.25 (3), Yb(1)–centroid(1) 2.490, Yb(1)–C(toluene)$_{range}$ 2.832(3)-2.872(3). Selected angles [°]: F(16)-Yb(1)-F(30) 114.11(6), F(16)-Yb(1)-F(1) 68.40(6), F(30)-Yb(1)-F(1) 144.58(6), F(16)-Yb(1)-F(6) 141.40(6), F(30)-Yb(1)-F(6) 69.06(6), F(1)-Yb(1)-F(6) 87.60(6), F(1)-Yb(1)-centroid(1) 95.72, H(1)-Yb(1)-H(2) 103 (1).

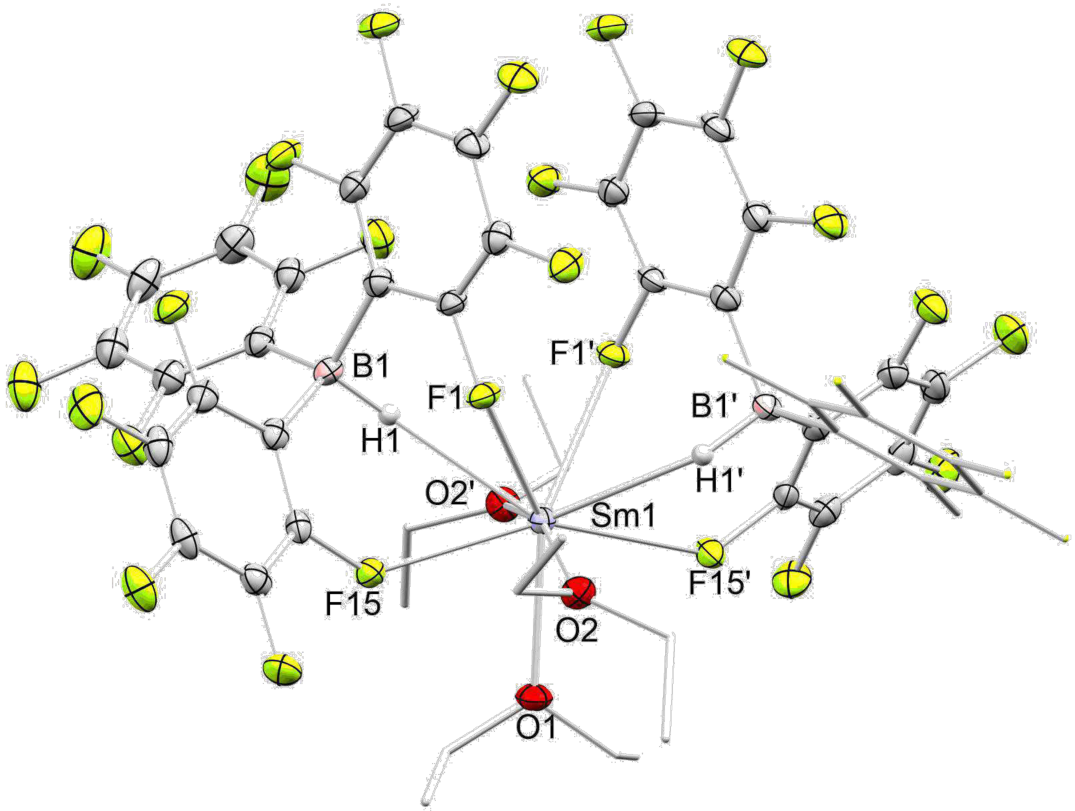

Figure S27. Crystal structure of [Sm{HB(C_6F_5)$_3$}$_2$(Et_2O)$_3$] (**8**). Ellipsoids are shown at the 50 % probability level. Hydrogen atoms are omitted for clarity. Selected interatomic distances [Å]: B(1)–H(1) 1.14(2), Sm(1)–H(1) 2.50(7), Sm(1)–O(1) 2.563(2), Sm(1)–O(2) 2.5182(15), Sm(1)–F(1) 2.6572(12), Sm(1)–F(15) 2.6514(12). Selected angles [°]: O(2)-Sm(1)-O(2)' 161.40(7), O(2)-Sm(1)-O(1) 80.70(4), O(2)-Sm(1)-F(15)' 97.12(5), O(2)-Sm(1)-F(15) 78.51(5), O(1)-Sm(1)-F(15) 76.54(3), F(15)'-Sm(1)-F(15) 153.08(5), O(2)-Sm(1)-F(1)' 122.70(4), O(2)'-Sm(1)-F(1)' 73.52(4), O(1)-Sm(1)-F(1)' 142.56(3), F(15)-Sm(1)-F(1)' 132.59(4), O(2)-Sm(1)-F(1) 73.52(4), O(2)'-Sm(1)-F(1) 122.71(4), O(1)-Sm(1)-F(1) 142.56(3), F(15)'-Sm(1)-F(1) 132.59(4), F(15)-Sm(1)-F(1) 72.12(4), F(1)'-Sm(1)-F(1) 74.87(5), H(1)-Sm(1)-H(1') 124.07.

' -x+1, y, -z+3/2

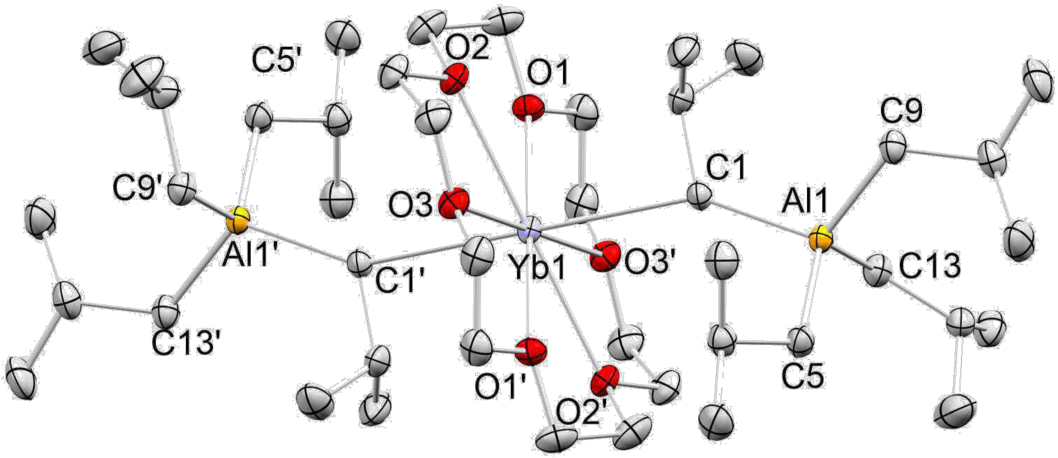

Figure S28. Crystal structure of [Yb(18-crown-6)(Al*i*Bu$_4$)$_2$] (**9**). Ellipsoids are shown at the 50% probability level. Hydrogen atoms are omitted for clarity. Selected interatomic distances [Å]: Yb(1)–C(1) 2.9159(19), Yb(1)–O(1) 2.6171(13), Yb(1)–O(2) 2.6549(13), Yb(1)–O(3) 2.6433(15), Al(1)–C(1) 2.0834(19), Al(1)–C(5) 2.0279(19), Al(1)–C(9) 2.0172(19), Al(1)–C(13) 2.025(2). Selected angles [°]: C(1)-Yb(1)-C(1)' 180.00(6), O(1)-Yb(1)-C(1) 81.21(5), O(1)-Yb(1)-C(1)' 98.79(5).

' -x+1, -y+1, -z+1

Table S1. Crystallographic Data for Compounds $\mathbf{1}^{Sm}$, $\mathbf{1}^{Eu}$, and $\mathbf{1}^{Yb}$

	$\mathbf{1}^{Sm}$	$\mathbf{1}^{Eu}$	$\mathbf{1}^{Yb}$
formula	$C_{32}H_{72}Al_2Sm$	$C_{32}H_{72}Al_2Eu$	$C_{32}H_{72}Al_2Yb$
M [g mol^{-1}]	661.20	662.81	683.89
color/shape	purple/block	colorless/block	colorless/needle
Crystal dimensions [mm]	0.202 x 0.120 x 0.103	0.175 x 0.109 x 0.100	0.248 x 0.101 x 0.063
cryst. system	triclinic	triclinic	triclinic
space group	$P\bar{1}$	$P\bar{1}$	$P\bar{1}$
a [Å]	9.6115(7)	9.5200(6)	10.926(6)
b [Å]	9.9347(8)	9.9034(6)	11.006(6)
c [Å]	10.6575(8)	10.6569(7)	18.097(10)
α [°]	73.645(2)	73.2920(10)	86.671(9)
β [°]	89.012(2)	89.4010(10)	87.375(10)
γ [°]	76.369(2)	76.4440(10)	61.432(9)
V [Å^3]	947.66(13)	933.76(10)	1907.6(18)
Z	1	1	2
T [K]	170(2)	100(2)	100(2)
wavelength [Å]	0.71073	0.71073	0.71073
ρ_{calcd} [Mg m^{-3}]	1.159	1.179	1.191
μ [mm^{-1}]	1.611	1.743	2.513
F (000)	352	353	720
θ range [°]	1.994/28.697	2.205/28.784	2.255/23.234
unique reflns	4896	4861	5137
observed reflns	38046	38936	11848
R_1[b]/wR_2[c](I>2σ)	0.0247/0.0649	0.0300/0.0715	0.0848/0.1698
R_1/wR_2 (all data)[a]	0.0248/0.0650	0.0308/0.0720	0.1271/0.1898
GOF[a]	1.019	1.037	1.184

[a]GOF = $[\Sigma w(F_0^2 - F_c^2)^2 / (n_0 - n_p)]^{1/2}$. [b]$R_1 = \Sigma(||F_0| - |F_c||) / \Sigma|F_0|$, $F_0 > 4\sigma(F_0)$. [c]$wR_2 = \{\Sigma[w(F_0^2 - F_c^2)^2 / \Sigma[w(F_0^2)^2]\}^{1/2}$.

Table S2. Crystallographic Data for Compounds **2^{Yb}**, **3**, **4**, and **5**

	2^{Yb}	**3**	**4**	**5**
formula	$C_{36}H_{66}AlYb$	$C_{102}H_{230}Al_6Cl_8Sm_6$	$C_{160}H_{360}Al_{10}Cl_8Yb_9$	$C_{43}H_{82}AlClO_6Sm$
M [g mol^{-1}]	698.90	2804.43	4395.22	907.86
color/shape	blue/plate	purple/block	yellow/needle	blue/block
crystal dimensions [mm]	0.251 x 0.143 x 0.138	0.239 x 0.141 x 0.086	0.100 x 0.095 x 0.029	0.216 x 0.131 x 0.094
cryst. system	orthorhombic	triclinic	trigonal	monoclinic
space group	*Pbcn*	$P\bar{1}$	*R-3c*	$P2_1/c$
a [Å]	10.6666(4)	15.812(2)	17.1133(8)	15.182(2)
b [Å]	21.0827(8)	15.871(2)	17.1133(8)	27.417(3)
c [Å]	15.50.69(6)	16.241(2)	119.378(8)	11.580(1)
α [°]	90	109.6480(10)	90	90
β [°]	90	91.5410(10)	90	102.925(2)
γ [°]	90	118.7660(10)	120	90
V [Å^3]	3.4872(2)	3275.7(6)	30278(3)	4697.9(9)
Z	4	1	6	4
T [K]	150(2)	100(2)	100(2)	173(2)
wavelength [Å]	0.71073	0.71073	0.71073	0.71073
ρ_{calcd} [Mg m^{-3}]	1.331	1.422	1.446	1.284
μ [mm^{-1}]	2.728	2.885	4.314	1.366
F (000)	1460	1428	13296	1920
θ range [°]	1.932/30.048	1.790/30.518	1.416/27.483	1.376/26.372
unique reflns	5102	19856	7556	9602
observed reflns	84408	148729	138704	92482
R_1[b]/wR_2[c](I>2σ)	0.0186/0.0407	0.0327/0.0733	0.0433/0.0912	0.0656/0.1241
R_1/wR_2 (all data)[a]	0.0280/0.0470	0.0424/0.0785	0.0785/0.1122	0.1210/0.1439
GOF[a]	1.029	1.065	1.014	1.027

[a]GOF = $[\Sigma w(F_0^2 - F_c^2)^2 / (n_0 - n_p)]^{1/2}$. [b]$R_1 = \Sigma(||F_0| - |F_c||) / \Sigma|F_0|$, $F_0 > 4\sigma(F_0)$. [c]$wR_2 = \{\Sigma[w(F_0^2 - F_c^2)^2 / \Sigma[w(F_0^2)^2]\}^{1/2}$.

Table S3. Crystallographic Data for Compounds **6**, **7**, **8**, and **9**

	6	**7**	**8**	**9**
formula	$C_{50}H_{18}B_2F_{30}Sm \cdot \frac{1}{2} C_7H_8 \cdot \frac{1}{2}C_6H_4F_2$	$C_{45}H_2B_2D_9F_{30}Yb$	$C_{48}H_{32}B_2F_{30}O_3Sm$	$C_{44}H_{96}Al_2O_6Yb$
M [g mol^{-1}]	1463.73	1325.25	1398.70	948.20
color/shape	orange/needle	yellow block	orange/needle	colorless columns
crystal dimensions [mm]	0.222 x 0.049 x 0.037	0.185 x 0.155 x 0.036	0.162 x 0.077 x 0.037	0.338 x 0.158 x 0.088
cryst. system	orthorhombic	triclinic	monoclinic	monoclinic
space group	*Pbca*	$P\bar{1}$	*C2/c*	$P2_1/c$
a [Å]	13.3766(12)	9.6701(6)	20.4277(14)	12.330(3)
b [Å]	19.6999(18)	11.0157(6)	13.6628(10)	13.406(3)
c [Å]	39.715(4)	21.675 (1)	18.1390(12)	15.383(3)
α [°]	90	78.266(2)	90	90
β [°]	90	89.119(2)	95.366(2)	97.637(4)
γ [°]	90	73.516(2)	90	90
V [Å^3]	10465.6(17)	2165.5(2)	5040.4(6)	2520.2(9)
Z	8	2	4	2
T [K]	100(2)	100(2)	100(2)	100(2) K
wavelength [Å]	0.71073	0.71073	0.71073	0.71073
ρ_{calcd} [Mg m^{-3}]	1.858	2.032	1.843	1.250
μ [mm^{-1}]	1.275	2.326	1.320	1.930
F (000)	5712	1262	2744	1008
θ range [°]	1.836/24.735	1.921/29.246	1.796/26.444	2.023/27.877
unique reflns	8923	11729	5201	5998
observed reflns	59914	80349	74083	46886
R_1[b]/wR_2[c](I>2σ)	0.0509/0.0968	0.0355/0.0720	0.0245/0.0565	0.0203/0.0494
R_1/wR_2 (all data)[a]	0.1158/0.1221	0.0400/0.0735	0.0291/0.0586	0.0292/0.0544
GOF[a]	1.017	1.216	1.035	1.062

[a]GOF = $[\Sigma w(F_0^2 - F_c^2)^2 / (n_0 - n_p)]^{1/2}$. [b]$R_1 = \Sigma(||F_0| - |F_c||) / \Sigma|F_0|$, $F_0 > 4\sigma(F_0)$. [c]$wR_2 = \{\Sigma[w(F_0^2 - F_c^2)^2 / \Sigma[w(F_0^2)^2]\}^{1/2}$.

Polymer Analysis

Exemplary polymer data including ^{1}H- and $^{13}C\{^{1}H\}$-NMR spectra, SEC measurements and standard reports, DSC curves, and ATR spectrum of the polymer given in Table 1, entry 6, are given in the following.

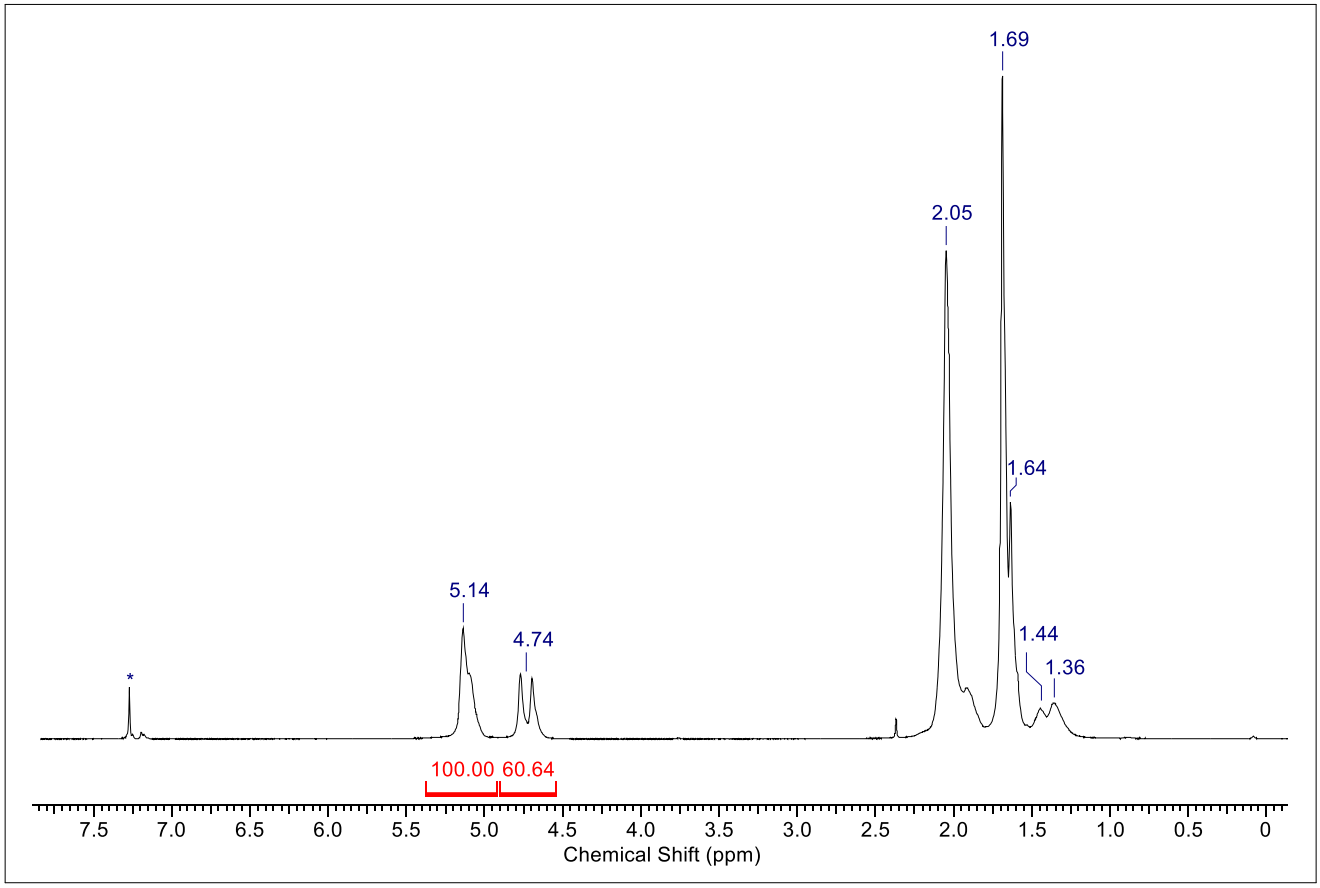

Figure S29. Exemplary ^{1}H-NMR spectrum of the polymer given in Table 1, entry 6.

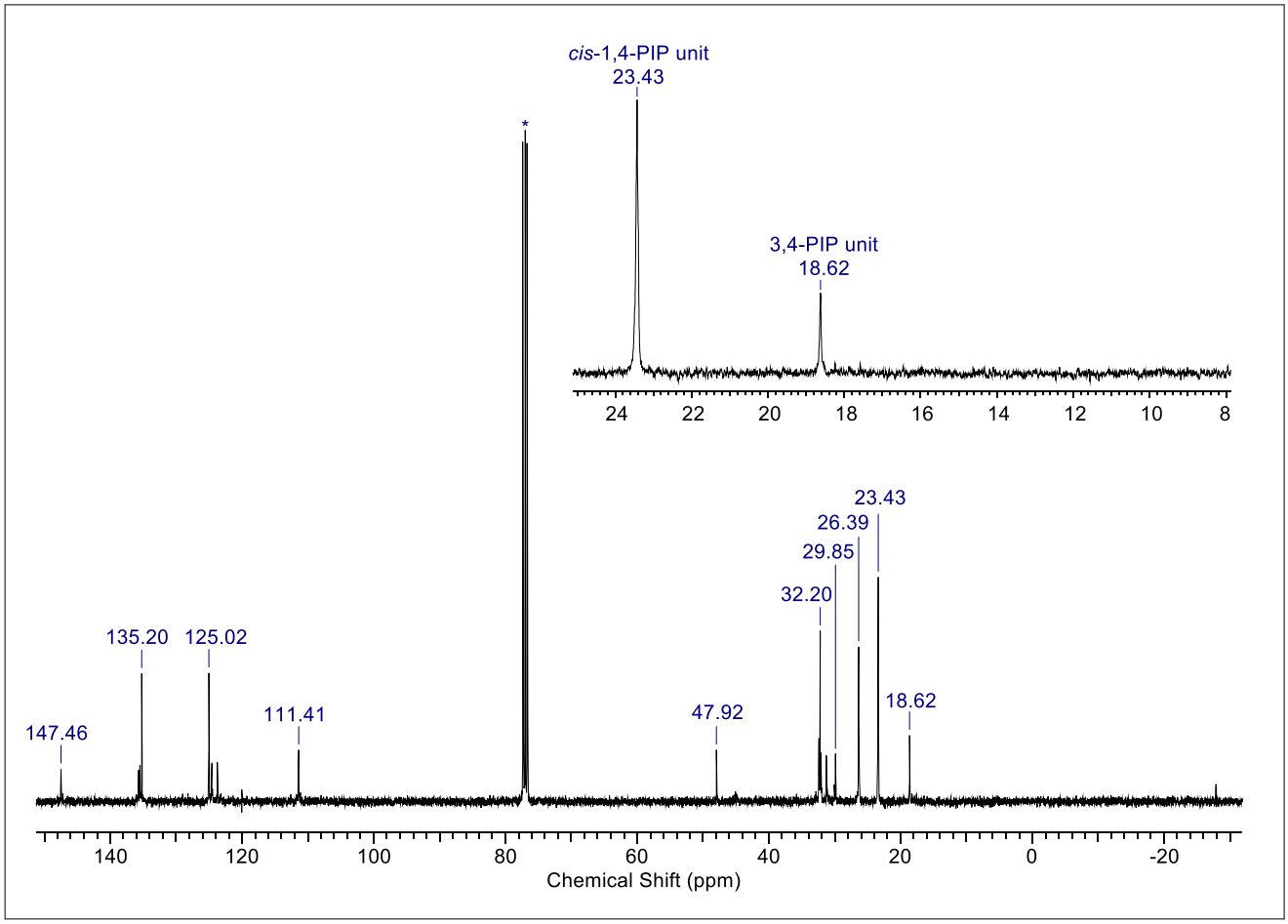

Figure S30. Exemplary $^{13}C\{^{1}H\}$-NMR spectrum of the polymer given in Table 1, entry 6.

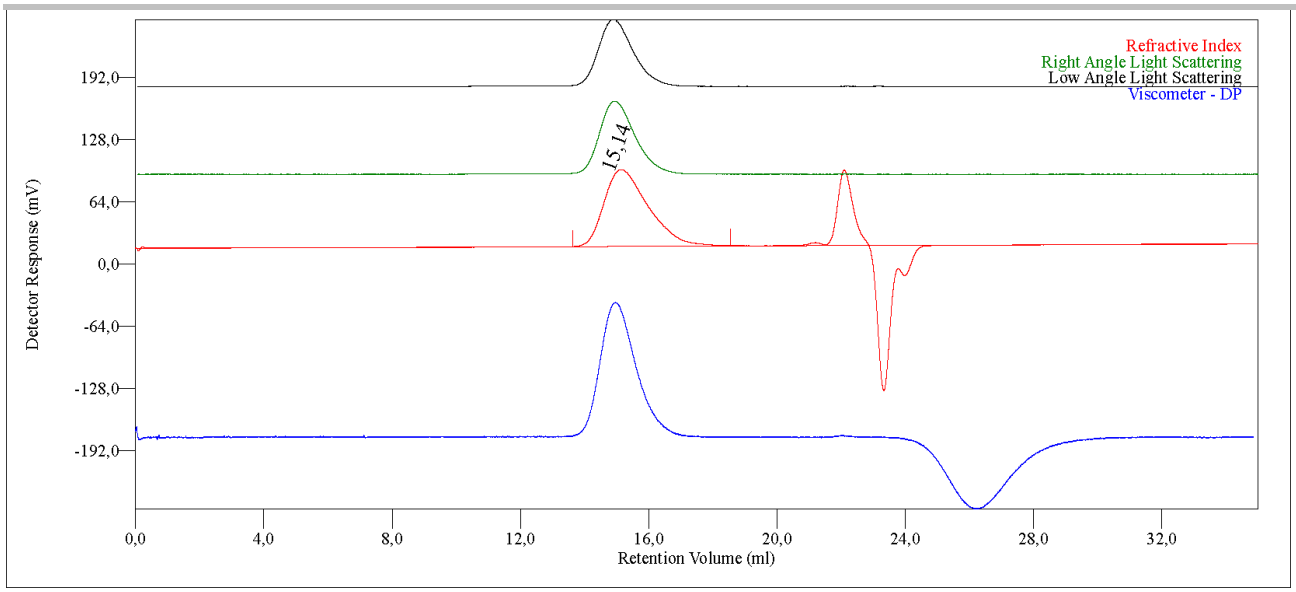

Multi-Detectors - Homopolymers : Results

Peak RV - (ml)	15,140
Mn - (Daltons)	393.413
Mw - (Daltons)	636.987
Mz - (Daltons)	838.690
Mp - (Daltons)	725.988
Mw / Mn	1,619
Percent Above Mw: 0	100,000
Percent Below Mw: 0	0,000
IV - (dl/g)	3,3120
Rh(w) - (nm)	31,152
Rg(w) - (nm)	39,259
Wt Fr (Peak)	1,000
Mark-Houwink a	0,788
Mark-Houwink logK	-4,037
Branches	0,000
Branch Freq.	0,000
RI Area - (mvml)	126,16
UV Area - (mvml)	0,00
RALS Area - (mvml)	98,80
LALS Area - (mvml)	88,62
IVDP Area - (mvml)	179,76

Sample Parameters	Input	Calculated
Sample Conc - (mg/ml)	0,840	0,000
Sample Recovery (%)	0,000	105,129
dn/dc - (ml/g)	0,1290	0,0000
dA/dc - (ml/g)	1,0000	0,0000

Annotation	
Method File	PIP105kvon Injek1 Meth09_10_20-0001.vcm
Limits File	
Date Acquired	Oct 09, 2020 - 01:34:18
Solvent	THF
Acquisition Operator	admin : Administrator
Calculation Operator	admin : Administrator
Column Set	GMHxl
System	System 1
Flow Rate - (ml/min)	1,000
Inj Volume - (ul)	100,0
Volume Increment - (ml)	0,00333
Detector Temp. - (deg C)	35,0
Column Temp. - (deg C)	35,0
OmniSEC Build Number	467

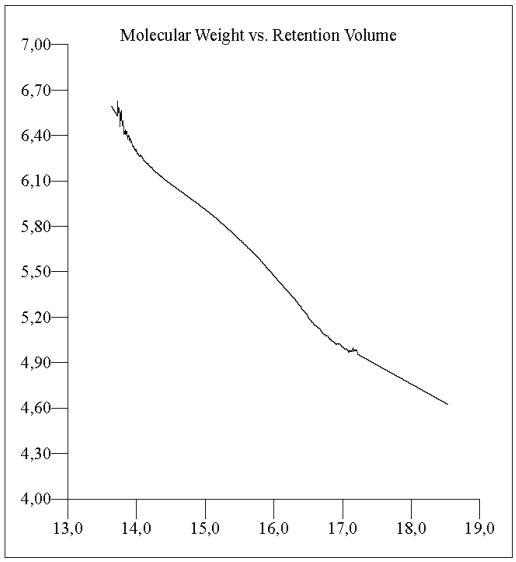

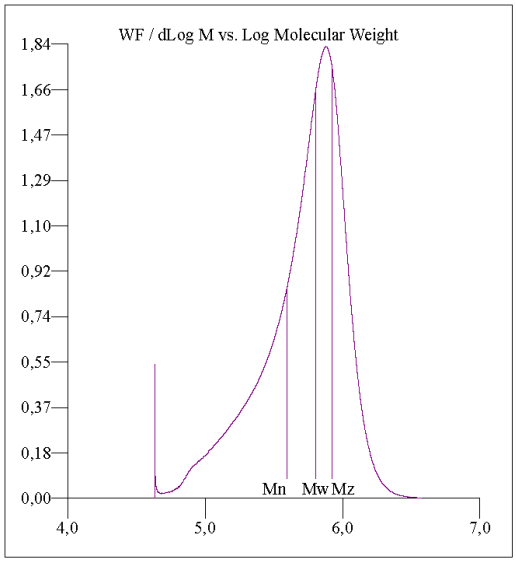

Figure S31. Exemplary SEC data of the polymer given in Table 1, entry 6.

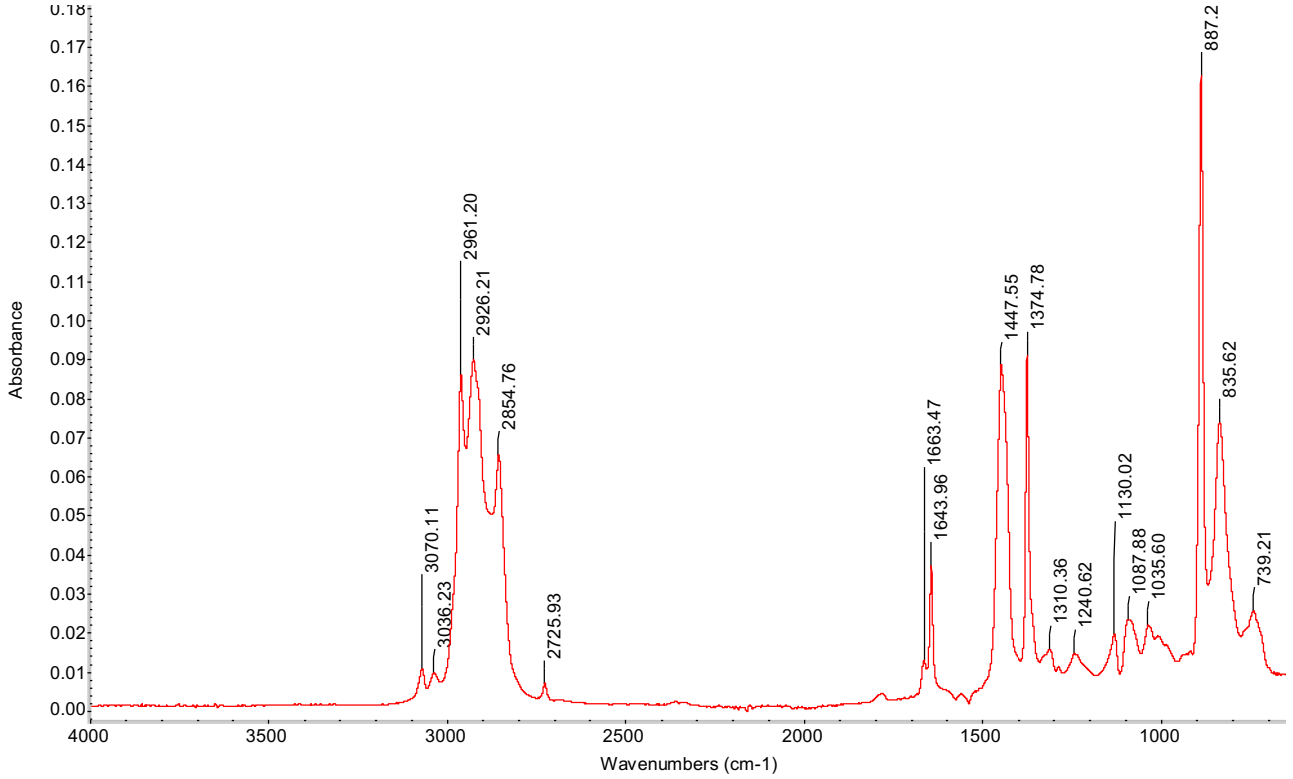

Figure S32. Exemplary ATR spectrum of polymer given in Table 1, entry 6, confirming essentially *trans*-free microstructure (lack of 1,4-*trans* specific signals (843 cm^{-1}: out-of-plane bending vibration of C–H in the –CH=CH– group of *trans*-1,4-unit; 1383 cm^{-1}: scissoring vibration of CH_3 in *trans*-1,4-unit).[13]

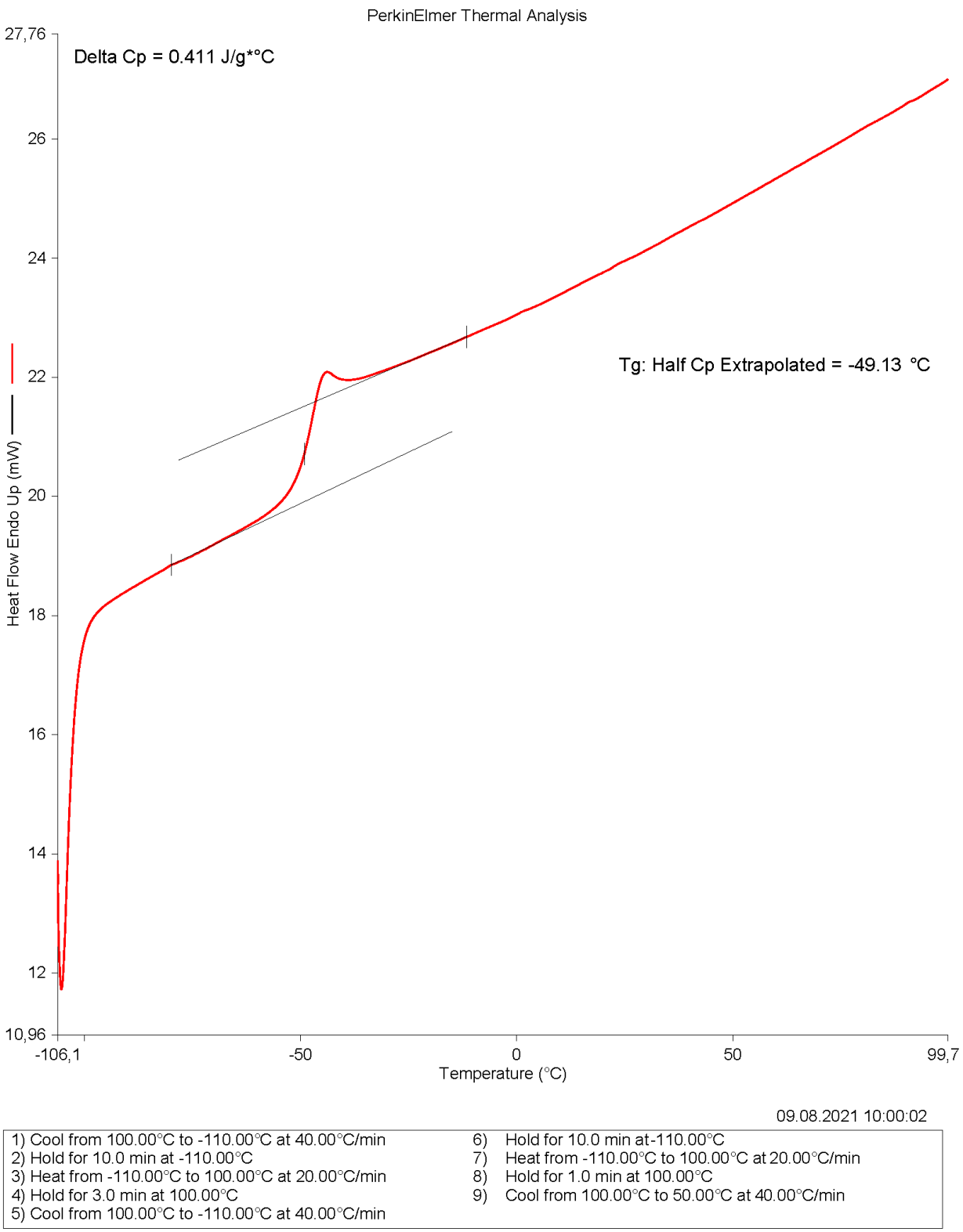

Figure S33. Exemplary DSC data of polymer given in Table 1, entry 6.

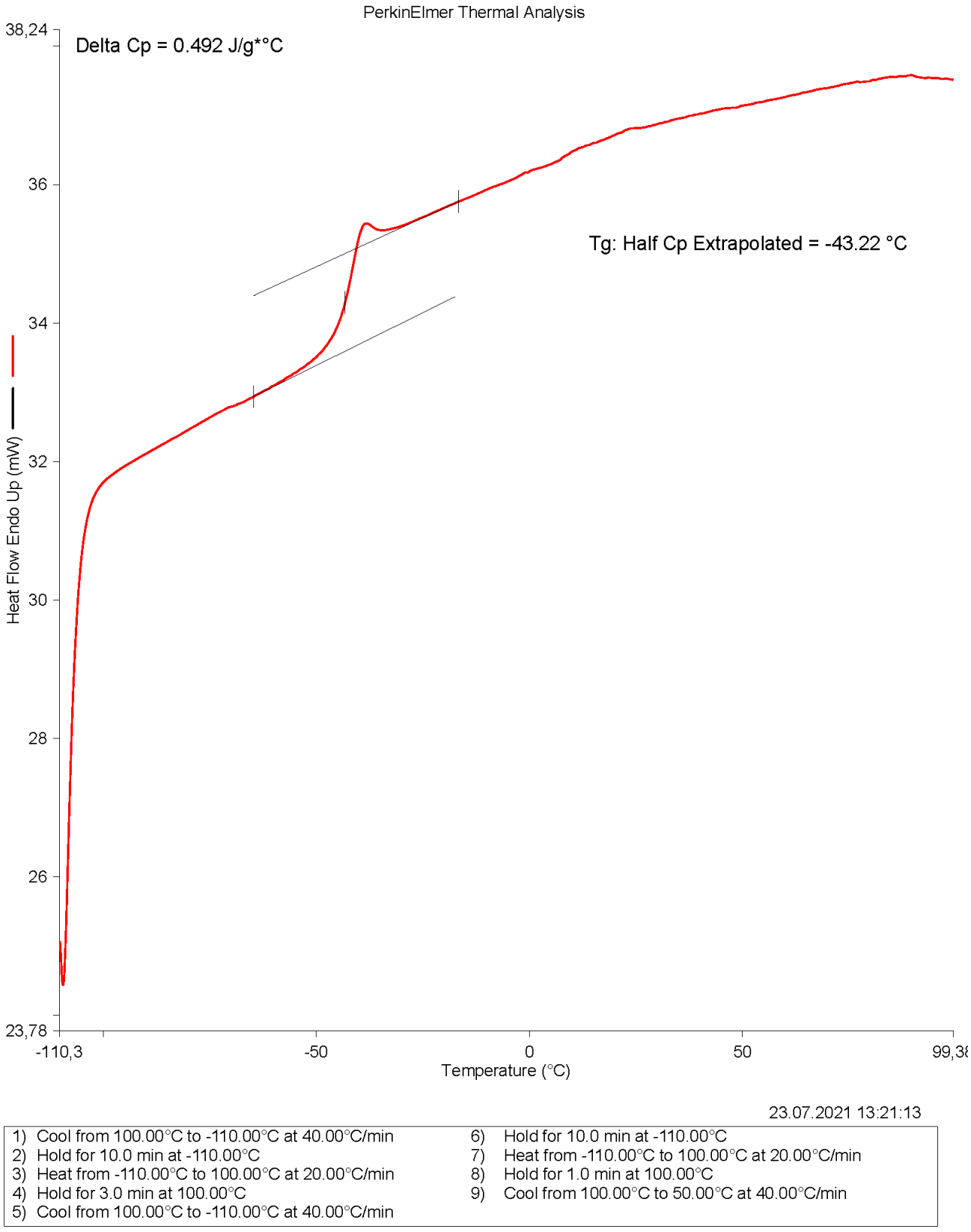

Figure S34. Exemplary DSC data of polymer obtained from **1**^{Yb}/**B**, four monomer additions (Table 1, entry 17).

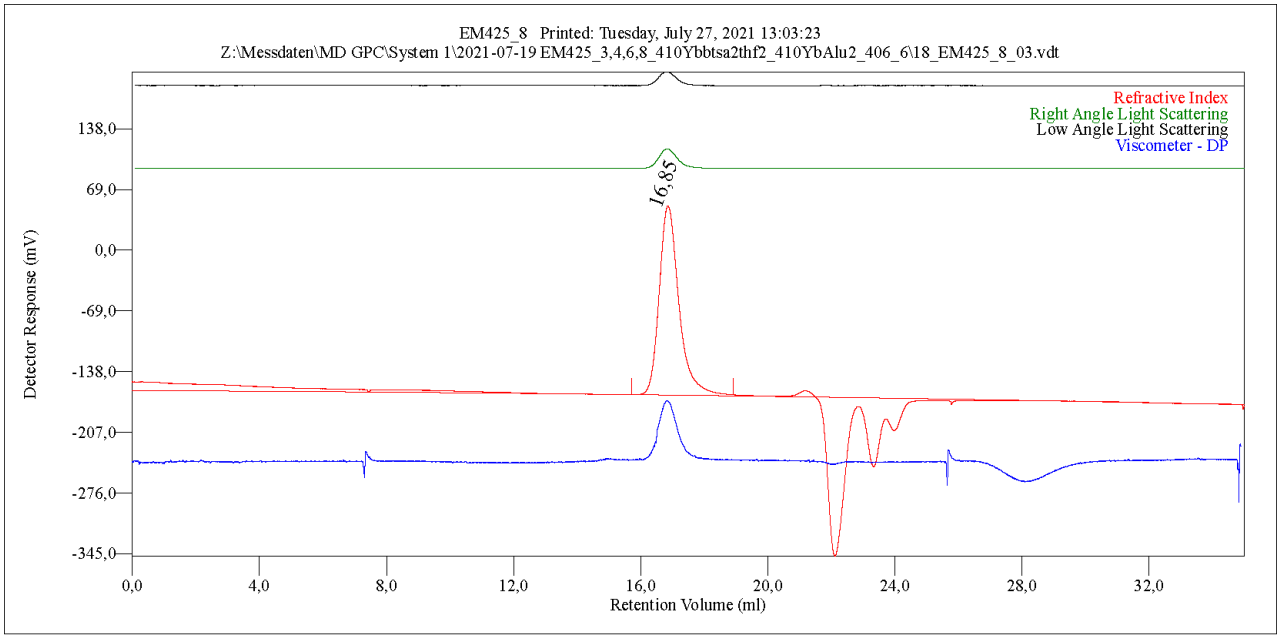

Multi-Detectors - Homopolymers : Results

Peak RV - (ml)	16,853
Mn - (Daltons)	48.723
Mw - (Daltons)	50.252
Mz - (Daltons)	51.426
Mp - (Daltons)	50.635
Mw / Mn	1,031
Percent Above Mw: 0	100,000
Percent Below Mw: 0	0,000
IV - (dl/g)	0,5973
Rh(w) - (nm)	7,738
Rg(w) - (nm)	No Calc
Wt Fr (Peak)	1,000
Mark-Houwink a	0,898
Mark-Houwink logK	-4,449
Branches	0,000
Branch Freq.	0,000
RI Area - (mvml)	155,56
UV Area - (mvml)	0,00
RALS Area - (mvml)	15,33
LALS Area - (mvml)	10,93
IVDP Area - (mvml)	48,32

Sample Parameters	Input	Calculated
Sample Conc - (mg/ml)	1,160	0,000
Sample Recovery (%)	0,000	96,431
dn/dc - (ml/g)	0,1290	0,0000
dA/dc - (ml/g)	1,0000	0,0000

Annotation	
Method File	PIP86k Meth10_06_21Vers3-0001.vcm
Limits File	
Date Acquired	Jul 20, 2021 - 00:53:19
Solvent	THF
Acquisition Operator	admin : Administrator
Calculation Operator	admin : Administrator
Column Set	GMHxl
System	System 1
Flow Rate - (ml/min)	1,000
Inj Volume - (ul)	100,0
Volume Increment - (ml)	0,00333
Detector Temp. - (deg C)	35,0
Column Temp. - (deg C)	35,0
OmniSEC Build Number	467

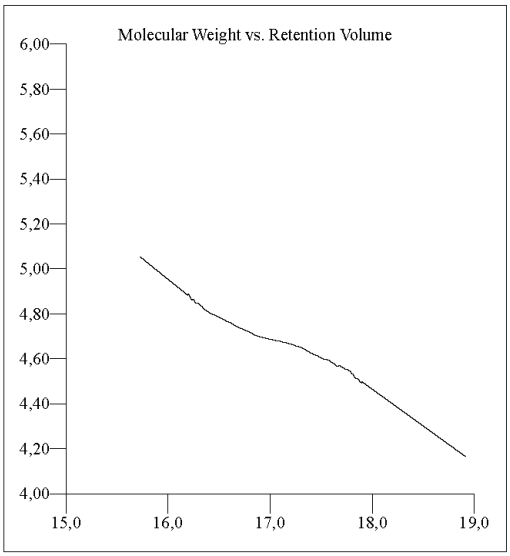

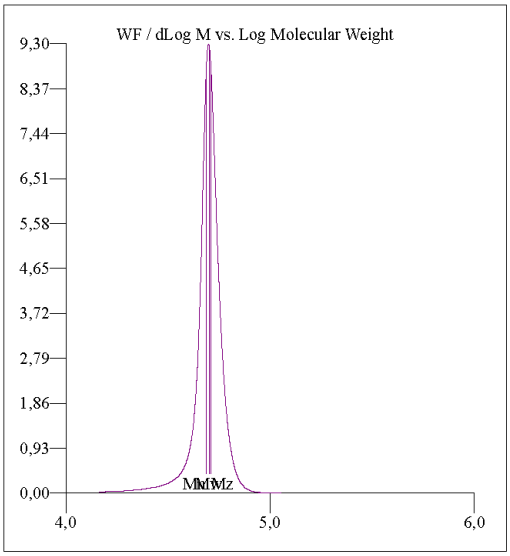

Figure S35. Exemplary SEC data polymer obtained from **1^{Yb}/B**, four monomer additions (Table 1, entry 17).

References

[1] W. J. Evans, D. K. Drummond, H. Zhang, J. L. Atwood, *Inorg. Chem.* **1988**, *27*, 575-579.
[2] P. Girard, J. L. Namy, H. B. Kagan, *J. Am. Chem. Soc.* **1980**, *102*, 2693-2698.
[3] M. G. Klimpel, R. Anwander, M. Tafipolsky, W. Scherer, *Organometallics* **2001**, *20*, 3983-3992.
[4] W. J. Evans, J. T. Leman, R. D. Clark, J. W. Ziller, *Main Group Met. Chem.* **2000**, *23*, 163-168.
[5] COSMO v. 1.61, Bruker AXS Inc., Madison, WI., **2012**.
[6] APEX 3 v. 2017.3-0, Bruker AXS Inc., Madison, WI., **2017**.
[7] L. Krause, R. Herbst-Irmer, G. M. Sheldrick, D. Stalke, *J. Appl. Crystallogr.* **2015**, *48*, 3-10.
[8] G. Sheldrick, *Acta Crystallogr. Sect. C.* **2015**, *71*, 3-8.
[9] C. B. Hübschle, G. M. Sheldrick, B. Dittrich, *J. Appl. Crystallogr.* **2011**, 1281-1284.
[10] D. Kratzert, J. J. Holstein, I. Krossing, *J. Appl. Crystallogr.* **2015**, *48*, 933-938.
[11] C. F. Macrae, P. R. Edgington, P. McCabe, E. Pidcock, G. P. Shields, R. Taylor, M. Towler, J. van de Streek, *J. Appl. Crystallogr.* **2006**, *39*, 453-457.
[12] POV-Ray v. 3.6, Persistence of Vision Pty. Ltd., Williamstown, Victoria, Australia, **2004**.
[13] R. Saunders, D. Smith, *J. Appl. Phys.* **1949**, *20*, 953-965.

Paper II

Triisobutylaluminium-promoted formation of lanthanide hydrides

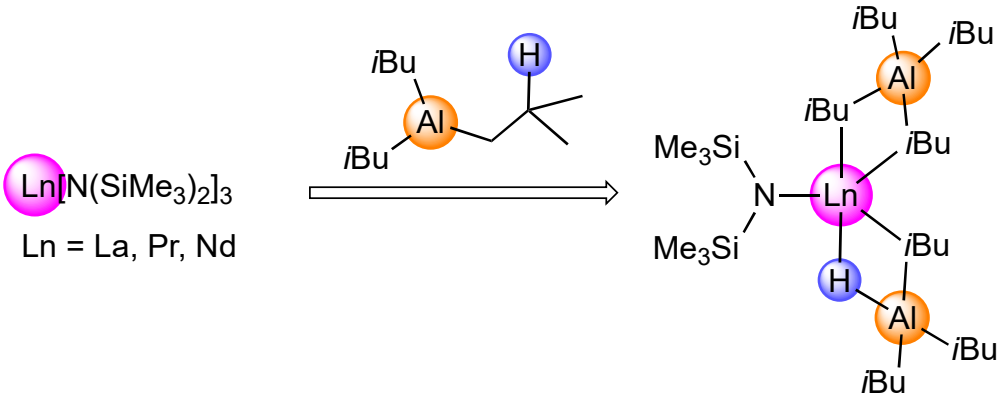

ChemComm

COMMUNICATION

View Article Online
View Journal | View Issue

Cite this: *Chem. Commun.*, 2023, 59, 5261

Received 17th March 2023,
Accepted 4th April 2023

DOI: 10.1039/d3cc01330h

rsc.li/chemcomm

Triisobutylaluminium-promoted formation of lanthanide hydrides†

Eric C. Moinet,[a] Olivier Tardif,[b] Cäcilia Maichle-Mössmer[a] and Reiner Anwander *[a]

Discrete lanthanide(III) isobutylaluminates Ln[N(SiMe$_3$)$_2$](HAliBu$_3$)(AliBu$_4$) (Ln = La, Pr, Nd) are obtained from Ln[N(SiMe$_3$)$_2$]$_3$ and triisobutylaluminium (TIBA). Nd[N(SiMe$_3$)$_2$](HAliBu$_3$)(AliBu$_4$) reacts with crown ether to give the ion pair [Nd(18-c-6){N(SiMe$_3$)$_2$}(HAliBu$_3$)][AliBu$_4$], featuring a strong Nd–H interaction in the solid state. The equimolar reaction of La[N(SiMe$_3$)$_2$](HAliBu$_3$)(AliBu$_4$) with fluorene resulted in the concomitant formation of [(μ-fluorenyl)$_3$La$_2$(μ-H)-(HAliBu$_3$)$_2$] and (fluorenyl)$_2$La[N(SiMe$_3$)$_2$]. [(μ-Fluorenyl)$_3$La$_2$(μ-H)(HAliBu$_3$)$_2$] features fluorenyl ligands with a μ-η^6:η^6 coordination around the hydrido-bridged dilanthanum core motif. The reported complexes are the first crystallographically characterized, ancillary ligand-free lanthanide(III) tetraisobutylaluminates, and display potential model systems for Ziegler-type polymerization catalysis.

Ziegler mixed catalysts play a major role in the large-scale production of synthetic rubber.[1,2] Of the early lanthanide metals, neodymium-based catalysts excel in 1,3-diene polymerization, in particular due to redox-stability (relative to cerium or samarium) and natural abundance/cost efficiency (relative to praseodymium), fabricating rubbers with the highest *cis*-1,4 contents.[3–6] State-of-the-art ternary catalysts consist of a neodymium compound (chloride, alkoxide, or carboxylate), a cocatalyst (diethyl- or diisopropylaluminium chloride), and triisobutylaluminium (AliBu$_3$ = TIBA), or diisobutylaluminium hydride (HAliBu$_2$ = DIBAH).[3–6] Academic research has also dealt with commercially available lanthanide silylamides Ln[N(SiMe$_3$)$_2$]$_3$ as catalyst precursors.[7–9] In contrast to industrially applied catalyst precursors, homoleptic Ln[N(SiMe$_3$)$_2$]$_3$ form discrete, monomeric species in aliphatic solvents, ideally suited for studying precatalyst/cocatalyst interactions and, hence, for elucidating the active species. Complexes Ln[N(SiMe$_3$)$_2$]$_3$ are favourably activated by TIBA, upon addition of a fluorinated borate cocatalyst[7–9] or silica grafting.[10–12] Both selectivity and activity of Ln[N(SiMe$_3$)$_2$]$_3$/TIBA-derived ternary mixtures are found to be superior or at least comparable with established catalyst systems based on lanthanide carboxylates.[7] Moreover, ternary system (2-Ph-indenyl)$_2$Gd-[N(SiMe$_3$)$_2$]/[Ph$_3$C][B(C$_6$F$_5$)$_4$]/TIBA bearing a silylamido ligand was described as a highly efficient catalyst for *cis*-1,4-selective polymerization of butadiene (>99%).[13] However, structural details of the species formed in Ln(III)–[N(SiMe$_3$)$_2$]/TIBA mixtures have remained elusive. This also applies to similar Ziegler–Natta catalysts derived from group 4 metals.[14] NMR-spectroscopic investigations of metal halide/TIBA-derived catalysts suggest the formation of metal hydride species (*via* β-H elimination) for both lanthanide and group 4 metals.[14,15] Only recently, the first structural proof of hydride formation has been revealed *via* treatment of divalent Ln(AliBu$_4$)$_2$ (Ln = Sm, Yb) with B(C$_6$F$_5$)$_3$ affording discrete hydroborates Ln[HB(C$_6$F$_5$)$_3$]$_2$(arene).[16] For comparison Ln(III)–[N(SiHMe$_2$)$_2$]→Ln(III)–H as well as Ln–benzoate→Ln–H and Ln–CH$_3$→Ln–H transformations are readily promoted by alkylaluminium hydrides like DIBAH or HAlMe$_2$.[17,18] Furthermore, (C$_5$Me$_5$)$_2$Sm[(μ-iBu)$_2$AliBu$_2$] is the only trivalent lanthanide complex containing a tetraisobutylaluminato moiety which has been crystallographically authenticated.[19] Two more types of trivalent lanthanide compounds containing a triisobutylaluminium moiety were reported to our knowledge, comprising (C$_5$Me$_5$)$_2$Ln[(μ-Cl)(μ-iBu)AliBu$_2$] (Ln = Sm, Y), and (C$_5$Me$_5$)$_2$Sm[(μ-O$_2$CPh)(μ-iBu)AliBu$_2$], both stabilized by pentamethylcyclopentadienyl ligands.[20,21]

Here, we present the synthesis, isolation and reactivity of the first ancillary ligand-free trivalent lanthanide isobutylaluminates. Unambiguous structural evidence for a TIBA-promoted Ln(III)-amido→Ln(III)-hydrido transformation is provided.

Aiming at putative homoleptic [La(AliBu$_4$)$_3$], silylamide La[N(SiMe$_3$)$_2$]$_3$ was treated with 6.5 equiv. TIBA (95%) at ambient temperature in *n*-pentane. Repeated re-crystallization of the concentrated reaction solution at −40 °C afforded single crystals of La[N(SiMe$_3$)$_2$](HAliBu$_3$)(AliBu$_4$) (**1^{La}**) (Scheme 1 and Fig. 1).

However, since excess TIBA and isobutylaluminium side products greatly hampered crystallization, the amount of added

[a] *Institut für Anorganische Chemie, Eberhard Karls Universität Tübingen, Auf der Morgenstelle 18, D-72076 Tübingen, Germany. E-mail: reiner.anwander@uni-tuebingen.de*

[b] *Bridgestone Corporation, Ogawahigashi-cho, Kodaira-shi, Tokyo, 187-8531, Japan*

† Electronic supplementary information (ESI) available. CCDC 2249265–2249269. For ESI and crystallographic data in CIF or other electronic format see DOI: https://doi.org/10.1039/d3cc01330h

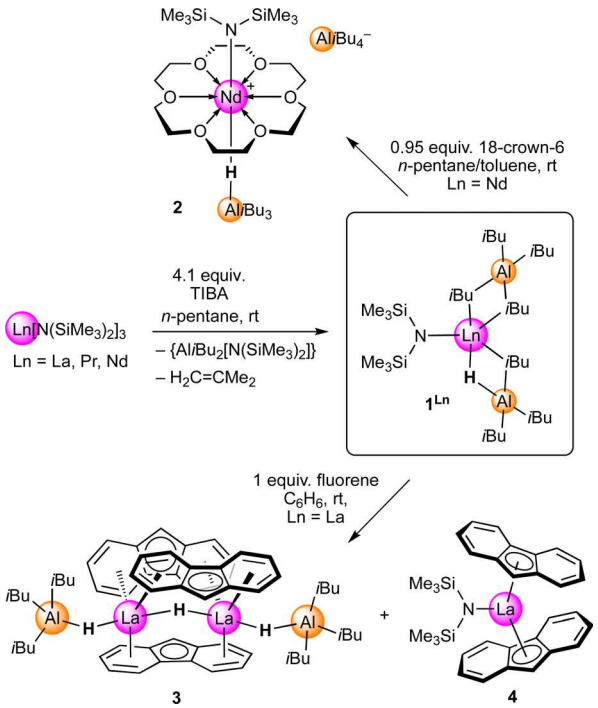

Scheme 1 Synthesis of $\mathbf{1}^{\mathbf{Ln}}$, and reactivity towards 18-crown-6 and fluorene with products [Nd(18-c-6){N(SiMe$_3$)$_2$}(HAliBu$_3$)][AliBu$_4$] (**2**), and [(μ-fluorenyl)$_3$La$_2$(μ-H) (HAliBu$_3$)$_2$]/(fluorenyl)$_2$La[N(SiMe$_3$)$_2$] (**3**/**4**).

TIBA was reduced to 4.1 equiv., thus facilitating crystallization/recrystallization processes (26% yield). Both 6.5 and 4.1 equiv. TIBA generated the same product $\mathbf{1}^{\mathbf{La}}$ (Scheme 1). Following similar procedures, isotypic compounds Ln[N(SiMe$_3$)$_2$](HAliBu$_3$)-(AliBu$_4$) of praseodymium ($\mathbf{1}^{\mathbf{Pr}}$, 28%) and neodymium ($\mathbf{1}^{\mathbf{Nd}}$, 33%) (Ln = La, Nd, Pr) were obtained under optimized conditions. The heteroleptic complexes $\mathbf{1}^{\mathbf{Ln}}$ feature one unreacted silylamido ligand along with homo- and heteroaluminato moieties [AliBu$_4$] and [HAliBu$_3$], respectively (Fig. 1).

A closer look at the solid-state structures revealed distinct tetraisobutylaluminato coordination. The largest rare-earth-metal centre exhibits a distorted η^3-coordination, with two

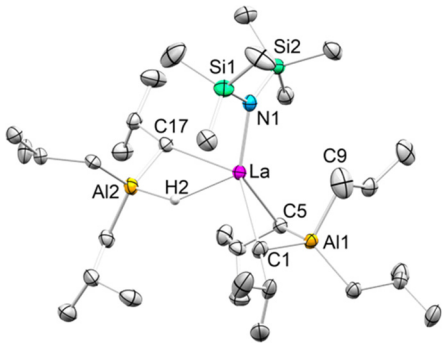

Fig. 1 Crystal structure of La[N(SiMe$_3$)$_2$](HAliBu$_3$)(AliBu$_4$) ($\mathbf{1}^{\mathbf{La}}$). Ellipsoids are shown at a 50% probability level. Hydrogen atoms except the hydrido ligand, and the disorder of the isobutyl groups are omitted for clarity. For detailed metrics, see the ESI.† The praseodymium and neodymium complexes $\mathbf{1}^{\mathbf{Pr}}$ and $\mathbf{1}^{\mathbf{Nd}}$ are isotypic (see ESI†).

similar and one La–C[AliBu$_4$] distance elongated (*i.e.* La(1)–C(1) 2.782(4) Å, La(1)–C(5) 2.755(4) Å, La(1)–C(9) 3.155(1) Å in $\mathbf{1}^{\mathbf{La}}$). For praseodymium and neodymium, one relatively short Ln–C1 distance (2.566(8) and 2.543(2) Å), a considerably longer (2.716(4) and 2.708(5) Å), and overlong distance are noticed (3.228(1) and 3.237(1) Å). The Ln–C[HAliBu$_3$] and Ln–N distances decrease with decreasing Ln(III) radii (La 2.823(4)/2.276(3), Pr 2.808(4)/2.246(9), Nd 2.763(7)/2.208(5) Å). Despite significant disorder in the crystal structure of the $\mathbf{1}^{\mathbf{Pr}}$ and $\mathbf{1}^{\mathbf{Nd}}$ (see ESI†), the structural data indicate that the distorted η^3-coordination of the [AliBu$_4$] moiety detected in $\mathbf{1}^{\mathbf{La}}$ gives way to a Ln–SiMe(silylamido) intramolecular interaction for the smaller rare-earth metals.[13]

The structural identification of an alkyl/hydrido heteroaluminato η^2-coordination in $\mathbf{1}^{\mathbf{Ln}}$ is unprecedented. It can be hypothesized that the hydrido moiety is formed by sterically enforced β-hydride elimination from an isobutyl moiety of putative [La{N(SiMe$_3$)$_2$}(AliBu$_4$)$_2$]. Alternatively or additionally, hydride formation might result from the presence of DIBAH. However, exclusive DIBAH-promoted formation of hydride species seems unlikely since commercial TIBA samples contain less than 5% DIBAH. Considering that TIBA and DIBAH are both used as cocatalysts for conjugated diene polymerization,[1–3] the hydride formation in $\mathbf{1}^{\mathbf{Ln}}$ may provide valuable insights on their activating nature. Hydride species are discussed as potential active sites in 1,3-diene polymerization,[22] generating allyl moieties with 1,3-dienes,[23] as widely proposed intermediates in 1,3-diene polymerization.[1–3] For example, Cui *et al.* proposed the formation of transient moieties [Y(μ-iBu)$_2$AliBu$_2$], [Y(μ-H)(μ-iBu)AliBu$_2$] and [Y(μ-H)$_2$AliBu$_2$] as active sites of the ternary mixture (PBNHC)-YBr$_2$(THF)/TIBA/[Ph$_3$C][B(C$_6$F$_5$)$_4$] (1 : 20 : 1; PBNHC = CCC pincer), by NMR spectroscopic analysis.[15] Similarly, [Zr(μ-H)AliBu$_3$] and [Zr(μ-H)$_2$AliBu$_2$] moieties could be identified in mixtures of (C$_5$H$_4$*n*Bu)$_2$ZrCl$_2$/TIBA (1 : 12) by means of NMR spectroscopy only.[14a]

The ^{1}H NMR spectrum of diamagnetic La[N(SiMe$_3$)$_2$]-(HAliBu$_3$)(AliBu$_4$) ($\mathbf{1}^{\mathbf{La}}$) revealed two nicely resolved isobutyl signal sets for the [AliBu$_4$] and [HAliBu$_3$] moieties. The La–H–Al-bridging hydrido resonance was detected at 6.46 ppm in C$_6$D$_6$ (*cf.* Fig. S2, ESI†), which corresponds well to the ^{1}H chemical shift of a terminal Sc–H proton (6.39 ppm at −60 °C in toluene-d_8) reported recently by Chen *et al.*[24] For further comparison, the Ln–H–Al hydrido resonances of complexes Tp$^{t\mathrm{Bu,Me}}$Ln[(μ-H)AlMe$_3$]$_2$ (Ln = Y, 5.05 ppm, toluene-d$_8$; Lu, 7.82 ppm, C$_6$D$_6$) and Tp$^{t\mathrm{Bu,Me}}$Ln[μ-N(C$_6$H$_3$Me$_2$-2,6)](μ-H)AlMe$_2$] (Ln = Y, 6.57 ppm, C$_6$D$_6$; Lu, 8.67 ppm; C$_6$D$_6$) are in a similar range.[25] Complex [La{(μ-H)[(μ-NC$_6$H$_3$iPr$_2$-2,6)(μ-H)AlMe$_2$](thf)$_3$}]$_2$ features a La–H–Al linkage, but NMR spectroscopic data were not provided.[26] Variable temperature ^{1}H-NMR spectra performed on $\mathbf{1}^{\mathbf{La}}$ revealed highly fluxional isobutyl groups, *i.e.* the resonances of bridging and terminal isobutyl groups do not exhibit decoalescence even at 193 K (*cf.* Fig. S7, ESI†), and sharpening of the La–H–Al resonance.

The excellent solubility of $\mathbf{1}^{\mathbf{Ln}}$ in aliphatic and aromatic solvents may explain why lanthanide tetraisobutylaluminates are difficult to crystallize. During the crystallization process of

$\mathbf{1^{Ln}}$ from the reaction mixture, enrichment of the highly soluble co-product, presumably diisobutylaluminium hexamethyldisilazide, hampered further isolation of product and limited the yield to approximately 30%. Species other than $\mathbf{1^{Ln}}$ could not be unequivocally identified, even though monitoring the reaction of $\mathbf{1^{La}}$ with additional TIBA by ^{1}H-NMR spectroscopy showed that the silylamido methyl resonance is shifted. This indicates further exchange of $[N(SiMe_3)_2]$ for another $[AliBu_4]$ or $[HAliBu_3]$ moiety (*cf.* Fig. S5 and S6, ESI†), as corroborated by the formation of additional isobutene. However, exchange products could not be isolated, most likely due to the very high mobility of the isobutylaluminato ligand impeding crystallization.

The ability of DIBAH to promote the formation of discrete rare-earth-metal hydride complexes has already been demonstrated.[17] The present work revealed that TIBA does engage in lanthanide hydride formation as well. Entities like $[Ln(\mu\text{-}H)(\mu\text{-}iBu)AliBu_2]$ featured by complexes $\mathbf{1^{Ln}}$ lend support to Cui's mechanistic proposal (*vide supra*)[15b] and make complexes $\mathbf{1^{Ln}}$ cogent models for poorly defined Ziegler mixed catalysts used in 1,3-diene polymerization. It is noteworthy that previous investigations into the active species, which are formed in mixtures of neodymium carboxylate $Nd(vers)_3$ (vers = neodecanoato), TIBA, and diisobutylaluminium chloride, using MALDITOF and XAFS techniques do not consider the formation of hydride species but very well alkylation.[27,28] Theoretical optimization of the EXAFS data assumes the presence of approx. 3–4 alkyl ligands at the neodymium centre, with a Nd–C distance of 2.58 Å, whereas addition of extra diisobutylaluminium chloride led to detection of two Al "neighbours" at a distance of 3.14 Å.[28] Compared to our work, this may suggest that two aluminato units may be involved. Further, the comparison of interatomic distances clearly shows similarities of $\mathbf{1^{Nd}}$ with the calculated parameters reported by Guo *et al.*[26,28] They describe substitution of the Nd–O for Nd–C bonds, which are in the range of 2.57–2.58 Å. We observed strikingly similar Nd–C interatomic distances in the range of 2.542–2.763 Å for $\mathbf{1^{Nd}}$. Additionally, the Nd---Al distances in $\mathbf{1^{Nd}}$ are 2.999(2) and 3.243(2) Å, which is comparable to the metrics for two aluminium neighbours given with average 3.14 Å.[28]

To probe the bonding and reactivity of the isobutylaluminates $\mathbf{1^{Ln}}$, an equimolar amount of 18-crown-6 was added to $\mathbf{1^{Nd}}$, which rapidly led to the precipitation of compound $[Nd(18\text{-}c\text{-}6)\{N(SiMe_3)_2\}(HAliBu_3)][AliBu_4]$ (**2**) (*cf.* Fig. 2). Compound **2** demonstrates the strong binding of the hydrido to the lanthanide centre, albeit the Nd–H bond is elongated with 2.39(3) Å, compared to 2.17(5) Å in $\mathbf{1^{Nd}}$. The $[AliBu_4]$ moiety is separated from the central ion, implying rather weak interactions with the Nd(III) centre. Given the 8-coordinate neodymium centre in **2**, the Nd(1)–N(1) distance of 2.329(2) Å is markedly increased to those in $\mathbf{1^{Nd}}$ (2.208(5) Å) or $Nd[N(SiMe_3)_2]_3$ and (2.29 (2) Å).[29]

Aiming at a half-sandwich complex, the equimolar reaction of $\mathbf{1^{La}}$ with fluorene at ambient temperature in benzene surprisingly led to the concurrent precipitation of orange-red complexes $[[(\mu\text{-fluorenyl})_3La_2(\mu\text{-}H)(HAliBu_3)_2]$ (**3**) (Scheme 1 and Fig. 3) and $(fluorenyl)_2La[N(SiMe_3)_2]$ (**4**) (Fig. S17, ESI†).

While the crystal structure of complex **4** shows the common metallocene motif with η^5-coordinated fluorenyl ligands

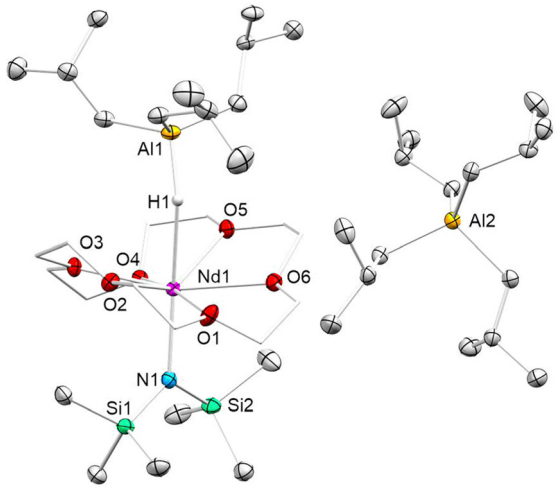

Fig. 2 Crystal structure of $[Nd(18\text{-}c\text{-}6)\{N(SiMe_3)_2\}(HAliBu_3)][AliBu_4]$ (**2**). Ellipsoids are shown at a 50% probability level. Hydrogen atoms expect the bridging hydrido ligand, as well as the disorder in isobutyl groups are omitted for clarity. For detailed metrics, see the ESI.†

(*cf.*, $(fluorenyl)_2La(AlMe_4)_2$),[30] the connectivity of tetrametallic **3** is rather unusual. The two lanthanum centres in **3** are encapsulated by three fluorenyl ligands in a $\mu\text{-}\eta^6\text{:}\eta^6$ fashion. The central cavity is occupied by a bridging hydrido anion, while the La–H–La axis is extended on both sides to $[(\mu\text{-}H)AliBu_3]$ ligands. The $[HAliBu_3]$ unit of precursor $\mathbf{1^{La}}$ remains coordinated while **3** is formed, which seems plausible considering the strong hydrido binding observed in complex **2**. The presence of hydrido ligands in **3** was confirmed by monitoring the protonolysis of compound **3** with isopropanol by ^{1}H-NMR spectroscopy, showing dihydrogen evolution. Referenced to the signal of hexamethyldisilazane (18 protons) co-formed in the mixture, the integral ratios of 6 hydrogen protons (or 3 of the non-binomial triplet observed when instead iPrOD-d_8 was used) corroborate the presence of three hydridos in **3** (*cf.* Fig. S11 and S12, ESI†).

η^6-Coordinated fluorenyl ligands as observed in **3** are very uncommon in rare-earth-metal chemistry. A similar structural motif was reported for orange-red lithium fluorenide, showing a dimer comprised of two lithium ions sandwiched by fluorenyls in $\mu\text{-}\eta^6\text{:}\eta^6$ fashion.[31] The latter are nearly planar, as

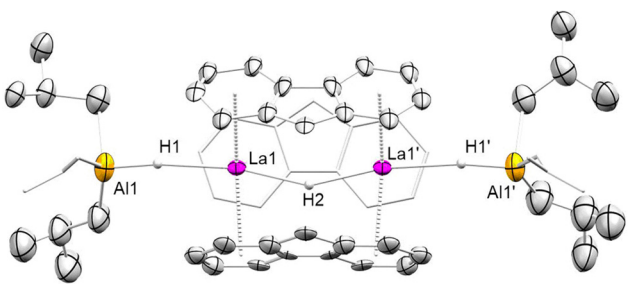

Fig. 3 Crystal structure of **3**. Ellipsoids are shown at a 50% probability level. Hydrogen atoms expect the bridging hydridos, as well as the disorder in the isobutyl and fluorenyl groups, and co-crystallized **4** are omitted for clarity. For detailed metrics, see the ESI.†

observed for the fluorenyl anions in **3**. Quantum chemical calculations for lithium fluorenide revealed that η^6-coordination is favoured over putative η^5-coordinated species since no donor molecules are available to complete the coordination sphere of lithium cations tentativley η^5-coordinated.[31,32] For lanthanides, η^6-fluorenyl coordination has so far only be reported for the divalent complexes η^6-bis(Me_3Si-fluorene-AlR_3)Sm (R = Me (**A**), Et).[33] Remarkably, η^6-bis(Me_3Si-fluorene-AlR_3)Sm can be converted into η^5-(Me_3Si-fluorenyl)$_2$Sm(THF)$_2$ by addition of THF, and the reaction can be reversed by addition of AlR_3.[33] A similar μ-η^6:η^6 bonding motif has been observed in $[(C_5Me_5)La]_3(\mu\text{-}Cl)_3(thf)(\mu\text{-}\eta^2\text{:}\eta^6\text{:}\eta^6\text{-}C_{16}H_{10})$ (**B**) featuring a trianionic pyrenyl ligand.[34] The La–centroid(η^6) distances in **4** range from 2.629 to 2.680 Å and, hence, are significantly longer than in complex **B**.

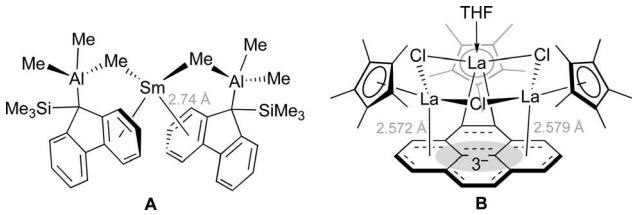

In summary, treatment of $Ln[N(SiMe_3)_2]_3$ with triisobutylaluminium (TIBA) affords crystalline heteroleptic lanthanide isobutylaluminates $Ln[N(SiMe_3)_2](HAliBu_3)(AliBu_4)$ (Ln = La, Pr, Nd). Their isolation provides credible evidence that $AliBu_3$ is both an alkylating agent and a potent hydride source for the generation of Ln-hydride complexes *via* β-hydride elimination from isobutyl moieties. The $[HAliBu_3]$ moiety interacts stronger with the lanthanide(III) centre than $[AliBu_4]$ as indicated by the formation of ion pair $[Nd(18\text{-}c\text{-}6)\{N(SiMe_3)_2\}(HAliBu_3)][AliBu_4]$. Separation of $AliBu_3$ from the $[HAliBu_3]$ ligand is evidenced by the barrel-shaped complex $[(\mu\text{-fluorenyl})_3La_2(\mu\text{-}H)(HAliBu_3)_2]$ featuring a rare μ-η^6:η^6 bonding motif of the fluorenyl ligands. Studies covering the use of $\mathbf{1^{Ln}}$ in 1,3-diene polymerization will be published soon.

We thank Bridgestone Corporation for generous support.

Conflicts of interest

There are no conflicts to declare.

Notes and references

1 T. Sone, *Int. Polym. Sci. Technol.*, 2016, **43**, 49–54.
2 G. Ricci, G. Pampaloni, A. Sommazzi and F. Masi, *Macromolecules*, 2021, **54**, 5879–5914.
3 L. Friebe, O. Nuyken and W. Obrecht, *Adv. Polym. Sci.*, 2006, **204**, 1–154.
4 A. Fischbach and R. Anwander, *Adv. Polym. Sci.*, 2006, **204**, 155–281.
5 Z. Zhang, D. Cui, B. Wang, B. Liu and Y. Yang, in *Molecular Catalysis of Rare-Earth Elements*, ed. P. W. Roesky, Springer, Berlin Heidelberg, 2010, pp. 49–108.
6 H. Wang, J. M. O. Cue, E. L. Calubaquib, R. N. Kularatne, S. Taslimy, J. T. Miller and M. C. Stefan, *Polym. Chem.*, 2021, **12**, 6790–6823.
7 C. Boisson, F. Barbotin and R. Spitz, *Macromol. Chem. Phys.*, 1999, **200**, 1163–1166.
8 V. Monteil, R. Spitz and C. Boisson, *Polym. Int.*, 2004, **53**, 576–581.
9 N. Martins, F. Bonnet and M. J. P. Visseaux, *Polymer*, 2014, **55**, 5013–5016.
10 T. J. Woodman, Y. Sarazin, G. Fink, K. Hauschild and M. Bochmann, *Macromolecules*, 2005, **38**, 3060–3067.
11 R. M. Gauvin, T. Chenal, R. A. Hassan, A. Addad and A. Mortreux, *J. Mol. Catal. A: Chem.*, 2006, **257**, 31–40.
12 A. Bathellier, D. Moreno, L. Maron, C. Dinoi and I. del Rosal, *Chem. – Eur. J.*, 2020, **26**, 13213–13225.
13 O. Tardif and S. Kaita, *Dalton Trans.*, 2008, 2531–2533.
14 (*a*) D. B. Culver, R. W. Dorn, A. Venkatesh, J. Meeprasert, A. J. Rossini, E. A. Pidko, A. S. Lipton, G. R. Lief and M. P. Conley, *ACS Cent. Sci.*, 2021, **7**, 1225–1231; (*b*) D. B. Culver, J. Corieri, G. R. Lief and M. P. Conley, *Organometallics*, 2022, **41**, 892–899.
15 (*a*) W. Gao and D. Cui, *J. Am. Chem. Soc.*, 2008, **130**, 4984–4991; (*b*) K. Lv and D. Cui, *Organometallics*, 2010, **29**, 2987–2993.
16 E. C. Moinet, B. M. Wolf, O. Tardif, C. Maichle-Mössmer and R. Anwander, *Angew. Chem., Int. Ed.*, 2023, e202219316.
17 M. G. Klimpel, P. Sirsch, W. Scherer and R. Anwander, *Angew. Chem., Int. Ed.*, 2003, **42**, 574–577.
18 (*a*) C. Schädle, A. Fischbach, E. Herdtweck, K. W. Törnroos and R. Anwander, *Chem. – Eur. J.*, 2013, **19**, 16334–16341; (*b*) C. Schädle, C. Maichle-Mössmer, K. W. Törnroos and R. Anwander, *Organometallics*, 2015, **34**, 2667–2675.
19 W. J. Evans, J. T. Leman, R. D. Clark and J. W. Ziller, *Main Group Met. Chem.*, 2000, **23**, 163–168.
20 W. J. Evans, T. M. Champagne, D. G. Giarikos and J. W. Ziller, *Organometallics*, 2005, **24**, 570–579.
21 W. J. Evans, T. M. Champagne and J. W. Ziller, *Chem. Commun.*, 2005, 5925–5927.
22 L. Friebe, O. Nuyken, H. Windisch and W. Obrecht, *Macromol. Chem. Phys.*, 2002, **203**, 1055–1064.
23 (*a*) G. Jeske, H. Lauke, H. Mmauermann, P. N. Swepston, H. Schumann and T. J. Marks, *J. Am. Chem. Soc.*, 1985, **107**, 8091–8103; (*b*) W. J. Evans, T. A. Ulibarri and J. W. Ziller, *J. Am. Chem. Soc.*, 1990, **112**, 2314–2324.
24 X. Han, L. Xiang, C. A. Lamsfus, W. Mao, E. Lu, L. Maron, X. Leng and Y. Chen, *Chem. – Eur. J.*, 2017, **23**, 14728–14732.
25 C. Schädle, D. Schädle, K. Eichele and R. Anwander, *Angew. Chem., Int. Ed.*, 2013, **52**, 13238–13242.
26 R. Thim, D. Schädle, C. Maichle-Mössmer and R. Anwander, *Chem. – Eur. J.*, 2019, **25**, 507–511.
27 (*a*) G. Kwag, H. Lee and S. Kim, *Macromolecules*, 2001, **34**, 5367–5369; (*b*) G. Kwag, *Macromolecules*, 2002, **35**, 4875–4879.
28 (*a*) H. Guo, J. Bi, J. Wang, X. Zhang, S. Jiang and Z. Wu, *Dalton Trans.*, 2015, **44**, 9130–9139; (*b*) H. Guo, J. Bi, Q. Wu, J. Wang, W. Shi, X. Zhang, S. Jiang and Z. Wu, *RSC Adv.*, 2017, **7**, 14413–14421.
29 R. A. Andersen, D. H. Templeton and A. Zalkin, *Inorg. Chem.*, 1978, **17**, 2317–2319.
30 D. Diether, K. Tyulyunov, C. Maichle-Mössmer and R. Anwander, *Organometallics*, 2017, **36**, 4649–4659.
31 C. Üffing, R. Köppe and H. Schnöckel, *Organometallics*, 1998, **17**, 3512–3515.
32 H. Jiao, P. v R. Schleyer, Y. Mo, M. A. McAllister and T. T. Tidwell, *J. Am. Chem. Soc.*, 1997, **119**, 7075–7083.
33 H. Nakamura, Y. Nakayama, H. Yasuda, T. Maruo, N. Kanehisa and Y. Kai, *Organometallics*, 2000, **19**, 5392–5399.
34 K.-H. Thiele, S. Bambirra, J. Sieler and S. Yelonek, *Angew. Chem., Int. Ed.*, 1998, **37**, 2886–2888.

Electronic Supplementary Material (ESI) for Chemical Communications.

Supporting Information

Triisobutylaluminium-promoted formation of lanthanide hydrides

Eric C. Moinet,[a] Olivier Tardif,[b] Cäcilia Maichle-Mössmer,[a] and Reiner Anwander[a,*]

[a] Institut für Anorganische Chemie, Eberhard Karls Universität Tübingen, Auf der Morgenstelle 18, D-72076 Tübingen, Germany. E-mail: reiner.anwander@uni-tuebingen.de

[b] Bridgestone Corporation, Ogawahigashi-cho, Kodaira-shi, Tokyo, 187-8531, Japan

Table of Contents

Experimental

General Considerations

All manipulations were performed under rigorous exclusion of air and moisture, using standard Schlenk, high-vacuum, and glovebox techniques (MBraun MB200B <1 ppm O_2, <1 ppm H_2O, argon atmosphere). Solvents were supplied by Merck KGaA, purified using a SPS solvent purification system (MBraun) and stored inside a glovebox. Benzene-d_6, toluene-d_8 and *o*-difluorobenzene were obtained from Merck KGaA and dried over Na/K alloy prior to use. Triisobutylaluminum (TIBA), and fluorene were purchased from Merck KGaA and used as received. 18-Crown-6 was purchased from abcr and used without further purification. Argon (99.999 Vol%) was supplied by Westfalen AG. Complexes $Ln[N(SiMe_3)_2]_3$ (Ln = La, Pr, Nd) were prepared following standard procedures.[1] Chemicals were stored at −40 °C. Glassware and polymer fittings were dried prior to use for several hours at 120 °C or 80 °C, respectively. IR spectra were recorded on a Nicolet 6700 FTIR spectrometer (Thermo Fisher Scientific), and samples were mixed with KBr powder and measured in a DRIFT cell equipped with KBr windows. Elemental analyses were performed on an Elementar vario MICRO cube. NMR spectra of air and moisture sensitive compounds were recorded using J. Young-valved NMR tubes on a Bruker AVII+400 spectrometer (^{1}H: 400.13 MHz; ^{13}C: 100.61 MHz). ^{1}H and ^{13}C NMR chemical shifts are referenced to solvent residual resonances and reported in parts per million, relative to tetramethylsilane.

Caution! Note that organoaluminum compounds may react violently with air or moisture and may explode with water.

Procedures

$La[N(SiMe_3)_2](HAl\mathit{i}Bu_3)(Al\mathit{i}Bu_4)$ (1^{La})

A solution of TIBA (20.478 g, 103.257 mmol, 4.1 equiv.) in *n*-pentane (30 mL) was added to $La[N(SiMe_3)_2]_3$ (15.616 g, 25.185 mmol, 1 equiv.) in *n*-pentane (100 mL) in portions under stirring at ambient temperature. After stirring overnight, the yellowish solution was concentrated and

cooled to −40° C. Repeated recrystallization afforded 4.945 g (6.558 mmol, 26%) of combined fractions of La[N(SiMe$_3$)$_2$](HAl*i*Bu$_3$)(Al*i*Bu$_4$) **(1^{La})** in the form of colourless, big crystals. DRIFT (KBr, cm^{-1}): 2947 (vs), 2860 (s), 2735 (w), 1457 (s), 1381 (w), 1360 (m), 1315 (w), 1249 (s), 1161 (m), 1060 (m), 1036 (m), 958 (s), 847 (vs), 824 (s), 736 (s), 677 (vs), 648 (vs), 439 (s). $C_{34}H_{82}Al_2LaNSi_2$ (754.06 g/mol): calcd. C 54.16, H 10.96, N 1.86; found C 53.97, H 11.13, N 1.81. ^{1}H NMR (400.1 MHz, C_6D_6, 26 °C): δ 6.46 (s, 1 H, *H*Al*i*Bu$_3$); 2.27 (m, 3 H, C*H* {HAl*i*Bu$_3$}); 1.97 (m, 4 H, C*H* {Al*i*Bu$_4$}); 1.25 (d, 18 H, C*H*$_3$ {HAl*i*Bu$_3$}); 1.14 (d, 24 H, C*H*$_3$ {Al*i*Bu$_4$}); 0.45 (d, 8 H, C*H*$_2$ {Al*i*Bu$_4$}); 0.42 (d, 6 H, C*H*$_2$ {HAl*i*Bu$_3$}); 0.32 (s, 18 H, C*H*$_3$ {N(SiMe$_3$)$_2$}) ppm. ^{13}C{^{1}H} NMR (100.6 MHz, 26 °C): δ 34.5 (*C*H$_2$ {Al*i*Bu$_4$}); 30.6 (*C*H$_2$ {HAl*i*Bu$_3$}); 29.1 (*C*H {Al*i*Bu$_4$}); 29.0 (*C*H {HAl*i*Bu$_3$}); 28.7 (*C*H$_3$ {HAl*i*Bu$_3$}); 28.5 (*C*H$_3$ {Al*i*Bu$_4$}); 3.9 (*C*H$_3$ {N(SiMe$_3$)$_2$}) ppm.

Pr[N(SiMe$_3$)$_2$](HAl*i*Bu$_3$)(Al*i*Bu$_4$) (1^{Pr})

To a solution of Pr[N(SiMe$_3$)$_2$]$_3$ (4.911 g, 7.895 mmol) in *n*-pentane (50 mL), TIBA (6.452 g, 32.533 mmol, 4.1 equiv.) in *n*-pentane (20 mL) was added in portions. After stirring 12 h at ambient temperature, the yellow-green solution was concentrated *in vacuo* and cooled to –40 °C. Repeated recrystallization afforded 1.674 g (2.214 mmol, 28%) yellow-green crystals of Pr[N(SiMe$_3$)$_2$](HAl*i*Bu$_3$)(Al*i*Bu$_4$). DRIFT (KBr, cm^{-1}): 2950 (vs), 2861 (s), 2732 (vw), 1463 (w), 1381 (vw), 1361 (vw), 1318 (vw), 1260 (w), 1250 (m), 1159 (vw), 1064 (w), 1017 (w), 943 (m), 859 (m), 835 (m), 814 (m), 779 (w), 734 (w), 682 (m), 656 (w), 619 (w), 572 (vw). $C_{34}H_{82}Al_2PrNSi_2$ (756.06 g/mol): calcd. C 54.01, H 10.93 N 1.85; found C 53.86, H 10.65, N 1.67.

Nd[N(SiMe$_3$)$_2$](HAl*i*Bu$_3$)(Al*i*Bu$_4$) (1Nd)

To a solution of Nd[N(SiMe$_3$)$_2$]$_3$ (2.624 g, 4.196 mmol) in *n*-hexane (100 mL), TIBA (4.161 g, 20.98 mmol, 5 equiv.) in *n*-hexane (20 mL) was added in portions. After stirring 12 h at ambient temperature, the solution was concentrated *in vacuo* to a volume of 10 mL. The red-green solution yielded dark blue crystals suitable for X-ray diffraction upon storage at –40 °C. The crystals were purified by recrystallization, yielding 1.060 g (1.396 mmol, 33%) big blue column-

shaped crystals (see Fig. S1). DRIFT (KBr, cm^{-1}): 2950 (vs), 2861 (s), 2729 (w), 1463 (vs), 1381 (m), 1359 (m), 1317 (m), 1249 (s), 1159 (m), 1051 (m), 1017 (m), 983 (w), 861 (s), 850 (s), 833 (s), 778 (s), 736 (m), 684 (m), 652 (m), 600 (m), 553 (w), 435 (w). $C_{34}H_{82}Al_2NdNSi_2$ (759.40 g/mol): calcd. C 53.77, H 10.88, N 1.84; found C 53.86, H 10.54, N 1.94.

Figure S1. Crystals of $\mathbf{1^{Nd}}$. The solution of pure $\mathbf{1^{Nd}}$ is deep blue, whereas minor contamination of $\mathbf{1^{Nd}}$ with TIBA/reaction side products results in a solution showing both blue and purple color (right). The reaction mixture containing $\mathbf{1^{Nd}}$ prior to crystallization exhibits both red and green color at the same time (left), a behavior known for other neodymium compounds.[2]

[Nd(18-C-6){N(SiMe$_3$)$_2$}(HAl*i*Bu$_3$)][Al*i*Bu$_4$] (2)

To a solution of 250 mg (0.329 mmol) Nd[N(SiMe$_3$)$_2$](HAl*i*Bu$_3$)(Al*i*Bu$_4$) ($\mathbf{1^{Nd}}$) in *n*-pentane (4 mL), a solution of 18-crown-6 (82.9 mg, 0.314 mmol, 0.95 equiv.) in toluene (1 mL) was added dropwise under stirring at ambient temperature. The immediately formed suspension was stirred for five minutes. Removal of the solvent in vacuum, and washing of the residue three times with cooled *n*-pentane yielded a sticky, pale bluish white powder (324 mg, 96%). Single crystals suitable for X-ray crystallography were grown from *o*-difluorobenzene at –40 °C. DRIFT (KBr, cm^{-1}): 2948 (vs), 2855 (vs), 2765 (m), 2581 (vw), 1457 (s), 1403 (w), 1369 (m), 1354 (s), 1289 (m), 1258 (s), 1201 (vw), 1161 (m), 1085 (s), 1009 (w), 962 (s), 914 (s), 859 (s), 776 (m), 696 (m), 666 (s), 617 (m), 430

(w). $C_{46}H_{106}Al_2NNdO_6Si_2$ (1023.52 g/mol): calcd. C 53.97, H 10.44, N 1.37; found C 53.97, H 10.38, N 1.17.

[(μ-fluorenyl)$_3$La$_2$(μ-H)(HAl*i*Bu$_3$)$_2$] (3) and (fluorenyl)$_2$La[N(SiMe$_3$)$_2$] (4)

A mixture of 500 mg (0.666 mmol) La[N(SiMe$_3$)$_2$](HAl*i*Bu$_3$)(Al*i*Bu$_4$) (**1^{La}**) and fluorene (222 mg, 0.666 mmol, 1 equiv.) was suspended in benzene and left in a sealed vial for ten days without stirring, after which crystalline product suitable for X-ray analysis was formed. The solvent of the obtained orange-red suspension was removed *in vacuo*, and the residue was washed twice with *n*-pentane (1 mL) and dried. The product mixture was obtained as orange-red powder (250.2 mg, 139 mmol, 63%). DRIFT (KBr, cm^{-1}): 3082 (w), 2942 (s), 2854 (m), 2769 (vw), 1594 (w), 1558 (m), 1472 (m), 1458 (m), 1431 (m), 1371 (m), 1355 (m), 1331 (m), 1243 (w), 1197 (w), 1156 (w), 1111 (vw), 1053 (w), 1015 (w), 974 (vw), 948 (w), 860 (w), 820 (m), 786 (vs), 754 (vs), 733 (m), 722 (m), 694 (m), 638 (w), 567 (w), 496 (vw), 434 (m), 425 (w). $C_{95}H_{120}Al_2La_3NSi_2$ (**3** and **4**,1802.83 g/mol): calcd. C 63.29, H 6.71, N 0.78; found C 63.71, H 6.76, N 0.56.

NMR Spectra

In general, solvent residual signals are labeled with an asterisk (*). In some cases, the paramagnetic nature of Pr(III), and Nd(III) (**1**^{Pr}, **1**Nd, **2**), or poor solubility (**3**) did not allow conclusive NMR analysis.

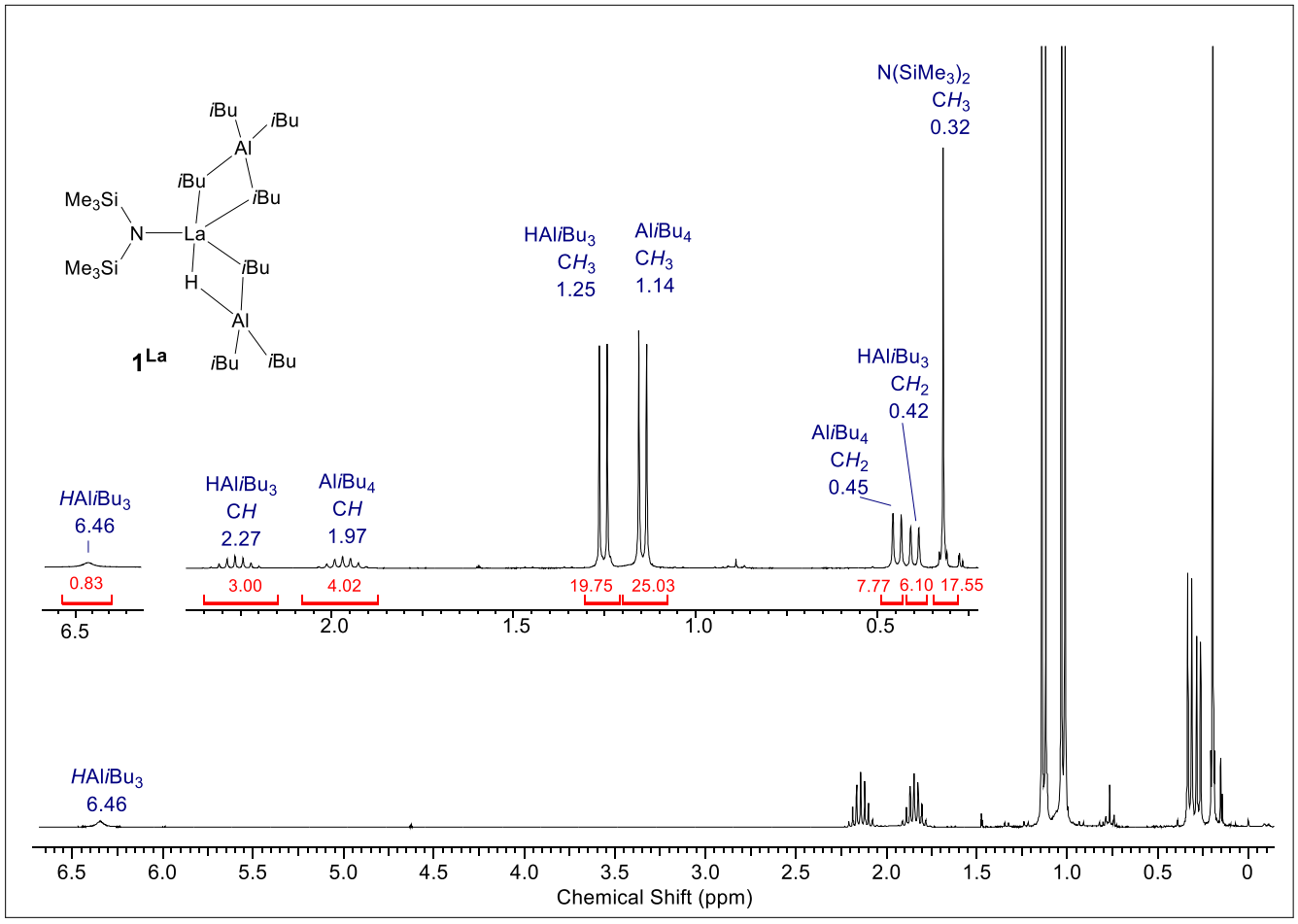

Figure S2. ^{1}H-NMR spectrum (400 MHz, C_6D_6, 26 °C) of La[N(SiMe$_3$)$_2$](HAl*i*Bu$_3$)(Al*i*Bu$_4$) (**1**^{La}).

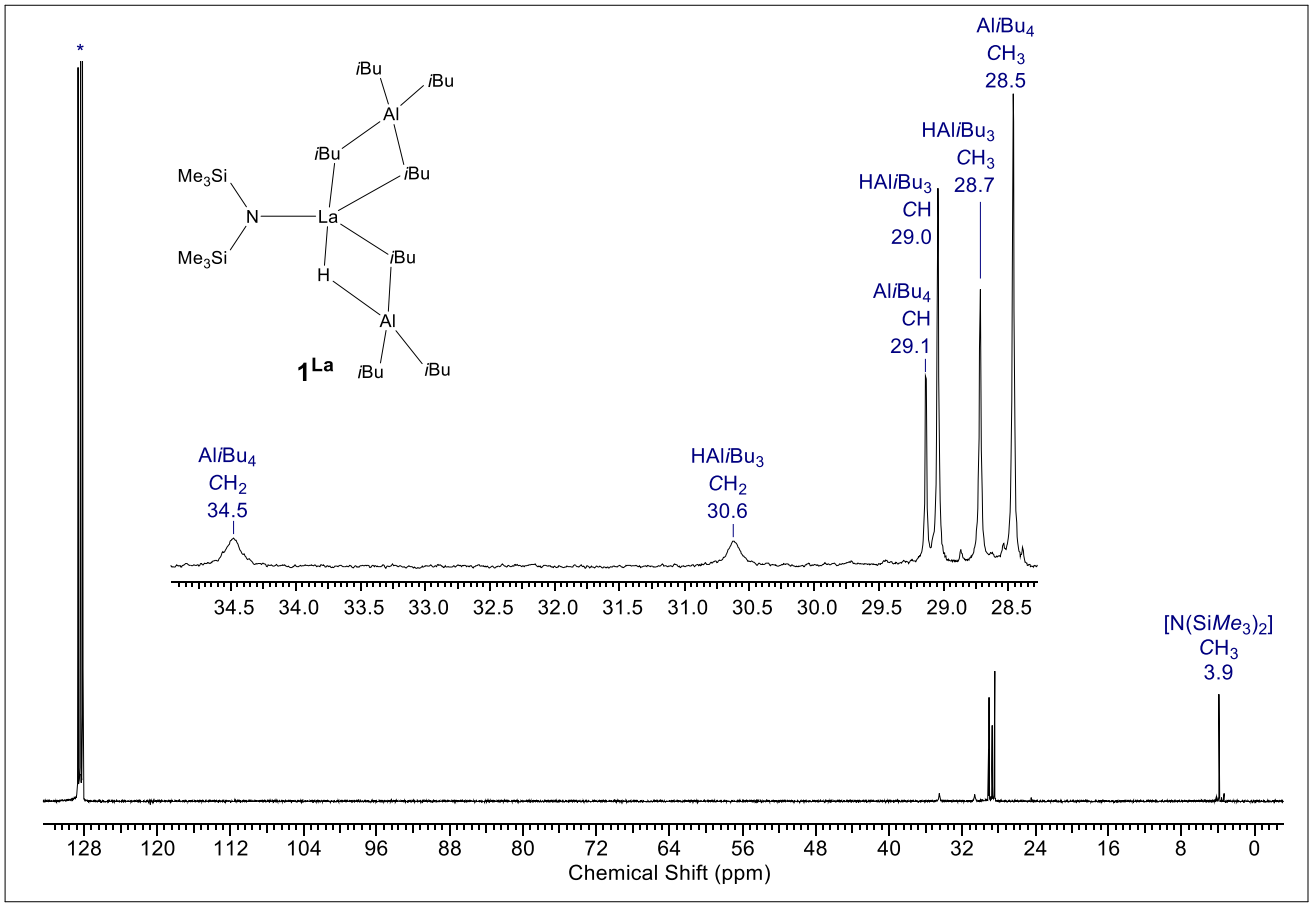

Figure S3. ^{13}C-NMR spectrum (101 MHz, C_6D_6, 26 °C) of La[N(SiMe$_3$)$_2$](HAl*i*Bu$_3$)(Al*i*Bu$_4$) (**1^{La}**).

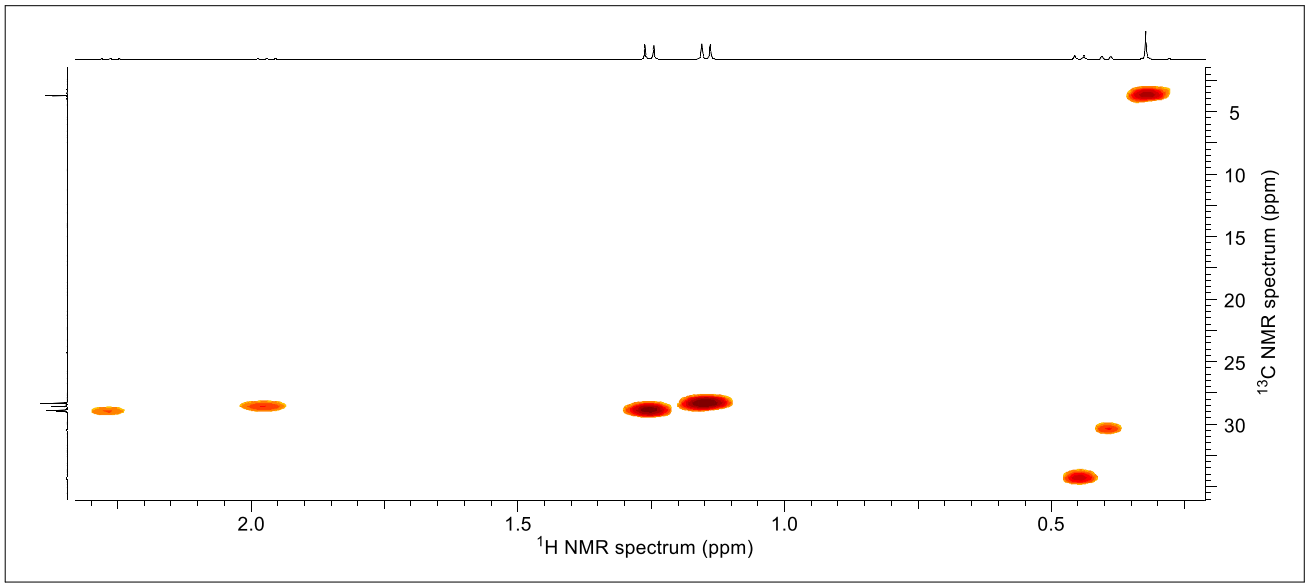

Figure S4. ^{1}H-^{13}C-HSQC NMR spectrum (400/101 MHz, C_6D_6, 26 °C) of La[N(SiMe$_3$)$_2$](HAl*i*Bu$_3$)(Al*i*Bu$_4$) (**1^{La}**).

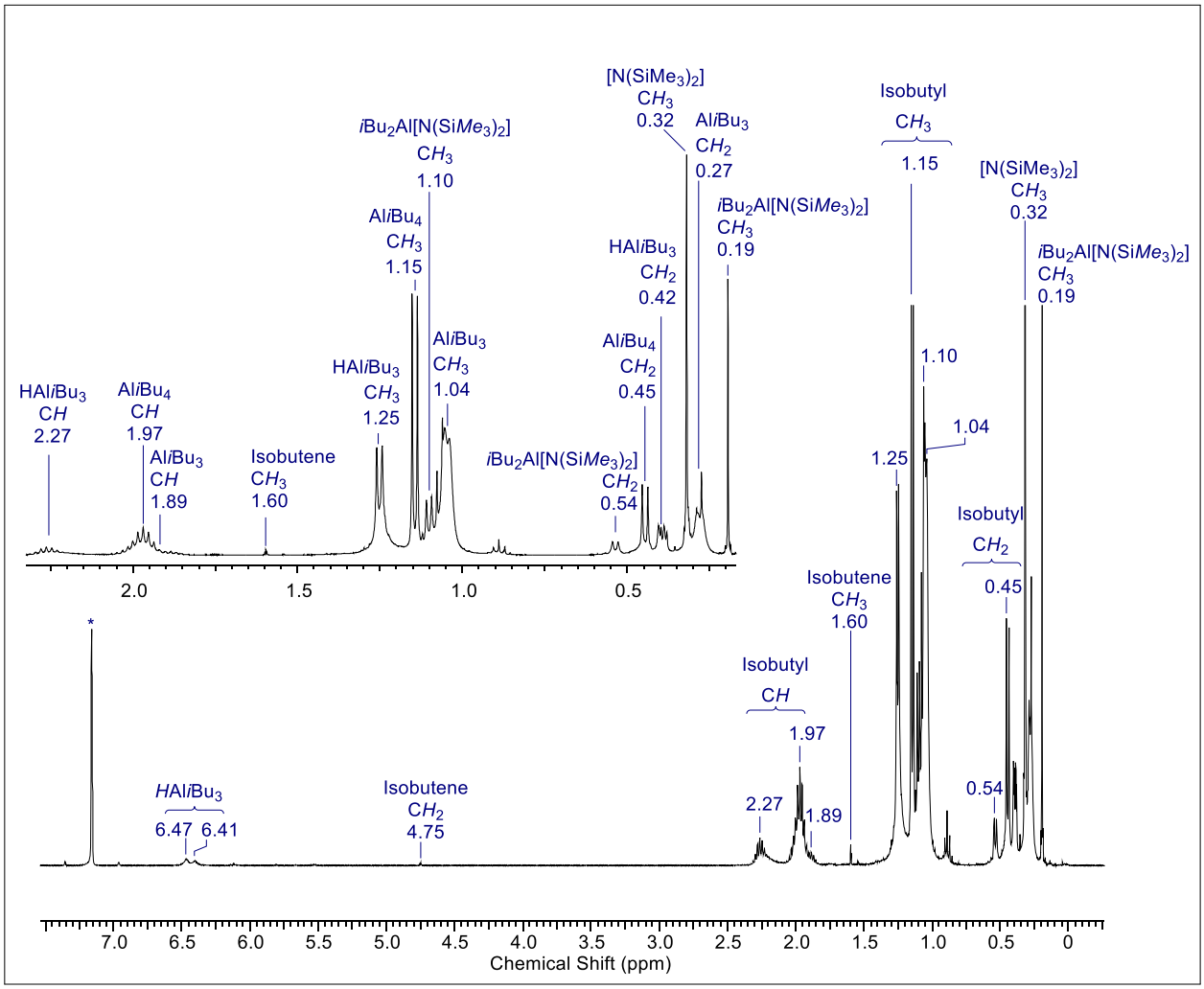

Figure S5. ^{1}H-NMR spectrum (400 MHz, C_6D_6, 26 °C) of the reaction of La[N(SiMe$_3$)$_2$](HAl*i*Bu$_3$)(Al*i*Bu$_4$) (**1^{La}**) with 2 equiv. TIBA in C_6D_6.

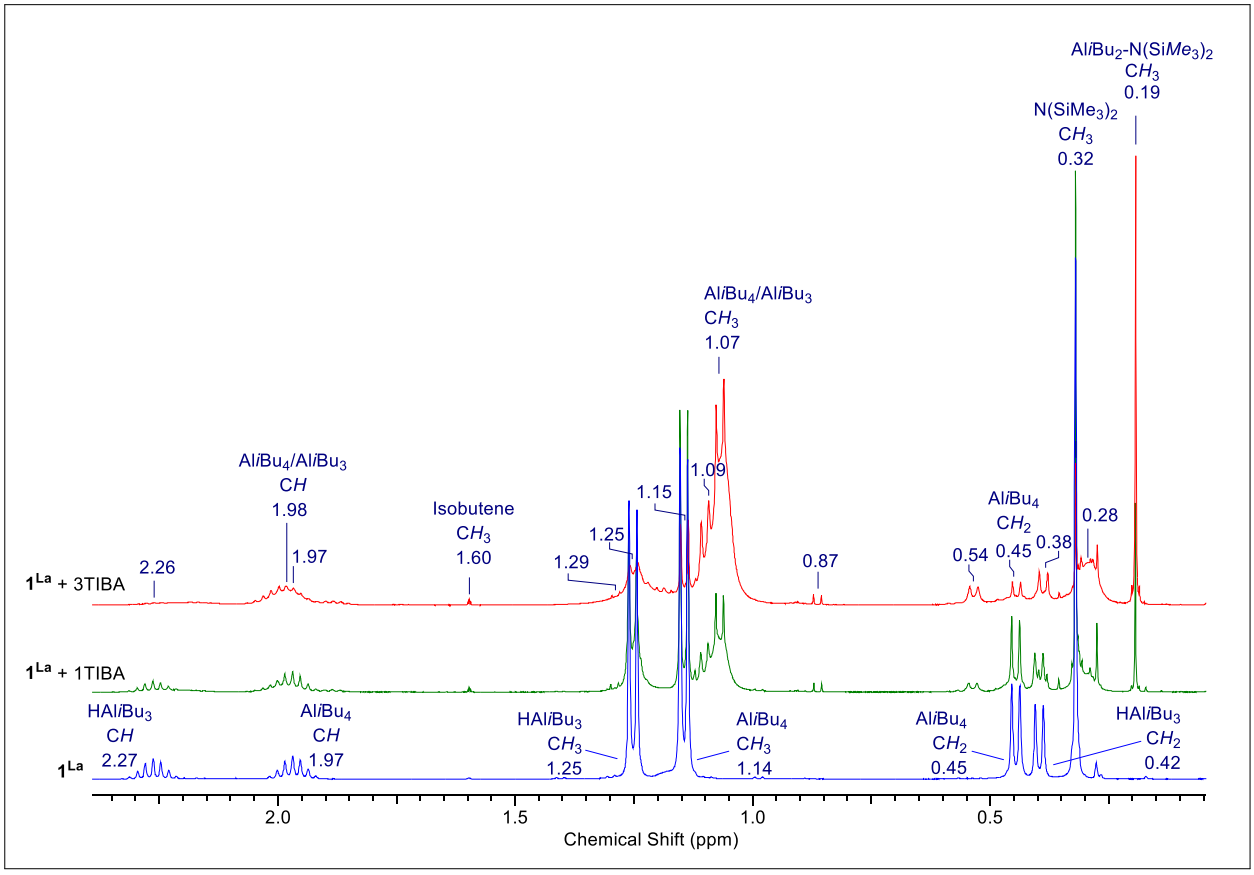

Figure S6. ^{1}H-NMR spectra (400 MHz, C_6D_6, 26 °C) of the reaction of La[N(SiMe$_3$)$_2$](HAl*i*Bu$_3$)(Al*i*Bu$_4$) (**1**^{La}) with 1, and 3 equiv. TIBA in C_6D_6, and **1**^{La} for comparison.

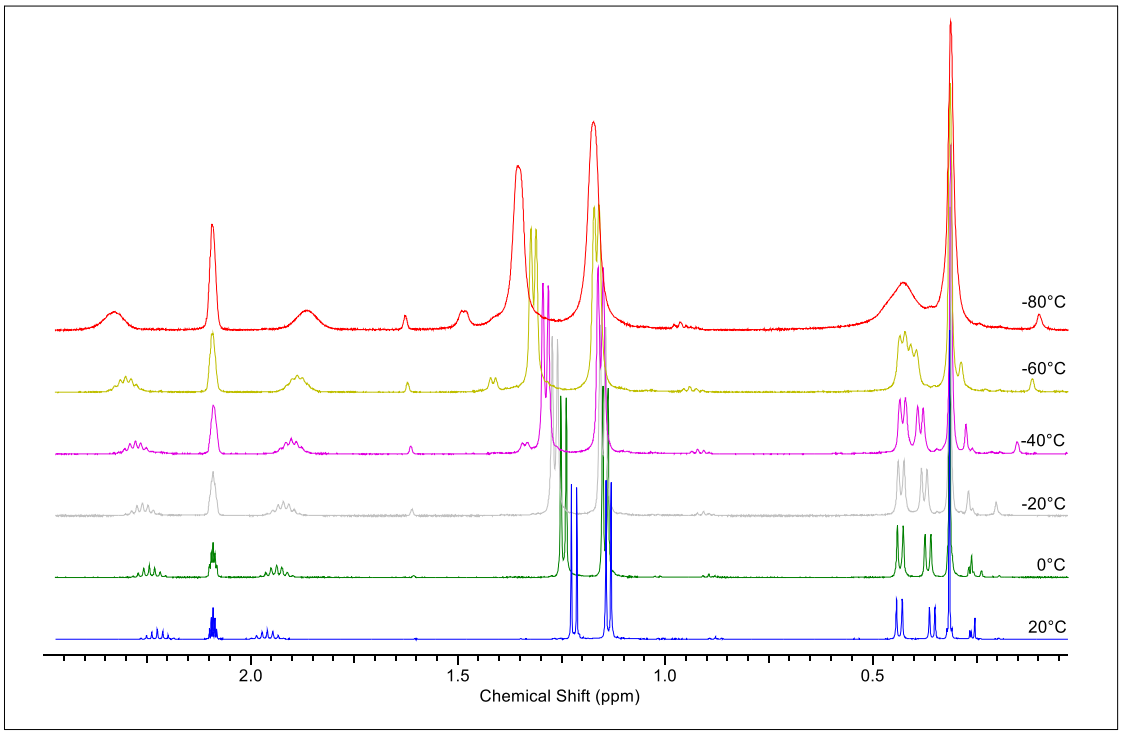

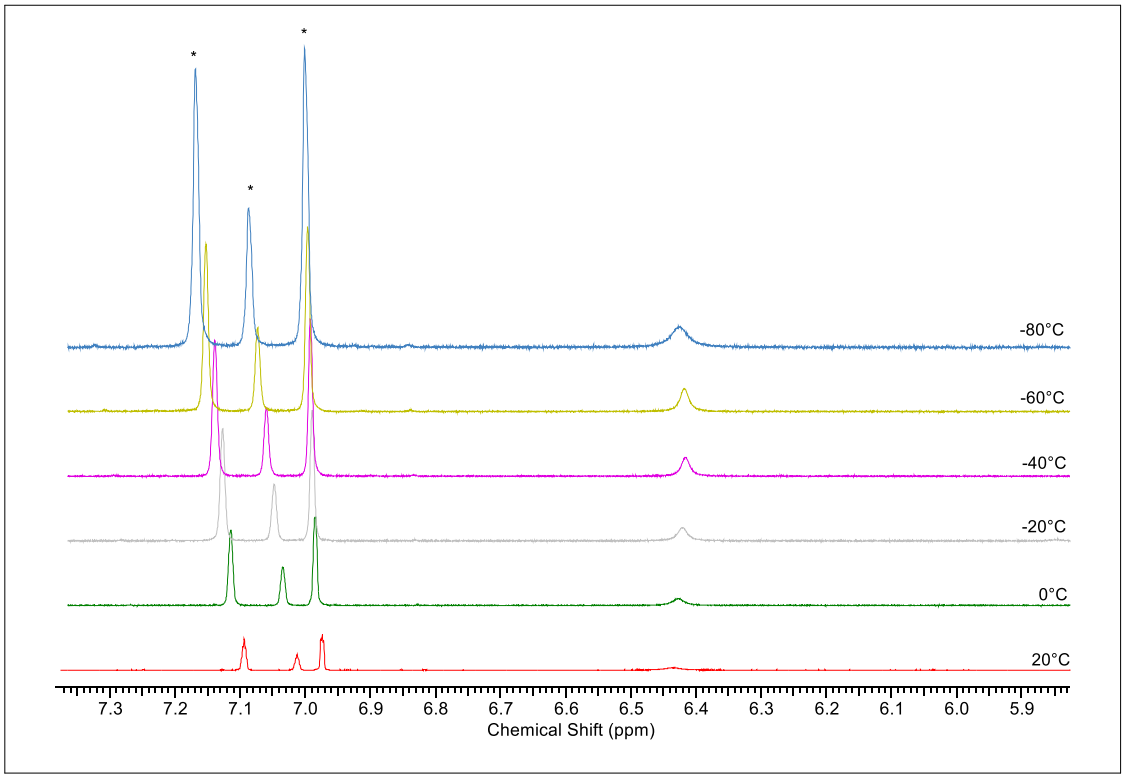

Figure S7. Variable temperature ^{1}H-NMR spectra (500 MHz, toluene-d_8) of La[N(SiMe$_3$)$_2$](HAl*i*Bu$_3$)(Al*i*Bu$_4$) (**1^{La}**).

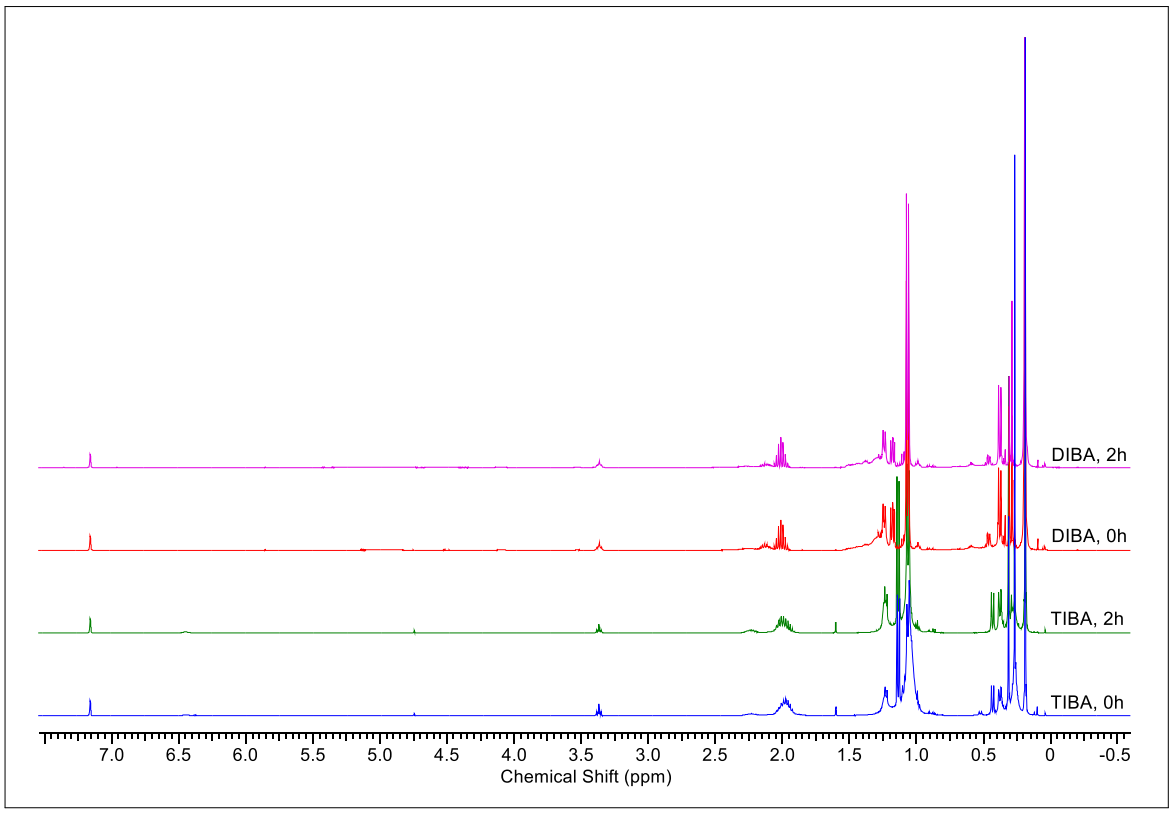

Figure S8. ^{1}H-NMR spectrum (400 MHz, C_6D_6, 26 °C) of the reaction of $La[N(SiMe_3)_2]_3$ with 4 equiv. of TIBA, or DIBAH.

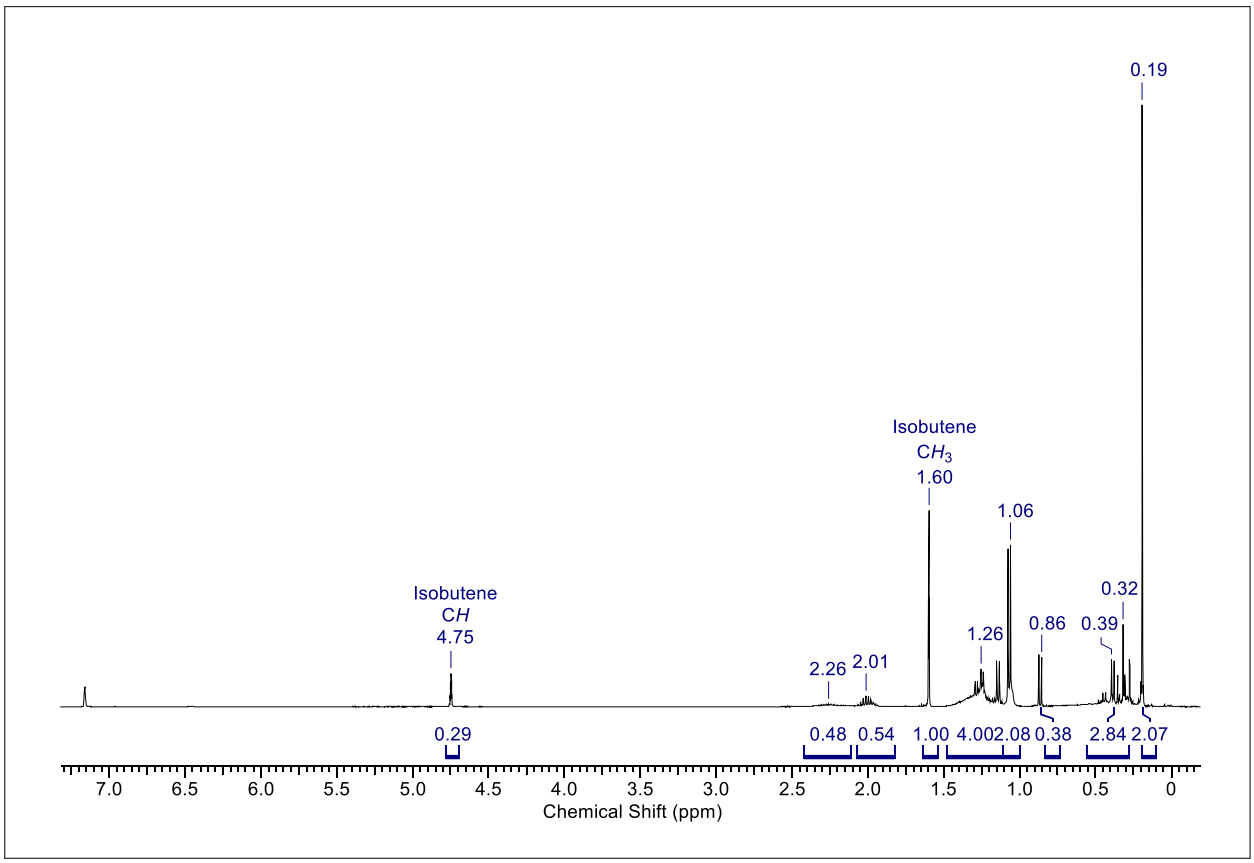

Figure S9. ^{1}H-NMR spectrum (400 MHz, C_6D_6, 26 °C) of La[N(SiMe$_3$)$_2$](HAl*i*Bu$_3$)(Al*i*Bu$_4$) (**1^{La}**) after heating for 1 h at 70°C.

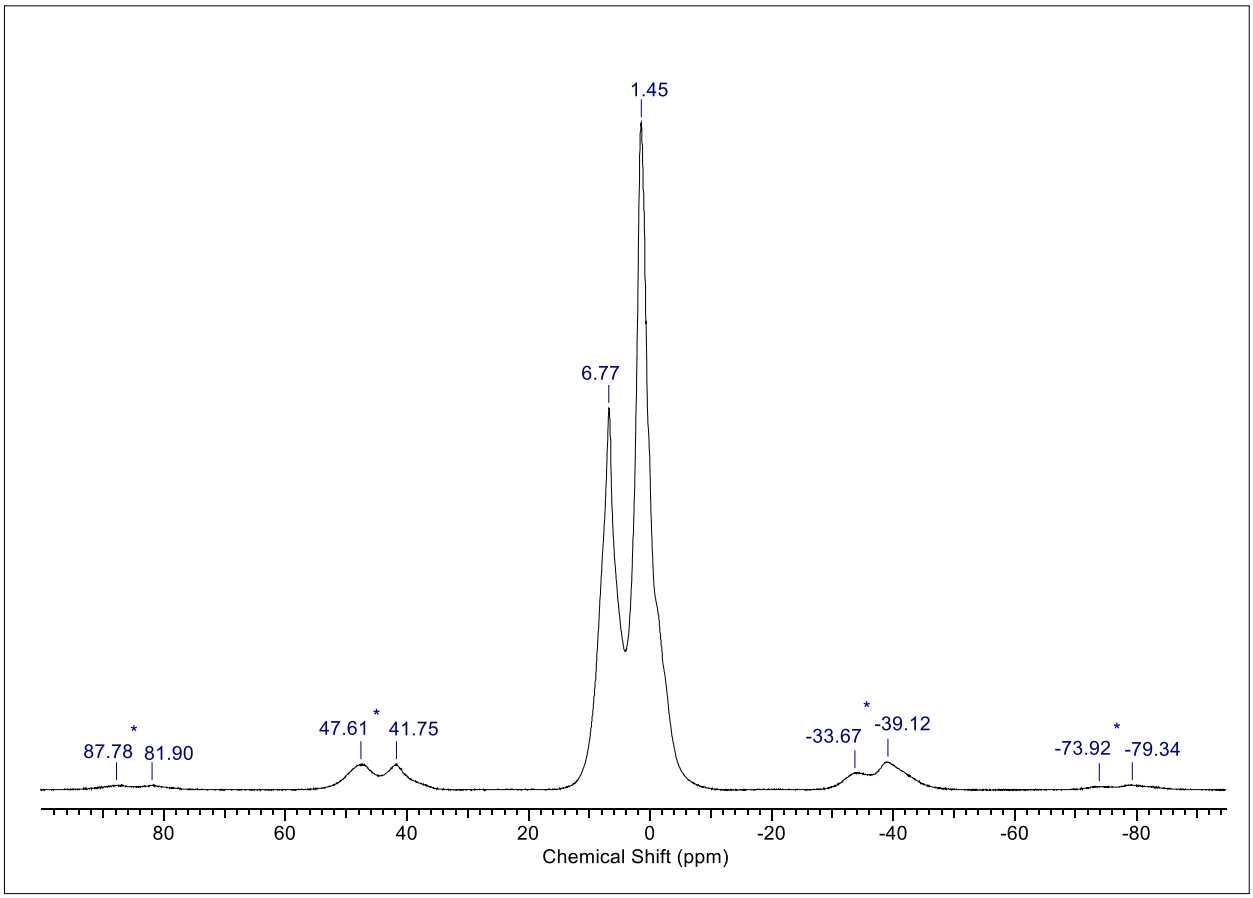

Figure S10. ^{1}H-MAS NMR spectrum (500 MHz, 26 °C) of (μ-fluorenyl)$_3$La$_2$(μ-H)(HAl*i*Bu$_3$)$_2$ (**3**) and (fluorenyl)$_2$La[N(SiMe$_3$)$_2$] (**4**) including spinning sidebands (*).

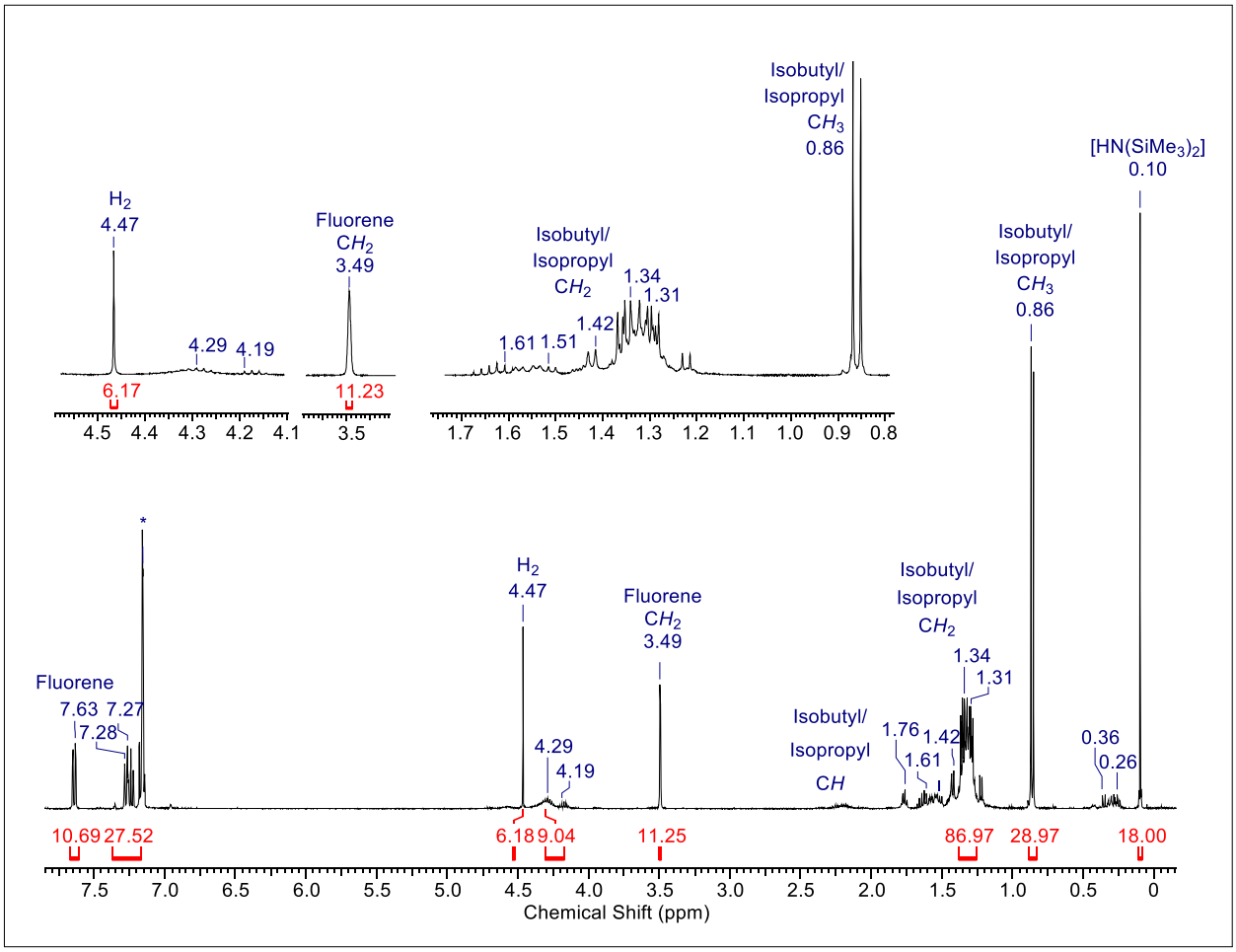

Figure S11. ^{1}H NMR spectrum (400 MHz, C_6D_6, 26 °C) of the reaction of (μ-fluorenyl)$_3$La$_2$(μ-H)(HAl*i*Bu$_3$)$_2$ (**3**) and (fluorenyl)$_2$La[N(SiMe$_3$)$_2$] (**4**) with 20 equiv. isopropanol in C_6D_6 showing the formation of hydrogen (4.47 ppm).

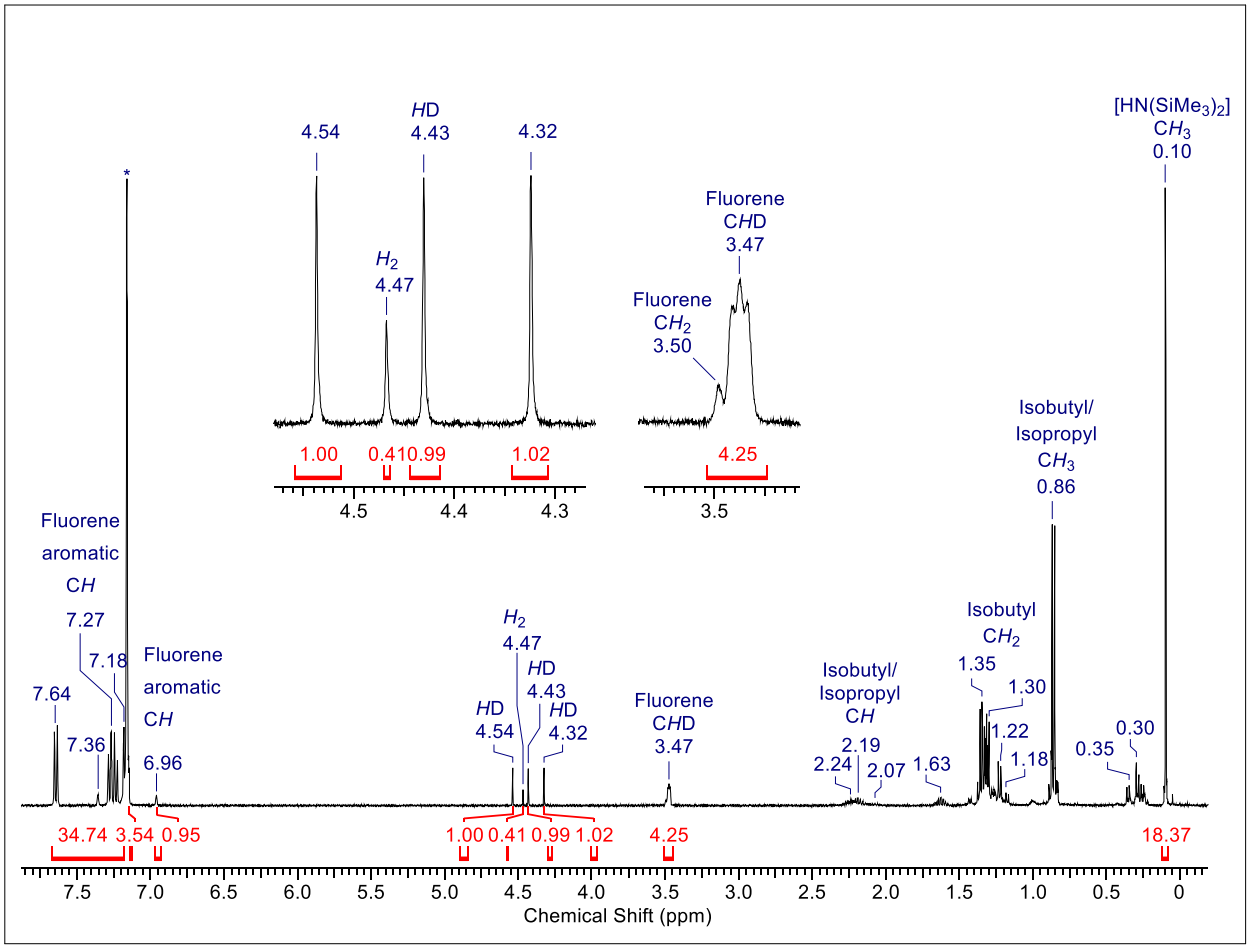

Figure S12. ^{1}H NMR spectrum (400 MHz, C_6D_6, 26 °C) of the reaction of (μ-fluorenyl)$_3$La$_2$(μ-H)(HAl*i*Bu$_3$)$_2$ (**3**) and (fluorenyl)$_2$La[N(SiMe$_3$)$_2$] (**4**) with 20 equiv. isopropanol-d_8 in C_6D_6, showing the formation of HD-gas (nonbinomial triplett; 4.43 ppm), and dihydrogen (singulett; 4.47 ppm).

Crystallography

Crystal Structure Determination and Crystallographic Data

Single crystals suitable for X-ray diffraction were selected in a glovebox, coated with Parabar 10312 (Hampton Research), and fixed on a nylon/loop glass fiber. X-ray data for all compounds were collected on a Bruker APEX II DUO diffractometer equipped with an IμS microfocus sealed tube and QUAZAR optics for MoK_α (λ = 0.71073 Å). The data collection strategy was determined using COSMO,[3] employing ω-scans. Raw data were processed using APEX[4], and SAINT[5]. Corrections for absorption effects were applied using SADABS.[6] The structures were solved by direct methods and refined against all data by full-matrix least-squares methods on F^2 using SHELXTL[7], and ShelXle.[8] All structures except **2** showed disorder. Compound **1-Pr** is not a single crystal, but it was not possible to refine the date as a twin or 'Drilling'. For compound **3**/**4** disorder was calculated using DSR, a program for refining structures in ShelXl.[9] For compound **3/4** a global restraint (RIGU/SIMU) was applied to all atoms to achieve a more chemically reasonable model, furthermore twinning was found. All graphics were produced employing Mercury 4.2.011[10] and POV-Ray12.[11]

For X-ray crystallography, single-crystalline of $\mathbf{1^{La}}$ and $\mathbf{1^{Pr}}$ were grown from saturated solutions in *n*-pentane at –40 °C, and of $\mathbf{1^{Nd}}$ from *n*-hexane at –40 °C. Single crystals of **2** suitable for X-ray crystallography were grown from *o*-difluorobenzene at –40 °C. (μ-fluorenyl)$_3$La$_2$(μ-H)(HAl*i*Bu$_3$)$_2$ (**3**) and (fluorenyl)$_2$La[N(SiMe$_3$)$_2$] (**4**) were crystallized from benzene at ambient temperature.

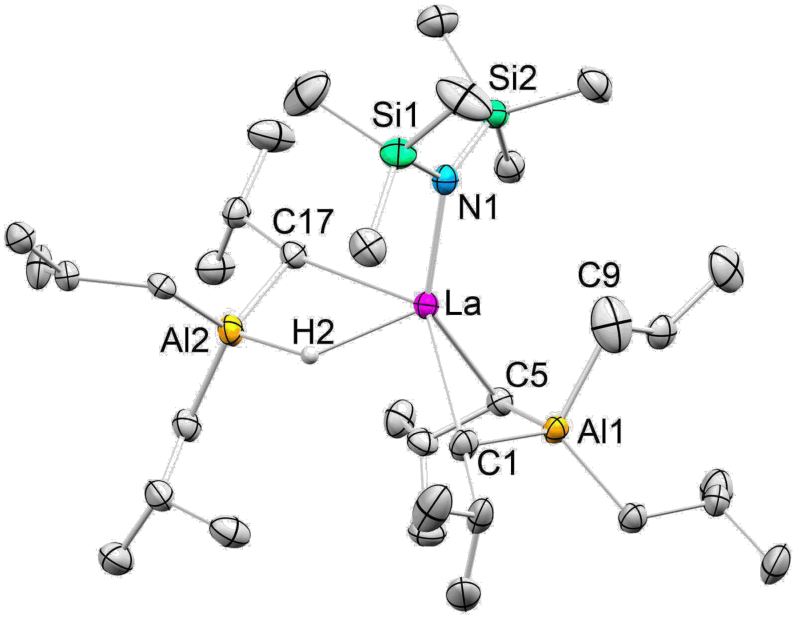

Figure S13. Crystal structure of 1^{La}. Hydrogen atoms except the bridging hydride are omitted for clarity. Atomic displacement ellipsoids were set at 50% probability. Selected interatomic distances [Å] and angles [°]: La(1)–C(1) 2.782(4), La(1)–C(5) 2.755(4), La(1)–C(9) 3.155(1), La(1)–C(17) 2.823(4), La(1)···Si(1) 3.432(1), La(1)···Si(2) 3.428(1), Al(1)–C(1) 2.078(4), Al(1)–C(5) 2.096(4), Al(1)–C(9) 2.024(4), Al(2)–C(17) 2.058(4), Al(2)–H(1) 1.66(3), La(1)–N(1) 2.276(3), La(1)···Al(1) 3.0243(1), La(1)···Al(2) 3.330(1), La(1)–H(1) 2.22(3), La(1)-Al(1)-C(1) 62.9(1), La(1)-Al(1)-C(5) 162.0(1), La(1)-Al(1)-C(9) 74.4(1), La(1)-Al(1)- C(9) 74.4(1), Al(2)-C(17)-La(1) 84.5(1), C(17)-Al(2)-La(1) 57.5(1), La(1)-Al(2)-H(1) 36.2(10), N(1)-La(1)-C(1) 126.12(11), N(1)-La(1)-C(5) 135.56(10), N(1)-La(1)-C(17) 90.75(10), C(1)-La(1)-Al(1) 41.69(8), C(5)-La(1)-Al(1) 42.20(8), C(17)-La(1)-Al(1) 140.79(8), N(1)-La(1)-Al(1) 123.02(7), N(1)-La(1)-Al(2) 106.69(7), N(1)-La(1)-H(1) 112.4(8), C(1)-La(1)-H(1) 75.4(8), C(5)-La(1)-H(1) 111.1(8), C(17)-La(1)-H(1) 64.1(8), La(1)-N(1)-Si(1) 117.64(14), La(1)-N(1)-Si(2) 117.27(15), Si(1)-N(1)-Si(2) 124.48(17).

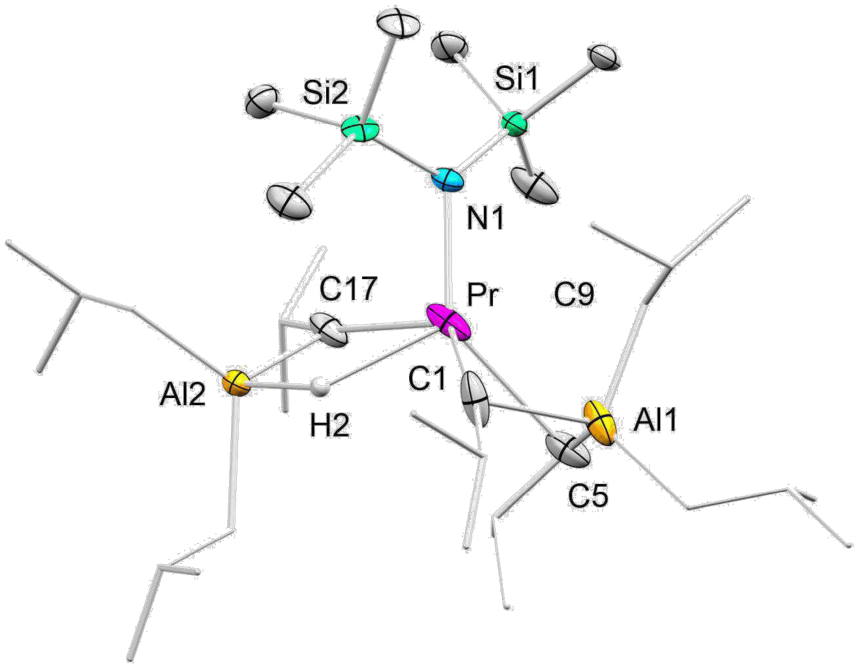

Figure S14. Crystal structure of **1**^{Pr}. Hydrogen atoms except the bridging hydride are omitted for clarity. Atomic displacement ellipsoids were set at 50% probability. Selected interatomic distances [Å] and angles [°]: Pr(1)–C(1) 2.565(8), Pr(1)–C(5) 2.715(4), Pr(1)–C(9) 3.2499(5), Pr(1)–C(17) 2.808(4), Pr(1)···Si(1) 3.434(3), Pr(1)···Si(2) 3.634(2), Al(1)–C(1) 2.173(8), Al(1)–C(5) 2.102(3), Al(1)–C(9) 2.158(13), Al(2)–C(17) 2.105(5), Al(2)–H(2C) 1.55(5), Pr(1)–N(1) 2.356(9), Pr(1)–N(1A) 2.136(8), Pr(1)···Al(1) 2.9944(12), Pr(1)···Al(2) 3.182(4), Pr(1)–H(1) 2.22(5), C(1)-Al(1)-Pr(1) 56.9(2), C(5)-Al(1)-Pr(1) 61.5(1), C(9)-Al(1)-Pr(1) 71.1(3), Al(2)-C(17)-Pr(1) 79.3(1), C(17)-Al(2)-Pr(1) 60.1(1), Pr(1)-Al(2)-H(2C) 39(2), N(1)-Pr(1)-C(1) 111.0(3), N(1)-Pr(1)-C(5) 146.1(2), N(1)-Pr(1)-C(17) 90.6(2), N(1)-Pr(1)-Al(1) 125.4(2), C(1)-Pr(1)-Al(1) 45.2(2), C(5)-Pr(1)-Al(1) 42.85(7), C(17)-Pr(1)-Al(1) 141.61(7), N(1)-Pr(1)-Al(1) 125.4(2), N(1)-Pr(1)-Al(2) 103.9(2), N(1)-Pr(1)-H(2C) 104.8(14), C(1)-Pr(1)-H(2C) 74.9(1), C(5)-Pr(1)-H(2C) 109.1(1), C(17)-Pr(1)-H(2C) 66.5(1). Pr(1)-N(1)- Si(1) 113.30 (4), Pr(1)-N(1)-Si(2) 124.81 (4), Si(1)-N(1)-Si(2) 121.73 (5).

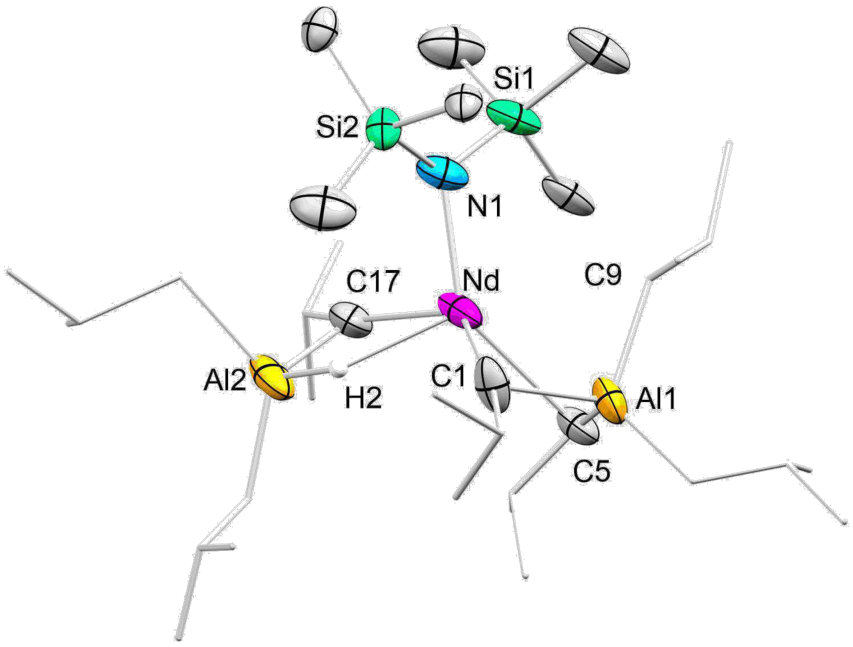

Figure S15. Crystal structure of $\mathbf{1}^{Nd}$. Hydrogen atoms except the bridging hydride are omitted for clarity. Atomic displacement ellipsoids were set at 50% probability. Selected interatomic distances [Å] and angles [°]: Nd(1)–C(1) 2.542(11), Nd(1)–C(5) 2.708(5), Nd(1)–C(9) 3.237(6), Nd(1)–C(17) 2.763(7), Nd(1)···Si(1) 3.277(6), Nd(1)···Si(2) 3.354(5), Al(1)–C(1) 2.101(16), Al(1)–C(5) 2.093(6), Al(1)–C(9) 2.019(6), Al(2)–C(17) 2.054(7), Al(2)–H(2) 1.63(5), Nd(1)–N(1) 2.208(5), Nd(1)···Al(1) 2.999(2), Nd(1)···Al(2) 3.243(2), Nd(1)–H(2) 2.17(5), Nd(1)-Al(1)-C(1) 56.5(3), Nd(1)-Al(1)-C(5) 61.3(2), Nd(1)-Al(1)-C(9) 77.6(2), Nd(1)-C(17)-Al(2) 83.3(2), Nd(1)-Al(2)-C(17) 57.8 (2), Nd(1)-Al(2)-H(2) 37.0(17), N(1)-Nd(1)-C(1) 111.6(5), N(1)-Nd(1)-C(5) 141.6(2), N(1)-Nd(1)-C(17) 94.3(2), N(1)-Nd(1)-Al(1) 120.7(1), C(1)-Nd(1)-Al(1) 43.6(4), C(5)-Nd(1)-Al(1) 42.6(1), C(17)-Nd(1)-Al(1) 141.2(2), N(1)-Nd(1)-Al(1) 120.7(1), N(1)-Nd(1)-Al(2) 103.5(2), N(1)-Nd(1)-H(2) 105.5(14), C(1)-Nd(1)-H(2) 78.6(14), C(1)-Nd(1)-H(2) 78.6(14), C(5)-Nd(1)-H(2) 112.9(13), C(17)-Nd(1)-H(2) 65.8(13). Nd(1)-N(1)-Si(1) 107.37(3), Nd(1)-N(1)-Si(2) 126.44(4), Si(1)-N(1)-Si(2) 125.99(4).

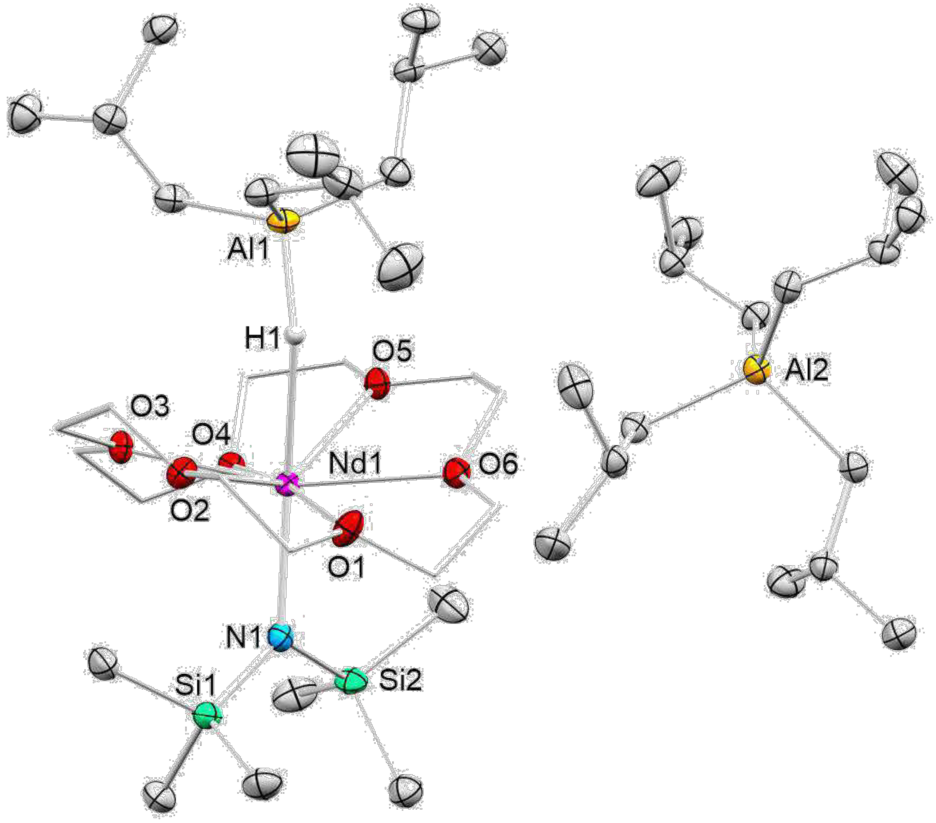

Figure S16. Crystal structure of **2**. Hydrogen atoms except the bridging hydride are omitted for clarity. Atomic displacement ellipsoids were set at 50% probability. Selected interatomic distances [Å] and angles [°]: Nd(1)–N(1) 2.329(2), Nd(1)···Si(1) 3.6329(9), Nd(1)···Si(2) 3.519(1), Nd(1)–O(1) 2.500(2), Nd(1)–O(2) 2.578(2), Nd(1)–O(3) 2.545(2), Nd(1)–O(4) 2.537(2), Nd(1)–O(5) 2.545(2), Nd(1)–O(6) 2.541(2), Nd(1)–H(1) 2.39(3), Al(1)–H(1) 1.70(3), N(1)-Nd(1)-H(1) 170.1(7), Nd(1)-H(1)-Al(1) 157.5(16), Nd(1)-N(1)-Si(1) 126.08(13), Nd(1)-N(1)-Si(2) 119.12(13), Si(1)-N(1)-Si(2) 114.78(14).

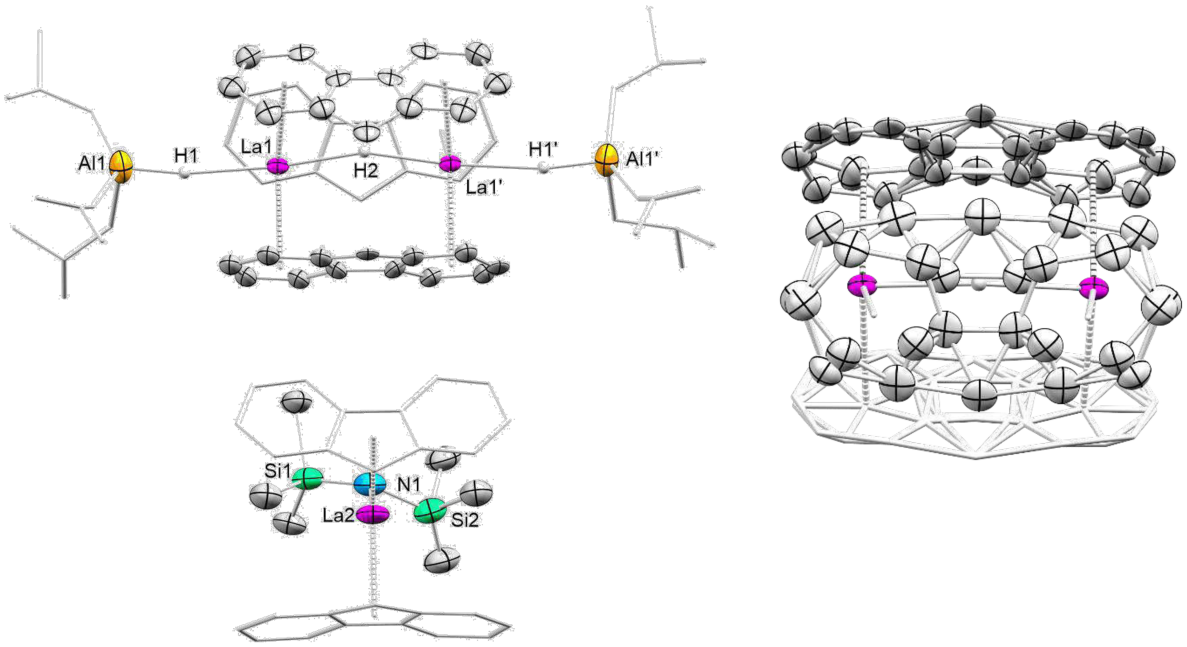

Figure S17. Crystal structure of **3** and **4** (left), core motif of **3** showing disorder of the fluorenyl rings (right). Hydrogen atoms except the bridging hydrides, as well as the disorder in fluorenyl ions are omitted for clarity; isobutyl moieties are displayed as capped sticks. Atomic displacement ellipsoids were set at 50% probability. Selected interatomic distances [Å] and angles [°] for **3**: La(1)–H(1) 2.39(1), La(1)–H(2) 2.29(2), Al(1)–H(1) 1.63(1), La(1)-centroid(1) 2.680, La(1)-centroid(2) 2.634, La(1)-centroid(3) 2.629, range La–C 2.893-3.018, La(1)-H(1)-Al(1) 169.4, H(1)-La(1)-H(2) 166(3). Selected interatomic distances [Å] for **4**: La(1)-N(1) 2.309(2), La(1)-centroid(1) 2.585, La(1)-centroid(2) 2.623.

Table S1. Crystallographic data for compounds $\mathbf{1}^{La}$, $\mathbf{1}^{Pr}$ and $\mathbf{1}^{Nd}$

	$\mathbf{1}^{La}$	$\mathbf{1}^{Pr}$	$\mathbf{1}^{Nd}$
formula	$C_{34}H_{82}Al_2LaNSi_2$	$C_{34}H_{82}Al_2NPrSi_2$	$C_{34}H_{82}Al_2NNdSi_2$
CCDC	2249268	2249269	2249266
M [g mol^{-1}]	754.05	756.05	759.38
color/shape	colourless/column	colourless/block	turquoise/needle
crystal dimensions [mm]	0.235 x 0.100 x 0.081	0.187 x 0.150 x 0.143	0.182 x 0.070 x 0.041
cryst. system	triclinic	triclinic	triclinic
space group	$P\bar{1}$	$P\bar{1}$	$P\bar{1}$
a [Å]	9.304(1)	9.309(1)	9.339 (1)
b [Å]	11.606(1)	11.525(2)	11.492(2)
c [Å]	21.098(2)	21.018(3)	20.898(3)
α [°]	93.848(2)	94.562(1)	94.846(2)°.
β [°]	102.114(2)	101.615(1)	101.606(2)°.
γ [°]	92.747(2)	92.784(1)°.	92.456(2)°.
V [Å^3]	2218.0(4)	2196.9(6)	2184.8(6)
Z	2	2	2
T [K]	100(2)	100(2)	100(2)
wavelength [Å]	0.71073	0.71073	0.71073
ρ_{calcd} [Mg m^{-3}]	1.129	1.143	1.154
μ [mm^{-1}]	1.077	1.224	1.304
F (000)	808	812	814
θ range [°]	2.089/27.138	1.776/30.640	2.124/24.806
unique reflns	9764	13495	7459
observed reflns	92155	126853	57683
R1[b]/wR2 (I>2σ)[c]	0.0420/0.0841	0.0456/0.1024	0.0558/0.1212
R1[b]/wR2 (all data)[c]	0.0645/0.0943	0.0609/0.1167	0.0817/0.1359
GOF[a]	1.036	1.131	1.040

[a]GOF = $[\Sigma w(F_0^2 - F_c^2)^2 / (n_0 - n_p)]^{1/2}$. [b]$R_1 = \Sigma(||F_0| - |F_c||) / \Sigma|F_0|$, $F_0 > 4\sigma(F_0)$. [c]$wR_2 = \{\Sigma[w(F_0^2 - F_c^2)^2 / \Sigma[w(F_0^2)^2]\}^{1/2}$.

Table S2. Crystallographic data for compounds **2**, and **3/4**

	2	**3/4**
formula	$C_{46}H_{106}Al_2NNdO_6Si_2$	$C_{95}H_{120}Al_2La_3NSi_2$
CCDC	2249267	2249265
M [g mol^{-1}]	1023.69	1802.78
color/shape	colourless/needle	orange/plate
crystal dimensions [mm]	0.187 x 0.097 x 0.051 mm3	0.079 x 0.068 x 0.048
cryst. system	monoclinic	monoclinic
space group	$P2_1/c$	$P2_1/m$
a [Å]	14.134(2)	9.0290(7)
b [Å]	15.570(2)	28.770(2)
c [Å]	26.282(3)	16.089(1)
α [°]	90	90
β [°]	91.616(2)°.	89.983(2)
γ [°]	90	90
V [Å^3]	5781(1)	4179.2(6)
Z	4	2
T [K]	100(2)	100(2)
wavelength [Å]	0.71073	0.71073
ρ_{calcd} [Mg m^{-3}]	1.176	1.433
μ [mm^{-1}]	1.009	1.601
F (000)	2204	1844
θ range [°]	1.441/28.342	1.266/26.390
unique reflns	14361	8677
observed reflns	90248	36003
R1[b]/wR2 (I>2σ)[c]	0.0395/0.0806	0.0738/0.1838
R1[b]/wR2 (all data)[c]	0.0633/0.0916	0.1027/0.2022
GOF[a]	1.020	1.035

[a]GOF = $[\Sigma w(F_0^2 - F_c^2)^2 / (n_0 - n_p)]^{1/2}$. [b]$R_1 = \Sigma(||F_0| - |F_c||) / \Sigma|F_0|$, $F_0 > 4\sigma(F_0)$. [c]$wR_2 = \{\Sigma[w(F_0^2 - F_c^2)^2 / \Sigma[w(F_0^2)^2]\}^{1/2}$.

References

[1] D. C. Bradley, J. S. Ghotra and F. A. Hart, *J. Chem. Soc., Dalton Trans.* 1973, 1021-1023.

[2] A. C. Fecker, M. Freytag, P. G. Jones and M. D. Walter, *Dalton Trans.* 2019, **48**, 8297-8302.

[3] COSMO v. 1.61, Bruker AXS Inc., Madison, WI, 2012.

[4] APEX3 V. 2019.11-0, Bruker AXS Inc., Madison, WI, 2019.

[5] SAINT V. 8.40B, Bruker Nano, Inc., 2019.

[6] L. Krause, R. Herbst-Irmer, G. M. Sheldrick and D. Stalke, *J. Appl. Crystallogr*. 2015, **48**, 3-10.

[7] G. Sheldrick, *Acta Crystallogr. Sect. C*. 2015, **71**, 3-8.

[8] C. B. Hübschle, G. M. Sheldrick and B. Dittrich, *J. Appl. Crystallogr.* 2011, **44**, 1281-1284.

[9] D. Kratzert, J. J. Holstein and I. Krossing, *J. Appl. Crystallogr.* 2015, **48**, 933-938.

[10] C. F. Macrae, P. R. Edgington, P. McCabe, E. Pidcock, G. P. Shields, R. Taylor, M. Towler and J. van de Streek, *J. Appl. Crystallogr.* 2006, **39**, 453-457.

[11] POV-Ray v.3.6, Persistence of Vision Pty. Ltd., POV-Ray Williamstown, Victoria, Australia. http://www.povray.org, 2004.

Paper III

Discrete Trivalent Lanthanide Isobutylaluminates in Isoprene Polymerization: Elucidation of Cationized Active Species

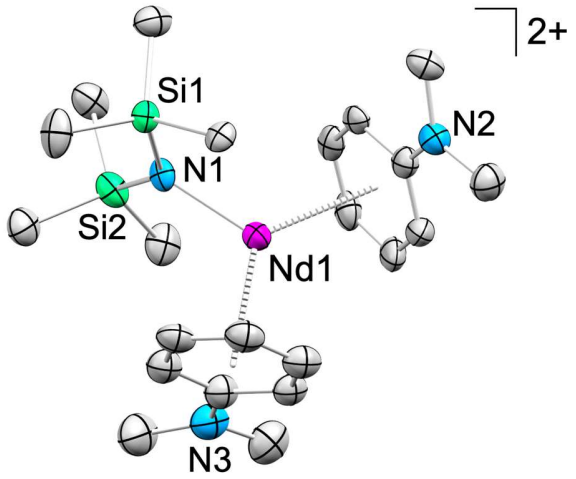

ACS Catalysis

pubs.acs.org/acscatalysis Research Article

Discrete Trivalent Lanthanide Isobutylaluminates in Isoprene Polymerization: Elucidation of Cationized Active Species

Eric C. Moinet, Olivier Tardif, Lea-Sophie Hornberger, Friederike Adams, Cäcilia Maichle-Mössmer, and Reiner Anwander*

Cite This: *ACS Catal.* 2023, 13, 12826−12834 Read Online

ACCESS | Metrics & More | Article Recommendations | Supporting Information

ABSTRACT: Triisobutylaluminum (TIBA) is a main component applied in industrial Ziegler-type mixed catalysts for conjugated diene polymerization. Despite this importance, discrete crystalline trivalent lanthanide tetraisobutylaluminates have not yet been examined in polymerization. The present study revealed that discrete complexes $Ln[N(SiMe_3)_2](HAliBu_3)(AliBu_4)$ (Ln = La, Pr, Nd, Gd) promote highly stereoselective isoprene polymerization with >99% *cis* selectivity. Mechanistic studies with borate cocatalysts, supported by single crystal X-ray diffraction, and NMR spectroscopy, disclose the formation of dicationic neodymium complex $[Nd\{N(SiMe_3)_2\}(PhNMe_2)_2][B(C_6F_5)_4]_2$ from the binary system $Nd[N(SiMe_3)_2](HAliBu_3)(AliBu_4)/[PhNMe_2H][B(C_6F_5)_4]$. Complex $[Nd\{N(SiMe_3)_2\}(PhNMe_2)_2][B(C_6F_5)_4]_2$ engages in single-component isoprene polymerization.

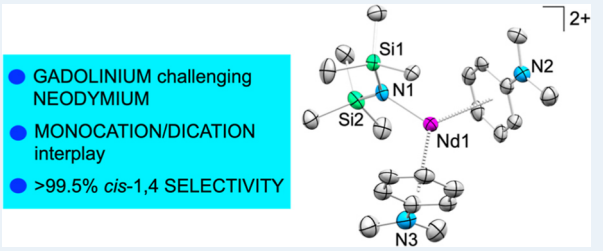

KEYWORDS: *lanthanides, triisobutylaluminum, isoprene, active species formation, X-ray diffraction*

INTRODUCTION

Stereoregular *cis*-1,4 polybutadiene and -isoprene are of high commercial relevance, especially for manufacturing high-performance tire components.[1−4] As such, synthetic polydienes are of growing importance as complement/replacement for natural rubber which faces environmental constraints, and hence limited supply.[5,6] Notwithstanding, natural rubber has remained unrivaled in terms of mechanical properties compared to synthetic polyisoprene.[6,7]

Large-scale fabrication of *cis*-1,4 polydiene rubbers is currently performed with mixed Ziegler-type catalysts. They stand out because of the very high *cis*-1,4 contents (∼98%) and high catalytic activities.[8] The routinely employed neodymium-based catalyst systems comprise a neodymium compound such as versatate $Nd(O_2CC_7H_{15})_3$, an alkylaluminum reagent (e.g., $AliBu_3$, $AliBu_2H$), and a chloride source (e.g., $AlEt_2Cl$).[5,8] For advanced technological product development, the understanding of how catalysts work is a desirable goal, since microstructure, stereoregularity, and tacticity can be controlled by selecting the proper method of polymerization, and catalyst.[1] One of the largest drawbacks in understanding polymerization mechanisms is that commonly used catalysts require additional activation with organoaluminum compound (e.g., dialkylaluminum), or methylaluminoxane (MAO) to achieve catalytic activity.[5] Such multinary systems greatly aggravate the identification of the catalytically active species as well as the elucidation of mechanistic details.[5] Highly active rare-earth-metal (or lanthanide, Ln) species tend to be of low stability, or display mixtures, making identification a very challenging task.[9] Although stereoregular polymers of butadiene and isoprene could be synthesized since the late 1950s,[8] neither the complicated mechanisms of active species formation in complex mixed catalysts nor the mechanisms of polymerization are yet fully understood.[2,10]

However, it is generally accepted that Ln(III)-alkyl, -hydride, or -allyl species are involved, and cationic species, generated by Al → Ln chloride transfer, add to possible candidates for active species.[2] Putative active catalyst species comprise an electron-deficient neodymium center coordinated by a reactive chain via multihapto interactions involving allyl and olefinic moieties.[10−13] To date, only very few active species formed in multinary Ziegler-type catalysts have been structurally authenticated, and initiating species are still ambiguous.[9] Especially, catalytically active species may be composed of higher aggregates.[14−16] The only product characterized in the solid state to our knowledge was obtained by Shan et al. after crystallization for several months from the ternary mixture $Nd(OiPr)_3/AlEt_3/AlEt_2Cl$ (1/10/1.5 ratio).[14] The crystallized polynuclear product $[Al_3Nd_6(\mu_2\text{-}Cl)_6(\mu_3\text{-}Cl)_6(\mu_2\text{-}Et)_9Et_5(OiPr)]_2$ was found to engage in single-component butadiene polymerization.[14] Other single-component catalysts

Received: May 18, 2023
Revised: August 30, 2023
Published: September 18, 2023

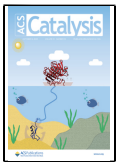

https://doi.org/10.1021/acscatal.3c02247
ACS Catal. 2023, 13, 12826−12834

include LnI_2 (Ln = Nd, Sm, Dy, Tm) or $LnI_2(thf)_x$ (Ln = Sm, Tm),[17] neutral or cationic allyl complexes,[18−22] cationic mixed aluminate/borate compounds previously reported by our group,[23−25] and the recently discovered divalent lanthanide aluminates $Ln(AliBu_4)_2$ (Ln = Sm, Eu, Yb).[26]

Ternary $Nd[N(SiMe_3)_2]_3/AliBu_3/AlEt_2Cl$ mixtures have been successfully examined for butadiene polymerization, affording polymers with high *cis*-1,4 contents.[27,28] The catalytic activity of $Nd[N(SiMe_3)_2]_3/AliBu_3/AlEt_2Cl$ systems generally excel those of carboxylate-based ones or are at least comparable.[27,29] It was stated that they do exhibit a higher activity than the system established by Kaita et al. consisting of $Nd[O_2CCCl_3]_3/AliBu_3/AlEt_2Cl$.[29] In contrast to industrially applied carboxylate components, homoleptic $Ln[N(SiMe_3)_2]_3$ are monomeric in aliphatic solvents and thus are ideally suited for studying precatalyst/cocatalyst interactions. Note that both amido/alkyl and carboxylato/alkyl exchange proceed effectively in the presence of organoaluminum reagents.[4] Monteil et al. also focused on $Nd[N(SiMe_3)_2]_3$ as a catalyst precursor.[28] Combined with MAO, or with $AliBu_3$, and the boron compounds $[CPh_3][B(C_6F_5)_4]$ (**A**), or $[C_6H_5NMe_2H][B(C_6F_5)_4]$ (**B**), or $B(C_6F_5)_3$ (**C**), the neodymium amide/cocatalyst mixtures were applied for the homopolymerization of butadiene, and the copolymerization of butadiene with styrene. This study also included compound $[Nd\{N(SiMe_3)_2\}_2(THF)_2][B(C_6F_5)_4]$ which was identified in the reaction of $Nd[N(SiMe_3)_2]_3$ with $[HNMe_2Ph][B(C_6F_5)_4]$,[28] while a cationic neodymium amide complex activated with AlR_3 was postulated as the active species. However, solid-state structures were not reported.

Moreover, Bochman et al. grafted rare-earth-metal bis(trimethylsilyl)amides (Ln = Sc, Y, La, Nd, Sm, Gd, Dy) onto silica and showed that the resulting hybrid species polymerize ethylene and 1,3-butadiene upon activation with TIBA.[30] Gauvin et al. applied similar materials TIBA@$Nd[N(SiMe_3)_2]_3$@silica (Ln = Y, La, Nd, Sm) as catalysts for the polymerization of methyl methacrylate, ethylene, ε-caprolactone, and isoprene.[31] A recent theoretical study examined the immobilization of $La[N(SiMe_3)_2]_3$ on graphene system and the catalytic activity of methylated species in ethylene and 1,3-butadiene polymerization.[32]

RESULTS AND DISCUSSION

Tetraisobutylaluminate Precursors. Complexes of the type $Ln[N(SiMe_3)_2](HAliBu_3)(AliBu_4)$ (Ln = La, Pr, Nd) ($\mathbf{1}^{Ln}$) recently reported by our group display the first examples of ancillary ligand-free, trivalent lanthanide isobutylaluminates.[33] Such discrete complexes feature a more intricate, but also a more realistic model system for isoprene polymerization catalysts than the frequently utilized lanthanide tetramethylaluminates, since commercially relevant mixed catalysts comprise "higher" organoaluminum compounds, such as diethylaluminum chloride, triethyl- or triisobutylaluminum (TIBA), as well as diisobutylaluminum hydride or -chloride. Early lanthanide metals were chosen due to their superior performance in industrial *cis*-1,4-selective diene polymerization catalysts. Crucially, all attempts to crystallize products from $Ln[N(SiMe_3)_2]_3/AliBu_3$ mixtures derived from lanthanides smaller than gadolinium were not successful. Luckily, single-crystalline $Gd[N(SiMe_3)_2](HAliBu_3)(AliBu_4)$ ($\mathbf{1}^{Gd}$) could be obtained (Figure 1), albeit in lower yields than the corresponding isostructural lanthanum, praseodymium, and neodymium congeners, corroborating the preferred formation of compounds $\mathbf{1}^{Ln}$ for the larger early lanthanides.

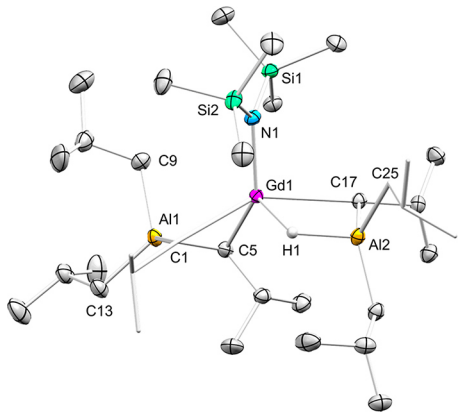

Figure 1. Crystal structure of $\mathbf{1}^{Gd}$. Ellipsoids are shown at the 50% probability level. Hydrogen atoms are omitted for clarity. Selected interatomic distances and angles: Gd(1)−C(1) 2.5793(16), Gd(1)−C(5) 2.6392(16), Gd(1)···C(9) 3.403(2), Gd(1)−C(17) 2.6806(15), Gd(1)−N(1) 2.1867(13), Gd(1)−H(1) 2.077(18).

Isoprene Polymerization in Toluene. Surprisingly, $\mathbf{1}^{Nd}$ exhibits a low polymerization activity already in the absence of any cocatalyst (Table 1, entry 1). The relatively high *trans* content of the polymer obtained is remarkable. Works by Taube et al. show that tris(allyl)neodymium(III) is a single-component catalyst for the *trans*-selective polymerization of butadiene (*trans* content 78−85%).[34] This might indicate that $\mathbf{1}^{Nd}$ is forming an active allyl species via the addition of the hydrido or alkyl group to the isoprene monomer. Similarly, allyl species are assumed intermediates throughout the catalyst activation process.[35] On the other hand, neodymium hydride complexes are discussed as possible initiators for ethylene-butadiene copolymerization,[36] while Lv and Cui propose the formation of a cationic hydrido-bridged lanthanide isobutylaluminate as the active species in the highly *cis*-1,4-selective polymerization of isoprene.[37]

In contrast to the low polymerization activity of non-activated $Nd[N(SiMe_3)_2](HAliBu_3)(AliBu_4)$ ($\mathbf{1}^{Nd}$), it forms species very active in isoprene polymerization, when a toluene solution is treated with equimolar amounts of borate cocatalysts $[CPh_3][B(C_6F_5)_4]$ (**A**), $[PhNMe_2H][B(C_6F_5)_4]$ (**B**), or $B(C_6F_5)_3$ (**C**). Quantitative polymer yields have been detected after 1 h (Table 1, entries 2−7). Interestingly, such binary mixtures feature generally higher *cis* selectivity in isoprene polymerization than the respective ones derived from homoleptic tetramethylaluminates $Nd(AlMe_4)_3$ (maximum *cis* content 44.3 (**A**), 46.8 (**B**), 68.0 (**C**)).[38] It is also notable that $Nd(AlMe_4)_3$/borate systems give lower yields (76−89%) under the same reaction conditions.[38] Interestingly, Martins et al. reported on a similar mixed catalyst system for isoprene polymerization, comprising $Nd[N(SiMe_3)_2]_3$/borate cocatalyst/10 TIBA at 50 °C (borate = **A**, **B**, or **C**).[39] However, also these systems gave lower yields after 24 h (**A** 62%, **B** 23%, **C** 89%).[39] Like $Nd(AlMe_4)_3$, isobutylaluminate $\mathbf{1}^{Nd}$, when activated with cocatalysts **D** (Me_2AlCl) or **E** (Et_2AlCl) fabricates polymers with high *cis*-microstructure (*cis* content >94.6%).[38] The $\mathbf{1}^{Nd}$/**1D** and $\mathbf{1}^{Nd}$/**1E** binary catalysts (Table 1, entries 8−9, and 10−12) generally yielded less polymer (74/81% after 24 h) than $Nd(AlMe_4)_3$ under the same conditions (40/57% after 1 h).[38] However, the corresponding PDIs of 3.71−3.74/3.20 are smaller compared to those obtained with

https://doi.org/10.1021/acscatal.3c02247
ACS Catal. 2023, 13, 12826−12834

Table 1. Isoprene Homopolymerization with Complexes 1^{Ln} (Ln = La, Nd, Pr, Gd) and 2^{Nd}

entry[a]	precatalyst	cocatalyst[b]	reaction time [h]	solvent	yield [%]	*cis*-1,4[c] [%]	*trans*-1,4[c] [%]	3,4[c] [%]	M_n[d] [10^4 g·mol^{-1}]	PDI[d]	T_G[e] [°C]
1	1^{Nd}	none	72	toluene	2	18.4	74.9	6.7	n.d.	n.d.	n.d.
2	1^{Nd}	1A	1	toluene	>99	86.1	5.9	8.0	6.3	1.49	−62
3[h]	1^{Nd}	1B	10 min	toluene	>99	82.1	9.2	8.7	4.0	1.64	n.d.
4[f,h]	1^{Nd}	1B	10 min	toluene	>99	70.4	21.6	8.0	2.7	1.44	n.d.
5	1^{Nd}	1B	1	toluene	>99	71.7	21.0	7.3	5.4	1.28	−62
6[f,h]	1^{Nd}	1B	1	toluene	>99	77.3	14.2	8.5	4.8	1.45	n.d.
7	1^{Nd}	1C	1	toluene	>99	92.7	2.6	4.7	8.8	3.48	−65
8[h]	1^{Nd}	1D	1	toluene	65	96.1	1.2	2.7	5.6	3.71	n.d.
9	1^{Nd}	1D	24	toluene	74	94.6	3.4	2.0	5.4	3.74	−65
10	1^{Nd}	1E	10 min	toluene	1	97.6		2.4	n.d.	n.d.	n.d.
11[h]	1^{Nd}	1E	1	toluene	84	97.7		2.3	n.d.	n.d.	n.d.
12	1^{Nd}	1E	24	toluene	81	96.0	1.9	2.1	5.6	3.20	−64
13[g]	1^{Nd}	2E	1	toluene	96	97.6		2.4	3.4	6.04	−64
14[g]	1^{Nd}	2E	10 min	toluene	25	97.7		2.3	4.4	5.63	−64
15	1^{Nd}	3E	30 min	toluene	34	96.4	0.9	2.7	1.8	3.66	−64
16	1^{Nd}	4E	24	toluene	<1	95.2		4.8	n.d.	n.d.	n.d.
17	1^{Nd}	1A	1	*n*-hexane	88	55.8	38.2	6.0	3.7	1.70	−64
18	1^{Nd}	1B	1	*n*-hexane	78	30.5	60.8	8.7	2.5	1.81	−65
19	1^{Nd}	1C	1	*n*-hexane	94	90.7	5.1	4.2	9.2	2.30	−64
20[g]	1^{Nd}	1D	1	*n*-hexane	17	97.3		2.7	5.1	8.31	−65
21[g,h]	1^{Nd}	1D	24	*n*-hexane	86	95.7	1.3	3.0	3.7	9.62	n.d.
22[g]	1^{Nd}	1E	1	*n*-hexane	10	97.0		3.0	3.2	9.54	−65
23	1^{Nd}	1E	24	*n*-hexane	>99	96.5	0.8	2.7	n.d.	n.d.	n.d.
24[g]	1^{Nd}	2E	10 min	*n*-hexane	93	97.0		3.0	4.7	4.27	−64
25	1^{Nd}	2E	1	*n*-hexane	>99	97.1		2.9	n.d.	n.d.	n.d.
26[g]	1^{Nd}	3E	10 min	*n*-hexane	87	97.1		2.9	7.1	6.48	−65
27[g,h]	1^{Nd}	3E	1	*n*-hexane	>99	97.4		2.6	3.4	8.09	n.d.
28[g]	1^{Nd}	1F	1	*n*-hexane	16	97.6		2.4	3.4	7.99	−64
29[g]	1^{La}	1F	2	toluene	5	92.6	3.9	3.5	1.1	4.00	−64
30[g]	1^{La}	2F	1	toluene	18	96.8		3.2	1.6	8.39	−63
31[g]	1^{Pr}	1F	1	toluene	7	97.4		2.6	1.6	5.88	−64
32[g]	1^{Pr}	2F	1	toluene	58	97.3		2.7	3.3	5.52	−63
33[g]	1^{Nd}	1F	1	toluene	22	97.7		2.3	2.0	4.68	−64
34[g]	1^{Nd}	2F	10 min	toluene	54	98.1		1.9	2.5	4.50	−63
35[g]	1^{Nd}	2F	30 min	toluene	>99	97.6		2.4	5.2	3.35	−63
36	1^{Nd}	3F	2	toluene	28	95.5	1.9	2.6	2.0	2.69	−64
37[g]	1^{Gd}	1F	1	toluene	32	>99.5			5.4	3.55	−63
38[g]	1^{Gd}	2F	30 min	toluene	89	>99.5			5.2	4.30	−63
39	2^{Nd}	none	10 min	1,2-difluoro-benzene	44	84.7		15.3	34.1	1.27	−58
40[h]	2^{Nd}	none	30 min	1,2-difluoro-benzene	>99	85.2		14.8	71.2	1.74	n.d.
41	2^{Nd}	none	30 min	toluene	17	82.2		17.8	46.9	1.12	−58
42	2^{Nd}	2 TIBA	30 min	toluene	23	84.6		15.4	14.9	1.49	−57
43[h]	$2^{Nd}/1^{Nd}$	none	10 min	toluene	>99	57.3	36.2	6.5	4.6	1.37	n.d.
44[f]	$2^{Nd}/1^{Nd}$	none	10 min	toluene	>99	69.4	23.3	7.3	2.1	1.16	−64
45	1^{Nd}	2B	10 min	toluene	>99	83.4	8.1	8.5	3.1	1.34	−63
46[g]	1^{Nd}	2B	<1 min	1,2-difluoro-benzene	>99	92.4		7.6	12.7	2.00	−61
47	none	B	24	toluene	none						

[a]Conditions: 20 μmol of precatalyst, 20 μmol of cocatalyst, 20 mmol of isoprene, 8 mL of solvent, 500 rpm stirring velocity. [b]Aged with cocatalyst at ambient temperature for 30 min: **A** = $[Ph_3C][B(C_6F_5)_4]$; **B** = $[PhNMe_2H][B(C_6F_5)_4]$; **C** = $B(C_6F_5)_3$; **D** = Me_2AlCl, **E** = Et_2AlCl, **F** = iBu_2AlCl, 1, 2, 3, or 4 equivalents. [c]Determined by $^1H/^{13}C$ NMR spectroscopy in $CDCl_3$. [d]Determined by SEC. [e]Determined by DSC. n.d. not determined. [f]0.04 mmol Nd in total. [g]pronounced bi- or multimodal molecular weight distribution detected. [h]Measured on a different GPC device.

$Nd(AlMe_4)_3$ (6.77/4.52). We also probed different amounts of diethylaluminum chloride cocatalyst **E** (Table 1, entries 10−16), with two equivalents of **E** affording the most active catalysts. A slightly lower yield was obtained with three equivalents, but still revealing very high activities. In contrast, using 4 equiv. of **E** yielded only 1% of polymer after 24 h, indicating deactivation of the catalyst via the formation of insoluble neodymium chloride species. This is in good accordance with a study by Boisson et al. reporting on a $Nd[N(SiMe_3)_2]_3/AliBu_3/AlEt_2Cl$ mixed catalyst system (e.g., 1/40/2 ratio; 70 °C in *n*-heptane), which achieved the highest monomer conversion at a 2−2.5 Cl/Nd ratio.[27] Overall, the binary catalyst systems under study produced polymers with relatively broad or multimodal molecular weight distributions. This is also observed for the conventional carboxylate-based catalysts. It can be explained by the formation and action of (a)

https://doi.org/10.1021/acscatal.3c02247
ACS Catal. 2023, 13, 12826−12834

mixtures of cationic/dicationic species, (b) distinct active sites at the same rare-earth-metal center, and (c) cluster and colloidal species.[3,4,16,35] Putative major active species of the present study might include monocationic "[Nd(PhNMe$_2$)-{N(SiMe$_3$)$_2$}{RAl*i*Bu$_3$}][B(C$_6$F$_5$)$_4$]" and "[Nd(Al*i*Bu$_4$)-(HAl*i*Bu$_3$)(Cl)]$_x$" (vide infra).

Isoprene Polymerization in *n*-Hexane. The polymerization performance of compound **1**Nd activated with one equivalent cocatalyst was also studied in *n*-hexane as a solvent (*cf.*, Table 1, entries 17−28). Overall, the polymer yield as well as the *cis* selectivity obtained with borate cocatalysts was generally lower than in toluene (Table 1, entries 17−19). However, **1**Nd/**D** and **1**Nd/**E** catalyst mixtures proved to be tentatively more active toward isoprene polymerization in *n*-hexane with similar *cis* selectivity (Table 1, entries 20−23) as found in toluene. This finding is in accordance with the aforementioned study by Boisson et al., who reported a similar behavior for the system Nd[N(SiMe$_3$)$_2$]$_3$/Al*i*Bu$_3$/AlEt$_2$Cl in heptane.[27] This can be explained by competitive coordination of diene and toluene to the active center, slowing down the polymerization rate in toluene compared to weaker coordinating aliphatic solvents.[40] Like in toluene, maximum polymerization activity in *n*-hexane was observed when using **1**Nd combined with two equivalents of **E** (Table 1, entries 24−25). Again, the broad MWD observed with **D** and **E** (*cf.* entries 21 and 22) may be attributed to higher aggregates or clusters formed due to the lower solubility in *n*-hexane.

Isoprene Polymerization with the Binary System Ln[N(SiMe$_3$)$_2$](HAl*i*Bu$_3$)(Al*i*Bu$_4$) (1^{Ln})/*i*Bu$_2$AlCl (F) (Ln = La, Pr, Nd, Gd). As shown before, the activation of **1**Nd with two equivalents diethylaluminum chloride (**E**) generated the most active catalyst system. Similarly, the binary system **1**Nd/*i*Bu$_2$AlCl (**F**) featured maximum activity with a chloride/neodymium ratio of 2:1 (Table 1, entries 34 and 35). To probe the effect of the lanthanide center, compounds Ln[N-(SiMe$_3$)$_2$](HAl*i*Bu$_3$)(Al*i*Bu$_4$) (**1**^{Ln}) (Ln = La, Pr, Nd, Gd) were activated with one or two equivalents of **F** (Table 1, *cf.*, entries 29−38). As observed with **1**Nd, compounds **1**^{La}, **1**^{Pr}, and **1**^{Gd} exhibited higher activities with 2 equiv. **F** compared to 1 equiv. **F**. More importantly, a clear trend was observed for the activity of both **1**^{Ln}/**F** and **1**^{Ln}/2**F**, increasing in the order La < Pr < Nd ≈ Gd. It needs to be noted that the polymer yield obtained with catalyst system **1**^{Gd}/2**F** is slightly lower than with **1**Nd/2**F** (entries 35 and 36). However, this can be ascribed to gel formation observed with **1**^{Gd}/2**F**, that hindered monomer diffusion, limiting overall conversion.

Remarkably, the *cis* selectivity was found to increase in the same order La < Pr < Nd < Gd. Polymers obtained with precatalyst **1**^{Gd} show almost perfect *cis* stereoselectivity (>99%), with no *trans*-linked isoprene resonances detectable by ^{13}C{^{1}H}-NMR spectroscopy (*cf.*, Figure 2). This is in good agreement with studies covering isoprene polymerization activity using lanthanide tetramethylaluminates, where the Gd(AlMe$_4$)$_3$/1**D** system gave *cis* contents as high as 99.9%.[38] Other examples of *cis*-1,4 specific (>99.9%) gadolinium catalysts affording polybutadiene with narrow MWD comprise [(C$_5$Me$_5$)$_2$Gd][B(C$_6$F$_5$)$_4$]/5TIBA (1.41−1.73) and [(Ind)Gd-{N(SiMe$_3$)$_2$}][B(C$_6$F$_5$)$_4$]/2TIBA (1.10−1.47) bearing cyclopentadienyl or indenyl ancillary ligands, respectively.[41,42] The catalyst mixtures **1**Nd/2**F**, and especially **1**^{Gd}/**F** (Table 1, entries 35, and 37−38) were shown to produce relatively high molecular weight *cis*-1,4 polyisoprene.

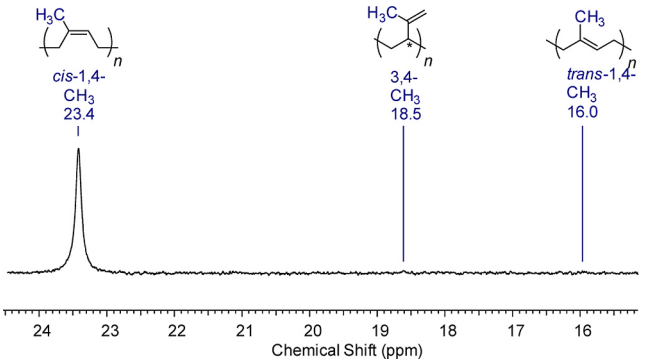

Figure 2. ^{13}C{^{1}H}-NMR spectrum of polyisoprene obtained with catalyst mixture **1**^{Gd}/2**F** (*cf.*, Table 1, entry 29).

It is notable that the polymer obtained with **1**^{Gd}/**F** and **1**^{Gd}/2**F** is very similar whereas the yield is smaller with one equivalent, which may indicate that two chloride ions are necessary to generate the active species (Table 1, entries 37 and 38).

Characterization of the Active Species. The reaction of diamagnetic **1**^{La} with each one equivalent of cocatalyst was monitored using ^{1}H NMR spectroscopy. With all cocatalysts, displacement of the silylamido ligand [N(SiMe$_3$)$_2$] is indicated by the appearance of a sharp singlet at 0.19 ppm assigned to *i*Bu$_2$Al[N(SiMe$_3$)$_2$] (see Supporting Information). Especially, treatment of **1**^{La} with one equivalent of *i*Bu$_2$AlCl (**F**) displayed silylamido/chlorido exchange, leading to the putative active species "[La(Al*i*Bu$_4$)(HAl*i*Bu$_3$)(Cl)]$_x$". It may be also hypothesized that displacement of TIBA leads to subsequent cationization of the complex. For example, cationization via TIBA-promoted chlorido abstraction and formation of the non-coordinating anion [Cl(Al*i*Bu$_3$)$_2$] has been reported.[9] The observation of amido displacement is in good agreement with NMR experiments performed by Boisson et al., revealing that AlEt$_2$[N(SiMe$_3$)$_2$] and AlEt[N(SiMe$_3$)$_2$]$_2$ are formed as coproducts of the reaction of Nd[N(SiMe$_3$)$_2$]$_3$ with Et$_2$AlCl.[27]

Attempts to crystallize reaction products from equimolar mixtures of **1**Nd and cocatalysts **A**, **C**, or **F** were unsuccessful; however, storing an equimolar mixture of **1**Nd and **B** for three months at −40 °C yielded crystals identified as [Nd{N-(SiMe$_3$)$_2$}(PhNMe$_2$)$_2$][B(C$_6$F$_5$)$_4$]$_2$ (**2**Nd) by X-ray diffraction (Figure 3).

Compound **2**Nd consists of the dicationic Nd[N(SiMe$_3$)$_2$]-(PhNMe$_2$)$_2$ fragment and two non-coordinating borate anions [B(C$_6$F$_5$)$_4$]. Little surprising, the Nd···N distance of 2.146(3) Å is considerably shortened compared to the 2.29 (2) Å in Nd[N(SiMe$_3$)$_2$]$_3$.[43] Spurred by the identification of **2**Nd, we wondered whether the same compound would be accessible by an aluminate-free synthesis employing Nd[N(SiMe$_3$)$_2$]$_3$ and **B**. The **1**Nd/**B** reaction yielded only very few crystals, and side products hampered any purification. In fact, **2**Nd could be obtained in almost quantitative yield following the synthesis from Nd[N(SiMe$_3$)$_2$]$_3$ and 2.5 equiv. **B**. Similarly, the 1:1, and 1:3 reactions yielded exclusively product **2**Nd.

[Nd{N(SiMe$_3$)$_2$}(PhNMe$_2$)$_2$][B(C$_6$F$_5$)$_4$]$_2$ (2Nd) in Isoprene Polymerization. Dicationic Ln(III) species have long been postulated and discussed as putative active species in homogeneous ethylene polymerization,[10,44−46] albeit further activation with borate or alkylaluminum cocatalysts seems inevitable. Additionally, the vast majority of such cationic rare-earth-metal alkyl complexes, examined in polymerization

https://doi.org/10.1021/acscatal.3c02247
ACS Catal. 2023, 13, 12826−12834

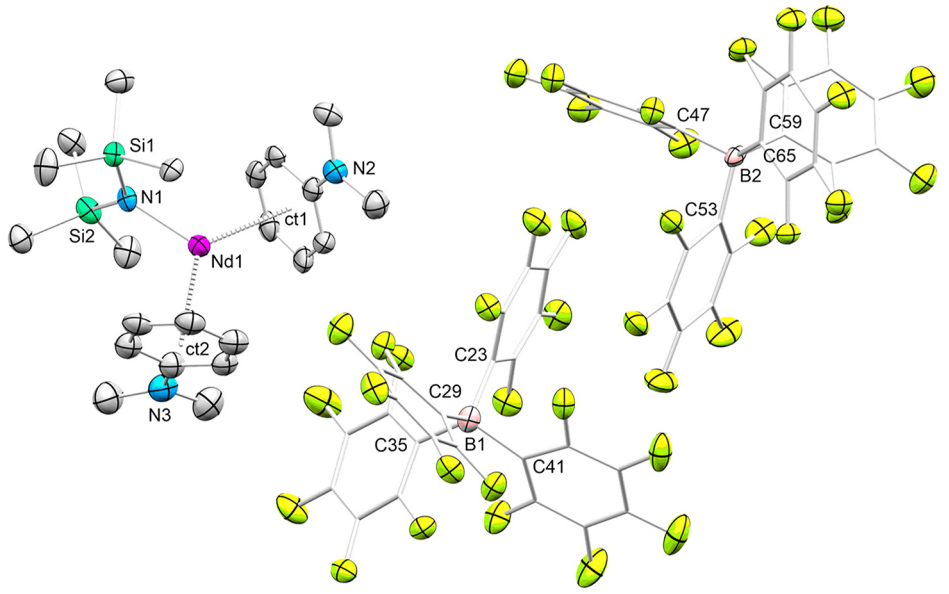

Figure 3. Crystal structure of 2^{Nd}. Ellipsoids are shown at the 50% probability level. Hydrogen atoms are omitted for clarity. Selected interatomic distances and angles: Nd(1)−N(1) 2.140(3), Nd(1)···Ct(1) 2.611, Nd(1)···Ct(2) 2.614, N(1)-Nd(1)-Ct(1) 116.37, N(1)-Nd(1)-Ct(2) 114.70, Ct(1)-Nd(1)-Ct(2) 127.61. Ct = $PhNMe_2$ ring centroid. For more metrics, see Supporting Information.

Scheme 1. Proposed Formation of Active Species in the Reaction of 1^{Ln} with B

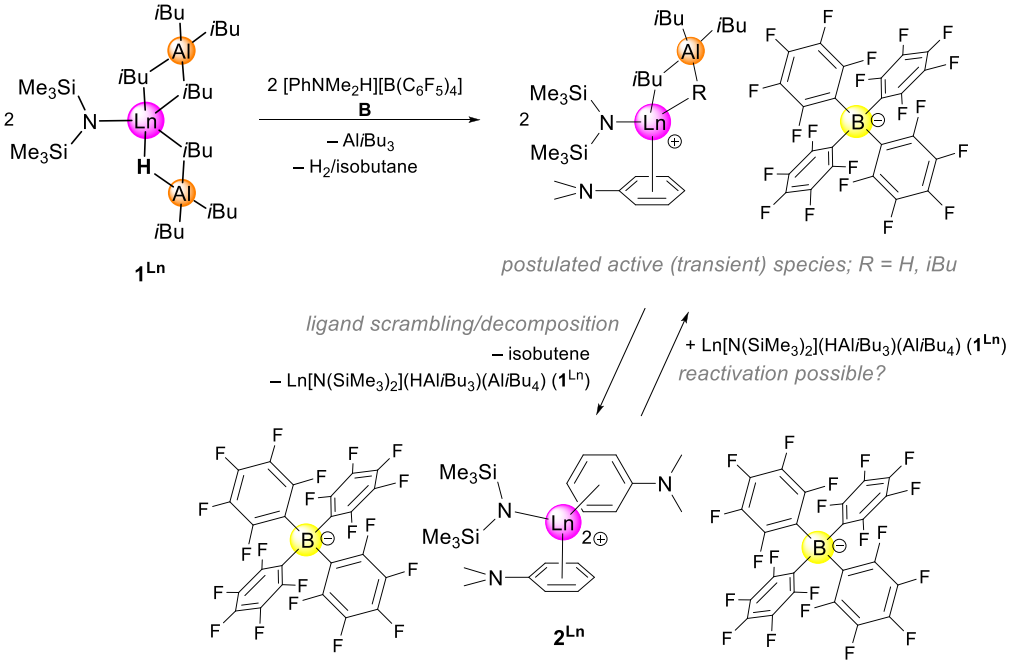

reactions, are generated in situ, and hence inaccessible for detailed mechanistic studies.[10] Similarly, cationic Ln(III) complexes generated in situ for 1,3-diene polymerization have escaped isolation and characterization.[5,10,47] For example, conjugated dienes can be efficiently polymerized *cis*-1,4 specifically using the binary system $Y(AlMe_4)_3/n[PhNMe_2H]$-$[B(C_6F_5)_4]$ (n = 1,2) involving in situ generated $[YMe_2(toluene)_x]^+$ and $[YMe(toluene)_x]^{2+}$ as probably active species.[12]

Remarkably, complex 2^{Nd} proved to be active in isoprene polymerization without further activation, or the presence of an alkylation agent (entries 39−41). Since 2^{Nd} is poorly soluble in toluene but soluble in *ortho*-difluorobenzene, it is plausible that the polymerization activity was higher in the latter solvent. Moreover, considering a competitive coordination of dienes and arenes,[40] diene coordination may become more favorable in the presence of the less electron-donating 1,2-difluorobenzene. In both cases, the obtained polymers feature a comparable microstructure and are essentially free of *trans* connectivities according to $^{13}C\{^1H\}$ NMR spectroscopy (Table 1, entries 39−41). In both cases, polymers with very high molecular weight were retrieved indicating that not all neodymium centers are active in polymerization. Several mechanistic scenarios may be considered, for example, the B

https://doi.org/10.1021/acscatal.3c02247
ACS Catal. 2023, 13, 12826−12834

→ Nd transfer of initiating pentafluorophenyl groups. Taking into account that the zirconium(IV) species $Zr[N(SiMe_3)_2]_3^+$ initiates the carbocationic isobutene/isoprene copolymerization,[48] a (coordinative) cationic polymerization may be occurring as well. The treatment of $\mathbf{2}^{Nd}$ with two equivalents of TIBA only led to a slight increase of activity (23 vs 17% yield; *cf.*, entries 42, and 41). Therefore, a further substitution of the silylamido ligand seems unlikely, since the substitution for an isobutyl(aluminato) moiety would very likely result in a higher catalytic activity. TIBA however clearly decreased the molecular weight (14.9 vs 46.9 × 10^4 g·mol^{-1}), arguing for TIBA to serve as a chain transfer agent.[49] This may proceed directly by exchange of an isobutyl group on TIBA for a polyisoprenyl chain on the Ln(III) center, or indirectly involving a hydride formed by isobutene elimination.[49]

Using the binary system $\mathbf{1}^{Nd}$/**2B** (entries 45−46) yielded polymers with a microstructure distinct from that obtained with compound $\mathbf{2}^{Nd}$. These findings suggest that $\mathbf{2}^{Nd}$ is not the (main) active species formed in the mixture $\mathbf{1}^{Nd}$/**B** (entry 5). Moreover, the system $\mathbf{1}^{Nd}$/2**B** (entries 45−46) features a much higher activity. It is thus likely that dicationic $\mathbf{2}^{Nd}$ is formed as a "decomposition product" from a putative monocationic species, initially emerging from the mixture $\mathbf{1}^{Nd}$/**B** (Scheme 1).

This scenario is also supported by the ^{1}H NMR spectrum of the equimolar reaction of $\mathbf{1}^{La}$ with **B** in deuterated benzene, showing that still a considerable amount of $\mathbf{1}^{La}$ prevailed. Comparison to literature ^{19}F NMR chemical shifts suggests borate coordination to the metal center in solution.[50] We favor the occurrence of an equilibrium between $\mathbf{2}^{Ln}$ and a possible active species. Since a catalytically active mixture, as for example formed by $\mathbf{1}^{Nd}$ and **B** (*cf.* entry 5) would contain both complexes $\mathbf{1}^{Nd}$, and complex $\mathbf{2}^{Nd}$, such a scenario might suggest a potential "reactivation" of complex $\mathbf{2}^{Nd}$ with $\mathbf{1}^{Nd}$. In other words, the binary system $\mathbf{1}^{Nd}$/**B** should lead to the same active species as a mixture of $\mathbf{1}^{Nd}$ and $\mathbf{2}^{Nd}$ (see Scheme 1). This would also imply the formation of polymers with the same microstructure. In fact, this is exactly what has been observed: (a) strikingly similar polymer microstructures using equimolar mixtures of $\mathbf{1}^{Nd}$/**B** or $\mathbf{1}^{Nd}$/$\mathbf{2}^{Nd}$ (71.7/21.0/7.3 (entry 5) vs 69.4/23.3/7.3 (entry 44) *cis*/*trans*/3,4), (b) almost identical molecular weight distributions (1.28 vs 1.16), and (c) molecular weights corresponding to the total amount of neodymium in each catalyst mixture (54,000 g/mol, 0.02 mmol Nd for $\mathbf{1}^{Nd}$/**B**, vs 21,000 g/mol, 0.04 mmol Nd for $\mathbf{1}^{Nd}$/$\mathbf{2}^{Nd}$).

Discrete cationic lanthanide amide species generated with cocatalyst **B** have already been reported.[22,42] The half−sandwich complex $[(2\text{-MeInd})Sc\{N(SiMe_3)_2\}(PhNMe_2)][B(C_6F_5)_4]$ (Ind = indenyl) displays coordination of *N*,*N*′-dimethylaniline to the small scandium center via the nitrogen atom instead of the aromatic ring as observed with $\mathbf{2}^{Nd}$.[42] Since this complex is engaging in single-component 1,3-butadiene polymerization, this may support the catalytic scenario proposed in this paper.

CONCLUSIONS

Discrete ancillary ligand-free lanthanide isobutylaluminate complexes $Ln[N(SiMe_3)_2](HAli\mathit{Bu}_3)(Ali\mathit{Bu}_4)$ (Ln = La, Pr, Nd, Gd) act as precatalysts for isoprene polymerization. Upon activation with borate cocatalysts, the binary system exhibits better *cis* stereoselectivity compared to homoleptic lanthanide tetramethylaluminates $Ln(AlMe_4)_3$. High *cis* stereoselectivity was observed upon treatment of complexes $Ln[N(SiMe_3)_2](HAli\mathit{Bu}_3)(Ali\mathit{Bu}_4)$ with dialkylaluminum chloride cocatalysts (alkyl = methyl, ethyl, isobutyl). Especially, $Gd[N(SiMe_3)_2](HAli\mathit{Bu}_3)(Ali\mathit{Bu}_4)$ afforded perfectly stereoregular *cis*-1,4 polyisoprene with no *trans*-1,4 or 3,4 portions detectable by $^{13}C\{^1H\}$ NMR spectroscopy. Generally, both the catalytic activity and stereoselectivity increased in the order La < Pr < Nd < Gd. Activation of diamagnetic $La[N(SiMe_3)_2](HAli\mathit{Bu}_3)(Ali\mathit{Bu}_4)$ with one equivalent of diisobutylaluminum chloride provided evidence of a silylamido-chlorido exchange, possibly forming $[LnCl(HAli\mathit{Bu}_3)(Ali\mathit{Bu}_4)]_x$. The reaction of $Nd[N(SiMe_3)_2](HAli\mathit{Bu}_3)(Ali\mathit{Bu}_4)$ with one equivalent of $[PhNMe_2H][B(C_6F_5)_4]$ led to the formation of the dicationic complex $[Nd\{N(SiMe_3)_2\}(PhNMe_2)_2][B(C_6F_5)_4]_2$. The latter was also obtained from $Nd[N(SiMe_3)_2]_3$ and $[PhNMe_2H][B(C_6F_5)_4]$. Compound $[Nd\{N(SiMe_3)_2\}(PhNMe_2)_2][B(C_6F_5)_4]_2$ combined with $Nd[N(SiMe_3)_2](HAli\mathit{Bu}_3)(Ali\mathit{Bu}_4)$ gave a polymer featuring an almost identical microstructure as obtained with a 1:1 mixture of $Nd[N(SiMe_3)_2](HAli\mathit{Bu}_3)(Ali\mathit{Bu}_4)$ and $[PhNMe_2H][B(C_6F_5)_4]$, which supports the proposed mechanism involving monocationic $[Nd(PhNMe_2)\{N(SiMe_3)_2\}\{RAli\mathit{Bu}_3\}][B(C_6F_5)_4]$ (R = H, or *i*Bu) as the active species. Complex $[Nd\{N(SiMe_3)_2\}(PhNMe_2)_2][B(C_6F_5)_4]_2$ proved to be active in isoprene polymerization without further activation with cocatalyst, forming high molecular weight polyisoprene with narrow molecular weight distribution.

EXPERIMENTAL SECTION

All manipulations were performed under rigorous exclusion of air and moisture unless indicated, using standard Schlenk, high-vacuum, and glovebox techniques (MBraun MB200B <1 ppm O_2, <1 ppm H_2O, argon atmosphere). Solvents were supplied by Merck KGaA, purified using a Grubbs-type solvent purification system (MBraun), and stored inside a glovebox. Benzene-d_6 was obtained from Merck KGaA and dried over Na/K alloy prior to use. Isoprene was purchased from Merck KGaA, dried with TIBA, and distilled under reduced pressure before use. Dimethylaluminum chloride (**D**), diethylaluminum chloride (**E**), diisobutyl aluminum (**F**), and TIBA were purchased from Merck KGaA. $[CPh_3][B(C_6F_5)_4]$ (**A**), $[C_6H_5NMe_2H][B(C_6F_5)_4]$ (**B**), and $[B(C_6F_5)_3]$ (**C**) were purchased from Boulder Scientific and used as received. Argon (99.999 vol %) was supplied by Westfalen AG. Complexes $Ln[N(SiMe_3)_2]_3$ (Ln = La, Pr, Nd) were prepared following standard procedures.[51] Complexes $\mathbf{1}^{Ln}$ were synthesized as previously reported by our group.[33] Glassware and polymer fittings were dried prior to use for several hours at 120 °C or 80 °C, respectively. IR spectra were recorded on a Vertex 70 spectrometer (Bruker) in Nujol and measured in a cell equipped with CsI windows. Elemental analyses were performed on an Elementar vario MICRO cube. NMR spectra of air and moisture-sensitive compounds were recorded using J. Young valve NMR tubes on a Bruker AVII+400 spectrometer (^{1}H: 400.13 MHz; ^{13}C: 100.61 MHz). ^{1}H and ^{13}C NMR chemical shifts are referenced to solvent residual resonances and reported in parts per million, relative to tetramethylsilane. Size-exclusion chromatography (SEC) was performed on a Viscotek GPCmax VE2001 device equipped with a TDA305 detector (Viscotek) against a polystyrene standard in THF (35 °C) with a flow rate of 1 mL/min. Sample solutions (1.0 mg polymer per mL THF) were filtered through a 0.45 μm syringe filter prior to injection. M_n and M_w

https://doi.org/10.1021/acscatal.3c02247
ACS Catal. 2023, 13, 12826−12834

were determined by means of the integrated OmniSec software. Due to technical challenges, polymers' data in entries marked with asterisk (Table 1) were determined using the Waters SEC system with a Waters 2414 Refractive Index Detector. M_n and M_w were determined by means of the Waters Empower 3 Software.

Glass transition temperatures T_g were determined by differential scanning calorimetry (DSC) under nitrogen atmosphere on a DSC8000 device equipped with a CLN2 cooler (PerkinElmer) calibrated with cyclohexane and indium standards, by scanning from −100 °C up to +100 °C with heating rates of 20 K/min and cooling rates of 60 K/min. The monomer conversion was determined gravimetrically. Note that isoprene is a volatile, toxic compound and should be handled in a well-ventilated fumehood. Organoaluminum compounds are pyrophoric and may react violently with moisture and air.

Gd[N(SiMe$_3$)$_2$](HAl*i*Bu$_3$)(Al*i*Bu$_4$) (1^{Gd}). A solution of TIBA (14.58 g, 73.15 mmol, 4 equiv.) in *n*-pentane (50 mL) was added to Gd[N(SiMe$_3$)$_2$]$_3$ (11.67 g, 18.29 mmol, 1 equiv.) in *n*-pentane (50 mL) in portions under stirring at ambient temperature. After stirring overnight, the clear yellowish solution was concentrated in a vacuum to 25 mL and cooled to −40 °C. Several recrystallization steps afforded 1.64 g (2.12 mmol, 12%) of combined fractions of Gd[N(SiMe$_3$)$_2$]-(HAl*i*Bu$_3$)(Al*i*Bu$_4$) (**1^{Gd}**) in the form of colorless, block-shaped crystals. IR (nujol) 1462 (vs), 1377 (m), 1316 (w), 1249 (vs), 1158 (m), 1096 (vw), 1060 (w), 1017 (m), 941 (m), 861 (s), 833 (s), 779 (w), 725 (m), 672 (m), 620 (w), 543 (s), 436 (s) cm^{-1}. Anal. Calcd for $C_{34}H_{82}Al_2GdNSi_2$ (772.41 g mol^{-1}): calcd. C. 52.87; H, 10.70; N, 1.81. Found C, 52.92; H, 10.62; N, 1.77.

Nd[N(SiMe$_3$)$_2$](PhNMe$_2$)$_2$[B(C$_6$F$_5$)$_4$]$_2$ (2Nd). Route 1: Nd-[N(SiMe$_3$)$_2$](HAl*i*Bu$_3$)(Al*i*Bu$_4$) (**1Nd**) (85 mg, 0.112 mmol, 1 equiv) was dissolved in 1,2-difluorobenzene (0.5 mL), and a solution of [PhNMe$_2$H][B(C$_6$F$_5$)$_4$] (108 mg, 0.135 mmol, 1.2 equiv.) in 1,2-difluorobenzene (1.5 mL) was added dropwise. After stirring the moss-green, clear solution for 10 min at ambient temperature, cooling to −40 °C afforded very few, colorless block-shaped crystals after three months identified as **2Nd** by X-ray crystallography. Route 2: A solution of [PhNMe$_2$H][B(C$_6$F$_5$)$_4$] (320 mg, 0.399 mmol, 2.5 equiv) in 1,2-difluorobenzene (3 mL) was added dropwise to a solution of Nd[N(SiMe$_3$)$_2$]$_3$ (100 mg, 0.160 mmol, 1 equiv) in 1,2-difluorobenzene (2 mL). After stirring for 30 min at ambient temperature, the solvent volume was reduced under vacuum to 1 mL. Cooling to −40 °C yielded **2Nd** as pale green, plate-shaped crystals (318.3 mg, 93%). IR (nujol) 1462 (m), 1589 (s), 1511 (s), 1376 (s), 1258 (m), 1195 (w), 1165 (vw), 1081 (s), 1023 (vw), 974 (vs), 910 (w), 830 (w), 755 (s), 724 (m), 684 (m), 660 (s), 610 (m), 574 (m), 522 (m) cm^{-1}. Anal. Calcd for $C_{82}H_{48}B_2F_{44}N_3NdSi_2$ (2133.24 g mol^{-1}): calcd C, 46.17; H, 2.27; N, 1.97. Found C, 46.08; H, 2.82; N, 2.12.

Representative Example of Isoprene Polymerization Provided Material Compiled in Table 1, Entry 2. Nd[N(SiMe$_3$)$_2$](HAl*i*Bu$_3$)(Al*i*Bu$_4$) (**1Nd**) (15.19 mg, 0.02 mmol), and [CPh$_3$][B(C$_6$F$_5$)$_4$] (**A**) (1 equiv, 18.45 mg, 0.02 mmol) were dissolved in toluene (8 mL), and stirred at ambient temperature for 30 min. After the addition of isoprene (20 mmol), the polymerization was carried out at ambient temperature for 1 h under stirring (500 rpm). The solution was quenched in methanol (20 mL) containing 0.1% (w/w) 2,6-di-*tert*-butyl-4-methylphenol as a stabilizer. The precipitated polymer was dried in vacuo at ambient temperature to constant weight.

■ ASSOCIATED CONTENT

Supporting Information

The Supporting Information is available free of charge at https://pubs.acs.org/doi/10.1021/acscatal.3c02247.

Supporting figures, detailed crystallographic data, spectroscopic data (NMR), polymer data (GPC traces) (PDF)
(CIF)
(CIF)

■ AUTHOR INFORMATION

Corresponding Author

Reiner Anwander − *Institut für Anorganische Chemie, Eberhard Karls Universität Tübingen, Tübingen 72076, Germany;* orcid.org/0000-0002-1543-3787; Email: reiner.anwander@uni-tuebingen.de

Authors

Eric C. Moinet − *Institut für Anorganische Chemie, Eberhard Karls Universität Tübingen, Tübingen 72076, Germany;* orcid.org/0009-0000-5035-5553

Olivier Tardif − *Bridgestone Corporation, Kodaira-shi, Tokyo 187-8531, Japan;* orcid.org/0000-0001-6297-9443

Lea-Sophie Hornberger − *Chair of Macromolecular Materials and Fiber Chemistry, Institute of Polymer Chemistry, University of Stuttgart, Stuttgart 70569, Germany*

Friederike Adams − *Chair of Macromolecular Materials and Fiber Chemistry, Institute of Polymer Chemistry, University of Stuttgart, Stuttgart 70569, Germany;* orcid.org/0000-0002-4362-0387

Cäcilia Maichle-Mössmer − *Institut für Anorganische Chemie, Eberhard Karls Universität Tübingen, Tübingen 72076, Germany;* orcid.org/0000-0001-7638-1610

Complete contact information is available at: https://pubs.acs.org/10.1021/acscatal.3c02247

Notes

The authors declare no competing financial interest.

■ ACKNOWLEDGMENTS

We thank Bridgestone Corporation for the generous support and Dr. Christoph O. Hollfelder for evaluating polymer data.

■ REFERENCES

(1) Sone, T. Industrial Synthetic Method of the Rubbers. 1. Butadiene Rubber. *Int. Polym. Sci. Technol.* **2016**, *43*, 49−54.

(2) Zhang, Z.; CuiWang, D. B.; Liu, B.; Yang, Y. In *Molecular Catalysis of Rare-Earth Elements*; Roesky, P. W., Ed.; Springer: Berlin Heidelberg, 2010; pp 49−108.

(3) Friebe, L.; Nuyken, O.; Obrecht, W. Neodymium-Based Ziegler/Natta Catalysts and their Application in Diene Polymerization. *Adv. Polym. Sci.* **2006**, *204*, 1−154.

(4) Fischbach, A.; Anwander, R. Rare-Earth Metals and Aluminum Getting Close in Ziegler-Type Organometallics. *Adv. Polym. Sci.* **2006**, *204*, 155−281.

(5) Zhang, L.; Suzuki, T.; Luo, Y.; Nishiura, M.; Hou, Z. Cationic Alkyl Rare-Earth Metal Complexes Bearing an Ancillary Bis(phosphinophenyl)amido Ligand: A Catalytic System for Living cis-1,4-Polymerization and Copolymerization of Isoprene and Butadiene. *Angew. Chem., Int. Ed.* **2007**, *46*, 1909−1913.

(6) Cornish, K. Alternative natural rubber crops: why should we care? *Technol. Innovat.* **2017**, *18*, 244−255.
(7) Puskas, J. E.; Gautriaud, E.; Deffieux, A.; Kennedy, J. P. Natural rubber biosynthesis-A living carbocationic polymerization? *Prog. Polym. Sci.* **2006**, *31*, 533−548.
(8) Ricci, G.; Pampaloni, G.; Sommazzi, A.; Masi, F. Dienes Polymerization: Where We Are and What Lies Ahead. *Macromolecules* **2021**, *54*, 5879−5914.
(9) Li, D.; Li, S.; Cui, D.; Zhang, X. *β*-Diketiminato Rare-Earth Metal Complexes. Structures, Catalysis, and Active Species for Highly *cis*-1,4-Selective Polymerization of Isoprene. *Organometallics* **2010**, *29*, 2186−2193.
(10) Arndt, S.; Okuda, J. Cationic Alkyl Complexes of the Rare-Earth Metals: Synthesis, Structure, and Reactivity. *Adv. Synth. Catal.* **2005**, *347*, 339−354.
(11) Taube, R. In *Metalorganic Catalysts for Synthesis and Polymerization*; Kaminisky, W., Ed.; Springer: Berlin Heidelberg New York, 1999; pp 531−547.
(12) Arndt, S.; Beckerle, K.; Zeimentz, P. M.; Spaniol, T. P.; Okuda, J. Cationic Yttrium Methyl Complexes as Functional Models for Polymerization Catalysts of 1,3-Dienes. *Angew. Chem., Int. Ed.* **2005**, *44*, 7473−7477.
(13) Schmidt, B. M.; Pindwal, A.; Venkatesh, A.; Ellern, A.; Rossini, A. J.; Sadow, A. D. Zwitterionic Trivalent (Alkyl)lanthanide Complexes in Ziegler-Type Butadiene Polymerization. *ACS Catal.* **2019**, *9*, 827−838.
(14) Shan, C.; Lin, Y.; Ouyang, J.; Fan, Y.; Yang, G. Single crystal structure of a polymerization active Nd-Al bimetallic complex. *Macromol. Chem.* **1987**, *188*, 629−635.
(15) Fischbach, A.; Meermann, C.; Eickerling, G.; Scherer, W.; Anwander, R. Discrete Lanthanide Aryl(alk)oxide Trimethylaluminum Adducts as Isoprene Polymerization Catalysts. *Macromolecules* **2006**, *39*, 6811−6816.
(16) Meermann, C.; Törnroos, K. W.; Nerdal, W.; Anwander, R. Rare-Earth Metal Mixed Chloro/Methyl Compounds: Heterogeneous−Homogeneous Borderline Catalysts in 1,3-Diene Polymerization. *Angew. Chem., Int. Ed.* **2007**, *46*, 6508−6513.
(17) Evans, W. J.; Giarikos, D. G.; Allen, N. T. Polymerization of Isoprene by a Single Component Lanthanide Catalyst Precursor. *Macromolecules* **2003**, *36*, 4256−4257.
(18) Taube, R.; Windisch, H.; Maiwald, S.; Hemling, H.; Schumann, H. XLVIII Synthese und struktur der ersten neutralen Tris(allyl) lanthanoid-komplexe La(η^3-C_3H_5)$_3$ · 1,5 Dioxan und Nd(η^3-C_3H_5)$_3$ · Dioxan und ihre Eignung als "single site" -Katalysatoren für die stereospezifische Butadienpolymerisation. *J. Organomet. Chem.* **1996**, *513*, 49−61.
(19) Li, X.; Nishiura, M.; Mori, K.; Mashiko, T.; Hou, Z. Cationic scandium aminobenzyl complexes. Synthesis, structure and unprecedented catalysis of copolymerization of 1-hexene and dicyclopentadiene. *Chem. Commun.* **2007**, 4137−4139.
(20) Rodrigues, A.-S.; Kirillov, E.; Vuillemin, B.; Razavi, A.; Carpentier, J.-F. Stereocontrolled styrene−isoprene copolymerization and styrene−ethylene−isoprene terpolymerization with a single-component allyl *ansa*-neodymocene catalyst. *Polymer* **2008**, *49*, 2039−2045.
(21) Annunziata, L.; Duc, M.; Carpentier, J.-F. Chain Growth Polymerization of Isoprene and Stereoselective Isoprene−Styrene Copolymerization Promoted by an *ansa*-Bis(indenyl)allyl−Yttrium Complex. *Macromolecules* **2011**, *44*, 7158−7166.
(22) Yu, N.; Nishiura, M.; Li, X.; Xi, Z.; Hou, Z. Cationic Scandium Allyl Complexes Bearing Mono (cyclopentadienyl) Ligands: Synthesis, Novel Structural Variety, and Olefin-Polymerization Catalysis. *Chem.−Asian J.* **2008**, *3*, 1406−1414.
(23) Zimmermann, M.; Törnroos, K. W.; Anwander, R. Cationic Rare-Earth-Metal Half-Sandwich Complexes for the Living trans-1,4-Isoprene Polymerization. *Angew. Chem., Int. Ed.* **2008**, *47*, 775−778.
(24) Barisic, D.; Lebon, J.; Maichle-Mössmer, C.; Anwander, R. Pentadienyl migration and abstraction in yttrium aluminabenzene complexes including a single-component catalyst for isoprene polymerization. *Chem. Commun.* **2019**, *55*, 7089−7092.
(25) Barisic, D.; Buschmann, D. A.; Schneider, D.; Maichle-Mössmer, C.; Anwander, R. Rare-Earth-Metal Pentadienyl Half-Sandwich and Sandwich Tetramethylaluminates−Synthesis, Structure, Reactivity, and Performance in Isoprene Polymerization. *Chem.—Eur. J.* **2019**, *25*, 4821−4832.
(26) Moinet, E. C.; Wolf, B.; Tardif, O.; Maichle-Mössmer, C.; Anwander, R. Divalent Lanthanide Tetraisobutylaluminates: Reactivity and Living Isoprene Polymerization. *Angew. Chem., Int. Ed.* **2023**, *62*, No. e202219316.
(27) Boisson, C.; Barbotin, F.; Spitz, R. Polymerization of butadiene with a new catalyst based on a neodymium amide precursor. *Macromol. Chem. Phys.* **1999**, *200*, 1163−1166.
(28) Monteil, V.; Spitz, R.; Boisson, C. Polymerization of butadiene and copolymerization of butadiene with styrene using neodymium amide catalysts. *Polym. Int.* **2004**, *53*, 576−581.
(29) Kaita, S.; Kobayashi, E.; Sakakibara, S.; Aoshima, S.; Furukawa, J. Homo- and copolymerizations of butadiene and styrene with Ln(OCOCCl$_3$)$_3$-based catalyst. *J. Polym. Sci., Part A: Polym. Chem.* **1996**, *34*, 3431−3434.
(30) Woodman, T. J.; Sarazin, Y.; Fink, G.; Hauschild, K.; Bochmann, M. Heterogenized "Ligand-Free" Lanthanide Catalysts for the Homo-and Copolymerization of Ethylene and 1,3-Butadiene. *Macromolecules* **2005**, *38*, 3060−3067.
(31) Gauvin, R. M.; Chenal, T.; Hassan, R. A.; Addad, A.; Mortreux, A. Grafted lanthanide amides: Versatile catalysts for various transformations. *J. Mol. Catal. A: Chem.* **2006**, *257*, 31−40.
(32) Bathellier, A.; Moreno, D.; Maron, L.; Dinoi, C.; Del Rosal, I. Grafting of lanthanum complexes on a functionalised graphene surface : theoretical investigation on Ethylene and 1,3-Butadiene homo- and co-polymerisation. *Chem.—Eur. J.* **2020**, *26*, 13213−13225.
(33) Moinet, E. C.; Tardif, O.; Maichle-Mössmer, C.; Anwander, R. Triisobutylaluminium-promoted formation of Lanthanide Hydrides. *Chem. Commun.* **2023**, *59*, 5261−5264.
(34) Maiwald, S.; Weißenborn, H.; Sommer, C.; Müller, G.; Taube, R. Komplexkatalyse: LIX Die Katalyse der 1,4-trans-Polymerisation des Butadiens mit Tris(allyl)neodym(III) Nd(η^3-C_3H_5)$_3$ als Einkomponentenkatalysator—Kinetik und Reaktionsmechanismus. *J. Organomet. Chem.* **2001**, *640*, 1−9.
(35) Fischbach, A.; Perdih, F.; Herdtweck, E.; Anwander, R. Structure−Reactivity Relationships in Rare-Earth Metal Carboxylate-Based Binary Ziegler-Type Catalysts. *Organometallics* **2006**, *25*, 1626−1642.
(36) Barbotin, F.; Monteil, V.; Llauro, M.-F.; Boisson, C.; Spitz, R. First Synthesis of Poly (ethene-co-1, 3-butadiene) with Neodymocene Catalysts. *Macromolecules* **2000**, *33*, 8521−8523.
(37) Lv, K.; Cui, D. CCC-Pincer Bis(carbene) Lanthanide Dibromides. Catalysis on Highly cis-1,4-Selective Polymerization of Isoprene and Active Species. *Organometallics* **2010**, *29*, 2987−2993.
(38) Hollfelder, C. O.; Jende, L. N.; Diether, D.; Zelger, T.; Stauder, R.; Maichle-Mössmer, C.; Anwander, R. 1,3-Diene Polymerization Mediated by Homoleptic Tetramethylaluminates of the Rare-Earth Metals. *Catalysts* **2018**, *8*, 61.
(39) Martins, N.; Bonnet, F.; Visseaux, M. J. P. Highly efficient cis-1, 4 polymerisation of isoprene using simple homoleptic amido rare earth-based catalysts. *Polymer* **2014**, *55*, 5013−5016.
(40) Friebe, L.; Müller, J. M.; Nuyken, O.; Obrecht, W. Comparison of the Solvents n-Hexane, tert-Butyl Benzene and Toluene in the Polymerization of 1,3-Butadiene with the Ziegler Catalyst System Neodymium Versatate/Diisobutylaluminum Hydride/Ethylaluminum Sesquichloride. *J. Macromol. Sci. A* . **2006**, *43*, 841−854.
(41) Kaita, S.; Hou, Z.; Nishiura, M.; Doi, Y.; Kurazumi, J.; Horiuchi, A. C.; Wakatsuki, Y. Ultimately Specific 1, 4-cis Polymerization of 1, 3-Butadiene with a Novel Gadolinium Catalyst. *Macromol. Rapid Commun.* **2003**, *24*, 179−184.
(42) Tardif, O.; Kaita, S. Generation of cationic indenyl silylamide gadolinium and scandium complexes [(Ind)Ln{N(SiMe$_3$)$_2$}]$^+$[B-

https://doi.org/10.1021/acscatal.3c02247
ACS Catal. 2023, 13, 12826−12834

$(C_6F_5)_4]^-$ and their reactivity for 1, 3-butadiene polymerization. *Dalton Trans.* **2008**, 2531−2533.
(43) Andersen, R. A.; Templeton, D. H.; Zalkin, A. Structure of tris(bis(trimethylsilyl)amido)neodymium(III), $Nd[N(Si(CH_3)_3)_2]_3$. *Inorg. Chem.* **1978**, *17*, 2317−2319.
(44) Hajela, S.; Schaefer, W. P.; Bercaw, J. E. Highly electron deficient group 3 organometallic complexes based on the 1, 4, 7-trimethyl-1, 4, 7-triazacyclononane ligand system. *J. Organomet. Chem.* **1997**, *532*, 45−53.
(45) Arndt, S.; Spaniol, T. P.; Okuda, J. Homogeneous Ethylene-Polymerization Catalysts Based on Alkyl Cations of the Rare-Earth Metals: Are Dicationic Mono(alkyl) Complexes the Active Species? *Angew. Chem., Int. Ed.* **2003**, *42*, 5075−5079.
(46) Ward, B. D.; Bellemin-Laponnaz, S.; Gade, L. H. C3 Chirality in Polymerization Catalysis: A Highly Active Dicationic Scandium-(III) Catalyst for the Isoselective Polymerization of 1-Hexene. *Angew. Chem., Int. Ed.* **2005**, *44*, 1668−1671.
(47) Taube, R.; Maiwald, S.; Sieler, J. Komplexkatalyse: LVII. Vereinfachte Synthese des $Nd(\pi\text{-}C_3H_5)_3{\cdot}C_4H_8O_2$ nach der Grignard-Methode und Darstellung der neuen Allylneodym(III)-Komplexe $[Nd(\pi\text{-}C_5Me_5)(\pi\text{-}C_3H_5)_2{\cdot}C_4H_8O_2]$ und $[Nd(\pi\text{-}C_3H_5)Cl(THF)_5]B(C_6H_5)_4{\cdot}$THF als Präkatalysatoren für die stereospezifische Butadien-polymerisation. *J. Organomet. Chem.* **2001**, *621*, 327−336.
(48) Carr, A. G.; Dawson, D. M.; Bochmann, M. The $[Zr(N\{SiMe_3\}_2)_3]^+$ cation as a novel initiator for carbocationic isobutene homo-and isobutene/isoprene co-polymerisations. *Macromol. Rapid Commun.* **1998**, *19*, 205−207.
(49) Friebe, L.; Windisch, H.; Nuyken, O.; Obrecht, W. Polymerization of 1,3-Butadiene Initiated by Neodymium Versatate/Triisobutylaluminum/Ethylaluminum Sesquichloride: Impact of the Alkylaluminum Cocatalyst Component. *J. Macromol. Sci., Part A: Pure Appl.Chem.* **2004**, *41*, 245−256.
(50) Horton, A. D. Direct Observation of β-Methyl Elimination in Cationic Neopentyl Complexes: Ligand Effects on the Reversible Elimination of Isobutene. *Organometallics* **1996**, *15*, 2675−2677.
(51) Bradley, D. C.; Ghotra, J. S.; Hart, F. A. Low co-ordination numbers in lanthanide and actinide compounds. Part I. The preparation and characterization of tris {bis(trimethylsilyl)amido} lanthanides. *Dalton Trans.* **1973**, 1021−1023.

https://doi.org/10.1021/acscatal.3c02247
ACS Catal. 2023, 13, 12826−12834

Supporting Information

Discrete Trivalent Lanthanide Isobutylaluminates in Isoprene Polymerization: Elucidation of Cationized Active Species

Eric C. Moinet,[a] Olivier Tardif,[b] Lea-Sophie Hornberger,[c] Friederike Adams,[c] Cäcilia Maichle-Mössmer,[a] and Reiner Anwander[a,*]

[a] Institut für Anorganische Chemie, Eberhard Karls Universität Tübingen, Auf der Morgenstelle 18, 72076 Tübingen, Germany

[b] Bridgestone Corporation, Ogawahigashi-cho, Kodaira-shi, Tokyo, 187-8531, Japan

[C] Chair of Macromolecular Materials and Fiber Chemistry, Institute of Polymer Chemistry, University of Stuttgart, Pfaffenwaldring 55, 70569 Stuttgart, Germany

*E-mail for R.A.: reiner.anwander@uni-tuebingen.de.

Table of Contents

NMR Spectra

In general, solvent residual signals are labeled with an asterisk (*). In some cases, the paramagnetic nature of Pr(III), Nd(III) and Gd(III) (**1**^{Pr}, **1**Nd, **1**^{Gd}), or poor solubility (compound **2**) did not allow any conclusive NMR analysis.

Activation of La[N(SiMe$_3$)$_2$](HAl*i*Bu$_3$)(Al*i*Bu$_4$) (**1**^{La}) with [CPh$_3$][B(C$_6$F$_5$)$_4$] (A)

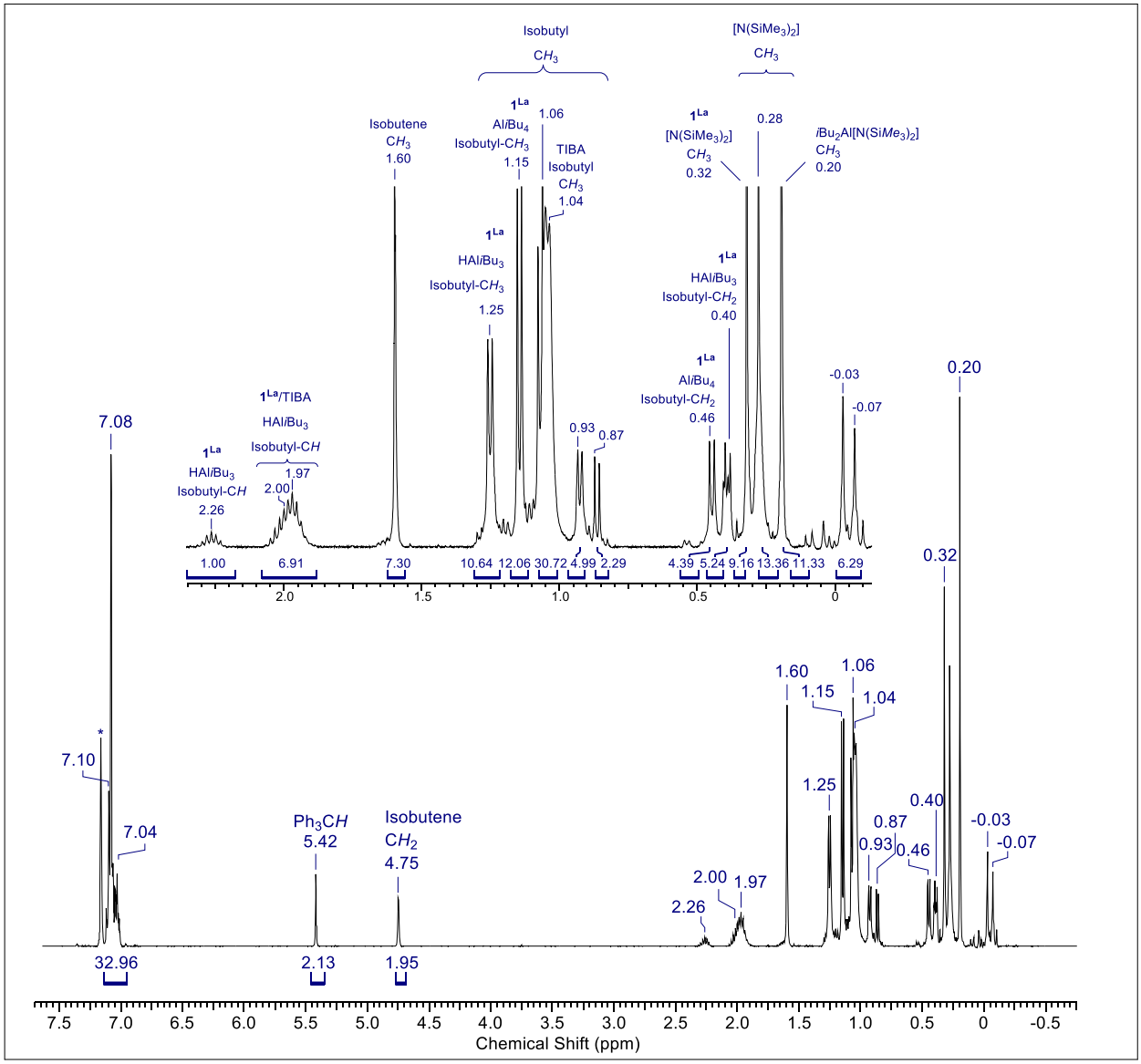

Figure 1. ^{1}H-NMR spectrum (400 MHz, C_6D_6, 26 °C) of the activation of **1**^{La} with one equivalent of cocatalyst **A**. Note that an oil is formed , which separates from the C_6D_6 solution.

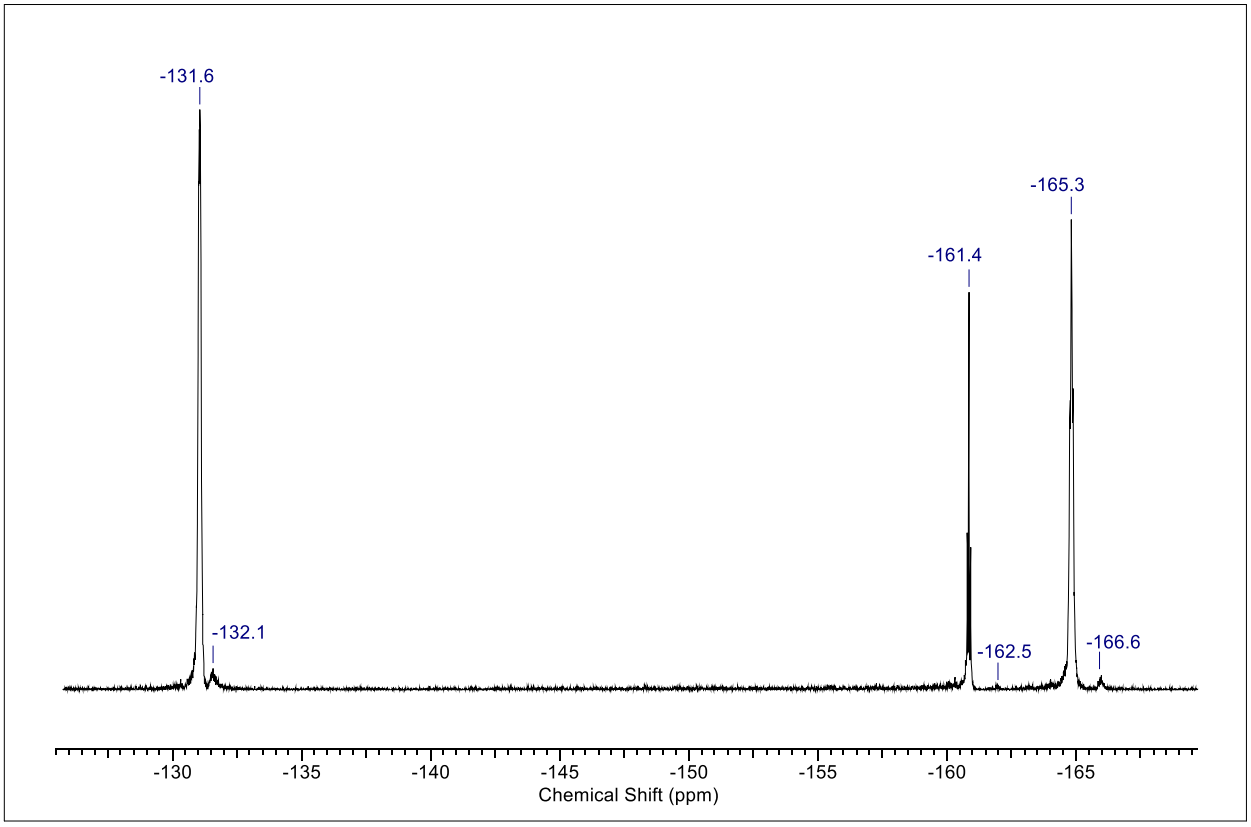

Figure 2. ^{19}F-NMR spectrum (400 MHz, C_6D_6, 26 °C) of the activation of **1**^{La} with one equivalent of cocatalyst **A**.

Activation of La[N(SiMe$_3$)$_2$](HAl*i*Bu$_3$)(Al*i*Bu$_4$) (1^{La}) with [C$_6$H$_5$NMe$_2$H][B(C$_6$F$_5$)$_4$] (B)

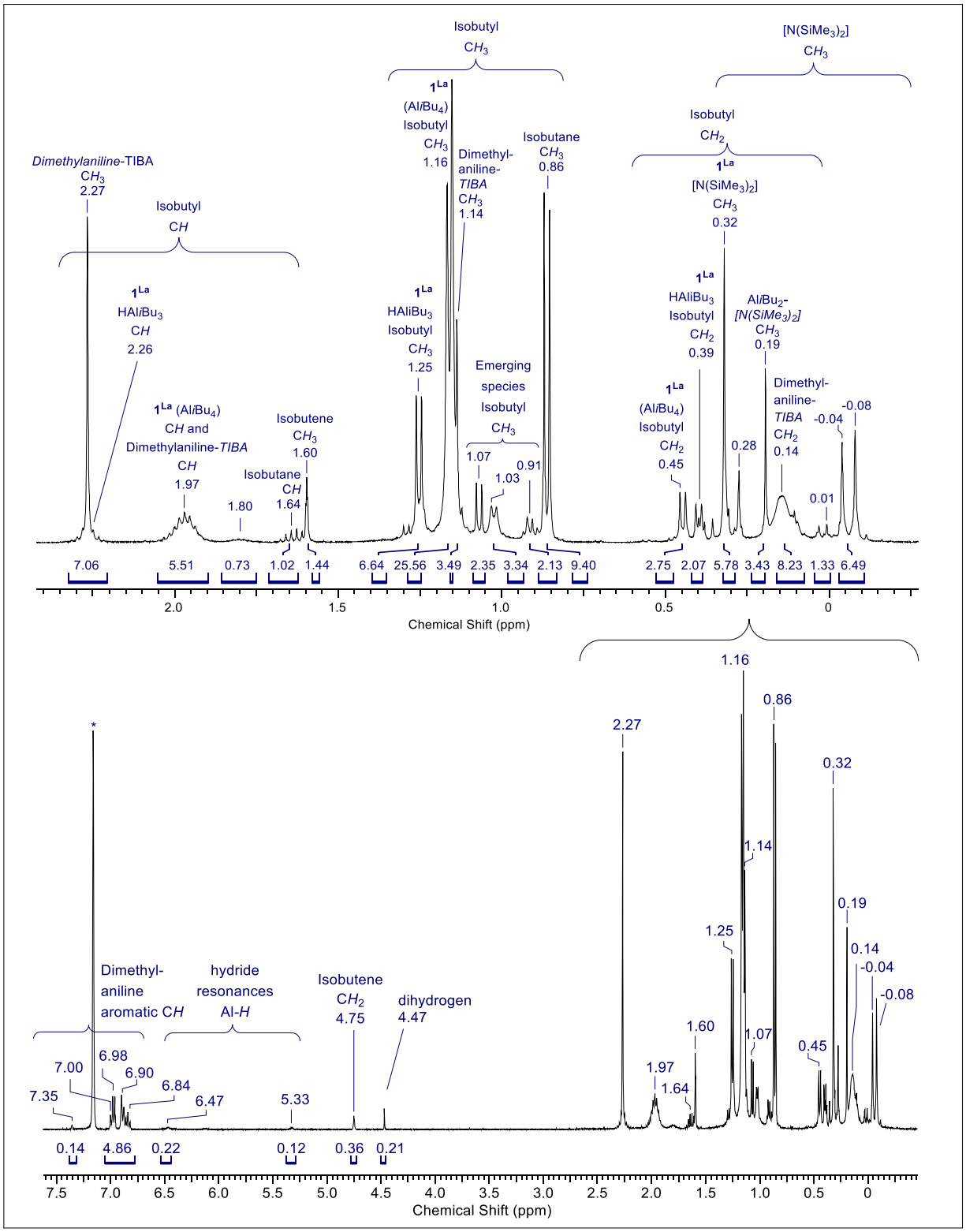

Figure 3. ^{1}H-NMR spectrum (400 MHz, 26 °C) of the activation of **1^{La}** with one equivalent of cocatalyst **B** in C_6D_6.

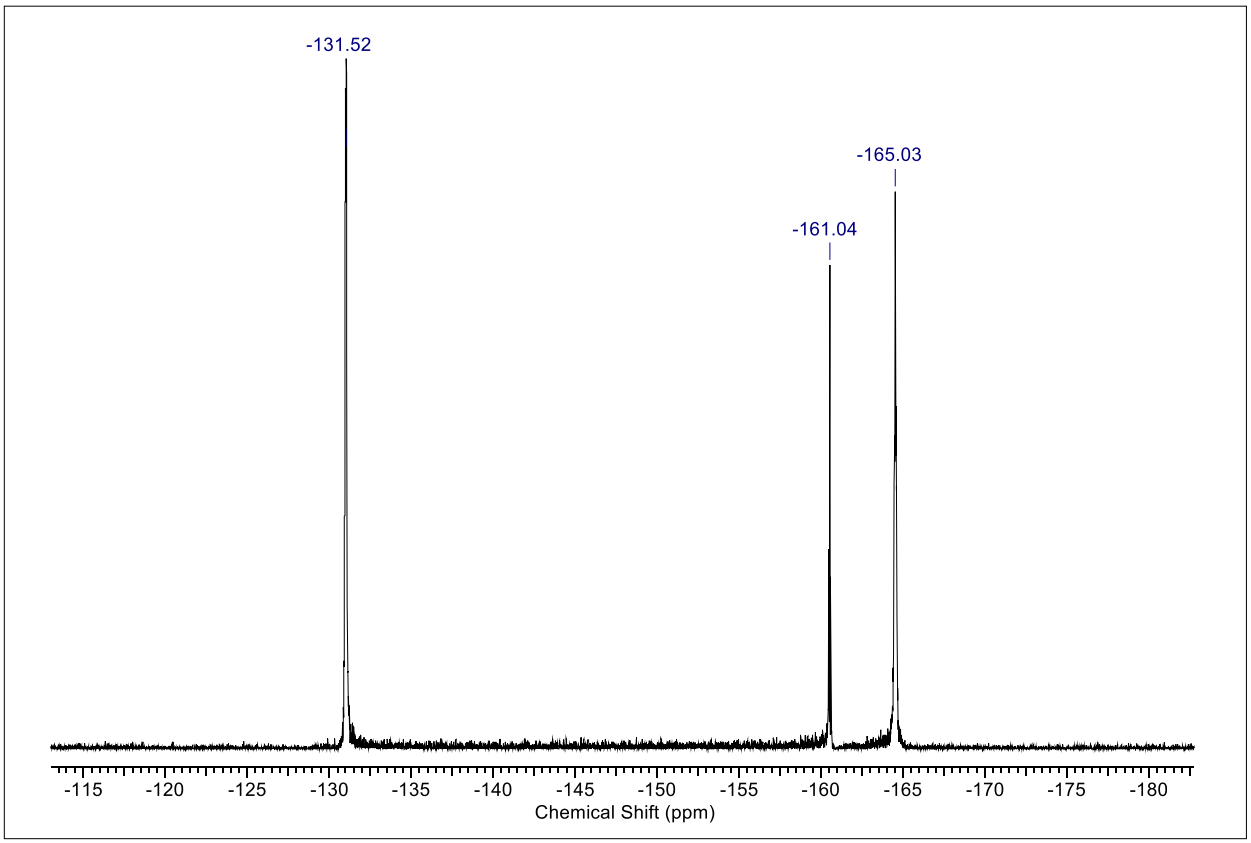

Figure 4. ^{19}F-NMR spectrum (400 MHz, C_6D_6, 26 °C) of the activation of **1**^{La} with one equivalent of cocatalyst **B**.

Activation of La[N(SiMe$_3$)$_2$](HAl*i*Bu$_3$)(Al*i*Bu$_4$) (1^{La}) with B(C$_6$F$_5$)$_3$ (C)

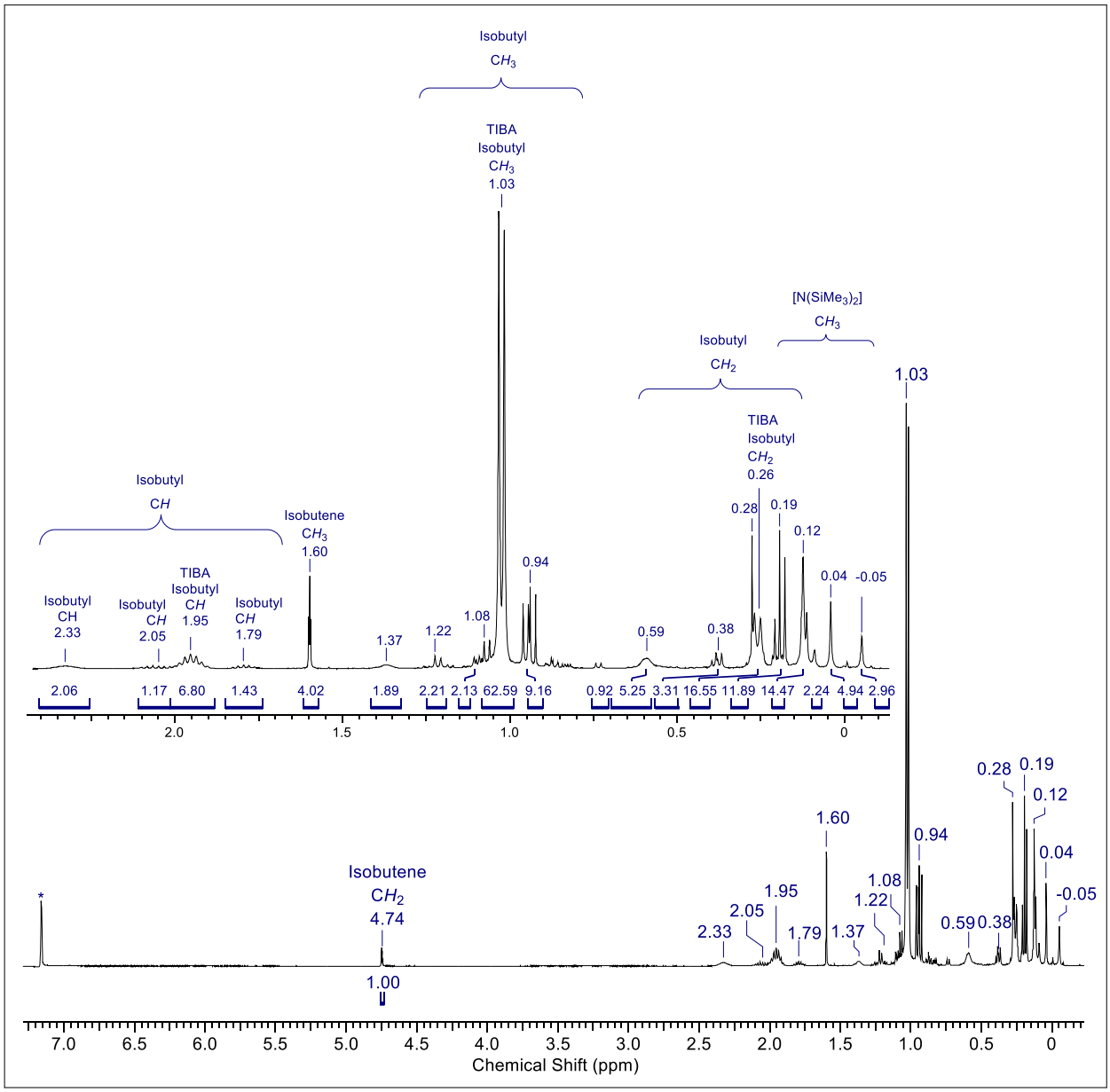

Figure 5. ^{1}H-NMR spectrum (400 MHz, C_6D_6, 26 °C) of the activation of **1^{La}** with one equivalent of cocatalyst **C** in C_6D_6.

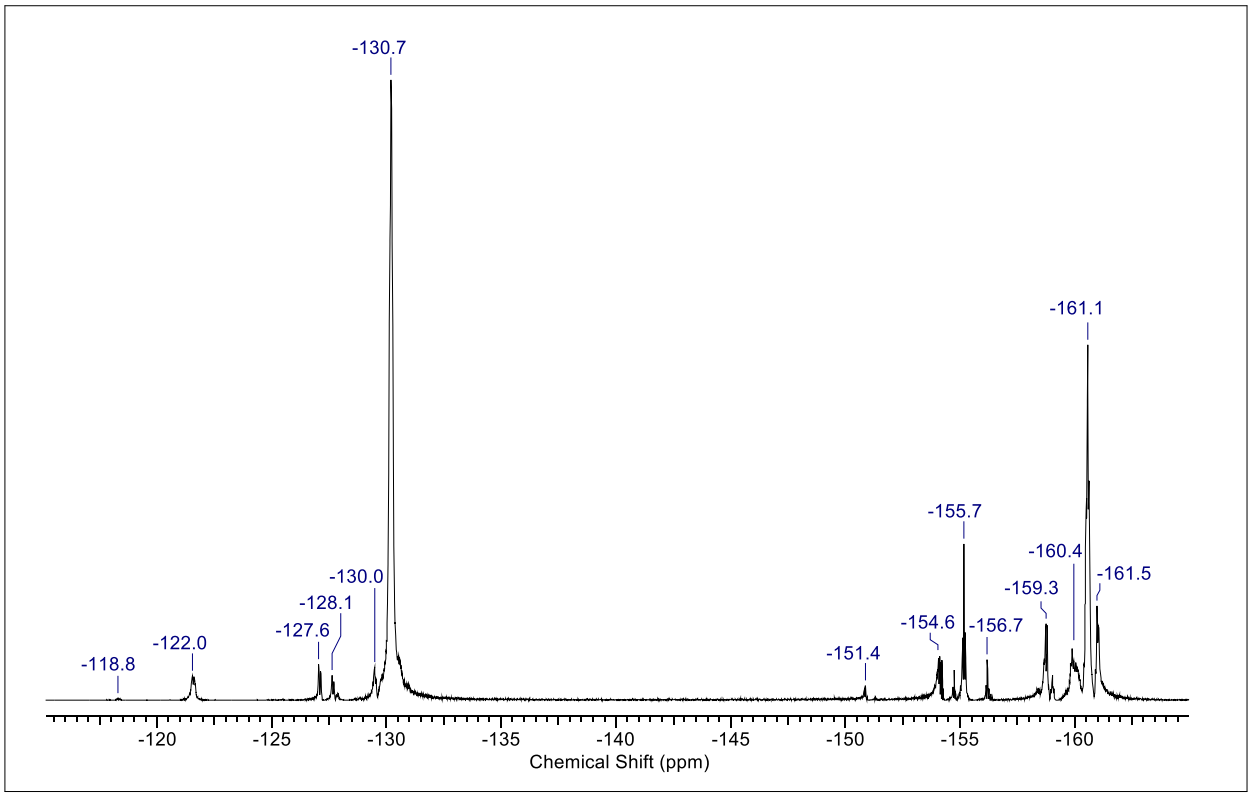

Figure 6. ^{19}F-NMR spectrum (400 MHz, C_6D_6, 26 °C) of the activation of **1**^{La} with one equivalent of cocatalyst **C**.

Activation of La[N(SiMe$_3$)$_2$](HAl*i*Bu$_3$)(Al*i*Bu$_4$) (1^{La}) with *i*Bu$_2$AlCl (F)

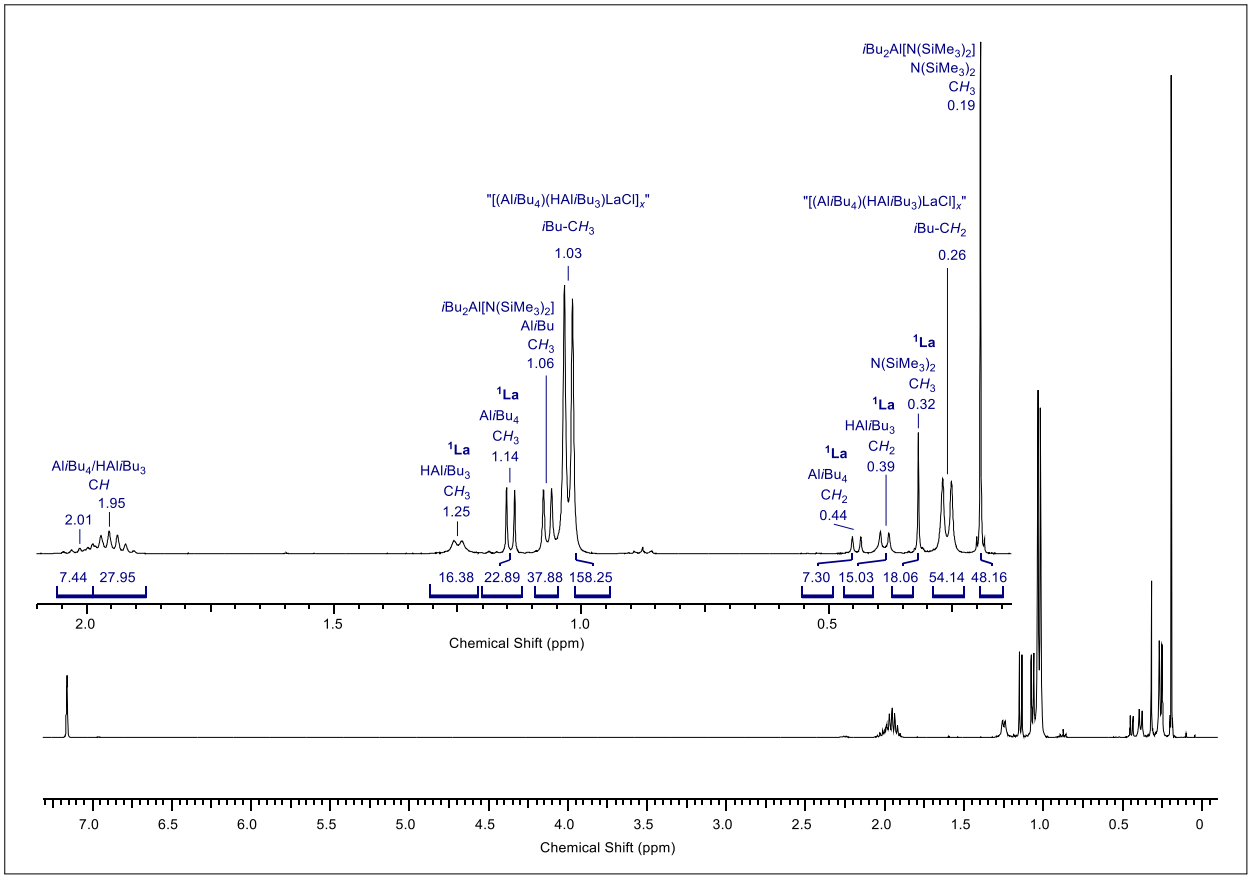

Figure 7. ^{1}H-NMR spectrum (400 MHz, C_6D_6, 26 °C) of the activation of **1^{La}** with one equivalent of cocatalyst **F**.

Crystallography

X-ray Crystallography and Crystal Structure Determination

For X-ray structure analyses, single crystals suitable for X-ray diffraction were selected in a glovebox, coated with Parabar 10312 (Hampton Research), and fixed on a nylon/ glass fiber loop. X-ray data for all compounds were collected on a Bruker APEX II DUO diffractometer equipped with an IμS microfocus sealed tube and QUAZAR optics for MoK_α (λ = 0.71073 Å). The data collection strategy was determined using COSMO, [1] employing ω-scans. Raw data were processed using APEX[2], and SAINT[2]. Corrections for absorption effects were applied using SADABS. [3] The structures were solved by direct methods and refined against all data by full-matrix least-squares methods on F^2 using SHELXTL[4], and SHELXLE. [5] Disorder models were calculated using (RIGU/SIMU) restrains. All graphics were produced employing Mercury 4.2.011[6] and POV-Ray12.[7]

For X-ray crystallography, single crystals of $\mathbf{1^{Gd}}$ were grown from saturated solutions in *n*-pentane at –40 °C. Single crystals of **2** suitable for X-ray crystallography were grown from *o*-difluorobenzene at –40 °C.

Table S1. Crystallographic Data for Compounds **1^{Gd}** and **2**

	1^{Gd}	**2**
formula	$C_{34}H_{82}Al_2GdNSi_2$	$C_{79}H_{46}B_2F_{43}N_3NdSi_2$
CCDC	2261600	2261599
M [g mol^{-1}]	772.39	2076.23
color/shape	colorless/column	pale green/plate
Crystal dimensions [mm]	0.143 x 0.137 x 0.101	0.227 x 0.138 x 0.035
cryst. system	triclinic	monoclinic
space group	$P\bar{1}$	$P2_1/c$
a [Å]	9.4526(4)	22.3405(13)
b [Å]	11.3615(4)	14.2454(9)
c [Å]	20.6916(8)	24.7367(15)
α [°]	95.3900(10)	90
β [°]	101.3940(10)	96.7684(16)
γ [°]	91.6540(10)	90
V [Å^3]	2166.20(15)	7817.6(8)
Z	2	4
T [K]	100(2)	100(2)
ρ_{calcd} [Mg m^{-3}]	1.184	1.764
μ [mm^{-1}]	1.647	0.846
F (000)	822	4104
θ range [°]	1.802/30.528	1.652/24.755
unique reflns	13242	12054
observed reflns	103983	77888
R1[b]/wR2 (I>2σ)[c]	0.0232/0.0532	0.0447/0.0758
R1[b]/wR2 (all data)[c]	0.0262/0.0548	0.0919/0.0870
GOF[a]	1.063	0.0825

[a]GOF = $[\Sigma w(F_0^2 - F_c^2)^2 / (n_0 - n_p)]^{1/2}$. [b]$R_1 = \Sigma(||F_0| - |F_c||) / \Sigma|F_0|$, $F_0 > 4\sigma(F_0)$. [c]$wR_2 = \{\Sigma[w(F_0^2 - F_c^2)^2 / \Sigma[w(F_0^2)^2]\}^{1/2}$.

Gd[N(SiMe$_3$)$_2$](HAl*i*Bu$_3$)(Al*i*Bu$_4$) (1^{Gd})

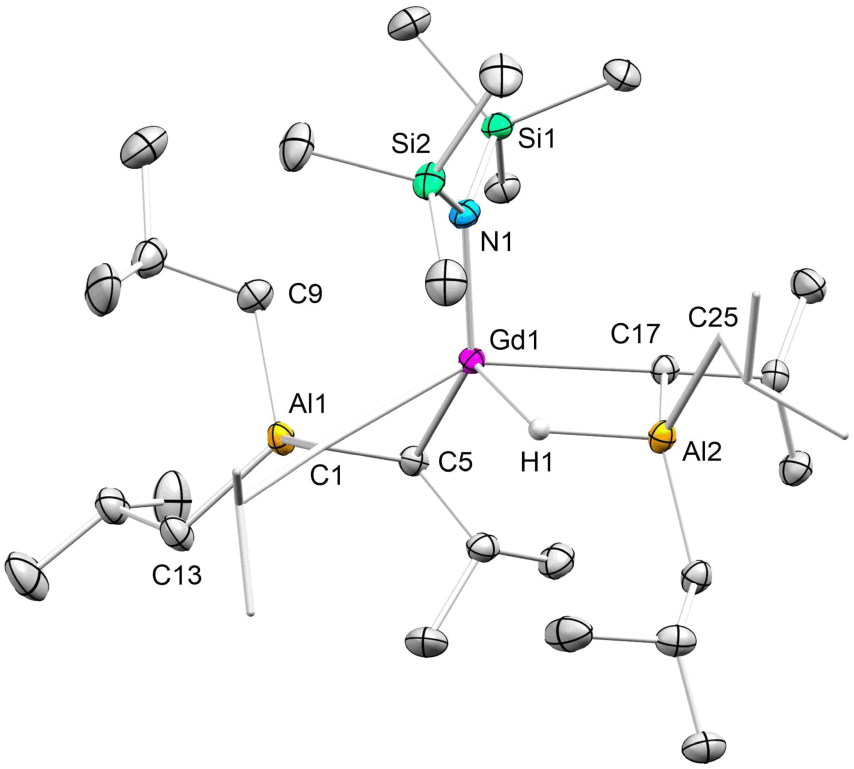

Figure 8. Crystal structure of **1^{Gd}**. Hydrogen atoms except the bridging hydride are omitted for clarity; two isobutyl moieties are displayed as capped sticks. Atomic displacement ellipsoids were set at 50% probability. Selected interatomic distances [Å] and angles [°]: Gd(1)–C(1) 2.5793(16), Gd(1)–C(5) 2.6392(16), Gd(1)···C(9) 3.403(2), Gd(1)–C(17) 2.6806(15), Al(1)–C(1) 2.1065(17), Al(1)–C(5) 2.1079(16), Al(1)–C(9) 2.0125(17), Al(2)–C(17) 2.0687(16), Al(2)–H(1) 1.698(18), Gd(1)–N(1) 2.1867(13), Al(1)···Gd(1) 3.0148(5), Al(2)···Gd(1) 3.1362(5), Gd(1)–H(1) 2.077(18), C(1)-Al(1)-Gd(1) 57.23(4), C(5)-Al(1)-Gd(1) 58.89(4), C(9)-Al(1)-Gd(1) 82.61(5), Al(2)-C(17)-Gd(1) 81.55(5), C(17)-Al(2)-Gd(1) 57.72(4), Gd(1)-Al(2)-H(1) 37.9(6), N(1)-Gd(1)-C(1) 103.96(5), N(1)-Gd(1)-C(5) 141.10(5), N(1)-Gd(1)-C(17) 98.83(5), N(1)-Gd(1)-Al(1) 115.26(3), C(1)-Gd(1)-Al(1) 43.37(4), C(5)-Gd(1)-Al(1) 43.14(4), C(17)-Gd(1)-Al(1) 140.82(3), N(1)-Gd(1)-Al(1) 115.26(3), N(1)-Gd(1)-Al(2) 99.54(3), N(1)-Gd(1)-H(1) 97.5(5), Gd(1)-N(1)-Si(1) 111.09(7), Gd(1)-N(1)-Si(2) 127.82(7).

Nd[N(SiMe$_3$)$_2$](N,N-dimethylaniline)$_2$[B(C$_6$F$_5$)$_4$]$_2$ (2)

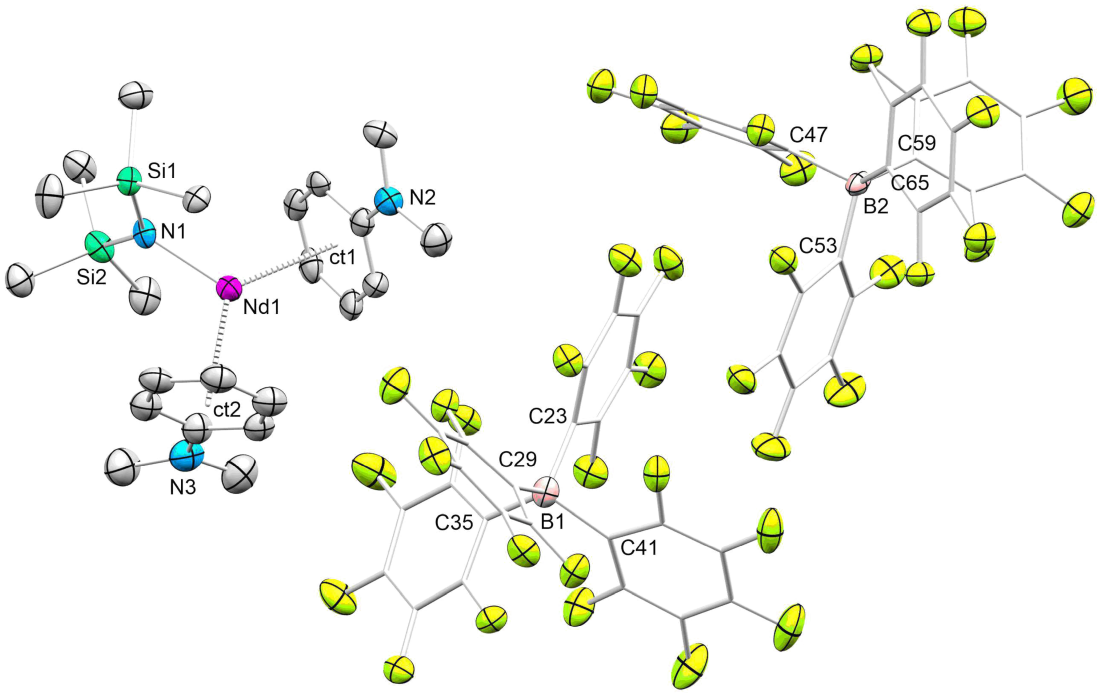

Figure 9: Crystal structure of **2**. Hydrogen atoms are omitted for clarity; carbon atoms of the borate anions are displayed as capped sticks. Atomic displacement ellipsoids were set at 50% probability. Selected interatomic distances [Å] and angles [°]: Nd(1)–N(1) 2.140(3), Nd(1)···N(2) 4.045, Nd(1)···N(3) 3.900, Nd(1)···Ct(1) 2.611, Nd(1)···Ct(2) 2.614, B(1)–C(23) 1.656(7), B(1)–C(29) 1.657(7), B(1)–C(35) 1.647(7), B(1)–C(41) 1.633(7), B(2)–C(47) 1.656(7), B(2)–C(53) 1.640(7), B(2)–C(59) 1.651(8), B(2)–C(65) 1.652(7), N(1)-Nd(1)-centroid(1) 116.37, N(1)-Nd(1)-centroid(2) 114.70, centroid(1)-Nd(1)-centroid(2) 127.61, Nd(1)-N(1)-Si(1) 111.06(18), Gd(1)-N(1)-Si(2) 120.2(2).

Polymer Analysis

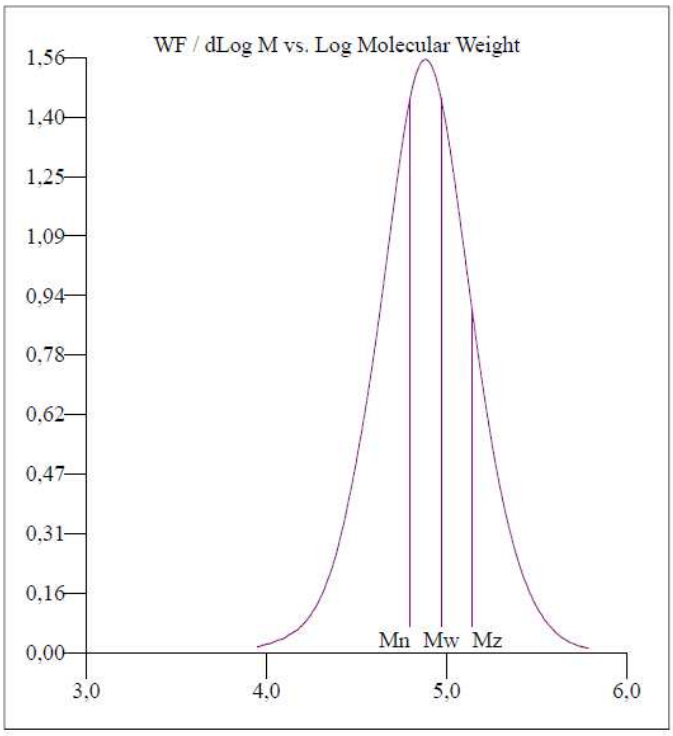

Molecular weight distribution plot for polymer obtained from **1Nd/A** (Table 1, entry 2).

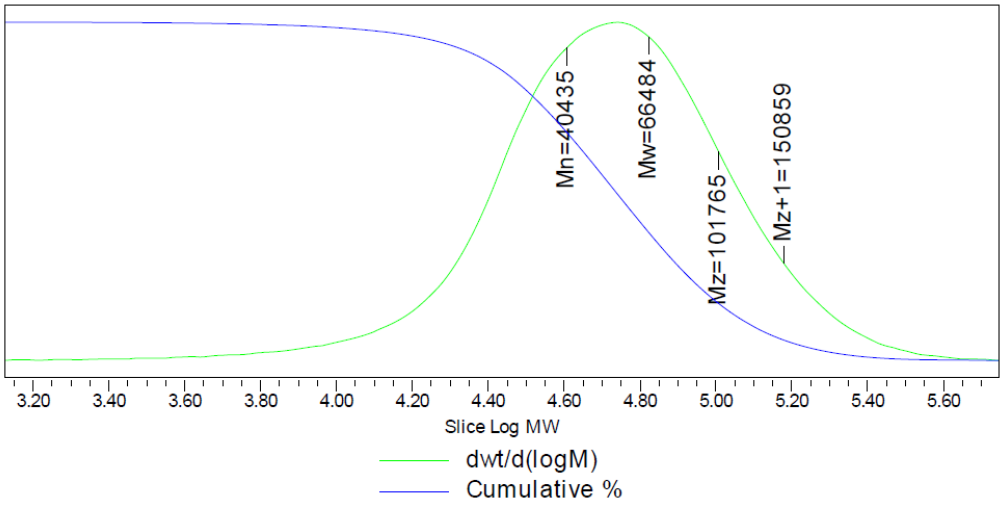

Molecular weight distribution plot for polymer obtained from **1Nd/B** (Table 1, entry 3).

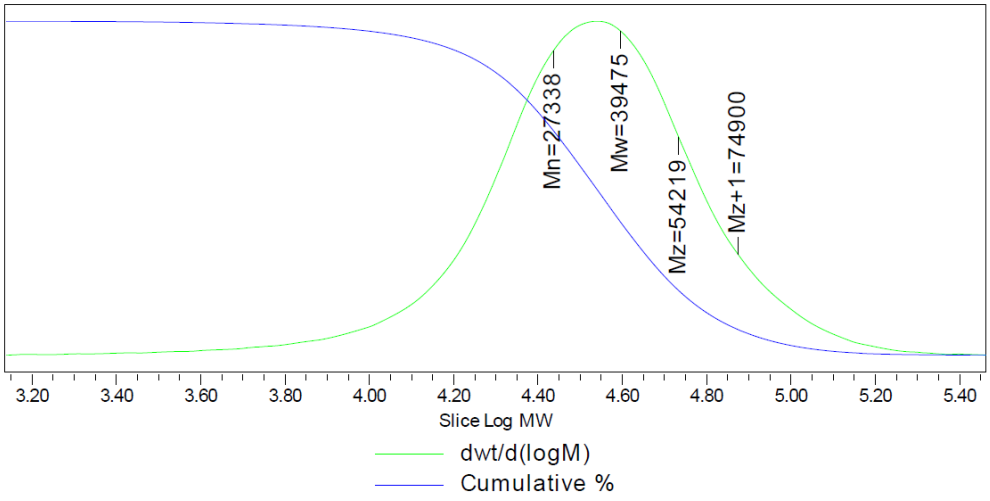

Molecular weight distribution plot for polymer obtained from **1Nd/B** (Table 1, entry 4).

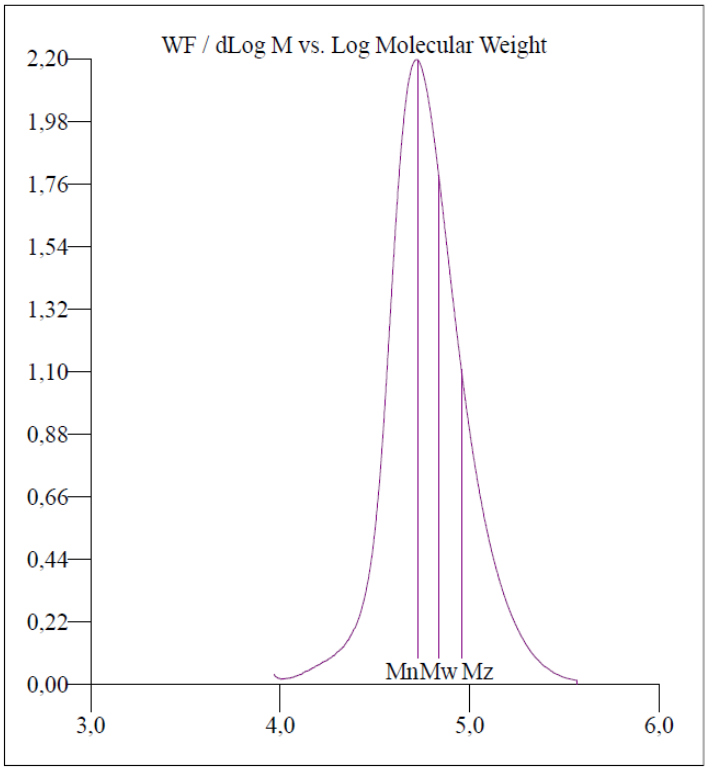

Molecular weight distribution plot for polymer obtained from **1Nd/B** (Table 1, entry 5).

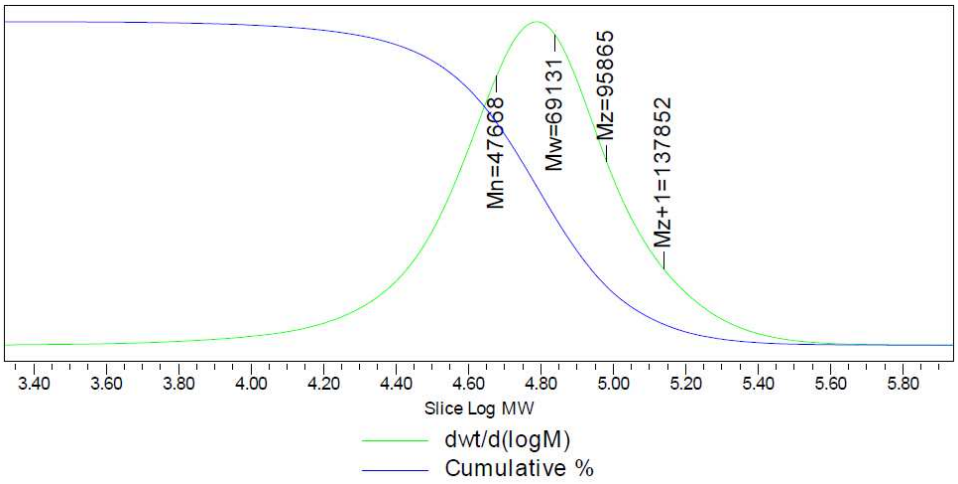

Molecular weight distribution plot for polymer obtained from **1Nd/B** (Table 1, entry 6).

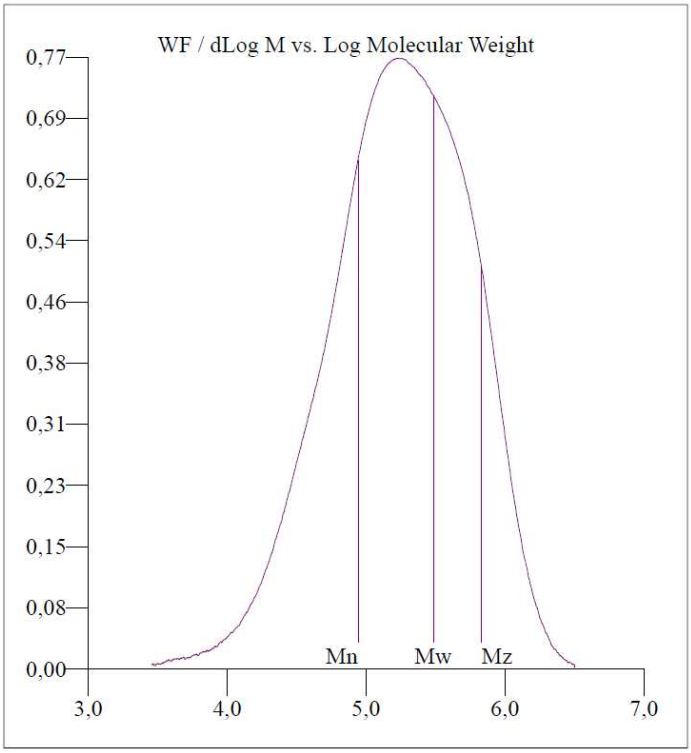

Molecular weight distribution plot for polymer obtained from **1Nd/C** (Table 1, entry 7)

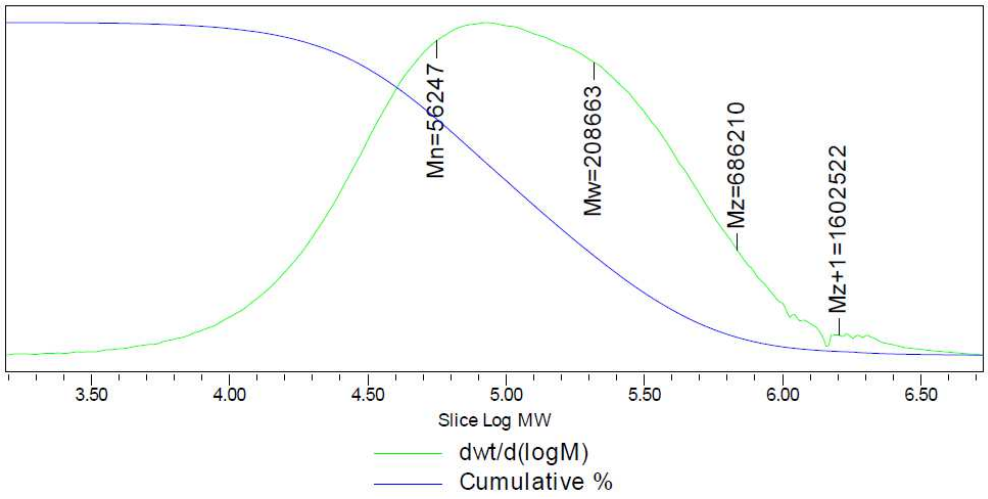

Molecular weight distribution plot for polymer obtained from **1Nd/D** (Table 1, entry 8).

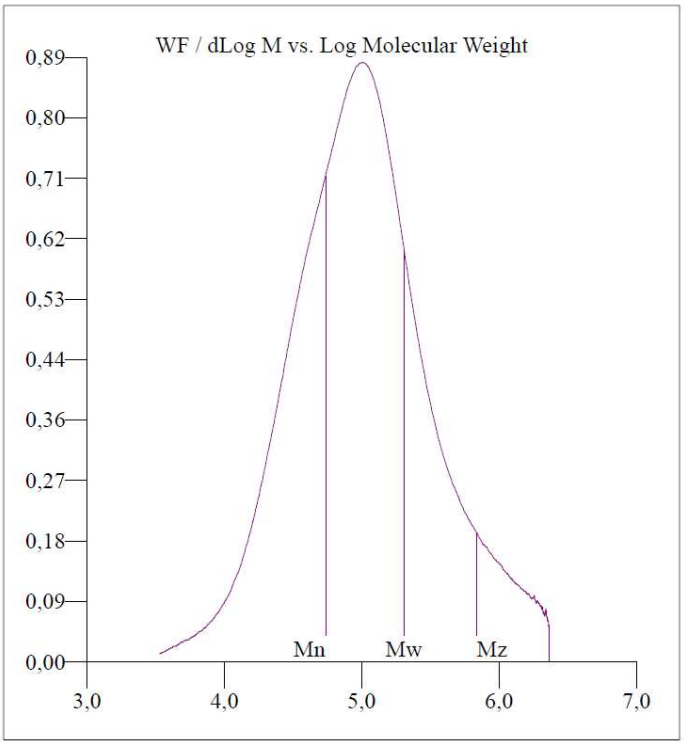

Molecular weight distribution plot for polymer obtained from **1Nd/D** (Table 1, entry 9)

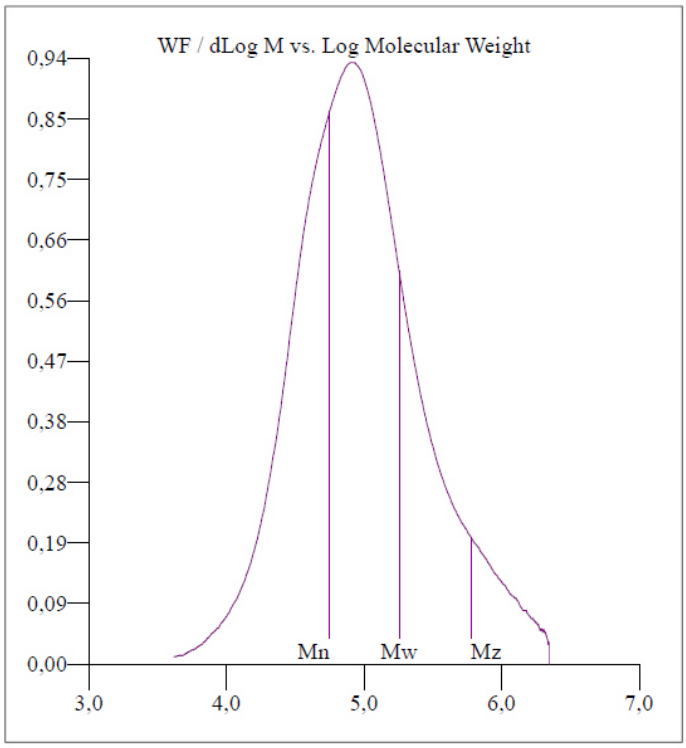

Molecular weight distribution plot for polymer obtained from **1**Nd**/E** (Table 1, entry 10)

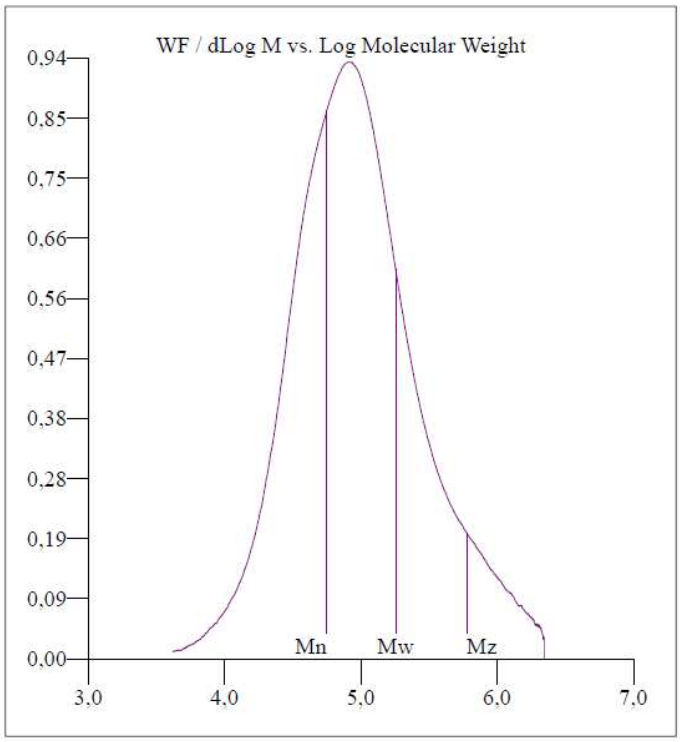

Molecular weight distribution plot for polymer obtained from **1**Nd**/E** (Table 1, entry 12).

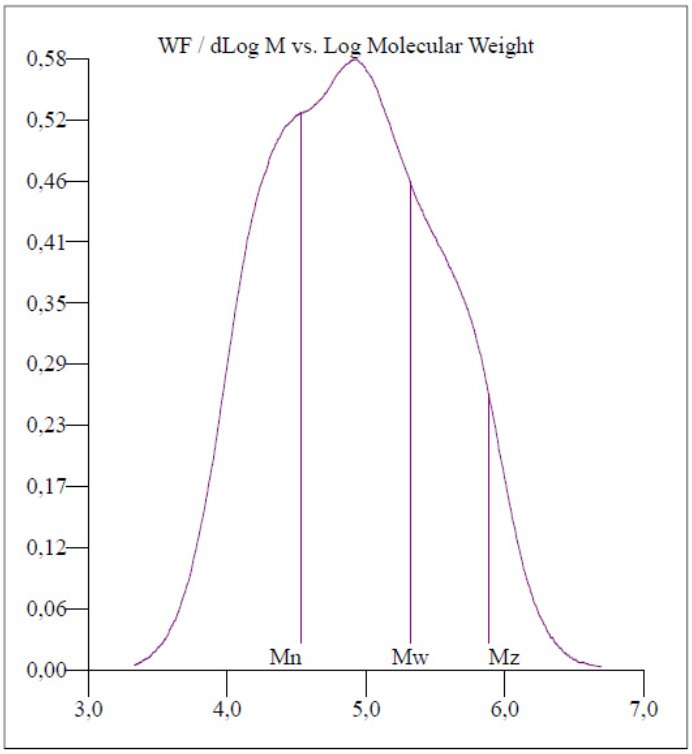

Molecular weight distribution plot for polymer obtained from **1Nd/2E** (Table 1, entry 13).

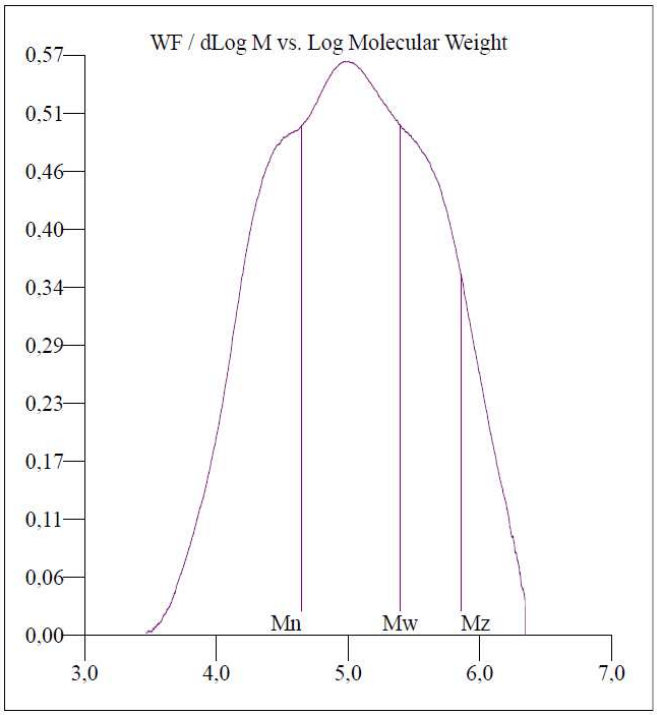

Molecular weight distribution plot for polymer obtained from **1Nd/2E** (Table 1, entry 14).

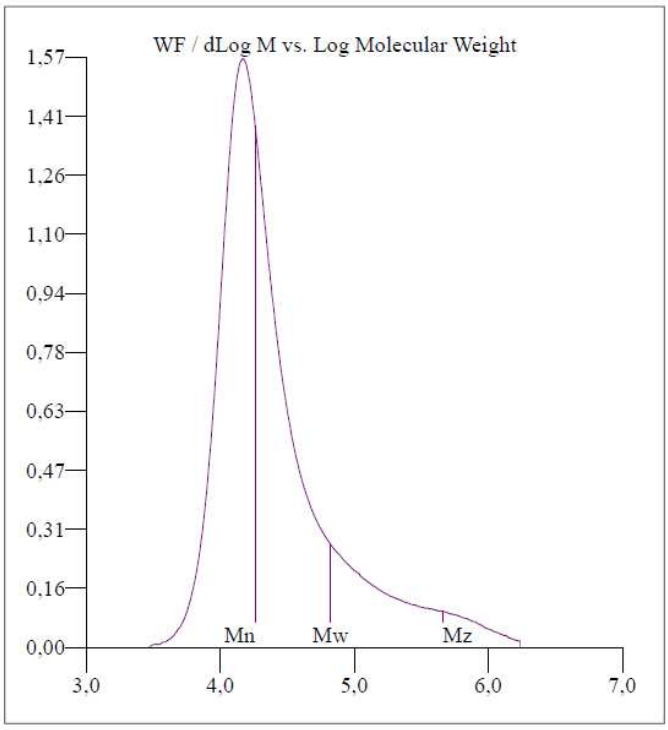

Molecular weight distribution plot for polymer obtained from **1^{Nd}/3E** (Table 1, entry 15).

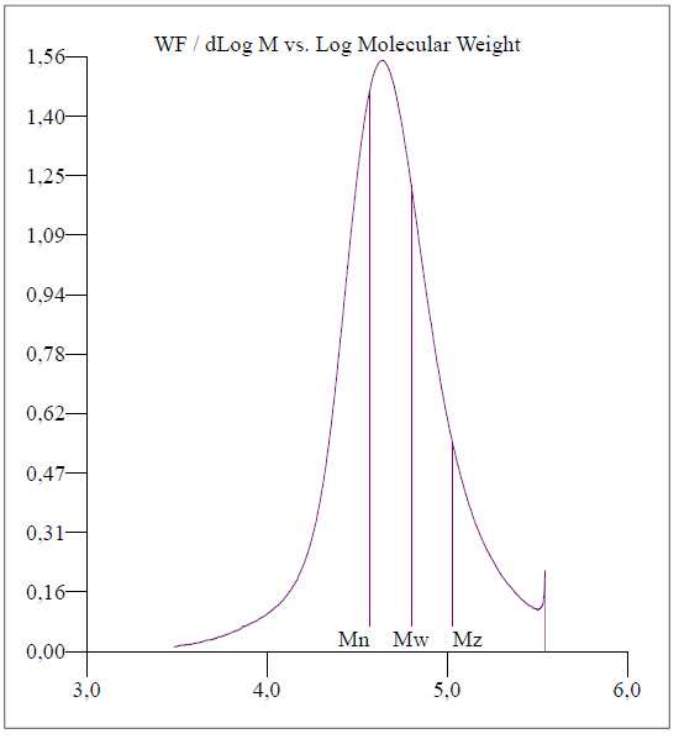

Molecular weight distribution plot for polymer obtained from **1^{Nd}/A** (Table 1, entry 17).

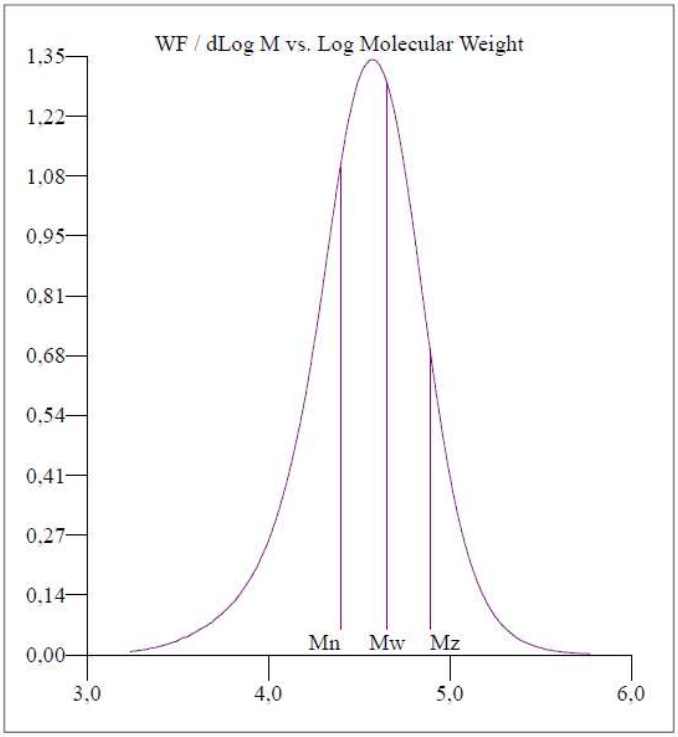

Molecular weight distribution plot for polymer obtained from **1Nd/B** (Table 1, entry 18).

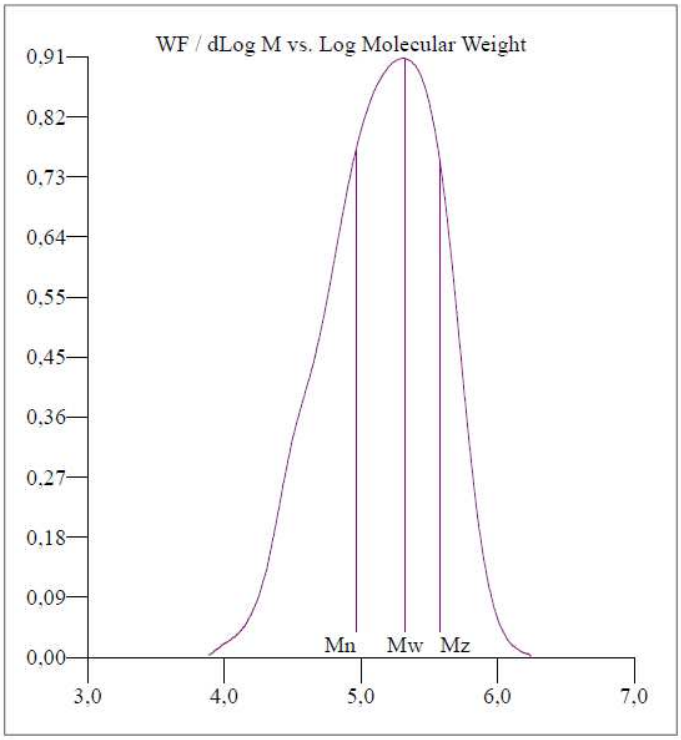

Molecular weight distribution plot for polymer obtained from **1Nd/C** (Table 1, entry 19).

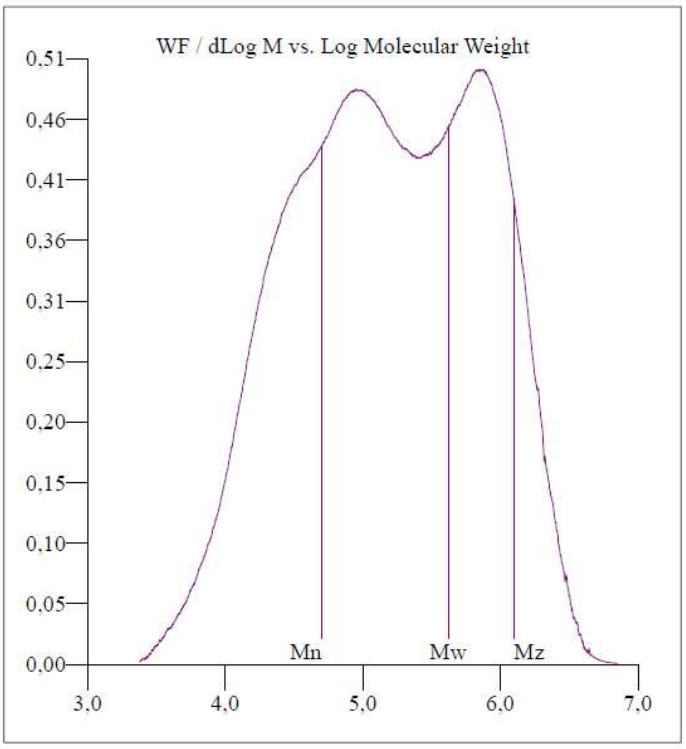

Molecular weight distribution plot for polymer obtained from **1Nd/D** (Table 1, entry 20).

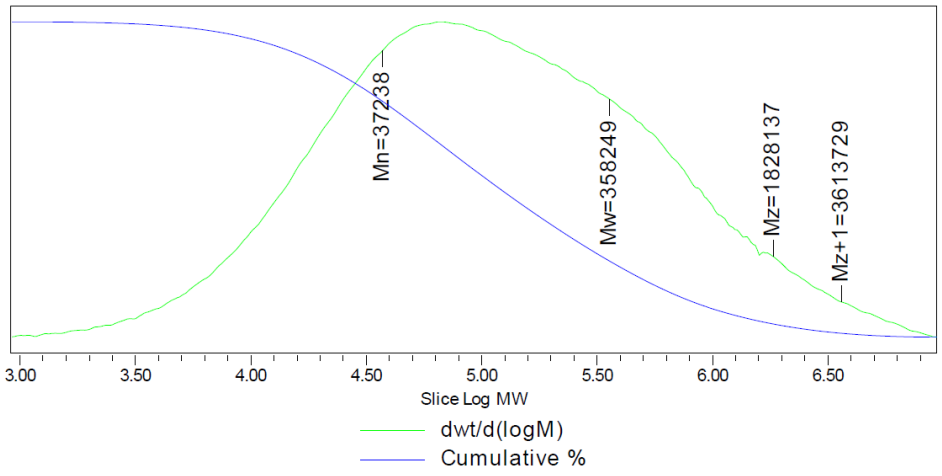

Molecular weight distribution plot for polymer obtained from **1Nd/D** (Table 1, entry 21).

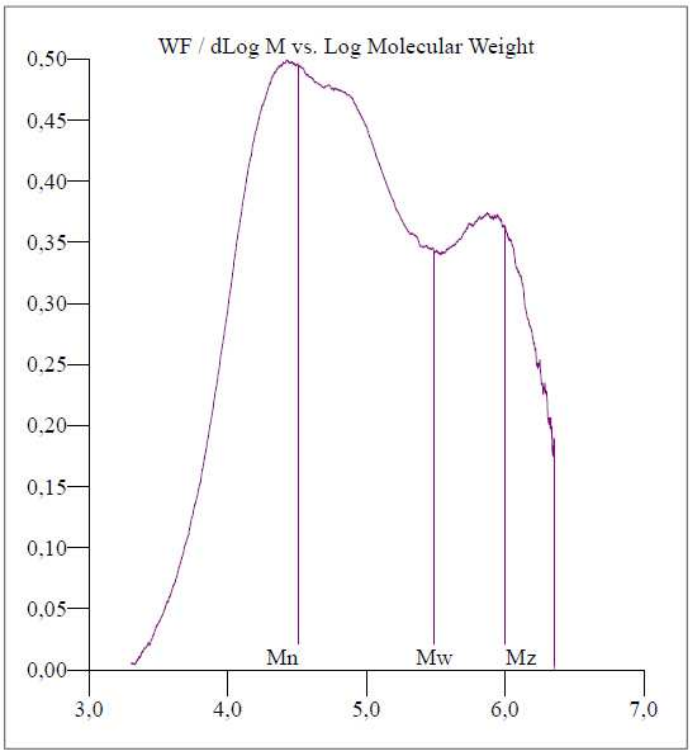

Molecular weight distribution plot for polymer obtained from **1**Nd**/E** (Table 1, entry 22).

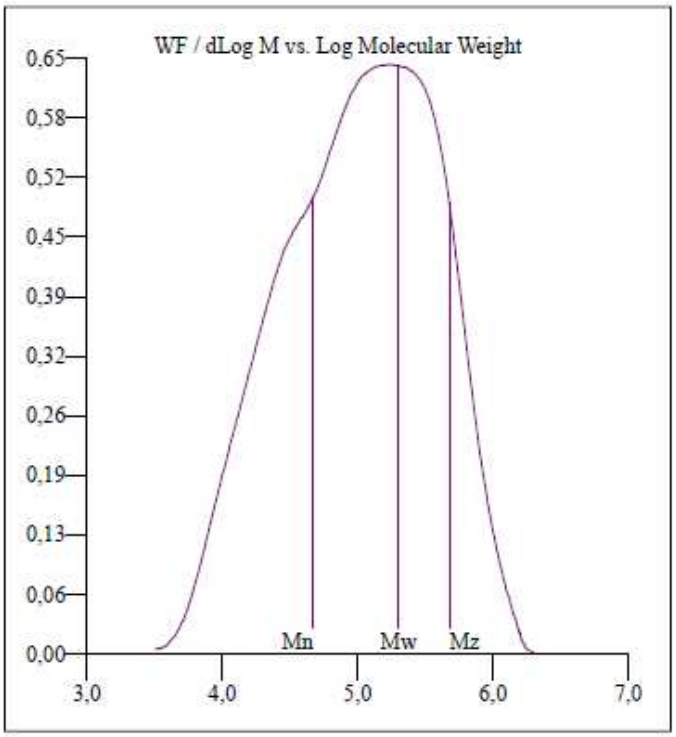

Molecular weight distribution plot for polymer obtained from **1**Nd/2**E** (Table 1, entry 24).

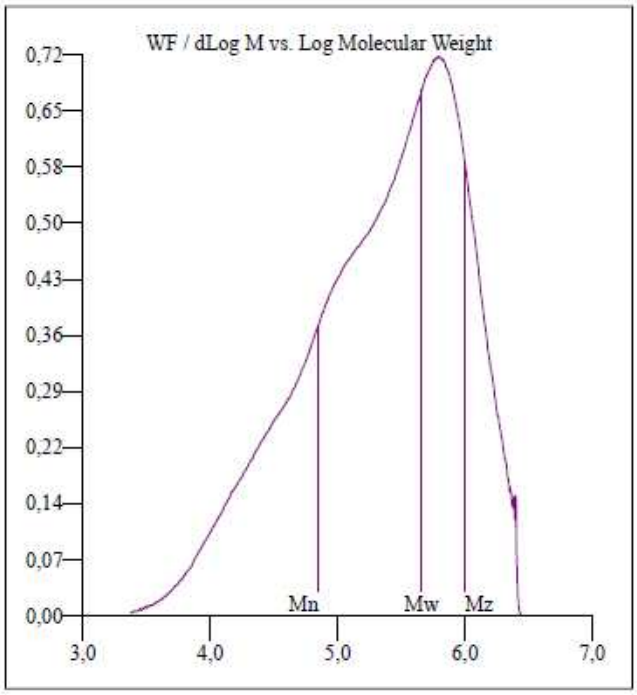

Molecular weight distribution plot for polymer obtained from **1**Nd/3**E** (Table 1, entry 26).

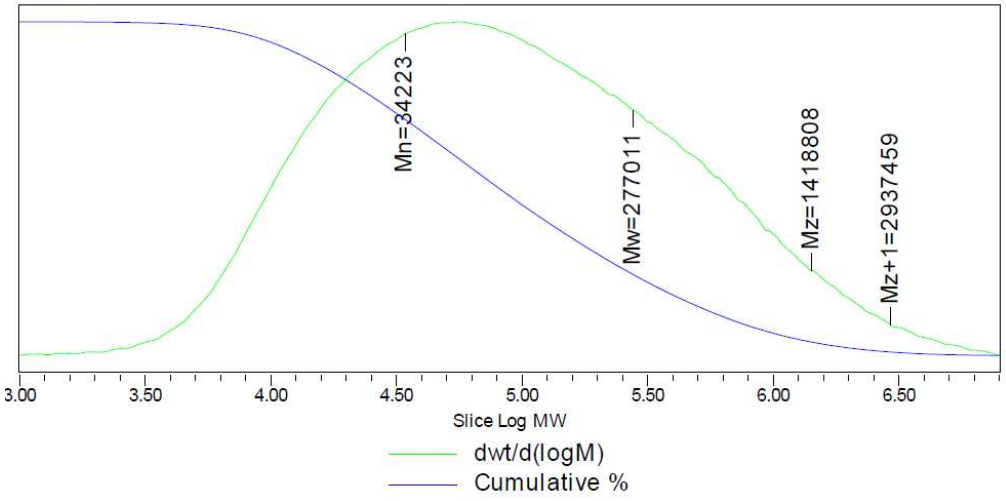

Molecular weight distribution plot for polymer obtained from **1**Nd/3**E** (Table 1, entry 27).

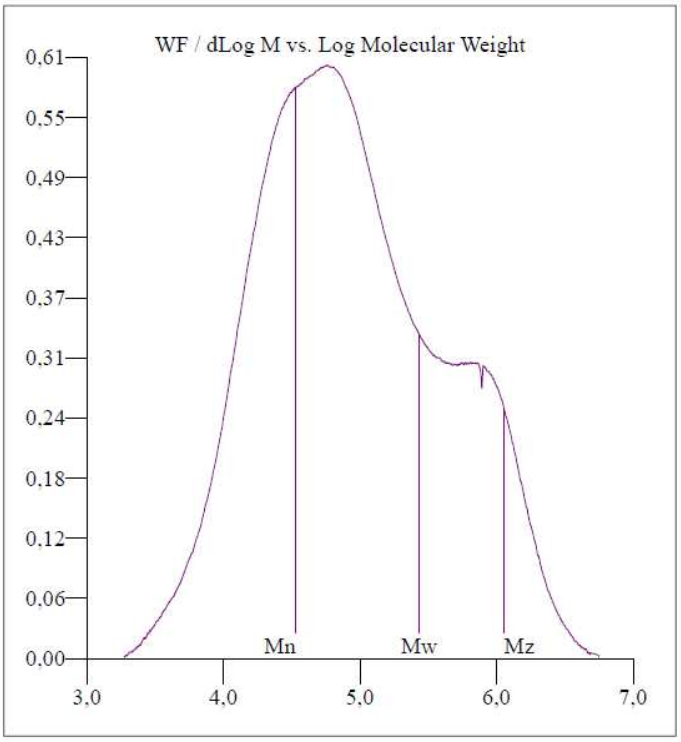

Molecular weight distribution plot for polymer obtained from **1**Nd**/F** (Table 1, entry 28).

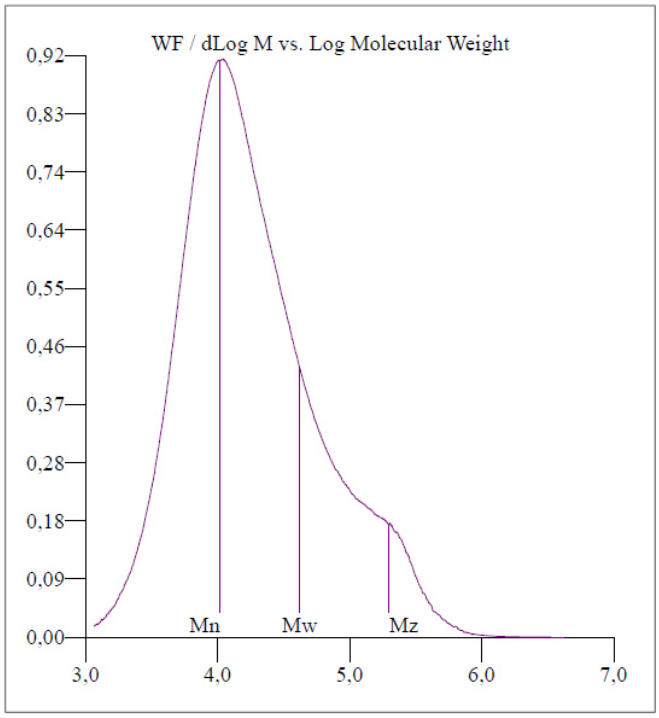

Molecular weight distribution plot for polymer obtained from **1**^{La}**/F** (Table 1, entry 29).

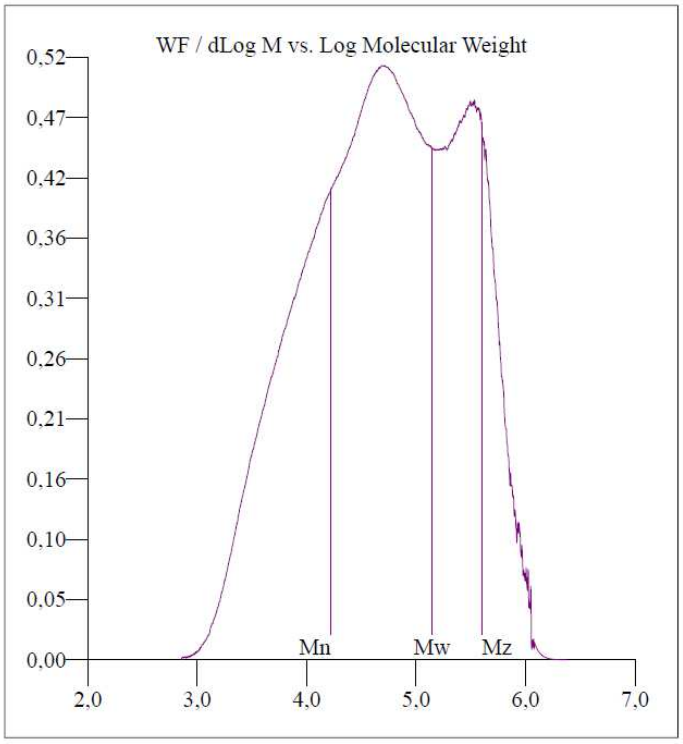

Molecular weight distribution plot for polymer obtained from **1**^{La}/2**F** (Table 1, entry 30).

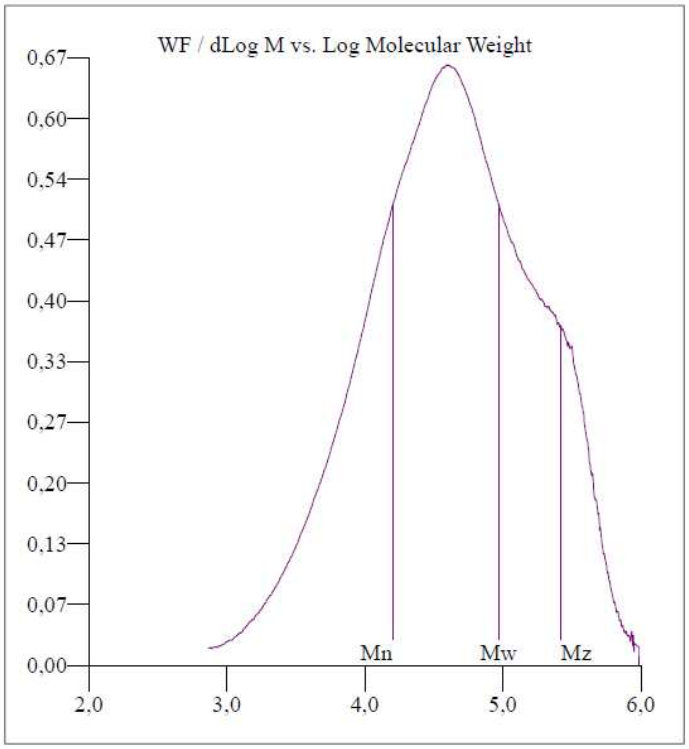

Molecular weight distribution plot for polymer obtained from **1**^{Pr}/**F** (Table 1, entry 31).

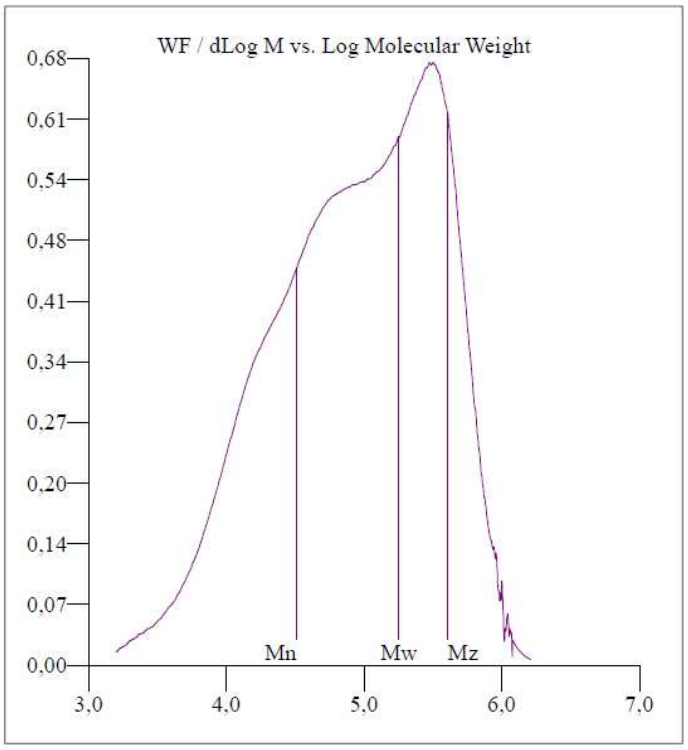

Molecular weight distribution plot for polymer obtained from **1**^{Pr}/2**F** (Table 1, entry 32).

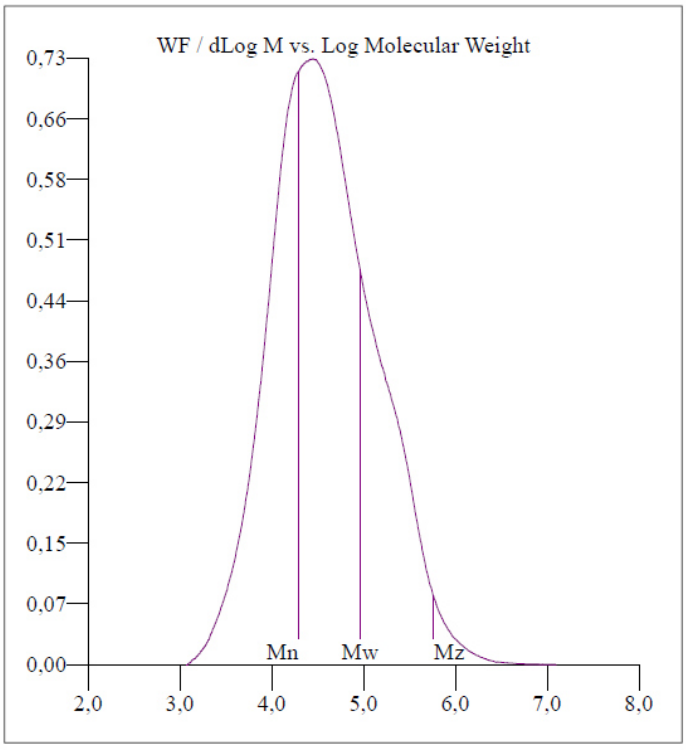

Molecular weight distribution plot for polymer obtained from **1**Nd/**F** (Table 1, entry 33).

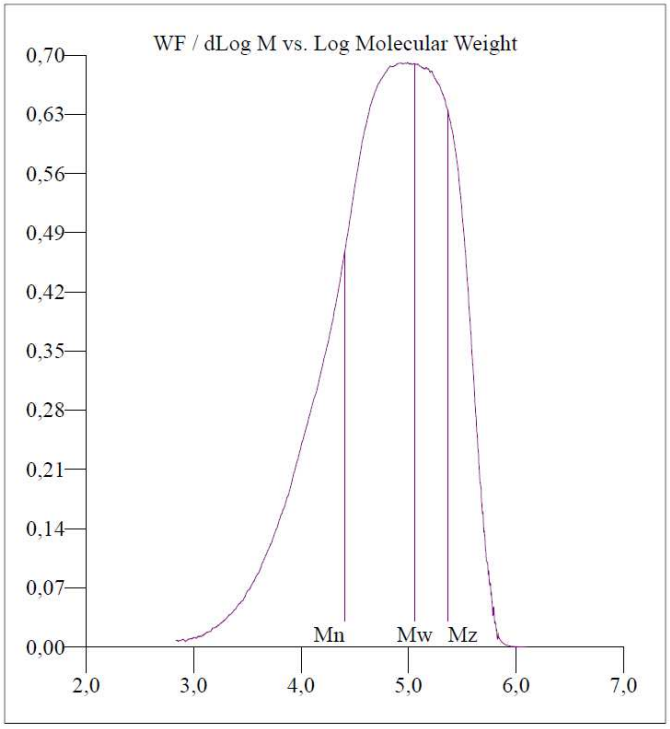

Molecular weight distribution plot for polymer obtained from **1**Nd/2**F** (Table 1, entry 34).

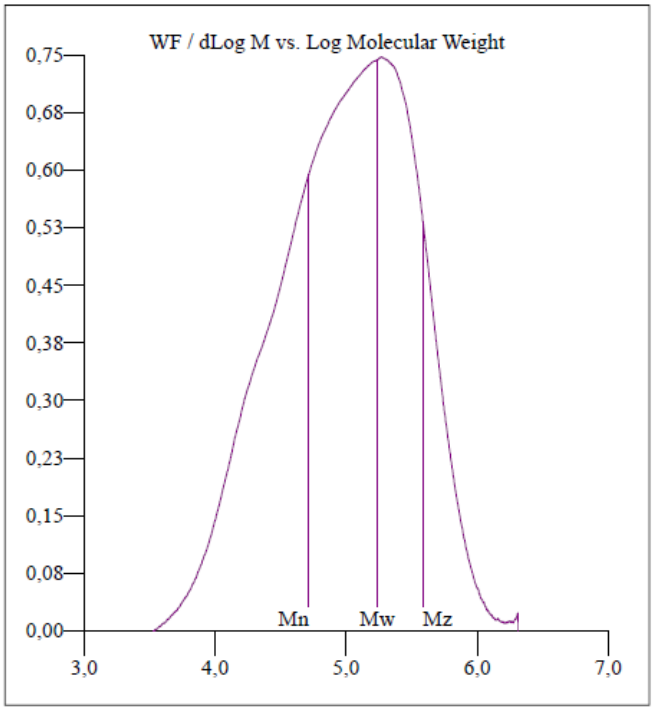

Molecular weight distribution plot for polymer obtained from **1**Nd/2**F** (Table 1, entry 35).

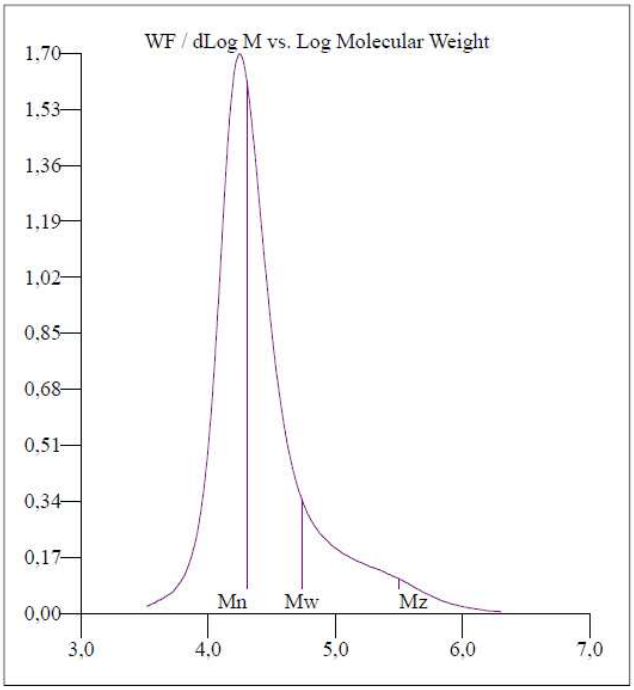

Molecular weight distribution plot for polymer obtained from **1**Nd/3**F** (Table 1, entry 36).

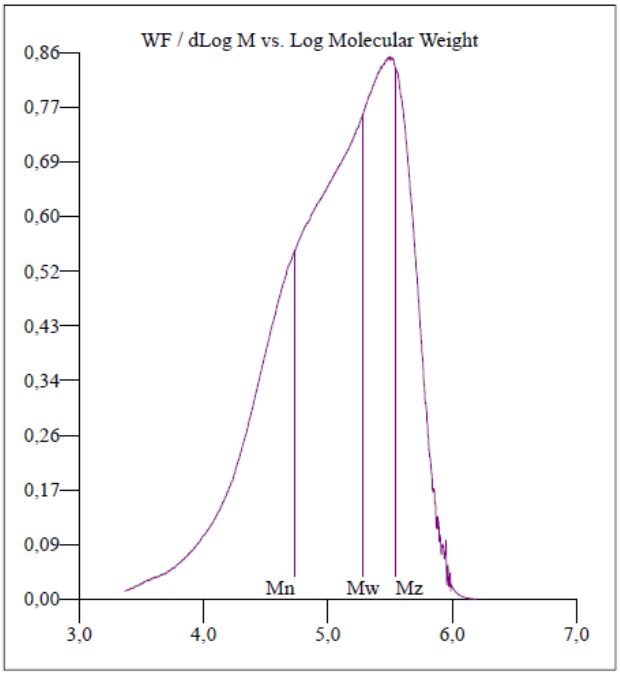

Molecular weight distribution plot for polymer obtained from **1**^{Gd}/**F** (Table 1, entry 37).

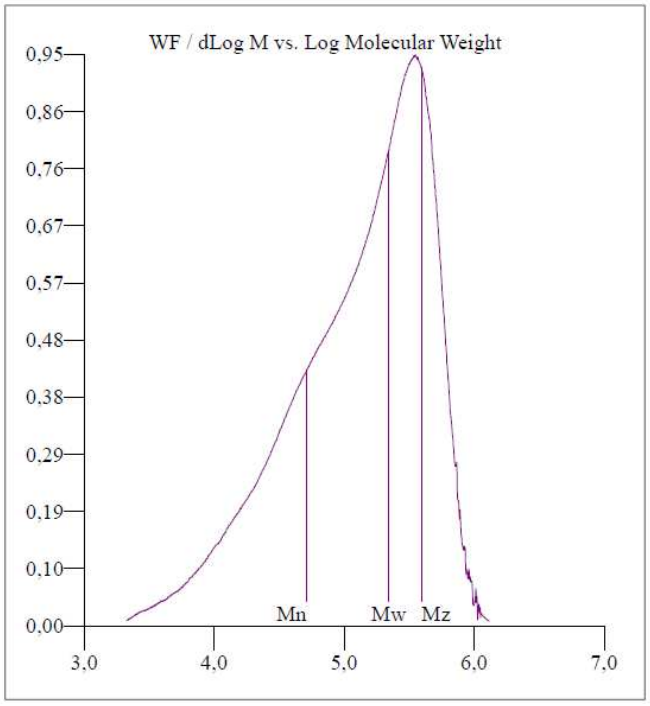

Molecular weight distribution plot for polymer obtained from **1**^{Gd}/2**F** (Table 1, entry 38).

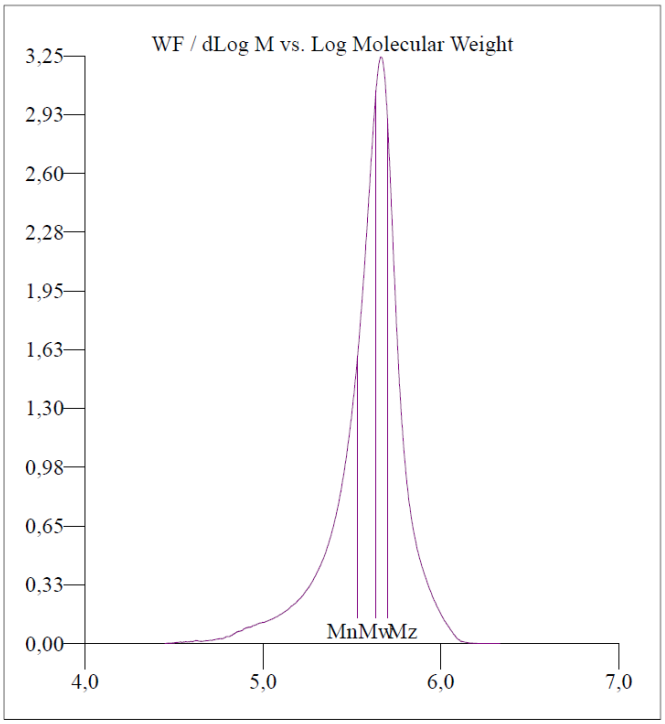

Molecular weight distribution plot for polymer obtained from **2**Nd (Table 1, entry 39).

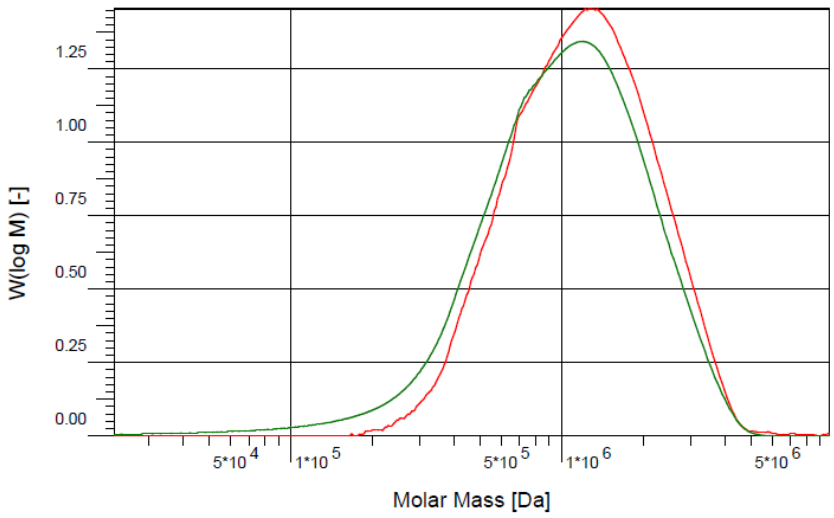

Molecular weight distribution plot for polymer obtained from **2**Nd (Table 1, entry 40).

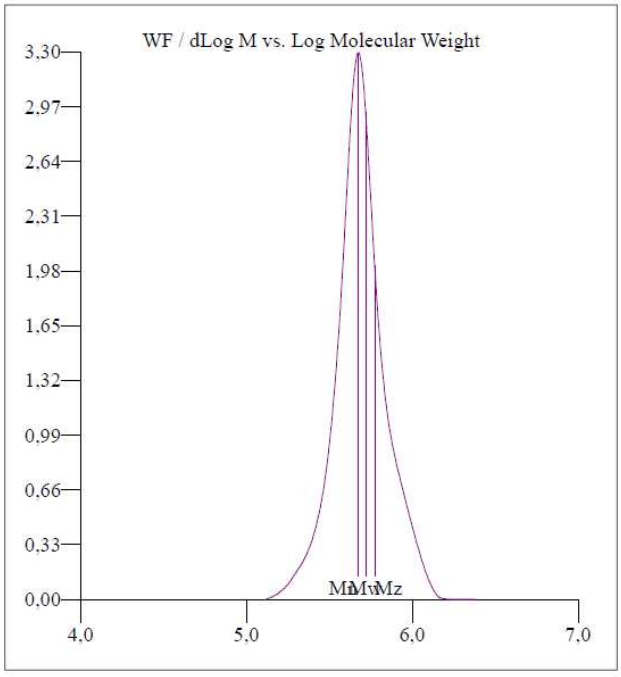

Molecular weight distribution plot for polymer obtained from **2**Nd (Table 1, entry 41).

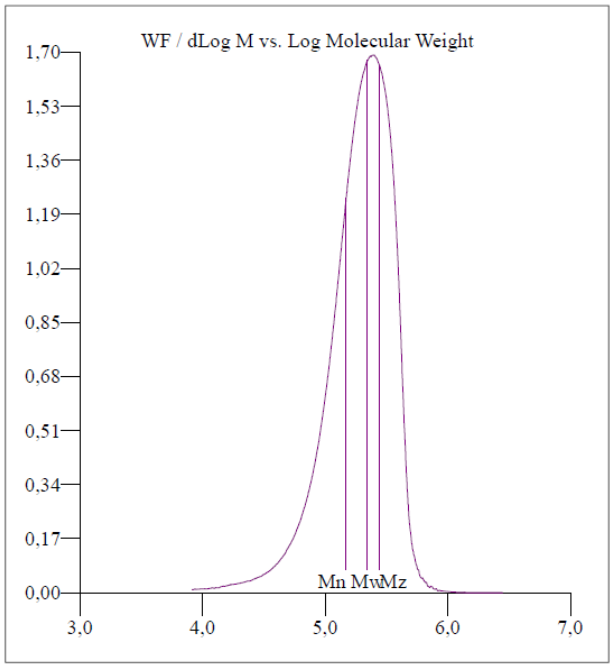

Molecular weight distribution plot for polymer obtained from **2**Nd/2 TIBA (Table 1, entry 42).

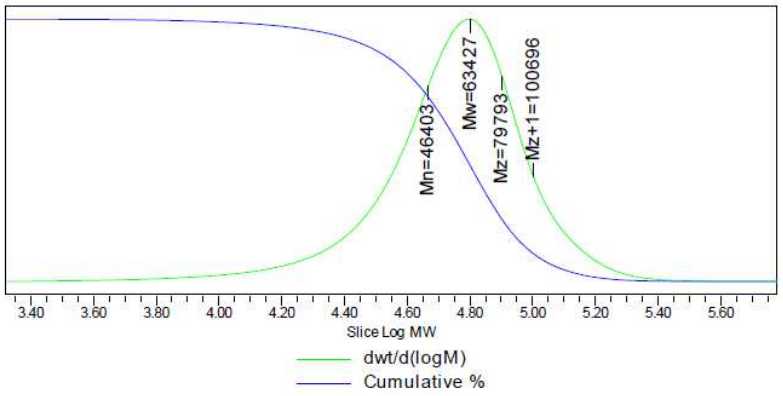

Molecular weight distribution plot for polymer obtained from **1**Nd/**2**Nd (Table 1, entry 43).

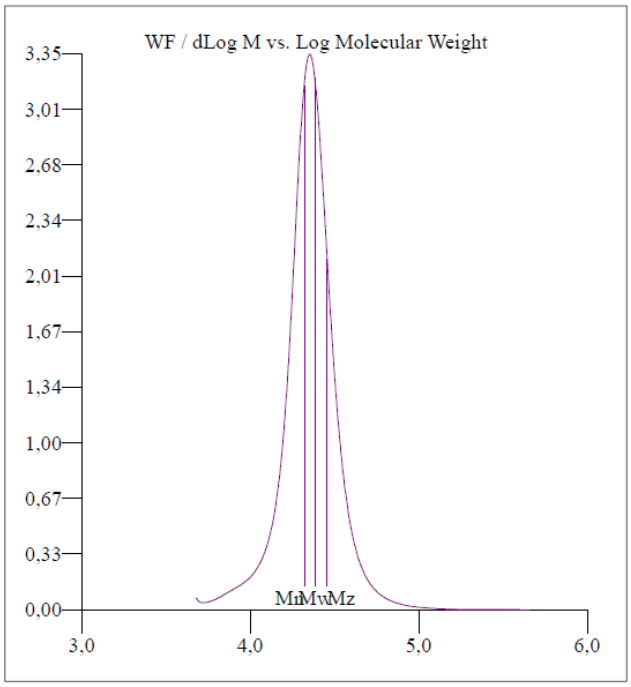

Molecular weight distribution plot for polymer obtained from **1**Nd/**2**Nd (Table 1, entry 44).

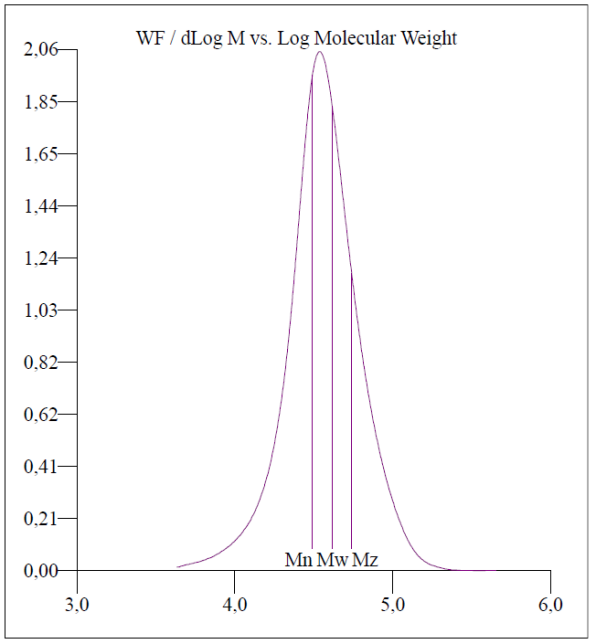

Molecular weight distribution plot for polymer obtained from **1**Nd/2**B** (Table 1, entry 45).

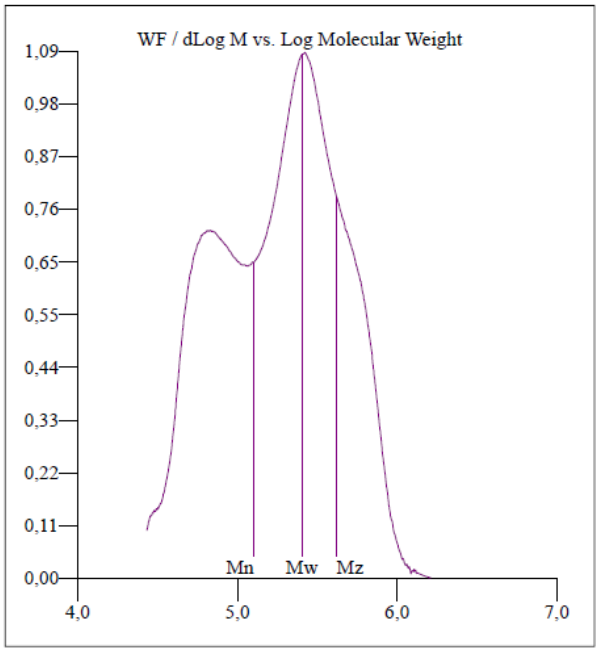

Molecular weight distribution plot for polymer obtained from **1**Nd/2**B** (Table 1, entry 46).

References

(1) COSMO v. 1.61, Bruker AXS Inc., Madison, WI., **2012**.

(2) APEX 3 v. 2017.3-0, Bruker AXS Inc., Madison, WI., **2017**.

(3) Krause, L.; Herbst-Irmer, R.; Sheldrick, G. M.; Stalke, D. Comparison of silver and molybdenum microfocus X-ray sources for single-crystal structure determination. *J. Appl. Crystallogr.* **2015**, *48*, 3-10.

(4) Sheldrick, G. Integrated space-group and crystal-structure determination. *Acta Crystallogr. Sect. C.* **2015**, *71*, 3-8.

(5) Hübschle, C. B.; Sheldrick, G. M.; Dittrich, B. ShelXle: a Qt graphical user interface for ShelXle. *J. Appl. Crystallogr.* **2011**, 44, 1281-1284.

(6) Macrae, C. F.; Edgington, P. R.; McCabe, P.; Pidcock, E.; Shields, G. P.; Taylor, R.; Towler, M.; J. van de Streek. Mercury: visualization and analysis of crystal structures. *J. Appl. Crystallogr.* **2006**, *39*, 453-457.

(7) POV-Ray v. 3.6, Persistence of Vision Pty. Ltd., Williamstown, Victoria, Australia, **2004**. http://www.povray.org

Manuscript

IV

Structurally Defined Chloride/Isobutylaluminato Lanthanide Complexes in Isoprene Polymerization

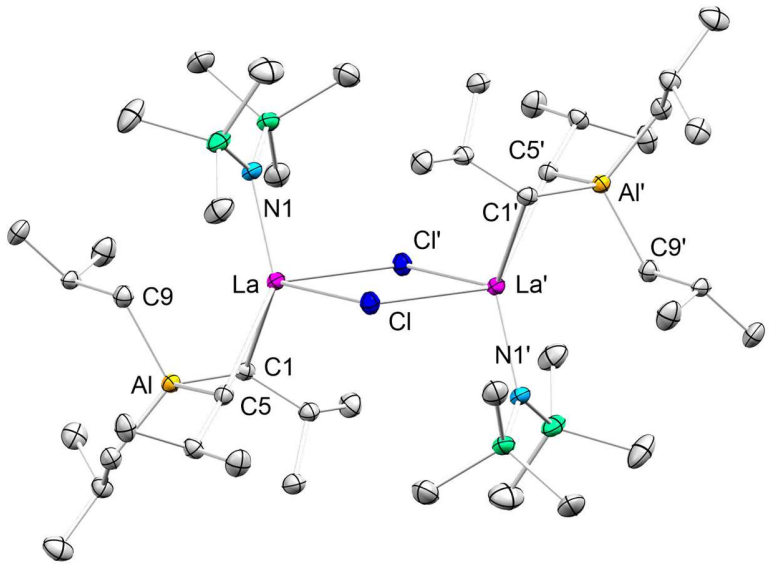

Structurally Defined Chloride/Isobutylaluminato Lanthanide Complexes in Isoprene Polymerization

Eric C. Moinet, Philipp Wetzel, Olivier Tardif, Cäcilia Maichle-Mössmer, and Reiner Anwander

Abstract

Heteroleptic lanthanide tetraisobutylaluminate complexes $[Ln\{N(SiMe_3)_2\}(Al\textit{i}Bu_4)(\mu\text{-}Cl)]_2$ (Ln = La, Nd) form when $[Ln\{N(SiMe_3)_2\}_2(\mu\text{-}Cl)(thf)]_2$ is treated with triisobutylaluminum. The $[La\{N(SiMe_3)_2\}_2(\mu\text{-}Cl)(thf)]_2/AlMe_3$ reaction afforded isolable $[La\{N(SiMe_3)_2\}\{(\mu\text{-}CH_3)(\mu\text{-}N(SiMe_3)_2)AlMe_2\}(\mu\text{-}Cl)]_2$, highlighting the distinct reactivity of TIBA species. Complex $[Nd\{N(SiMe_3)_2\}(Al\textit{i}Bu_4)(\mu\text{-}Cl)]_2$ features catalyst activity in isoprene polymerization for the fabrication of high *cis*-selective polyisoprene and displays single component polymerization activity.

Despite of decades of intensive research, the structures of active species in Ziegler mixed catalysts have remained elusive. Catalytic systems for isoprene polymerization usually consist of a neodymium salt precursor, chloride donors such as R_2AlCl (R = Me, Et, *i*Bu), and other additives such as organoaluminum compounds like triisobutylaluminum (TIBA), diisobutylaluminum hydride (DIBAH), or methylaluminum oxane (MAO).[1] Only very few active compounds formed within such multinary mixtures have been authenticated, and initiating species are still ambiguous.[2] However, it is generally accepted that Ln-alkyl, or Ln-H species are involved, whereas strongly polarized or cationic species generated *i.e*. by Al→Ln chlorido transfer are also possible candidates for active species.[3] Involved species tend to get very complex, as shown by Shan *et al*., who managed to crystallize a product from the highly polymerization active ternary mixture comprised of $Nd(O\textit{i}Pr_3/AlEt_3/AlEt_2Cl$ 1/10/1.5 ratio).[4] The polynuclear product identified as $[Al_3Nd_6(\mu_2\text{-}Cl)_6(\mu_3\text{-}Cl)_6(\mu_2\text{-}Et)_9Et_5(O\textit{i}Pr)]_2$, engages in single-component polymerization of butadiene.[4] Few other single-component catalysts active without additional cocatalyst or alkylaluminum compound have been reported.[5] [6] [7] [8] [9] [10] [11] [12] Unfortunately, different organoaluminum compounds affect catalytic behavior which further

adds to the level of complexity.[13] One strategy to avoid complex ternary mixtures by pre-formed compounds is to follow a chlorination/alkylation sequence, or an alkylation/chlorination (*cf*. Scheme 1).[14]

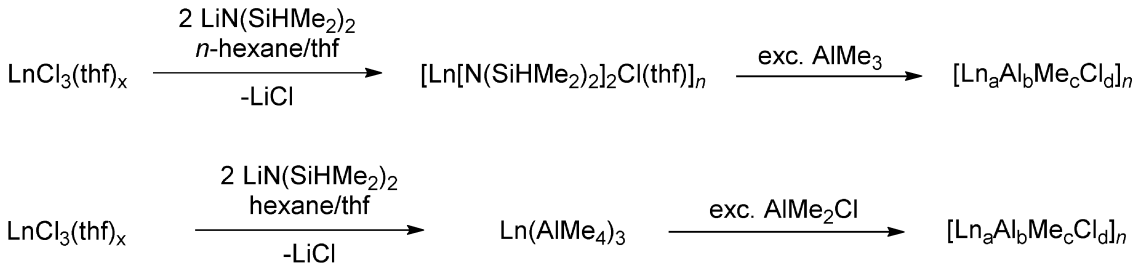

Scheme 1. Examples for chlorination/alkylation sequence (top), or an alkylation/chlorination sequence (bottom).[14]

Only recently, we have reported on a series of divalent, homoleptic tetraisobutylaluminates [Ln(Al*i*Bu$_4$)$_2$] (Ln = Sm, Eu, Yb),[15] [16] and trivalent mixed hydrido/isobutylaluminato lanthanide complexes.[17] However, heteroleptic rare-earth-metal complexes are usually difficult to synthesize. Major challenges include fast ligand redistribution, and the tendency to form homoleptic complexes. Here, we report the synthesis of chlorido-containing, heteroleptic lanthanide isobutylaluminates that serve as single component catalysts.

To elucidate whether chlorido-containing isobutylaluminato complexes can be obtained for early lanthanide metals, we envisaged hitherto unpublished complex [La{N(SiMe$_3$)$_2$}$_2$(μ-Cl)(thf)]$_2$ (**1^{La}**) as a precursor according to the previously reported chlorination-alkylation sequence.[14] Following a similar procedure as was applied for the neodymium complex [Nd{N(SiMe$_3$)$_2$}$_2$(μ-Cl)(thf)]$_2$ (**1Nd**) by Berg and coworkers,[18] the lanthanum congener was obtained quantitatively by heating a mixture of La[N(SiMe$_3$)$_2$]$_3$ (1.5 equiv.) with LaCl$_3$(thf) in THF to 70 °C for several days. It is noteworthy that [La{N(SiMe$_3$)$_2$}$_2$(μ-Cl)(thf)]$_2$ (**1^{La}**) displays the first diamagnetic compound of the type [Ln{N(SiMe$_3$)$_2$}$_2$(μ-Cl)(thf)]$_2$ (**1^{Ln}**) for early lanthanides. Complexes [Ln{N(SiMe$_3$)$_2$}$_2$(μ-Cl)(thf)]$_2$ (**1^{Ln}**) have been known for decades, and are now available for the entire size range including structurally characterized Y,[19] Ce,[20] Pr,[21] Nd,[22] Gd,[23] Sm,[24] [25] Eu,[23] [25] Tb,[25] Dy,[26] Tm,[27] and Yb.[23] [28]

[Ln{N(SiMe$_3$)$_2$}$_2$(μ-Cl)(thf)]$_2$ (**1**^{Ln}) (Ln = La, Nd) react with 6.5 equiv. TIBA to form isostructural [Ln{N(SiMe$_3$)$_2$}(Al*i*Bu$_4$)(μ-Cl)]$_2$ (**2**^{Ln}) (Scheme 2). Both Complexes display a distorted η^3-coordination of the tetraisobutylaluminato ligand, with one Ln–C distance (Ln–C9) significantly elongated compared to the other two Ln–C bonds (i.e. 2.782(3), 2.809(2), and 3.132(3) Å for **2**^{La}). In contrast, the reaction of [La{N(SiMe$_3$)$_2$}$_2$(μ-Cl)(thf)]$_2$ (**1**^{La}) with 6 equiv. trimethylaluminum did not lead to the displacement of the silylamido ligands as observed with triisobutylaluminum. A crystallization attempt afforded [La{N(SiMe$_3$)$_2$}{(μ-CH$_3$)(μ-N(SiMe$_3$)$_2$)AlMe$_2$}(μ-Cl)]$_2$ (**3**^{La}) (Figure 1), featuring two Me$_3$Al–N(SiMe$_3$)$_2$ moieties. In contrast to TIBA, trimethylaluminum engaged with [La{N(SiMe$_3$)$_2$}$_2$(μ-Cl)(thf)]$_2$ (**1**^{La}) in the formation of an Lewis acid-base adduct, instead of displacing the silylamido ligand. The methyl homologue to [La{N(SiMe$_3$)$_2$}(Al*i*Bu$_4$)(μ-Cl)]$_2$ (**2**^{La}) could not be obtained. Compound [La{N(SiMe$_3$)$_2$}{(μ-CH$_3$)(μ-N(SiMe$_3$)$_2$)AlMe$_2$}(μ-Cl)]$_2$ (**3**^{La}) features a significant elongation of the two La–N distances in case of the TMA-silylamido moiety (2.677(2) Å), indicating weaker interactions due to a less basic silylamido ligand. In contrast, the other two La–N distances are much shorter with 2.285(2) Å, which could even indicate a strengthening of this bond. The Al(1)–N(2) interatomic distance amounts 1.972(3) Å, which matches the Al–N distance in [Li{N(SiMe$_3$)$_2$}AlMe$_3$] 1.944(3).[29] For selected interatomic distances *cf*. Table 1.

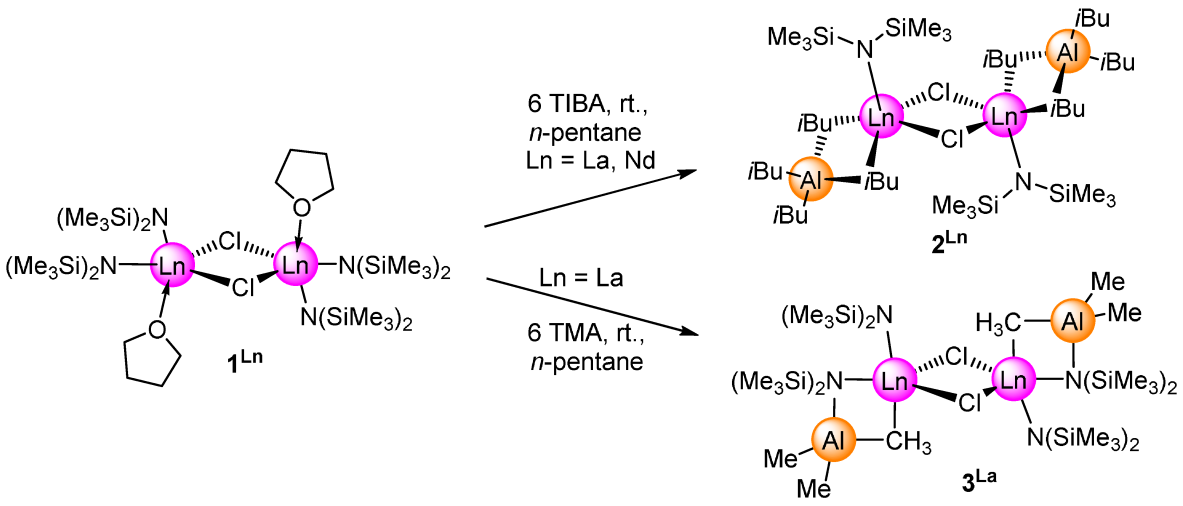

Scheme 2. Synthesis of [La{N(SiMe$_3$)$_2$}$_2$(μ-Cl)(thf)]$_2$ (**1**^{La}) and products [La{N(SiMe$_3$)$_2$}(Al*i*Bu$_4$)(μ-Cl)]$_2$ (**2**^{La}) and [La{N(SiMe$_3$)$_2$}{(μ-CH$_3$)(μ-N(SiMe$_3$)$_2$)AlMe$_2$}(μ-Cl)]$_2$ (**3**^{La}) obtained with tri*iso*butylaluminum, and trimethylaluminum.

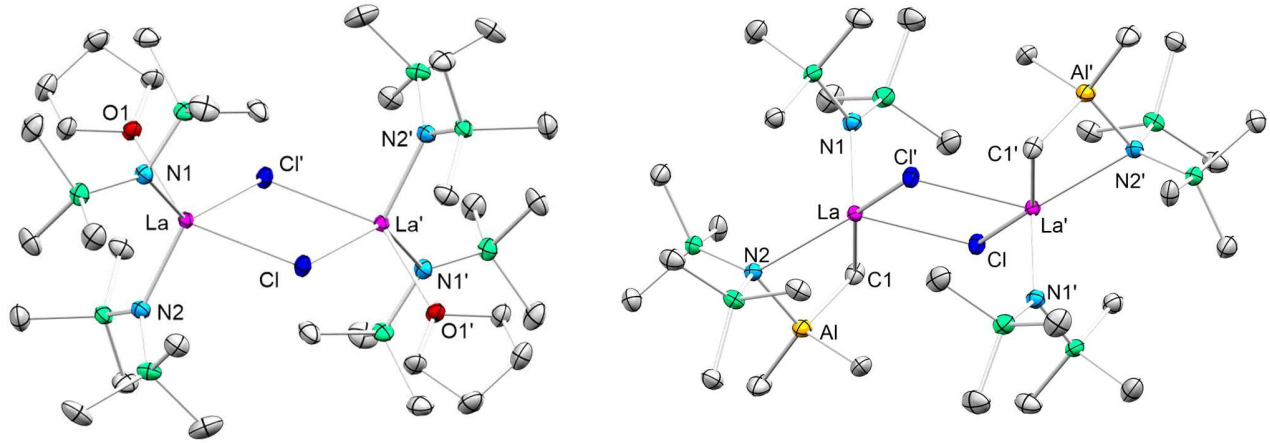

Figure 1. Crystal structures of complexes [La{N(SiMe$_3$)$_2$}$_2$(μ-Cl)(thf)]$_2$ (**1^{La}**), and [La{N(SiMe$_3$)$_2$}{(μ-CH$_3$)(μ-N(SiMe$_3$)$_2$)AlMe$_2$}(μ-Cl)]$_2$ (**3^{La}**). Hydrogen atoms are omitted for clarity. Atomic displacement ellipsoids were set at 50% probability. For detailed metrics and angles, see SI.

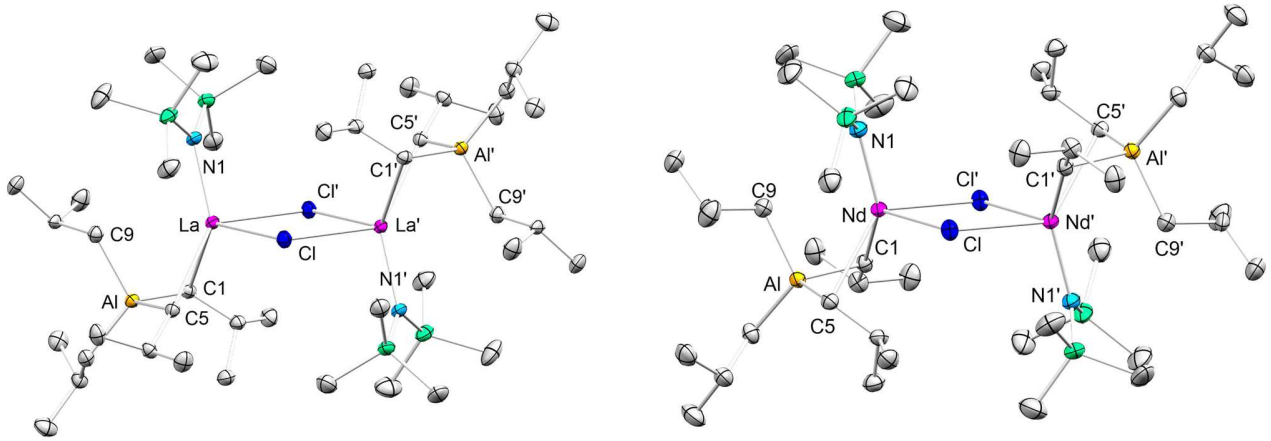

Figure 2. Crystal structures of [La(Al*i*Bu$_4$){N(SiMe$_3$)$_2$}(μ-Cl)]$_2$ (**2^{La}**), and [Nd(Al*i*Bu$_4$)[N(SiMe$_3$)$_2$](μ-Cl)]$_2$ (**2Nd**). Hydrogen atoms are omitted for clarity. Atomic displacement ellipsoids were set at 50% probability. For detailed metrics and angles, see SI.

Table 1. Selected interatomic distances for the compounds $\mathbf{1}^{La}$, $\mathbf{1}^{Nd}$, $\mathbf{2}^{La}$, $\mathbf{2}^{Nd}$, and $\mathbf{3}^{La}$ in Å. Interatomic distances of [Nd{N(SiMe$_3$)$_2$}$_2$(μ-Cl)(thf)]$_2$ ($\mathbf{1}^{Nd}$) are adapted from [18].

	$\mathbf{1}^{La}$	$\mathbf{1}^{Nd}$ [18]	$\mathbf{2}^{La}$	$\mathbf{2}^{Nd}$	$\mathbf{3}^{La}$
Ln–N	2.340(1)-2.379(1)	2.300(8)-2.335(8)	2.279(2)	2.220(1)	2.285(2) [N(SiMe$_3$)$_2$] 2.677(2) [N(SiMe$_3$)$_2$-AlMe$_3$]
Ln–O	2.566(1)	2.496(7)	-	-	-
Ln–C	-	-	2.782(3) 2.809(2) 3.132(3)	2.723(2) 2.746(2) 3.101(2)	2.769(3)
Ln–Cl	2.8531(4)-2.9031(5)	2.791(3)-2.854(3)	2.8397(6)-2.8514(6)	2.7804(5)-2.8000(5)	2.8513(8)-2.8631(7)
Ln···Al	-	-	3.0321(8)	2.9817(6)	3.144(1)

The [AlMe$_3$N(SiMe$_3$)$_2$] motif in [La{N(SiMe$_3$)$_2$}{(μ-CH$_3$)(μ-N(SiMe$_3$)$_2$)AlMe$_2$}(μ-Cl)]$_2$ ($\mathbf{3}^{La}$) does have relevance for the formation of aluminates according to the amide-elimination route as shown in Scheme 2, since it provides evidence for the two-stage mechanism of tetraalkylaluminate formation, which involves trimethylaluminum-amide adduct formation, followed by elimination of the alkylaluminum-amide moiety.[30] Silylamido-trimethylaluminum adducts similar to the [AlMe$_3$N(SiMe$_3$)$_2$] motif in [La{N(SiMe$_3$)$_2$}{(μ-CH$_3$)(μ-N(SiMe$_3$)$_2$)AlMe$_2$}(μ-Cl)]$_2$ ($\mathbf{3}^{La}$) have already been reported. For example, Andersen and Boncella described the formation of Yb{N(SiMe$_3$)$_2$}$_2$(AlMe$_3$)$_2$ from donor-free ytterbium bis(trimethylsilyl)amide, and trimethylaluminum[31], whereas trimethylaluminum reacts with Mn{N(SiMe$_3$)$_2$}$_2$(thf) to form the methyl-bridged compound [{Mn(μ-Me){N(SiMe$_3$)$_2$AlMe$_3$}}$_2$].[32]

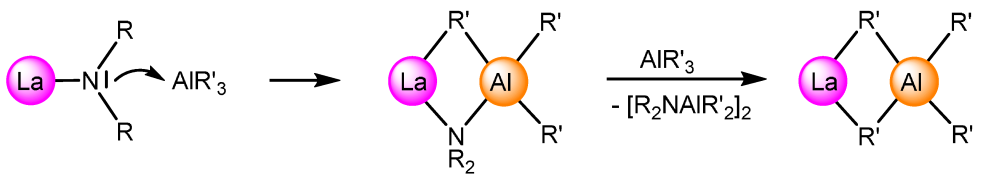

Scheme 3. Proposed two-stage amide elimination mechanism for tetralkylaluminate formation. Figure is adapted from [30].

The ^{1}H NMR spectrum of [La{N(SiMe$_3$)$_2$}(Al*i*Bu$_4$)(μ-Cl)]$_2$ (**2^{La}**) at 26°C in C_6D_6 revealed a mixture of products, albeit **2^{La}** proved to be pure by elemental analysis. This indicated rapid decomposition in deuterated benzene, leading to the formation of decomposition products identified as La[N(SiMe$_3$)$_2$](HAl*i*Bu$_3$)(Al*i*Bu$_4$),[17] La[N(SiMe$_3$)$_2$]$_3$, and isobutene by ^{1}H NMR resonances (see supporting information, Fig. S2). This decomposition scenario possibly involves the formation $LaCl_3$. Since no precipitate of $LaCl_3$ was observed, this may indicate that [$LaCl_2${N(SiMe$_3$)$_2$}] is formed, which is a possible explanation for the silylamido resonance observed at 0.33 ppm. Similar equilibrium phenomena are known for neodymium silylamido/chlorido complexes in solution as detected by ^{1}H NMR spectroscopy.[18] [22] The observed decomposition of [La(Al*i*Bu$_4$){N(SiMe$_3$)$_2$}(μ-Cl)]$_2$ (**2^{La}**) is little surprising, given the tendency of heteroleptic rare-earth-metal complexes to undergo fast ligand redistribution, forming homoleptic complexes. In contrast, ^{1}H-NMR spectroscopy of [La(Al*i*Bu$_4$){N(SiMe$_3$)$_2$}(μ-Cl)]$_2$ (**2^{La}**) in deuterated toluene at -50 °C revealed that the complex **2^{La}** is stable in solution at low temperatures (*cf.* supporting information, Fig. S1).

In contrast, attempts to generate [La{N(SiMe$_3$)$_2$}$_2$(μ-Cl)(thf)]$_2$ (**1^{La}**) by salt metathesis from $LaCl_3$(thf) and potassium hexamethyldisilazide led to product contaminated with the precursors. Reaction of the obtained product with TIBA allowed the isolation of potassium hydrido/isobutylaluminato [K(*i*Bu$_3$Al-μ-H-Al*i*Bu$_3$)]$_n$ (**4**) upon cooling to –40°C in the form of thin colorless needles. In the solid state, compound **4** exhibits a polymeric structure, with the CH_2-moieties of the isobutyl groups bridging to potassium ions (Figure 3). Similar structures have been reported, including K[(AlMe$_3$)$_2$-μ-F][33], and K[(AlEt$_3$)$_2$-μ-F].[34] ^{1}H NMR spectroscopy revealed the hydride resonance at 2.55 ppm, alongside with one set of isobutyl resonances (see supporting information, Figure S3).

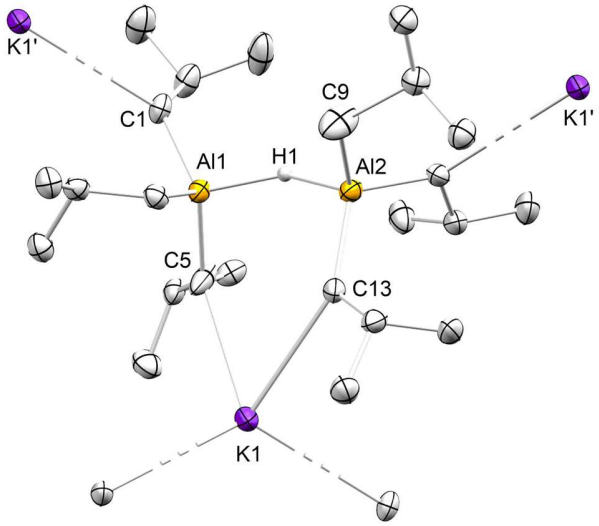

Figure 3. Connectivity of polymeric $[K(iBu_3Al\text{-}\mu\text{-}H\text{-}AliBu_3)]_n$ (**4**). Hydrogen atoms are omitted for clarity. Atomic displacement ellipsoids were set at 50% probability.

Polymerization with $[Nd\{N(SiMe_3)_2\}(AliBu_4)(\mu\text{-}Cl)]_2$ ($\mathbf{2^{Nd}}$)

Compound $[Nd\{N(SiMe_3)_2\}(AliBu_4)(\mu\text{-}Cl)]_2$ ($\mathbf{2^{Nd}}$) was found to polymerize isoprene as a single-component catalyst without the necessity of additional cocatalyst, and/or organoaluminum species (*cf*. Table 2, entry 1). As with neodymium tetramethylaluminate/organoaluminum chloride cocatalysts, high *cis*-1,4-selective polymerization was observed. The addition of an additional chloride source proved pivotal for the overall polymerization activity. Addition of one equivalent [Cl]/[Nd] in the form of diisobutylaluminum chloride increased the yield to 69% (entry 2; compared to 24% without addition of diisobutylaluminum chloride in entry 1). These findings are consistent with the results of $[Nd\{N(SiMe_3)_2\}(AliBu_4)(HAliBu_3)]$ activated with dialkylaluminum chloride systems, showing highest activities in isoprene polymerization with 2-3 [Cl]/[Nd]. Similar findings have been reported for neodymium-catalyzed polymerization with the ill-defined mixture $[Nd\{N(SiMe_3)_2\}_3]$/x Et_2AlCl/40 $AliBu_3$ showing a maximum activity for x = 2-2.5 in heptane.[35] Although this polymerization is conducted at 70 °C, it is notable that a 93.1 *cis*/6.0 trans/0.9% 1,2 microstructure was observed in toluene (15 min, 38% conversion), whereas $[Nd\{N(SiMe_3)_2\}(AliBu_4)(\mu\text{-}Cl)]_2$ ($\mathbf{2^{Nd}}$) produces essentially *trans*-free polyisoprene.

Generally, addition of two equivalents triisobutylaluminum enhance the polymerization activity of [Nd{N(SiMe$_3$)$_2$}(Al*i*Bu$_4$)(μ-Cl)]$_2$ (**2Nd**), to 31% vs. 24% without triisobutylaluminum (*cf*. entries 1, and 3). The addition of two equivalents triisobutylaluminum also increased the yield of [Nd{N(SiMe$_3$)$_2$}(Al*i*Bu$_4$)(μ-Cl)]$_2$ (**2Nd**)/2 equiv. *i*Bu$_2$AlCl (1 equiv. [Cl]/[Nd]) from 69 to 79% (*cf*. entries 2, and 4). This may suggest that further replacement of the remaining silylamido ligand still enhances the overall polymerization activity. It is remarkable that the polymer shown in entry 2 features similar microstructure (98/0/2 *vs*. 99/0/0) and relatively high molecular weight (19.2 *vs*. 22.3 x 10^4 [g x mol^{-1}]), but a narrower PDI (1.57 *vs*. 2.10) than with comparable neodymium-based catalysts generated via chlorination/alkylation sequences employing methylaluminum and ethylaluminum reagents.[14]

Table 2. Isoprene polymerization using [Nd{N(SiMe$_3$)$_2$}(AliBu$_4$)(μ-Cl)]$_2$ (**2Nd**) as precatalyst.

entry[a]	pre-catalyst	co-catalyst[b]	reaction time [h]	yield [%]	*cis*-1,4[c] [%]	*trans*-1,4[c] [%]	3,4[c] [%]	M_n[d] [10^4 g·mol^{-1}]	PDI[d]	T_G[e] [°C]
1	**2Nd**	none	1	24	98.0	0	2.0	3.2	3.69	-66
2	**2Nd**	1 **F**	1	69	98.0	0	2.0	19.2	1.57	-65
3	**2Nd**	2 TIBA	1	31	98.0	0	2.0	2.1	4.36	-67
4	**2Nd**	1**F**/2TIBA	1	79	98.0	0	2.0	11.3	2.04	-64

[a] Conditions: 10 μmol of precatalyst, 20 μmol of cocatalyst, 20 mmol of isoprene, 8 mL of toluene, 500 rpm stirring velocity. [b] Aged with cocatalyst at ambient temperature for 30 min: **F** = *i*Bu$_2$AlCl, equivalents are given as [Cl]/[Nd]. [c] Determined by ^{1}H, ^{13}C NMR in CDCl$_3$. [d] Determined by SEC. [e] Determined by DSC.

References

[1] G. Ricci, G. Pampaloni, A. Sommazzi, F. Masi, *Macromolecules* **2021**, *54*, 5879-5914.
[2] D. Li, S. Li, D. Cui, X. Zhang, *Organometallics* **2010**, *29*, 2186-2193.
[3] D. Cui, *Vol. 137, Molecular catalysis of rare-earth elements* (Ed.: P. W. Roesky), Springer Science & Business Media, **2010**.
[4] C. Shan, Y. Lin, J. Ouyang, Y. Fan, G. Yang, *Macromol. Chem.* **1987**, *188*, 629-635.
[5] D. Barisic, J. Lebon, C. Maichle-Mössmer, R. Anwander, *Chem. Comm.* **2019**, *55*, 7089-7092.
[6] W. J. Evans, D. G. Giarikos, N. T. Allen, *Macromolecules* **2003**, *36*, 4256-4257.
[7] R. Taube, H. Windisch, S. Maiwald, H. Hemling, H. Schumann, *J. Organomet. Chem.* **1996**, *513*, 49-61.
[8] X. Li, M. Nishiura, K. Mori, T. Mashiko, Z. Hou, *Chem. Comm.* **2007**, 4137-4139.
[9] A.-S. Rodrigues, E. Kirillov, B. Vuillemin, A. Razavi, J.-F. Carpentier, *Polymer* **2008**, *49*, 2039-2045.
[10] N. Yu, M. Nishiura, X. Li, Z. Xi, Z. Hou, *Chem. Asian J.* **2008**, *3*, 1406-1414.
[11] L. Annunziata, M. Duc, J.-F. Carpentier, *Macromolecules* **2011**, *44*, 7158-7166.
[12] M. Zimmermann, K. W. Törnroos, R. Anwander, *Angew. Chem. Int. Ed.* **2008**, *47*, 775-778.
[13] A. D. Oswald, L. Verrieux, P.-A. R. Breuil, H. Olivier-Bourbigou, J. Thuilliez, F. Vaultier, M. Taoufik, L. Perrin, C. Boisson, *Organometallics* **2022**, *41*, 2106-2118.
[14] C. Meermann, K. W. Törnroos, W. Nerdal, R. Anwander, *Angew. Chem. Int. Ed.* **2007**, *46*, 6508-6513.
[15] E. C. Moinet, B. Wolf, C. Maichle-Mössmer, O. Tardif, R. Anwander, *Angew. Chem. Int. Ed.* **2023**, *62*.
[16] E. C. Moinet, B. Wolf, C. Maichle-Mössmer, O. Tardif, R. Anwander, *Angewandte Chemie* **2023**, *135*.
[17] E. C. Moinet, O. Tardif, C. Maichle-Mössmer, R. Anwander, *Chem. Comm.* **2023**, *59*, 5261-5264.
[18] D. J. Berg, R. A. L. Gendron, *Can. J. Chem.* **2000**, *78*, 454-458.
[19] A. A. Trifonov, D. M. Lyubov, G. G. S. E. A. Fedorova, G. K. Fukin, Y. A. Kurskii, M. N. Bochkarev, *Russ. Chem. Bull.* **2006**, .
[20] P. B. Hitchcock, A. G. Hulkes, M. F. Lappert, *Inorg. Chem.* **2004**, *43*, 1031-1038.
[21] E. Hemmer, C. Cavelius, V. Huch, S. Mathur, *Inorg. Chem.* **2015**, *54*, 6267-6280.
[22] D. J. Berg, R. A. L. Gendron, *Can. J. Chem.* **2000**, *78*, 454-458.
[23] H. C. Aspinall, D. C. Bradley, M. B. Hursthouse, K. D. Sales, N. P. C. Walker, B. Hussain, *Dalton Trans.* **1989**, 623-626.
[24] M. Karl, G. Seybert, W. Massa, S. Agarwal, A. Greiner, K. Dehnicke, *Z. Anorg. Allg. Chem.* **1999**, *625*, 1405-1407.
[25] A. M. Bienfait, B. M. Wolf, K. W. Törnroos, R. Anwander, *Chem. Eur. J.* **2018**, *57*, 5204-5212.
[26] F. Zhou, S. Zhang, Y. Zhao, C. Zhang, X. Cheng, L. Zheng, Y. Zhang, Y. Li, *Z. Anorg. Allg. Chem.* **2009**, *635*, 2636-2641.
[27] A. M. Bienfait, B. M. Wolf, K. W. Törnroos, R. Anwander, *Inorg. Chem.* **2018**, *57*, 5204-5212.
[28] M. Niemeyer, *Z. Anorg. Allg. Chem.* **2002**, *628*, 647-657.
[29] M. Niemeyer, P. P. Power, *Organometallics* **1995**, *14*, 5488-5489.
[30] M. G. Klimpel, Technische Universität München, PhD Thesis, **2001**.
[31] J. M. Boncella, R. A. Andersen, *Organometallics* **1985**, *4*, 205-206.
[32] M. Niemeyer, P. P. Power, *Chem. Comm.* **1996**, 1573-1574.
[33] J. L. Atwood, W. R. Newberry, *J. Organomet. Chem.* **1974**, *66*, 15-21.
[34] G. Allegra, G. Perego, *Acta Cryst.* **1963**, *16*, 185-190.
[35] C. Boisson, F. Barbotin, R. Spitz, *Macromol. Chem. Phys.* **1999**, *200*, 1163-1166.

Structurally Defined Chlorido/Isobutylaluminato Lanthanide Complexes in Isoprene Polymerisation

Eric C. Moinet, Philipp Wetzel, Olivier Tardif, Cäcilia Maichle-Mössmer, and Reiner Anwander

Contents

Experimental Procedures

General Considerations

All manipulations were performed under rigorous exclusion of air and moisture, using standard Schlenk, high-vacuum, and glovebox techniques (MBraun MB200B <1 ppm O_2, <1 ppm H_2O, argon atmosphere). Glassware and polymer fittings were dried prior to use for several hours at 120 °C or 80 °C, respectively. Solvents were supplied by Merck KGaA, purified using a SPS solvent purification system (MBraun) and stored inside a glovebox. Argon (99.999 Vol%) was supplied by Westfalen AG. Tetrahydrofuran was dried over molecular sieves (3 Å). Benzene-d_6 and toluene-d_8 were obtained from Merck KGaA and dried over Na/K alloy prior to use. Isoprene was purchased from Merck KGaA, dried with trioctylaluminum and distilled under reduced pressure before polymerization. Dimethylaluminum chloride, diethylaluminum chloride, potassium bis(trimethylsilyl)amide, and triisobutylaluminum (TIBA), trioctylaluminum were purchased from Merck KGaA and used as received. Trimethylaluminum, lanthanum- and neodymium trichloride were purchased from abcr and used without further purification. $[CPh_3][B(C_6F_5)_4]$, $[C_6H_5NMe_2H][B(C_6F_5)_4]$, and $[B(C_6F_5)_3]$ were purchased from Boulder Scientific and used as received. $[Nd\{N(SiMe_3)_2\}_2(thf)(\mu\text{-}Cl)]_2$ (**1**Nd) was prepared following the procedures reported by Berg and coworkers.[1]

IR spectra were recorded on a Nicolet 6700 FTIR spectrometer (Thermo Fisher Scientific), and samples were mixed with KBr powder and measured in a DRIFT cell equipped with KBr windows. Elemental analyses were performed on an Elementar vario MICRO cube. NMR spectra of air and moisture sensitive compounds were recorded using J. Young-valved NMR tubes on a Bruker AVII+400 spectrometer (^{1}H: 400.13 MHz; $^{13}C\{^1H\}$: 100.61 MHz). ^{1}H and $^{13}C\{^1H\}$ NMR chemical shifts are referenced to solvent residual resonances and reported in parts per million, relative to tetramethylsilane. Coupling constants are given in Hertz. The microstructures of polyisoprenes were determined by ^{1}H and $^{13}C\{^1H\}$ NMR spectroscopy in $CDCl_3$ on a Bruker AVBII+400 spectrometer (^{1}H: 400.13 MHz) at ambient temperatures. Low temperature NMR spectra were recorded on Bruker AVII+500 spectrometer (^{1}H: 500.13 MHz). Size-exclusion chromatography (SEC) was performed on a Viscotek GPCmax VE2001 device equipped with a TDA305 detector (Viscotek) against a polystyrene standard in THF (35 °C) with a flow rate of 1 mL/min. Sample

solutions (1.0 mg polymer per mL THF) were filtered through a 0.45 µm syringe filter prior to injection. M_n and M_w were determined by means of the integrated OmniSec software. Glass-transition temperatures T_g were determined by differential scanning calorimetry (DSC) under nitrogen atmosphere on a DSC8000 device equipped with a CLN2 cooler (PerkinElmer) calibrated with cyclohexane and indium standards, by scanning from –100 °C up to +100 °C with heating rates of 20 K/min and cooling rates of 60 K/min. The monomer conversion was determined gravimetrically.

Caution! Note that organoaluminum compounds react very vigorously upon contact with air or moisture and may explode with water!

Syntheses

[La{N(SiMe$_3$)$_2$}$_2$(thf)(μ-Cl)]$_2$ (**1^{La}**)

The protocol follows a slightly modified procedure reported by Berg and coworkers.[1] In a thick-walled glass flask, a mixture of La[N(SiMe$_3$)$_2$]$_3$ (9.000 g, 14.515 mmol) and LaCl$_3$(thf)$_1$ (3.471 g, 10.886 mmol, 1.5 equiv.) was suspended in THF (200 mL). The suspension was heated overnight under stirring to 70 °C, whereupon a clear solution was obtained. After heating for additional six days, the solvent was removed. The remaining solid was extracted three times with *n*-pentane, and the combined extracts were dried *in vacuo*, leaving 11.505 g (10.159 mmol, 93%) product as white solid. DRIFT (KBr, cm^{-1}): 2949 (w), 2895 (vw), 1246 (s), 1020 (w), 967 (m), 862 (vs), 837 (vs), 768 (m), 666 (m), 600 (m). $C_{32}H_{88}Cl_2La_2N_2O_2Si_8$ (1134.47 g/mol): calcd. C 33.88, H 7.82, N 4.94; found C 33.99, H 7.68, N 5.34.

[La(Al*i*Bu$_4$){N(SiMe$_3$)$_2$}(μ-Cl)]$_2$ (**2^{La}**)

A solution of TIBA (1.241 g, 6.257 mmol, 6.5 equiv.) in *n*-pentane (3 mL) was added to a stirred suspension of [La[N(SiMe$_3$)$_2$]$_2$(thf)(μ-Cl)]$_2$ (**1^{La}**) (1.136 g, 0.962 mmol, 1 equiv.) in *n*-pentane (3 mL), yielding a clear solution. After reduction of the solvent volume, cooling to –40 °C yielded clear, colorless, block-shaped crystals. Recrystallization afforded 489 mg (0.415 mmol, 43%) of **2^{La}**. ^{1}H NMR (400.1 MHz, toluene-d$_8$, -50 °C): δ 1.99 (s, 4 H, C*H*); 1.24 (d, 24 H, C*H*$_3$), 0.53 (d, 8 H, C*H*$_2$), 0.43 (s, 18 H, C*H*$_3$). ^{13}C{^{1}H} NMR (100.6 MHz, toluene-d$_8$, -50 °C): δ 34.5 (*C*H$_2$), 28.6 (*C*H), 28.0 (*C*H$_3$), 3.63 [Si(*C*H$_3$)$_2$]. DRIFT (KBr, cm^{-1}): 2956 (vs), 2886 (w), 2862 (w), 2740 (vw), 1461 (w), 1381 (vw), 1247 (s), 1181 (vw), 1160 (vw), 1065 (w), 954 (vs), 860 (vs), 839 (vs), 775 (m), 680 (s), 613 (m), 588 (w), 428 (vw). $C_{44}H_{108}Al_2Cl_2La_2N_2Si_4$ (1180.36 g/mol): calcd. C 44.77, H 9.22, N 2.37; found C 44.78, H 9.29, N 2.37.

[Nd(Al*i*Bu$_4$)[N(SiMe$_3$)$_2$](μ-Cl)]$_2$ (2Nd)

The precursor [Nd{N(SiMe$_3$)$_2$}$_2$(thf)(μ-Cl)]$_2$ (**1Nd**) was synthesized following literature procedures.[1] [Nd(Al*i*Bu$_4$)[N(SiMe$_3$)$_2$](μ-Cl)]$_2$ was prepared analogously to the lanthanum congener [La(Al*i*Bu$_4$){N(SiMe$_3$)$_2$}(μ-Cl)]$_2$ (**2^{La}**), yielding 31% crystalline product. DRIFT (KBr, cm^{-1}): 2951 (vs), 2887 (m), 2861 (m), 2734 (vw), 1462 (w), 1381 (w), 1363 (w), 1247 (m), 1182 (vw), 1166 (w), 1063 (w), 1022 (vw), 938 (m), 834 (s), 778 (m), 679 (m), 618 (w), 587 (w), 439 (vw). $C_{44}H_{108}Al_2Cl_2N_2Nd_2Si_4$ (1191.04 g/mol): calcd. C 44.37, H 9.14, N 2.35; found C 44.21, H 8.98, N 2.32.

[La{N(SiMe$_3$)$_2$}{(μ-CH$_3$)(μ-N(SiMe$_3$)$_2$)AlMe$_2$}(μ-Cl)]$_2$ (3^{La})

Following the procedure as applied for the synthesis of [La(Al*i*Bu$_4$){N(SiMe$_3$)$_2$}(μ-Cl)]$_2$ (**2^{La}**), the utilization of trimethylaluminum instead of triisobutylaluminum led to the formation of very few crystals, which were identified as the Lewis (acid base) adduct [La{N(SiMe$_3$)$_2$}{(μ-CH$_3$)(μ-N(SiMe$_3$)$_2$)AlMe$_2$}(μ-Cl)]$_2$ (**3^{La}**). However, compound [La{N(SiMe$_3$)$_2$}{(μ-CH$_3$)(μ-N(SiMe$_3$)$_2$)AlMe$_2$}(μ-Cl)]$_2$ (**3^{La}**) could not be obtained in pure form, and attempts to synthesize the adduct with 4 equivalents of trimethylaluminum failed to yield the pure substance. The elemental analysis features large deviations in nitrogen content (measured C 32.31, H 8.53, N 3.63; calculated C 31.76, H 8.00, N 4.94). For this reason, it was not employed in catalysis.

[K(*i*Bu$_3$Al-μ-H-Al*i*Bu$_3$)]$_n$ (4)

Crystals of [K(*i*Bu$_3$Al-μ-H-Al*i*Bu$_3$)]$_n$ (**4**) were obtained when treating precursors contaminated with potassium hexamethyldisilazide with TIBA in *n*-hexane. Thin crystals precipitated upon cooling to –40 °C in the form of thin colorless needles prior to crystallization of other products. ^{1}H NMR (400.1 MHz, C_6D_6, 26 °C): δ 2.55 (s, 1 H, H), δ 2.14 (m, 2H, C*H*), δ 1.22 (d, 36 H, C*H*$_3$), δ -0.01 (d, 12H, C*H*$_2$) ppm. ^{13}C{^{1}H} NMR (100.6 MHz, 26 °C): δ 29.5 (*C*H$_3$); 28.0 (*C*H), 25.1 (*C*H$_2$) ppm. DRIFT (KBr, cm^{-1}): 2947 (vs), 2860 (vs), 2765 (m), 1461 (s), 1376 (w), 1358 (w), 1314 (w), 1163 (m), 1060 (m), 1039 (m), 1012 (w), 946 (vw), 814 (w), 739 (m), 665 (m), 644 (m), 478 (vw). $C_{24}H_{55}Al_2K$ (436.76 g/mol): calcd. C 66.00, H 12.69; obs. C 65.81, H 12.55.

Polymerization

Detailed procedures are described as typical examples.

Polymerization of Isoprene (Entry 2, Table 1).

[Nd(Al*i*Bu$_4$)[N(SiMe$_3$)$_2$](μ-Cl)]$_2$ (**2Nd**) (11.91 mg, 0.01 mmol) and Al*i*Bu$_2$Cl (**F**) (1 equiv. Cl/Nd, 2.41 mg, 0.02 mmol) were dissolved in toluene (8 mL), and stirred at ambient temperature for 30 minutes. After addition of isoprene (20 mmol), the polymerization was carried out at ambient temperature for 1 h under stirring (500 rpm). The solution was quenched in methanol (20 mL) containing 0.1% (w/w) 2,6-di-*tert*-butyl-4-methylphenol as a stabilizer. The precipitated polymer was dried *in vacuo* at ambient temperature to constant weight.

NMR Spectra

In general, solvent residual signals are labeled with an asterisk (*). In some cases, the paramagnetic nature of Nd(III) did not allow a conclusive interpretation of the recorded NMR spectra.

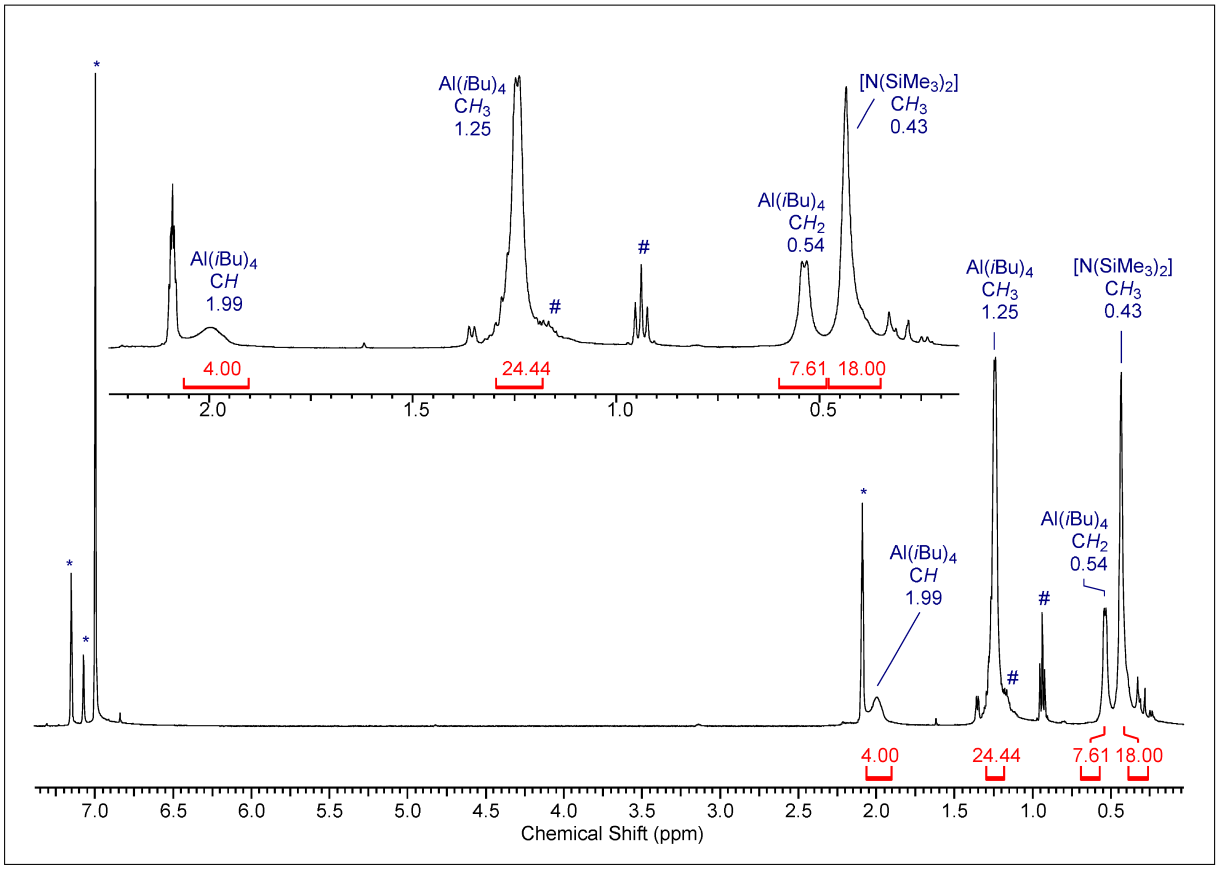

Figure S1: Low-temperature ^{1}H NMR spectrum (-50°C, 500 MHz) of [La(Al*i*Bu$_4$){N(SiMe$_3$)$_2$}(μ-Cl)]$_2$ (**2^{La}**) in deuterated toluene. The signal of the solvent is marked with an asterisk, # denotes aliphatic alkane, resulting from the contamination of commercial toluene-d$_8$.

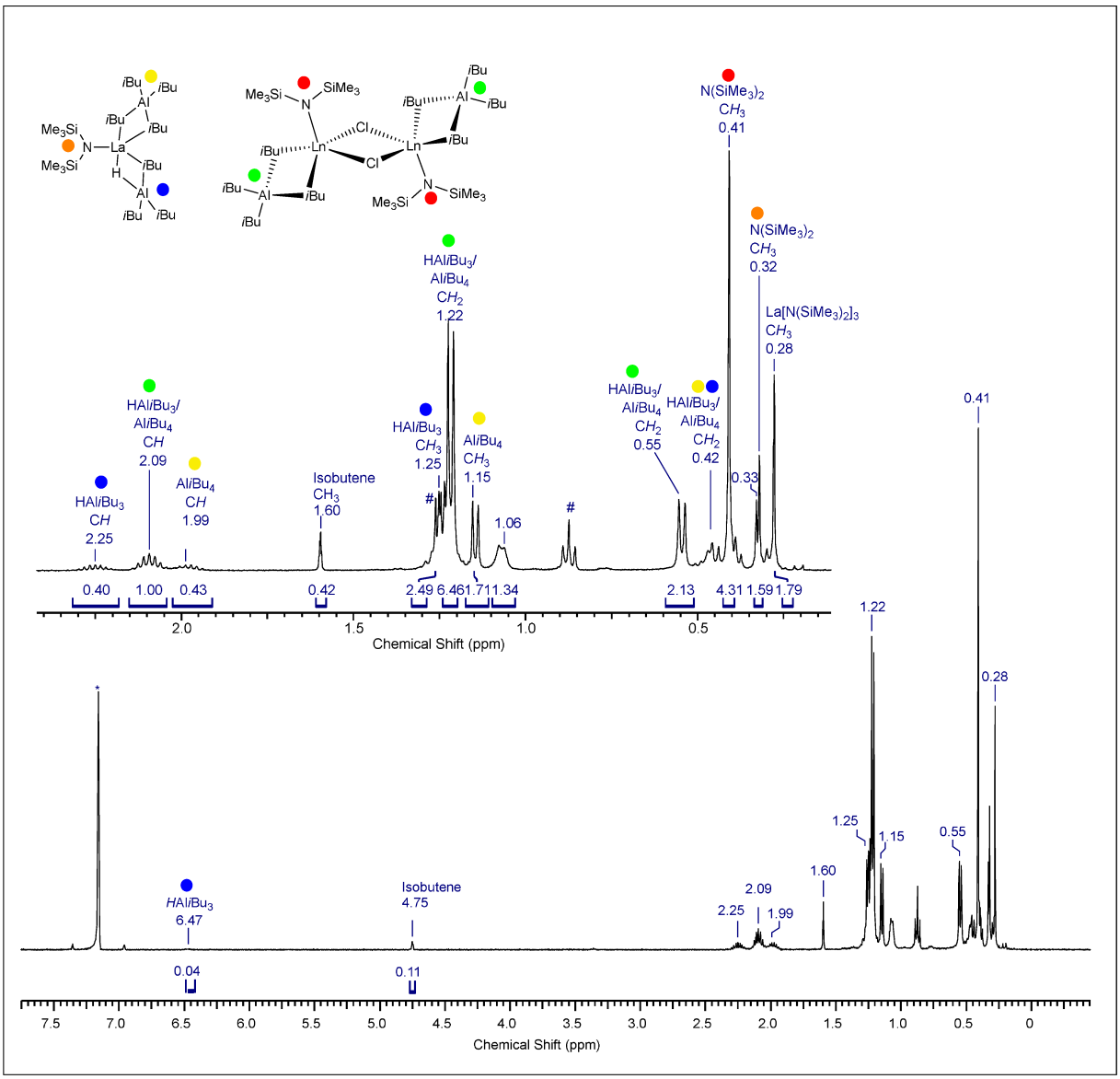

Figure S2: ^{1}H NMR spectrum (25°C, 500 MHz) of [La(Al*i*Bu$_4$){N(SiMe$_3$)$_2$}(μ-Cl)]$_2$ (**2^{La}**) in deuterated benzene. Resonances assigned to [La(Al*i*Bu$_4$){N(SiMe$_3$)$_2$}(μ-Cl)]$_2$ (**2^{La}**) and the decomposition product La[N(SiMe$_3$)$_2$](HAl*i*Bu$_3$)(Al*i*Bu$_4$) are labeled with colored dots. The signal of the solvent is marked with an asterisk, # denotes aliphatic alkane, resulting from the contamination of commercial C_6D_6.

[K(*i*Bu$_3$Al-μ-H-Al*i*Bu$_3$)]$_n$ (4).

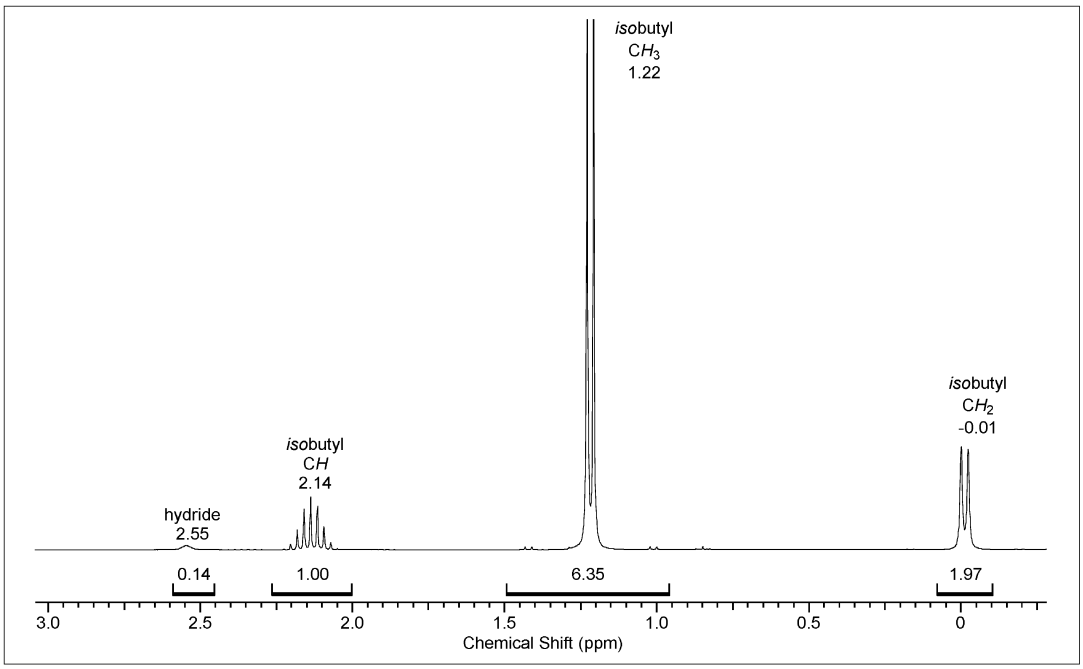

Figure S3. ^{1}H NMR spectrum (400 MHz, C_6D_6, 25 °C) of [K(*i*Bu$_3$Al-μ-H-Al*i*Bu$_3$)]$_n$ (**4**).

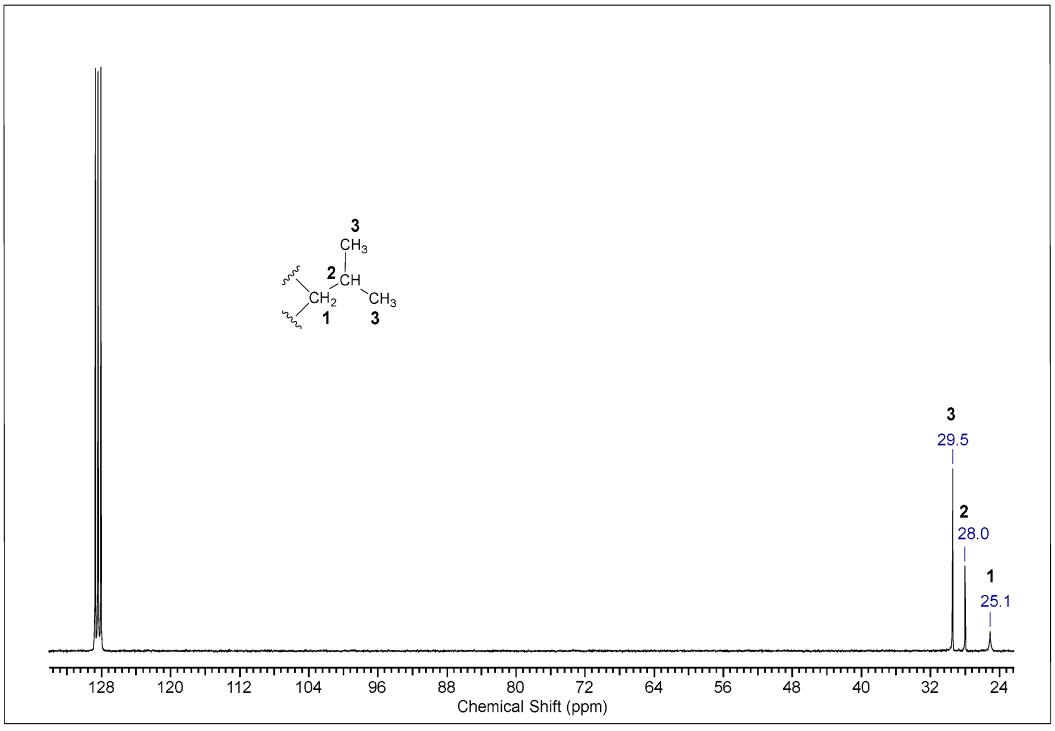

Figure S4. ^{13}C NMR spectrum (101 MHz, C_6D_6, 25 °C) of [K(*i*Bu$_3$Al-μ-H-Al*i*Bu$_3$)]$_n$ (**4**).

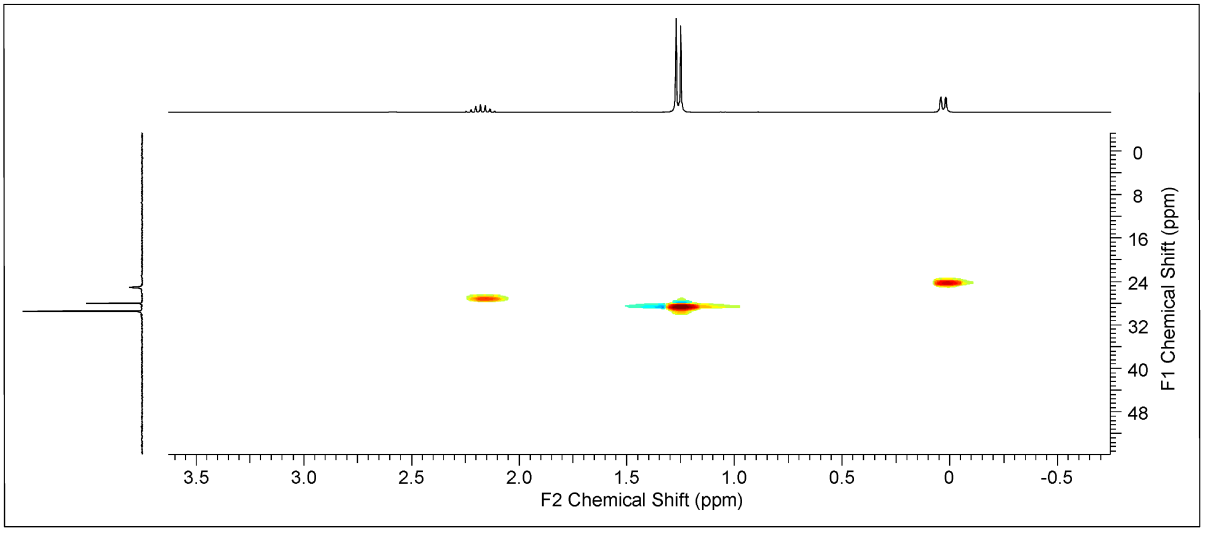

Figure S5. ^{1}H-^{13}C HSQC NMR spectrum (400/101 MHz, C_6D_6, 25 °C) of $[K(iBu_3Al\text{-}\mu\text{-}H\text{-}AliBu_3)]_n$ (**4**).

Crystallography

X-ray Crystallography and Crystal Structure Determination

For X-ray structure analyses, crystals suitable for X-ray diffraction were selected in a glovebox, coated with Parabar 10312 (Hampton Research), and fixed on a nylon/loop glass fiber. X-ray data for all compounds was collected on a Bruker APEX II DUO diffractometer equipped with an IμS microfocus sealed tube and QUAZAR optics for MoK_α (λ = 0.71073 Å). The data collection strategy was determined using COSMO,[2] employing ω-scans. Raw data were processed using APEX[3], and SAINT[3]. Corrections for absorption effects were applied using SADABS.[4] The structures were solved by direct methods and refined against all data by full-matrix least-squares methods on F2 using SHELXTL[5], and ShelXle.[6] Disorder models were calculated using DSR, a program for refining structures in ShelXl.[7] All graphics were produced employing Mercury 4.2.011[8] and POV-Ray12.[9] For X-ray crystallography, single crystalline material of $\mathbf{1}^{La}$, $\mathbf{2}^{La}$, $\mathbf{2}^{Nd}$, and $\mathbf{2}^{La}$ was grown from *n*-hexane at –40°C.

[La{N(SiMe$_3$)$_2$}$_2$(thf)(μ-Cl)]$_2$ (1)

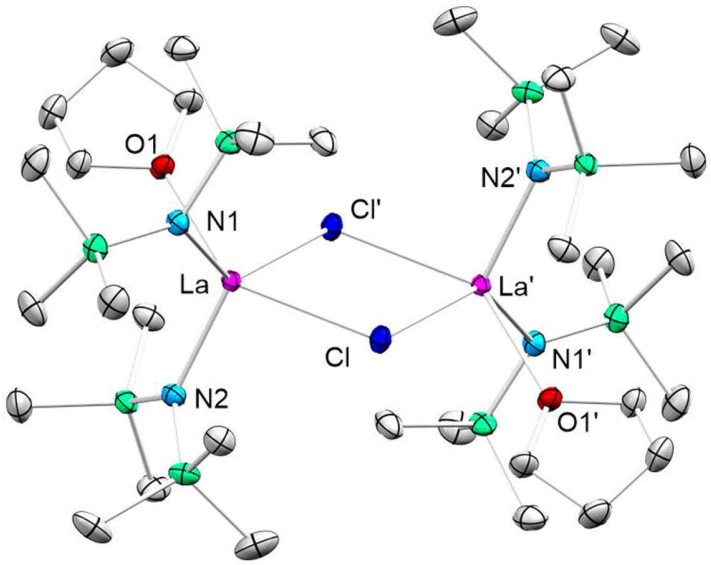

Figure S6. Crystal structure of complex [La{N(SiMe$_3$)$_2$}$_2$(μ-Cl)(thf)]$_2$ (**1^{La}**). Hydrogen atoms are omitted for clarity. Atomic displacement ellipsoids were set at 50% probability. Selected interatomic distances [Å]: La(1)–N(1) 2.3791(12), La(1)–N(2) 2.3396(13), La(1)–O(1) 2.5659(11), La(1)–Cl(1) 2.8531(4), Cl(1)-La(1)' 2.9031(5). Selected angles [°]: N(2)-La(1)-N(1) 116.42(4), N(2)-La(1)-O(3) 109.13(4), N(1)-La(1)-O(3) 80.62(4), N(2)-La(1)-Cl(1) 98.79(3), N(1)-La(1)-Cl(1) 108.90(3), O(1)-La(1)-Cl(1) 142.68(3), N(2)-La(1)-Cl(1)' 108.01(3), N(1)-La(1)-Cl(1)' 133.89(3), O(1)-La(1)-Cl(1)' 73.67(3), Cl(1)-La(1)-Cl(1)' 74.464(13).

[La(Al*i*Bu$_4$){N(SiMe$_3$)$_2$}(μ-Cl)]$_2$ ($\mathbf{2}^{La}$)

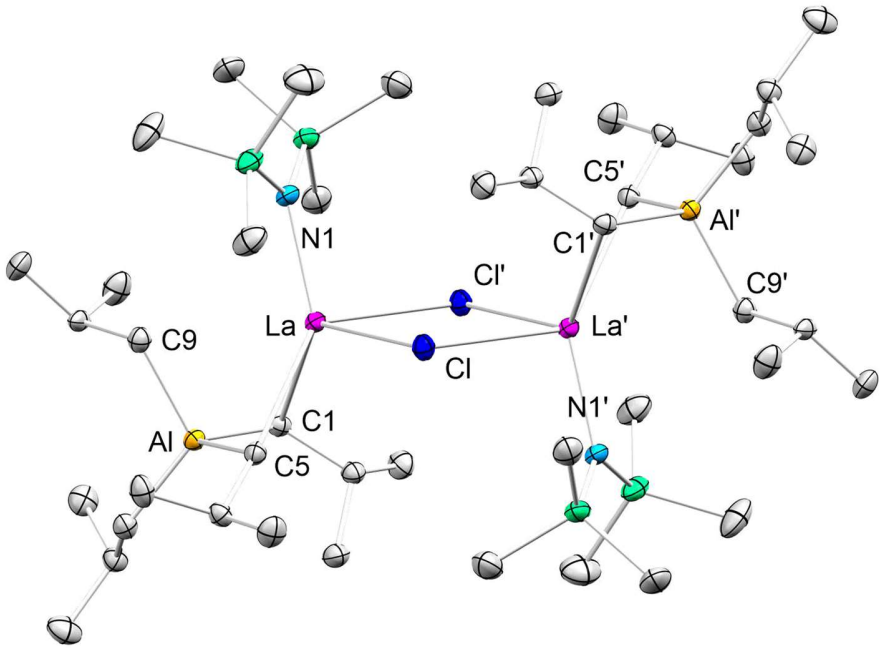

Figure S7. Crystal structure of [La(AliBu$_4$){N(SiMe$_3$)$_2$}(μ-Cl)]$_2$ ($\mathbf{2}^{La}$). Hydrogen atoms are omitted for clarity. Atomic displacement ellipsoids were set at 50% probability. Selected interatomic distances [Å]: La(1)–C(1) 2.782(3), La(1)–C(5) 2.809(2), La(1)–C(9) 3.132(3), La(1)–N(1) 2.279(2), La(1)···Al(1) 3.0321(8), La(1)'–Cl(1) 2.8397(6), Cl(1)-La(1) 2.8514(6), Selected angles [°]: N(1)-La(1)-Cl(1) 106.68(6), C(1)-La(1)-C(5) 71.27(7), C(1)-La(1)-C(9) 68.94(7), C(1)-La(1)-Cl(1) 124.90(5).

[Nd(Al*i*Bu$_4$)[N(SiMe$_3$)$_2$](*μ*-Cl)]$_2$ (2Nd)

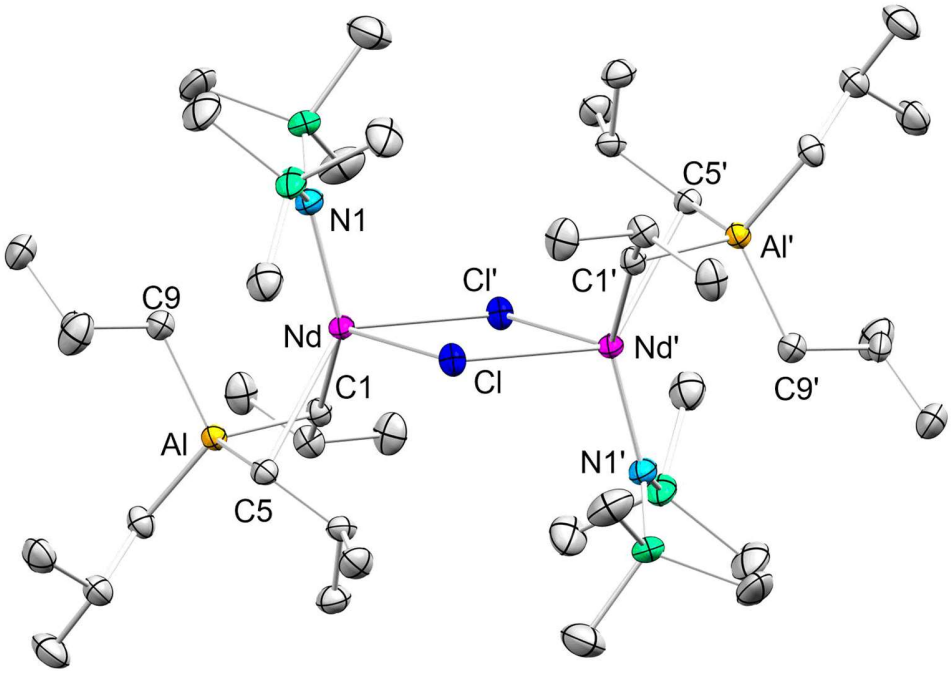

Figure S8. Crystal structure of [Nd(AliBu$_4$)[N(SiMe$_3$)$_2$](μ-Cl)]$_2$ (**2Nd**). Hydrogen atoms are omitted for clarity. Atomic displacement ellipsoids were set at 50% probability. Selected interatomic distances [Å]: Nd(1)–C(1) 2.7456(19), Nd(1)–C(5) 2.723(2), Nd(1)–C(9) 3.101(2), Nd(1)–N(1) 2.2197(17), Nd(1)···Al(1) 2.9817(6), Nd(1)'–Cl(1) 2.7804(5), Nd(1)–Cl(1) 2.8000(5). Selected angles [°]: N(1)-Nd(1)-Cl(1) 126.82(6), C(1)-Nd(1)-C(5) 72.92(6), C(1)-Nd(1)-Cl(1)' 87.77(4).

[La{N(SiMe$_3$)$_2$}{(μ-CH$_3$)(μ-N(SiMe$_3$)$_2$)AlMe$_2$}(μ-Cl)]$_2$ (3^{La})

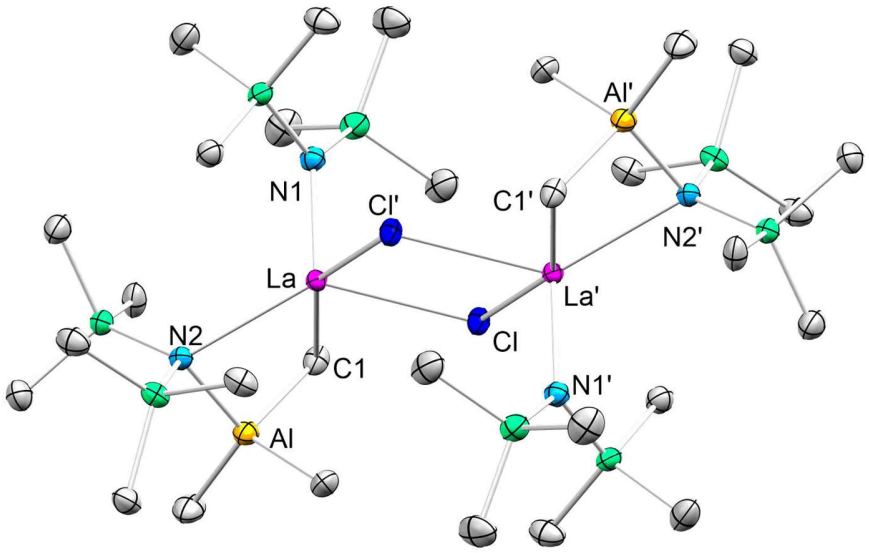

Figure S9. Crystal structure of [La{N(SiMe$_3$)$_2$}{AlMe$_3$N(SiMe$_3$)$_2$}(μ-Cl)]$_2$ (**3^{La}**). Hydrogen atoms are omitted for clarity. Atomic displacement ellipsoids were set at 50% probability. Selected interatomic distances [Å]: La(1)–N(1) 2.285(2), La(1)–N(2) 2.677(2), C(1)–La(1) 3.138(3), La(1)–Cl(1) 2.8513(8), La(1)'–Cl(1) 2.8631(7), Al(1)–N(2) 1.972(3), Al(1)···La(1) 3.1439(10). Selected angles [°]: N(1)-La(1)-N(2) 112.37(8), N(2)-Al(1)-C(1) 102.69(12), Al(1)-C(1)-La(1) 79.87(10), Cl(1)-La(1)-Cl(1)' 72.05(2), N(2)-La(1)-Cl(1) 135.12(5).

[K(*i*Bu$_3$Al-μ-H-Al*i*Bu$_3$)]$_n$ (4).

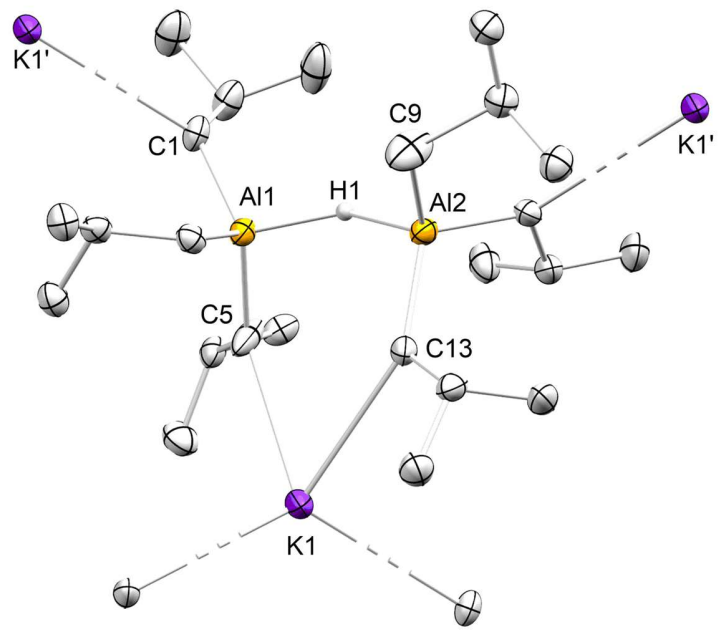

Figure S10. Connectivity of polymeric [K(*i*Bu$_3$Al-μ-H-Al*i*Bu$_3$)]$_n$ (**4**). Hydrogen atoms are omitted for clarity. Atomic displacement ellipsoids were set at 50% probability. Selected interatomic distances [Å]: Al(1)–H(1) 1.72(2), Al(2)–H(1) 1.69(3), Al(1)–C(1) 1.992(3), Al(1)–C(5) 2.009(3), Al(2)–C(9) 1.985(3), Al(2)–C(1) 2.004(3), Al(2)–C(17) 2.006(3). Selected angles [°]: Al(1)-H(1)-Al(2) 144(2).

Table S1. Crystallographic Data for Compounds **1**^{La}, **2**^{La}, **2**Nd and **3**

	1^{La}	**2**^{La}	**2**Nd	**3**
formula	$C_{32}H_{88}Cl_2La_2N_4O_2Si_8$	$C_{44}H_{108}Al_2Cl_2La_2N_2Si_4$	$C_{44}H_{108}Al_2Cl_2N_2Nd_2Si_4$	$C_{30}H_{90}Al_2Cl_2La_2N_4Si_8$
M [g mol^{-1}]	1134.50	1180.36	1191.02	1134.45
color/shape	colorless/column	colorless/block	blue/block	colorless/rhombus
crystal dimensions [mm]	0.103 x 0.088 x 0.068	0.084 x 0.034 x 0.027	0.212 x 0.189 x 0.050	0.108 x 0.085 x 0.045
cryst. system	monoclinic	triclinic	triclinic	monoclinic
space group	*P2₁/n*	$P\bar{1}$	$P\bar{1}$	*P2₁/n*
a [Å]	14.9648(16)	9.4385(6)	9.4739(7)	12.0030(11)
b [Å]	12.0481(13)	11.8337(7)	11.7807(9)	13.4833(12)
c [Å]	16.5884(17)	15.7759(10)	15.6528(12)	17.8972(16)
α [°]	90	73.425(2)	73.332(2)	90
β [°]	112.7580(10)	88.626(2)	88.335(2)	108.630(2)
γ [°]	90	68.093(2)	68.347(2)	90
V [Å^3]	2758.0(5)	1560.13(17)	1549.7(2)	2744.7(4)
Z	2	1	1	2
T [K]	100(2)	100(2)	150(2)	100(2)
wavelength [Å]	0.71073	0.71073	0.71073	0.71073
ρ_{calcd} [Mg m^{-3}]	1.366	1.256	1.276	1.373
μ [mm^{-1}]	1.828	1.568	1.876	1.863
F (000)	1168	616	622	1168
θ range [°]	2.152 to 30.568	1.353 to 28.377	2.019/30.507	2.343 to 26.472
unique reflns	8456	7775	9462	5648
observed reflns	60352	47692	74607	37489
R1/*w*R2 (I>2σ)[a]	0.0209/0.0481	0.0315/0.0619	0.0266/0.0594	0.0284/0.0636
R1/*w*R2 (all data)[a]	0.0243/0.0499	0.0414/0.0659	0.0341/0.0631	0.0370/0.0678
GOF[a]	1.066	1.023	1.047	1.028

[a] $R1 = \Sigma(||F_0|-|F_c||)/\Sigma|F_0|$, $F_0 > 4\sigma(F_0)$. $wR2 = \{\Sigma[w(F_0^2-F_c^2)^2/\Sigma[w(F_0^2)^2]\}^{1/2}$.

Table S2. Crystallographic Data for Compound **4**

	26
formula	$C_{24}H_{55}Al_2K$
M [g mol^{-1}]	436.74
color/shape	colorless/column
crystal dimensions [mm]	0.308 x 0.147 x 0.093
cryst. system	monoclinic
space group	*P21/c*
a [Å]	8.9053(10)
b [Å]	17.4906(19)
c [Å]	18.541(2)
α [°]	90
β [°]	90.394(2)
γ [°]	90
V [Å^3]	2887.8(6)
Z	4
T [K]	100(2)
wavelength [Å]	0.71073
ρ_{calcd} [Mg m^{-3}]	1.005
μ [mm^{-1}]	3.269
F (000)	976
θ range [°]	1.601/24.919
unique reflns	5031
observed reflns	33739
R1/*w*R2 (I>2σ)[a]	0.0514/0.1141
R1/*w*R2 (all data)[a]	0.0735/0.1288
GOF[a]	1.050

[a] $R1 = \Sigma(||F_0|-|F_c||)/\Sigma|F_0|$, $F_0 > 4\sigma(F_0)$. $wR2 = \{\Sigma[w(F_0^2-F_c^2)^2/\Sigma[w(F_0^2)^2]\}^{1/2}$.

References

References

[1] D. J. Berg, R. A. L. Gendron, *Can. J. Chem.* **2000**, *78*, 454-458.

[2] COSMO v. 1.61, Bruker AXS Inc., Madison, WI., **2012**.

[3] APEX 3 v. 2017.3-0, Bruker AXS Inc., Madison, WI., **2017**.

[4] L. Krause, R. Herbst-Irmer, G. M. Sheldrick, D. Stalke, *J. Appl. Crystallogr.* **2015**, *48*, 3-10.

[5] G. Sheldrick, *Acta Crystallogr. Sect. C.* **2015**, *71*, 3-8.

[6] C. B. Hübschle, G. M. Sheldrick, B. Dittrich, *J. Appl. Crystallogr.* **2011**, 1281-1284.

[7] D. Kratzert, J. J. Holstein, I. Krossing, *J. Appl. Crystallogr.* **2015**, *48*, 933-938.

[8] C. F. Macrae, P. R. Edgington, P. McCabe, E. Pidcock, G. P. Shields, R. Taylor, M. Towler, J. van de Streek, *J. Appl. Crystallogr.* **2006**, *39*, 453-457.

[9] POV-Ray v. 3.6, Persistence of Vision Pty. Ltd., Williamstown, Victoria, Australia, **2004**.

F

F.

Appendix

F. Appendix

Molecules in Paper I

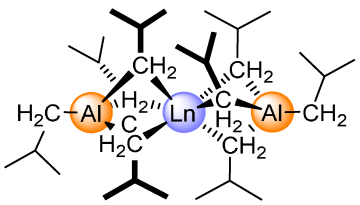

1^{Ln}

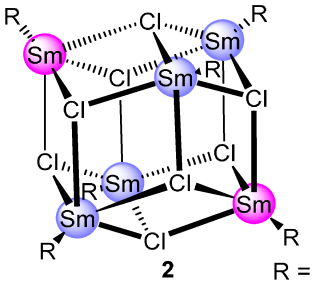

2

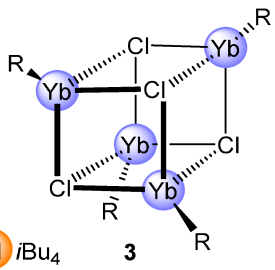

R = Al *i*Bu$_4$ **3**

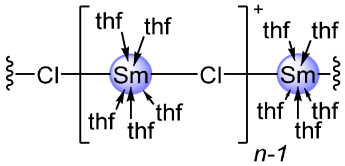

4

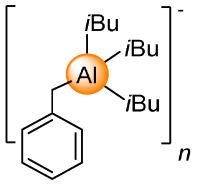

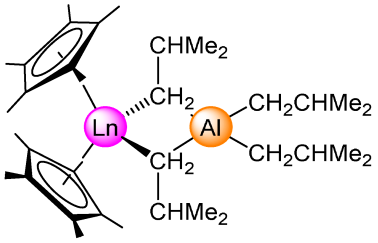

5^{Ln}, Ln = Sm, Yb

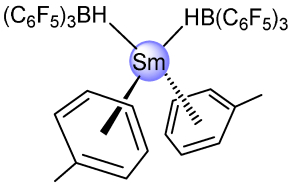

6

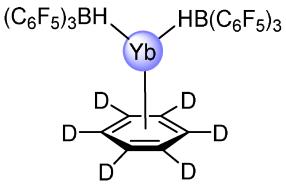

7

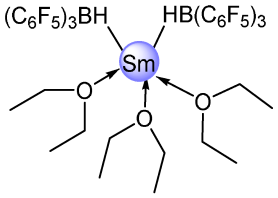

8

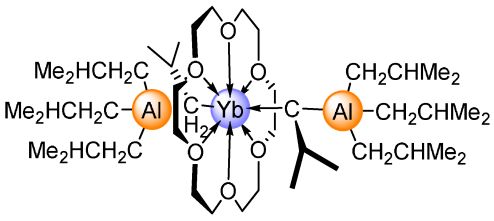

9

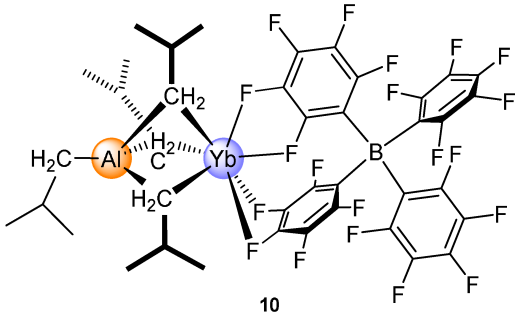

10

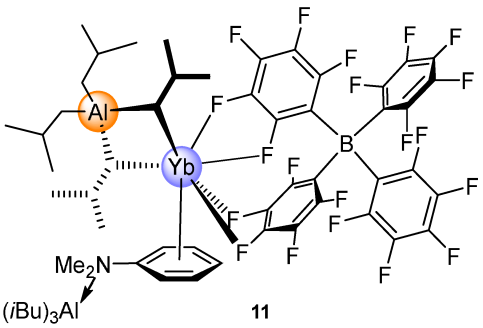

11

Molecules in Paper II

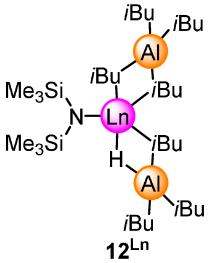

12^{Ln}

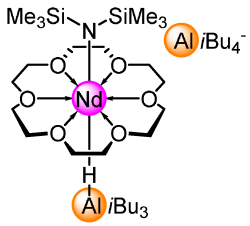

13

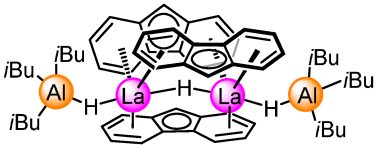

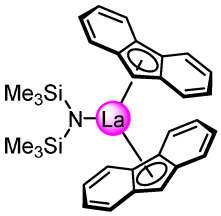

14

Molecules in Paper III

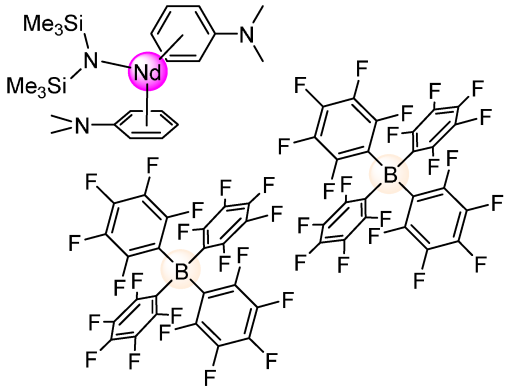

15

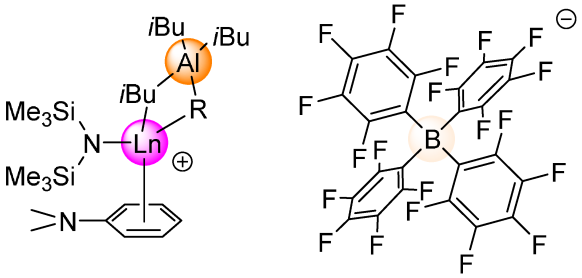

R = H, iBu **16**

Molecules in Manuscript IV

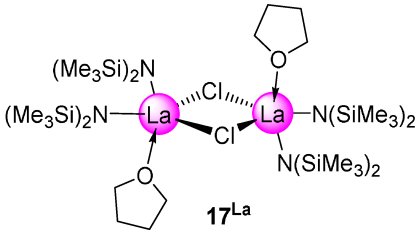

17^{La}

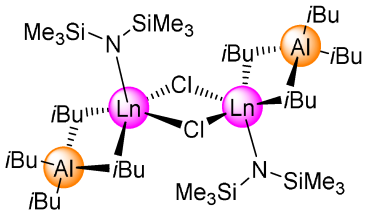

Ln = La, Nd

18

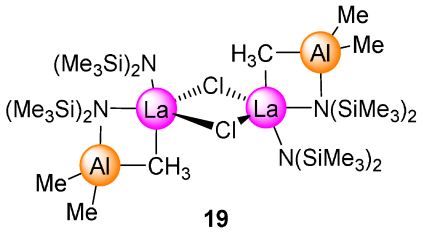

19

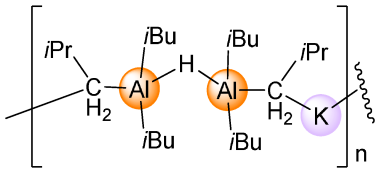

20

Structures from unpublished results

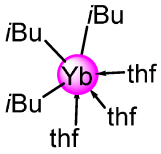

21

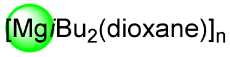

22

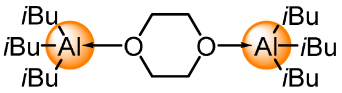

23

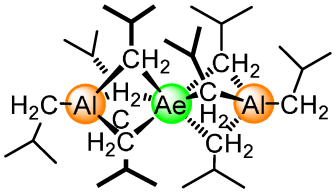

24^{Ae} (Ae = Ca, Sr, Ba)

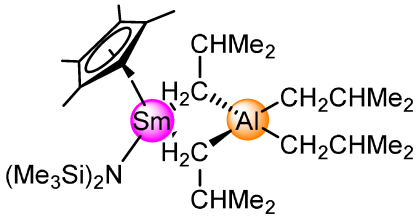

25

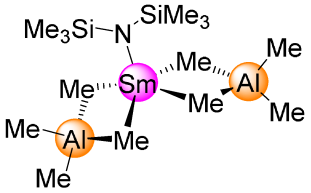

26

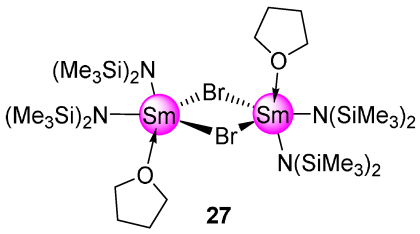

27

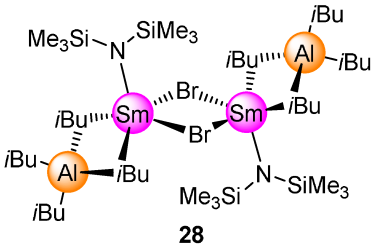

28

Structures from unpublished results

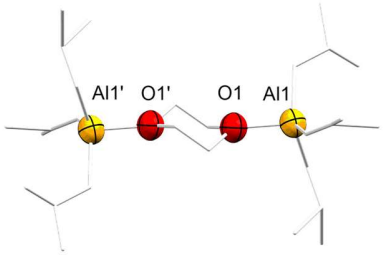

Connectivity of compound **23**.

Complexes neither included in the manuscripts nor in the Unpublished Results

[Ba(thf){N(SiMe$_3$)$_2$}μ-{N(SiMe$_3$)$_2$}$_2$K(thf)$_2$] AL01

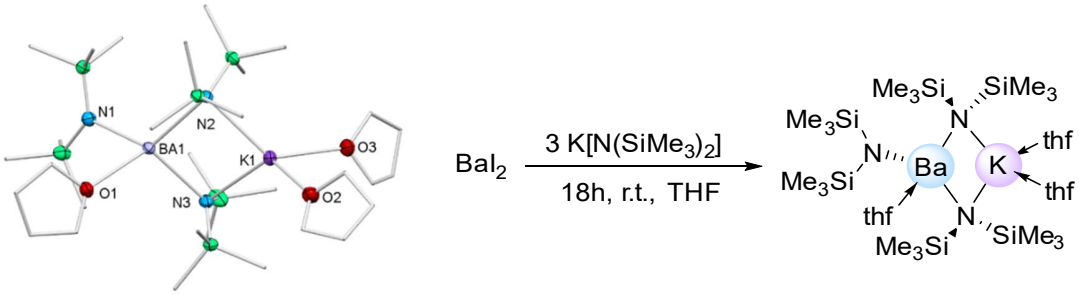

R1[I>sigma(I)] 2.76%, wR2(all data) 6.65%.

Monoclinic *P2$_1$/c*

a = 16.7200(11) Å α = 90°

b = 16.0261(11) Å β = 113.4540(10)°

c = 19.4621(13) Å γ = 90°

V = 4784.1(6) Å^3

[Ba(18-crown-6)(Al*i*Bu$_4$)$_2$] EM231

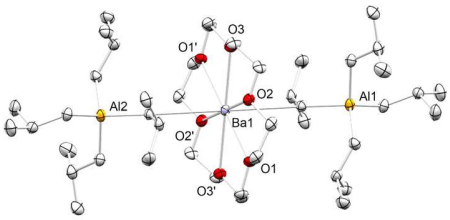

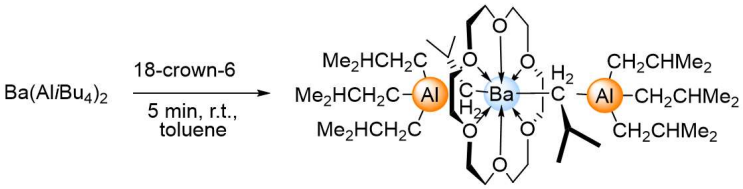

R1[I>sigma(I)] 5.00%, wR2(all data) 13.74%.

Monoclinic *P2$_1$/c*

a = 12.4330(18) Å α = 90°

b = 13.4377(19) Å β = 98.658(4)°

c = 15.700(2) Å γ = 90°

V = 2593.1(6) Å^3

[Sm(18-crown-6)(Al*i*Bu$_4$)$_2$] EM245

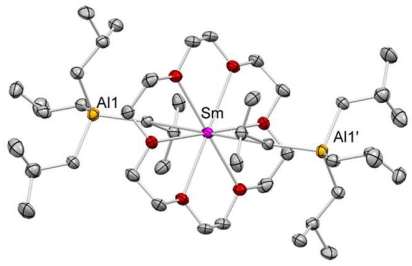

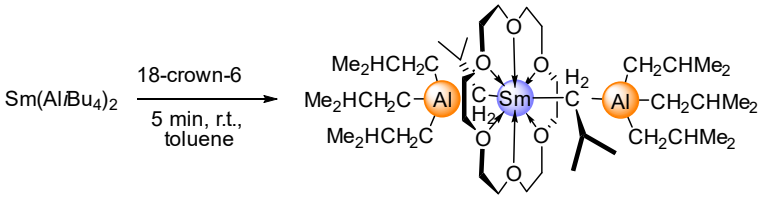

R1[I>sigma(I)] 4.30%, wR2(all data) 10.35%.

Monoclinic *P2$_1$/c*

a = 12.403(2) Å α = 90°

b = 13.436(3) Å β = 98.110(3)°

c = 15.540(3) Å γ = 90°

V = 2563.7(9) Å^3

[K_2Cp^*][iBu_3Al-μ-H–AliBu_3]$_n$ EM204

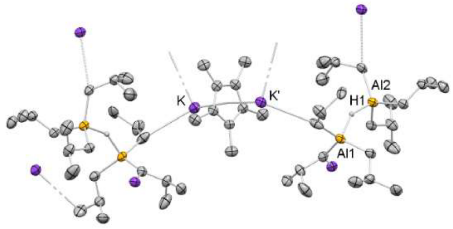

$[K(iBu_3\text{-}\mu\text{-H-}iBu_3)]_n$ —(0.27 equiv. Cp^*_2Pb, *n*-hexane, rt, 24h; $-Pb^0$)→ $[K_2Cp^*(AliBu_3\text{-}\mu\text{-H-}AliBu_3)]_n$

R1[I>sigma(I)] 5.24%, wR2(all data) 11.52%.

Trigonal $P3_121$

a = 17.092(3) Å α = 90°

b = 17.092(3) Å β = 90°

c = 26.548(5) Å γ = 120°

V = 6717(3) Å^3

[$K(thf)_5Yb\{N(SiMe_3)_2\}_3$] EM347

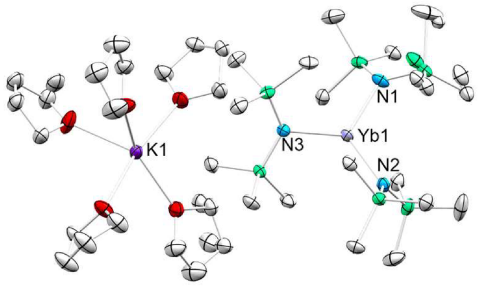

YbI_2 —(2 $K[N(SiMe_3)_2]$, 18h, r.t., THF)→

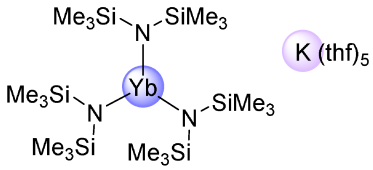

R1[I>sigma(I)] 3.29%, wR2(all data) 7.98%.

Triclinic $P\bar{1}$

a = 12.2311(11) Å α = 94.496(2)°

b = 14.3801(13) Å β = 94.183(2)°

c = 16.1903(14) Å γ = 96.655(2)°

V = 2810.0(4) Å^3

[Cp*$_2$Nd{N(SiMe$_3$)$_2$}] EM350

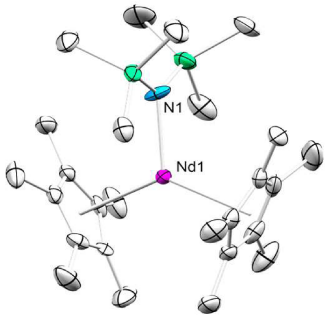

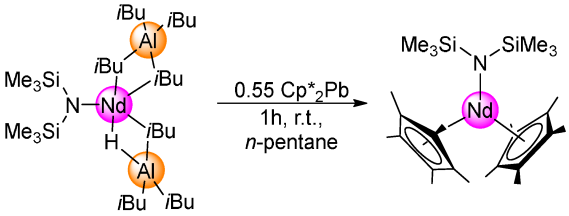

R1[I>sigma(I)] 3.17%, wR2(all data) 9.31%.

Trigonal $R\bar{1}$

a = 17.6948(6) Å α = 90°

b = 17.6948(6) Å β = 90°

c = 47.117(2) Å γ = 120°

V = 12776.2(11) Å^3

[*i*Bu$_2$Al-*μ*-H,{N(SiMe$_3$)$_2$}-Al*i*Bu$_2$] EM361

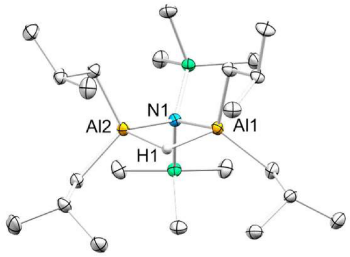

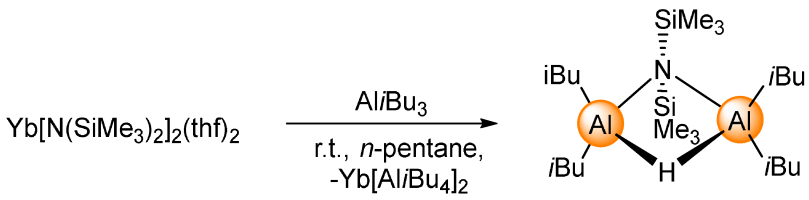

R1[I>sigma(I)] 3.10%, wR2(all data) 9.07%.

Triclinic $P\bar{1}$

a = 9.5029(4) Å α = 89.4390(10)°

b = 11.4520(5) Å β = 81.8950(10)°

c = 14.5393(6) Å γ = 67.9820(10)°

V = 1450.62(11) Å^3

$[(NEt_2)_2Gd(\mu\text{-}Cl)(thf)]_2$ EM 197

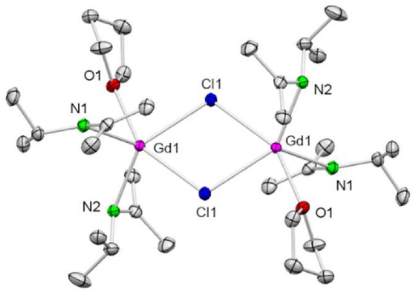

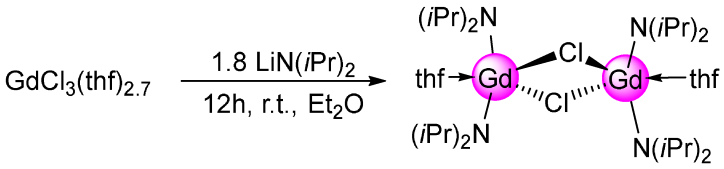

R1[I>sigma(I)] 2.24%, wR2(all data) 6.25%.

Monoclinic $P2_1/c$

a = 9.7613(14) Å α = 90°

b = 11.2450(16) Å β = 91.021(2)°

c = 18.080(3) Å γ = 90°

V = 1984.2(5) $Å^3$

Further analyses: EA, DRIFTS

$YCl_2(thf)_2(L3H)$ EM482

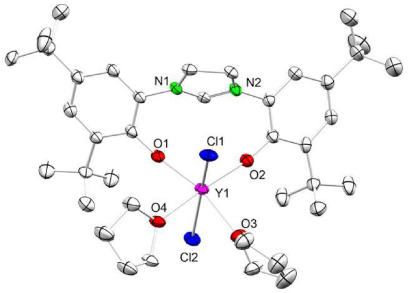

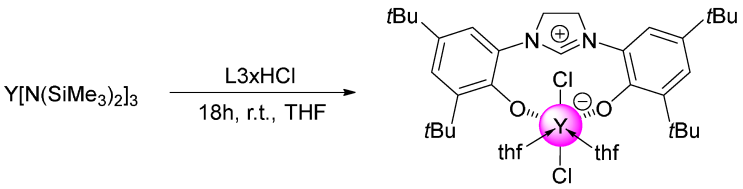

Connectivity of $YCl_2(thf)_2(L3H)$; L3 = 1,3-bis[O-4,6-di-*t*Bu-C_6H_2-2-CH_2][$C(NCH_2CH_2N)$].

Monoclinic $P2_1/c$

a = 18.2144(15) Å α = 90°

b = 19.2522(16) Å β = 99.761(2)°

c = 31.516(3) Å γ = 90°

V = 10892(16) $Å^3$

HoCl(thf)$_3$(L3) EM486

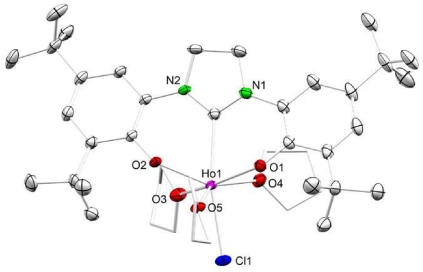

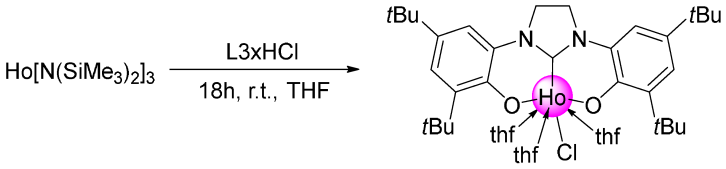

HoCl(thf)$_3$(L3); L3 = 1,3-bis[O-4,6-di-*t*Bu-C_6H_2-2-CH_2][C(NCH_2CH_2N)]

R1[I>sigma(I)] 3.36%, wR2(all data) 8.18%.

Monoclinic $P2_1/c$

a = 13.841(4) Å α = 90°

b = 10.4740(17) Å β = 92.692(11)°

c = 35.500(6) Å γ = 90°

V = 5140.7(18) Å^3

[(NEt_2)$_2$La(μ-NEt_2)(thf)]$_2$ PS28

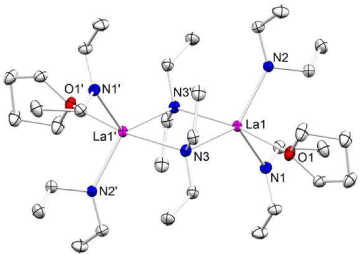

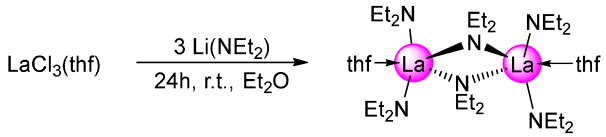

R1[I>sigma(I)] 1.96%, wR2(all data) 4.83%.

Triclinic $P\bar{1}$

a = 9.0669(8) Å α = 90.403(2)°

b = 9.5122(8) Å β = 103.864(2)°

c = 13.1984(12) Å γ = 113.268(2)°

V = 1008.64(15) Å^3

Further analyses: EA, DRIFTS

[(NEt$_2$)$_2$Sm(μ-NEt$_2$)(thf)]$_2$ PS33

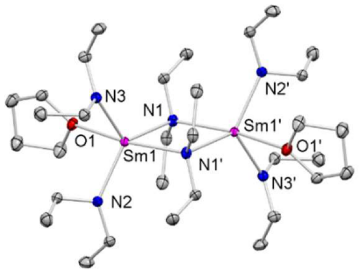

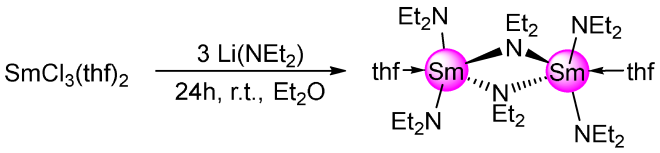

R1[I>sigma(I)] 2.62%, wR2(all data) 6.15%.

Triclinic $P\bar{1}$

a = 9.0566(15) Å α = 90.143(2)°

b = 9.4875(16) Å β = 104.235(2)°

c = 12.925(2) Å γ = 113.457(2)°

V = 981.2(3) Å^3 Further analyses: EA, DRIFTS

[(NEt$_2$)$_2$Gd(μ-NEt$_2$)(thf)]$_2$ PS15

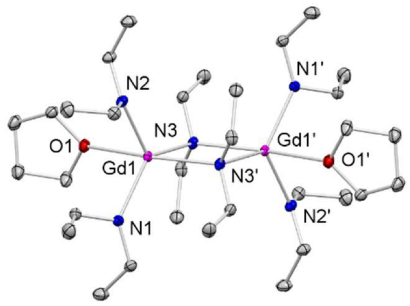

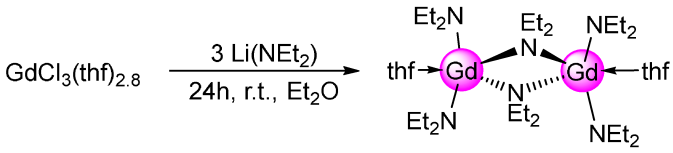

R1[I>sigma(I)] 1.12%, wR2(all data) 2.75%.

Triclinic $P\bar{1}$

a = 9.0558(4) Å α = 89.8580(10)°

b = 9.4771(4) Å β = 75.6140(10)°

c = 12.8916(5) Å γ = 66.5840(10)°

V = 977.66(7) Å^3